

MACONDO WELL INCIDENT
Transocean Investigation Report
Volume II

Appendices

- Appendix A.** Abbreviations and Acronyms
- Appendix B.** Macondo Casing Calculations
- Appendix C.** Testing of Cementing Float
- Appendix D.** Centralization Plan at Macondo
- Appendix E.** Review of Macondo #1 7" x 9-7/8" Production Casing Cementation
- Appendix F.** Lock-Down Sleeve Decision
- Appendix G.** Hydraulic Analysis of Macondo #252 Well Prior to Incident of April 20, 2010
- Appendix H.** BOP Modifications
- Appendix I.** BOP Maintenance History
- Appendix J.** BOP Testing
- Appendix K.** BOP Leaks
- Appendix L.** Drill Pipe in the BOP
- Appendix M.** Structural Analysis of the Macondo #252 Work String
- Appendix N.** AMF Testing
- Appendix O.** Analysis of Solenoid 103
- Appendix P.** *Deepwater Horizon* Investigation: Gas Dispersion Studies
- Appendix Q.** Possible Ignition Sources

Appendix A

Abbreviations and Acronyms

Appendix A Abbreviations and Acronyms

ABS	American Bureau of Shipping	DPO	dynamic positioning operator
AMF	automatic mode function	DTD	diverter test device
API	American Petroleum Institute	DWS	driller's work station
APM	application for permit to modify	ECD	equivalent circulating density
ASME	American Society of Mechanical Engineers	ECR	engine control room
Bankston	<i>Damon B. Bankston</i>	EDS	emergency disconnect system
bbbl	barrel or barrels	ESD	emergency shutdown
Bc	Bearden units of consistency	°F	degrees Fahrenheit
BHCT	bottom hole circulating temperature	FRC	fast rescue craft
BHST	bottom hole static temperature	ft.	foot or feet
BML	below mud line	gal	gallons
BOEMRE	Bureau of Ocean Energy Management, Regulation and Enforcement; formerly MMS	GMDSS	Global Maritime Distress Safety System
BOP	blowout preventer	gps	gallons per sack
bpm	barrels per minute	H₂S	hydrogen sulfide
BSR	blind shear ram	Hitec	NOV Hitec Cyberbase drilling rig control system
°C	degrees Celsius	HP	high pressure
C.F.R.	Code of Federal Regulations	HPHT	high pressure/high temperature
CBL	cement bond log	HVAC	heating, ventilation, and air conditioning
CCTV	closed-circuit television	HWDP	heavyweight drill pipe
CSR	casing shear ram	IADC	International Association of Drilling Contractors
DC	direct current	in.	inch or inches
DCP	driller's control panel	KCl	potassium chloride
DER	driller's equipment room	lb.	pound or pounds
DP	dynamically positioned	lbf	pounds (force)
		LCM	lost-circulation material

LIT	lead impression tool	ppg	pounds per gallon
LMRP	lower marine riser package	psi	pounds per square inch
LWD	Logging While Drilling	PWD	Pressure While Drilling
MAYDAY	emergency code word used as a distress signal	ROV	remotely operated vehicle
Marshall Islands (MI)	Republic of the Marshall Islands, the flag state of the <i>Deepwater Horizon</i>	RTE	rotary table elevation
MC252	Mississippi Canyon block 252, where the Macondo prospect is located	SBM	synthetic-based mud
MD	measured depth	SEM	subsea electronic module
MGS	mud-gas separator	sk	sack
MMS	Minerals Management Service, now BOEMRE	SOBM	synthetic oil-based mud
MOC	management of change	SOLAS	International Standards of Safety of Life at Sea (1974)
MODU	mobile offshore drilling unit	SSP	selected standpipe (drill pipe) pressure
MOU	mobile offshore unit	SSS	Simrad Safety System
MUX	multiplex	ST Lock	hydro-mechanical ram locking mechanism
MWD	Measurement While Drilling	STM	subsea transducer module
NDT	non-destructive testing	SVC	Simrad Vessel Control
No	number	TA	temporary abandonment
OBM	oil-based mud	TD	total depth
OCS	outer continental shelf	TVD	total vertical depth
OD	outside diameter	UCA	ultrasonic cement analyzer
OEM	original equipment manufacturer	USCG	United States Coast Guard
OIM	offshore installation manager	V	volt
PA	public address	VBR	variable bore ram
PETU	portable electronic test unit	VHF	very-high frequency radio
PLC	Programmable Logic Controller		

Appendix B

Macondo Casing Calculations



Macondo Casing Calculations

SES DOCUMENT NO.: 1101190-ST-RP-0001

Prepared for

**TRANSOCEAN OFFSHORE DEEPWATER
DRILLING, INC.**

Houston, Texas

REV	DATE	DESCRIPTION	ORIGINATOR	REVIEWER	APPROVER
C	24-Feb-11	Issued for Client Review	DLG/DK	RDY	
B	05-Nov-10	Issued for Client Review	DLG / DK	RDY	N/A
A	20-Oct-10	Issued for Internal Review	DLG / DK	N/A	N/A

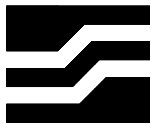
MACONDO CASING CALCULATIONS

SES DOCUMENT NO.: 1101190-ST-RP-0001

Prepared By: David L. Garrett
David L. Garrett, Ph.D.
Principal

Prepared By: Daniel Kluk
Daniel Kluk
Associate

Reviewed By: Ronald D. Young
Ronald D. Young, P.E.
Vice President



Stress Engineering Services, Inc.
13800 Westfair East Drive
Houston, Texas 77041-1101
281-955-2900 / www.stress.com

FEBRUARY 2011

EXECUTIVE SUMMARY

Transocean Offshore Deepwater Drilling, Inc., retained Stress Engineering Services, Inc. (SES) to provide technical assistance to the Macondo incident investigation. The assistance includes calculations that may be useful in the investigation. Calculations pertaining to casing are reported here. Structural analyses were limited to the 9-7/8" x 7" production casing. Load cases considered include (1) as installed, (2) pressure test, (3) the intended negative test, (4) case 3 with the addition of pressure on the annulus to reduce the casing hanger load to zero, (5) a modification of case 3 such that 16 ppg spacer is below the annular, and (6) a load case to represent flowing conditions. For each load case, the tension distribution in the casing, the pressure inside the casing, the pressure outside the casing, the load on the casing hanger, and stress in the casing are calculated. The load cases and the calculated results are presented here.

LIMITATIONS OF THIS REPORT

The scope of this report is limited to the matters expressly covered. This report is prepared for the sole benefit of Transocean. In preparing this report, Stress Engineering Services, Inc. (SES) has relied on information provided by Transocean Offshore Deepwater Drilling, Inc. Stress Engineering Services, Inc. (SES) has made no independent investigation as to the accuracy or completeness of such information and has assumed that such information was accurate and complete. Further, Stress Engineering Services, Inc. (SES) is not able to direct or control the operation or maintenance of client's equipment or processes.

All recommendations, findings and conclusions stated in this report are based upon facts and circumstances, as they existed at the time that this report was prepared. A change in any fact or circumstance upon which this report is based may adversely affect the recommendations, findings, and conclusions expressed in this report.

NO IMPLIED WARRANTY OF MERCHANTABILITY OR FITNESS FOR A PARTICULAR PURPOSE SHALL APPLY. STRESS ENGINEERING SERVICES, INC. MAKES NO REPRESENTATION OR WARRANTY THAT THE IMPLEMENTATION OR USE OF THE RECOMMENDATIONS, FINDINGS, OR CONCLUSIONS OF THIS REPORT WILL RESULT IN COMPLIANCE WITH APPLICABLE LAWS OR PERFECT RESULTS.

TABLE OF CONTENTS

	<u>Page No.</u>
EXECUTIVE SUMMARY	iii
1.0 INTRODUCTION.....	1
2.0 CASING	2
3.0 ANALYTICAL MODEL.....	6
4.0 LOAD CASES	7
5.0 RESULTS	9

LIST OF TABLES

	<u>Page No.</u>
Table 1: Macondo Casing Program	3
Table 2: Casing Properties for Drilling Strings	4
Table 3: Casing Properties for Production Casing.....	5
Table 4: Casing Segments in Model	6
Table 5: Load Cases for Structural Analysis of Production Casing	8
Table 6: Summary Structural Analysis Results	9
Table 7: Detailed Structural Analysis Results	10

LIST OF FIGURES

	<u>Page No.</u>
Figure 1: Macondo Well Schematic	2

1.0 INTRODUCTION

Transocean Offshore Deepwater Drilling, Inc., retained Stress Engineering Services, Inc. (SES) to provide technical assistance to the Macondo incident investigation. The assistance includes calculations that may be useful in the investigation.

Calculations pertaining to casing are reported here. Structural analyses were limited to the 9-7/8" x 7" production casing. Load combinations for the production casing were selected to represent, or be similar to, loading that may have occurred after installation of the production casing. Load cases considered include (1) as installed, (2) pressure test, (3) the intended negative test, (4) case 3 with the addition of pressure on the annulus to reduce the casing hanger load to zero, (5) a modification of case 3 such that 16 ppg spacer is below the annular, and (6) a load case to represent flowing conditions. For each load case, the tension distribution in the casing, the pressure inside the casing, the pressure outside the casing, the load on the casing hanger, and stress in the casing are calculated. The load cases and the calculated results are presented here.

A summary of the casing in the well is presented and properties for structural analyses are presented. The analytical model of the production casing used for structural analysis is described. Specifics for the load cases considered are listed and described. Results of the structural calculations are presented.

2.0 CASING

Transocean Offshore Deepwater Drilling, Inc., provided the well schematic shown in Figure 1 and the casing summary in Table 1.

Figure 1: Macondo Well Schematic

MACONDO WELL CASING & CEMENTING STATUS		CASING SIZE (")	WEIGHT (PPF)	GRADE	CASING CONNECTION	SHOE DEPTH (MD BRT)	HANG OFF POINT (MD BRT)	LOT / FIT (PPG EMW)	CASING TEST (PSI)	DRILLING FLUID BEHIND CASING / LINER (PPG)	Cement
	5067ft Scaled	36	2.0" / 1.5" wall	X-56	HC-100 / D90	5335	5071	8.7	N/A	N/A	N/A
		28	218.27	X-52	S60	6231	5076	9.8	N/A	N/A	389bbbls 13.5ppg foamed lead Unfoamed tail cement
		22	277 / 224.28	X-80	H90 / S90	7952	5068	10.3	N/A	N/A	243 bbbls 16.74 lead #1 567 bbbls 14.5ppg lead #2 14.5 ppg tail cement
		18	117	P-110	Hydril 511	8963	7503	11.7		10.1 SOBM	160bbbls 16.4ppg (tail only)
		16	97	P-110	Hydril 511	11585	5241	12.5	1125	11.2 SOBM	16.4ppg (tail only)
	9 7/8" x 7" X/O @ 12,487ft - 12,483ft	13 5/8"	88.2	Q-125	SLU-II	13145	11153	14.5	2400	12.4 SOBM	16.4ppg (tail only)
		11 7/8"	71.8	HCG-125	Hydril 513	15103	12817	14.7	1800	13.4 SOBM	16.4ppg (tail only)
		9 7/8"	65	Q-125	Hydril 523	17168	14759	16	914	14.1 SOBM	16.4ppg (tail only)
		7" x 9 7/8"	32 / 62.8	Q-125	Hydril 523	18285	5054	N/A	2700	14.0 SOBM	12bbbl @ 16.74ppg 48bbbl @ 14.5ppg
	18,300ft Well TD										

Table 1: Macondo Casing Program

Macondo MC 252 #1 Well Casing Summary Table

Size	Weight (ppf)	Grade	Couplings	Set From MDBRT (ft)	Set To MDBRT (ft)
36"	2" / 1.5" wall	X65	HC-100 / D90	5071	5335
28"	218.3	X52	S60	5076	6231
22"	277 / 224.28	X80	H90 / S90	5068	7952
18"	117.0	P110	Hydril 511	7503	8983
16"	97.0	P110	Hydril 511	5241	11585
13.625"	88.2	Q125	SLIJ-II	11153	13145
11.875"	71.8	Q125	Hydril 513	12817	15103
9.875"	65.0	Q125	Hydril 523	14759	17168
7 x 9.875"	32 / 62.8	Q125	Hydril 523	5054	18285

SES used calculations and catalog values to determine casing properties for structural analysis. The properties for the drilling casing strings are in Table 2 and the properties for the production casing are in Table 3.

Table 2: Casing Properties for Drilling Strings

Pipe OD, in.	22.000	18.000	16.000
Pipe wall, t, in.	1.250	0.625	0.575
Pipe ID, in.	19.500	16.750	14.850
A_o , in ²	380.133	254.469	201.062
A_i , in ²	298.648	220.353	173.198
A , in ²	81.485	34.116	27.864
AE, lb	2.44E+09	1.02E+09	8.36E+08
EI, lb-ft ²	9.17E+08	2.69E+08	1.73E+08
Weight, lb/ft	277	117	97
SMYS, psi	80,000	110,000	110,000
t_{min}/t	0.875	0.875	0.875
Capped end yield pressure, CEYP, psi	8,663	7,450	7,701
Yield tension, T_y , lb	6,518,805	3,752,731	3,065,036
Collapse pressure, psi	7,270	2,110	2,340
Connection	H90/S90	Hydril 511	Hydril 511
Connection yield tension, lb		2,331,000	1,916,000

Pipe OD, in.	13.625	11.875	9.875
Pipe wall, t, in.	0.625	0.582	0.650
Pipe ID, in.	12.375	10.711	8.575
A_o , in ²	145.802	110.753	76.589
A_i , in ²	120.276	90.105	57.751
A , in ²	25.525	20.648	18.838
AE, lb	7.66E+08	6.19E+08	5.65E+08
EI, lb-ft ²	1.13E+08	6.88E+07	4.20E+07
Weight, lb/ft	88.2	71.8	65
SMYS, psi	125,000	125,000	125,000
t_{min}/t	0.875	0.875	0.875
Capped end yield pressure, CEYP, psi	11,055	11,773	15,532
Yield tension, T_y , lb	3,190,680	2,581,025	2,354,722
Collapse pressure, psi	4,800	5,630	12,160
Connection	SLIJ-II	Hydril 513	Hydril 523
Connection yield tension, lb	2,393,000	1,595,000	1,681,000

Table 3: Casing Properties for Production Casing

Pipe OD, in.	9.875	7.000
Pipe wall, t, in.	0.625	0.453
Pipe ID, in.	8.625	6.094
A _o , in ²	76.589	38.485
A _i , in ²	58.426	29.167
A, in ²	18.162	9.317
AE, lb	5.45E+08	2.80E+08
EI, lb-ft ²	4.07E+07	1.05E+07
Weight, lb/ft	62.8	32
SMYS, psi	125,000	125,000
t _{min} /t	0.875	0.875
Capped end yield pressure, CEYP, psi	14,975	15,288
Yield tension, T _y , lb	2,270,292	1,164,663
Collapse pressure, psi	11,140	11,710
Connection	Hydril 523	Hydril 523
Connection yield tension, lb	1,682,000	843,000

In the tables, capped end yield pressure (CEYP) is the internal pressure required to yield a capped end tube. The theoretical value is reduced by 0.875 to account for a -12.5% wall tolerance. Pressure differential (inside to outside the tube) and effective tension can be combined to determine the von Mises stress using the formulae;

$$CEYP = \frac{SMYS}{\sqrt{3}} \frac{A}{A_o} \frac{t_{min}}{t}$$

$$T_y = SMYS \times A$$

$$\sqrt{\left(\frac{\Delta p}{CEYP}\right)^2 + \left(\frac{T_{effective}}{T_y}\right)^2} = \frac{\sigma_{von Mises}}{SMYS}$$

3.0 ANALYTICAL MODEL

The production casing was modeled analytically. The model extends from the subsea wellhead (depth = 5,054 ft) to the top of cement (TOC depth = 17,300 ft). A work string, supported at the rig, extends to a depth of 8,367 ft (shown as 8,637 ft in Figure 1). Since the portion of the 9.875” casing above 8,367 ft may have a different fluid than the portion below 8,367 ft, the model consists of three segments as listed in Table 4.

Table 4: Casing Segments in Model

Segment	From	To	Casing OD
1	5,054	8,367	9.875
2	8,367	12,485	9.875
3	12,485	17,300	7

The ends of the casing at the casing hanger and at TOC are assumed restrained.

For analysis, the internal and external pressure at the wellhead, the temperature at the wellhead, and the fluid density inside and outside each casing segment are specified. The temperature distribution is assumed linear with a bottom hole temperature of 242°F at a depth of 18,124 ft. The initial condition assumes the casing is suspended in 14.17 ppg mud. The initial effective tension at the TOC is assumed to be 25 kips, which corresponds to 1,000 ft of 7” casing in mud. The initial temperature at the wellhead is 40°F.

The casing hanger seal diameter used for hanger load calculations is 18.635 in.

4.0 LOAD CASES

Load combinations for the production casing were selected to represent, or be similar to, loading that may have occurred after installation of the production casing. The load cases are listed in Table 5.

The As Landed case provides the initial tension, pressure and stress distributions, as well as the initial hanger load. The pressure at the wellhead, inside and outside, corresponds to a 5,054 ft head of 14.17 ppg mud. The casing and annulus are filled with 14.17 ppg mud.

The Pressure Test case increases the internal pressure by 2,700 psi. The internal pressure at the wellhead corresponds to a 5,054 ft head of mud plus 2,700 psi.

The Intended Negative Test has mud and spacer displaced with water from the bottom of the work string to above the wellhead. The annular is closed and the surface pressure is bled off. The pressure at the wellhead corresponds to a 5,054 ft head of sea water.

The next case adds 398 psi to the casing annulus. The increase in annulus pressure was calculated to result in a zero casing hanger load.

The next case replaces the water in the casing above 8,367 ft with 16 ppg fluid (spacer). The pressure inside the casing at the wellhead is calculated assuming 1,400 psi on the work string at the surface plus an 8,367 ft head of seawater less a (8,367-5,054) ft head of 16 ppg spacer.

The last case assumes 4,400 psi at the wellhead, which was observed on May 25, 2010. A temperature increase from 40°F to 160°F was assumed. A pressure increase of 1,500 psi on the annulus, to account for thermal expansion, was assumed.

Table 5: Load Cases for Structural Analysis of Production Casing

As landed	P _i	3717	psi		
	P _o	3717	psi		
	T	40	deg F		
	Segment	1	2	3	
	MW _i	14.17	14.17	14.17	
	MW _o	14.17	14.17	14.17	
Pressure test	P _i	6,417	psi		
	P _o	3,717	psi		
	T	40	deg F		
	Segment	1	2	3	
	MW _i	14.17	14.17	14.17	
	MW _o	14.17	14.17	14.17	
Intended negative test	P _i	2,244	psi		
	P _o	3,717	psi		
	T	40	deg F		
	Segment	1	2	3	
	MW _i	8.556	14.17	14.17	
	MW _o	14.17	14.17	14.17	
Intended negative test + 398 psi on annulus	P _i	2,244	psi		
	P _o	4,115	psi		
	T	40	deg F		
	Segment	1	2	3	
	MW _i	8.556	14.17	14.17	
	MW _o	14.17	14.17	14.17	
Negative test (16 ppg to bottom of work string)	P _i	2,364	psi		
	P _o	3,717	psi		
	T	40	deg F		
	Segment	1	2	3	
	MW _i	16	14.17	14.17	
	MW _o	14.17	14.17	14.17	
May 25 pressure and estimated temperature	P _i	4,400	psi		
	P _o	5,217	psi		
	T	160	deg F		
	Segment	1	2	3	
	MW _i	4	4	4	
	MW _o	14.17	14.17	14.17	

5.0 RESULTS

Summary results are in Table 6. The hanger load is in kips; the sign convention is such that, if the hanger load is negative, the hanger may move up if unrestrained. VME is the maximum calculated von Mises stress in the casing expressed as a percentage of yield. If the internal pressure exceeds the external pressure, the Burst load (internal pressure minus external pressure) is expressed as a percentage of Capped End Yield Pressure (CEYP). If the external pressure exceeds the internal pressure, the Collapse load (external pressure minus internal pressure) is expressed as a percentage of the casing collapse pressure. The Burst and Collapse values are the maximum values. The maximum effective tension is expressed as a percentage of connection yield tension, which is lower than pipe body yield tension.

The effective tension distribution, internal pressure and external pressure distributions, and the von Mises stress distribution (as a percentage of yield) are in Table 7.

Table 6: Summary Structural Analysis Results

Case	Hanger load (kips)	VME (% yield)	Burst (% CEYP)	Collapse (%)	Tension (% Connection)
As landed	513	23%	0%	0%	30%
Pressure test	1,204	27%	18%	0%	28%
Intended negative test	100	24%	0%	22%	30%
Intended negative test + 398 psi on annulus	0	26%	0%	25%	30%
Negative test (16 ppg to bottom of work string)	179	26%	0%	12%	33%
May 25 pressure and estimated temperature	-7	48%	0%	62%	13%

Table 7: Detailed Structural Analysis Results

	Depth	T _{eff}	P _i	P _o	VME
As landed	5,054	513	3,717	3,717	23%
	8,367	349	6,153	6,153	15%
	8,367	349	6,153	6,153	15%
	12,485	145	9,182	9,182	6%
	12,485	145	9,182	9,182	12%
	17,300	25	12,723	12,723	2%
Pressure test	5,054	468	6,417	3,717	27%
	8,367	304	8,853	6,153	22%
	8,367	304	8,853	6,153	22%
	12,485	100	11,882	9,182	19%
	12,485	100	11,882	9,182	20%
	17,300	-20	15,423	12,723	18%
Intended negative test	5,054	501	2,244	3,717	24%
	8,367	394	3,715	6,153	24%
	8,367	394	3,715	6,153	24%
	12,485	190	6,744	9,182	18%
	12,485	190	6,744	9,182	23%
	17,300	69	10,285	12,723	17%
Intended negative test + 398 psi on annulus	5,054	510	2,244	4,115	26%
	8,367	403	3,715	6,551	26%
	8,367	403	3,715	6,551	26%
	12,485	199	6,744	9,580	21%
	12,485	199	6,744	9,580	25%
	17,300	78	10,285	13,121	20%
Negative test (16 ppg to bottom of work string)	5,054	548	2,364	3,717	26%
	8,367	366	5,115	6,153	18%
	8,367	366	5,115	6,153	18%
	12,485	162	8,144	9,182	10%
	12,485	162	8,144	9,182	15%
	17,300	41	11,685	12,723	8%
May 25 pressure and estimated temperature	5,054	215	4,400	5,217	11%
	8,367	153	5,088	7,653	18%
	8,367	153	5,088	7,653	18%
	12,485	76	5,943	10,682	32%
	12,485	76	5,943	10,682	32%
	17,300	30	6,942	14,223	48%

Appendix C

Testing of Cementing Float

TESTING OF CEMENTING FLOAT

Prepared for

**Transocean Offshore
Deepwater Drilling, Inc.
Houston, TX**

February, 2011

PN1101190DLG

**Stress Engineering Services, Inc.
Houston, Texas**

Testing of Cementing Float

SES PN 1101190DLG

Prepared for
Transocean Offshore Deepwater Drilling, Inc.
Houston, TX

Prepared By: *Brent Vyvial*
Brent Vyvial
Associate

Reviewed By: *George Ross*
George Ross, Ph.D, P.E.
Principal

David L. Garrett
David L. Garrett, Ph.D.
Principal



February, 2011

EXECUTIVE SUMMARY

Stress Engineering Services, Inc. was contracted by Transocean Offshore Deepwater Drilling, Inc. to test two exemplar cementing floats. SES understands that the exemplar floats were the same type as the float used in the MC252 well. During the cementing operation, there were indications that the pressure to convert the float was higher than what was expected. The purpose of the testing program is to gain a better understanding of the operation of this type of cementing float and identify potential causes for such a cementing float to require larger than expected pressures to convert the float (i.e. release the tube) and allow the flappers to close.

Due to the limited number of exemplar floats available for testing, bench testing of the floats was conducted in order to test the float performance in a more controlled manner. This testing program was performed in four phases. The first phase involved applying a load to the tube and measuring the load required to fail the tube retainer. The second phase of testing measured the load required to push the ball out of the tube. These loads were used to calculate equivalent pressures. The third phase tested the sealing ability of the flappers at ambient and elevated temperature. The fourth phase of testing measured the load required to push the flapper assembly out of the float.

Floats #1 and #2 converted at equivalent pressures of 410 and 406 psi, respectively. The equivalent pressure required to fail the seat at the end of the tube was 1,477 psi for Float #1 and 1,840 psi for Float #2. The flappers in both floats held a pressure of 3,000 psi of synthetic oil-based mud at a temperature of 225 °F. An equivalent pressure of 10,155 psi was required to fail the flapper assembly of Float #1.

LIMITATIONS OF THIS REPORT

The scope of this report is limited to the matters expressly covered. This report is prepared for the sole benefit of Transocean Offshore Deepwater Drilling, Inc. In preparing this report, Stress Engineering Services, Inc. (SES) has relied on information provided by Transocean Offshore Deepwater Drilling, Inc. SES has made no independent investigation as to the accuracy or completeness of such information and has assumed that such information was accurate and complete. Further, SES is not able to direct or control the operation or maintenance of client's equipment or processes.

All recommendations, findings and conclusions stated in this report are based upon facts and circumstances, as they existed at the time that this report was prepared. A change in any fact or circumstance upon which this report is based may adversely affect the recommendations, findings, and conclusions expressed in this report.

NO IMPLIED WARRANTY OF MERCHANTABILITY OR FITNESS FOR A PARTICULAR PURPOSE SHALL APPLY. STRESS ENGINEERING SERVICES, INC. MAKES NO REPRESENTATION OR WARRANTY THAT THE IMPLEMENTATION OR USE OF THE RECOMMENDATIONS, FINDINGS, OR CONCLUSIONS OF THIS REPORT WILL RESULT IN COMPLIANCE WITH APPLICABLE LAWS OR PERFECT RESULTS.

TABLE OF CONTENTS

	<u>Page No.</u>
EXECUTIVE SUMMARY	i
TABLE OF CONTENTS.....	iii
LIST OF TABLES.....	iv
LIST OF FIGURES	iv
1.0 INTRODUCTION	1
2.0 TEST METHODS AND SET-UP	2
2.1 <i>Float Conversion Test</i>	2
2.2 <i>Tube Seat Shear Test</i>	3
2.3 <i>Flapper Pressure Test</i>	4
2.4 <i>Flapper Assembly Shear Test</i>	6
3.0 TEST RESULTS.....	7
3.1 <i>Float Conversion Test</i>	7
3.2 <i>Tube Seat Shear Test</i>	11
3.3 <i>Flapper Pressure Test</i>	15
3.4 <i>Flapper Assembly Shear Test</i>	18
3.5 <i>Float Ball Dissection</i>	21
4.0 CONCLUSIONS.....	22
APPENDIX A: CALIBRATION CERTIFICATES	23
APPENDIX B: MUD TEST REPORT	43

LIST OF TABLES

	<u>Page No.</u>
Table 3.1: Float Conversion Loads and Pressures	10
Table 3.2: Tube Seat Shear Loads and Pressures	14

LIST OF FIGURES

	<u>Page No.</u>
Figure 2.1: Float Conversion Test Set-up Diagram	2
Figure 2.2: Tube Seat Shear Test Set-up Diagram	3
Figure 2.3: Flapper Pressure Test Set-Up	5
Figure 2.4: Flapper Assembly Shear Test Set-up	6
Figure 3.1: Load vs. Displacement Plot for Float Conversion on Float #1	7
Figure 3.2: Post-test Photographs for Float Conversion on Float #1	8
Figure 3.3: Retaining Screw Removed from Float #1 after Conversion Test	8
Figure 3.4: Load vs. Displacement Plot for Float Conversion on Float #2	9
Figure 3.5: Post-test Photographs for Float Conversion on Float #2	9
Figure 3.6: Photograph of Gluing Tube into Plate	11
Figure 3.7: Load vs. Displacement Plot for Tube Seat Shear Test on Float #1	12
Figure 3.8: Post-test Photographs for Tube Seat Shear Test on Float #1	12
Figure 3.9: Load vs. Displacement Plot for Tube Seat Shear Test on Float #2	13
Figure 3.10: Post-test Photographs for Tube Seat Shear Test on Float #2	13
Figure 3.11: Photograph of Flapper Pressure Test	15
Figure 3.12: Pressure Plot for Ambient Temperature Pressure Test of Float #1	16
Figure 3.13: Pressure Plot for Elevated Temperature Pressure Test of Float #1	16
Figure 3.14: Pressure Plot for Ambient Temperature Pressure Test of Float #2	17
Figure 3.15: Pressure Plot for Elevated Temperature Pressure Test of Float #2	17
Figure 3.16: Photograph of Flapper Assembly Shear Test	18
Figure 3.17: Load vs Displacement Plot for Flapper Assembly Shear Test of Float #1	19
Figure 3.18: Photograph of Flapper Assembly Failure	19
Figure 3.19: Close-up Photograph of Flapper Assembly Failure	20

Figure 3.20: Halves of Float Ball..... 21
Figure 3.21: Close-up of Float Ball 21

1.0 INTRODUCTION

Stress Engineering Services, Inc. (SES) was contracted by Transocean Offshore Deepwater Drilling, Inc. to test two exemplar cementing floats. SES understands that the exemplar floats were the same type as the float used in the MC252 well. During the cementing operation, there were indications that the pressure to convert the float was higher than what was expected. The purpose of the testing program is to gain a better understanding of the operation of this type of cementing float and identify potential causes for such a cementing float to require larger than expected pressures to convert the float (i.e. release the tube) and allow the flappers to close.

Due to the limited number of exemplar floats available for testing, bench testing of the floats was conducted in order to test the float performance in a more controlled manner. This testing program was performed in four phases. The first phase involved applying a load to the tube and measuring the load required to fail the tube retainer. The second phase of testing measured the load required to push the ball out of the tube. These loads were used to calculate the equivalent pressure. The third phase tested the sealing ability of the flappers at ambient and elevated temperature. The fourth phase of testing measured the load required to push the flapper assembly out of the float.

Measurements of floats and additional photographs are included in a separate report. The following sections of this report detail the test set-ups, methods, and results for the tests conducted on the cementing floats.

2.0 TEST METHODS AND SET-UP

2.1 Float Conversion Test

1. Determine load at which plug shears (set-up shown in Figure 2.1)
 - a. Begin recording data on DAQ system
 - b. Apply load to ball using pushrod
 - c. Increase load until plug shears
 - d. Stop test and remove float from test set-up
 - e. Photo document float condition
2. Set plug and any other loose components aside

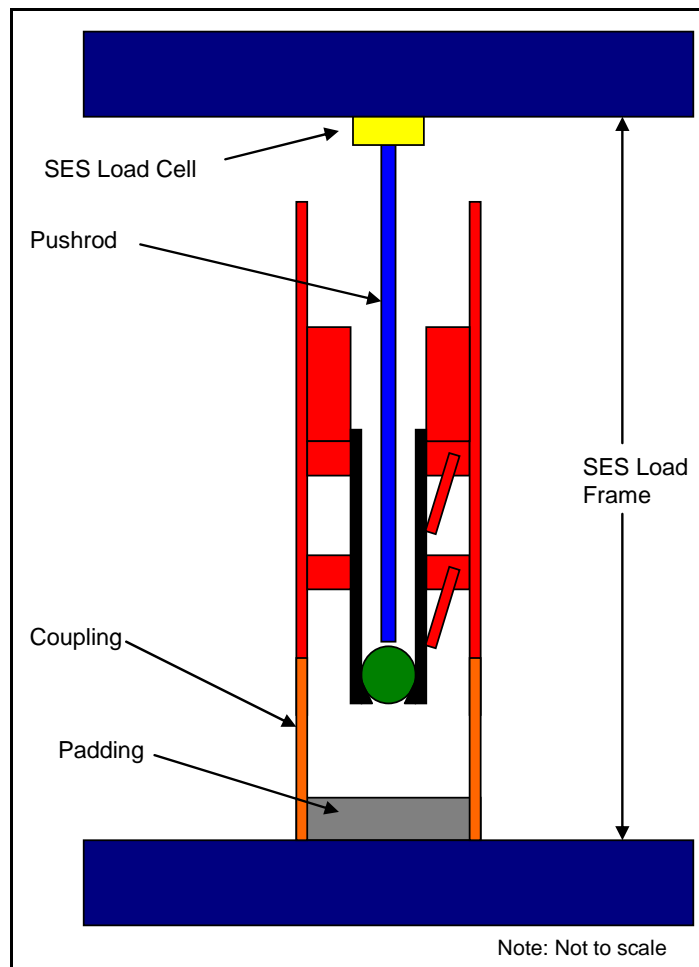


Figure 2.1: Float Conversion Test Set-up Diagram

2.2 Tube Seat Shear Test

1. Determine load at which seat shears (set-up shown in Figure 2.2)
 - a. Begin recording data on DAQ system
 - b. Apply load to ball using pushrod
 - c. Increase load until seat shears
 - d. Stop test and remove tube from test set-up
2. Set tube and any other loose components aside

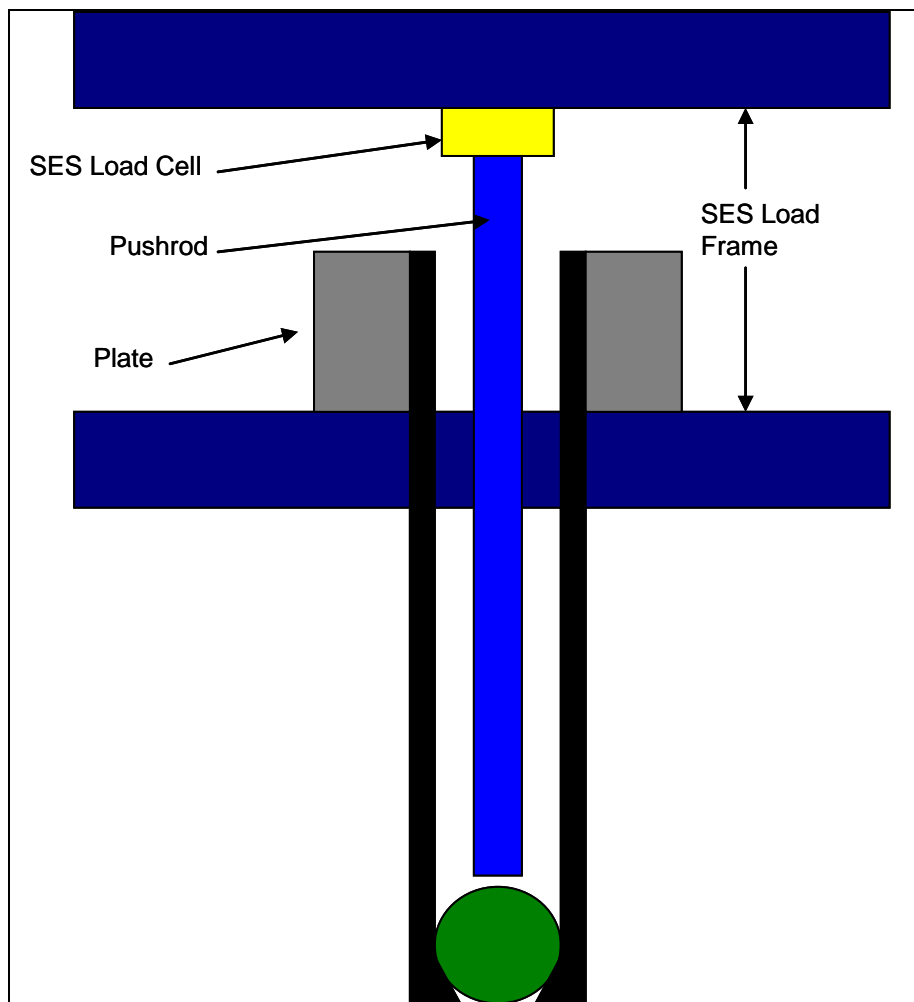


Figure 2.2: Tube Seat Shear Test Set-up Diagram

2.3 Flapper Pressure Test

1. With float vertical, fill float past top flapper with drilling fluid
2. Begin recording data on DAQ system
3. Apply internal pressure of 10 psi to float
4. Hold 2 minutes
5. Apply internal pressure of 20 psi to float
6. Hold 2 minutes
7. Apply internal pressure of 50 psi to float
8. Hold 2 minutes
9. Increase internal pressure to 100 psi
10. Hold 2 minutes
11. Increase internal pressure to 250 psi
12. Hold 2 minutes
13. Increase internal pressure to 500 psi
14. Hold 2 minutes
15. Remove pressure
16. Heat float to 225°F
17. Repeat Steps 3 through 14
18. Increase internal pressure to 1,000 psi
19. Hold 2 minutes
20. Increase internal pressure to 1,500 psi
21. Hold 2 minutes
22. Increase internal pressure to 2,000 psi
23. Hold 2 minutes
24. Increase internal pressure to 2,500 psi
25. Hold 2 minutes
26. Increase internal pressure to 3,000 psi
27. Hold for a minimum of 2 minutes
28. Remove pressure
29. Stop data acquisition

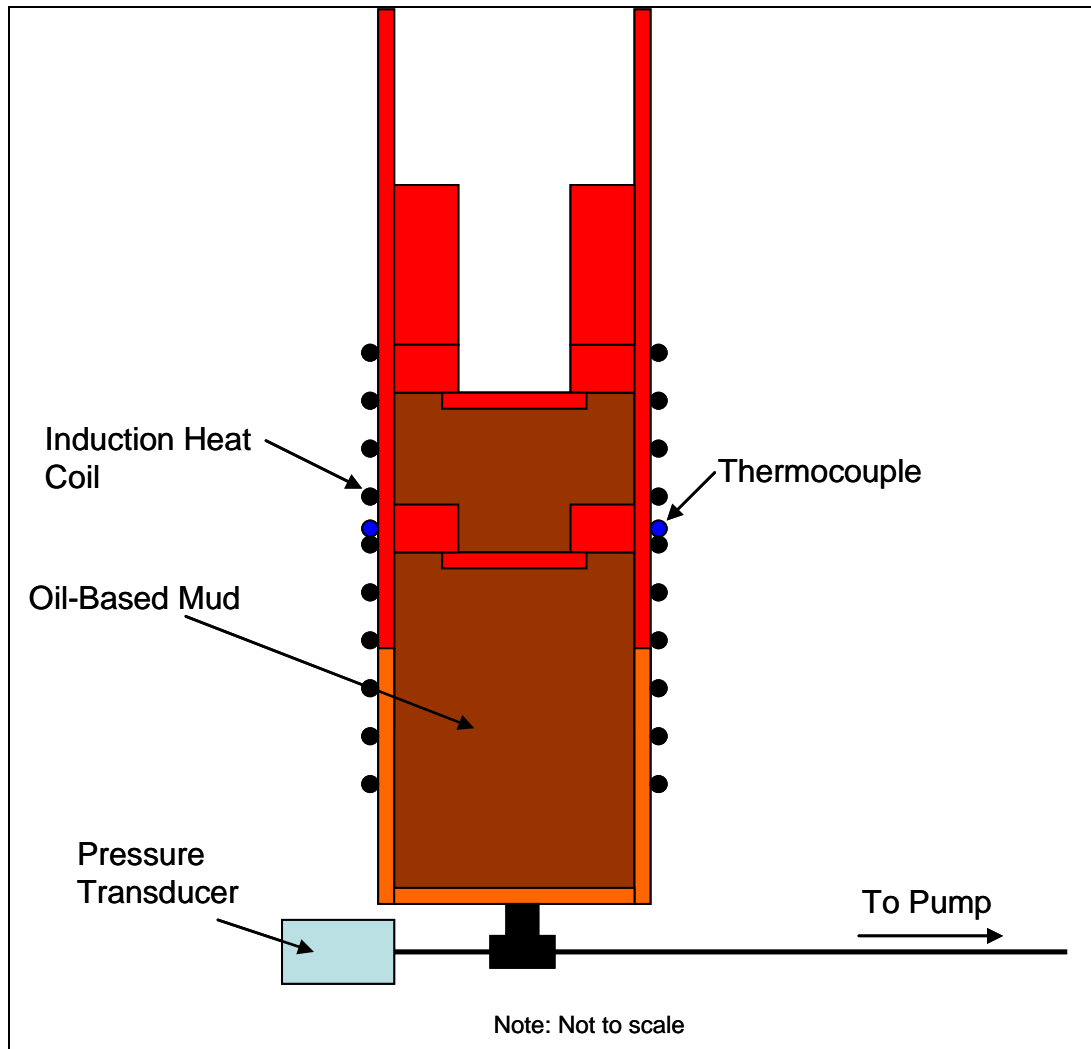


Figure 2.3: Flapper Pressure Test Set-Up

2.4 Flapper Assembly Shear Test

1. Cut float above top of tube retainer ring
2. Set-up test as shown in Figure 2.4
3. Start data acquisition to record load and displacement
4. Increase load until flapper assembly fails
5. Stop data acquisition

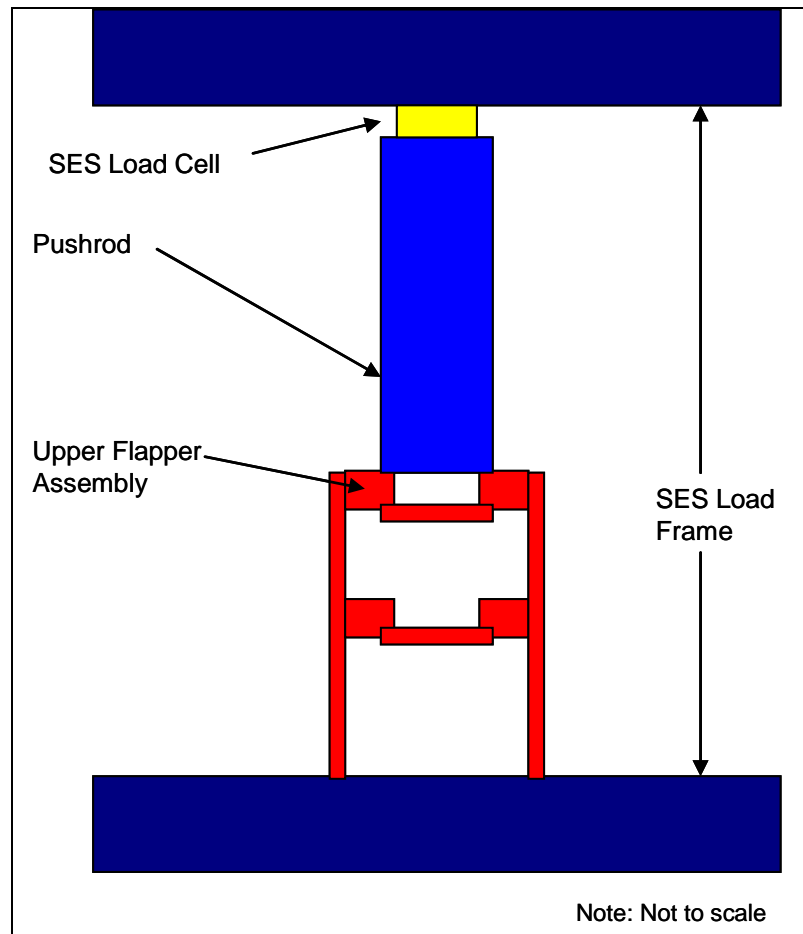


Figure 2.4: Flapper Assembly Shear Test Set-up

3.0 TEST RESULTS

3.1 Float Conversion Test

The float conversion test was set-up to simulate the pressure applied to the ball for conversion of the float. The load was applied to the ball with a load bar with a concave surface machined to match the curvature of the ball in order to evenly distribute the load over the surface of the ball. The float was placed in the frame vertically and load was applied to the ball until failure occurred. The results of the conversion tests for the two floats are plotted in Figure 3.1 and 3.4. The equivalent pressure required for conversion of the float was calculated using the applied load and the cross-sectional area of the inside of the tube. A summary of the maximum loads and equivalent pressures is listed in Table 3.1. For both exemplar floats, the retaining screws at the top of the tube did not shear; however the ring that holds the screws failed under the screws. An example of the retaining screws removed after the conversion test of Float #1 is shown in Figure 3.3. This allowed the screws to rotate down and out of the holes in the tube, and then drag along the surface of the tube. The photographs in Figure 3.2 and Figure 3.5 show the failure of the retainer ring and drag marks on the outside of the tube.

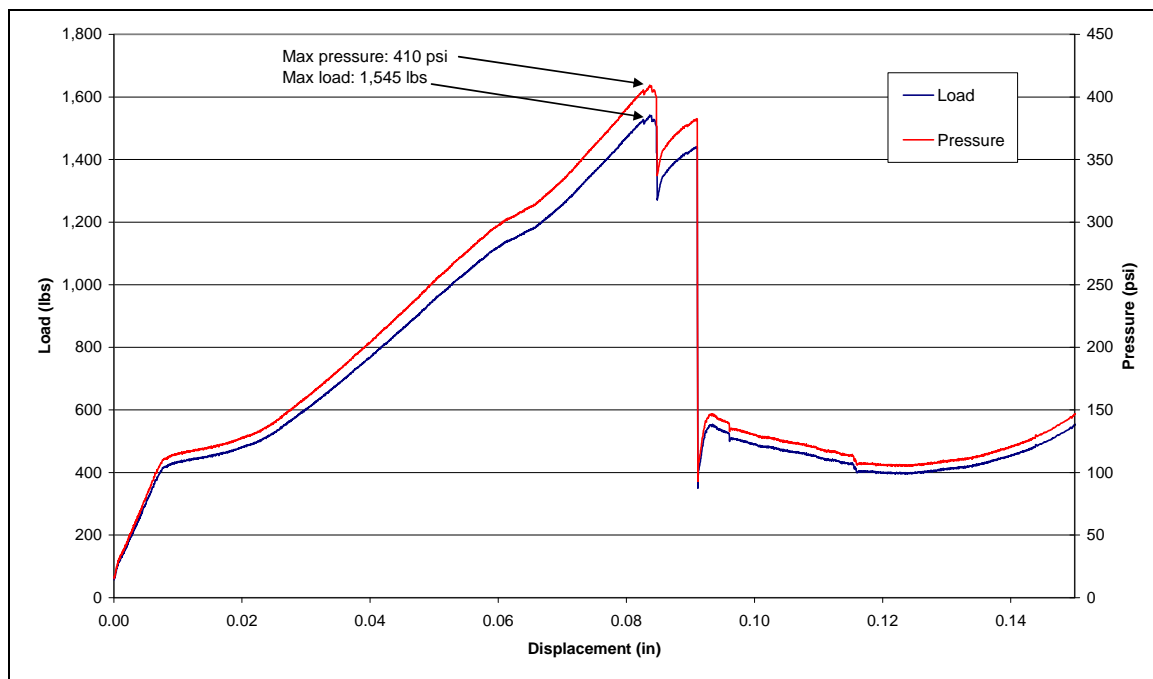


Figure 3.1: Load vs. Displacement Plot for Float Conversion on Float #1

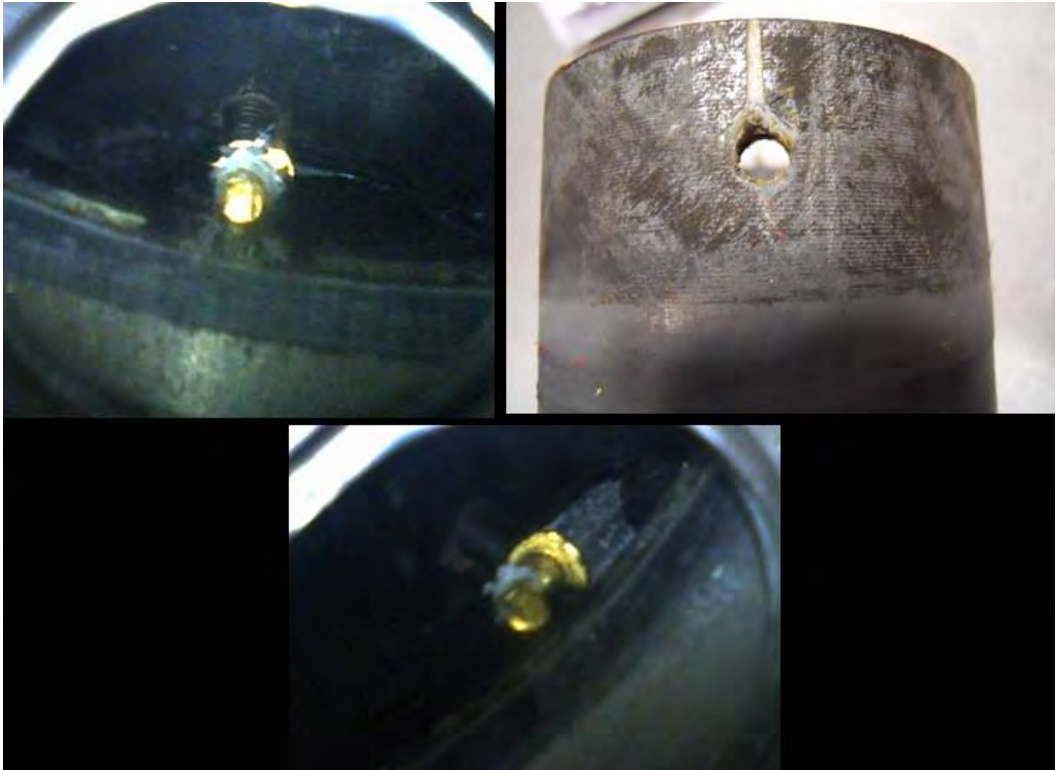


Figure 3.2: Post-test Photographs for Float Conversion on Float #1



Figure 3.3: Retaining Screw Removed from Float #1 after Conversion Test

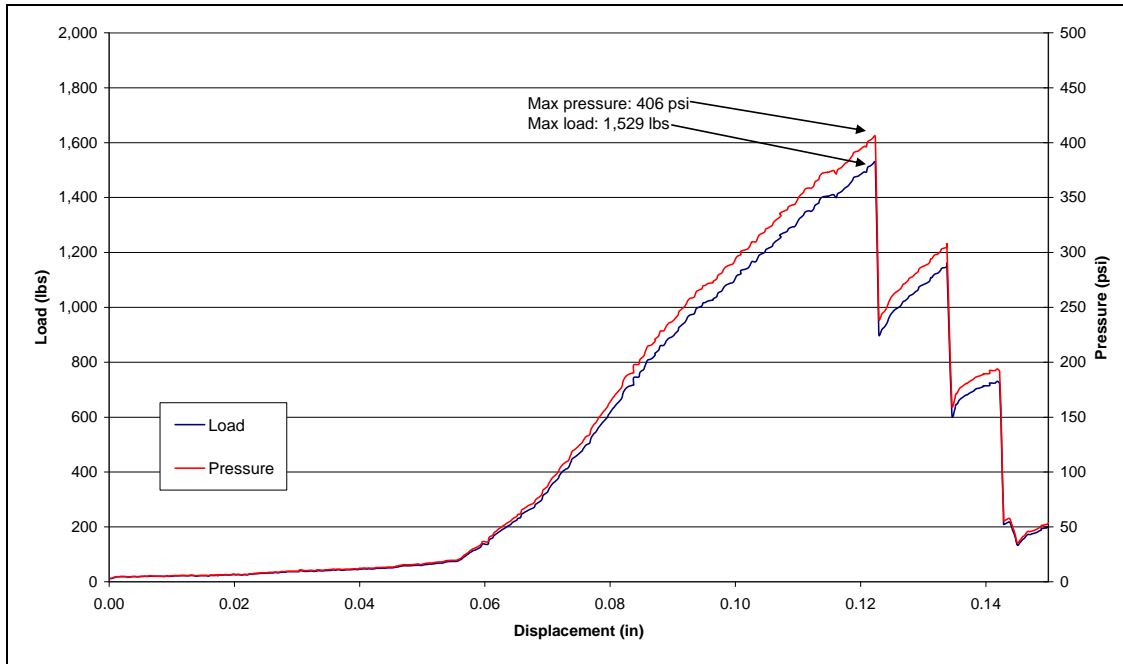


Figure 3.4: Load vs. Displacement Plot for Float Conversion on Float #2



Figure 3.5: Post-test Photographs for Float Conversion on Float #2

Table 3.1: Float Conversion Loads and Pressures

	Failure Load (lbs)	Pressure* (psi)
Float #1	1,545	410
Float #2	1,529	406

*Pressure calculated from load and cross-sectional area of 2.19 in ID tube

3.2 Tube Seat Shear Test

The second test was conducted to determine the load capacity of the ball seat located at the bottom of the tube. The tube was installed in a plate with a hole slightly larger than the outer diameter of the tube using a two part epoxy (Figure 3.6). The ball was loaded in the same manner as in the float conversion test. Load was applied until failure of the seat occurred. The results for the two floats are plotted in Figures 3.7 and 3.9. The equivalent pressures were calculated using the same method as in the float conversion test. The maximum loads and equivalent pressures for the two tests are listed in Table 3.2. The photographs in Figures 3.8 and 3.10 show the failure of the seat. In both tests, the seat failed and opened enough to allow the ball to pass through and out of the tube, with the ball remaining intact.

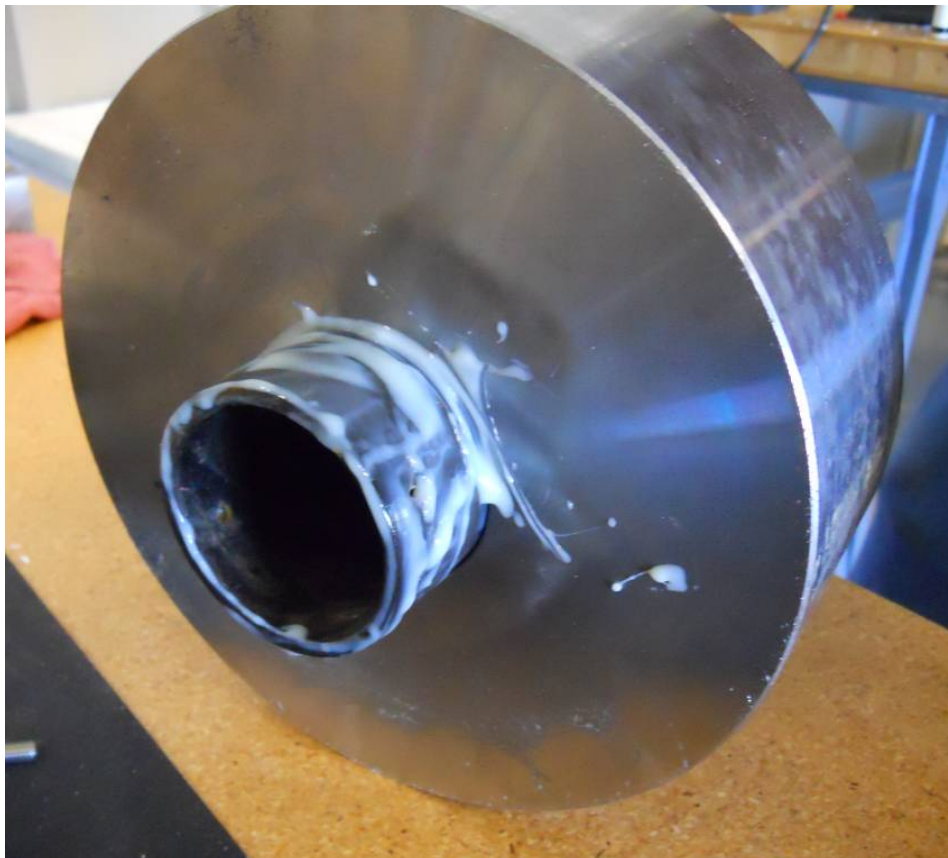


Figure 3.6: Photograph of Gluing Tube into Plate

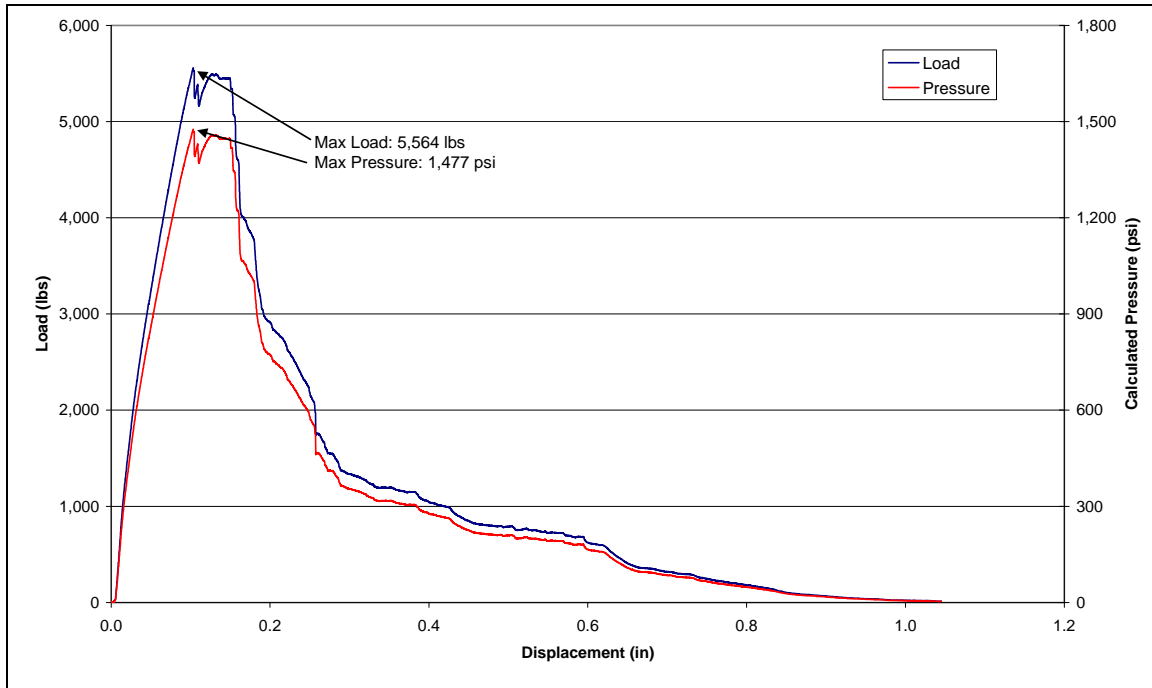


Figure 3.7: Load vs. Displacement Plot for Tube Seat Shear Test on Float #1



Figure 3.8: Post-test Photographs for Tube Seat Shear Test on Float #1

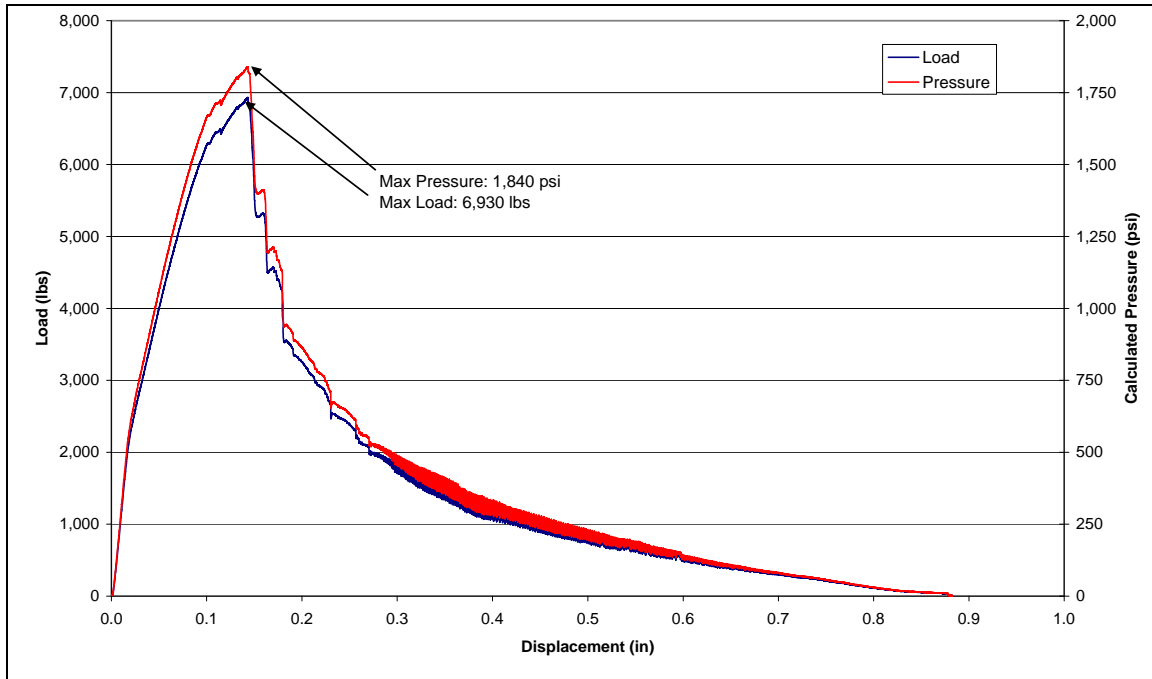


Figure 3.9: Load vs. Displacement Plot for Tube Seat Shear Test on Float #2



Figure 3.10: Post-test Photographs for Tube Seat Shear Test on Float #2

Table 3.2: Tube Seat Shear Loads and Pressures

	Failure Load (lbs)	Pressure* (psi)
Float #1	5,564	1,477
Float #2	6,930	1,840

*Pressure calculated from load and cross-sectional area of 2.19 in ID tube

3.3 Flapper Pressure Test

After the conversion tests, the floats were tested to check the sealing capability of the flappers. The pressure medium for the tests was 12 pound per gallon synthetic oil based mud. The floats were oriented vertically and filled with the mud. Both floats were pressure tested to 500 psi at ambient temperature. The ambient temperature pressure test results for the floats are plotted in Figures 3.12 and 3.14. The floats were then heated to 225°F and allowed to reach steady state prior to pressure testing to 3,000 psi. The results from the elevated temperature tests are plotted in Figures 3.13 and 3.15.



Figure 3.11: Photograph of Flapper Pressure Test

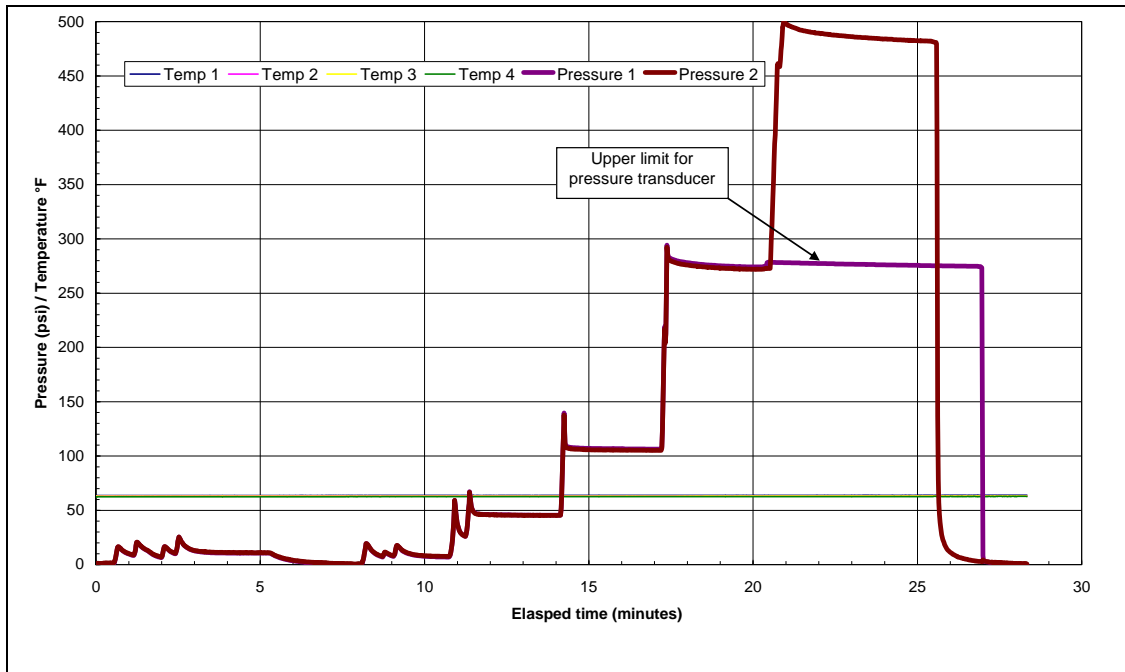


Figure 3.12: Pressure Plot for Ambient Temperature Pressure Test of Float #1

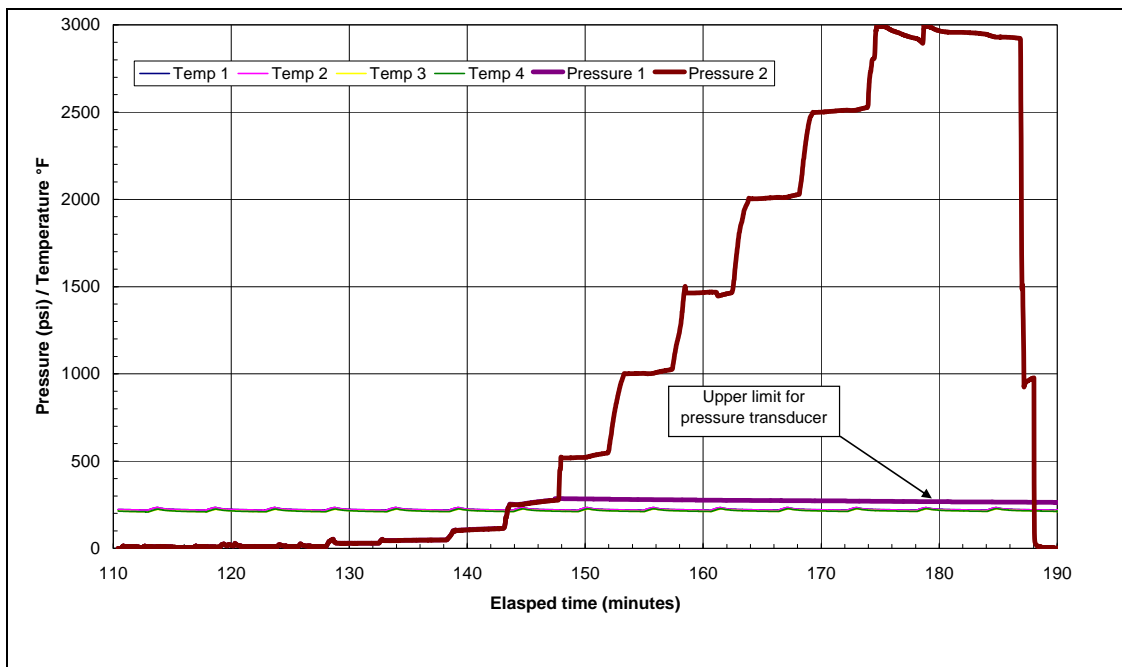


Figure 3.13: Pressure Plot for Elevated Temperature Pressure Test of Float #1

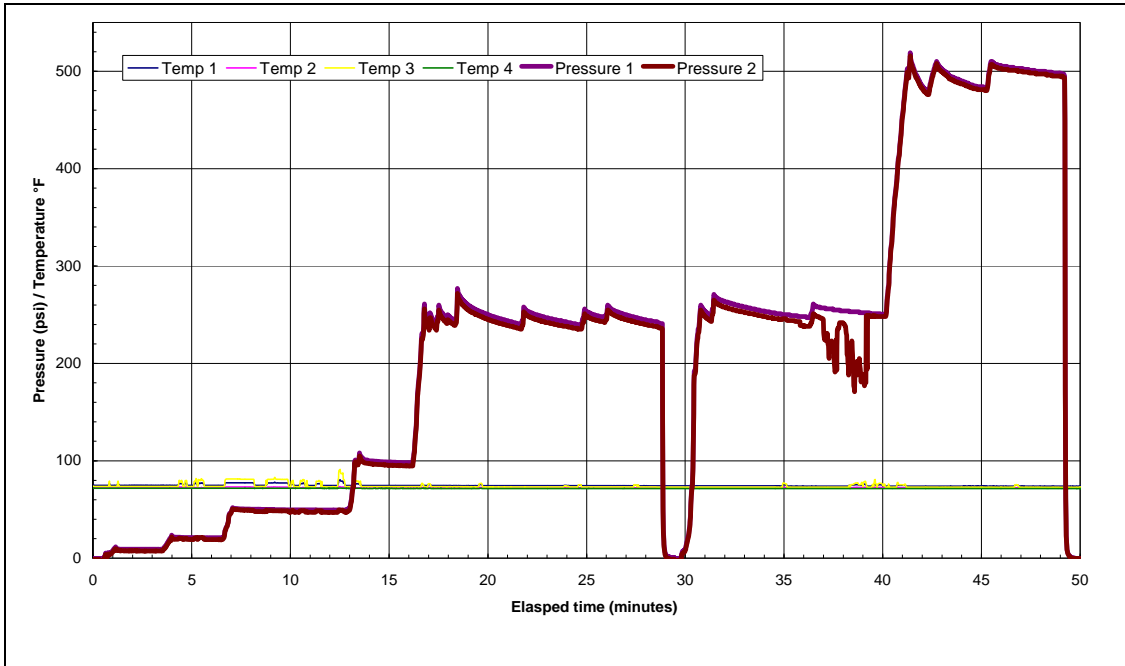


Figure 3.14: Pressure Plot for Ambient Temperature Pressure Test of Float #2

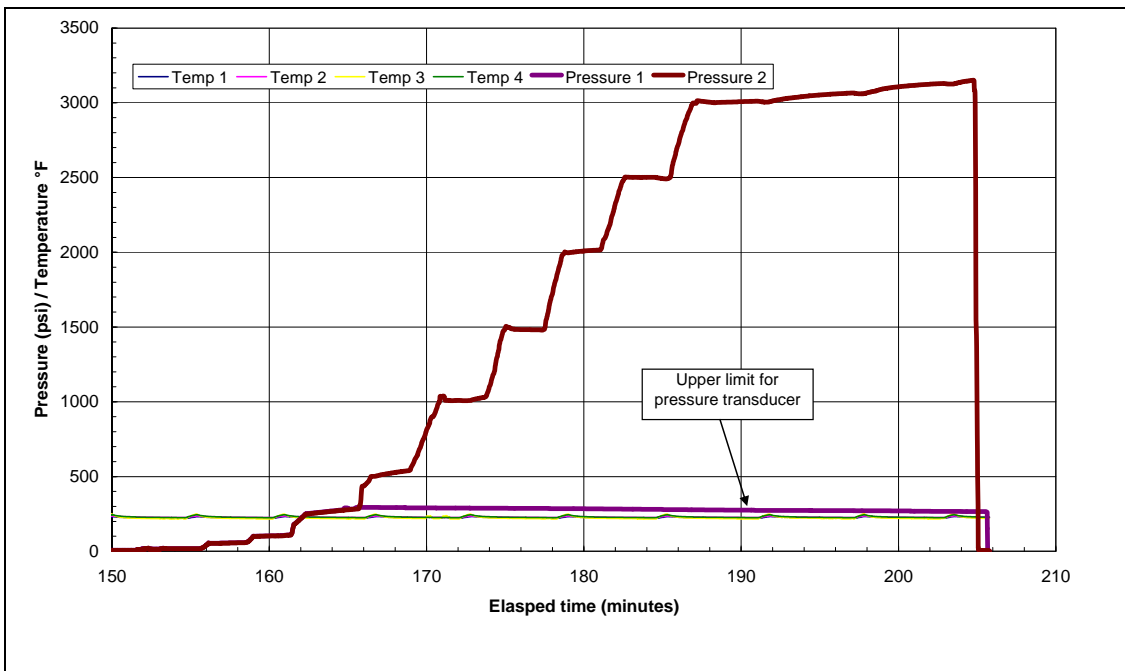


Figure 3.15: Pressure Plot for Elevated Temperature Pressure Test of Float #2

3.4 Flapper Assembly Shear Test

After the pressure test, Float #1 was cut above the top of the tube mounting ring. The ring and retaining screws were removed from the float and the upper flapper assembly was loaded until failure occurred. The test set-up is shown in Figure 3.16. The results from the test are shown in Figure 3.17. The equivalent pressure was calculated using the load and the cross-sectional area of the ring with an outer diameter of 3.2 in. The flapper assembly failed at 81,847 lbs which corresponds to an equivalent pressure of 10,155 psi. Photographs of the failed flapper assembly are shown in Figures 3.18 and 3.19.



Figure 3.16: Photograph of Flapper Assembly Shear Test

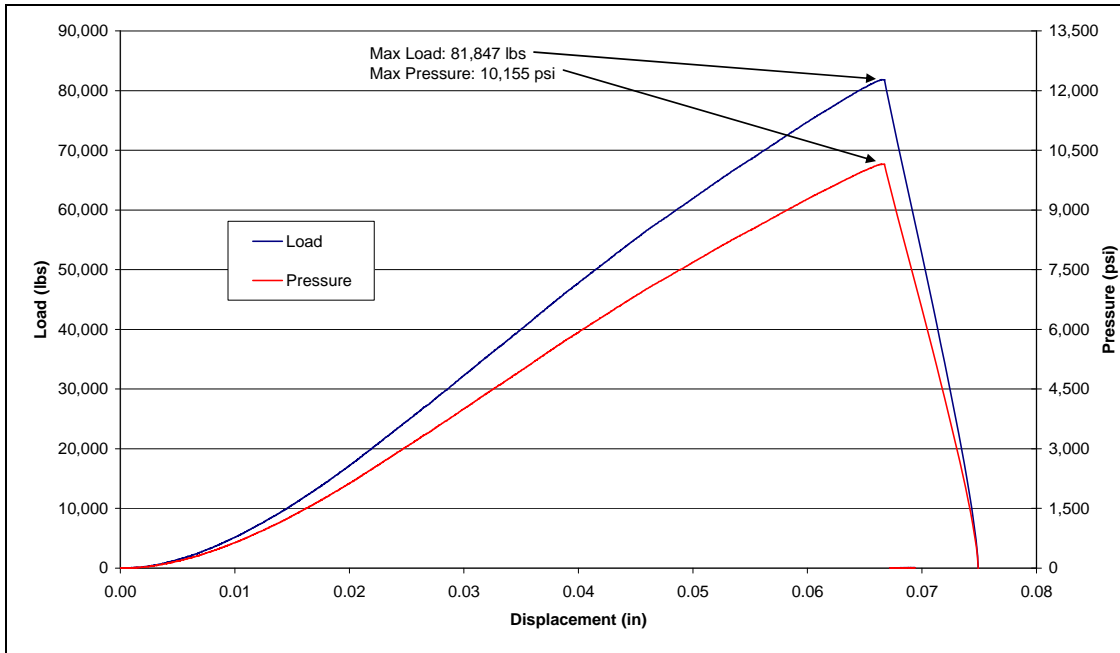


Figure 3.17: Load vs Displacement Plot for Flapper Assembly Shear Test of Float #1



Figure 3.18: Photograph of Flapper Assembly Failure



Figure 3.19: Close-up Photograph of Flapper Assembly Failure

3.5 Float Ball Dissection

After testing was completed, the ball from Float #1 was cut in half. The two halves are shown in Figure 3.20. A close-up photograph of one half of the ball is shown in Figure 3.21. The ball appears to contain powdered metal. The ball was checked with a magnet and confirmed to contain a ferrous material. The balls from both floats were confirmed to be 2 inches in diameter.



Figure 3.20: Halves of Float Ball



Figure 3.21: Close-up of Float Ball

4.0 CONCLUSIONS

Both exemplar floats tested in this program converted at pressures near the conversion pressure listed on the body of the float (300 – 400 psi). The three retaining screws holding the tube in place did not shear during the conversion tests for the floats, but the outer ring holding the screws failed at the bottom of the hole. This allowed the screws to rotate out of the holes in the tube, releasing the tube from the float. The equivalent pressure required to fail the ball seat at the end of the tube was over three times higher than the pressure required to convert the float. The balls from both floats remained intact for both the conversion and seat shear tests.

The floats tested in this program held pressures of up to 3,000 psi with minimal pressure drop when tested with 12 pound per gallon synthetic oil-based mud at a temperature of 225 °F. The flapper assembly failed in the cast portion at an equivalent pressure of 10,155 psi.

APPENDIX A: CALIBRATION CERTIFICATES



PO Box 355 Dobbin, Tx 77333
 Phone - 713-515-3619

CALIBRATION CERTIFICATE

CUSTOMER: Stress Engineering Services			
13800 WESTFAIR EAST DR			
Transducer Make:	Dynisco	Transducer Model:	A830-000-2.5C-K73
Transducer S/N:	250438178	Transducer Range:	0 - 250 psi
Reference and testing conditions:		979.312 gals	18°C +/- 1.5 deg
		Excitation	5.0013 volts
CALIBRATION READINGS (as left)			
ACTUAL (psi)	READING 1 (mv)	CONVERTED (psi)	PERCENT ERROR % of FS
0	0.710	0.0	0.00
25	2.183	25.0	-0.01
50	3.662	50.1	0.03
100	6.619	100.2	0.09
150	9.527	149.6	-0.17
200	12.516	200.3	0.11
250	15.447	250.0	0.00
All readings within manufacturer tolerance (+/- .5% F.S.)			
CONVERSION FACTORS (Reading - Offset)*gain			
Shunt Reading (millivolts)	Shunt Reading (psi)	Offset (millivolts)	Gain (psi/mv)
12.673	202.9	0.71	16.96
Calibration performed per STS document PTC1001 and is traceable to N.I.S.T.			
Equipment used: Pressurements Ametek 10-5525 SN:585-4, Keithly 2000 Sn: 1068367			
Technician	L. Wilson	DATE:	January 7, 2010
SIGNED:		RECALL:	January 7, 2011



PO Box 355 Dobbin, Tx 77333
 Phone - 713-515-3619

CALIBRATION CERTIFICATE

CUSTOMER: Stress Engineering Services			
13800 WESFAIR EAST BLVD			
Transducer Make:	Dynisco	Transducer Model:	G830-300-5C-K73
Transducer S/N:	240333574	Transducer Range:	0 - 500 psi
Reference and testing conditions:		979.312 gals	24°C +/- 1.5 deg
		Excitation	5 003
CALIBRATION READINGS (as found as left)			
ACTUAL (psi)	READING 1 (mv)	CONVERTED (psi)	PERCENT ERROR % of FS
0	0.510	0.0	0.00
50	2.049	50.7	0.15
100	3.570	100.9	0.17
200	6.610	201.1	0.22
300	9.643	301.1	0.21
400	12.668	400.8	0.15
500	15.682	500.1	0.02
All readings within manufacturer tolerance (+/- .5% F.S.)			
CONVERSION FACTORS (Reading - Offset)*gain			
Shunt Reading (millivolts)	Shunt Reading (psi)	Offset (millivolts)	Gain (psi/mv)
12.65	400	0.51	32.96
Calibration performed per STS document PTC1001 and traceable to N.I.S.T.			
Equipment used: Amtek S/N 585-5, Keithley 2000 Sn: 1068367			
Technician L. Wilson		DATE: April 23, 2010	
SIGNED:		RECALL: April 23, 2011	



PO Box 355 Dobbin, Tx 77333
 Phone - 713-515-3619

Specialized Test Services

CALIBRATION CERTIFICATE

CUSTOMER: Stress Engineering Services			
13800 WESTFAIR EAST DR			
Transducer Make:	Dynisco	Transducer Model:	G830-300-3M-K73
Transducer S/N:	220948983	Transducer Range:	0 - 3000 psi
Reference and testing conditions:		979.312 gals	31°C +/- 1.5 deg
		Excitation	5.043 volts
CALIBRATION READINGS (as left)			
ACTUAL (psi)	READING 1 (mv)	CONVERTED (psi)	PERCENT ERROR % of FS
0	1.585	0	0.00
50	1.828	48	-0.05
100	2.078	98	-0.06
300	3.079	297	-0.09
600	4.582	596	-0.12
1200	7.593	1195	-0.15
1800	10.610	1796	-0.14
2400	13.634	2398	-0.08
3000	16.662	3000	0.00
All readings within manufacturer tolerance (+/- .5% F.S.)			
CONVERSION FACTORS (Reading - Offset)*gain			
Shunt Reading (millivolts)	Shunt Reading (psi)	Offset (millivolts)	Gain (psi/mv)
13.626	2396	1.585	198.98
Calibration performed per STS document PTC1001 and traceable to N.I.S.T.			
Equipment used: Pressuremeat: Ametek 10-5525 SN:585-4, HP Model 34401A Sn: MY47007060			
Technician: L. Wilson		DATE: August 17, 2010	
SIGNED:		RECALL: August 17, 2011	

RCN Enterprises, Inc.
 371 Bowler Road
 Waller Texas 77484

21 September 2010

C A L I B R A T I O N R E P O R T

OWNER: SES - Stress Engineering Services, Inc.
 13800 Westfair East Drive
 Houston Texas 77041

MACHINE: Lebow - Daytronics 10,000lb Load Cell System
 Lebow Load Cell M/ 3124-10K S/ 1257516
 Daytronics Ind. Model: 3270 Serial: S02648
 Shunt Cal: 6630 Calibration in TENSION

CALIBRATION DATA:	RANGE LB	Positive Output		MACHINE ERROR	
		LOAD INDICATED	TRUE LB	LB	PERCENT
	10000	1000.	1008.	-8.	0.84
		2000.	2007.	-7.	0.33
		3000.	3002.	-2.	0.08
		4000.	3997.	3.	0.08
		5000.	4989.	11.	0.23
		6000.	5983.	17.	0.28
		7000.	6976.	24.	0.35
		8000.	7967.	33.	0.42
		9000.	8959.	41.	0.45
		10000.	9951.	49.	0.49
		1000.	1007.	-7.	0.71
		2000.	2008.	-8.	0.40
		3000.	3002.	-2.	0.08
		4000.	3995.	5.	0.11
		5000.	4991.	9.	0.17
		6000.	5983.	17.	0.28
		7000.	6976.	24.	0.35
		8000.	7968.	32.	0.40
		9000.	8961.	39.	0.44
		10000.	9952.	48.	0.48

True loads were recorded at the values of indicated load listed above according to the current ASTM Standard E-4.

DEVICE DATA:	INSTRUMENTS USED.....	SERIAL NO	CLASS 'A' RANGE.....	LOADING LB.....	VERIFIED DATE.....
	B L H Load Cell	18223	178 -	2,400	24 Aug 10
	Sensotec Cell	658345	1,560 -	25,000	16 Oct 08

Instruments were verified as noted above by National Standards Testing Laboratory according to current ASTM Standard E-74. Instruments were compensated for effect of temperature on zero and span by the manufacturer(s).

C E R T I F I C A T E O F V E R I F I C A T I O N

THIS IS TO CERTIFY THAT THE

Lebow - Daytronics 10,000lb Load Cell System
Lebow Load Cell M/ 3124-10K S/ 1257516
Daytronics Ind. Model: 3270 Serial: S02648
Shunt Cal: 6630 Calibration in TENSION
- - - Positive Output - - -

LOCATED AT

SES - Stress Engineering Services, Inc.
13800 Westfair East Drive
Houston Texas 77041

was calibrated on 21 September 2010 according to the current ASTM Standard E-4 as applied to load cells and determined to indicate load within the specified 1.0 percent tolerance on the ranges listed below. Maximum error observed was 0.84 percent.

MACHINE RANGE, LB	LOADING RANGE, LB MINIMUM - MAXIMUM
10,000	1,000 - 10,000

Ambient temperature recorded during the calibration: 82.2 F.

Devices used were verified as noted below by National Standards Testing Laboratory according to the current ASTM Standard E-74.

INSTRUMENTS USED.....	SERIAL NO	CLASS 'A' RANGE.....	LOADING RANGE.....LB	VERIFIED.DATE
B L H Load Cell	18223	178 -	2,400	24 Aug 10
Sensotec Cell	658345	1,560 -	25,000	16 Oct 08

RCN Enterprises, Inc.
371 Bowler Road
Waller Texas 77484

21 September 2010



RCN Enterprises, Inc.
 371 Bowler Road
 Waller Texas 77484

21 September 2010

C A L I B R A T I O N R E P O R T

OWNER: SES - Stress Engineering Services, Inc.
 13800 Westfair East Drive
 Houston Texas 77041

MACHINE: Lebow - Daytronics 10,000lb Load Cell System
 Lebow Load Cell M/ 3124-10K S/ 1257516
 Daytronics Ind. Model: 3270 Serial: S02648
 Shunt Cal: 6610 Calibration in COMPRESSION
 - - - Negative Output - - -

CALIBRATION DATA:	RANGE LB	LOAD.....LB		MACHINE ERROR	
		INDICATED	TRUE	LB	PERCENT
	10000	1000.	1004.	-4.	0.44
		2000.	2000.	0.	0.00
		3000.	3000.	0.	0.01
		4000.	3994.	6.	0.15
		5000.	4994.	6.	0.12
		6000.	5993.	7.	0.12
		7000.	6992.	8.	0.12
		8000.	7989.	11.	0.13
		9000.	8982.	18.	0.20
		10000.	9989.	11.	0.11
		1000.	1003.	-3.	0.31
		2000.	2000.	0.	0.00
		3000.	2997.	3.	0.10
		4000.	3995.	5.	0.11
		5000.	4995.	5.	0.09
		6000.	5989.	11.	0.19
		7000.	6990.	10.	0.14
		8000.	7989.	11.	0.13
		9000.	8993.	7.	0.08
		10000.	9991.	9.	0.09

True loads were recorded at the values of indicated load listed above according to the current ASTM Standard E-4.

DEVICE DATA:	INSTRUMENTS USED.....	SERIAL NO	CLASS 'A' RANGE.....	LOADINGLB	VERIFIED.DATE
	B L H Load Cell	18223	163 -	2,400	24 Aug 10
	Sensotec Cell	658345	1,560 -	25,000	16 Oct 08

Instruments were verified as noted above by National Standards Testing Laboratory according to current ASTM Standard E-74. Instruments were compensated for effect of temperature on zero and span by the manufacturer(s).

C E R T I F I C A T E O F V E R I F I C A T I O N

THIS IS TO CERTIFY THAT THE

Lebow - Daytronics 10,000lb Load Cell System
Lebow Load Cell M/ 3124-10K S/ 1257516
Daytronics Ind. Model: 3270 Serial: S02648
Shunt Cal: 6610 Calibration in COMPRESSION
- - - Negative Output - - -

LOCATED AT

SES - Stress Engineering Services, Inc.
13800 Westfair East Drive
Houston Texas 77041

was calibrated on 21 September 2010 according to the current ASTM Standard E-4 as applied to load cells and determined to indicate load within the specified 1.0 percent tolerance on the ranges listed below. Maximum error observed was 0.44 percent.

MACHINE RANGE, LB	LOADING RANGE, LB MINIMUM - MAXIMUM
10,000	1,000 - 10,000

Ambient temperature recorded during the calibration: 84.2 F.

Devices used were verified as noted below by National Standards Testing Laboratory according to the current ASTM Standard E-74.

INSTRUMENTS USED.....	SERIAL NO	CLASS 'A' RANGE.....	LOADING RANGE.....LB	VERIFIED.DATE
B L H Load Cell	18223	163 -	2,400	24 Aug 10
Sensotec Cell	658345	1,560 -	25,000	16 Oct 08

RCN Enterprises, Inc.
371 Bowler Road
Waller Texas 77484

21 September 2010





MTS Systems Corporation
 14000 Technology Drive
 Eden Prairie, MN 55344-2590

Calibration Report



Customer Name: Stress Engineering System: 30852D Page: 2 of 2 CALIBRATION CERT #1145.01
 Report Number: 1194-1723
 Site: 521917
 System ID: 22 KIP Sta #11 Location: Lab Country Code: USA

Equipment Device Type: Length Model: LVDT Serial No.: 782
 Controller/Conditioner Model: 493.25 Serial No.: 02047795P
 Readout Device Model: 493.25 Serial No.: 02047795P Channel: Disp

Procedure MTS Procedure: FS-CA 2124 Rev. A ACS Version: 7.02
 Calibration has been performed in accordance with: (none)
 Method of Verification:

Calibration Equipment Asset No. High Level Board: Low Level Board: Standard Asset No.: 17519
 DW Compensation: DMM: 16850 Digital Indicator: Lower Limit:
 Temperature Readout: 13662 Additional Equipment: Standardizer:

Conditions Ambient Temperature: 71.60 °F Polarity(+): Retraction Bidirectional: Cable Length: 25 Feet

In Tolerance As Found: Tolerances: +/-1.0% of Length 10% to 100%, +/-0.1% of range < 10%
 Out of Tolerance As Adjusted: As Found System Condition: Good

Conditioner Parameters Excitation: 10.000 Delta K: 1.0094 Zero Offset: 0.0000 Multiplier: 63.0003
 Cal Factor: Positive: Negative: Range Gain: Post Amp Gain: 1 Post Amp Fine Gain: 0.98694 Polarity: Normal

Calibration Data Range: 1 Full Scale: 6
 Extension Resolution: 0.0003 Report Units: Inch 0.0000

Applied Percent of Full Scale Length	Series 1		Series 1 Errors				Series 2		Series 2 Errors				Repeatability	
	Indicated Reading Ascending	Indicated Reading Descending	Units Error Asc	Percent Error Asc	Units Error Desc	Percent Error Desc	Indicated Reading Ascending	Indicated Reading Descending	Units Error Asc	Percent Error Asc	Units Error Desc	Percent Error Desc	Asc	Desc
	0	0.00000	-0.00019	0.00000	0.00	0.00019	0.00							
-2	-0.12043		0.00043	0.01										
-4	-0.23964		0.00036	-0.01										
-6	-0.35961		0.00039	-0.01										
-8	-0.48002		0.00002	0.00										
-10	-0.60032		0.00032	0.05										
-20	-1.20230		0.00230	0.19										
-30	-1.80070		0.00070	0.04										
-40	-2.40230		0.00230	0.10										
-50	-3.00470		0.00470	0.16										

Retraction Range: 1 Report Units: Inch

Applied Percent of Full Scale Length	Series 1		Series 1 Errors				Series 2		Series 2 Errors				Repeatability	
	Indicated Reading Ascending	Indicated Reading Descending	Units Error Asc	Percent Error Asc	Units Error Desc	Percent Error Desc	Indicated Reading Ascending	Indicated Reading Descending	Units Error Asc	Percent Error Asc	Units Error Desc	Percent Error Desc	Asc	Desc
	0	0.00000	0.00067	0.00000	0.00	0.00067	0.01							
2	0.12131		0.00131	0.02										
4	0.24166		0.00166	0.03										
6	0.36149		0.00149	0.02										
8	0.48171		0.00171	0.03										
10	0.60191		0.00191	0.32										
20	1.20330		0.00330	0.27										
30	1.80260		0.00260	0.14										
40	2.39810		0.00190	-0.08										
50	3.00070		0.00070	0.02										

Errors at zero are compared to 1% of Range.
 Uncertainty of the calibration data supplied is equal to or less than the greater of, ±0.25% of reading or ±50 μ inches, for a confidence level of 95%.
 This report shall not be reproduced except in full, without the written approval of the laboratory.
 Calibrations are performed with standards whose values and measurements are traceable to the National Institute of Standards and Technology.
 American Association of Laboratory Accreditation Certificate Number: 1145.01

Notes:

Performed By: Steve Brian Field Service Engineer Date: 17-Nov-09

Signature: Next Customer Agreed Upon Calibration Date: 17-Nov-10 ACSRepRevU
 GLD 14-Jul-09



MTS Systems Corporation
 14000 Technology Drive
 Eden Prairie, MN 55344-2290

Calibration Report



Customer Name: Stress Engineering System: 30852D Page: 2 of 2 CALIBRATION CERT #1145.01
 Report Number: 1194-1722
 Site: 521917
 System ID: 22 KIP Sta #11 Location: Lab Country Code: USA

Equipment
 Device Type: Force Model: 661.20C-03 Serial No.: 49417
 Controller/Conditioner Model: 493.25 Serial No.: 02048028P
 Readout Device Model: 493.25 Serial No.: 02048028P Channel: Force

Procedure
 MTS Procedure: FS-CA 2122 Rev. A ACS Version: 7.02
 Calibration has been performed in accordance with: ASTM E4-09
 Method of Verification: Set-the-Force Method using Elastic Calibration Devices

Calibration Equipment Asset No.
 Dead Weight Set: High Level Board: Low Level Board: Standard Asset No.: 12719
 DW Compensation: DMM: 16350 Digital Indicator: 16469 Lower Limit: 4 kip
 Temperature Readout: 13662 Additional Equipment: Standardizer: 16804

Conditions
 Ambient Temperature: 71.10 °F Polarity(+): Tension Bidirectional: Cable Length: 25 Feet

In Tolerance As Found: Tolerance: +/-1.0% of Applied Force
 Out of Tolerance As Adjusted: As Found System Condition: Good

Conditioner Parameters
 Excitation: 10.0000 Delta K: 1.0012 Zero Offset: 0.0000 Multiplier: Cal Res: 80.6 kohms
 Shunt Cal: Postive: 11.1315 Negative: Range Gain: PreAmp Gain: 240 Post Amp/FineGain: 1.93428 Polarity: Normal

Calibration Data
 Range: 1
 Resolution: 0.001 Full Scale: 22

Report Units: kip

Applied Percent of Full Scale Force	Series 1		Series 1 Errors				Series 2		Series 2 Errors				Repeatability Percent Error	
	Indicated Reading Ascending	Indicated Reading Descending	Units Error Asc	Percent Error Asc	Units Error Desc	Percent Error Desc	Indicated Reading Ascending	Indicated Reading Descending	Units Error Asc	Percent Error Asc	Units Error Desc	Percent Error Desc	Asc	Desc
	0	0.0000	0.0008	0.0000	0.00	0.0008	0.00	0.0000	0.0004	0.0000	0.00	0.0004	0.00	0.00
-2	-0.4406		0.0006	0.14			-0.4409		0.0009	0.20				0.07
-4	-0.8801		0.0001	0.01			-0.8816		0.0016	0.18				0.17
-6	-1.3194		0.0006	-0.05			-1.3199		0.0001	-0.01				0.04
-8	-1.7588		0.0012	-0.07			-1.7590		0.0010	-0.06				0.01
-10	-2.1986		0.0014	-0.06			-2.1995		0.0005	-0.02				0.04
-20	-4.3988		0.0012	-0.03			-4.3991		0.0009	-0.02				0.01
-40	-8.7978		0.0022	-0.02			-8.7986		0.0014	-0.02				0.01
-70	-15.4000		0.0000	0.00			-15.4010		0.0010	0.01				0.01
-100	-22.0050		0.0050	0.02			-22.0060		0.0060	0.03				0.00

Tension Range: 1
 Report Units: kip

Applied Percent of Full Scale Force	Series 1		Series 1 Errors				Series 2		Series 2 Errors				Repeatability Percent Error	
	Indicated Reading Ascending	Indicated Reading Descending	Units Error Asc	Percent Error Asc	Units Error Desc	Percent Error Desc	Indicated Reading Ascending	Indicated Reading Descending	Units Error Asc	Percent Error Asc	Units Error Desc	Percent Error Desc	Asc	Desc
	0	0.0000	-0.0008	0.0000	0.00	0.0008	0.00	0.0000	0.0002	0.0000	0.00	0.0002	0.00	0.00
2	0.4391		0.0009	-0.20			0.4403		0.0003	0.07				0.27
4	0.8790		0.0010	-0.11			0.8803		0.0003	0.03				0.15
6	1.3185		0.0015	-0.11			1.3196		0.0004	-0.03				0.08
8	1.7588		0.0012	-0.07			1.7599		0.0001	-0.01				0.06
10	2.1968		0.0032	-0.15			2.1983		0.0017	-0.08				0.07
20	4.3967		0.0033	-0.08			4.3982		0.0018	-0.04				0.03
40	8.7960		0.0040	-0.05			8.7974		0.0026	-0.03				0.02
70	15.4000		0.0000	0.00			15.4010		0.0010	0.01				0.01
100	22.0070		0.0070	0.03			22.0080		0.0080	0.04				0.00

Errors at zero are computed in % of Range.
 Uncertainty of the data supplied is equal to or less than ±0.25% of reading for a confidence level of 95%.
 This report shall not be reproduced except in full, without the written approval of the laboratory.

Calibrations are performed with standards whose values and measurements are traceable to the National Institute of Standards and Technology.
 American Association of Laboratory Accreditation Certificate Number: 1145.01
 MTS Reference Force Transducers are temperature compensated over the range of use.

Notes:

Performed By: Steve Broten Field Service Engineer Date: 17-Nov-09

Signature: Next Customer Agreed Upon Calibration Date: 17-Nov-10 ACSRP/Rev U GLD 14-Jul-09



MTS Systems Corporation

14000 Technology Drive
 Eden Prairie, MN 55344-2290

MTS Field Service



Certificate of Calibration

Page: 1 of 2
 Certificate Number: 1194-1722
 Site: 521917
 Country Code: USA

Customer Name: Stress Engineering

System: 30852D
 Location: Lab

System ID: 22 KIP Sta #11

Equipment

Device Type: Force	Model: 661.20C-03	Serial No.: 49417
Controller/Conditioner Model: 493.25	Serial No.: 02048028P	
Readout Device Model: 493.25	Serial No.: 02048028P	Channel: Force

MTS Field Service is accredited by the American Association for Laboratory Accreditation (A2LA Cert. No. 1145.01).
 The basis for this accreditation is the international standard for calibration laboratories, ISO/IEC 17025 "General Requirements for the Competence of Calibration and Testing Laboratories".
 Defined and documented measurement assurance techniques or uncertainty analyses are used to verify the adequacy of the measurement processes.

Calibrations are performed with standards whose values and measurements are traceable to the National Institute of Standards and Technology.
 MTS Reference Force Transducers are calibrated in compliance with ASTM E74.

When parameter(s) are certified to be within specified tolerance(s), the measured value(s) shall fall within the appropriate specification limit and the uncertainty of the measured value(s) shall be stated and provided to the customer for evaluation.

CALIBRATION INFORMATION

As Found: In Tolerance Max. Error As Found: 0.27 % Calibration Date: 17-Nov-09
 As Left: In Tolerance Max. Error As Left: 0.27 % Calibration Due: 17-Nov-10
 Tolerance: +/-1.0% of Applied Force
 Calibration Procedure: FS-CA 2122 Rev. A ASTM E4-09
 Full Scale Ranges: 22 kip
 Note:

STANDARDS USED FOR CALIBRATION

<u>MTS Asset Number</u>	<u>Manufacturer</u>	<u>Model Number</u>	<u>Description</u>	<u>Cal. Date</u>	<u>Cal. Due</u>
16469	Interface Inc.	9840	Readout	27-Feb-09	26-Feb-10
16850	Fluke	189	Multimeter	27-Feb-09	26-Feb-10
13662	Fluke	80T-150U	Temperature Probe	27-Feb-09	27-Feb-10
16804	Interface	CX-0220-1	Bridge Box	27-Feb-09	26-Feb-10
12719	Interface	1220AJF	22 KIP Load Cell	27-Feb-09	27-Aug-10

Certified by: Issued on: 17-Nov-09

ACS Version: 7.02

ACSRepRevU
 GLD 14-Jul-09



MTS Systems Corporation
 14000 Technology Drive
 Eden Prairie, MN 55344-2200

Calibration Report



Customer Name: Stress Engineering
 System: 30852D
 System ID: 22 KIP Sta #11
 Location: Lab
 Country Code: USA
 Page: 2 of 2
 Report Number: 1194-1947
 Site: 521917
 CALIBRATION CERT #1145.01

Equipment
 Device Type: Length
 Model: LVDT
 Serial No.: 782
 Controller/Conditioner Model: 493.25
 Serial No.: 02047795P
 Readout Device Model: 493.25
 Serial No.: 02047795P
 Channel: Disp

Procedure
 MTS Procedure: FS-CA 2124
 ACS Version: 8.1
 Calibration has been performed in accordance with: (none)

Method of Verification:
 Calibration Equipment Asset No.
 Dead Weight Set: HighLevel Board: LowLevel Board: Standard Asset No.: 17519
 DW Compensation: DMM: 16850 Digital Indicator: Lower Limit:
 Temperature Readout: 13662 Additional Equipment: Standardizer:

Conditions
 Ambient Temperature: 73.60 °F
 Polarity(+): Retraction
 Bidirectional:
 Cable Length: 25 Feet

In Tolerance:
 Out of Tolerance:
 As Found:
 As Adjusted:
 Tolerance: +/-1.0% of Length 10% to 100%, +/-0.1% of range < 10%
 As Found System Condition: Good

Conditioner Parameters
 Excitation: 10.000
 Cal Factor: Positive: Delta K: 1.0034 Zero Offset: 0.0000 Multiplier: Phase: 63.0003
 Negative: Range Gain: Post Amp/Phase Gain: 0.98694 Polarity: Normal

Calibration Data
 Range: 1
 Resolution: 0.0001 Full Scale: 6
 Report Units: inch 0.0000

Applied Percent of Full Scale Length	Series 1		Series 1 Errors				Series 2		Series 2 Errors				Repeatability Percent Error	
	Indicated Reading	Indicated Reading	Units Error	Percent Error	Units Error	Percent Error	Indicated Reading	Indicated Reading	Units Error	Percent Error	Units Error	Percent Error	Asc	Desc
	Ascending	Descending	Asc	Asc	Desc	Desc	Ascending	Descending	Asc	Asc	Desc	Desc		
0	0.00000	-0.00023	0.00000	0.00	0.00023	0.00								
-2	-0.11993		0.00007	0.00										
-4	-0.23985		0.00105	-0.02										
-6	-0.35974		0.00106	-0.02										
-8	-0.47931		0.00069	-0.01										
-10	-0.59939		0.00061	-0.10										
-20	-1.20050		0.00050	0.04										
-30	-1.79760		0.00240	-0.13										
-40	-2.39810		0.00190	-0.08										
-50	-2.99950		0.00050	-0.02										

Retraction Range: 1
 Report Units: inch

Applied Percent of Full Scale Length	Series 1		Series 1 Errors				Series 2		Series 2 Errors				Repeatability Percent Error	
	Indicated Reading	Indicated Reading	Units Error	Percent Error	Units Error	Percent Error	Indicated Reading	Indicated Reading	Units Error	Percent Error	Units Error	Percent Error	Asc	Desc
	Ascending	Descending	Asc	Asc	Desc	Desc	Ascending	Descending	Asc	Asc	Desc	Desc		
0	0.00000	0.00023	0.00000	0.00	0.00023	0.00								
2	0.12105		0.00105	0.02										
4	0.24131		0.00131	0.02										
6	0.36104		0.00104	0.02										
8	0.48114		0.00114	0.02										
10	0.60138		0.00138	0.23										
20	1.20270		0.00270	0.23										
30	1.80240		0.00240	0.13										
40	2.39870		0.00190	-0.05										
50	3.00240		0.00240	0.08										

Errors at zero are compensated to 0.01 Range.
 Uncertainty of the calibration data supplied is equal to or less than the greater of, +0.25% of reading or +50µ inches, for a confidence level of 95%.
 This report shall not be reproduced except in full, without the written approval of the laboratory.
 Calibrations are performed with standards whose values and measurements are traceable to the National Institute of Standards and Technology.
 American Association of Laboratory Accreditation Certificate Number: 1145.01

Notes:
 Performed By: Steve Broken
 Field Service Engineer
 Date: 17-Nov-10
 Signature:
 Next Customer Agreed Upon Calibration Date: 17-Nov-11
 ACSRepRev's



MTS Systems Corporation
 14000 Technology Drive
 Eden Prairie, MN 55344-2290

Calibration Report



Customer Name: Stress Engineering
 System ID: 22 KIP Sta #11
 Location: Lab
 Country Code: USA
 Page: 2 of 2
 Report Number: 1194-1948
 Site: 521917
 CALIBRATION CERT #1145.01

Equipment
 Device Type: Force
 Controller/Conditioner Model: 493.25
 Readout Device Model: 493.25
 Model: 661.20C-03
 Serial No.: 02048028P
 Serial No.: 02048028P
 Channel: Force
 Serial No.: 49417

Procedure
 MTS Procedure: FS-CA 2122
 Calibration has been performed in accordance with: ASTM E4-10
 Method of Verification: Set-the-Force Method using Elastic Calibration Devices
 ACS Version: 8.1

Calibration Equipment Asset No.
 Dead Weight Set: HighLevel Board: LowLevel Board: Standard Asset No.: 12719
 DW Compensation: DMM: 16850 Digital Indicator: 16489 Lower Limit: .44 kip
 Temperature Readout: 13662 Additional Equipment: Standardizer: 16804

Conditions
 Ambient Temperature: 74.40 °F Polarity(+): Tension Bidirectional: Cable Length: 25 Feet

In Tolerance: As Found: Tolerance: +/-1.0% of Applied Force
 Out of Tolerance: As Adjusted: As Found System Condition: Good

Conditioner Parameters
 Excitation: 10.0000 Delta K: 1.0012 Zero Offset: 0.0000 Multiplier: Cal Res: 80.6 kohms
 Shunt Cal: Positive: 11.1315 Negative: Range Gain: PreAmp Gain: 240 Post Amp/FineGain: 1.93428 Polarity: Normal

Calibration Data
 Range: 1
 Resolution: 0.001 Full Scale: 22
 Report Units: kip

Applied Percent of Full Scale Force	Series 1		Series 1 Errors				Series 2		Series 2 Errors				Repeatability Percent Error	
	Indicated Reading Ascending	Indicated Reading Descending	Units Error Asc	Percent Error Asc	Units Error Desc	Percent Error Desc	Indicated Reading Ascending	Indicated Reading Descending	Units Error Asc	Percent Error Asc	Units Error Desc	Percent Error Desc	Asc	Desc
	0	0.0000	0.0022	0.0000	0.00	0.0022	0.01	0.0000	0.0024	0.0000	0.00	0.0024	0.01	0.00
-2	-0.4398		0.0002	-0.05			-0.4408		0.0008	0.18				0.23
-4	-0.8809		0.0009	-0.10			-0.8794		0.0006	-0.07				0.17
-6	-1.3179		0.0021	-0.16			-1.3182		0.0018	-0.14				0.02
-8	-1.7580		0.0020	-0.11			-1.7581		0.0019	-0.11				0.01
-10	-2.2002		0.0002	0.01			-2.1979		0.0021	-0.10				0.10
-20	-4.3954		0.0046	-0.10			-4.3959		0.0041	-0.09				0.01
-40	-8.7928		0.0072	-0.08			-8.7934		0.0066	-0.08				0.01
-70	-15.3920		0.0080	-0.05			-15.3910		0.0090	-0.06				0.01
-100	-21.9950		0.0050	-0.02			-21.9940		0.0060	-0.03				0.00

Tension Range: 1
 Report Units: kip

Applied Percent of Full Scale Force	Series 1		Series 1 Errors				Series 2		Series 2 Errors				Repeatability Percent Error	
	Indicated Reading Ascending	Indicated Reading Descending	Units Error Asc	Percent Error Asc	Units Error Desc	Percent Error Desc	Indicated Reading Ascending	Indicated Reading Descending	Units Error Asc	Percent Error Asc	Units Error Desc	Percent Error Desc	Asc	Desc
	0	0.0000	0.0001	0.0000	0.00	0.0001	0.00	0.0000	-0.0009	0.0000	0.00	0.0009	0.00	0.00
2	0.4411		0.0011	0.25			0.4409		0.0009	0.21				0.05
4	0.8820		0.0020	0.23			0.8812		0.0012	0.14				0.09
6	1.3213		0.0013	0.10			1.3234		0.0034	0.26				0.16
8	1.7611		0.0011	0.06			1.7608		0.0008	0.05				0.02
10	2.2019		0.0019	0.09			2.2001		0.0001	0.00				0.08
20	4.4006		0.0006	0.01			4.4006		0.0006	0.01				0.00
40	8.7997		0.0003	0.00			8.7968		0.0032	-0.04				0.03
70	15.3960		0.0040	-0.03			15.3960		0.0040	-0.03				0.00
100	21.9990		0.0010	0.00			21.9980		0.0020	-0.01				0.00

Errors at zero are computed in % of Range.
 Uncertainty of the data supplied is equal to or less than ±0.25% of reading for a confidence level of 95%.
 This report shall not be reproduced except in full, without the written approval of the laboratory.
 Calibrations are performed with standards whose values and measurements are traceable to the National Institute of Standards and Technology,
 American Association of Laboratory Accreditation Certificate Number: 1145.01
 MTS Reference Force Transducers are temperature compensated over the range of use.

Notes:
 Performed By: Steve Broten Field Service Engineer Date: 17-Nov-10
 Signature: Next Customer Agreed Upon Calibration Date: 17-Nov-11 ACSRepRevYa



MTS Systems Corporation

14000 Technology Drive
 Eden Prairie, MN 55344-2290

MTS Field Service



Certificate of Calibration

Customer Name: Stress Engineering	System: 00552D	Page: 1 of 2
System ID: 22 KIP Slave 11	Location: Lab	Certificate Number: 1194-1948
Equipment:		Site: 021917
Device Type: Force	Model: 661.20C-05	Country Code: USA
Control/Conditioner Model: 455.25	Serial No.: 02046025P	
Readout Device Model: 455.25	Serial No.: 02046025P	Serial No.: 49417
		Channel: Force

MTS Field Service is accredited by the American Association for Laboratory Accreditation (A2LA Cert. No. 1145.01). The basis for this accreditation is the international standard for calibration laboratories, ISO/IEC 17025 "General Requirements for the Competence of Calibration and Testing Laboratories". Defined and documented measurement assurance techniques or uncertainty analyses are used to verify the adequacy of the measurement processes.

Calibrations are performed with standards whose values and measurements are traceable to the National Institute of Standards and Technology. MTS Reference Force Transducers are calibrated in compliance with ASTM E74.

When parameters are certified to be within specified tolerance(s), the measured value(s) shall fall within the appropriate specification limit and the uncertainty of the measured value(s) shall be stated and provided to the customer for evaluation.

CALIBRATION INFORMATION

As Found: In Tolerance	Max. Error As Found: 0.25 %	Calibration Date: 17-Nov-10
As Left: In Tolerance	Max. Error As Left: 0.25 %	Calibration Due: 17-Nov-11
Tolerance: +/-1.0% of Applied Force		
Calibration Procedure: FS-CA 2122	ASTM E4-10	
Full Scale Ranges: 22 Mp		
Note:		

STANDARDS USED FOR CALIBRATION

MTS Asset Number	Manufacturer	Model Number	Description	Cal. Date	Cal. Due
1 6469	Interface Inc.	0640	Readout	22-Feb-10	22-Feb-11
1 6850	Ruke	189	Multimeter	22-Feb-10	22-Feb-11
1 3662	Ruke	20T-150J	Temperature Probe	22-Feb-10	22-Feb-11
1 6804	Interface	0C-0020-1	Bridge Box	22-Feb-10	22-Feb-11
1 2719	Interface	1220A.F	22 KIP Load Cell	24-Aug-10	22-Jun-12

Certified by: Issued on: 17-Nov-10

ACS Version: 8.1

ACS Rep 7/06



MTS Systems Corporation
 14000 Technology Drive
 Eden Prairie, MN 55344-2290

Calibration Report



Page: 2 of 2 CALIBRATION CERT #1145.01

Customer Name: Stress Engineering System: 30852B Report Number: 1194-1719
 System ID: 55 KIP Sta #8 Location: Lab Site: 521917
 Country Code: USA

Equipment
 Device Type: Length Model: LVDT Serial No.: 361
 Controller/Conditioner Model: 493.25 Serial No.: 02047882P
 Readout Device Model: 493.25 Serial No.: 02047882P Channel: Disp

Procedure
 MTS Procedure: FS-CA 2124 Rev. A ACS Version: 7.02
 Calibration has been performed in accordance with: (none)
 Method of Verification:

Calibration Equipment Asset No.
 Dead Weight Set: HighLevel Board: LowLevel Board: Standard Asset No.: 17519
 DW Compensation: DMM: 16850 Digital Indicator: Lower Limit:
 Temperature Readout: 13662 Additional Equipment: Standardizer:

Conditions
 Ambient Temperature: 78.10 °F Polarity(+): Retraction Bidirectional: Cable Length: 25 Feet

In Tolerance As Found: Tolerance: +/-1.0% of Length 10% to 100%, +/-0.1% of range < 10%
 Out of Tolerance As Adjusted: As Found System Condition: Good

Conditioner Parameters
 Excitation: 10.0000 Delta K: 1.0051 Zero Offset: 0.0000 Multiplier: Phase: 48.60001
 Cal Factor: Positive: Negative: Range Gain: PreAmp Gain: 1 PostAmp/FineGain: 1.06038 Polarity: Normal

Calibration Data
 Range: 1 Full Scale: 6
 Extension Resolution: 0.0001 Report Units: inch 0.0000

Applied Percent of Full Scale Length	Series 1		Series 1 Errors				Series 2		Series 2 Errors				Repeatability Percent Error	
	Indicated Reading Ascending	Indicated Reading Descending	Units Error Asc	Percent Error Asc	Units Error Desc	Percent Error Desc	Indicated Reading Ascending	Indicated Reading Descending	Units Error Asc	Percent Error Asc	Units Error Desc	Percent Error Desc	Asc	Desc
	0	0.00000	-0.00055	0.00000	0.00	0.00055	-0.01							
-2	-0.12051		0.00051	0.01										
-4	-0.24054		0.00054	0.01										
-6	-0.36058		0.00058	0.01										
-8	-0.48089		0.00089	0.01										
-10	-0.60100		0.00100	0.17										
-20	-1.19890		0.00110	-0.09										
-30	-1.79970		0.00030	-0.02										
-40	-2.40650		0.00650	0.27										
-50	-3.01660		0.01660	0.55										

Retraction Range: 1
 Report Units: inch

Applied Percent of Full Scale Length	Series 1		Series 1 Errors				Series 2		Series 2 Errors				Repeatability Percent Error	
	Indicated Reading Ascending	Indicated Reading Descending	Units Error Asc	Percent Error Asc	Units Error Desc	Percent Error Desc	Indicated Reading Ascending	Indicated Reading Descending	Units Error Asc	Percent Error Asc	Units Error Desc	Percent Error Desc	Asc	Desc
	0	0.00000	0.00002	0.00000	0.00	0.00002	0.00							
2	0.12124		0.00124	0.02										
4	0.24220		0.00220	0.04										
6	0.36293		0.00293	0.05										
8	0.48352		0.00352	0.06										
10	0.60362		0.00362	0.60										
20	1.20060		0.00060	0.05										
30	1.79920		0.00080	-0.04										
40	2.40480		0.00480	0.20										
50	3.01620		0.01620	0.54										

Errors at Zero are compiled in % of Range.
 Uncertainty of the calibration data supplied is equal to or less than the greater of ±0.25% of reading or ±50µ inches, for a confidence level of 95%. Out of Tolerance in % column
 This report shall not be reproduced except in full, without the written approval of the laboratory.
 Calibrations are performed with standards whose values and measurements are traceable to the National Institute of Standards and Technology.
 American Association of Laboratory Accreditation Certificate Number: 1145.01

Notes:

Performed By: Steve Broten Field Service Engineer Date: 16-Nov-09
 Signature: Next Customer Agreed Upon Calibration Date: 16-Nov-10 ACSRepRevU
 GLD 14-Jul-09



MTS Systems Corporation

14000 Technology Drive
Eden Prairie, MN 55344-2290

MTS Field Service



Certificate of Calibration

Customer	Name: Stress Engineering	System: 30852B	Page: 1 of 2 Certificate Number: 1194-1719
	System ID: 55 KIP Sta #8	Location: Lab	Site: 521917 Country Code: USA
Equipment	Device Type: Length Controller/Conditioner Model: 493.25 Readout Device Model: 493.25	Model: LVDT Serial No.: 02047882P Serial No.: 02047882P	Serial No.: 381 Channel: Disp

MTS Field Service is accredited by the American Association for Laboratory Accreditation (A2LA Cert. No. 1145.01). The basis for this accreditation is the international standard for calibration laboratories, ISO/IEC 17025 "General Requirements for the Competence of Calibration and Testing Laboratories". Defined and documented measurement assurance techniques or uncertainty analyses are used to verify the adequacy of the measurement processes.

Calibrations are performed with standards whose values and measurements are traceable to the National Institute of Standards and Technology.

When parameter(s) are certified to be within specified tolerance(s), the measured value(s) shall fall within the appropriate specification limit and the uncertainty of the measured value(s) shall be stated and provided to the customer for evaluation.

CALIBRATION INFORMATION

As Found: In Tolerance Max. Error As Found: 0.60 % Calibration Date: 16-Nov-09
 As Left: In Tolerance Max. Error As Left: 0.60 % Calibration Due: 16-Nov-10
 Tolerance: +/-1.0% of Applied Length from 10% to 100% and +/-0.1% of range below 10%
 Calibration Procedure: FS-CA 2124 Rev. A
 Full Scale Ranges: 6 inch
 Note:

STANDARDS USED FOR CALIBRATION

MTS Asset Number	Manufacturer	Model Number	Description	Cal. Date	Cal. Due
16850	Fluke	189	Multimeter	27-Feb-09	26-Feb-10
13662	Fluke	80T-150U	Temperature Probe	27-Feb-09	27-Feb-10
17519	Boeckeler (9 pin)	DLG-460	18 Inch Boeckeler	2-Sep-09	2-Sep-10

Certified by: Issued on: 16-Nov-09

ACS Version: 7.02

ACSRepRevU
GLD 14-Jul-09



MTS Systems Corporation
14000 Technology Drive
Eden Prairie, MN 55344-2200

Calibration Report



Customer

Name: Stress Engineering

System: 30852B

Page: 2 of 2 CALIBRATION CERT #1145.01

Report Number: 1194-1718

Site: 521917

System ID: 55 KIP Sta #8

Location: Lab

Country Code: USA

Equipment

Device Type: Force Model: 3156 Serial No.: 2224
Controller/Conditioner Model: 493.25 Serial No.: 02047774P
Readout Device Model: 493.25 Serial No.: 0204774P Channel: Force

Procedure

MTS Procedure: FS-CA 2122 Rev. A ACS Version: 7.02

Calibration has been performed in accordance with: ASTM E4-09

Method of Verification: Set-the-Force Method using Elastic Calibration Devices

Calibration Equipment Asset No.

Dead Weight Set: HighLevel Board: LowLevel Board: Standard Asset No.: 18326
DW Compensation: DMM: 16850 Digital Indicator: 16469 Lower Limit: 1 kip
Temperature Readout: 13662 Additional Equipment: Standardizer: 16804

Conditions

Ambient Temperature: 78.10 °F Polarity(+): Tension Bidirectional: Cable Length: 25 Feet

In Tolerance

As Found:

Tolerance: +/-1.0% of Applied Force

Out of Tolerance

As Adjusted:

As Found System Condition: Good

Conditioner Parameters

Excitation: 10.0000 Delta K: 0.9966 Zero Offset: 0.0000 Multiplier: Cal Res: 80.6 kohms
Shunt Cal: Positive: 39.8084 Negative: Range Gain: PreAmp Gain: 240 Post Amp/FineGain: 1.623 Polarity: Normal

Calibration Data

Range: 1 Resolution: 0.002 Full Scale: 55

Compression

Report Units: kip

Applied Percent of Full Scale Force	Series 1		Series 1 Errors				Series 2		Series 2 Errors				Repeatability	
	Indicated Reading Ascending	Indicated Reading Descending	Units Error Asc	Percent Error Asc	Units Error Desc	Percent Error Desc	Indicated Reading Ascending	Indicated Reading Descending	Units Error Asc	Percent Error Asc	Units Error Desc	Percent Error Desc	Asc	Desc
	0	0.0000	-0.0014	0.0000	0.00	0.0014	0.00	0.0000	-0.0024	0.0000	0.00	0.0024	0.00	0.00
-2	-1.0939		0.0061	-0.55			-1.0944		0.0056	-0.51			0.05	
-4	-2.1853		0.0147	-0.67			-2.1872		0.0128	-0.58			0.09	
-6	-3.2831		0.0169	-0.51			-3.2843		0.0157	-0.48			0.04	
-8	-4.3786		0.0214	-0.49			-4.3766		0.0234	-0.53			0.05	
-10	-5.4773		0.0227	-0.41			-5.4778		0.0222	-0.40			0.01	
-20	-10.9790		0.0210	-0.19			-10.9780		0.0220	-0.20			0.01	
-40	-21.9870		0.0130	-0.06			-21.9880		0.0120	-0.05			0.00	
-70	-38.4760		0.0240	-0.06			-38.4750		0.0250	-0.06			0.00	
-100	-54.9400		0.0600	-0.11			-54.9430		0.0570	-0.10			0.01	

Tension

Range: 1

Report Units:

kip

Applied Percent of Full Scale Force	Series 1		Series 1 Errors				Series 2		Series 2 Errors				Repeatability	
	Indicated Reading Ascending	Indicated Reading Descending	Units Error Asc	Percent Error Asc	Units Error Desc	Percent Error Desc	Indicated Reading Ascending	Indicated Reading Descending	Units Error Asc	Percent Error Asc	Units Error Desc	Percent Error Desc	Asc	Desc
	0	0.0000	0.0005	0.0000	0.00	0.0005	0.00	0.0000	-0.0058	0.0000	0.00	0.0058	-0.01	0.00
2	1.1005		0.0005	0.05			1.0951		0.0049	-0.45			0.49	
4	2.1989		0.0011	-0.05			2.1926		0.0074	-0.34			0.29	
6	3.2987		0.0013	-0.04			3.2923		0.0077	-0.23			0.19	
8	4.4025		0.0025	0.06			4.3963		0.0037	-0.08			0.14	
10	5.5016		0.0016	0.03			5.4935		0.0065	-0.12			0.15	
20	11.0000		0.0000	0.00			10.9940		0.0060	-0.05			0.05	
40	21.9970		0.0030	-0.01			21.9910		0.0090	-0.04			0.03	
70	38.5010		0.0010	0.00			38.4950		0.0050	-0.01			0.02	
100	55.0160		0.0160	0.03			55.0110		0.0110	0.02			0.01	

Errors at zero are computed in % of Range.

Uncertainty of the data supplied is equal to or less than +/-0.25% of reading for a confidence level of 95%.

This report shall not be reproduced except in full, without the written approval of the laboratory.

Calibrations are performed with standards whose values and measurements are traceable to the National Institute of Standards and Technology.

American Association of Laboratory Accreditation Certificate Number: 1145.01

MTS Reference Force Transducers are temperature compensated over the range of use.

Notes:

Performed By:

Steve Broten

Field Service Engineer

Date: 16-Nov-09

Signature:

Next Customer Agreed Upon Calibration Date: 16-Nov-10

ACSRepRevU
GLD 14-Jul-09



MTS Systems Corporation

14000 Technology Drive
Eden Prairie, MN 55344-2290

MTS Field Service



Certificate of Calibration

Customer	Name: Stress Engineering	System: 30852B	Page: 1 of 2 Certificate Number: 1194-171B Site: 521917
	System ID: 55 KIP Sta #8	Location: Lab	Country Code: USA
Equipment	Device Type: Force	Model: 3156	Serial No.: 2224
	Controller/Conditioner Model: 493.25	Serial No.: 02047774P	
	Readout Device Model: 493.25	Serial No.: 0204774P	Channel: Force

MTS Field Service is accredited by the American Association for Laboratory Accreditation (A2LA Cert. No. 1145.01).

The basis for this accreditation is the international standard for calibration laboratories, ISO/IEC 17025

"General Requirements for the Competence of Calibration and Testing Laboratories".

Defined and documented measurement assurance techniques or uncertainty analyses are used to verify the adequacy of the measurement processes.

Calibrations are performed with standards whose values and measurements are traceable to the National Institute of Standards and Technology.

MTS Reference Force Transducers are calibrated in compliance with ASTM E74.

When parameter(s) are certified to be within specified tolerance(s), the measured value(s) shall fall within the appropriate specification limit and the uncertainty of the measured value(s) shall be stated and provided to the customer for evaluation.

CALIBRATION INFORMATION

As Found:	In Tolerance	Max. Error As Found:	-0.67 %	Calibration Date:	16-Nov-09
As Left:	In Tolerance	Max. Error As Left:	-0.67 %	Calibration Due:	16-Nov-10
Tolerance:	+/-1.0% of Applied Force				
Calibration Procedure:	FS-CA 2122 Rev. A	ASTM E4-09			
Full Scale Ranges:	55 kip				
Note:					

STANDARDS USED FOR CALIBRATION

MTS Asset Number	Manufacturer	Model Number	Description	Cal. Date	Cal. Due
16469	Interface Inc.	9840	Readout	27-Feb-09	26-Feb-10
16850	Fluke	189	Multimeter	27-Feb-09	26-Feb-10
13662	Fluke	80T-150U	Temperature Probe	27-Feb-09	27-Feb-10
16804	Interface	CX-0220-1	Bridge Box	27-Feb-09	26-Feb-10
18326	Interface	50 KIP	55 KIP Load Cell	10-Sep-08	10-Mar-10

Certified by: Issued on: 16-Nov-09

ACS Version: 7.02

ACSRepRevU
GLD 14-Jul-09

APPENDIX B: MUD TEST REPORT

Drilling Assembly						Casing/Riser			Volumes		Pump Information						
Hole Size	Depth		Bit Type			OD	ID	Set @	Hole	Model	Stroke	Liner	Eff.	bbf/stk	stk/min	l/min	gpm
in	0	ft															
Drill Collars			Drill Pipe						Pits								
OD	ID	Length ft	OD	ID	Length ft				Total Vol.								
					0				In Storage								
						Hole Information											
						Hole Inclination			deg			Water Depth			ft		
						Circulating Pressure			psi			Total Flow			0.00 bpm		
Mud Properties						Drill Collar Ann. Vel.			Circulation Times								
Sample Number						1	2	3	4	DC#1 ft/min			Surface to bit min		Full Cycle Time min		
Source						Pits			DC#2 ft/min			Btms up min		Mud Type			
Time						08:00			DC#3 ft/min			Solids Analysis					
Sample Temp F						150			DC#4 ft/min			Sample Number		1	2	3	4
Flowline Temp F									Drill Pipe Ann. Vel.			ASG		4.13			
Depth MD ft						0			DP#1 ft/min			LGS ppb		6.93			
Mud weight ppg						12.1			DP#2 ft/min			HGS ppb		254.95			
Funnel vis. sec/qt						50			DP#3 ft/min			LGS Pctvol.		0.76			
Plastic Viscosity cp						31			DP#4 ft/min			HGS Pctvol.		17.34			
Yield Point lbs/100R2						7			Bit Information			LGS Pctwt.		1.36			
Gels 10 sec lbs/100ft2						10			Size in			HGS Pctwt.		50.17			
Gels 10 min lbs/100ft2						35			Type								
Gels 30 min lbs/100ft2									Number								
API Filtrate cc									Depth in ft			Rheology					
HTHP API						8			RPM			600 RPM		69			
HTHP Temp. F						200			WOB lb			300 RPM		38			
Cake API									Nozzles			200 RPM		30			
Cake HTHP									Bit Hydraulics			100 RPM		19			
% Solids						19.00			TFA in2			6 RPM		8			
% Corr. Solids						18.11			Nozzle velocity ft/sec			3 RPM		5			
% Water						13.00			Pressure Drop			Hydraulic Analysis					
% Oil						68.00			Hydraulic HP			n Annulus		0.381			
Oil Ratio						84.0			HHP/sq in			k Annulus		13.720			
Water Ratio						16.0			Impact Force lbf			System Hydraulic Horsepower					
Sand Content									Nozzle Diam. in			ECD @ TD ppg					
Electrical Stability						600			Pressure Drop%			Velocity in Riser ft/min					
Pom ml 0.1N H2SO4						1.9			Mud Property Specification								
Excess Lime ppb						2.46			Weight ppg			Viscosity			Filtrate		
Tot.Hdnss ml 0.1M EDTA									Recommendations								
Ca++ ml 0.1 M EDTA						3											
AgNo3 ml 0.282N						2.2											
NaCl pctwt.						0.71											
CaCl2 pctwt.						20.24											
MgCl2 pctwt.						0.00											
Brine Density sg.						1.18											
Nacl mg/l						8,447											
CaCl2 mg/l						239,576											
MgCl2 mg/l									Remarks								

PHOTO DOCUMENTATION AND MEASUREMENTS OF CEMENTING FLOATS

Prepared for

**Transocean Offshore Deepwater
Drilling, Inc.
Houston, TX**

January, 2011

PN1101190DLG

**Stress Engineering Services, Inc.
Houston, Texas**

Photo Documentation and Measurements of Cementing Floats

SES PN 1101190DLG

Prepared for
Transocean Offshore Deepwater Drilling, Inc.
Houston, TX

Prepared By: *Lisa M. Ely*
Lisa M. Ely
Analyst

Brent Vyvial
Brent Vyvial
Associate

Reviewed By: *George Ross*
George Ross, Ph.D, P.E.
Principal

David L. Garrett
David L. Garrett, Ph.D.
Principal



LIMITATIONS OF THIS REPORT

The scope of this report is limited to the matters expressly covered. This report is prepared for the sole benefit of Transocean Offshore Deepwater Drilling, Inc. In preparing this report, Stress Engineering Services, Inc. (SES) has relied on information provided by Transocean Offshore Deepwater Drilling, Inc. Stress Engineering Services, Inc. (SES) has made no independent investigation as to the accuracy or completeness of such information and has assumed that such information was accurate and complete. Further, Stress Engineering Services, Inc. (SES) is not able to direct or control the operation or maintenance of client's equipment or processes.

All recommendations, findings and conclusions stated in this report are based upon facts and circumstances, as they existed at the time that this report was prepared. A change in any fact or circumstance upon which this report is based may adversely affect the recommendations, findings, and conclusions expressed in this report.

NO IMPLIED WARRANTY OF MERCHANTABILITY OR FITNESS FOR A PARTICULAR PURPOSE SHALL APPLY. STRESS ENGINEERING SERVICES, INC. MAKES NO REPRESENTATION OR WARRANTY THAT THE IMPLEMENTATION OR USE OF THE RECOMMENDATIONS, FINDINGS, OR CONCLUSIONS OF THIS REPORT WILL RESULT IN COMPLIANCE WITH APPLICABLE LAWS OR PERFECT RESULTS.

TABLE OF CONTENTS

	<u>Page No.</u>
TABLE OF CONTENTS.....	ii
LIST OF FIGURES	iii
LIST OF TABLES	iii
INTRODUCTION	1
AS-RECEIVED	2
GREASE SAMPLES.....	5
BOROSCOPE EXAMINATION.....	6
MEASUREMENTS.....	8
APPENDIX A: FLOAT UNPACKING PHOTO DOCUMENTATION	12
APPENDIX B: GREASE AND RESIDUE SAMPLE COLLECTION	18
APPENDIX C: CALIBRATED MEASUREMENT DEVICES	20
APPENDIX D: MEASUREMENT DATA	25

LIST OF FIGURES

Figure 1: As-received Sample 1.....	2
Figure 2: Sample 1 Label and Stamping.....	2
Figure 3: As-received Sample 2.....	3
Figure 4: Sample 2 Labels and Stamped Markings	3
Figure 5: Flapper and Ball Position as-received Sample 1	4
Figure 6: Flapper and Ball Position as-received Sample 2	4
Figure 7: Grease and Residue Sample Collection.....	5
Figure 8: Caliper Manufacturer	8
Figure 9: ID Micrometer	9
Figure 10: ID Micrometer Manufacturer and Calibration Information	9
Figure 11: UT Meter	10
Figure 12: UT Meter Calibration Block.....	10
Figure 13: UT Meter Calibration and Model Information.....	11

LIST OF TABLES

Table 1: Boroscope Measurements.....	7
--------------------------------------	---

INTRODUCTION

Stress Engineering Services, Inc. was contracted by Transocean Offshore Deepwater Drilling, Inc. to test two exemplar cementing floats. SES understands that the exemplar floats were the same type as the float used in the MC252 well. The exemplars provided by Transocean Offshore Deepwater Drilling, Inc. for the test program were photo documented and measured prior to testing.

Photographs of the floats were taken upon receipt by SES. The internals of the floats were also inspected using a boroscope. In addition to photographing the floats, measurements were taken for each float. Grease and residue samples were collected from the floats for possible analysis at a later date.

This report details the photo documentation and measurements of the exemplars. The testing program is detailed in another report.

AS-RECEIVED

On September 1, 2010, an exemplar cementing float was delivered to Stress Engineering by the Transocean Investigation Team. It is the understanding of SES that this float has never been used in an on-site drilling application. The sample was packaged in a wooden crate secured with a metal band; see Figure 1. The box and pin ends were protected with paper and masking tape. The label on the end of the crate was identical to the label on the float. The impression on the float reiterated the information found on the paper label; see Figure 2. The crate was disassembled so the float could be photo documented under Transocean Offshore Deepwater Drilling, Inc.'s supervision. See Appendix A for complete unpacking pictures.



Figure 1: As-received Sample 1

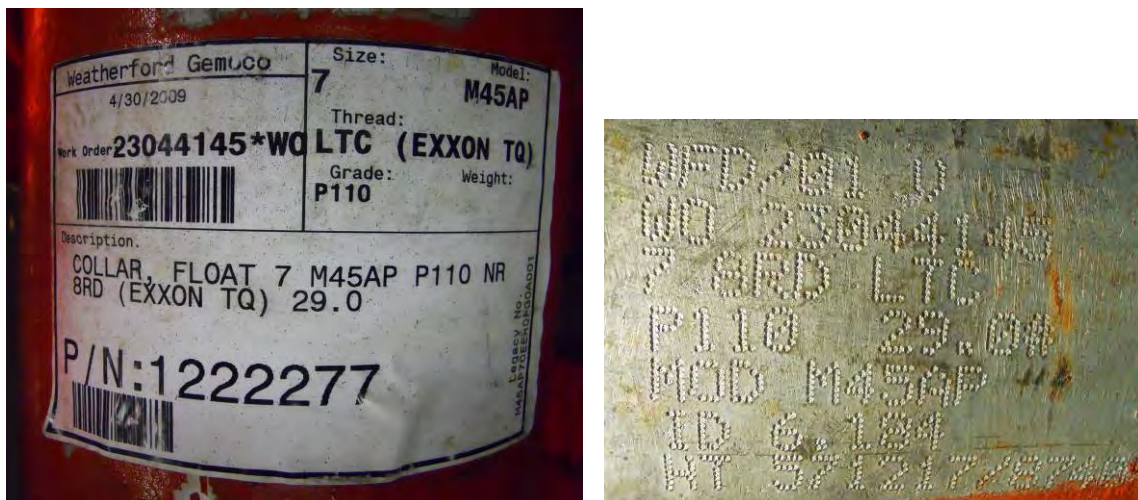


Figure 2: Sample 1 Label and Stamping

Sample 2 was delivered on September 13, 2010, by the Transocean Investigation Team. It is the understanding of SES that this float has never been used in an on-site drilling application. The sample was packaged in a wooden crate secured with a metal band; see Figure 3. The box and pin ends were protected with paper and masking tape. The label on the end of the crate was identical to the label on the float. The impression on the float reiterated the information found on the paper label; see Figure 4. The crate was disassembled so the float could be photo documented under Transocean Offshore Deepwater Drilling, Inc.'s supervision. See Appendix A for complete unpacking pictures.



Figure 3: As-received Sample 2



Figure 4: Sample 2 Labels and Stamped Markings

Once the protective tape was removed, the flapper and ball positions were easily visible. The flappers of both samples were in the open position as the inner tube was still inserted. Both balls were resting inside the cage and were mobile. See Figures 5 and 6.



Figure 5: Flapper and Ball Position as-received Sample 1

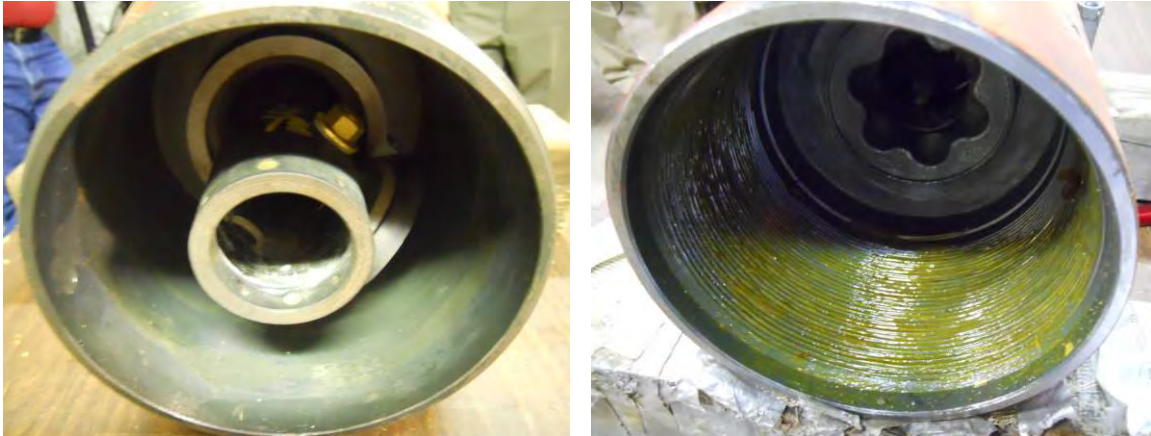


Figure 6: Flapper and Ball Position as-received Sample 2

GREASE SAMPLES

Before measurements began, grease samples from the pin exterior and box interior were collected as well as residue from the cage and ball. The samples were collected in large-mouth glass jars qualified by EPA specifications using sterile cotton cloth swabs. These samples can be submitted to a third party laboratory for chemical analysis if necessary, but at this time, the samples are being held by SES. An attempt was made to collect all of the grease, but any remaining material was wiped clean. See Appendix B for complete picture documentation of the grease sample collection process.



Figure 7: Grease and Residue Sample Collection

BOROSCOPE EXAMINATION

A detailed inspection of the interior cavity, shear pins, and ball were completed using a calibrated boroscope before measurements of the inner tube were collected. The examination was recorded on DVD and is available if needed. The boroscope, Model XL, is manufactured by Everest Imaging. The scope is calibrated before each use using a verification block; the verification block is calibrated to NIST calibration standards every five years by the Everest VIT Service Department. At the time of use, the boroscope is due for calibration on January 27, 2011.



Figure 8: Boroscope Verification Box for Calibration

Both samples had three shear pins in place, although four holes exist. The boroscope was used to measure diameters of outer seat pins, shear pins, and distance between the inner tube and flapper opening. Measurements collected by the boroscope are accurate to 0.0002 inches (0.005 mm).

Table 1: Boroscope Measurements

Location	Position	Sample 1	Sample 2
Outer ball seat pins	0°	5.97 mm	6.06 mm
	90°	6.14 mm	6.32 mm
	180°	6.27 mm	6.35 mm
	270°		6.17 mm
Shear pins	0°	3.65 mm	4.13 mm
	120°	3.72 mm	3.63 mm
	240°	3.81 mm	3.94 mm
Distance btw Inner pipe and flapper opening	0°	1.36 mm	2.38 mm
	120°	0.63 mm	
	180°		0.00 mm
	240°	0.82 mm	

The samples were rotated 180 degrees and the spacing did not change indicating that the inner tube is secure.

MEASUREMENTS

Calipers manufactured by Starrett were used to collect exterior measurement data. The calibration certificate for the calipers is found in Appendix C.

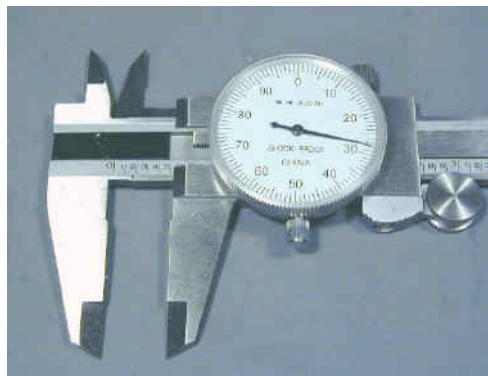


Figure 9: Calibrated Calipers



Figure 8: Caliper Manufacturer

An ID micrometer manufactured by Starrett was used to collect interior diameter measurements. The micrometer is calibrated annually by Precision Calibration & Repair. At the time of use, the micrometer is due for calibration on June 18, 2011.



Figure 9: ID Micrometer

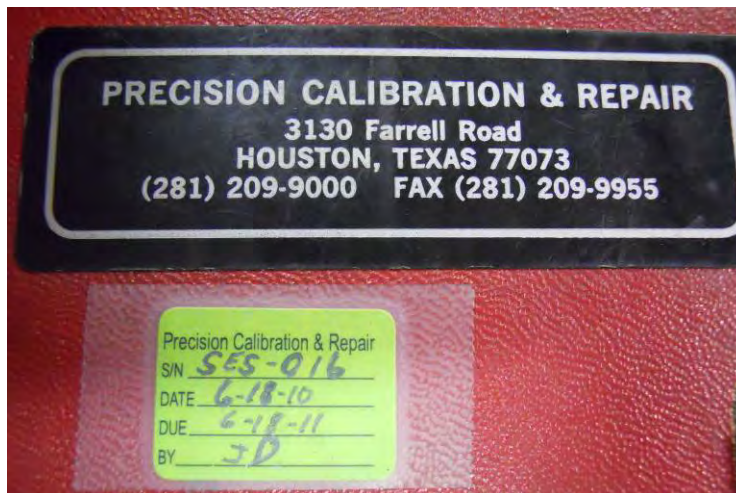


Figure 10: ID Micrometer Manufacturer and Calibration Information

Nondestructive inspection of a few exterior thicknesses was completed using a UT meter; the UT meter, Model EHC 09B, is manufactured by Datatronics.



Figure 11: UT Meter

The meter is calibrated before each use using a calibration block with steps of varying thickness.



Figure 12: UT Meter Calibration Block

The meter is also calibrated once a year by Datatronics. At the time of use, the meter is due for calibration on February 23, 2011.



Figure 13: UT Meter Calibration and Model Information

See Appendix C for measurement instruments. See Appendix D for measurement data and photographs.

APPENDIX A: FLOAT UNPACKING PHOTO DOCUMENTATION

FLOAT 1: As-received September 1, 2010



Sample 1 As-received



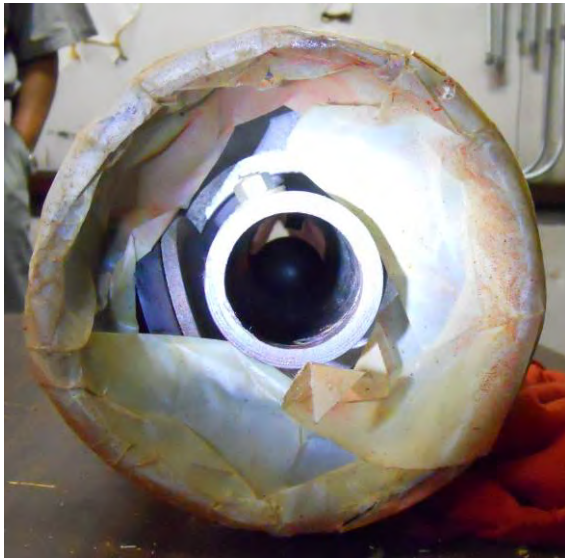
End of Crate



Removing Metal Strap



Removing Shipping Crate



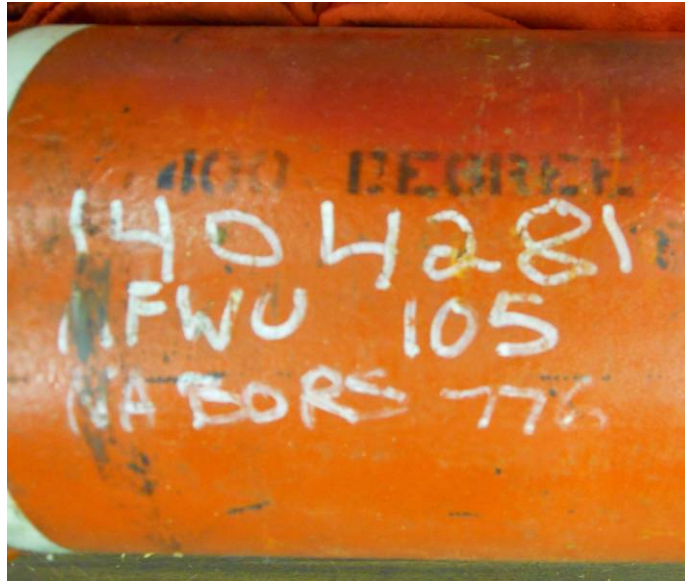
Protective Tape on Pin



Box End is Open



Exterior Marking



Additional Exterior Markings

FLOAT 2: As-received September 13, 2010



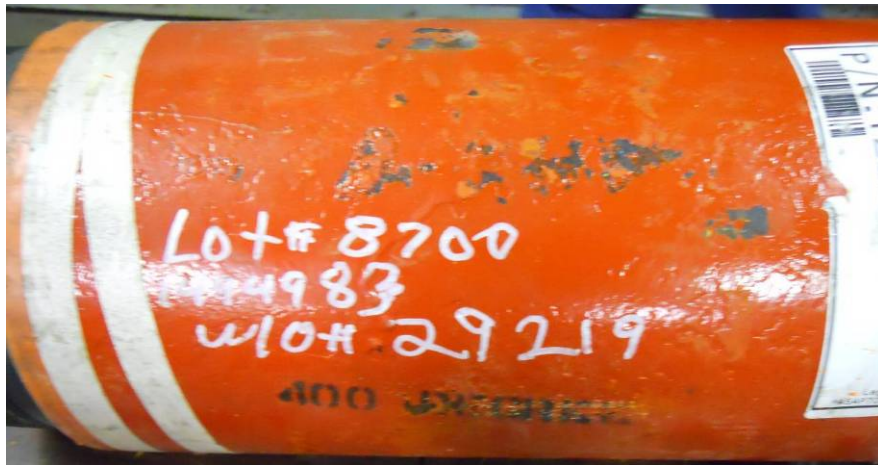
Sample 2 As-Received



End of Crate



Crate Removal



Exterior Marking



Pin End with Ball Visible

** Float was tilted; ball rolled to front but did not fall out.

APPENDIX B: GREASE AND RESIDUE SAMPLE COLLECTION



Collecting Grease from Pin



Collecting Grease from Box



Collecting Residue from Cage Opening



Collecting Residue from under Ball



Collecting Residue from Inner Tube



Collecting Residue from Under Ball

APPENDIX C: CALIBRATED MEASUREMENT DEVICES



Boroscope Instruction Manual



Boroscope Verification Box



Boroscope Calibration Opening



Boroscope Calibration Instructions

*** PCR *** PCR *** PCR *** PCR *** PCR *** PCR *** PCR *** PCR *** PCR *** PCR *** PCR *** PCR *** PCR *** PCR *** PCR ***
 * CERT NO:102710439850
 * PAGE 1 OF 1

PRECISION CALIBRATION & REPAIR 3130 FARRELL ROAD HOUSTON, TEXAS 77073
 PHONE: 281-209-9000 FAX: 281-209-9955 www.precal.net

FORM C071297R5

NIST TEST NUMBERS FOR PRIMARY STANDARDS
 821/274298 821/274921 821/273187 821/276493 821/278015
 443863 822/266926 09-221-01167 09-237-01524 10921-1 120408-1

PURCHASE ORDER: 9110305
 METROLOGIST: BEH
 DATE ISSUED: 10/27/10
 CALIBRATION SPECS: MFG TOL
 AS FOUND CONDITION: NON FUNCTIONAL

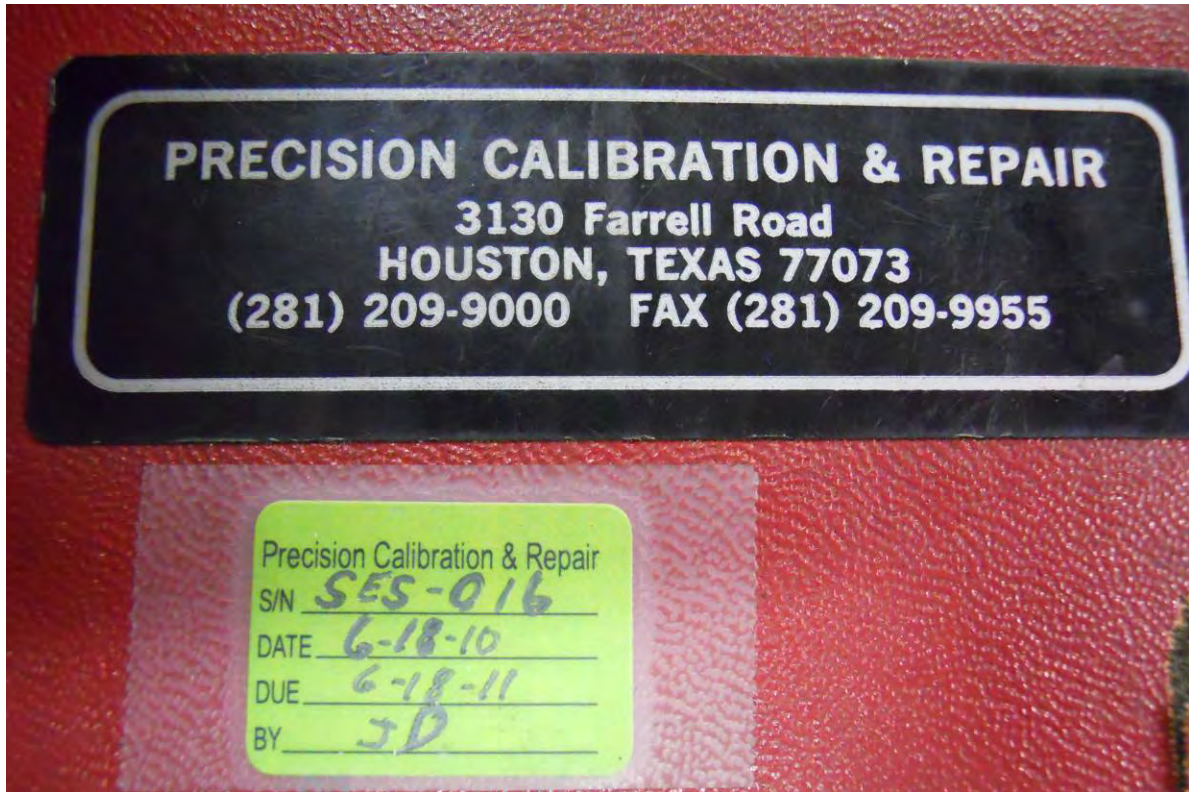
CERTIFICATE OF CALIBRATION
 ISSUED TO: STRESS ENGINEERING
 HOUSTON TX

QUALITY MANAGER: *Charlie Oakley*
 DATE RECEIVED: 10/11/10
 DATE CALIBRATED: 10/26/10
 FREQUENCY: 12
 DATE DUE: 10/26/11

ALL CALIBRATIONS ARE PERFORMED IN ACCORDANCE WITH PCR'S QUALITY PROGRAM DATED 03/01/86, LATEST REVISION "10/01/98".
 ALL CALIBRATIONS ARE PERFORMED IN ACCORDANCE WITH ISO 9000, ISO 17025, ISO 10012-1, ANSI Z540.1 AND MIL-STD 45662A
 AND ARE TRACEABLE TO NIST. ALL CALIBRATIONS ARE PERFORMED AT SIXTY-EIGHT (68) DEGREES PLUS OR MINUS ONE (1) DEGREE
 AND FIFTY-FIVE (55) PERCENT OR LESS HUMIDITY. THE COLLECTIVE UNCERTAINTY OF THE MEASUREMENT STANDARDS DOES NOT
 EXCEED TWENTY-FIVE (25) PERCENT OF THE ACCEPTABLE TOLERANCE FOR EACH CHARACTERISTIC OF THE MEASURING AND TEST
 EQUIPMENT BEING CALIBRATED OR VERIFIED. THESE RESULTS ARE RELATED ONLY TO THE INSTRUMENT(S) CALIBRATED. THIS
 CERTIFICATE SHALL NOT BE REPRODUCED EXCEPT IN FULL WITHOUT WRITTEN APPROVAL OF PCR.

*SERIAL NO	DESCRIPTION	MANUFACTURER	SIZE	MASTER SERIAL NO	ACTUAL SIZE
SES-046	DIAL CALIPER	STARRETT	6"	850783, 724, 5561	6
SES-056	DIAL CALIPER	STARRETT	6"	850783, 724, 5561	6
BD019117	DIAL CALIPER	MITUTOYO	8"	216667, 724, 5561	8
SES-059	DIAL CALIPER	MITUTOYO	12"	850783, 724, 5561	12
SES-032	DIAL CALIPER	MITUTOYO	12"	850783, 724, 5561	12
6062923	DIAL CALIPER	MITUTOYO	12"	216667, 724, 5561	12
SES-020	DIGITAL CALIPER	MITUTOYO	24"	216667, 724, 5561	24

Caliper Calibration Information



ID Micrometer Manufacturer and Calibration Information



ID Micrometer



UT Meter Manufacturer



UT Meter

APPENDIX D: MEASUREMENT DATA

Photo 1



Exterior Measurements

- (a) length of tube
- (b) length of shoulder (transition)
- (c) length of threads

	Position	Sample 1	Sample 2
a	0° - 180°	21.25"	21.25"
	90° - 270°	21.25"	21.25"
b	0° - 180°	0.5"	0.503"
	90° - 270°	0.5"	0.503"
c	0° - 180°	4.44"	4.47"
	90° - 270°	4.44"	4.48"

Photo 2



Pin End Measurements

- (a) pin thickness at edge
- (b) depth of pin tube
- (c) thickness of inner tube
- (d) distance from ID of outer tube to OD of inner tube
- (e₁) diameter of inner tube – at edge
- (e₂) diameter of inner tube – after transition

	Position	Sample 1	Sample 2
a	0° - 180°	0.179"	0.205"
	90° - 270°	0.167"	0.200"
b	0° - 180°	5.9375"	6.00"
	90° - 270°	5.8125"	5.9375"
c	0° - 180°	0.394"	0.281"
	90° - 270°	0.394"	0.295"
d	0° - 180°	1.888"	1.974"
	90° - 270°	1.862"	1.848"
e1	0° - 180°	1.935"	1.921"
	90° - 270°	1.921"	1.922"
e2	0° - 180°	2.190"	2.189"
	90° - 270°	2.179"	2.188"

Photo 3



Inner Tube Measurements

- (a) small threaded hole diameter
- (b) brass set screw pin diameter
- (c) distance from set screw to inner tube edge
- (d) distance from screw hole to inner tube edge
- (e) depth
- (f) thread depth

	Position	Sample 1	Sample 2
a	0°	0.15625"	0.15625"
	90°	0.15625"	0.15625"
	180°	0.15625"	0.15625"
	270°	0.15625"	0.15625"
b	0°	0.25"	0.25"
	90°	0.25"	0.25"
	180°	0.25"	0.25"
	270°	0.25"	0.25"
c		1.75"	1.75"
d		1.6875"	1.6875"
e		0.50"	0.50"
f		0.50"	0.50"

Photo 4



Box End Measurements

- (a) box thickness
- (b) distance to thread
- (c) length of thread

	Position	Sample 1	Sample 2
a	0° - 180°	0.323"	0.339"
	90° - 270°	0.330"	0.314"
b	0° - 180°	0.732"	0.662"
	90° - 270°	0.712"	0.635"
c	0° - 180°	3.9375"	3.925"
	90° - 270°	3.9375"	3.905"

Tube Measurements

	Sample #1	Sample #2
OD	0 deg	2.512"
	90 deg	2.515"
ID	0 deg	2.189"
	90 deg	2.19"
Retaining screw hole diameter	0 deg	0.162"
	90 deg	0.163"
	180 deg	0.163"
L	270 deg	0.164"
	0 deg	13.021"
	180 deg	13.032"
		12.972"

Appendix D
Centralization Plan at Macondo

APPENDIX D Centralization Plan at Macondo

The Centralization Plan

The original Macondo 9-7/8-in. production casing design called for bow-spring centralizer subs to be installed at every joint for the first five joints, followed by one at every other joint up to 500 ft. above the productive interval.¹ This would have required a minimum of 14 centralizers to 17,280 ft.^A A revision on April 15, 2010, altered the program to use six bow-spring subs and 15 slip-on centralizers supplied by Weatherford (21 in total).² The slip-on centralizers were to be installed on every joint from joint 7 to joint 21.³

To: Hafle, Mark E; Morel, Brian P; Cocales, Brett W; Walz, Gregory S
Subject: OptiCem Report

Attached is the updated OptiCem report & lab test. The items that I updated in OptiCem are below; everything else is the same from the one we ran together yesterday.

- Imported caliper data
- Imported directional data
- Entered in centralizer info
- Updated Cement RPM data from lab test

Updating the above info now shows the cement channeling and the ECD going up as a result of the channeling. I'm going to run a few scenarios to see if adding more centralizers will help us or not.

Below is what the standoff looks like with the current centralizer plan. Let me know if you have any questions. Thanks!!

Halliburton Energy Services
 OptiCem v6.4.8
 Centralizer Calculations Report
 This report was created 04/15/2010 15:31:57.
 GetCentNumber = 10

n	Spacing ft	MD ft	Dev. %	Az. °	Stand. %	Rest. Force lbf	Tension lbf	Centralizer
10	48.0	18300.0 18276.0	0.9	219.9	80.73 77.23	11	0	B 7.000x8.500
9	45.0	18252.0 18229.5	0.9	219.9	80.31 79.77	21	1356	B 7.000x8.500
8	45.0	18207.0 18184.5	0.9	219.9	80.33 79.80	20	2627	B 7.000x8.500
7	45.0	18162.0 18139.5	0.9	219.9	91.47 90.86	20	3899	B 7.000x8.500
6	48.0	18117.0 18093.0	0.9	219.9	91.44 90.66	21	5170	B 7.000x8.500
5	84.0	18069.0 18027.0	0.9	219.9	63.91 59.77	27	6526	B 7.000x8.500
4	45.0	17985.0 17962.5	0.9	219.9	45.09 44.83	25	8590	B 7.000x8.500
3	84.0	17940.0 17898.0	0.9	219.9	45.09 42.29	25	9696	B 7.000x8.500
2	45.0	17856.0 17833.5	0.9	219.9	43.95 43.70	25	11760	B 7.000x8.500
1	17811.0	17811.0 17810.0 17790.0	0.9	219.9	13.98 13.98 50.00	3399	12865	B 7.000x8.500
	0.0	0.0			50.00			

Jesse Gagliano
 Halliburton Energy Services
 Account Representative - Cementing
 Office - 281-366-6106
 Cell - 281-635-4798
 Fax - 713-583-9700
 E-mail - jesse.gagliano@halliburton.com

Figure 1 Halliburton Centralizer Report, April 15, 2010

A Fourteen centralizers would put the top centralized joint at 17,280 ft. The depth to 500 ft. above the productive interval is 17,288 ft.

Halliburton runs models using its proprietary OptiCem software for each cement job. The model uses the specifications of the well and other data to determine how many centralizers will be needed for optimum cement flow around the casing. For the 9-7/8-in. x 7-in. production casing, the model specified that 21 centralizers would be required.⁴ With 21 centralizers installed, the model predicted only a minor gas flow potential.⁵ Halliburton's modeling on April 15 had predicted cement channeling with 10 centralizers installed, and Halliburton notified the BP well team of this.⁶ In the model, stand-off varied from as low as 13.98% (where the last centralizer was installed) to as high as 91.47% throughout the centralized interval, from 18,300 ft. to 17,810 ft.⁷ See Figure 1. For adequate centralization, a minimum stand-off of 80% would be required.

The model used a centralizer size of 7 in. x 8-1/2 in., which was not the size of centralizers run on the well. An 8-1/2 in. centralizer would have been unsuitable because the open-hole section was larger than 8-1/2 in. over the entire callipered hole interval.

The Centralization Plan Changed

In response to these results presented by Halliburton, a BP onshore drilling engineer advised the Halliburton cementing coordinator that BP had six centralizers it was planning on running, and recommended placement depths for each centralizer, from the estimated shoe depth of 18,300 ft. to 17,835 ft.⁸

Halliburton performed additional modeling on April 15 after updating its model with final directional survey data, open-hole caliper data and the six centralizers BP had proposed. Results verified that channeling would occur, which would place cement higher than the planned top of cement in the well and increase the equivalent circulating density at the base of the sand to 15.06 pounds per gallon (ppg).⁹ This equivalent mud weight would exceed the formation fracture pressure; however, running an additional 14 centralizers (20 in total) would reduce the ECD to 14.65 ppg — less than the 14.7-ppg ECD, at which mud losses occurred near completion of drilling.¹⁰ Whether Halliburton used the correct size of centralizer for their modeling in this instance is unknown. The BP well team was notified of these findings the same day.¹¹

To align with the modeling performed by Halliburton, BP mobilized 15 additional centralizers and stop collars to the rig prior to job commencement. These specific centralizers raised concerns within the BP well team, as they were not integral centralizers; the stop collars and centralizers were separate pieces that have a risk of slipping when run downhole.¹² The BP Macondo well team erroneously believed they had received the wrong centralizers.¹³ BP was also reluctant to install the additional centralizers due to time concerns, as installation of the additional hardware had been estimated at about 10 hours.¹⁴

The Halliburton 9-7/8-in. x 7-in. production casing design report, dated April 18, 2010, showed a severe gas flow potential with seven centralizers installed on the casing.¹⁵ It is unknown why seven centralizers instead of six were used in the model. Again, the centralizers were incorrectly stated as being 8-1/2 in.¹⁶

Ultimately, only six 7-in. centralizer subs pre-installed on the lower 7-in. interval of the production casing string were run in the well. Whether centralization was adequate to get good cement around the casing annulus and across the reservoir formations is unknown, as no post-cement job logging was performed.

The post-incident OptiCem model performed by Halliburton on May 12, 2010, shows an indication of good centralization over the lower interval, across the productive formations with six centralizers installed. Where the effective casing stand-off is 80% or above, there should be relatively good mud removal and cement coverage. Adequate stand-off over the centralized interval should have ensured mud removal was sufficient over this short section of pipe, therefore mitigating against mud contamination. Above the centralized zone, the casing may be resting on or close to the borehole wall, which would result in the onset of channeling and cement contamination, adversely impacting the quality of the cement in the annulus.

APPENDIX D Centralization Plan at Macondo

1. MC 252 # 1 - Macondo Prospect 9-7/8 Casing Interval, BP-HZN-CEC 8848.
2. 7" x 9 7/8" Casing Interval, BP-HZN-CEC021281, 85.
3. *Ibid.*
4. 9 7/8" x 7" Production Casing Report, April 15, 2010, HAL_0010699, 713.
5. 9 7/8" x 7" Production Casing Report, April 15, 2010, HAL_0010699, 715.
6. Jesse Gagliano e-mail to Mark Hafle, et. al., April 15 2010, HAL_0010648, 50.
7. *Ibid.*
8. Brian Morel e-mail to Jesse Gagliano, et. al., April 15, 2010, HAL_0010648, 49.
9. Greg Walz e-mail to John Guide, April 16, 2010, BP-HZN-CEC022433.
10. *Ibid.*
11. *Ibid.*
12. John Guide e-mail to Greg Walz, April 16, 2010, BP-HZN-CEC022433.
13. *Ibid.*
14. *Ibid.*
15. 9 7/8" x 7" Production Casing Design Report, April 18, 2010, HAL_0010988.
16. *Ibid.*

Appendix E
Review of Macondo #1 7" x 9-7/8"
Production Casing Cementation

BP and Halliburton have produced information including cement testing reports, production casing reports, modeling, and other information in connection with the ongoing multi-district litigation proceedings pertaining to Macondo. Appendix E is based in part on information produced during litigation that BP and Halliburton have marked as "confidential" and not for public disclosure pursuant to the pretrial order of the Court.

For this reason, Appendix E is being withheld at this time.

Should the parties come to an agreement regarding the status of the data, Appendix E will be supplemented.

Transocean has sought and will continue to seek permission to release this information.

Appendix F
Lock-Down Sleeve Decision

Appendix F Lock-Down Sleeve Decision

After the production casing has been installed in the well and cemented in place, the operator may elect to run a lock-down sleeve. A lock-down sleeve locks the casing hanger to the wellhead housing, which prevents upward movement of the casing system and typically is installed prior to completion operations. The lock-down sleeve on Macondo was positioned inside the well on top of the 9-7/8-in. casing hanger and latches into the 18-3/4-in. wellhead housing, thus securing the casing from potentially lifting upwards after it is landed.

Lock-Down Sleeve Procedures

Initially, BP's temporary abandonment procedure (as proposed on April 12) specified setting the lock-down sleeve before commencing temporary abandonment operations.¹ Figure 1 represents a typical lock-down sleeve. BP modified the procedure twice and then submitted to the Minerals Management Service (MMS) an Application for Permit to Modify on April 16.² The modified procedure directed that the lock-down sleeve be set last, after displacing the kill line to seawater, conducting a negative pressure test and setting a surface cement plug for the temporary abandonment.³

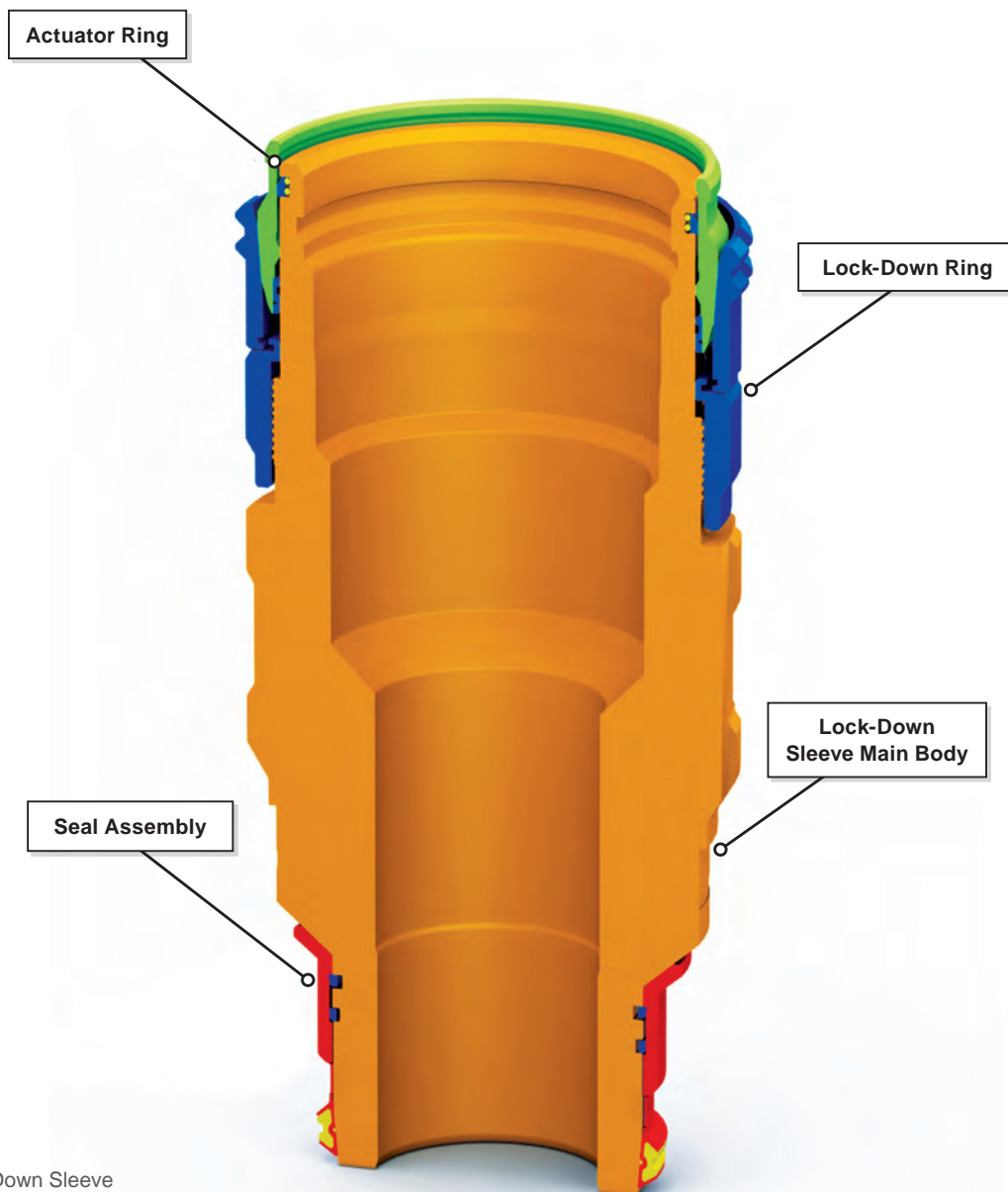


Figure 1 Lock-Down Sleeve

Changing the sequence in which the sleeve would be set from first to last eliminated the risk of damaging the internal sealing areas of the lock-down sleeve while running drill pipe into the well to set the surface cement plug.⁴ However, setting the lock-down sleeve last impacted other well activities during the abandonment phase of the well and increased other risks.

The lock-down sleeve is set in position with a running tool by applying weight. To set the lock-down sleeve, Dril-Quip recommended running 100,000 lb. of weight below the running tool. The weight below the running tool is known as the tailpipe. To achieve the 100,000 lb., there had to be enough space left below the wellhead and above the top of the surface cement plug, which under the final plan would be set in place prior to the lock-down sleeve being installed. Alternatively, Dril-Quip stated in their manual that weight above the running tool could be substituted for weight below the running tool.

BP's lock-down sleeve running procedure, as revised on April 13, called for assembling 24 joints of 5-1/2-in heavyweight drill pipe (HWDP) and 6-1/2-in. drill collars as a tailpipe section to achieve this required weight. The tailpipe would have been run to approximately 1,350 ft. below the wellhead utilizing this configuration.

In an April 15 version of the 9-7/8-in. x 7-in. casing program, BP specified that six joints of 6-1/2-in. collars; 28 joints of 5-1/2 in. HWDP; and about 36 joints of 5-1/2 in., 21.9-pound-per-foot drill pipe (standard drill pipe) would be used to provide the tailpipe weight.⁵ As standard drill pipe provides less weight than heavyweight drill pipe, this tailpipe would have been run to approximately 2,700 ft. below the wellhead.

BP's final abandonment procedure provided to the drill crew on the morning of April 20, 2010, noted that the cement plug would be set at 8,367 ft. (3,300 ft. below the wellhead), or 600 ft. deeper than the 2,700 ft. of tailpipe in the casing program of April 15.⁶ The April 15 version had a tailpipe weight that was much closer to the required amount to set the lock-down sleeve per Dril-Quip procedures. It is unknown why this depth was changed from the previous procedure.⁷ The investigation team noted that the 5-1/2-in. standard drill pipe was available in the derrick while the HWDP and drill collars were on the rig's pipe deck.⁸ Picking up the HWDP and drill collars from the deck to the drill floor could be performed offline, meaning the operation could be conducted at the same time as other main operations and not directly impact the rig time and costs. However, at the end of operations, the pipe would need to be laid back on the deck, which could not be done at the same time that the riser and BOP stack was being pulled, and would thus increase operational time and cost.

BP's decision to set the cement plug deeper, at 8,367 ft., was not critical until BP decided to change the sequence of its abandonment procedures and set its final abandonment cement plug in seawater to minimize contamination of cement with the drilling mud. BP had it classified as a "surface plug." This waiver likely saved 8 to 12 hours of rig time that would have been necessary to wait for the cement to harden prior to testing the plug, as there were no MMS weight testing or pressure testing requirements for plugs classified as surface plugs.⁹

There is no evidence that BP conducted any formal risk assessment to evaluate the increased risks associated with removing additional amounts of heavy mud in the well and replacing it with lighter seawater before the negative test was performed. Also, no management of change or other risk assessment documents appear to have been prepared.

Casing Hanger Load Summary

The investigation evaluated the potential for the production casing hanger to be unseated, thereby enabling a flow path for hydrocarbons up the production casing annulus. The tension loads experienced by the casing hanger were evaluated by Stress Engineering Services, the findings of which are summarized in *Appendix B*.¹⁰ The known and anticipated loads on the production casing and casing hanger revealed that the casing hanger likely had some positive tension load throughout the incident, but this was dependent upon the annulus pressure which, if sufficiently high, could have moved the tension load to neutral or slightly negative.^A

^A Since the wellhead and casing temperatures experienced during the time the well was flowing can only be roughly estimated, any annulus pressure due to the thermal effects likewise would be only rough estimates. It is theoretically possible that the casing hanger and seal assembly could have experienced enough of an uplift force from the combination of thermal effects on the casing and annulus pressure below the casing hanger to temporarily unseat the seal assembly. This would have relieved the annulus pressure and the casing hanger and seal assembly would have re-seated in the wellhead.

Appendix F Lock-Down Sleeve Decision

After successfully killing the Macondo well, the seal assembly and casing hanger were found to be in the correct position when located with the Dril-Quip Lead Impression Tool (LIT) during the course of the abandonment operations.¹¹ The 9-7/8-in. casing was perforated, and there was no indication of pressure or gas in the casing annulus.¹²

Both the seal assembly and casing hanger were recovered prior to permanently abandoning the Macondo well.¹³ Photographs of the casing hanger and seal assembly show the erosion effects of the well flow path to be from the interior of the casing and not from the casing annulus.^B

^B During the Macondo abandonment operations, a 1-5/8-in. brass setting ball was recovered from a section of the marine riser. It is believed this was the ball utilized to activate the Allamon Diverter Test Device and Diverter Sub. Once activated, the ball will drop down hole to the float collar. The presence of this ball in the riser section confirms that the flow path must have been from the bottom of the casing, rather than up the annulus.

1. See Section 3.2, Temporary Abandonment.
2. Brian Morel e-mail to James Wilson and Ronald Sepulvado, April 14, 2010, BP-HZN-MBI00126928; Application for Permit to Modify, April 16, 2010, BP-HZN-MBI00023711,13.
3. Application for Permit to Modify, April 16, 2010, BP-HZN-MBI00023711,13.
4. *Ibid.*
5. 7" x 9 7/8" Interval, April 15, 2010, BP-HZN-CEC017621, 30.
6. BP-HZN-CEC020165, Email from Brian Morel to Robert Kaluza, et al.
7. 7" x 9 7/8" Interval, April 15, 2010, BP-HZN-CEC017621, 30.
8. Transocean *Deepwater Horizon* Morning Report, April 18, 2010, TO-DHTF-00005081.
9. 30 C.F.R. 250 § 1715.; 30 C.F.R. 250 § 1721.
10. See Appendix B.
11. Development Driller II Daily Drilling Report, Sept. 9, 2010.
12. Development Driller II Daily Drilling Report, Oct. 6, 2010; Development Driller II Daily Drilling Report, Oct. 7, 2010; Development Driller II Daily Drilling Report, Oct. 8, 2010; Development Driller II Daily Drilling Report, Oct. 9, 2010; Development Driller II Daily Drilling Report, Oct. 10, 2010.
13. Development Driller II Daily Drilling Report, Oct. 11, 2010; Development Driller II Daily Drilling Report, Oct. 12, 2010; Development Driller II Daily Drilling Report, Oct. 13, 2010.

Appendix G
Hydraulic Analysis of Macondo
#252 Well Prior to
Incident of April 20, 2010



Hydraulic Analysis of Macondo #252 Well Prior to Incident of April 20, 2010

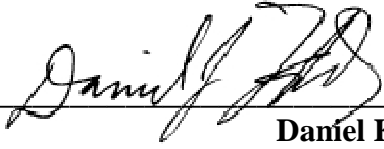
SES Document No.: 1101190-ST-RP-0002


Prepared for:
Transocean Offshore Deepwater Drilling, Inc.

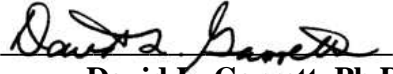
REV	DATE	DESCRIPTION	ORIGINATOR	REVIEWER	APPROVER
1	27-Apr-11	Revised	DJK	DLG/KPM	W. Bell
0	04-Apr-11	Issued for Use	DJK	DLG/KPM	M. Thibodeaux D. Farr
B	15-Mar-11	Issued for Client Review	DJK	DLG/KPM	N/A
A	15-Feb-11	Issued for Internal Review	DJK	N/A	N/A

HYDRAULIC ANALYSIS OF MACONDO #252 WELL PRIOR TO INCIDENT OF APRIL 20, 2010

SES DOCUMENT NO.: 1101190-ST-RP-0002

Prepared By: 
Daniel Kluk
Associate

Reviewed By: 
Kenneth P. Malloy, P.E.
Staff Consultant

Reviewed By: 
David L. Garrett, Ph.D.
Principal



Stress Engineering Services, Inc.
13800 Westfair East Drive
Houston, Texas 77041-1101
281-955-2900 / www.stress.com

APRIL 2011

EXECUTIVE SUMMARY

This report documents data review and analysis work performed by Stress Engineering Services, Inc. (SES) on behalf of Transocean Offshore Deepwater Drilling, Inc. The objective of the analysis was to determine the hydraulic state of the Macondo Prospect Mississippi Canyon #252 exploration well during the events leading up to the blowout, explosion, and subsequent fire aboard the *Deepwater Horizon* mobile offshore drilling unit on April 20, 2010. The analysis is focused primarily on the events which occurred on the day of the blowout between 3:00 pm (15:00) to the last recorded data transmission at 9:49 pm (21:49) CDT.

SIGNIFICANT FINDINGS from the analysis are as follows:

1. Lower than expected rig pump volumetric output is calculated over the time interval of interest.
2. Well return volumes were obscured during initial displacement activity due to transfers out of the active pits at an unknown rate.
3. The spacer pumped into the well was not displaced above the BOP prior to beginning the negative test.
4. During the negative testing, the well was underbalanced, with potential influx from the pay zone, on three separate occasions.
5. During the second seawater displacement, the well was underbalanced to the hydrocarbon formations by 20:52.
6. The spacer was not at the top of the riser upon shutting down the pumps for the static sheen test at 21:09.
7. By 21:39, 501 bbl of hydrocarbon influx was taken into the well and reached the end of the work string.
8. It is estimated that an annular preventer was closed on the BOP stack at 21:43:40, but the closure failed to seal the well.
9. Hydrocarbon gas reached the rig surface (emerging from the mud gas separator vent outlets) at 21:46:40. At this time, the volume gain was 2,510 bbl.
10. A variable bore ram was closed on the BOP stack at 21:47:00, which temporarily shut in the well.
11. The final recorded data transmission from the *Deepwater Horizon* occurred at 21:49:15.

LIMITATIONS OF THIS REPORT

The scope of this report is limited to the matters expressly covered. This report is prepared for the sole benefit of Transocean Offshore Deepwater Drilling, Inc. (“Transocean”). In preparing this report, Stress Engineering Services, Inc. (SES) has relied on information provided by Transocean. Stress Engineering Services, Inc. (SES) has made no independent investigation as to the accuracy or completeness of such information and has assumed that such information was accurate and complete. Further, Stress Engineering Services, Inc. (SES) is not able to direct or control the operation or maintenance of client’s equipment or processes.

All recommendations, findings and conclusions stated in this report are based upon facts and circumstances, as they existed at the time that this report was prepared. A change in any fact or circumstance upon which this report is based may adversely affect the recommendations, findings, and conclusions expressed in this report.

NO IMPLIED WARRANTY OF MERCHANTABILITY OR FITNESS FOR A PARTICULAR PURPOSE SHALL APPLY. STRESS ENGINEERING SERVICES, INC. MAKES NO REPRESENTATION OR WARRANTY THAT THE IMPLEMENTATION OR USE OF THE RECOMMENDATIONS, FINDINGS, OR CONCLUSIONS OF THIS REPORT WILL RESULT IN COMPLIANCE WITH APPLICABLE LAWS OR PERFECT RESULTS.

TABLE OF CONTENTS

	<u>Page No.</u>
EXECUTIVE SUMMARY	III
LIMITATIONS OF THIS REPORT.....	IV
1 INTRODUCTION.....	12
1.1 Definition of Terms.....	13
1.2 Definition of Symbols.....	19
1.3 Accuracy and Precision of Reported Results.....	20
2 SCOPE.....	23
2.1 Well Status During Events of Interest.....	24
3 PLANNED DISPLACEMENT PROCEDURE AND HYPOTHETICAL HYDRAULIC RESPONSE.....	26
3.1 Overview.....	26
3.2 Hypothetical Pump Schedule.....	27
3.3 Discussion.....	28
4 TIMELINE OF OBSERVED EVENTS WITH SUPPORTING ANALYSIS.....	35
4.1 Displacement of Auxiliary Lines.....	39
4.1.1 Booster Line.....	41
4.1.2 Choke Line.....	46
4.1.3 Kill Line.....	50
4.2 First Displacement of 16 ppg Spacer and Seawater Prior to Negative Testing.....	54
4.2.1 Strokes Pumped.....	54
4.2.2 Measured Spacer Volume Pumped.....	56
4.2.3 Riser Flow Out.....	57
4.2.4 Pressure Response.....	60
4.2.5 Fluid Boundary Positions.....	62
4.2.6 Pit Returns.....	64
4.2.7 Well Fluid State.....	64
4.3 Hydrostatic Analysis of Negative Testing.....	67
4.3.1 Observed Standpipe and Kill Line Pressures.....	68

4.3.2	Well State Calculations	73
4.3.3	Kill Line Valve Status Summary	90
4.4	Second Displacement of Seawater after Negative Testing	91
4.4.1	Strokes Pumped.....	92
4.4.2	Pit Returns	93
4.4.3	Riser Flow Out	95
4.4.4	Pressure Response	97
4.4.5	Estimated Hydrocarbon Influx Volume	102
4.5	Static Sheen Test	102
4.5.1	Pressure Response	105
4.5.2	Estimated Hydrocarbon Influx Volume	105
4.6	Final Displacement of Seawater After Static Sheen Test	106
4.6.1	Strokes Pumped.....	106
4.6.2	Pressure Response	107
4.6.3	Estimated Hydrocarbon Influx Volume	109
4.7	20 Minutes Prior to Explosion	111
4.7.1	Observed Standpipe, Kill Line, and Trip Tank Signals	113
4.7.2	Hydrostatic Calculations	121
4.7.3	Well Flow Calculations.....	126
4.7.4	Frictional Pressure Drop Calculations.....	132
4.7.5	Flow through Diverter and Mud-Gas Separator System.....	134
4.7.6	Work String Displacement Analysis	141
4.7.7	Flow Velocities Around and Through Work String at Selected Times	143
5	DISCUSSION	145
5.1	Key Observations	145
5.2	Comparison of Hypothetical Displacement Scenario to Actual Events.....	148
5.3	Summary of Pump Efficiency Estimates	149
5.4	Hydrocarbon Flow Path	151
6	REFERENCES	155

APPENDICES

	<u>Page No.</u>
Appendix A: Analysis Input Parameters	157
Appendix B: Time-Domain Hydraulic Models.....	160
Appendix C: Detailed Charts and Supporting Calculations.....	168
Appendix D: MI-Swaco Rheliant Displacement Procedure	231
Appendix E: Comparison of Input Data Sets	233

LIST OF TABLES

	<u>Page No.</u>
Table 1: Precision of reported quantities.....	20
Table 2: Standpipe and kill line pressures, hypothetical displacement.....	30
Table 3: Calculated pressure differences for various fluids	33
Table 4: Equivalent mud weight at 12.6 ppg formation depth, hypothetical displacement.....	34
Table 5: Description of events from 15:00 to 17:00	36
Table 6: Description of events from 17:00 to 20:00	37
Table 7: Description of events from 20:00 to 21:49	38
Table 8: Description of events from 15:00 to 15:55	40
Table 9: Pump output summary, booster line displacement	41
Table 10: Pump analysis summary, booster line displacement	44
Table 11: Pump output summary, choke line displacement.....	46
Table 12: Pump analysis summary, choke line displacement	49
Table 13: Pump output summary, kill line displacement.....	50
Table 14: Pump analysis summary, kill line displacement.....	53
Table 15: Pump output summary, spacer displacement.....	54
Table 16: Pump output summary, seawater displacement	54
Table 17: Description of events from 15:55 to 17:00	55
Table 18: Pump analysis summary, spacer displacement.....	58
Table 19: Pump analysis summary, first seawater displacement.....	58
Table 20: Formation pressure data used for well simulations, obtained from [6]	61
Table 21: Spacer position and final standpipe pressure for various displacement cases	63
Table 22: Description of events from 16:54 to 17:35	68
Table 23: Description of events, first 40 minutes of negative test.....	69
Table 24: Description of events from 17:32 to 20:00	70
Table 25: Description of events, final 150 minutes of negative test.....	71

Table 26: Summary of inferred kill line valve status during negative testing	90
Table 27: Description of events from 20:00 to 21:08	92
Table 28: Pump output summary, seawater displacement through work string	92
Table 29: Pump output summary, seawater displacement through booster line	92
Table 30: Pit return volume tally during second seawater displacement	94
Table 31: Pump analysis summary, second seawater displacement	95
Table 32: Description of events from 21:08 to 21:30	104
Table 33: Pump output summary, seawater displacement through work string	106
Table 34: Pump output summary, seawater displacement through auxiliary lines	107
Table 35: Description of events from 21:30 to 21:49	112
Table 36: Description of events 20 minutes prior to explosion	112
Table 37: Volume and standpipe pressure results comparison, hydrostatic analysis	121
Table 38: Tabulated flow and volume gain estimates, final 20 minutes	131
Table 39: Initial flow estimates through MGS	138
Table 40: Flow estimates through MGS, all outlets flowing	138
Table 41: Estimate of hydrocarbons in riser	139
Table 42: Gas flow distribution through MGS outlets	140
Table 43: Estimated steady state mass flow rate; equivalent representations	140
Table 44: Pressure responses, hypothetical scenario vs. actual	148
Table 45: Summary of rig pump volumetric efficiency analyses	149
Table 46: Pump output summary, second seawater displacement	150
Table 47: Drill Pipe Specifications	158
Table 48: Wellbore Fluid Capacities and Volumes	158
Table 49: Wellbore Equipment Depths	159
Table 50: Other Well Specifications	159
Table 51: Mud Pump Specifications	159
Table 52: Model A fluid properties	164
Table 53: Model B fluid properties	165
Table 54: Characteristics of reported telemetry signals	236

LIST OF FIGURES

	<u>Page No.</u>
Figure 1: Diagram of Macondo well #252, April 20th 2010, 15:00 to end of transmission.....	25
Figure 2: Graph of prescribed flow rates for hypothetical riser displacement.....	29
Figure 3: Expected standpipe and kill line pressures during hypothetical displacement.....	29
Figure 4: Fluid states during hypothetical displacement procedure: Initial state (left); after spacer displacement (middle); after first seawater displacement (right).....	31
Figure 5: Fluid states during hypothetical displacement procedure: After second seawater displacement (left); after final seawater displacement (right).....	32
Figure 6: Overview of auxilliary line and riser displacement, 15:00 to 17:00.....	36
Figure 7: Overview of negative testing activity, 17:00 to 20:00.....	37
Figure 8: Overview of final riser displacement and activity prior to explosion, 20:00 to 21:49.	38
Figure 9: Pressure and flow signals recorded during auxiliary line displacement.....	40
Figure 10: Simulated line pressure, booster line displacement.....	42
Figure 11: Simulated flow out vs. measured flow sensor data, booster line displacement.....	43
Figure 12: Pit activity during auxiliary line displacement	45
Figure 13: Simulated (calculated) vs. measured choke line pressure during displacement.....	47
Figure 14: Simulated flow out vs. measured flow sensor data, choke line displacement.....	48
Figure 15: Simulated (calculated) vs. measured kill line pressure during displacement	51
Figure 16: Simulated flow out vs. measured flow sensor data, kill line displacement	52
Figure 17: Pressure, flow, and hook load signals recorded during riser displacement with spacer and seawater	55
Figure 18: Pressure, flow, and pit signals during spacer displacement.....	56
Figure 19: Simulated vs. measured flow out of riser during spacer and seawater displacement.	59
Figure 20: Simulated vs. measured standpipe pressure during spacer and seawater displacement	60
Figure 21: Simulated bottom hole pressures during spacer and seawater displacement	61
Figure 22: Simulated spacer-to-mud and spacer-to-seawater liquid boundary positions during spacer and seawater displacement.....	62
Figure 23: Pit transfer activity during spacer displacement.....	64
Figure 24: Well fluid states before and after spacer displacement:	65
Figure 25: Well fluid state after first displacement at 16:53 (left);.....	66
Figure 26: Negative test data telemetry, first 40 minutes	68
Figure 27: Negative test data telemetry, final 150 minutes.....	70
Figure 28: Schematic of rig surface piping arrangement during negative test.....	72
Figure 29: Plot of cement pump pressure recorded during positive pressure test on April 20th.	75
Figure 30: Standpipe pressure signal during annular preventer closure	76
Figure 31: Well fluid states during negative testing: 16:57 (left); 17:26 (right).....	78

Figure 32: Trip tank activity following annular preventer leakage.....	79
Figure 33: Well fluid states during negative testing: 17:28 (left); 17:33 (right).....	82
Figure 34: Well fluid states during negative testing: 18:00 (left); 18:31 (right).....	84
Figure 35: Detailed view of pressure signals recorded during build-up, 18:00 to 18:31	85
Figure 36: Well fluid states during negative testing: 18:37 (left); 19:50 (right).....	87
Figure 37: Overview of signals recorded during second seawater displacement	91
Figure 38: Pit and flow sensor return data during second seawater displacement.....	94
Figure 39: Simulated vs. measured flow out of riser during second seawater displacement.....	96
Figure 40: Simulated vs. measured standpipe pressure during second seawater displacement, with tubing washout scenario	97
Figure 41: Simulated bottom hole pressures during second seawater displacement, with formation balance points labeled.....	99
Figure 42: Simulated spacer-to-mud and spacer-to-seawater liquid boundary positions during second seawater displacement.....	100
Figure 43: Well fluid states during the post-negative test seawater displacment:	101
Figure 44: Well state diagrams before and after the static sheen test, with hydrocarbon influx: 21:09 (left); 21:13 (right)	103
Figure 45: Overview plot of signals recorded during static sheen test and final seawater displacement.....	104
Figure 46: Simulated vs. measured pressure reponse, second seawater displacement	107
Figure 47: Well state diagram following final seawater displacement, 21:30	110
Figure 48: Plot of telemetry signals 20 minutes prior to explosion	111
Figure 49: Detail of pressure signals recorded from 21:42 to 21:47.....	116
Figure 50: Diagram of BOP showing kill line entry locations (circled). Excerpted from [8].	117
Figure 51: Well state diagrams during final 20 minutes of data: 21:30 (left); 21:34 (right)	122
Figure 52: Well state diagrams during final 20 minutes of data: 21:39 (left); 21:42 (right)	123
Figure 53: Comparison of measured and calculated kill line pressures	124
Figure 54: Diagram of theoretical riser model	126
Figure 55: Liquid free-body diagram with relevant equations and values.....	127
Figure 56: Theoretical gas rise velocity plot.....	128
Figure 57: Hydrocarbon volume above work string and surface liquid flow, starting at 21:39	130
Figure 58: Calculated work string-to-casing annulus pressure drop (starting at 21:39)	133
Figure 59: Hydrostatic and frictional pressures in diverter, flow line and gumbo box.....	135
Figure 60: Diagram of mud-gas separator and adjacent piping	136
Figure 61: Expanded view of MGS system indicating scale of vent and vacuum breaker lines	137
Figure 62: Frictional loading of the work string below the BOP, starting at 21:39.....	142
Figure 63: Hypothetical displacement procedure at static sheen test. Formation exposure to production casing only with sealed annulus (left); exposure to open annulus only (right)	153
Figure 64: Model A Geometric Diagram and Variable Labeling	162

Figure 65: Model B Geometric Diagram and Variable Labeling..... 163
Figure 66: Mud viscosity comparison: 204 cP (top); 28 cP (bottom)..... 166
Figure 67: Comparison of simulation outputs: Model A (top); Model B (bottom) 167
Figure 68: Comparison of filtered and unfiltered data sets, example 1 234
Figure 69: Comparison of filtered and unfiltered data sets, example 2 235

1 INTRODUCTION

This report documents data review and analysis work performed by Stress Engineering Services, Inc. (SES) on behalf of Transocean Offshore Deepwater Drilling, Inc. (“Transocean”). The objective of the analysis was to determine the hydraulic state of the Macondo Prospect Mississippi Canyon #252 exploration well during the events leading up to the blowout, explosion, and subsequent fire aboard the *Deepwater Horizon* mobile offshore drilling unit on April 20, 2010. The analysis is focused primarily on the events which occurred on the day of the blowout between 3:00 pm (15:00) to the last recorded data transmission at 9:49 pm (21:49) CDT (this period is referred to as the “time interval of interest” in the discussion herein).

This document constitutes our report in this matter. SES has reviewed all materials provided, which are listed in the references (Section 6). The content of the report is limited to factual statements regarding the information contained in the references, and presentation of analysis results derived therefrom. These results are presented as a means to: a) assess the validity of the input data sets; and b) to provide estimates of well state quantities that were not recorded (and/or measured) in the data sets. When provided, observations are limited to an assessment of the plausibility of the analysis results. SES does not attempt to discern specific actions taken by personnel aboard the rig or elsewhere, or assign culpability in any case.

The findings from our investigation are based on years of formal training, practical field experience, knowledge of current recommended practices, witness testimony, and interview notes, along with associated records. Accordingly, SES reserves the right to modify this report based upon further study or if additional information becomes available.

This report is prepared exclusively for the benefit of Transocean Offshore Deepwater Drilling, Inc. under Work Order #DWH-417803-001 and Confidentiality Agreement, both dated May 20th, 2010.

1.1 Definition of Terms

- **Annular:** An annular blowout preventer device installed as part of a BOP stack, consisting of a toroidal- or annular-shaped rubber element supported by steel guides. When activated, the element is compressed via hydraulic pressure into the bore of the BOP, thereby forming a seal. Also called “annular preventer”.
- **Annulus:** A ring-shaped space formed between two concentric pipes of unequal size.
- **Anticipated:** In the context of this report, “anticipated” refers to pump volumes derived from stroke counts. These volumes are obtained by multiplying the measured stroke count by the theoretical pump output, scaled by a fixed volumetric efficiency ratio.
- **Assumed:** In the context of this report, “assumed” refers to physically plausible operations or events for which no direct evidence is available, but which are consistent with adjoining established events. Physical plausibility is assigned based on professional common practice and experience.
- **bbbl:** Abbreviation for “barrel”, a common unit of volume in drilling operations. One barrel (bbl) is equal to 42 US gallons.
- **Booster Line:** A small-diameter line that runs along the outside of the riser and terminates just above the BOP stack. Allows extra fluid flow to be pumped into the riser during a displacement.
- **Blind Shear Ram:** A blowout preventer device installed as part of a BOP stack, intended to seal the BOP bore via the closure of opposing ram elements. The rams are fitted with hardened steel blades designed to sever (shear) any drill pipe present in the bore upon closing, although the device is not powerful enough to sever casing.
- **BOP:** BlowOut Preventer. Specifically, an individual blowout preventer device.
- **BOP Stack:** A series of individual BOP devices, usually of varying design functions, assembled in a vertical stack configuration. The BOP stack is installed onto a wellhead to facilitate well control and testing operations. See Figure 50 (page 117) for a diagram of the *Deepwater Horizon* BOP stack.
- **Calculated:** In the context of this report, “calculated” refers to estimates of well state quantities generated by means of a spreadsheet or other engineering calculation software, or a hand calculation.

- Casing: Large-diameter piping segments installed into a wellbore after drilling. Once installed, the casing segments are cemented in place to provide structural support and pressure containment to the well.
- Casing Shear Ram: A blowout preventer device installed as part of a BOP stack, intended to close (but not necessarily seal) the BOP bore via the closure of opposing ram elements. The rams are fitted with hardened steel blades designed to sever (shear) any drill pipe or casing present in the bore upon closing.
- Cement: A material pumped as a fluid that develops compressive strength, sets and hardens due to hydration involving chemical reactions of certain materials with water. Once hardened, it provides a hydraulic seal preventing fluid channels within the cement sheath between the casing-formation annulus. This achieves zonal isolation of formation fluids, containing them within a specific zone of interest.
- Cementing Unit: A high-pressure triplex pump capable of pumping cement slurries. Also has the capability to pressure test casing, BOPs, and formation for integrity.
- Chiksan Lines: A collection of rigid piping segments joined by swivel joints, intended for temporarily deployment to connect two or more fluid systems.
- Choke Line: One of two medium-diameter lines that run along the outside of the riser and terminate at various points within the BOP stack. The primary purpose of the choke line is to direct wellbore fluids into the surface choke manifold during well control operations. See also “Kill Line”.
- Corrected: In the context of this report, “corrected” refers to measured flow sensor signals from which the trip tank outlet flow rate (obtained by differentiating the measured volume) is subtracted. Because the trip tank flow may include a portion of the active well outlet flow that bypasses the flow sensor, the corrected signal is a more accurate representation of the total well outlet flow.
- Crossover: A pipe segment designed to join drill pipe, tubing, or casing having dissimilar diameters or thread forms.
- Diverter: A hydraulically actuated annular sealing element, similar to an annular blowout preventer, installed at the top of a riser just beneath the drill floor. When activated, the annular element is compressed via hydraulic pressure into the bore of the diverter,

thereby forming a seal, and riser outlet flow is redirected from the flow line to the divert piping system. The flow then proceeds either overboard or to a mud gas separator, depending on a pre-selected valve configuration.

- Drill Pipe: Specialized piping segments designed to be run through a wellbore to deploy drill bits and other tools and pump various fluids into the well.
- EMW: Equivalent Mud Weight. A method of expressing downhole pressures as an effective liquid density, relative to a specified reference depth.
- Final Displacement: In the context of this report, “final displacement” refers to the continued displacement of the casing and riser annulus created by the work string with seawater following the static sheen test. This activity occurred from 21:13 to 21:30 on April 20, 2010.
- First Displacement: In the context of this report, “first displacement” refers to the initial displacement of the casing annulus and riser with 16 ppg spacer and seawater prior to the negative test. This activity occurred from 15:55 to 16:53 on April 20, 2010.
- FOSV: Full Open Safety Valve with full open bore.
- Gumbo Box: A hopper-like device into which mud returning from the riser flows prior to reaching the shale shakers and mud pits. The gumbo box performs initial separation of solids from the mud.
- Hypothetical: In the context of this report, “hypothetical” refers to the output of an analytical reconstruction of the mud displacement procedure [9] used aboard the *Deepwater Horizon* on April 20, 2010. The reconstruction is employed as a case study for comparison purposes, and does not reflect the actual state of the Macondo well. See Section 3 for further information.
- IBOP: Inside BlowOut Preventer. A valve installed in the work string designed to prevent uncontrolled flow up the work string.
- Influx: Movement of fluid from rock formations outside of the wellbore into the wellbore.
- Kelly Hose: A high-pressure flexible hose connecting the standpipe to a string of drill pipe through a swivel.

- **Kill Line:** One of two medium-diameter lines that run along the outside of the riser and terminate at various points within the BOP stack. The primary purpose of the kill line is to pump kill fluid into the well during well control operations. See also “Choke Line”.
- **Measured:** In the context of this report, “measured” refers to signals recorded in one of the rig telemetry data files [12, 13, 14, 17]. These signals serve as the basis for deriving calculated and simulated quantities.
- **MGS:** Mud Gas Separator. A pressure vessel used to separate entrained gas from mud returning from a well.
- **Mud Line:** Depth of the sea floor.
- **Overbalanced:** A condition in which the hydrostatic pressure of the drilling fluid within the wellbore exceeds the fluid pressures from the surrounding rock formation(s).
- **PBTD:** Plug Back Total Depth. The total depth of a well as measured to the lowest seal obstruction or plug. For purposes of this report, PBTD refers to the float collar installed at 18,115 feet below RKB.
- **Plug:** A cylindrical device, often made of rubber, installed into a wellbore to seal fluids at the installation point. See Wiper Plug.
- **ppg:** Pounds (mass) Per Gallon. A unit of liquid density commonly referenced in drilling operations. One ppg is approximately equal to 0.1198 grams per cubic centimeter.
- **Rig Personnel:** In the context of this report, “rig personnel” refers to all persons aboard the *Deepwater Horizon* mobile offshore drilling unit on April 20, 2010. No distinction is made between employers, guest or crew status, or job functions.
- **Riser:** A large diameter vertical pipe connecting a drilling or production vessel to equipment at the seafloor (often a BOP stack). The riser provides a conduit to the wellhead for fluids and tools during drilling and / or production operations.
- **RKB:** A vertical point of reference at (or in close proximity to) the drill floor relative to which well and downhole equipment depths are measured.
- **Second Displacement:** In the context of this report, “second displacement” refers to the continued displacement of the casing annulus and riser with seawater following the negative test, prior to the static sheen test. This activity occurred from 20:02 to 21:08 on April 20, 2010.

- Simulated: In the context of this report, “simulated” refers to the output from independent mathematical time-domain hydraulic models of the Macondo wellbore, which use pump flow rates as input and produce dynamic estimates of resulting well state quantities. For further information, see Appendix B.
- SOBM: Synthetic Oil-Based Mud.
- Spacer: A fluid placed between two dissimilar fluids to prevent them from mixing.
- Standpipe: A surface pipe that carries drilling fluids up the derrick into the kelly hose prior to entering the drill pipe. The standpipe pressure is an indicator of the drill pipe pressure.
- Static Sheen Test: A test designed to indicate the presence of oil in mud or other fluids discharged from a well into offshore waters.
- STB: Stock Tank Barrel. A liquid volume equal to one barrel (42 US gallons) at specified standard pressure and temperature conditions. For purposes of this report, standard conditions are defined as 15.025 psia and 60°F, per [10].
- Stick-Slip: An erratic velocity behavior sometimes observed when two objects engage in sliding motion under heavy friction. The effect is observed as alternating periods of low (or zero) and high velocity as the objects transition between static and kinetic friction regimes.
- TOC: Top Of Cement.
- Test Sub: A tee-shaped manifold installed at the top of the work string at the rig floor. The manifold contains valves that allow pressure and flow to be directed to various locations for testing purposes.
- Time interval of interest: In the context of this report, the time interval of interest is defined from 15:00 to 21:49 CDT, April 20, 2010.
- Underbalanced: A condition in which the fluid pressures from the rock formation(s) surrounding a well exceed the hydrostatic pressure of the drilling fluid within the wellbore.
- VBR: Variable Bore Ram. A blowout preventer device installed as part of a BOP stack, intended to seal the annular space via the closure of opposing ram elements around drill pipe. These specific rams are designed to seal around a range of drill pipe diameters.

- Volumetric Efficiency: The ratio of a pump's actual fluid volume output to its theoretical volumetric displacement.
- Wiper Plug: A specialized plug used in cementing operations. The plug is designed to isolate the cement slurry from surrounding fluids. See Plug.
- Work String: A generic term referring to the combination of drill pipe, tubing, and tools deployed into the wellbore.

1.2 Definition of Symbols

<i>Symbol</i>	<i>Description</i>	<i>Unit</i>
<i>A</i>	Cross sectional area	in ²
<i>D</i>	Diameter	in
<i>f</i>	Flow friction factor	Dimensionless
<i>g</i>	Gravitational constant	32.174 ft/sec ²
<i>h</i>	Vertical height (or depth)	ft
<i>ID</i>	Inside diameter	in
<i>OD</i>	Outside diameter	in
<i>P</i>	Pressure	lb _f /in ² (psi)
<i>q</i>	Flow	gal/min or bbl/min
<i>Re</i>	Reynolds number	Dimensionless
<i>V</i>	Velocity	ft/sec
<i>ε</i>	Pipe surface roughness	ft
<i>ν</i>	Kinematic viscosity	ft ² /sec
<i>ρ</i>	Density	lb _m /gal or lb _m /ft ³

1.3 Accuracy and Precision of Reported Results

SES received no calibration certificates, maintenance records, or other information pertaining to the accuracy of the rig telemetry data files and other inputs utilized herein (such as mud densities, pipe diameters, pump parameters, etc.). Accordingly, SES makes no claims regarding the accuracy of the analysis results obtained from these inputs, and does not attempt to conform to standard reporting practices such as ASTM E29-08 [4]. Results herein are reported to varying levels of precision as listed in Table 1, which are generally chosen for readability and ease of duplication.

Table 1: Precision of reported quantities

Quantity	Reported Precision
Pressure	Nearest pound per square inch (psi)
Volume	Nearest barrel (bbl) or tenth of a barrel
Liquid Flow	Nearest gallon or barrel per minute (gpm or bpm)
Density	Nearest hundredth of a pound mass per gallon (ppg)
Distance or Depth	Nearest foot (ft)
Diameter	Nearest hundredth of an inch (in)

Additionally, it should be noted that the results reported herein were generally obtained using engineering calculation software, employing built-in constant terms (such as the gravitational constant g) and automatic unit conversion. Internal calculations were performed to machine precision and the results rounded to the reported precisions listed above. This fact should be kept in mind when attempting to duplicate the reported values.

For example, a recurring calculation herein is the computation of hydrostatic pressure of a static liquid column, given the column height and liquid density. In fundamental units, the hydrostatic pressure is given by

$$P = \rho gh$$

where P is the hydrostatic pressure, ρ is the liquid density, g is the gravitational constant, and h is the column height. This is the equation employed in the engineering calculation software. However, performing the same calculation by hand using the common oilfield units of psi, ppg, and ft requires a number of unit conversions, which in practice are combined with g into a single constant, allowing for quick field computations. With the oilfield units above, the conversion constant is typically expressed to two significant figures as $0.052 \text{ psi(ppg)}^{-1}(\text{ft})^{-1}$. A hand calculation performed in this manner may produce a result that is not equal to the corresponding software-computed value.

As a specific example, consider the computation of bottom-hole pressure (BHP) of the Macondo well at its initial state at 15:00, filled with 14.17 ppg mud to a depth of 18,115 ft. Using the typical oilfield conversion constant, the pressure computes as:

$$BHP = (18,115 \text{ ft})(14.17 \text{ ppg})(0.052 \text{ psi(ppg)}^{-1}(\text{ft})^{-1}) = 13,348 \text{ psi}$$

However, using fundamental units, the engineering calculation software computes the same value as 13,335 psi—a slight difference. To duplicate the software-computed value exactly, the conversion constant must be expanded to $0.051948 \text{ psi(ppg)}^{-1}(\text{ft})^{-1}$ (five significant figures). This produces a revised result of

$$BHP = (18,115 \text{ ft})(14.17 \text{ ppg})(0.051948 \text{ psi(ppg)}^{-1}(\text{ft})^{-1}) = 13,335 \text{ psi}$$

which is sufficient for comparison purposes.

A final note concerns the documentation of event times in this report. With certain exceptions, event times are reported to the nearest whole minute, even though the telemetry data entries are resolved in ten-, five-, or one-second intervals. This is done for two reasons:

1. Some of the data sets (specifically [12] and [14]) have been time-averaged (filtered) over an unknown interval. The filtering has the effect of smoothing rapid changes in the data over a longer interval than the actual event duration. It is therefore difficult to resolve the exact time at which certain events occur, such as changes in pit volume and pump flow, to finer than one minute. For further discussion of the signal characteristics of the data sets employed, see Appendix E.
2. Due to the issue above, in combination with other sources of error (such as imprecise volume, flow, or density information), the times at which certain calculated or simulated hydraulic state events occur (for example, the well flow rates near the end of transmission) cannot be reported to finer than one-minute accuracy.

2 SCOPE

The overarching goal of the various analyses presented herein is to ascertain the hydraulic state of the Macondo Prospect Mississippi Canyon #252 exploration well from approximately 3 pm (15:00) to 9:49 pm (21:49) CDT on April 20, 2010. “Hydraulic state” refers to the following dynamic quantities:

- Standpipe (work string) pressure;
- Cement pump pressure;
- Auxiliary line (booster, choke, kill) pressure;
- Flow into work string;
- Flow into auxiliary line(s);
- Flow out of riser;
- Fluid type and composition;
- Fluid boundary position(s) relative to the drill floor (RKB);
- Hydrostatic and frictional pressure gradients in work string, riser, and wellbore;
- Well bottom hole pressure (BHP);
- Flow of hydrocarbon flux into wellbore.

Some of the above quantities (such as standpipe pressure) were measured explicitly during the times of interest, and were recorded in the rig telemetry data files, which were transmitted to shore during the event. These telemetry data, given in [13], [14], and [17], comprise the primary reference for this report. Another primary reference for deriving flow rate information is the electronic log of rig pit data [12]. In addition, important supporting and contextual information was provided by an interim incident investigation presentation given during congressional testimony on May 25th, 2010 [7], a formal report issued by BP on September 8th, 2010 [6], and other supporting information provided by Transocean via internal sources.

2.1 Well Status During Events of Interest

The events analyzed within this report occurred from approximately 3 pm (15:00) to the last recorded data transmission at 9:49 pm (21:49) CDT on April 20, 2010. During this time, the well and riser system were maintained in a single mechanical configuration in terms of the equipment deployed downhole (i.e. work string, casing, plugs, and cement). Only the hydraulic configuration, in terms of the fluids, pressures, and flow rates through the various pipe and annulus sections of the well, varied during this time. As such, the models and calculations provided herein are based on a common wellbore geometry, depicted schematically in Figure 1. This mechanical configuration serves as the basis for all simulations, observations and assessments during the time period considered.

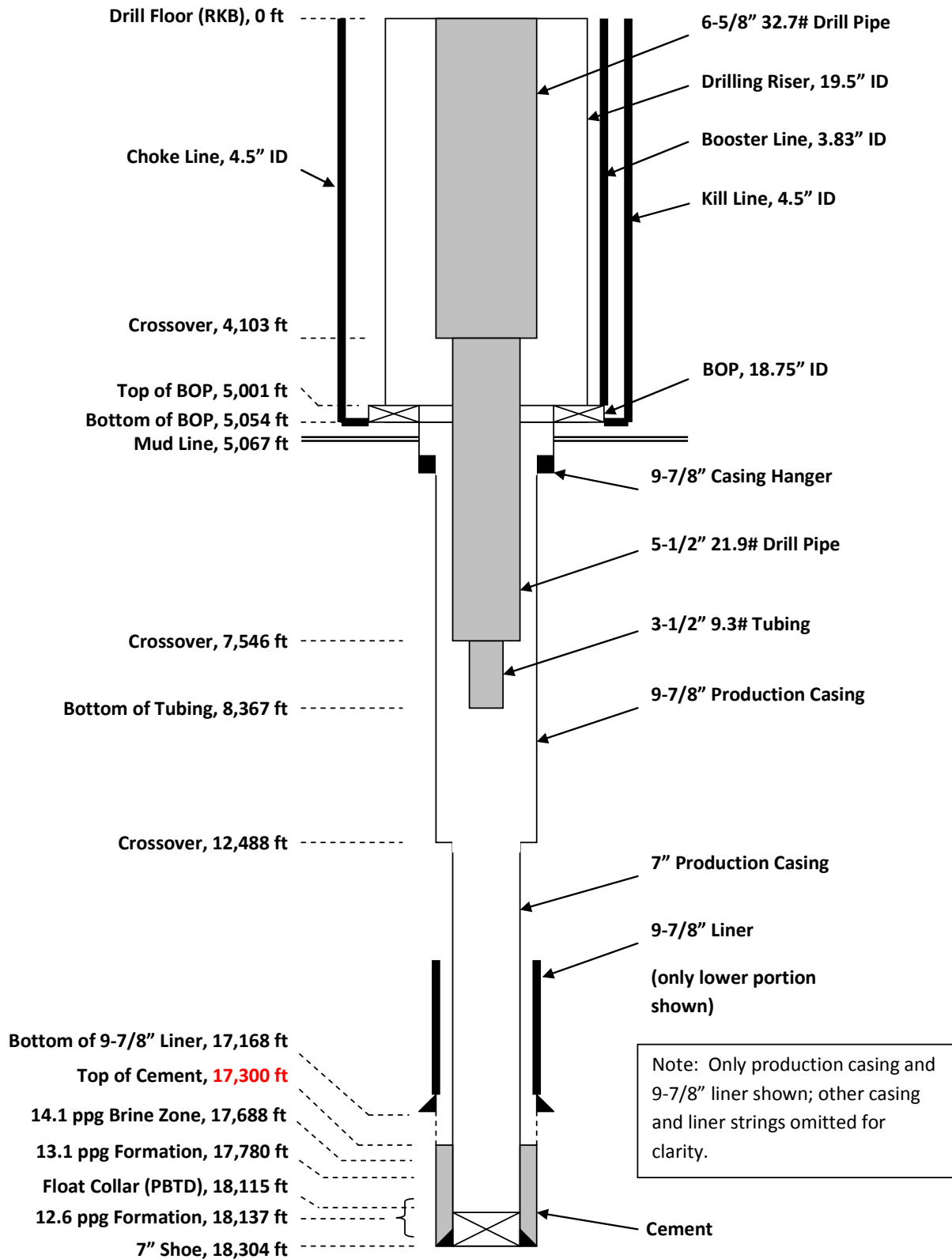


Figure 1: Diagram of Macondo well #252, April 20th 2010, 15:00 to end of transmission

3 PLANNED DISPLACEMENT PROCEDURE AND HYPOTHETICAL HYDRAULIC RESPONSE

Before proceeding with the hydraulic analysis of the actual events of April 20, 2010, it is instructive to examine the planned procedure for displacing and testing the well prior to temporary abandonment. Doing so provides a hypothetical benchmark of the planned process, against which the actual hydraulic responses within the well may be evaluated and compared.

3.1 Overview

As part of the temporary abandonment procedures at the Macondo well, the riser and a portion of the well were to be displaced with seawater prior to disconnecting the BOP and riser [9]. This activity would reduce the pressure profile in the casing to less than the pressure when the casing and riser were filled with drilling mud. A spacer was to be pumped ahead of the seawater to separate the mud and seawater.

The written procedure used aboard the *Deepwater Horizon* on April 20th [9] was prepared and documented on the rig and disseminated to the rig personnel. The instructions relevant to the displacement itself are paraphrased in the list below. Other instructions are omitted; see Appendix D for a copy of the original document.

- Build 425 bbl spacer in pit #5;
- During pumping, direct fluid returns from the well directly to the pits, bypassing the sand traps;
- Pump excess pit return volume to a nearby offshore supply vessel;
- Displace the boost, choke, and kill lines with seawater;
- Pump 425 bbl spacer down work string;
- After pumping spacer, continue pumping seawater to a total volume of 775 bbl (350 bbl seawater);
- Conduct a negative pressure test on the production casing, which simulates the pressure in the casing following full riser displacement;
- Open annular preventer and continue displacing the riser with seawater;

- Add booster line flow at 950 bbl, when interface is well above the BOP;
- Shut down for static sheen test when spacer-mud interface returns to surface;
- After passing the static sheen test, route remaining spacer returns overboard. The riser is now filled with seawater.

3.2 Hypothetical Pump Schedule

A reconstructed hypothetical schedule for riser displacement, which is representative of the actual procedure outlined above, is presented in this section. Calculations are performed for the schedule to provide expected pressures and volumes that may be useful in understanding the displacement process. As such, the presentation in this section is an idealized scenario and does not attempt to replicate the actual events aboard the *Deepwater Horizon*, only the basic procedural intent.

The hole is initially filled with 14.17 ppg mud¹. A tapered work string (6-5/8" x 5-1/2" x 3-1/2") is run in the hole to 8,367 ft. The choke, kill and boost lines are displaced to seawater. The riser and casing annulus above the work string are then displaced to seawater. Volumes for the displacement include:

- Work string plus annulus volume = 2,016 bbl
- Spacer volume = 425 bbl
- Total displacement = 2,445 bbl

Displacement is carried out in steps as follows:

- First displacement (places the bottom of the spacer about 8 bbl, or 25 ft, above BOP)
 - o 425 bbl 16 ppg spacer
 - o 385 bbl seawater²

¹ Note that the nominal surface density of the SOBMs is 14.00 ppg; however, its actual measured average density in the well, which is used for all calculations herein, is 14.17 ppg (due to compressibility). The terms 'SOBM', 'mud', '14 ppg mud', etc. are used interchangeably herein; all refer to 14.17 ppg synthetic oil-based mud.

² The initial seawater displacement volume specified in the procedure (350 bbl) was insufficient to place the spacer above the BOP (see Section 4.2.5 for further details). Therefore, in the hypothetical displacement procedure the volume is increased to 385 bbl to achieve the correct placement.

- o 810 bbl total
- Negative test
- Second displacement (puts top of spacer at surface)
 - o 1,210 bbl seawater
- Static Sheen test
- Final displacement (removes all spacer from the riser; riser and work string are now filled with seawater)
 - o 425 bbl seawater

Prescribed pump rates are

- Down work string = 630 gpm (15 bpm)
- Boost line = 378 gpm (9 bpm) after 950 bbl pumped

Prescribed hold times are

- Hydrostatics = 3 minutes each time pumps are stopped
- Negative test = 30 minutes
- Sheen test = 15 minutes
- Total time = 188 minutes from start of spacer pumping

3.3 Discussion

A graph of the prescribed pump flow rate is shown in Figure 2. Calculated standpipe pressure and kill line pressure are shown in Figure 3. After the first displacement, pressures are allowed to reach static equilibrium. The annular preventer is then closed and pressure is bled off, reducing the standpipe and kill line pressures to zero to begin the negative test. At the end of the negative test, standpipe pressure is increased to equalize the pressure (differential) across the annular preventer. The annular preventer is opened and pressures are allowed to reach static equilibrium. The second displacement is pumped and there is a 15-minute hold for the static sheen test. The final displacement completes the process and leaves the work string and riser filled with seawater.

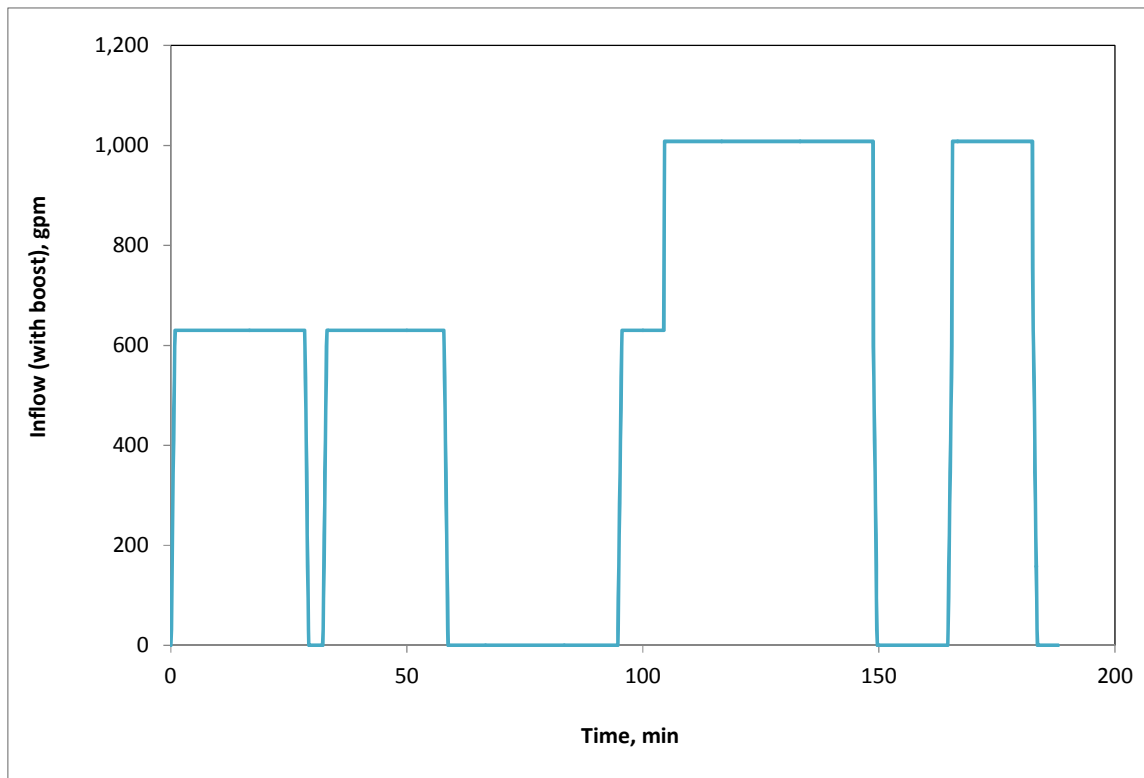


Figure 2: Graph of prescribed flow rates for hypothetical riser displacement

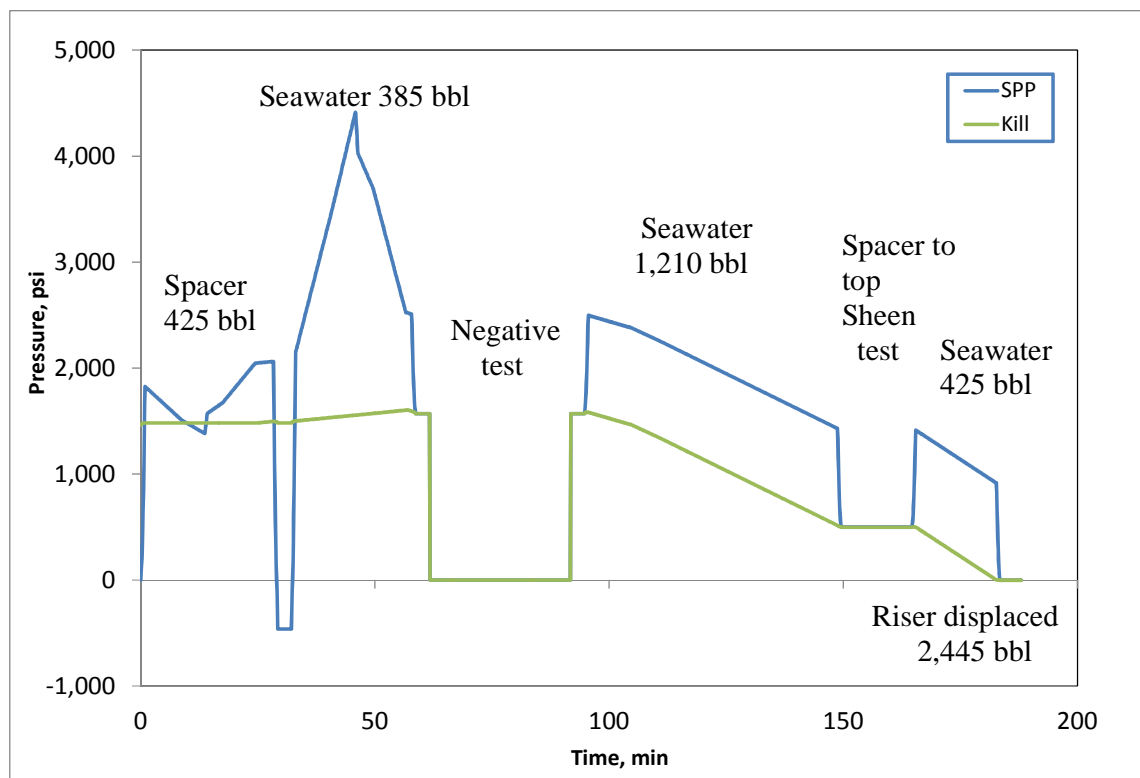


Figure 3: Expected standpipe and kill line pressures during hypothetical displacement

Static pressures on the standpipe and on the kill line for each of the steps are given in the table below:

Table 2: Standpipe and kill line pressures, hypothetical displacement

Step	Static Pressure, psi	
	<i>SPP</i>	<i>Kill</i>
Kill line displacement	0	1,465
End of First Displacement	1,572	1,572
Negative Test	0	0
Prior to Second Displacement	1,572	1,572
End of Second Displacement	500	500
Final Displacement	0	0

A significant observation from the table above is that after the spacer is displaced with seawater above the kill line entry point at the BOP, the static pressures at the standpipe and kill lines are always equal. This serves as a simple check for proper displacement any time the pumps are stopped. While pumping, the pressures are unequal due to frictional pressure drop through the work string and casing annulus, as shown in Figure 3.

Graphical presentations of the well fluid states during the various displacement operations are given in Figure 4 and Figure 5. Wellbore components are labeled in the first diagram and are consistent throughout the remaining figures in this report. The vertical axes of the diagrams are approximately to scale. Larger, more detailed versions of these diagrams, along with supporting calculations, may be found in Appendix C.

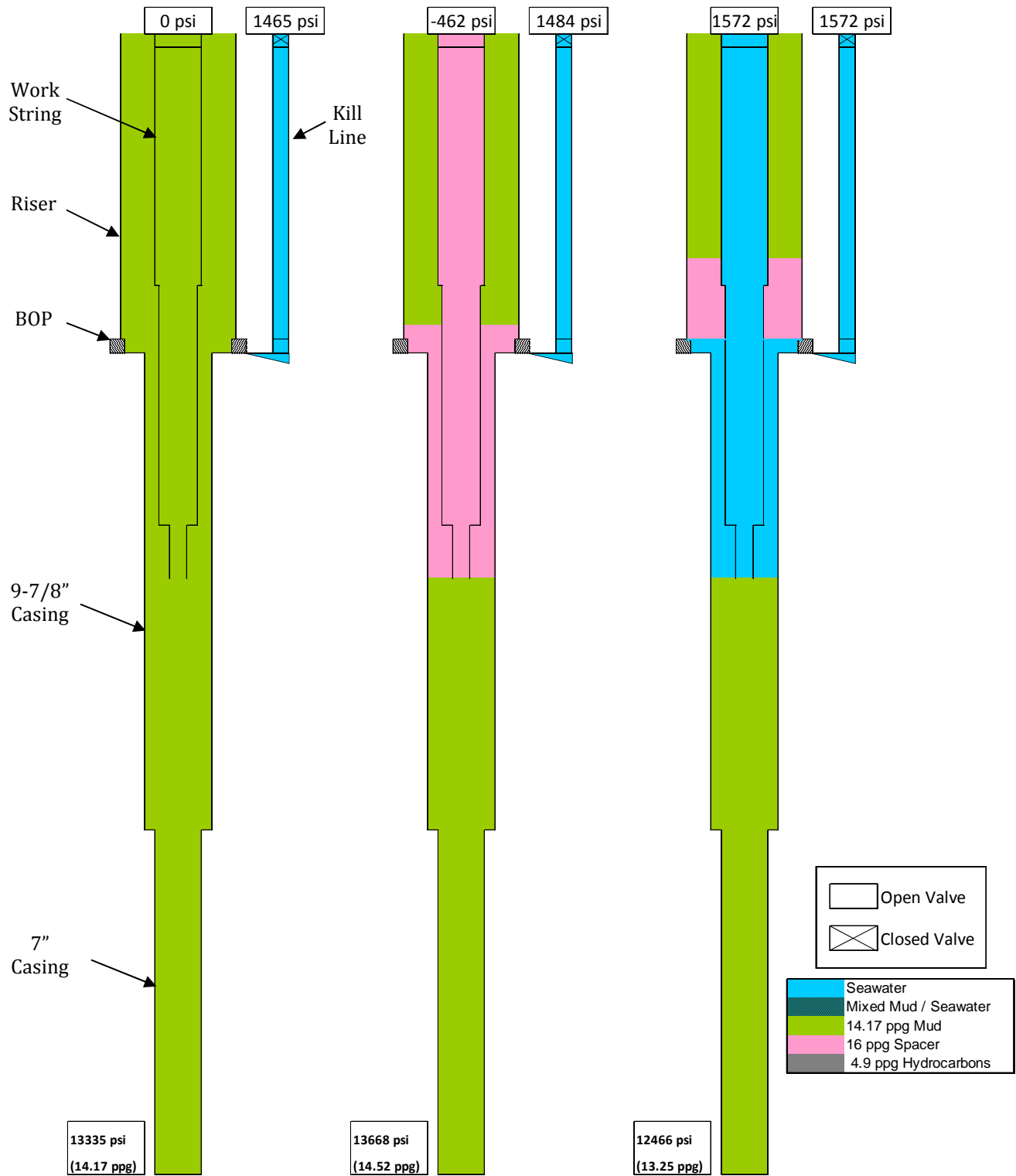


Figure 4: Fluid states during hypothetical displacement procedure: Initial state (left); after spacer displacement (middle); after first seawater displacement (right).

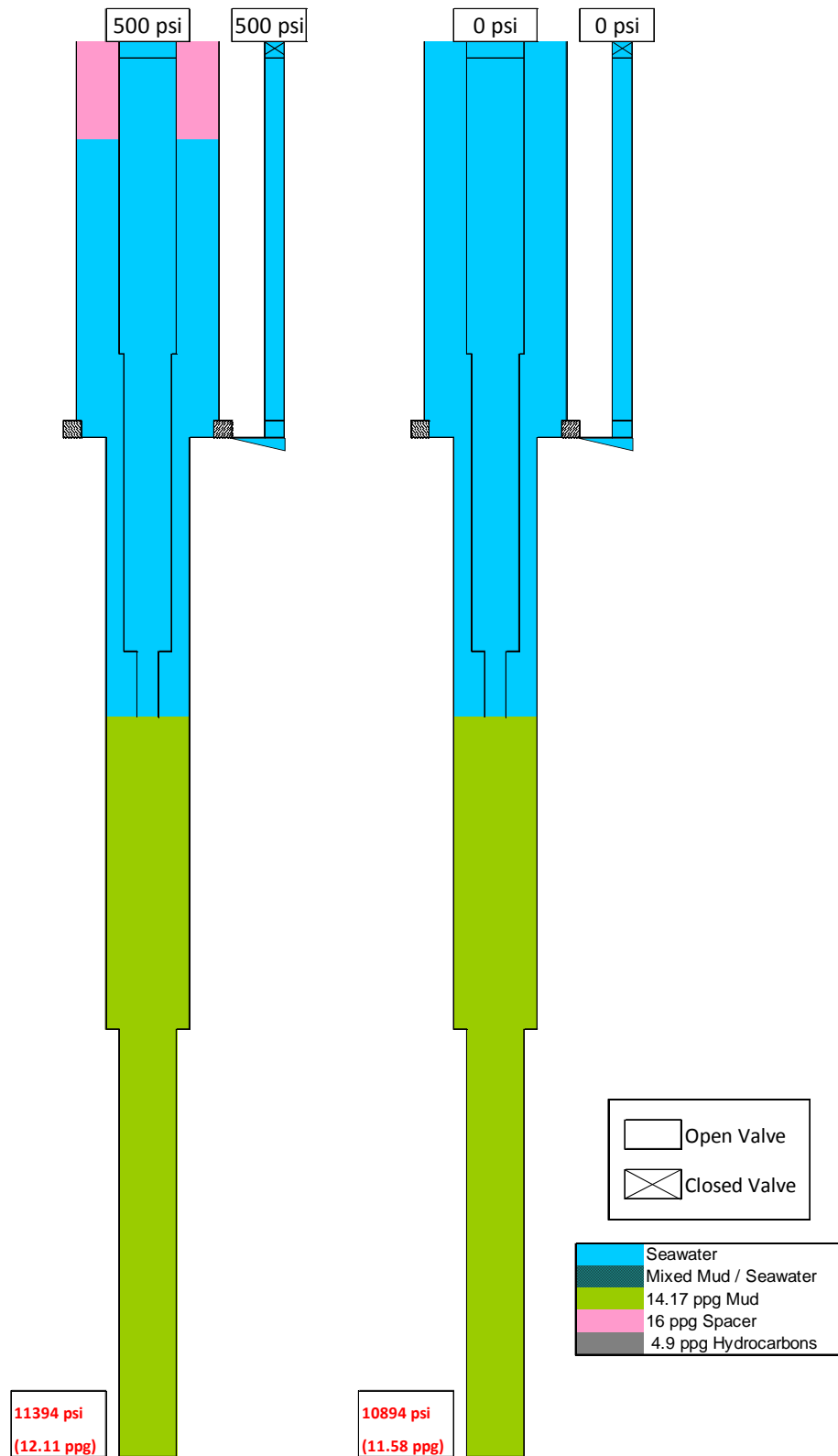


Figure 5: Fluid states during hypothetical displacement procedure: After second seawater displacement (left); after final seawater displacement (right).

After the first displacement, the standpipe pressure tracks the kill line pressure since the work string and the annulus below the kill line to the bottom of the work string is filled with seawater. The difference in standpipe pressure and kill line pressure is an indication of the average density of the fluid between the two measurement points. The differences in pressure for seawater, mud and spacer in the work string-to-casing annulus (with the work string filled with seawater) are given in Table 3.

Table 3: Calculated pressure differences for various fluids

Fluid in annulus	SPP- Kill, psi
Seawater	0
Mud	970
Spacer	1,290

Replacing mud with seawater reduces the pressure in the well. The maximum pressure reduction is:

$$Pressure\ reduction = (8,367\ ft)(14.17 - 8.556\ ppg)(0.051948\ psi(ppg)^{-1}(ft)^{-1}) = 2,440\ psi$$

This is the pressure reduction below the work string during the negative test, and after completion of the displacement.

Hydrostatic pressure can also be represented as Equivalent Mud Weight (EMW), referenced to a particular depth. A useful reference is the float collar at 18,115 ft, which is within the 12.6 ppg hydrocarbon formation. The equivalent mud weights are calculated by computing the heights of the various fluids in the wellbore, multiplying by their densities, and summing the results over the total wellbore depth. An example calculation for the first displacement is

$$EMW = \frac{(14.17 \text{ ppg})(3706 \text{ ft} + 9748 \text{ ft}) + (16.00 \text{ ppg})(1270 \text{ ft}) + (8.556 \text{ ppg})(3391 \text{ ft})}{18115 \text{ ft}} = 13.25 \text{ ppg}$$

The EMW results for the hypothetical displacement are given in the table below.

Table 4: Equivalent mud weight at 12.6 ppg formation depth, hypothetical displacement

Step	EMW, ppg
Initial	14.17
First Displacement	13.25
Negative Test	11.58
Second Displacement	12.11
Final Displacement	11.58

Thus, the negative test and subsequent displacement and abandonment activity underbalance the well by a maximum of 1.02 ppg, or approximately 960 psi, relative to the 12.6 ppg formation.

4 TIMELINE OF OBSERVED EVENTS WITH SUPPORTING ANALYSIS

The actual execution of the displacement procedure on the *Deepwater Horizon* took place from 15:00 to 21:49 following completion of run-in-hole with a tapered work string to 8,367 feet per the established procedure. At the beginning of this interval the entire wellbore, BOP, riser, and auxiliary lines (boost, choke, and kill lines) were filled with 14.17 ppg synthetic oil-based mud (SOBM).

Overview plots of selected signals obtained from the rig telemetry data are shown in the figures on pages 36 through 38. Relevant events are labeled and described in the tables accompanying the figures. Each event is described and analyzed in detail in the sections that follow.

Note that the work string was fitted on the surface (i.e., the rig floor) with a test sub after it was run, and chiksan lines were run from the test sub to the cement manifold (see Figure 28, page 72). This allowed the pressure in the work string to be monitored at the cement unit, in addition to the typical measurement at the standpipe manifold. Allowing for frictional pressure losses proportional to flow rate, pipe diameter, and length, the cement pump pressure data generally tracks the standpipe pressure throughout the time interval of interest, except for the time between 17:52 to 19:54. During this period, the standpipe pressure gauge was isolated from the work string, with only the cement pump pressure as the remaining measurement.

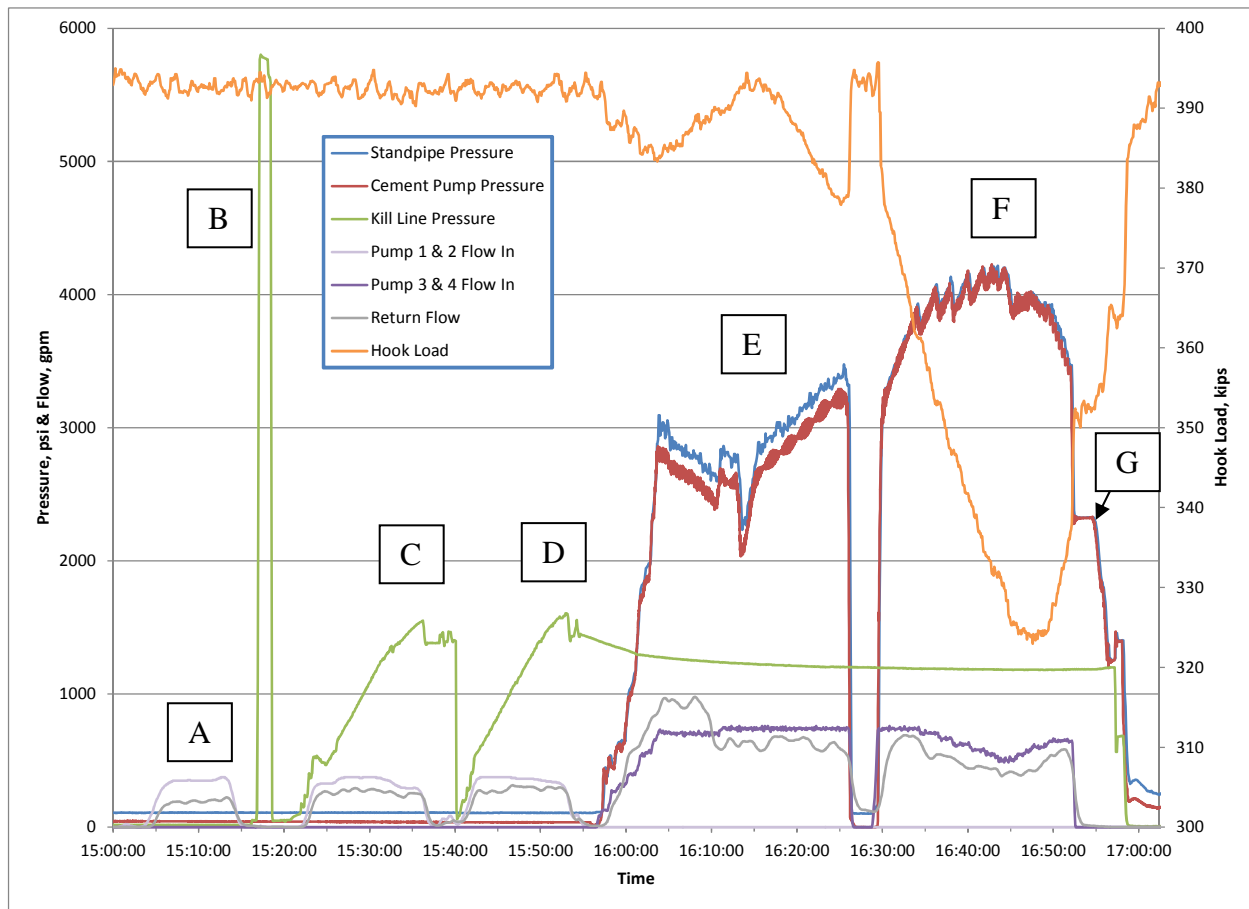


Figure 6: Overview of auxiliary line and riser displacement, 15:00 to 17:00

Table 5: Description of events from 15:00 to 17:00

Event	Description	Time
A	Displacement of booster line with seawater	15:03 to 15:15
B	Pressure test of surface lines	15:17 to 15:19
C	Displacement of choke line with seawater	15:21 to 15:38
D	Displacement of kill line with seawater	15:38 to 15:55
E	Displacement of riser with 16 ppg spacer	15:55 to 16:27
F	Displacement of riser with seawater	16:28 to 16:53
G	Pumps stopped; annular BOP closed	16:53 to 16:54

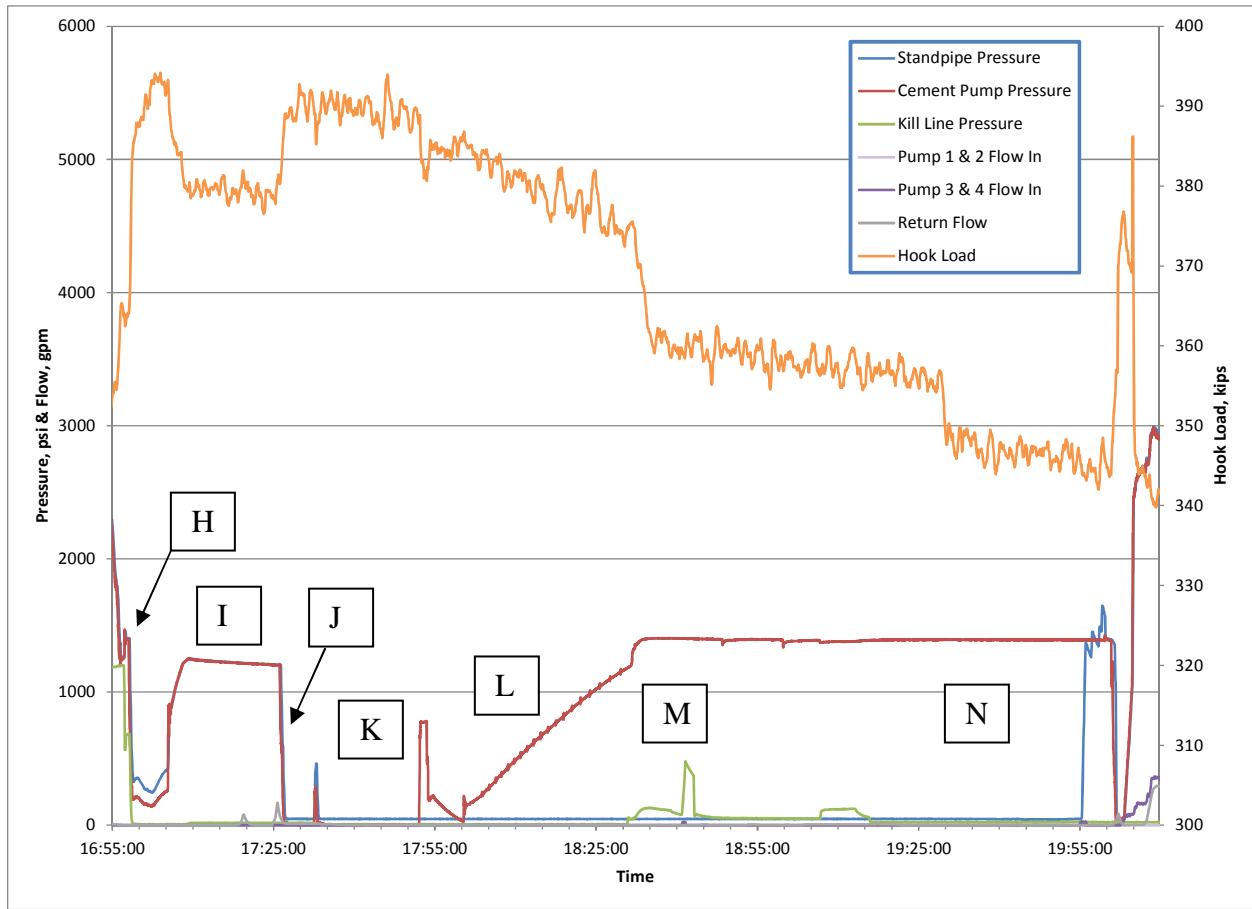


Figure 7: Overview of negative testing activity, 17:00 to 20:00

Table 6: Description of events from 17:00 to 20:00

Event	Description	Time
H	Bleed work string and equalize with kill line	16:53 to 16:58
I	Observe annular preventer leakage, seal annular and work string	16:58 to 17:24
J	Bleed work string to cement unit	17:24 to 17:26
K	Switch lineup to kill line; gauges isolated	17:26 to 17:52
L	Bleed work string, shut in, observe cement unit pressure build	17:53 to 18:30
M	Pump on kill line to ensure full (valve closed)	18:30 to 19:12
N	Conduct negative test with no flow from kill line	19:16 to 20:00

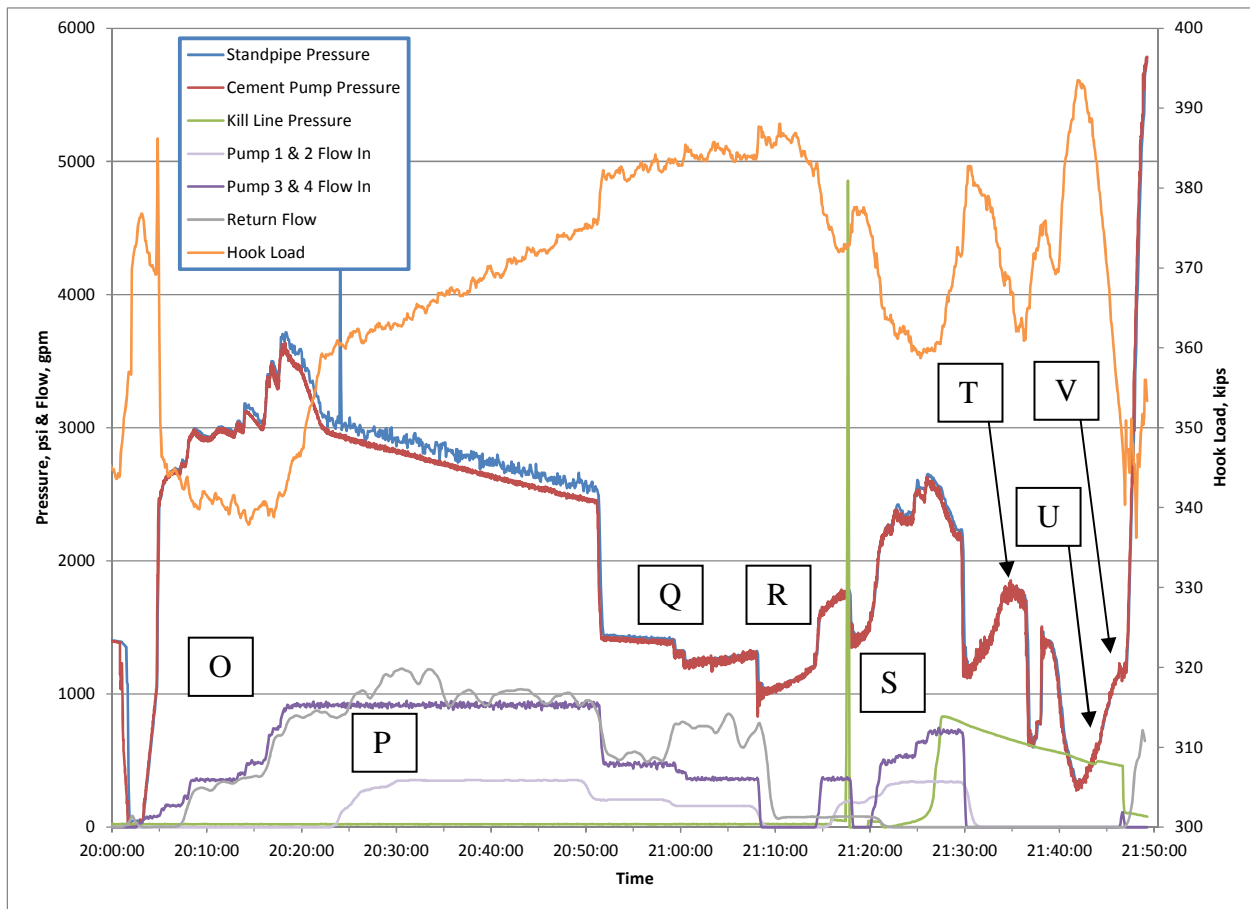


Figure 8: Overview of final riser displacement and activity prior to explosion, 20:00 to 21:49

Table 7: Description of events from 20:00 to 21:49

Event	Description	Time
O	Open annular preventer and resume seawater displacement	20:02 to 20:22
P	Activate booster line pump; dump trip tank	20:22 to 20:52
Q	Slow pump rates; dump trip tank, standpipe pressure builds	20:52 to 21:08
R	Static sheen test; standpipe pressure builds	21:08 to 21:13
S	Resume seawater displacement; relief valve blows on pump 2	21:13 to 21:30
T	Observe differential pressure; bleed and shut in work string	21:30 to 21:42
U	Drill floor overflows; well control actions taken	21:42 to 21:46
V	Gas flows onto rig; power loss; end of transmission	21:46 to 21:49

4.1 Displacement of Auxiliary Lines

As described in the displacement procedure [9], seawater was pumped down the three riser auxiliary lines in order to displace the SOBM in preparation for the riser displacement and negative testing starting at approximately 15:03. A plot of the pressure and flow signals recorded during the auxiliary line displacement is given in Figure 9 (expanded from Figure 6).

Note that the spike in kill line pressure between 15:17 and 15:19 was a planned pressure test of the choke manifold lineup prior to displacing the choke and kill lines. This event will not be analyzed in further detail in the discussion of surrounding events.

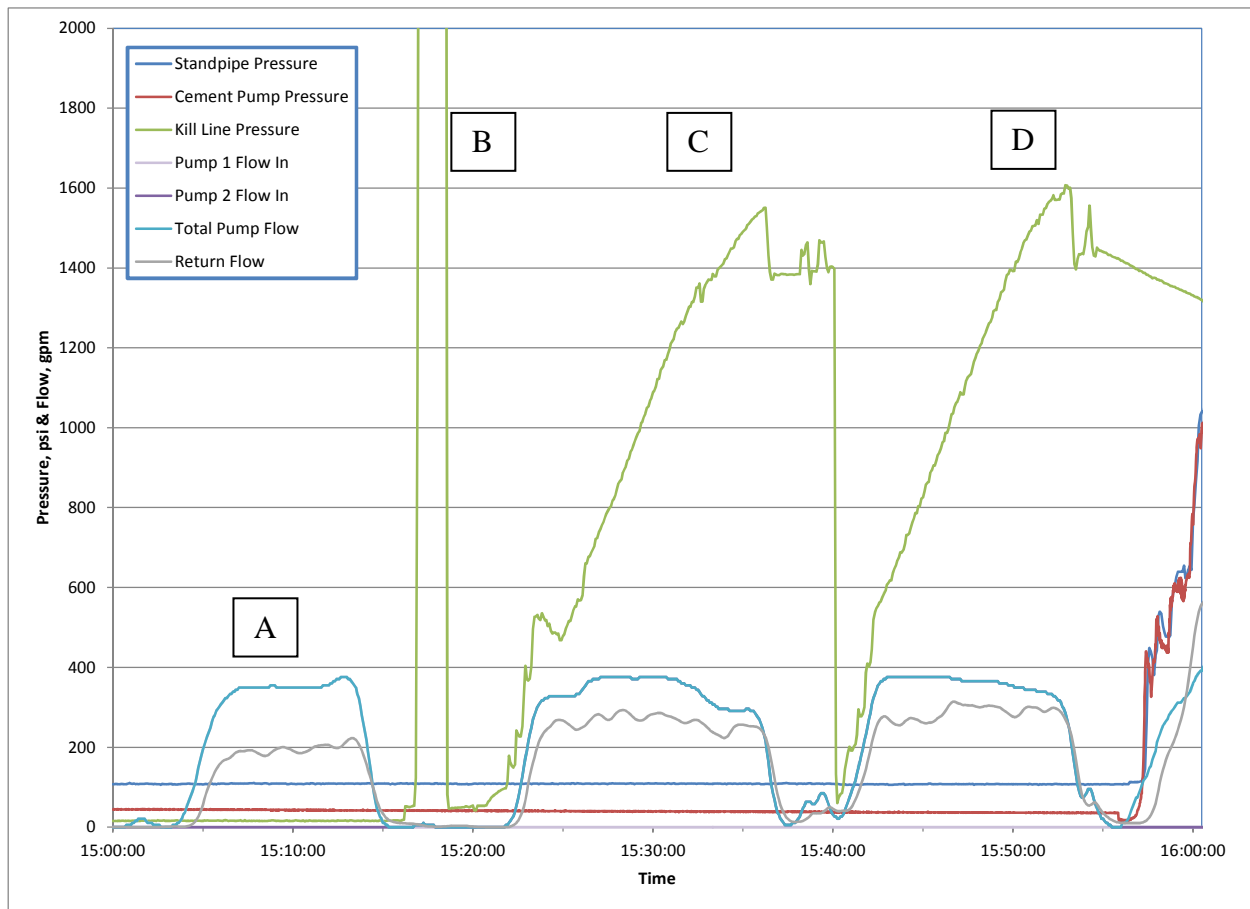


Figure 9: Pressure and flow signals recorded during auxiliary line displacement

Table 8: Description of events from 15:00 to 15:55

Event	Description	Time
A	Displacement of booster line with seawater	15:03 to 15:15
B	Pressure test of surface lines	15:17 to 15:19
C	Displacement of choke line with seawater	15:21 to 15:38
D	Displacement of kill line with seawater	15:38 to 15:55

4.1.1 *Booster Line*

Pumping down the mud booster line commenced at approximately 15:03 and ended at 15:15 (see Figure 9, Event A).

4.1.1.1 *Strokes Pumped*

Rig pump #1 was used to displace the booster line. The telemetry data files indicate that 623 strokes were pumped (see summary table below). Referring to the mud pump anticipated efficiency in Table 51 (see Appendix A), the anticipated pump volume³ was 78.5 bbl. The booster line capacity is 71.3 bbl, which suggests a 7.2 bbl over-displacement (not including drape hose and surface volume).

Table 9: Pump output summary, booster line displacement

Time	Pump Strokes (Pump 1)	Theoretical Output	Anticipated Output	Anticipated Volume
15:03	5	0.13113 bbl/stk	0.126 bbl/stk	0.6 bbl
15:15	628	0.13113 bbl/stk	0.126 bbl/stk	79.1 bbl
<i>Interval</i>	<i>623</i>	<i>0.13113 bbl/stk</i>	<i>0.126 bbl/stk</i>	<i>78.5 bbl</i>

³ Pump volumes derived from stroke counts are reported as “anticipated pump volume” herein. These quantities, which are obtained by multiplying the stroke count by the theoretical pump output scaled by the volumetric efficiency used by the rig personnel, are not necessarily an accurate representation of the true pump output volume. This is because the calculation assumes the pump efficiency remains constant at the specified input value during the pumping interval(s).

Both the MI Swaco displacement procedure [9] and the pump output volume fields recorded in the rig telemetry data files ([14], [17]) utilize the same volumetric efficiency of 96.1% to calculate anticipated pump volumes based on stroke counts throughout the time interval of interest. This value is the “anticipated efficiency” reported in Table 51.

4.1.1.2 Pressure Response

No recorded pressure data for the booster line pumping is available. For a line depth of 5,001 ft, the expected surface pressure for a full displacement of the booster line is 1,458 psi:

$$\text{Pressure increase} = (5,001 \text{ ft})(14.17 - 8.556 \text{ ppg})(0.051948 \text{ psi(ppg)}^{-1}(\text{ft})^{-1}) = 1,458 \text{ psi}$$

A simulated pressure response, using the pump stroke data from pump #1 as input, is shown below in Figure 10. The simulated pressure of 1,460 psi at the end of the displacement closely matches the expected pressure.

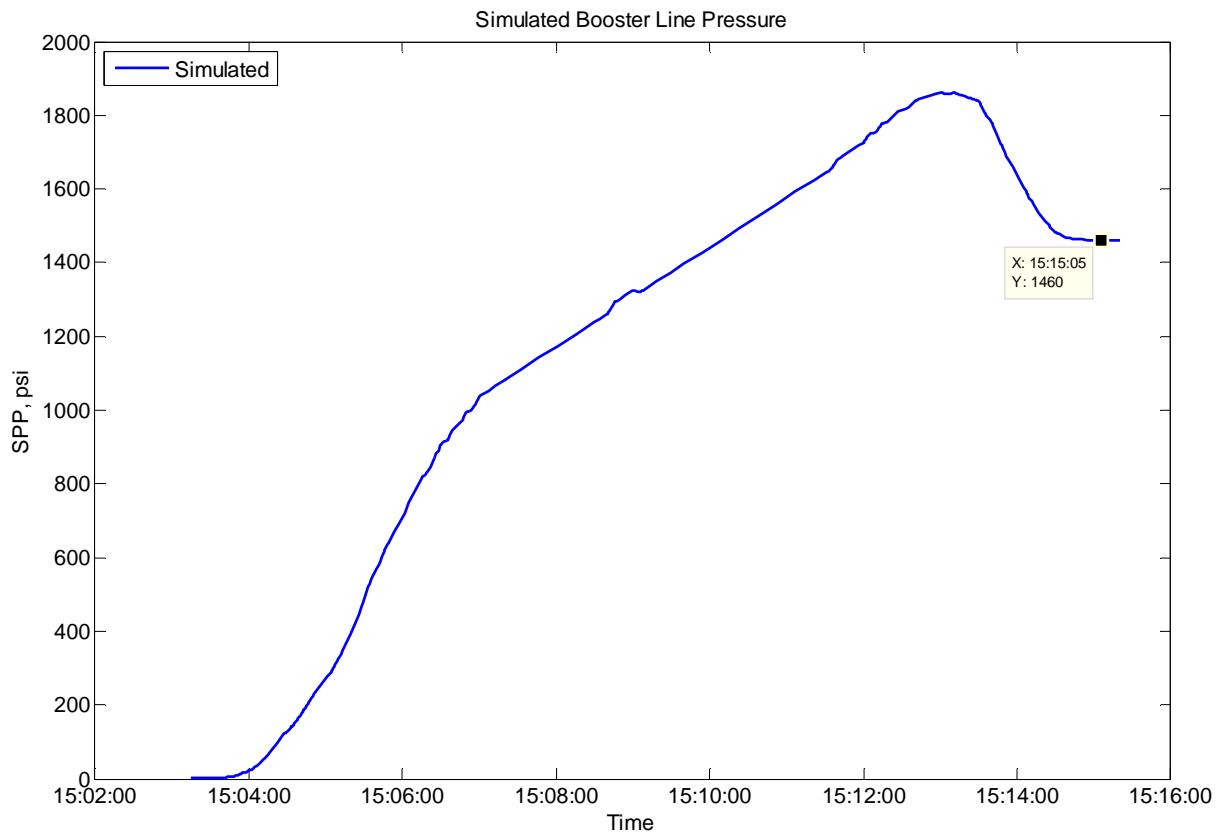


Figure 10: Simulated line pressure, booster line displacement

4.1.1.3 Riser Flow Analysis

The Sperry-Sun flow sensor⁴ data indicates that the return volume out of the riser was significantly less than the expected volume into the line from the pump. This discrepancy is illustrated in Figure 11, which compares the simulated output to the measured flow sensor returns. Integrating the sensor data over the pumping interval indicates a return volume of 42.6 bbl, compared to the anticipated pump volume of 78.5 bbl. Thus, the flow sensor data suggests a volumetric efficiency for rig pump #1 of 52.2% (see Table 10).

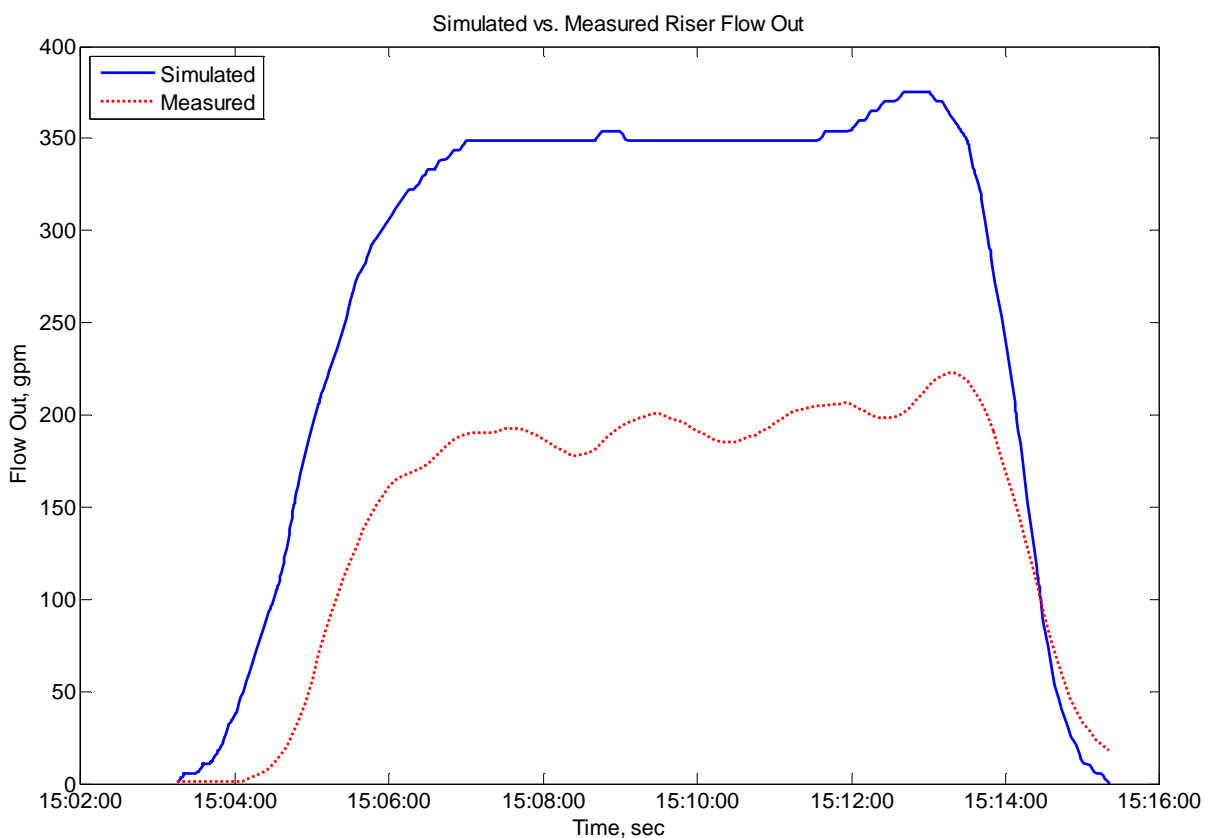


Figure 11: Simulated flow out vs. measured flow sensor data, booster line displacement

⁴ Two flow sensors measured the liquid flow out of the riser through the flow line. The first, provided by Sperry-Sun, was installed at the end of the flow line, just after the point of entry into the gumbo box. The signal from this sensor, recorded in the rig telemetry files transmitted to shore, was provided by Transocean for analysis. The recorded telemetry is referenced simply as “flow sensor data” herein.

A second sensor, referred to as the “Hi-Tec” sensor, was installed at a point in the flow line upstream of the Sperry-Sun sensor. The signal from this unit was available to all rig personnel during the time interval of interest, but was not transmitted off the rig or recorded in telemetry files, and is not accessible for analysis.

Table 10: Pump analysis summary, booster line displacement

Strokes Pumped (Pump 1)	623
Return Volume (from flow sensor)	42.6 bbl
Return Volume (from pit returns)	N/A
Theoretical Pump Output (Pump 1)	0.13113 bbl/stk
Volumetric Efficiency (based on flow sensor)	52.2%
Volumetric Efficiency (based on pit returns)	N/A

4.1.1.4 Pit Returns

During displacement of the booster line, riser flow return data were available only from the Sperry-Sun flow sensor installed in the rig's flow line. Although data is available from the active pits (9 & 10) to which the return flow was taken during this time, the true returns are obscured because mud was being transferred out of the active system into auxiliary pits, and then to a nearby offshore supply vessel, at an unknown rate. This activity continued throughout the displacement of all three auxiliary lines, as shown in Figure 12.

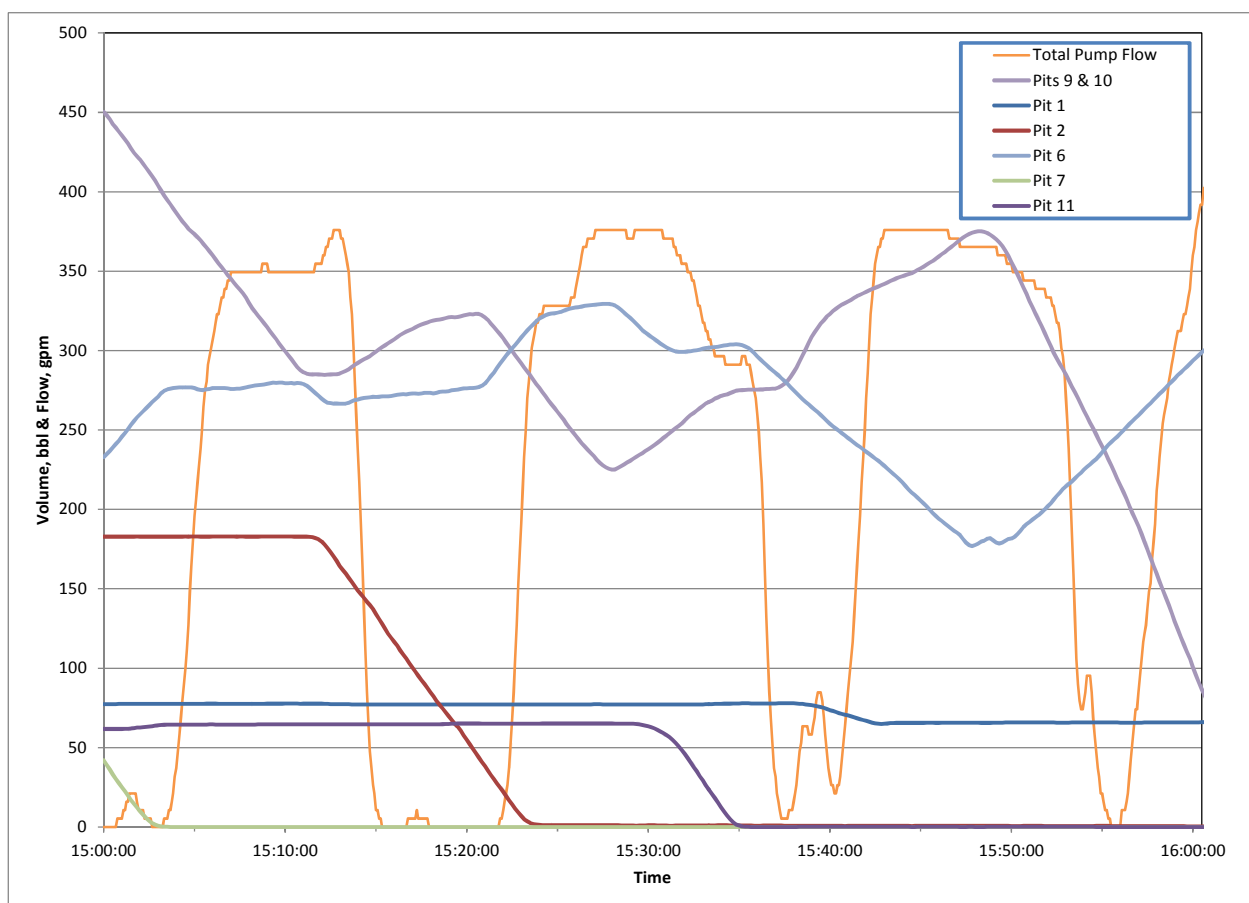


Figure 12: Pit activity during auxiliary line displacement

4.1.2 Choke Line

Pumping down the choke line commenced at approximately 15:21 and ended at 15:38 (see Figure 9, Event C).

4.1.2.1 Strokes Pumped

Rig pump #2 was used to displace the choke line. The telemetry data files indicate that 872 strokes were pumped (see summary table below). Referring to the mud pump anticipated efficiency in Table 51 (see Appendix A), the anticipated pump volume was 109.9 bbl. The choke line capacity is 99.1 bbl, indicating a 10.8 bbl over-displacement (not including drape hose and surface volume).

Table 11: Pump output summary, choke line displacement

Time	Pump Strokes (Pump 2)	Theoretical Output	Anticipated Output	Anticipated Volume
15:21	1	0.13113 bbl/stk	0.126 bbl/stk	0.1 bbl
15:38	873	0.13113 bbl/stk	0.126 bbl/stk	110.0 bbl
<i>Interval</i>	<i>872</i>	<i>0.13113 bbl/stk</i>	<i>0.126 bbl/stk</i>	<i>109.9 bbl</i>

4.1.2.2 Pressure Response

For a line depth⁵ of 5,045 ft, the expected surface pressure for a full displacement of the choke line is 1,471 psi:

$$\text{Pressure increase} = (5,045 \text{ ft})(14.17 - 8.556 \text{ ppg})(0.051948 \text{ psi(ppg)}^{-1}(\text{ft})^{-1}) = 1,471 \text{ psi}$$

Pressure data from the choke manifold was recorded during the displacement. A simulated pressure response using the pump stroke data as input is compared to the recorded data in Figure 13. Although the simulated pressure at the end of the event closely matches the expected value, the measured pressure is about 100 psi lower than expected. This may indicate that full displacement of the choke line was not achieved.

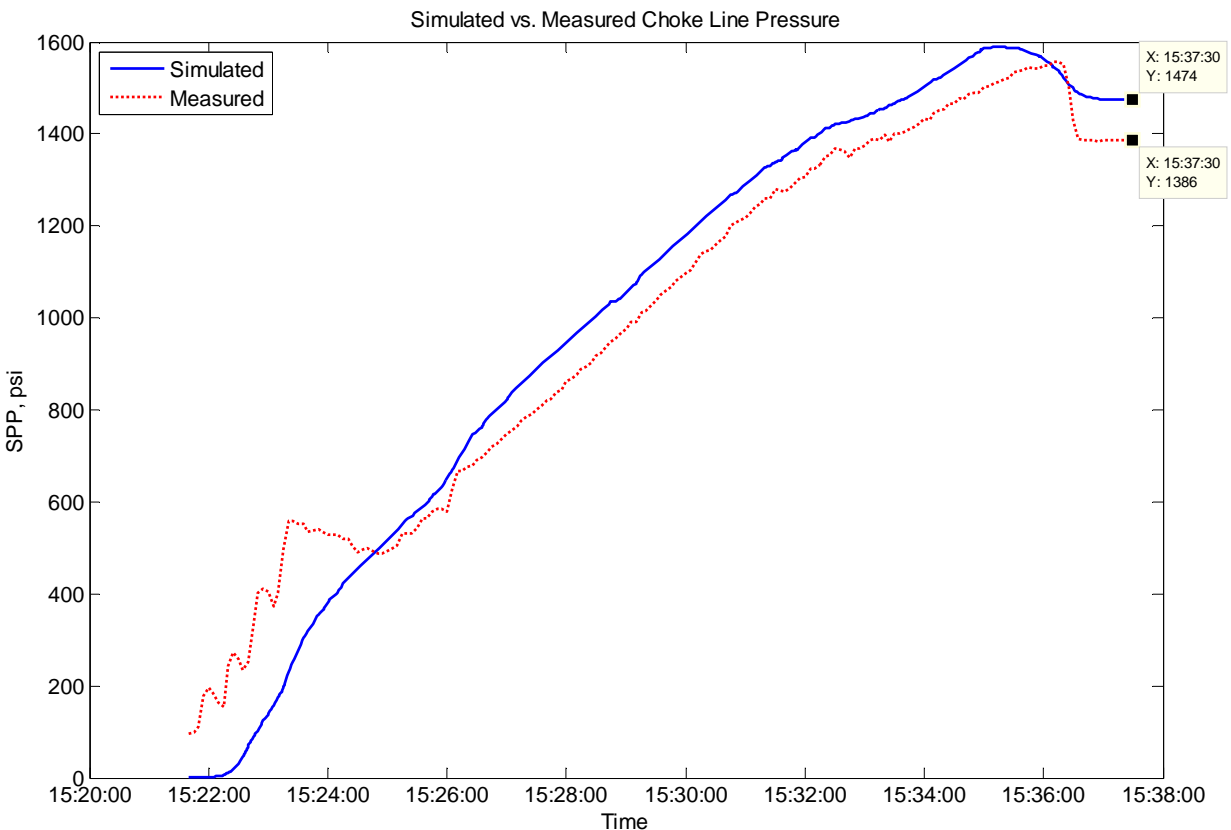


Figure 13: Simulated (calculated) vs. measured choke line pressure during displacement

⁵ The choke and kill lines have multiple entry points into the BOP at varying depths. It is assumed that the lower entry points (5,045 ft in both cases) were opened to achieve full line displacement.

4.1.2.3 Riser Flow Out

The Sperry-Sun flow sensor data indicates that the return volume out of the riser was less than the expected volume into the line from the pump, although on a percentage basis the discrepancy was not as severe as that observed on pump #1. Figure 14 compares the simulated output to the measured flow sensor returns. Integrating the sensor data over the pumping interval indicates a return volume of 84.8 bbl, compared to the anticipated pump volume of 109.8 bbl. This suggests a volumetric efficiency for rig pump #2 of 74.2% (see Table 12).

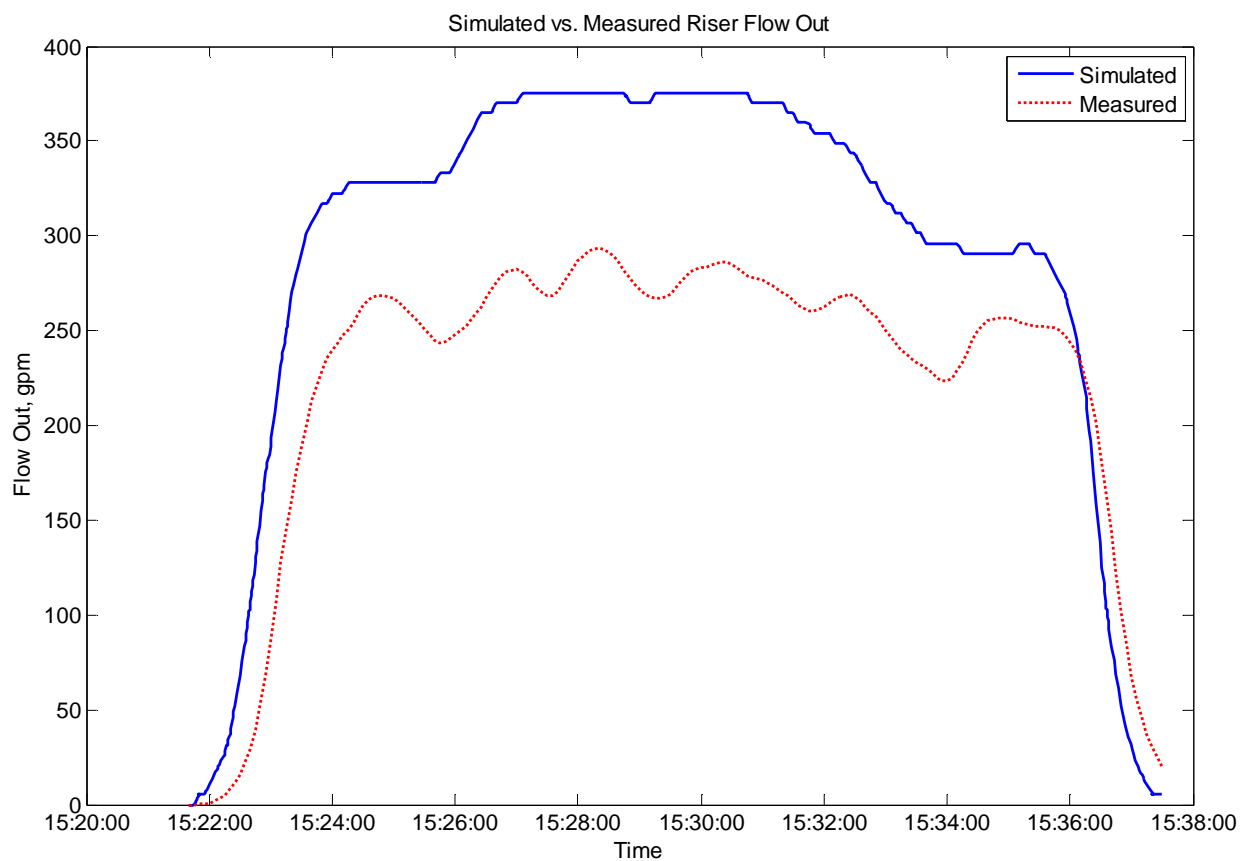


Figure 14: Simulated flow out vs. measured flow sensor data, choke line displacement

Table 12: Pump analysis summary, choke line displacement

Strokes Pumped (Pump 2)	872
Return Volume (from flow sensor)	84.8 bbl
Return Volume (from pit returns)	N/A
Theoretical Pump Output (Pump 2)	0.13113 bbl/stk
Volumetric Efficiency (based on flow sensor)	74.2%
Volumetric Efficiency (based on pit returns)	N/A

4.1.2.4 Pit Returns

Transfer of volume between the active pits, auxiliary pits, and the offshore supply vessel continued during this period (see Figure 12); therefore, the returns based on available pit data are inconclusive.

4.1.3 Kill Line

Pumping down the kill line commenced at approximately 15:38 and ended at 15:55 (see Figure 9, Event D).

4.1.3.1 Strokes Pumped

Rig pump #2 was used to displace the kill line. The telemetry data files indicate that 842 strokes were pumped (see summary table below). Referring to the mud pump anticipated efficiency in Table 51 (see Appendix A), the anticipated pump volume was 106.1 bbl. The kill line capacity is 99.0 bbl, which suggests a 7.1 bbl over-displacement (not including drape hose and surface volume).

Table 13: Pump output summary, kill line displacement

Time	Pump Strokes (Pump 2)	Theoretical Output	Anticipated Output	Anticipated Volume
15:38	873	0.13113 bbl/stk	0.126 bbl/stk	110.0 bbl
15:55	1715	0.13113 bbl/stk	0.126 bbl/stk	216.1 bbl
<i>Interval</i>	<i>842</i>	<i>0.13113 bbl/stk</i>	<i>0.126 bbl/stk</i>	<i>106.1 bbl</i>

4.1.3.2 Pressure Response

For a line depth⁶ of 5,045 ft, the expected surface pressure for a full displacement of the kill line is 1,471 psi.

$$\text{Pressure increase} = (5,045 \text{ ft})(14.17 - 8.556 \text{ ppg})(0.051948 \text{ psi(ppg)}^{-1}(\text{ft})^{-1}) = 1,471 \text{ psi}$$

Pressure data from the choke manifold was recorded during the displacement. A simulated pressure response using the pump stroke data as input is compared to the recorded data in Figure 15. The simulation tracks closely with the actual pressure response, and the final surface pressures are very similar to the expected value. This suggests that a full line displacement was achieved in this case.

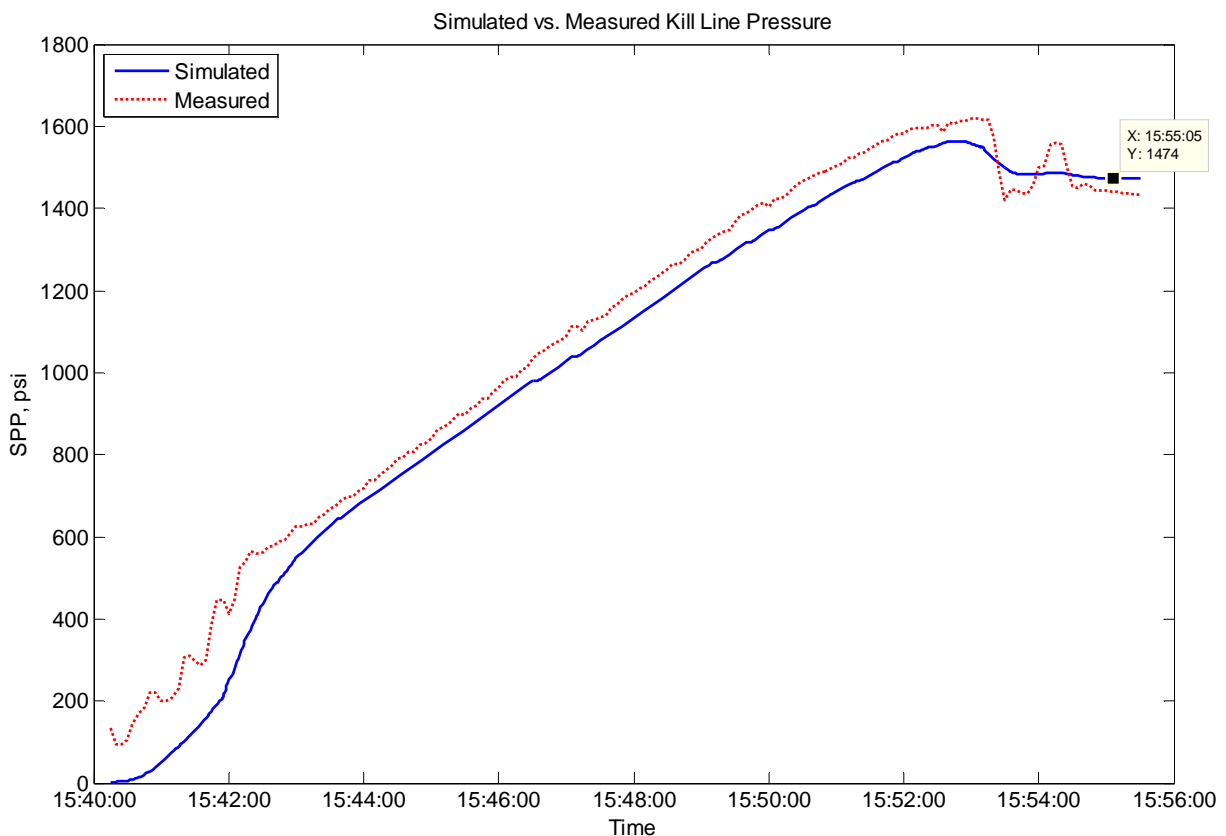


Figure 15: Simulated (calculated) vs. measured kill line pressure during displacement

⁶ The choke and kill lines have multiple entry points into the BOP at varying depths. It is assumed that the lower entry points (5,045 ft in both cases) were opened to achieve full line displacement.

Note that although the expected kill line pressure was achieved initially, the pressure did not remain stable. During the subsequent riser displacement, the kill line pressure decayed slowly, eventually settling out at about 1,200 psi (see Figure 6). The cause of this behavior is unknown, but a leaking valve or thermal effects are possible explanations.

4.1.3.3 Riser Flow Out

The Sperry-Sun flow sensor data indicates a response similar to that observed for the choke line displacement. Figure 16 compares the simulated output to the measured flow sensor returns. Integrating the sensor data over the pumping interval indicates a return volume of 84.8 bbl, compared to the anticipated pump volume of 106.1 bbl. This suggests a volumetric efficiency for rig pump #2 of 76.8% (see Table 14).

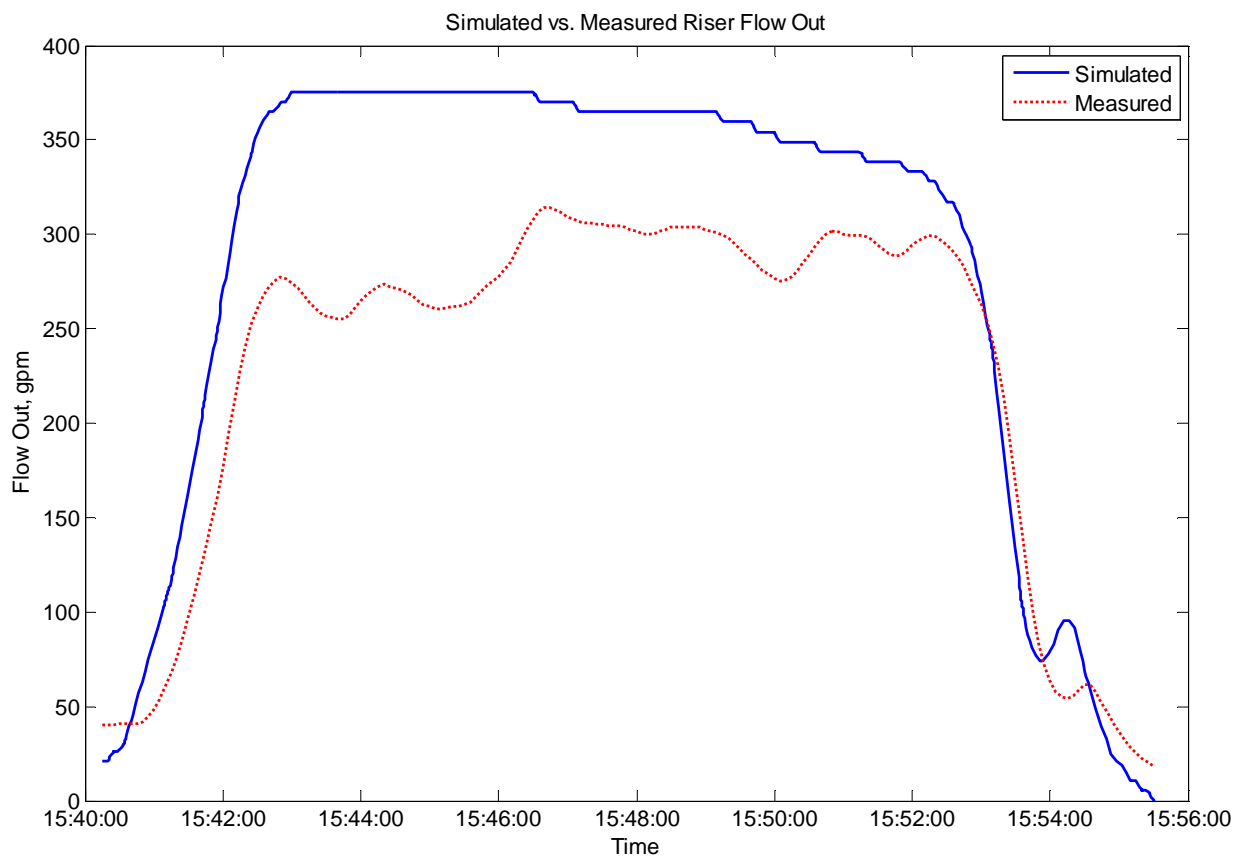


Figure 16: Simulated flow out vs. measured flow sensor data, kill line displacement

Table 14: Pump analysis summary, kill line displacement

Strokes Pumped (Pump 2)	842
Return Volume (from flow sensor)	84.8 bbl
Return Volume (from pit returns)	N/A
Theoretical Pump Output (Pump 2)	0.13113 bbl/stk
Volumetric Efficiency (based on flow sensor)	76.8%
Volumetric Efficiency (based on pit returns)	N/A

4.1.3.4 Pit Returns

Transfer of volume between the active pits, auxiliary pits, and the offshore supply vessel continued during this period (see Figure 12); therefore, the returns based on available pit data are inconclusive.

4.2 First Displacement of 16 ppg Spacer and Seawater Prior to Negative Testing

Following the auxiliary line displacements, displacement of the riser with a 16 ppg spacer composed of lost-circulation material (LCM) commenced. Pumping began at 15:55 and ended at 16:27 (see Figure 6, Event E). Pumping of the spacer was immediately followed by displacement with seawater from 16:28 to 16:53 (see Figure 6, Event F).

A plot of selected signals recorded during the initial riser displacement is given in Figure 17.

4.2.1 Strokes Pumped

Rig pumps #3 and #4 were utilized in parallel for all of the main riser displacements. During the spacer displacement, the telemetry data files indicate that 3609 strokes were pumped (see summary tables below). Referring to the mud pump anticipated efficiency in Table 51 (see Appendix A), the anticipated pump volume was 454.7 bbl.

During the subsequent seawater displacement, the telemetry data files indicate 2800 strokes pumped, corresponding to a pumped volume of 352.8 bbl.

Table 15: Pump output summary, spacer displacement

Time	Pump Strokes (Pump 3 & 4)	Theoretical Output	Anticipated Output	Anticipated Volume
15:55	0	0.13113 bbl/stk	0.126 bbl/stk	0 bbl
16:27	3609	0.13113 bbl/stk	0.126 bbl/stk	454.7 bbl
Interval	3609	0.13113 bbl/stk	0.126 bbl/stk	454.7 bbl

Table 16: Pump output summary, seawater displacement

Time	Pump Strokes (Pump 3 & 4)	Theoretical Output	Anticipated Output	Anticipated Volume
16:28	3609	0.13113 bbl/stk	0.126 bbl/stk	454.7 bbl
16:53	6409	0.13113 bbl/stk	0.126 bbl/stk	807.5 bbl
Interval	2800	0.13113 bbl/stk	0.126 bbl/stk	352.8 bbl

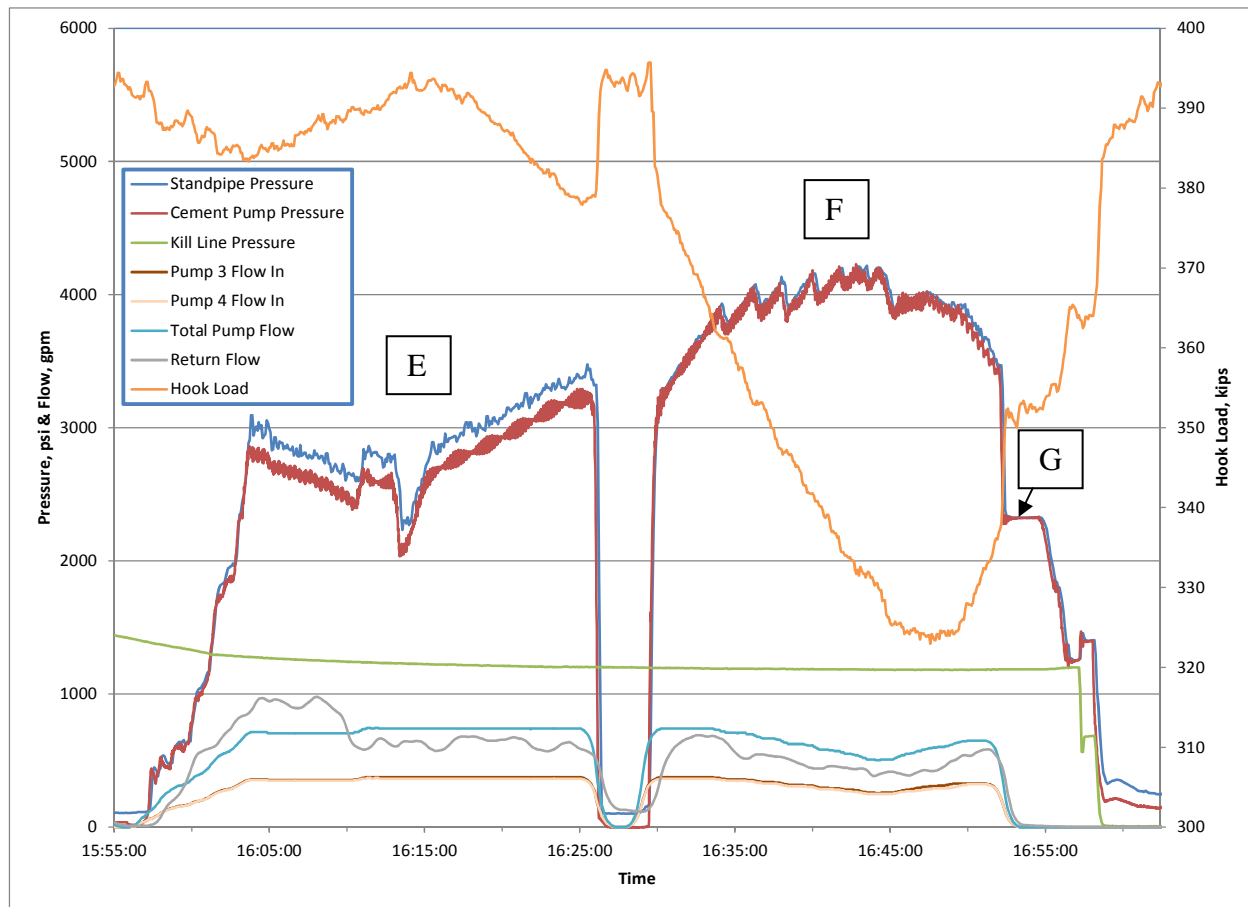


Figure 17: Pressure, flow, and hook load signals recorded during riser displacement with spacer and seawater

Table 17: Description of events from 15:55 to 17:00

Event	Description	Time
E	Displacement of riser with 16 ppg spacer	15:55 to 16:27
F	Displacement of riser with seawater	16:28 to 16:53
G	Pumps stopped; annular BOP closed	16:53 to 16:54

4.2.2 Measured Spacer Volume Pumped

Because the spacer pumped into the well was drawn from a mud pit, a direct measurement of the actual displacement volume is available from the pit data in this case⁷. As instructed in the displacement procedure [9], the spacer was mixed in pit #5. Plotting the data from pit #5 against the pump flow data over the spacer pumping duration indicates that 428 bbl of spacer were available prior to the displacement, and 7 bbl remained in the pit after completion of pumping (see Figure 18). Therefore, 421 bbl of spacer was pumped into the well.

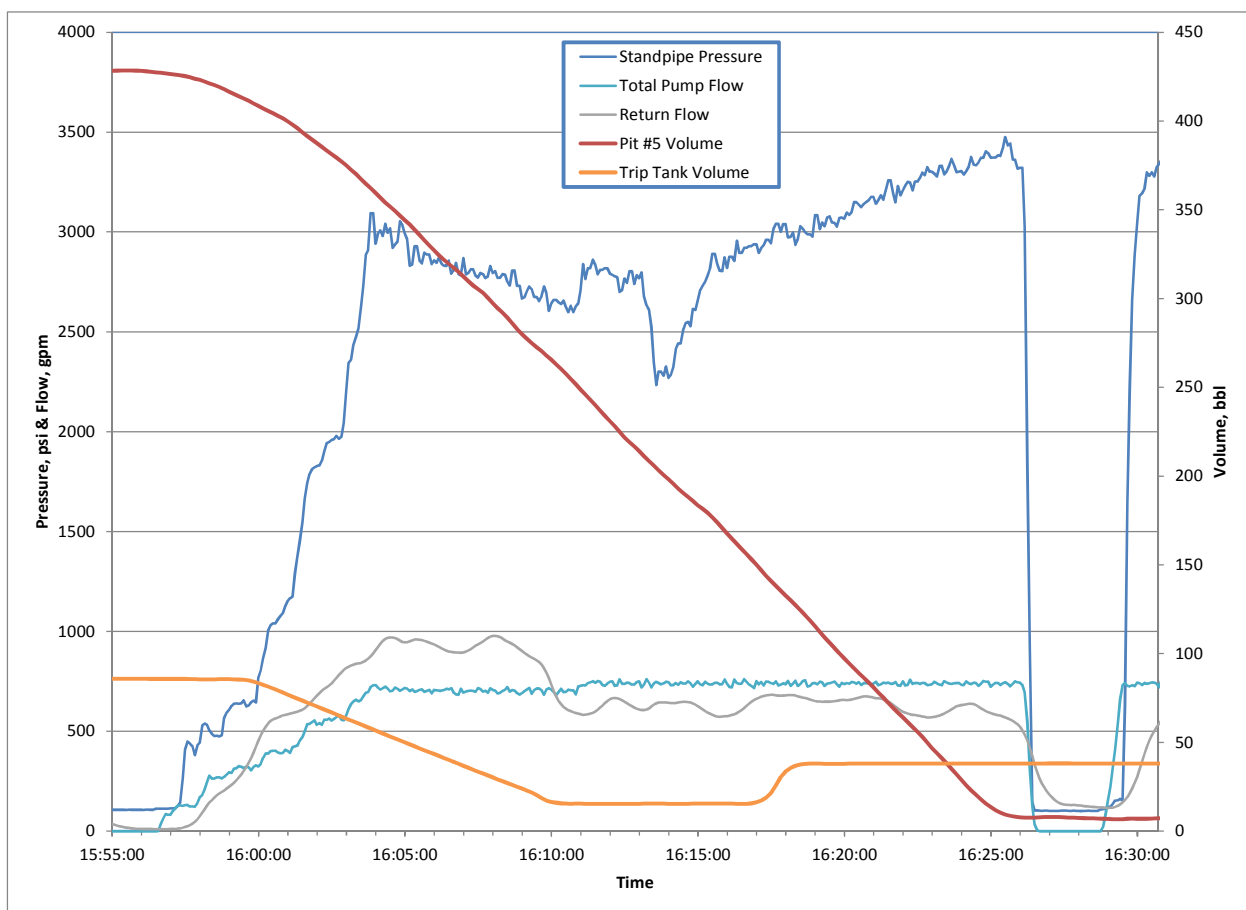


Figure 18: Pressure, flow, and pit signals during spacer displacement

⁷ All other displacements during the time interval of interest were of unknown volumes of seawater drawn from the rig sea chest; thus, the pump strokes provide the only indication of input volume for these cases.

The pit #5 volume signal serves as the only reference in the time interval of interest against which the rig pump efficiency may be directly computed. Given the observed volume, the volumetric efficiency for rig pumps #3 and #4 during the spacer displacement is calculated at 89.0%⁸.

4.2.3 Riser Flow Out

Integrating the Sperry-Sun flow sensor data over the spacer displacement interval indicates a return volume of 459.8 bbl, compared to the anticipated pump volume of 454.7 bbl. This puzzling result seems to indicate a pumping efficiency of greater than 100%; however, further examination of the data reveals that the measured flow rate was artificially increased at the beginning of the spacer displacement because the trip tanks were emptied into the flow line. It may be observed in Figure 18 that the increase of return flow in excess of the pump flow into the well corresponds to the drop in the trip tank volume.

The initial trip tank volume was 85.6 bbl at the onset of the displacement, and was 15.4 bbl after the tank was emptied; therefore, an extra volume of 70.2 bbl flowed through the flow line into the active pits (9 & 10). Accounting for this, the remaining flow sensor volume over the spacer displacement is 389.6 bbl. This implies a pumping volumetric efficiency of 82.3% (see Table 18).

Using the pit #5 measured volume as a reference and assuming no lost returns, the corrected flow sensor returns appear to be in error by approximately -7.5%.

Integrating the flow sensor data over the seawater displacement interval indicates a return volume of 280.9 bbl, compared to the anticipated pump volume of 352.8 bbl, which suggests a pump volumetric efficiency of 76.5% (see Table 19).

⁸ The analysis presented in [6] does not attribute the difference in pit volume and pump stroke volume to a reduced pumping efficiency. Rather, the document suggests (in Appendix Q and elsewhere) that 30 bbl of fresh water were pumped along with 424 bbl of spacer, summing to a total volume of 454 bbl. SES found no evidence of this fresh water volume in its review. Indeed, a strong contraindication to this claim is the fact that the pumps were not stopped to change the inlet lineup during the interval that the spacer was pumped (over which 454 bbl of pump strokes were accumulated).

Table 18: Pump analysis summary, spacer displacement

Strokes Pumped (Pump 3 & 4)	3609
Pumped Volume (from Pit #5)	421 bbl
Return Volume (from flow sensor)	389.6 bbl
Return Volume (from pit returns)	N/A
Theoretical Pump Output (Pump 2)	0.13113 bbl/stk
Volumetric Efficiency (based on pumped volume)	89.0%
Volumetric Efficiency (based on flow sensor)	82.3%
Volumetric Efficiency (based on pit returns)	N/A

Table 19: Pump analysis summary, first seawater displacement

Strokes Pumped (Pump 3 & 4)	2800
Return Volume (from flow sensor)	280.9 bbl
Return Volume (from pit returns)	N/A
Theoretical Pump Output (Pump 2)	0.13113 bbl/stk
Volumetric Efficiency (based on flow sensor)	76.5%
Volumetric Efficiency (based on pit returns)	N/A

Simulation results of riser outlet flow over the spacer and seawater displacement, using the pump stroke data scaled by a pumping efficiency of 89.0% (calculated from the pit volume data) as input, are presented in Figure 19. The measured flow sensor data are indicated in red, while a corrected version of the data in which the flow rate from the emptying of the trip tanks is subtracted, is shown in green. The simulated results match the corrected measurements well over the spacer displacement interval. However, the simulated returns are higher than the measurements during the subsequent seawater displacement.

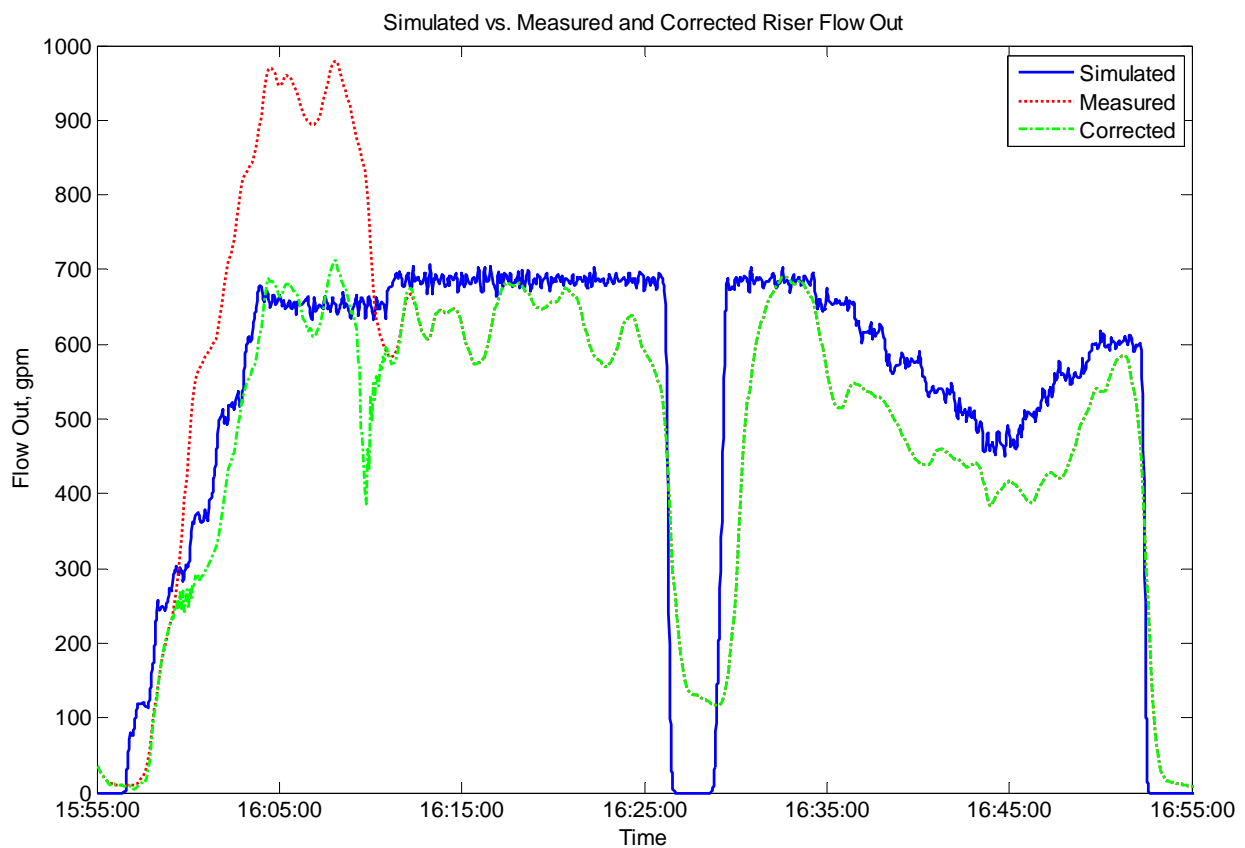


Figure 19: Simulated vs. measured flow out of riser during spacer and seawater displacement

4.2.4 Pressure Response

The pressure response from the same simulation, plotted against the measured standpipe pressure, is presented in Figure 20. Included in the figure are annotations indicating key events that occurred during the displacement.

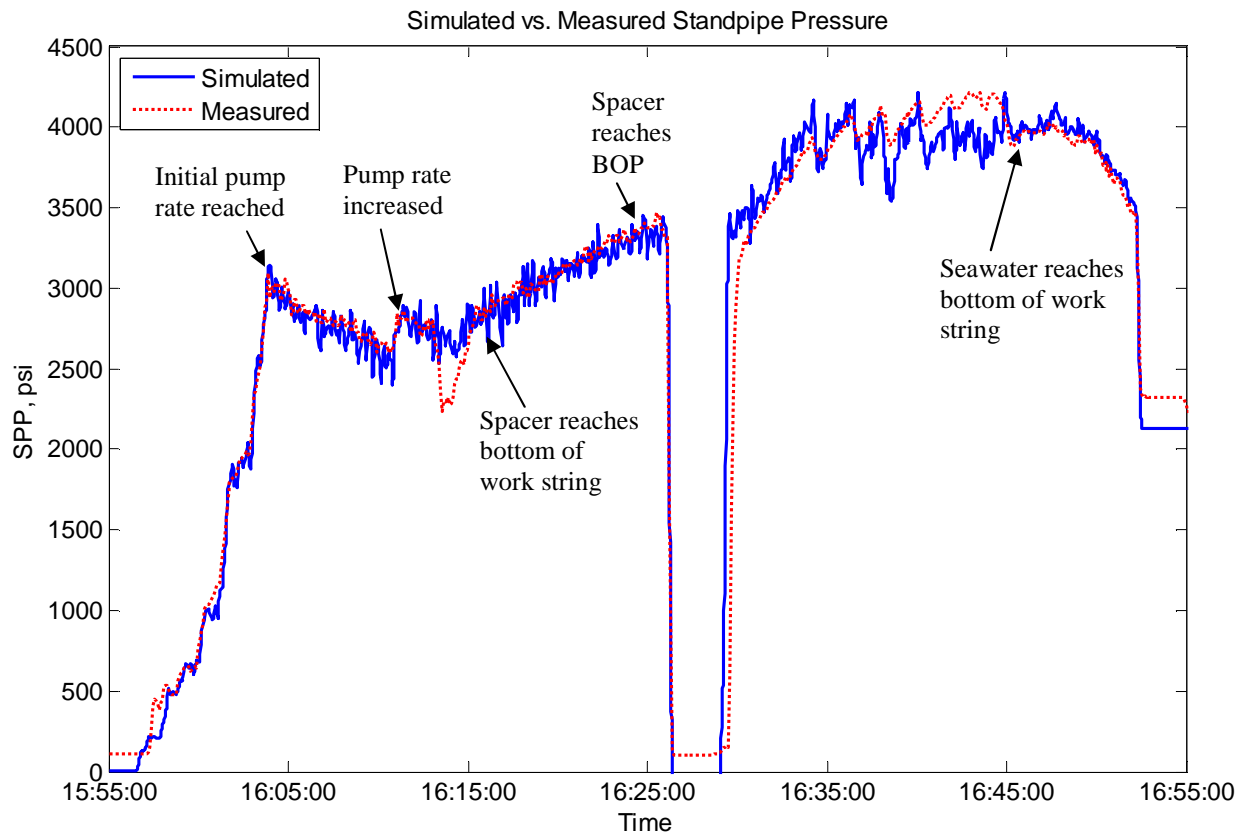


Figure 20: Simulated vs. measured standpipe pressure during spacer and seawater displacement

The simulated pressure response closely matches the measured pressures. However, to obtain this match it was necessary to introduce a larger than expected volume delay parameter into the simulation. The volume delay parameter accounts for the surface piping volume on the rig between the pits and the point where the drill pipe passes the RKB on the drill floor. Based on information provided by Transocean, the expected volume delay was nominally 10 bbl [21], but the best match was obtained with 26 bbl. SES currently has no information to account for the 16 bbl difference.

Simulated bottom-hole pressures, relative to the various pressures present in the formation, are presented in Figure 21 over the spacer and seawater displacement interval. Well pressures are designated as “WP”, while formation pore pressures (plotted as horizontal lines) are designated as “PP”. Formation depths and pressures used in the simulation, obtained from [6], are presented in Table 20.

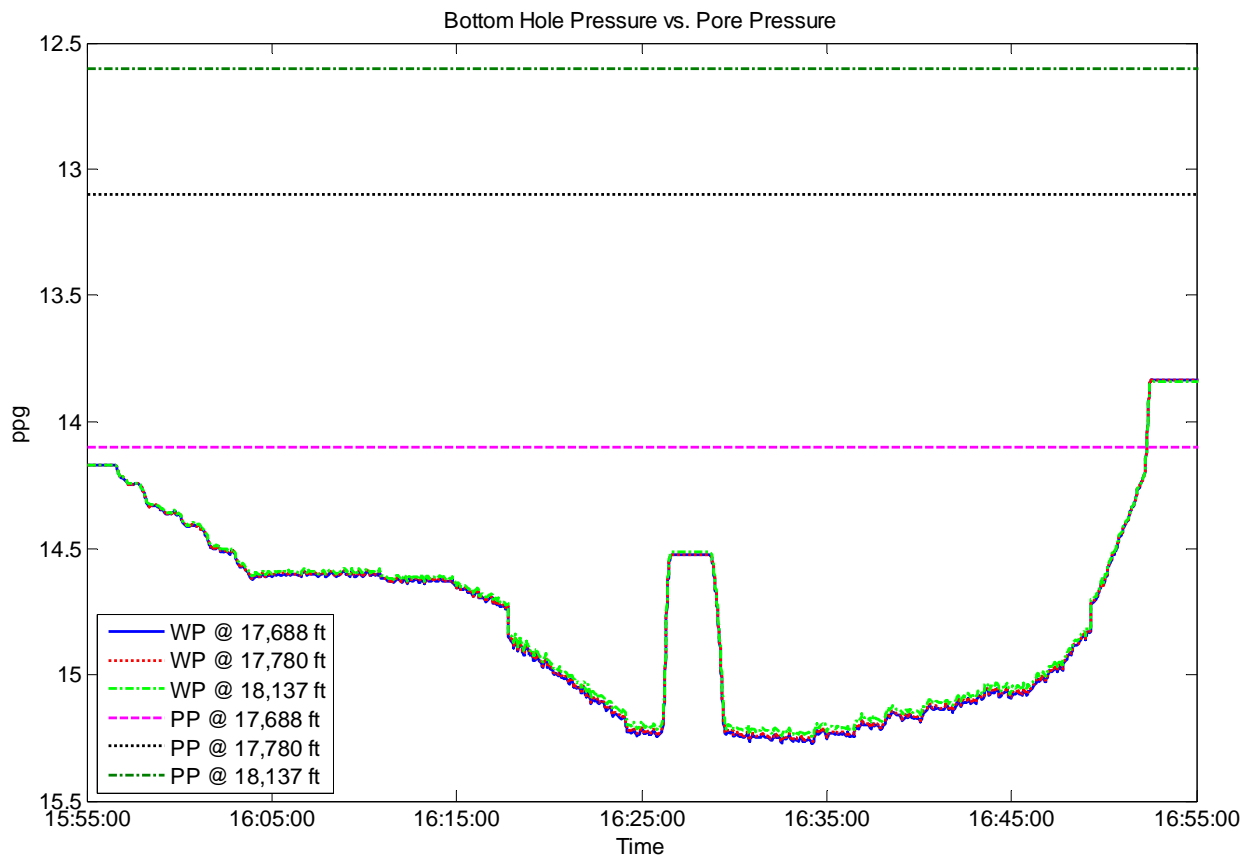


Figure 21: Simulated bottom hole pressures during spacer and seawater displacement

Table 20: Formation pressure data used for well simulations, obtained from [6]

Formation	Average Depth	Pore Pressure
14.1 ppg Brine	17,688 ft	12,956 psi
13.1 ppg Hydrocarbons	17,780 ft	12,099 psi
12.6 ppg Hydrocarbons	18,137 ft	11,871 psi

The results indicate that the well was underbalanced to the 14.1 ppg brine zone following the initial displacement, but remained overbalanced to the 13.1 and 12.6 ppg hydrocarbon-bearing formations.

4.2.5 Fluid Boundary Positions

The annotations of Figure 20 are echoed in Figure 22, which plots the simulated liquid boundary positions (mud-to-spacer and spacer-to-seawater) in the well over time. The key observation from the plot is that the bottom of the spacer does not arrive at the BOP prior to shutting in for the negative test. The final position of the spacer-to-seawater boundary of 6,488 feet places it 1,487 feet below the BOP's upper annular preventer (depth 5,001 ft), or approximately 71 bbl short of the intended displacement volume (see also Figure 25, left diagram, and Table 23, Event #1).

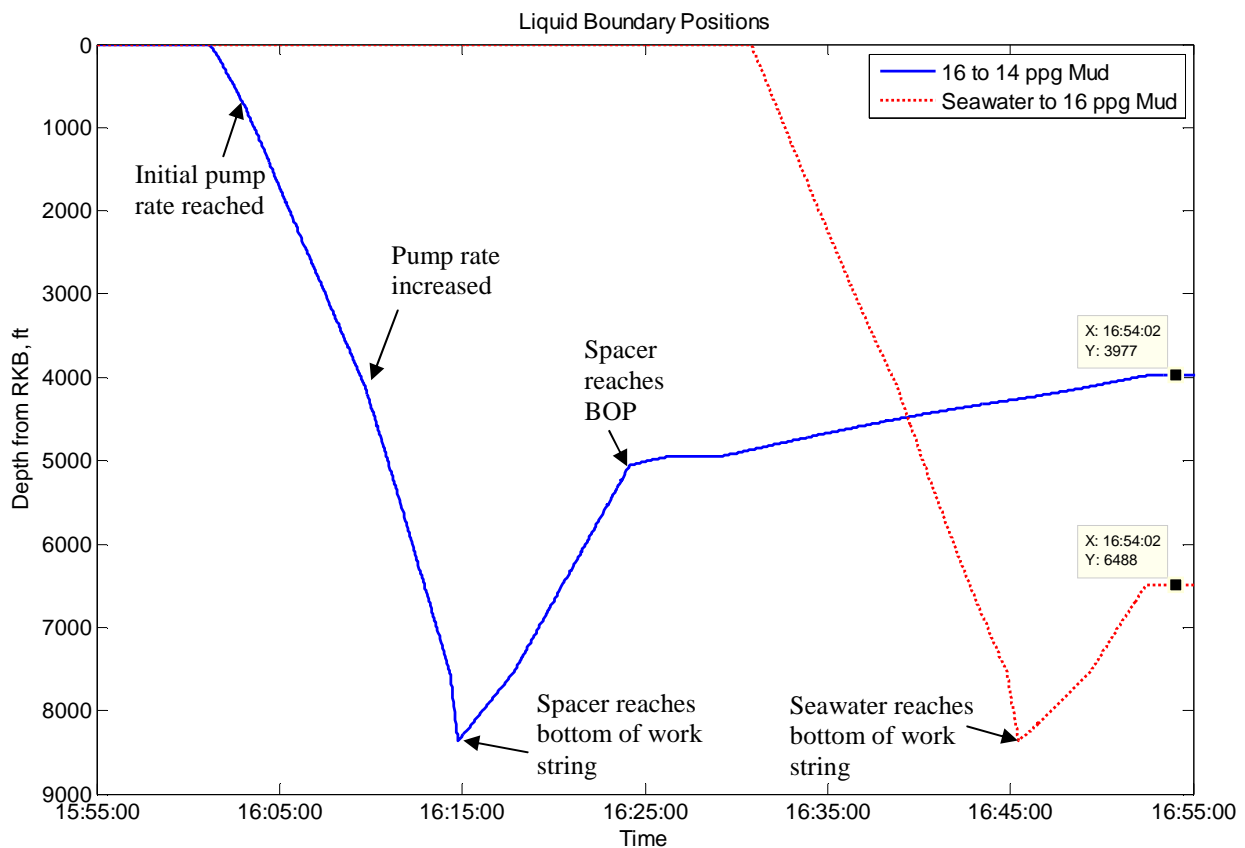


Figure 22: Simulated spacer-to-mud and spacer-to-seawater liquid boundary positions during spacer and seawater displacement

Simulated and / or calculated scenarios were run for four different displacement cases to determine the final spacer placement relative to the BOP for each:

- A. Pump strokes as measured, but with volumetric efficiency reduced to 89.0% and 26 bbl surface delay (as presented in this section);
- B. Volumes pumped as specified in the displacement procedure [9] with 26 bbl surface delay;
- C. Pump strokes as measured, with the full anticipated volumetric efficiency of 96.1% and 0 bbl surface delay. This case places the spacer at the highest possible elevation consistent with recorded evidence.
- D. Volumes pumped described by the hypothetical displacement procedure outlined in Section 3 of this report. This case is listed for reference, and does not reflect actual events on the rig.

The upper and lower spacer boundaries for each case are given in Table 21, below:

Table 21: Spacer position and final standpipe pressure for various displacement cases

Case	Spacer Volume Pumped	Seawater Volume Pumped	Upper Spacer Boundary Position	Lower Spacer Boundary Position	Final Standpipe Pressure
A	421 bbl	327 bbl	3,977 ft	6,488 ft	2,131 psi
B	425 bbl	350 bbl	3,896 ft	5,930 ft	1,923 psi
C	455 bbl	353 bbl	3,715 ft	5,250 ft	1,677 psi
D	425 bbl	385 bbl	3,706 ft	4,976 ft	1,572 psi

Of these cases, only in Case D is the bottom of the spacer displaced above the BOP upper annular preventer at 5,001 ft. The other cases, which could have occurred aboard the rig, do not displace the spacer high enough to clear the BOP. Therefore, SES concludes that at the cessation of pumping at 16:53, the BOP annulus, along with a portion of the work string-to-casing annulus below it, were filled with 16 ppg spacer.

4.2.6 Pit Returns

Transfer of volume between the active pits, auxiliary pits, and the offshore supply vessel continued during the spacer and seawater displacement, as shown in Figure 23. Therefore, the returns based on available pit data for this period are inconclusive.

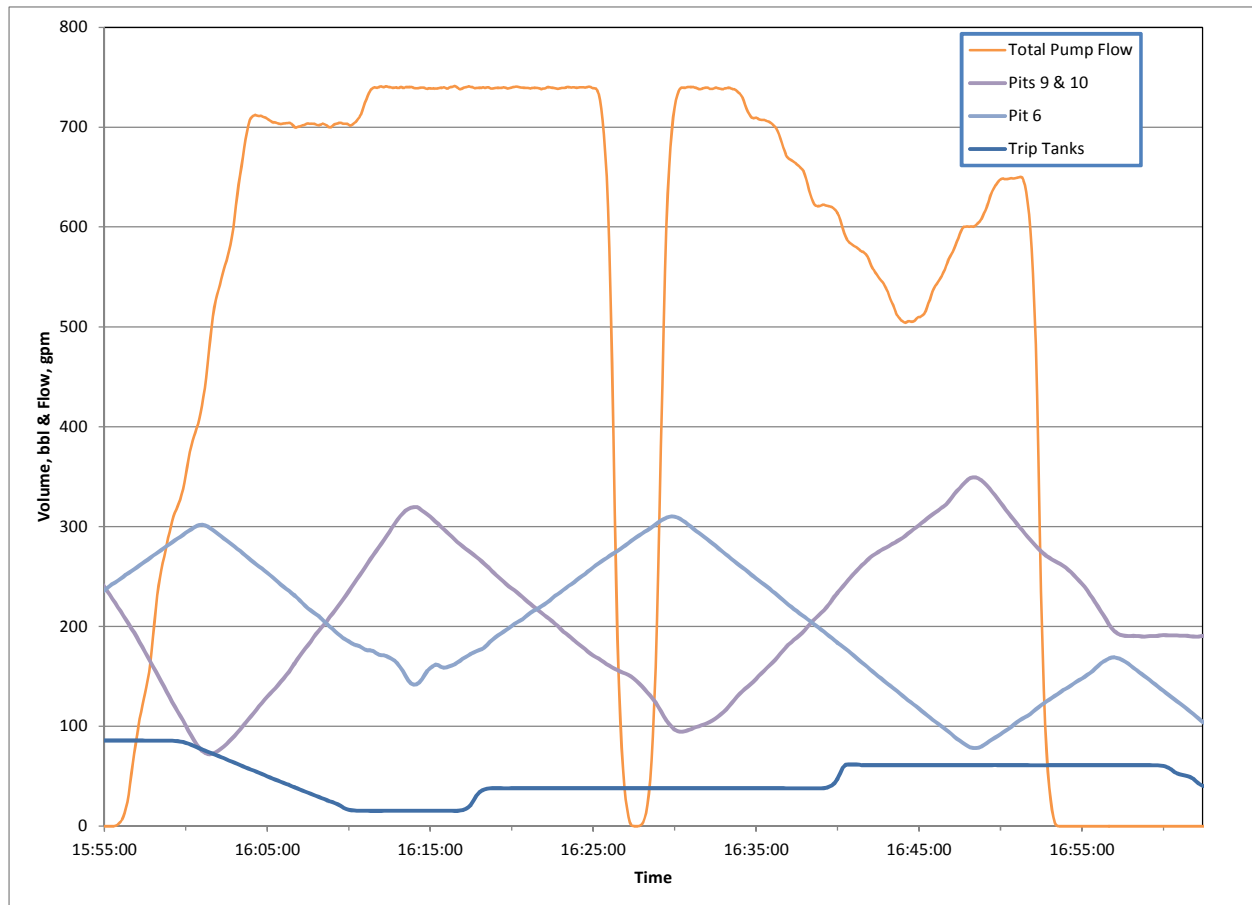
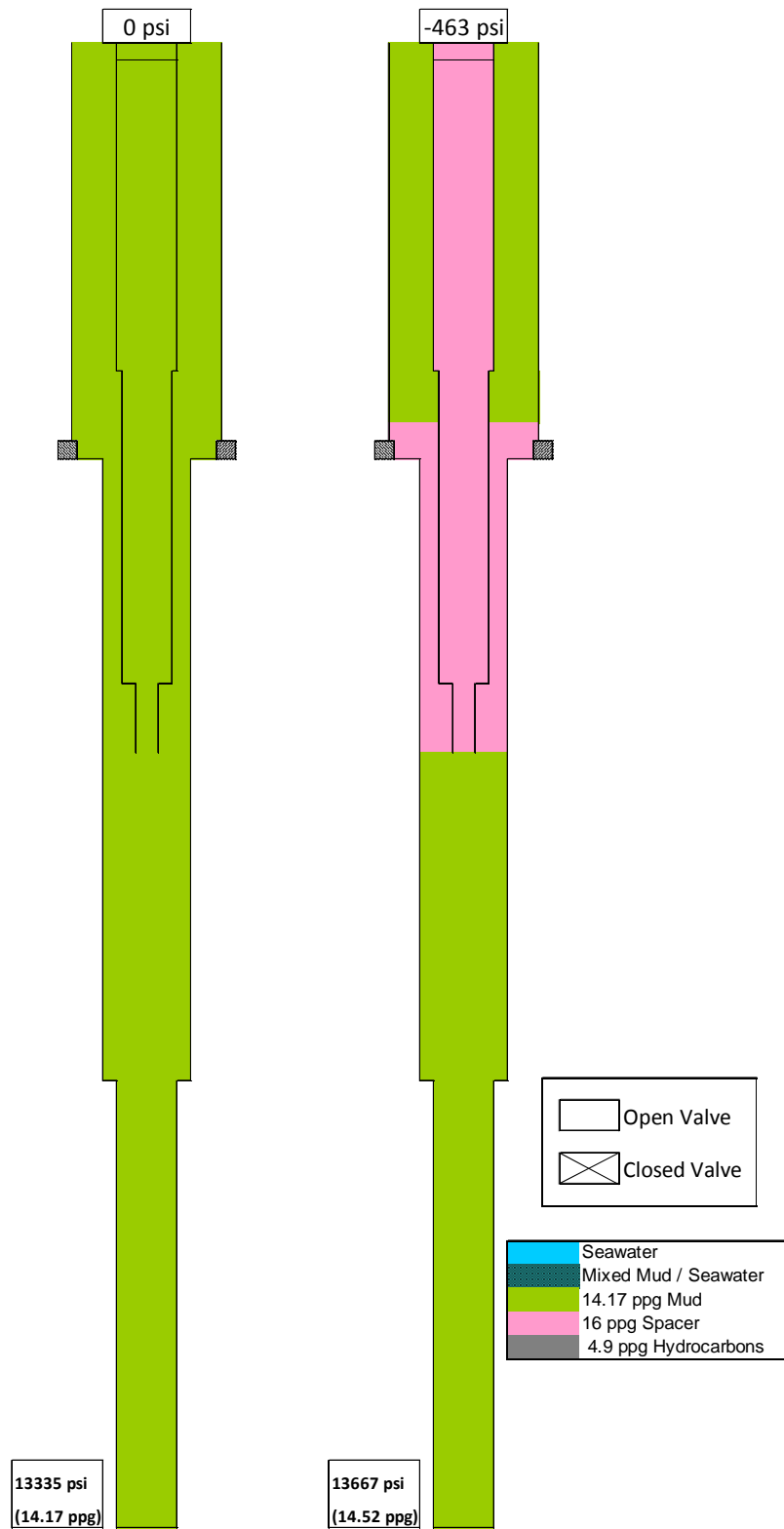


Figure 23: Pit transfer activity during spacer displacement

4.2.7 Well Fluid State

Based on the analyses presented above, illustrations of the well fluid state before and after the spacer displacement are given in Figure 24. The well state following the first seawater displacement is presented in Figure 25 (left diagram), compared with the theoretical state (right diagram; highlighted in yellow) at the same point in the hypothetical displacement procedure presented in Section 3. The comparison emphasizes the under-displacement of the spacer in the actual case.



**Figure 24: Well fluid states before and after spacer displacement:
15:55 (left); 16:28 (right)**

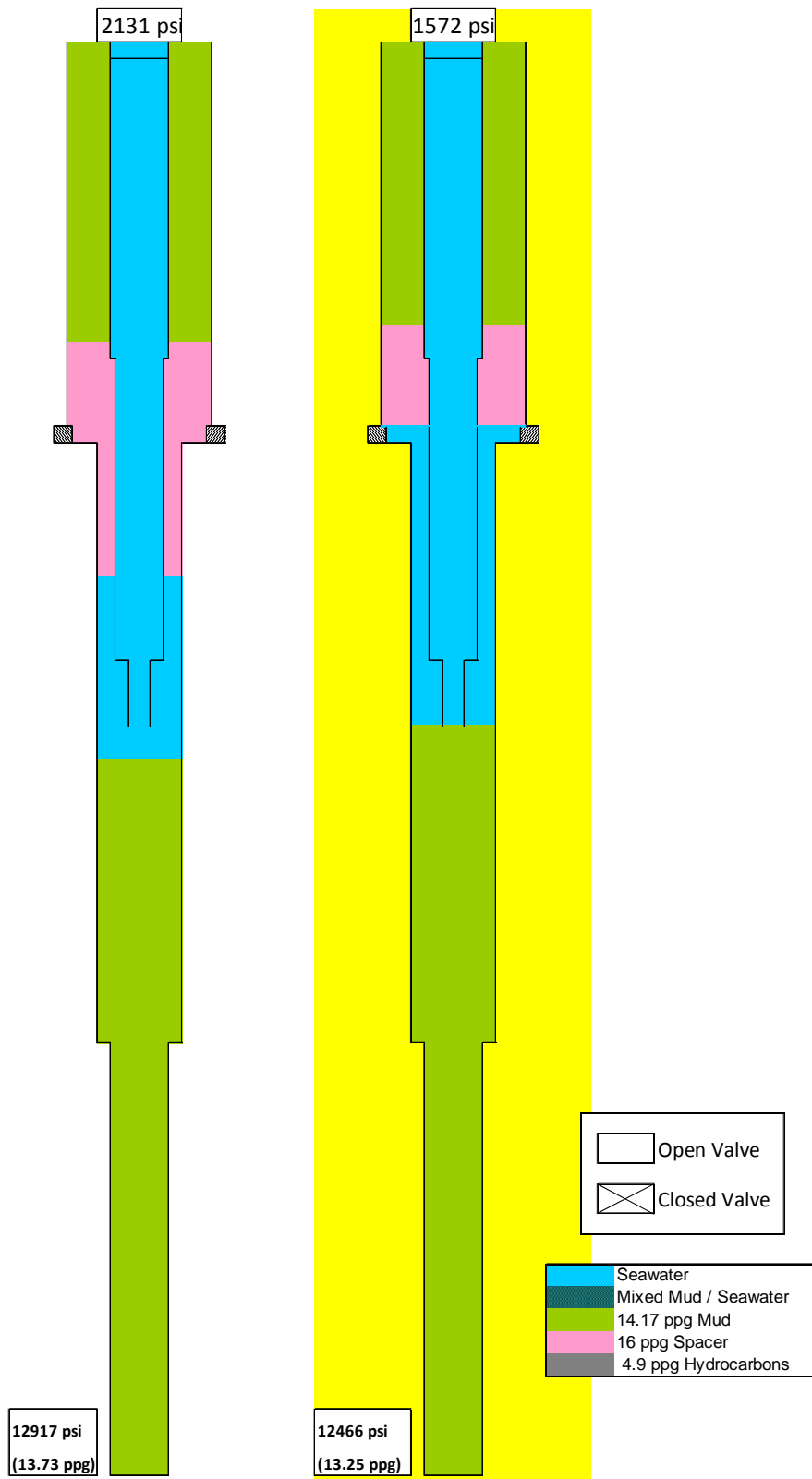


**Figure 25: Well fluid state after first displacement at 16:53 (left);
 Hypothetical well state after first displacement, from Section 3 analysis (right)**

4.3 Hydrostatic Analysis of Negative Testing

Following the spacer and seawater displacement, well activity proceeded to the execution of the negative testing. As discussed in Section 3, the objective of the test is to simulate the seawater gradient to which the well will be exposed during the subsequent temporary abandonment procedure, thereby verifying the pressure integrity of the downhole equipment (in this case, float collar, casing, and seal assembly⁹).

The presentation of this section consists of a review of the observed telemetry data during the negative testing, followed by a hydrostatic analysis of well states during this time.

Note that the well state analysis presented is the one that SES considers most plausible given the information available, including telemetry data and witness accounts. At present, there is not enough information available to perform a precise reconstruction of the well state, and assumptions are required where information is lacking. These assumptions are noted in the presentation. The general objective is to derive a set of assumptions that may be employed consistently over both the negative test and the larger time interval of interest.

⁹ In the event of a leak in the float collar, the cement is also tested.

4.3.1 Observed Standpipe and Kill Line Pressures

Relevant pressure and pump flow data recorded during the negative test period (approximately 16:53 to 20:02) are given in Figure 26 and Figure 27 (expanded from Figure 7), with accompanying descriptions in Table 23 and Table 25. Supporting information for the descriptions is presented in the following section.

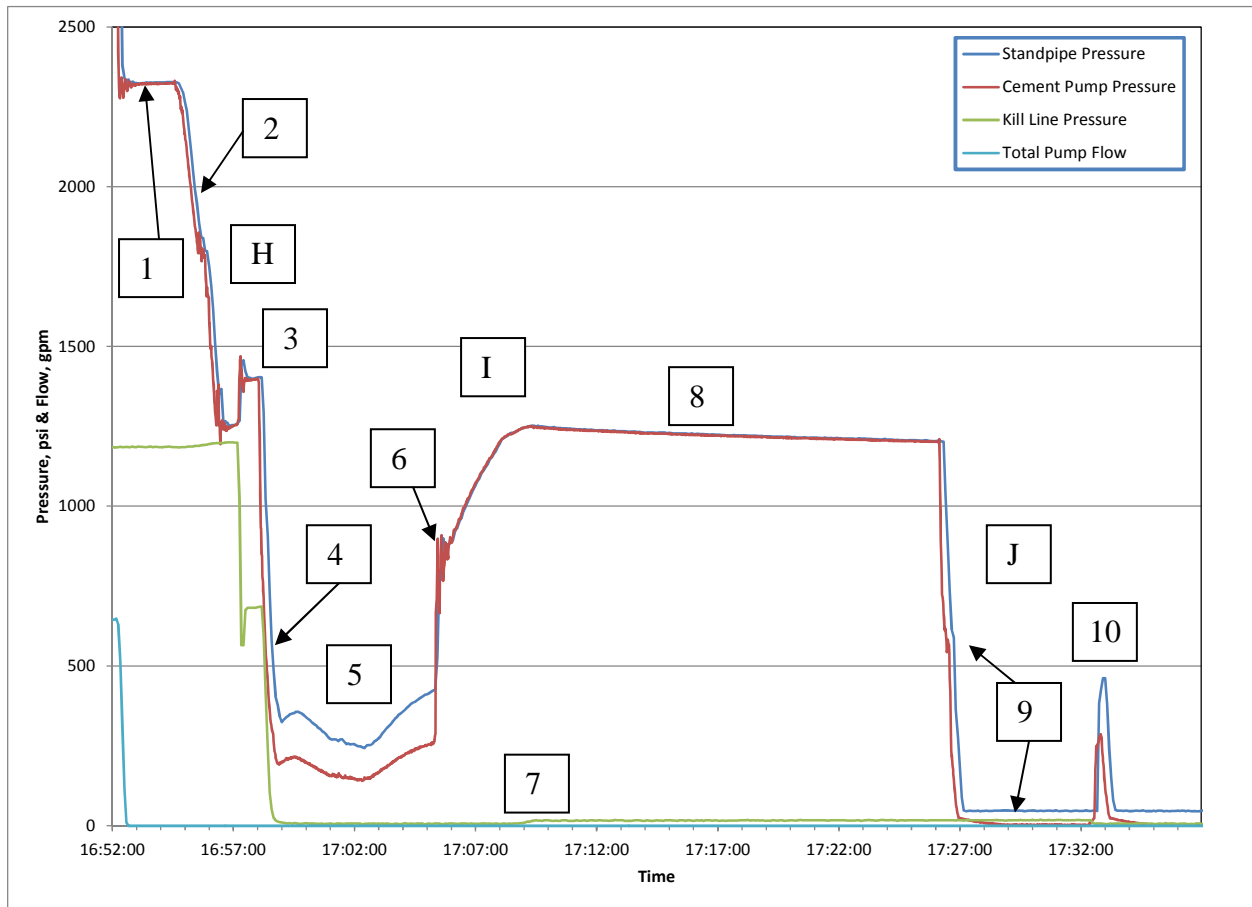


Figure 26: Negative test data telemetry, first 40 minutes

Table 22: Description of events from 16:54 to 17:35

Event	Description	Time
H	Bleed work string and equalize with kill line	16:53 to 16:58
I	Observe annular preventer leakage, seal annular and work string	16:58 to 17:24
J	Bleed work string to cement unit	17:24 to 17:26

Table 23: Description of events, first 40 minutes of negative test

Event	Description	Time
1	Annular preventer closed, residual pump pressure trapped	16:53 to 16:54
2	Bleed work string pressure to cement unit, spacer begins leaking through annular preventer from riser into BOP (18 bbl); shut in work string	16:55 to 16:57
3	Open kill valve at BOP; equalize work string pressure (1,395 psi) with kill line pressure (682 psi)	16:57 to 16:58
4	Bleed work string pressure with kill valve at BOP open (surface kill valve closed), results in a vacuum drawn on kill line	16:58 to 16:59
5	Spacer continues leaking through annular preventer from riser into BOP (47 bbl); riser fluid level dropping; well underbalanced; possible influx	16:59 to 17:05
6	Shut in work string; increase annular preventer closing pressure to seal	17:05 to 17:06
7	Formation pressure causes standpipe and kill line pressures to increase; BOP kill valve closed	17:06 to 17:10
8	Riser filled with 65 bbl mud; standpipe pressure stabilizes at 1,202 psi (well balanced with formation pressure)	17:10 to 17:26
9	Bleed work string pressure (15 bbl taken at cement unit); well underbalanced; possible influx;	17:26 to 17:32
10	Kill valves at BOP and surface opened; u-tube flow from kill line into work string; air taken into kill line; kill valves closed	17:32 to 17:33

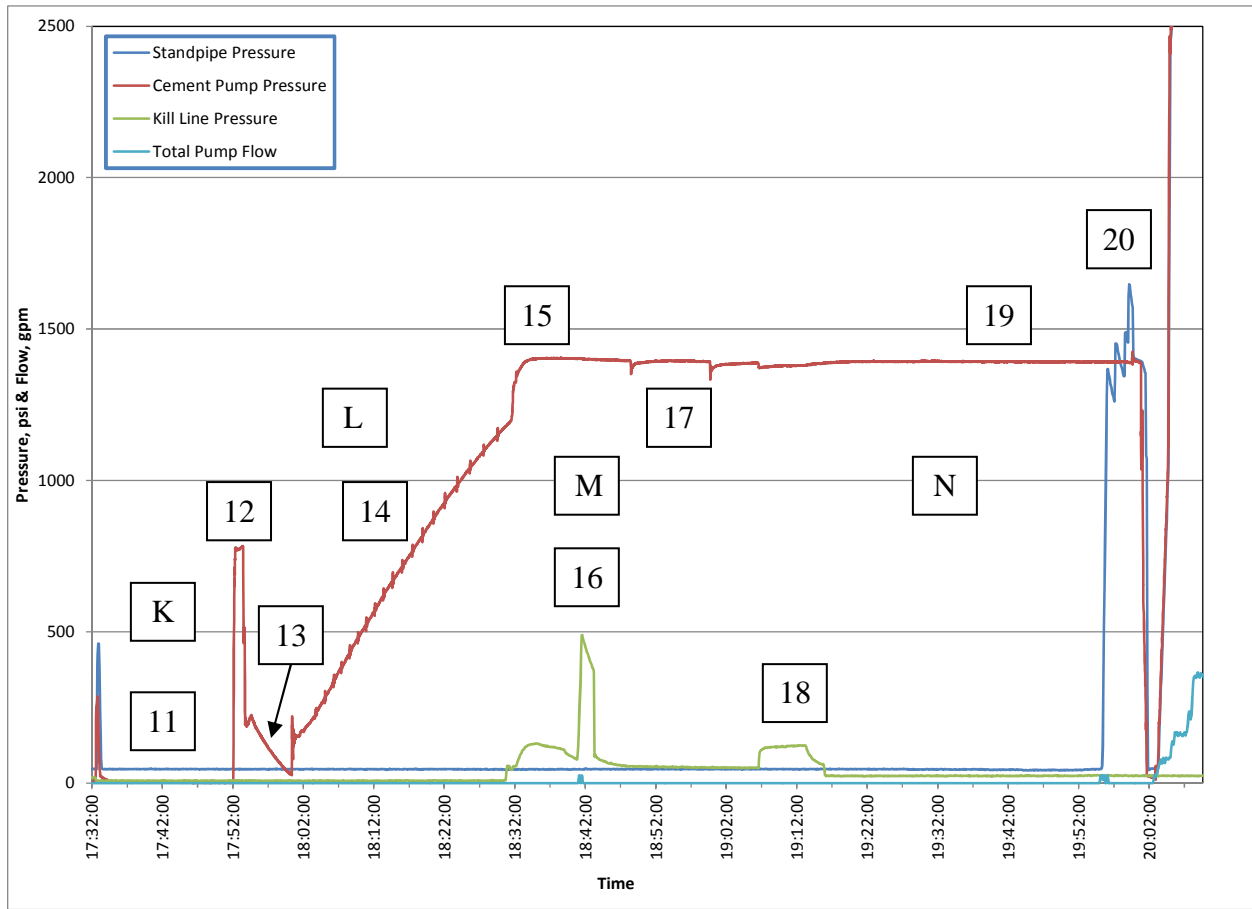


Figure 27: Negative test data telemetry, final 150 minutes

Table 24: Description of events from 17:32 to 20:00

Event	Description	Time
K	Switch lineup to kill line; gauges isolated	17:26 to 17:52
L	Bleed work string, shut in, observe standpipe pressure build	17:53 to 18:30
M	Pump on kill line to ensure full (valve closed)	18:30 to 19:12
N	Conduct negative test with no flow from kill line	19:16 to 20:00

Table 25: Description of events, final 150 minutes of negative test

Event	Description	Time
11	Test sub valves and IBOP closed; gauges isolated; line up to conduct negative test on kill line; well pressure builds behind isolated gauges	17:33 to 17:52
12	Test sub valves opened to cement unit; pressure gauge spikes to 770 psi	17:52 to 17:53
13	Bleed work string pressure at cement unit (3-15 bbl); shut in	17:53 to 18:00
14	Well pressure builds to 1,182 psi	18:00 to 18:31
15	Open kill valve at BOP; standpipe pressure increases to 1,404 psi; kill line pressure increases to 121 psi	18:31 to 18:40
16	Pump against closed valve on kill line; bleed off	18:40 to 18:47
17	Bleed work string briefly at cement unit; pressure builds to prior level; repeat bleed with same result	18:48 to 19:04
18	Open kill valve at BOP, then open surface kill valve; air bubble and 0.2 bbl liquid bled back; spacer drawn up kill line	19:07 to 19:15
19	Conduct negative test with no flow on kill line	19:15 to 19:54
20	Open test sub valves to standpipe manifold; bleed pressure before resuming displacement	19:54 to 20:00

Based on an analysis of rig piping drawings and conversations with rig personnel, Transocean prepared a schematic, presented in Figure 28, of the probable surface piping configuration during the negative test.

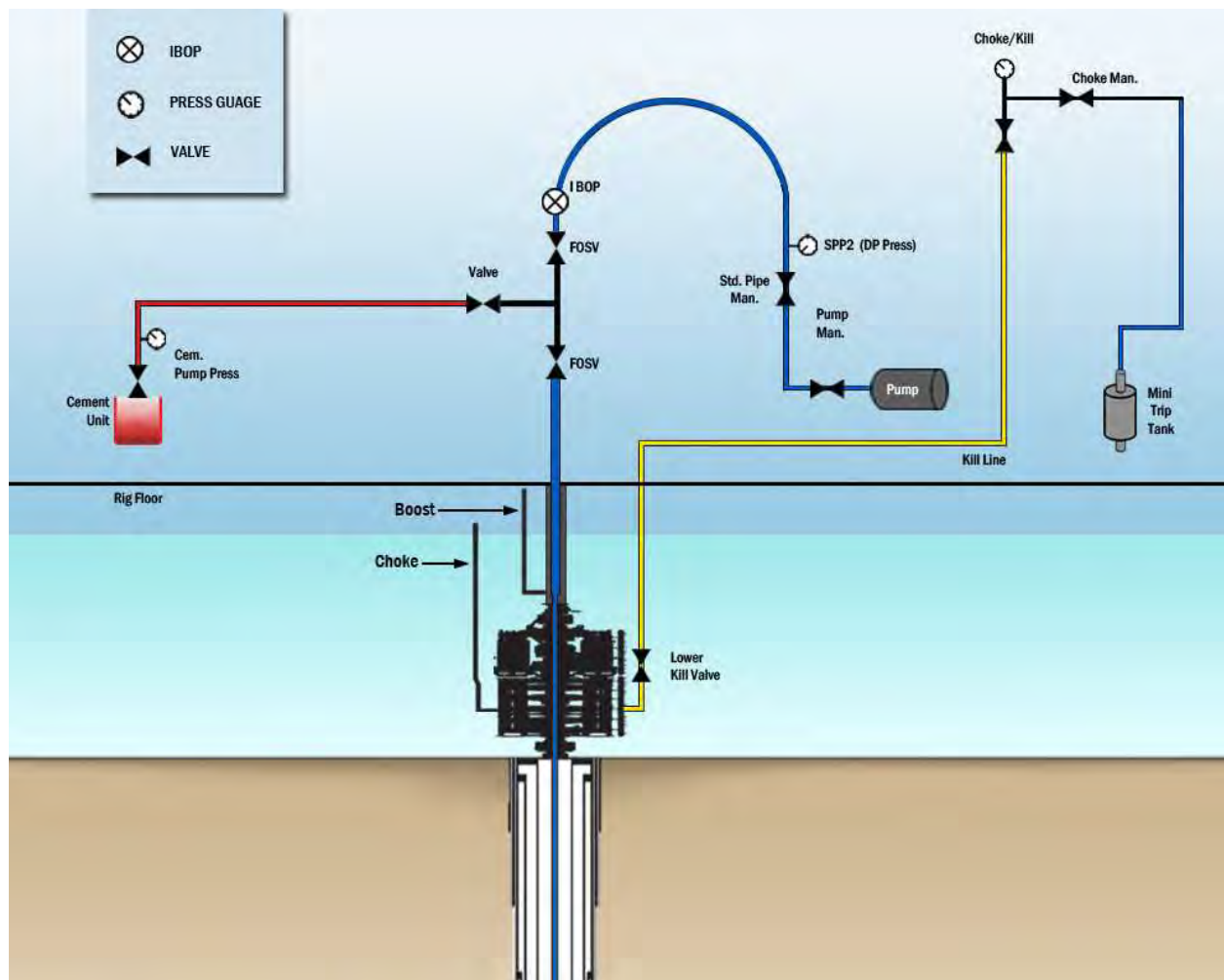


Figure 28: Schematic of rig surface piping arrangement during negative test

4.3.2 Well State Calculations

Before proceeding with individual well state descriptions for the negative testing events, a discussion of a significant assumption made in the hydrostatic analysis is warranted.

Examining the collected data set as a whole, certain portions of the negative test may be interpreted as instances in which the well was in fluidic communication with one or more of the hydrocarbon-bearing sands. One of these is the standpipe pressure build-up to 1,250 psi with eventual decay to 1,202 psi (see Event 8, Figure 26); another is a similar build-up to approximately 1,400 psi prior to and during the actual negative test (See Events 15, 17, 18, and 19, Figure 27). In each of these cases, SES could find no valid hydrostatic solution that matched the measured surface pressure data in which the casing was completely isolated from the formation pressures. In other words, formation pressure acting into the wellbore was the only physically plausible mechanism that could produce the recorded surface pressure responses on the standpipe and kill line.

A hydrostatic analysis which assumes exposure to the 12.6 ppg formation, the work string filled with seawater, and the entire casing below the work string filled with 14.17 SOBM produces a standpipe pressure which is too low (966 psi) to match the recorded pressures of Event 8 (1,202 to 1,250 psi). Conversely, assuming exposure to the 13.1 ppg formation and the same fluid state in the well gives a standpipe pressure which is too high (1,433 psi) to match the Event 8 pressures, although it is reasonably close to the measurements from later events (15, 17, 18, 19).

Additionally, as was noted in Section 4.2, when simulating the seawater displacement a good match was obtained between simulated and measured standpipe pressures; however, a mismatch was noted between simulated and measured flow returns (see Figure 19 and Figure 20). SES calculates that based on the efficiency established during the spacer pumping, the amount of seawater pumped is in error with respect to the negative test hydrostatics by 20 to 50 bbl.

Rather than reducing the pumping efficiency to account for the volume discrepancy (which results in a mismatch in standpipe pressure during the pumping, both in time and magnitude), SES considered the possibility that the extra volume was instead lost to the formation through a

leak in either the casing or the wiper plug and lower shoe. Such a leak would leave a portion of the pumped seawater volume below the work string at the end of the prior seawater displacement.

The seawater leakage scenario resolves several issues with prior and subsequent analyses as follows:

1. Introducing lost circulation to the model resolves the flow discrepancy in the seawater displacement simulation, because the return flow is less than the input flow for such a case.
2. The simulated standpipe pressure at the end of the seawater displacement (2,131 psi) is a closer match to the observed pressure (2,325 psi);
3. Seawater is drawn into the work string during the bleeds that occurred during the negative testing, instead of mud. This results in analytical hydrostatic states that provide a better match to the measured data throughout the negative test interval.
4. When calculating bottom-hole pressures, the seawater volume in the casing below the work string provides calculated results that are closer to the measured pore pressures in the well (12.6 and 13.1 ppg).

The strongest counter to the assertion of formation losses is the fact that the casing, seal, and wiper plugs were subjected to, and passed, a positive pressure test on the morning of April 20th. The pressure telemetry from this test is shown in Figure 29. The well was subjected to a surface pressure greater than 2,560 psi, which translates to a downhole EMW of approximately 16.89 ppg. This pressure is much greater than the maximum downhole pressure of approximately 15.25 ppg experienced during the spacer and seawater displacement (see Figure 21).

In light of the above, for the fluid loss scenario to be plausible, a leak would need to have developed in the wiper plug or casing subsequent to the positive pressure test, and prior to the negative test. The most likely time for such an event would be during the seawater displacement between 16:28 and 16:53, as the highest bottom-hole pressures (about 15.3 ppg EMW; see Figure 21) were experienced in this interval. The hydrostatic analysis presented in this section

assumes a loss volume of 27 bbl, resulting in an equal volume of seawater just below the work string. It is also assumed that the 27 bbl of mud lost to the formation is returned into the production casing prior to the ingress of other fluids (such as hydrocarbons, base oil, cement, etc.) when influx from the formation takes place.



Figure 29: Plot of cement pump pressure recorded during positive pressure test on April 20th

Event 1 (see Figure 26 and Table 23): At the cessation of the seawater displacement, the spacer was across the BOP with its upper boundary at 3,977 ft and lower boundary at 6,488 ft, as described in Section 4.2. The calculated hydrostatic standpipe pressure for this case is 2,131 psi and the bottom-hole EMW (assuming 27 bbl seawater below the work string as discussed above) is 13.73 ppg. See Figure 25, left diagram for a sketch of this fluid state.

The measured standpipe pressure of 2,325 psi was higher than the calculated value. Based on the shape of the pressure decay just prior to reaching this point, it is surmised that the annular BOP was closed prior to reaching hydrostatic equilibrium; hence the discrepancy in pressures. See Figure 30.

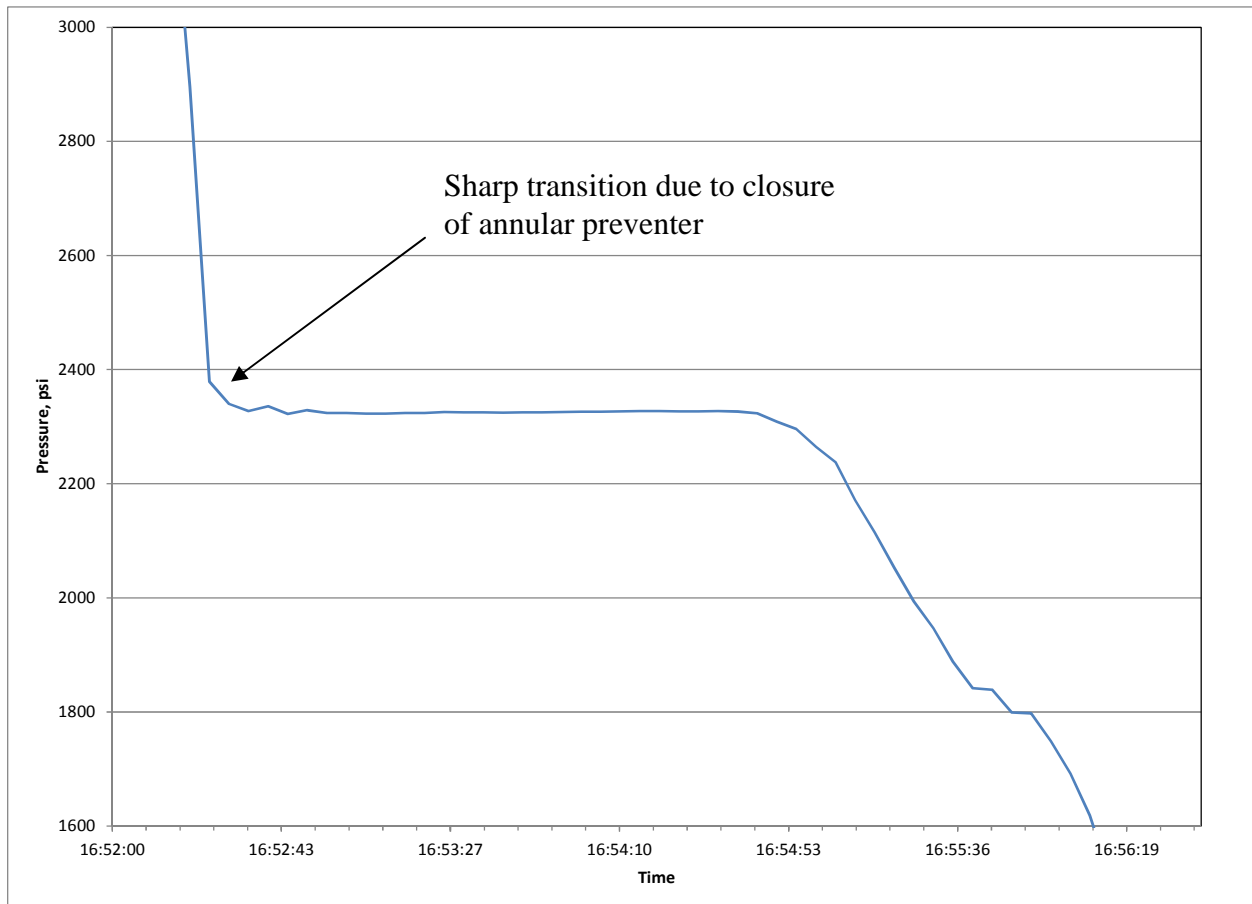


Figure 30: Standpipe pressure signal during annular preventer closure

Event 2 (see Figure 26 and Table 23): After a short wait period, the work string was bled to the cement unit over a period of about three minutes. Based on information provided by Transocean, 25 bbl of fluid was taken during this bleed [21]. Because the well was overbalanced during this event, it is surmised that the large bleed volume is due to leakage flow downward through the annular BOP from the riser into the production casing¹⁰. SES calculates a bleed volume through the annular preventer of 18 bbl, which does not include the effects of fluid compressibility. This leakage moved the spacer further down the annulus, displacing seawater back through the work string. The standpipe pressure at the end of the bleed was 1,250 psi. The measured kill line pressure at this time was 1,197 psi.

Event 3 (see Figure 26 and Table 23): Following the bleed, the kill valve at the BOP was opened, allowing fluidic communication between the kill line and work string through the work string-to-casing annulus. Because of the heavy fluid in the work string-to-casing annulus and BOP, the standpipe pressure increased to 1,395 psi and the kill line pressure decreased to 682 psi.

A hydrostatic solution for this event was found, which is shown schematically in Figure 31, left diagram. The solution indicates that 88 bbl of spacer and 77 bbl of seawater were in the work string-to-casing annulus below the annular BOP at this time. The calculated bottom-hole EMW is 12.94 ppg, which is overbalanced to the 12.6 ppg formation but slightly underbalanced to the 13.1 ppg formation.

Event 4 (see Figure 26 and Table 23): At 16:58 the work string was again opened to the cement unit to bleed pressure. The kill valve at the BOP was left open during this bleed, and as such, the kill line pressure was bled off as well. Because of the extra weight of the spacer in the annulus, the kill line pressure measurement dropped to zero psi, and hydrostatic analysis indicates a vacuum was present in the kill line thereafter. The standpipe pressure immediately following the bleed was 341 psi.

¹⁰ The annular preventer was confirmed to be leaking by the rig personnel shortly after this event [21].

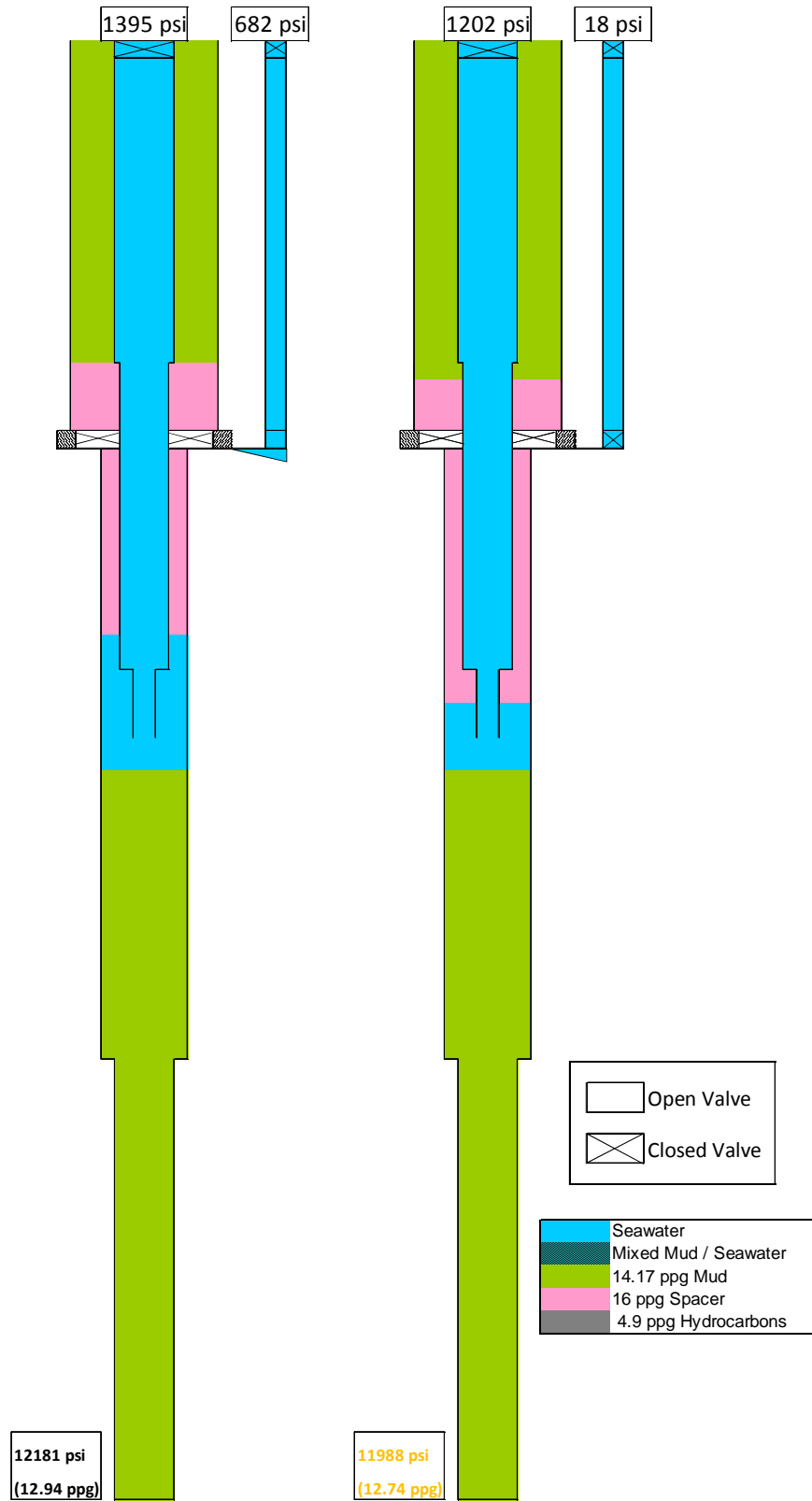


Figure 31: Well fluid states during negative testing: 16:57 (left); 17:26 (right)

Event 5 (see Figure 26 and Table 23): Following the initial bleed, the work string was left open to the cement unit for several minutes. The annular preventer continued to leak spacer from the riser into the BOP during this period. SES calculates based on an analysis of the trip tank data (see Figure 32, expanded from Figure 26) that an additional 46 bbl of fluid was taken at the cement unit. The total bleed volume between Events 2 and 5 was 65 bbl, which may be attributed (in total or in part) to the leakage through the annular. During this time, the well was underbalanced (bottom-hole EMW of 11 ppg or less), with a possible influx from the formation.

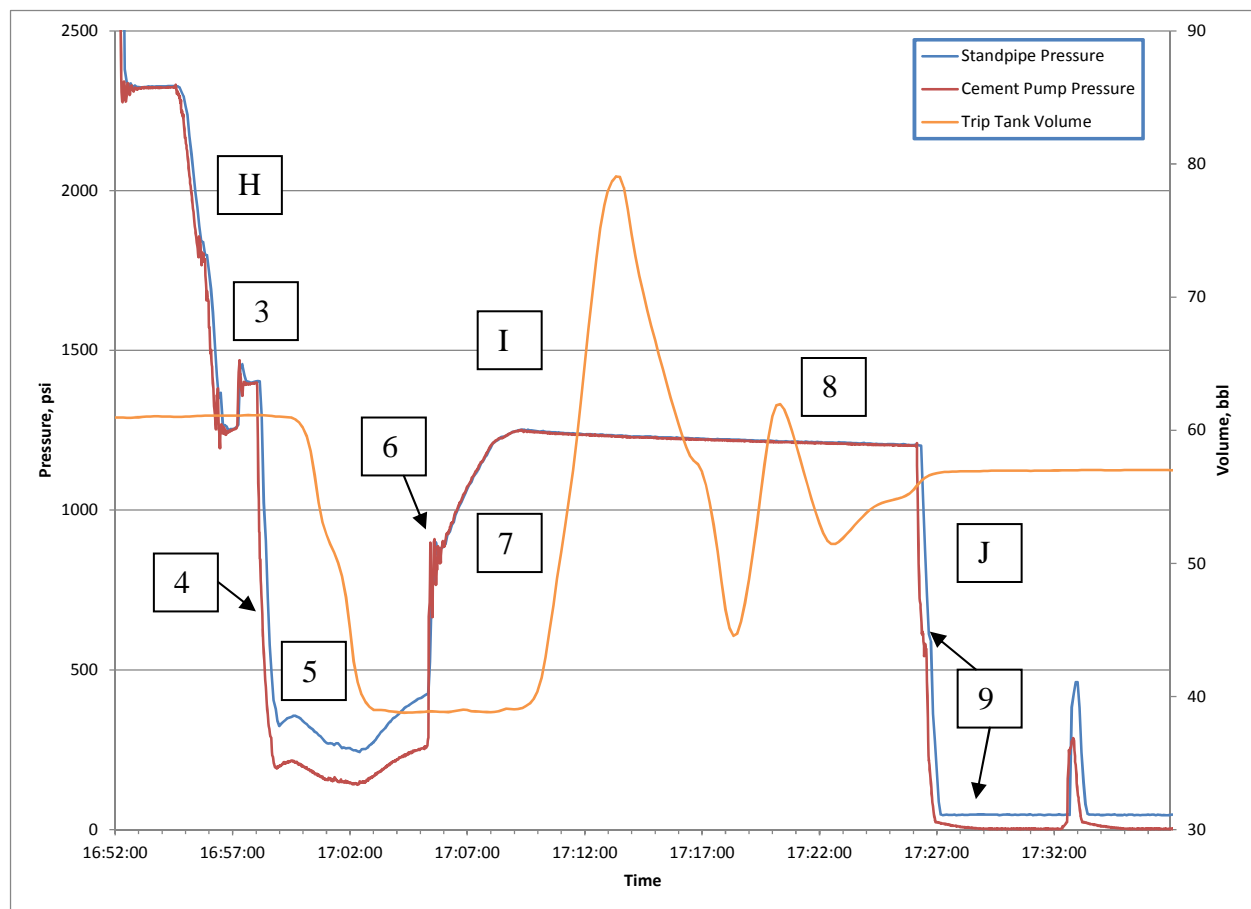


Figure 32: Trip tank activity following annular preventer leakage

Examination of the standpipe and cement pump pressures provides evidence of significant flows during this period. Since neither pressure reached zero psi during the bleed interval from 16:59 to 17:05, it is likely that fluid was flowing through the work string and chiksan lines. Additionally, the two pressure signals differed by approximately 150 psi over the interval,

whereas they are closely matched during other periods (see Figure 32). Since the two pressure gauges are physically separated by a long line length, the pressure difference is an indicator of flow through the line.

Event 6 (see Figure 26 and Table 23): At 17:05 the work string was shut in, causing a rebound in standpipe pressure. In addition, the closing hydraulic pressure on the annular preventer was increased, causing it to seal and halting the leakage flow from the riser into the BOP.

Event 7 (see Figure 26 and Table 23): With the work string shut in, flow from the well (and possibly residual leakage through the annular preventer) caused an additional increase in standpipe pressure. From 17:06 to 17:10, the pressure increased from 900 to 1,250 psi.

The BOP kill line valve remained open during this time. As the well pressure increased, the kill line manifold pressure transitioned from vacuum to a slight positive pressure of 18 psi. At some point after this time, the kill valve was closed.

Event 8 (see Figure 26 and Table 23): From the peak of 1,250 psi the standpipe pressure gradually decayed over 17 minutes, reaching a final value of 1,202 psi before being bled off. The calculated well state for this point is 136 bbl spacer and 29 bbl seawater in the work string-to-casing annulus below the annular preventer. The calculated bottom-hole EMW is 12.74 ppg, slightly above the formation pressure of 12.6 ppg. A sketch of the fluid positions for this state is given in Figure 31, right diagram.

Event 9 (see Figure 26 and Table 23): At 17:26 the work string was again opened to bleed it to the cement unit. This time the standpipe pressure dropped to zero psi, presumably due to the lack of annular preventer leakage flow. Following the bleed, the work string was left open to the cement unit for several minutes, from 17:27 to 17:32. No direct measure of the total bleed volume is available; however, information provided by Transocean indicated a volume of approximately 15 bbl at this time [21].

During this event, the well was again in an underbalanced state, with a calculated bottom-hole EMW of 11.53 ppg. As such, it is likely that some or all of the volume taken during the bleed was pushed up the work string from below by the formation pressure. A diagram of this well state is given in Figure 33 (left).

Event 10 (see Figure 26 and Table 23): At approximately 17:32, with the work string open and flowing, both the upper and lower kill valves (surface and BOP) were opened, placing the kill line in fluidic communication with the work string through the work string-to-casing annulus. Due to the heavy fluid weight in the annulus, fluid began to flow out the kill line, into the BOP and work string-to-casing annulus, and out through the work string (“U-tube” flow). This created an air pocket in the upper portion of the kill line. Shortly after opening, the kill valves were closed again.

As in the analysis of Event 5, unequal standpipe and cement unit pressure readings provide evidence of flow to the cement unit during this period (see Figure 32).

Information provided by Transocean indicates that the volume that flowed out of the kill line (into the BOP and annulus and taken at the surface through the work string) during this period was 3 to 4 bbl [21]. Figure 33, right diagram illustrates this fluid position.

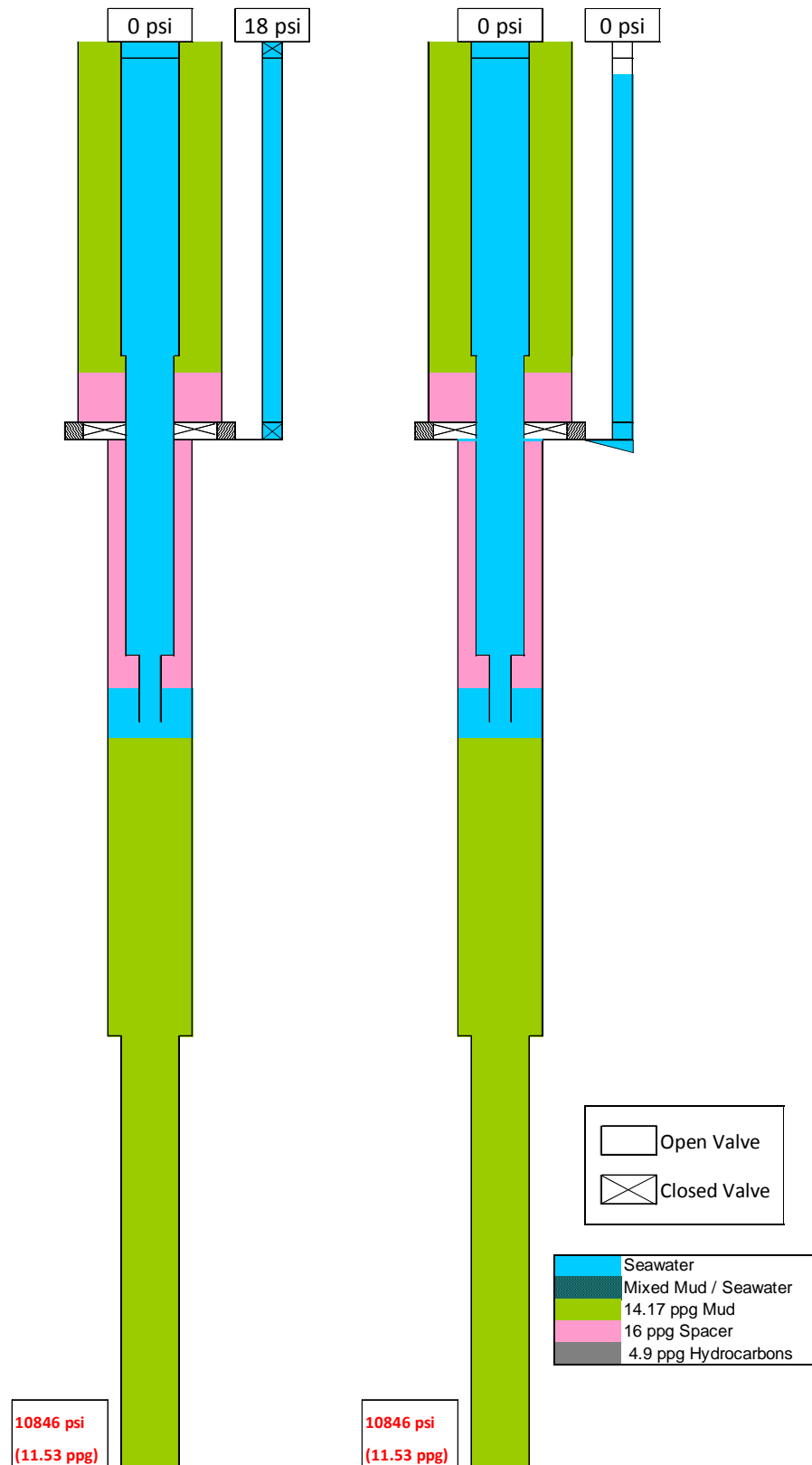


Figure 33: Well fluid states during negative testing: 17:28 (left); 17:33 (right)

Event 11 (see Figure 27 and Table 25): After the kill line U-tube, the lineup was changed to perform the negative test on the kill line rather than on the work string (the lineup to this point had been for the latter case) [21]. During the change, it is likely that both the standpipe and cement unit pressure gauges were isolated from the work string via closure of one or more test sub valves and / or the IBOP between the work string and standpipe manifold (see Figure 28).

Because the well was underbalanced at the time the gauges were isolated, it is probable that pressure in the well and work string was building during the 19-minute interval, following a trend similar to that observed in a later pressure build-up (Event 14).

Event 12 (see Figure 27 and Table 25): Evidence for the pressure build-up suggested in Event 11 was provided when the test sub was opened again after the lineup change at 17:52. At this time, the cement pump pressure spiked rapidly to approximately 770 psi. No commensurate pressure response was measured at the standpipe manifold, presumably because the IBOP was still closed (see Figure 28).

Event 13 (see Figure 27 and Table 25): After observing the spike, the pressure was bled off by opening the work string to the cement unit. Information provided by Transocean indicates that approximately 3-15 bbl were bled back at this time [21] (SES uses a volume of 7 bbl herein for calculation purposes). Following the bleed, the cement unit was shut in at 18:00.

Hydrostatic analysis of the wellbore at 18:00 indicates a bottom-hole EMW of 11.56 ppg, which is underbalanced to both hydrocarbon formations. A sketch of this state is shown in Figure 34, left diagram.

Event 14 (see Figure 27 and Table 25): With the cement unit shut in, the formation pressure again acted to increase the pressure in the wellbore. Over a period of 31 minutes, the cement pump pressure increased from zero to 1,182 psi. This surface pressure corresponds to a bottom-hole EMW of 12.81 ppg, partway between the two formation pressures (see Figure 34, right diagram).

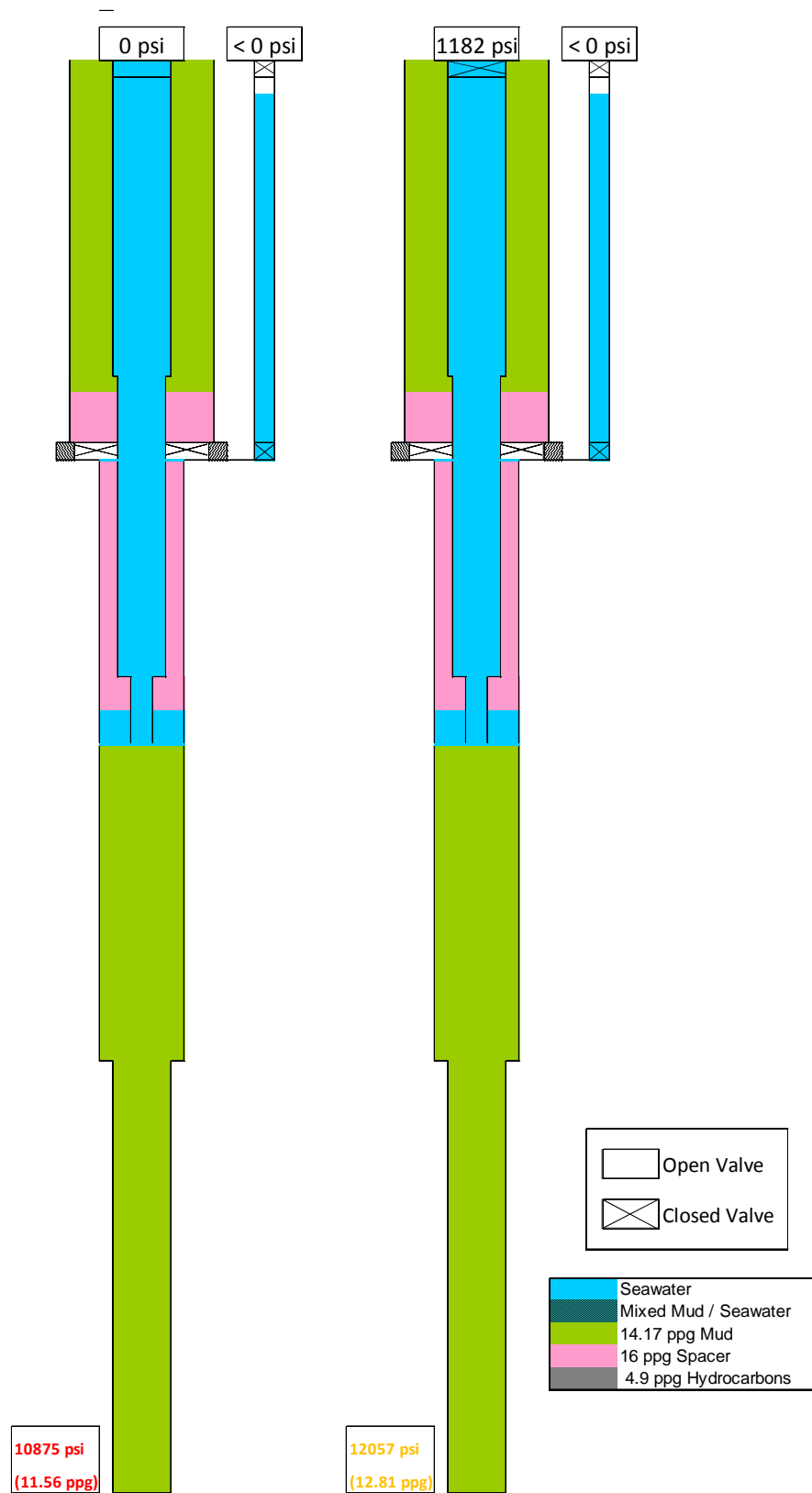


Figure 34: Well fluid states during negative testing: 18:00 (left); 18:31 (right)

A notable observation regarding the build-up from 18:00 to 18:31 is the short pressure transients occurring at regular intervals of 1 to 2 minutes over the duration (see Figure 35). A possible physical explanation for these transients is a “stick-slip” behavior from the wiper plug being pushed up the casing by formation pressure from below.

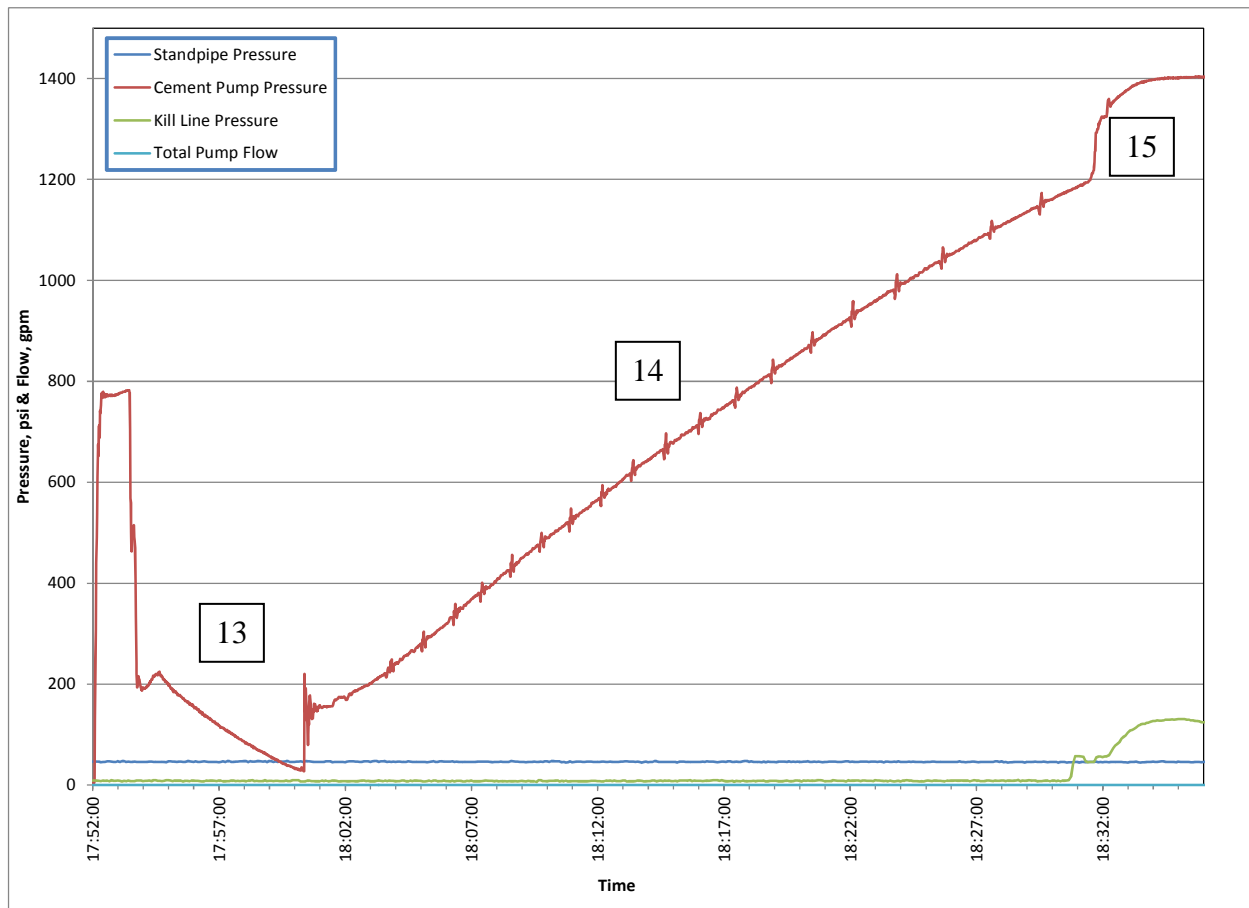


Figure 35: Detailed view of pressure signals recorded during build-up, 18:00 to 18:31

Event 15 (see Figure 27 and Table 25): At 18:31, the kill valve at the BOP was opened, adding the weight of the fluids in the kill line to the annulus. At this point, a peculiar pressure response was observed: Both the work string pressure (measured at the cement unit) and the kill line pressure increased, to 1,404 and 137 psi, respectively (see Figure 35).

An expected response for this type of action would be a pressure increase in one line and a decrease in the other, similar to the behavior recorded during Event 3. Physically, the only

mechanism to produce a pressure increase on both these lines is the application of a common pressure to the wellbore via some source. SES found no evidence of such a pressure being applied from the surface; for example, from a pump or a release of trapped pressure on the rig.

Discounting a source of pressure from the surface, the only remaining source is from the formation itself. Reviewing the calculations from prior negative test events with the work string shut in at the surface, the bottom-hole EMW is generally seen to increase over time. The calculated bottom-hole EMW for Event 15 is 13.05 ppg, a further increase, and very close to the formation pore pressure of 13.1 ppg. See Figure 36, left diagram.

A physical explanation for this increasing trend is a progressively exposed pay zone. Under this scenario, during the first underbalance of the well at approximately 17:00 a small portion of the formation was in communication through the well via some mechanism (for example, a channel in the cement). During successive pressurizations and bleeds (Events 6, 8, 9, 11, 13, 14), formation exposure incrementally increased due to the varying pressure differential across the cement, float equipment, and casing.

Employing this physical scenario, the sudden increase in work string and kill line surface pressures may be explained by a corresponding increase in formation exposure to the well, via some mechanical means. Subsequent to this point, the cement pump pressure remained relatively stable, indicating that “full” exposure to the formation had likely been achieved.

Based on hydrostatic analysis, the calculated increase in kill line pressure that matches the observed work string pressure (as measured at the cement unit) of 1,404 psi is 298 psi. The measured kill line pressure is lower: 137 psi. A possible explanation for the difference is the fact that the spacer in the annulus and BOP had been left in a relatively static state for over an hour at seafloor temperatures (approximately 40°F); thus, it is likely that it had built up gel strength by this time. The gelled spacer may have formed a plug that prevented full transmission of the well pressure up the kill line.

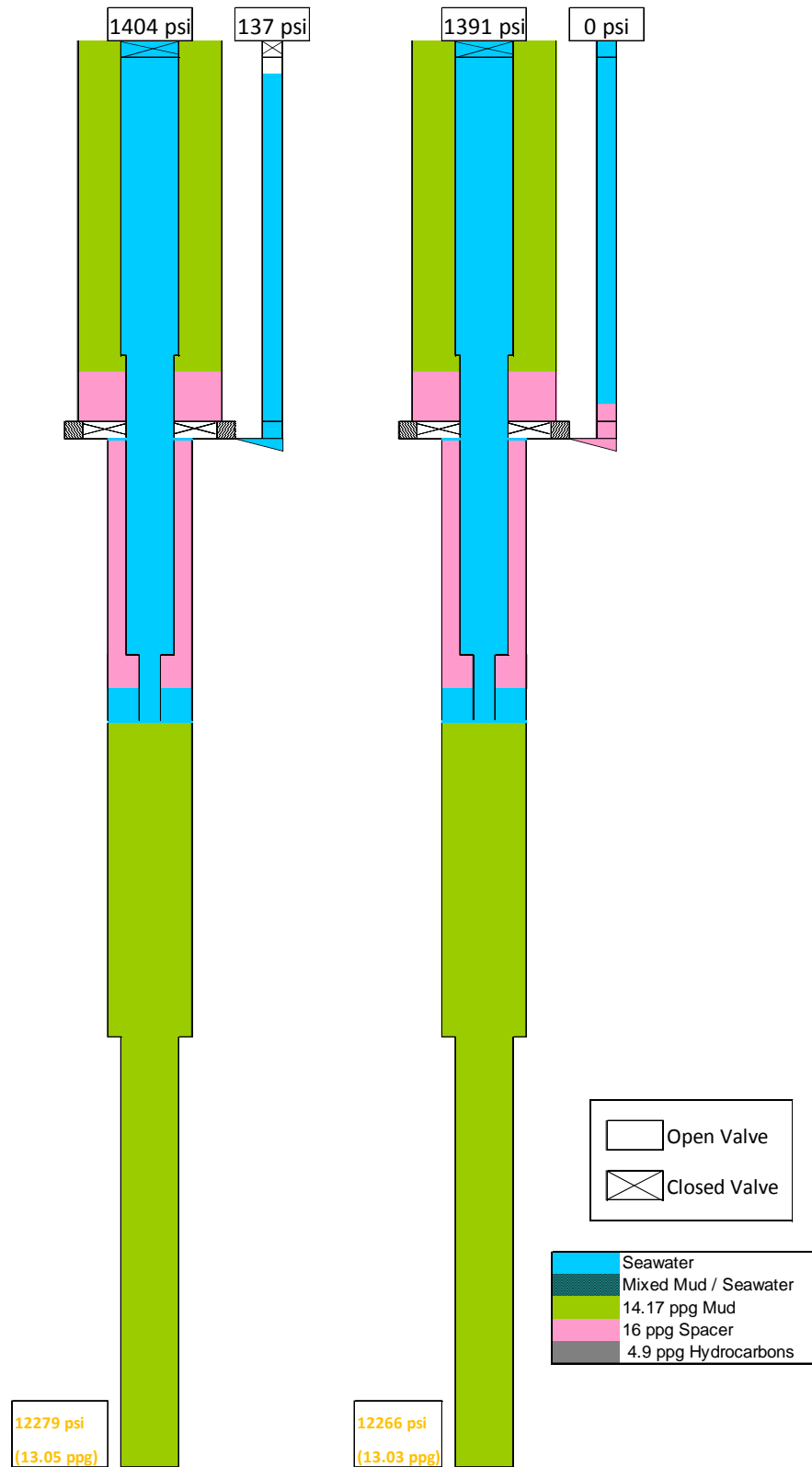


Figure 36: Well fluid states during negative testing: 18:37 (left); 19:50 (right)

Event 16 (see Figure 27 and Table 25): At approximately 18:42, a sudden spike in kill line pressure to 489 psi was recorded, accompanied by minor pump activity (2 strokes pumped on rig pump #3; theoretical volume of 0.25 bbl). This activity has been identified as pumping into the kill line, based on information provided by Transocean [21]. However, because no pressure response was observed on the cement pump pressure during the kill line pumping, SES concludes that one or more kill line valves were closed during this event: either a surface valve and / or the lower valve at the BOP. In either case, it is unlikely that any significant flow into the kill line occurred.

Immediately after pumping, the kill line pressure was bled off at the surface, stabilizing at approximately 53 psi.

Event 17 (see Figure 27 and Table 25): During the pumping of Event 16, the cement pump pressure remained stable at approximately 1,400 psi. At 18:48 and 19:00, two nearly identical perturbations occurred in the cement pump pressure signal: The pressure suddenly dropped to 1,350 psi, then built back up to 1,390 psi over a two-minute period. No corresponding response from the kill line was observed.

Even though no supporting information exists, SES interprets these events as mechanical interventions on the work string by the rig personnel at the surface (i.e. brief bleeds and closures). In each case, well pressure caused the cement pump pressure to recover after the initial bleed.

The lack of response in the kill line pressure provides further evidence that the BOP kill valve was indeed closed during the pumping of Event 16 (implying that it remained closed during this event). Alternatively, if the surface kill valve had been left open after the bleed-off following pumping, a relief path may have been present which prevented pressure changes in the kill line as the work string was bled. In this case, the surface valve would need to have been closed prior to Event 18 (see next section).

Event 18 (see Figure 27 and Table 25): At 19:07, the kill line pressure increased to 122 psi, accompanied by a small drop in cement pump pressure to 1,371 psi (from 1,390 psi). The response here is similar to Event 16; therefore, SES interprets this event as the opening of the kill valve at the BOP, against an initially closed surface valve.

At approximately 19:12 the surface kill line valve was opened, opening a flow path to the well through the work string-to-casing annulus. According to information provided by Transocean, a small amount of liquid (approximately 0.2 bbl) flowed out the kill line, and reportedly stopped [21].

The most likely explanation of the recorded behavior is that the opening of the surface kill valve resulted in some amount of 16 ppg spacer being drawn into the kill line, providing additional head to balance the pressure from the wellbore. Via this action, the volume from the air pocket created in the kill line (see Event 10) was forced out, followed by a small amount (0.2 bbl) of seawater.

Event 19 (see Figure 27 and Table 25): From 19:15 to 19:54, the cement pump and kill line pressures remained steady at 1,391 and 25 psi, respectively. This event is interpreted to be the actual negative test, as conducted on the open kill line. The flow and cement pump pressure appear to have been monitored for more than 30 minutes, with no flow increase or pressure change. This outcome was interpreted as a passing negative test.

SES was able to find a precise hydrostatic solution for this event; however, the volume of spacer drawn up the kill line (during the bleed of Event 18) required to achieve this result was 22 bbl. This large volume is not corroborated by witness accounts, either for this event or for Event 10 (in which the air pocket volume was created). In light of this, a more consistent explanation would involve either a plug of gelled spacer in the kill line (as explained in Event 15), or possibly the accidental re-closure of the BOP kill line valve. A schematic of the former scenario is given in Figure 36, right diagram.

Event 20 (see Figure 27 and Table 25): After the negative test was deemed successful, the rig pumps were activated briefly to equalize the standpipe manifold pressure with the cement unit (and work string) pressure. At this point, the IBOP and / or test sub valves were opened (see Figure 28) and the work string pressure was bled off, which briefly returned the well to an underbalanced condition.

4.3.3 Kill Line Valve Status Summary

In the preceding discussion, references to kill line valves which were opened or closed are inferred (by SES) from the measured pressure responses, hydrostatic calculations, and witness statements as appropriate. For reference, Table 26 indicates the inferred status of the surface and BOP kill line valves during the negative testing events.

Table 26: Summary of inferred kill line valve status during negative testing

Time	Event (s)	Surface Kill Valve Status	BOP Kill Valve Status
16:54	1, 2	Closed	Closed
16:57	3 – 5	Closed	Open
17:10	6 – 9	Closed	Closed
17:32	10	Open	Open
17:33	11 – 14	Closed	Closed
18:30	15	Closed	Open
18:40	16	Open	Closed
18:48	17	Closed*	Closed
19:07	18	Closed	Open
19:15	19	Open	Open*
~20:00	20	Closed	Closed

* Valve status at this time is not definitive. See prior event discussion for further details.

4.4 Second Displacement of Seawater after Negative Testing

Following the negative test activity, pumping of seawater was resumed at 20:02 in order to complete the displacement of the riser. As the pumps were brought up, the annular BOP was opened, bringing the well back to an overbalanced state. At approximately 21:09, the pumps were shut down for the static sheen test.

An overview plot of the pressure, flow, and hook load signals recorded during the displacement is given in Figure 37.

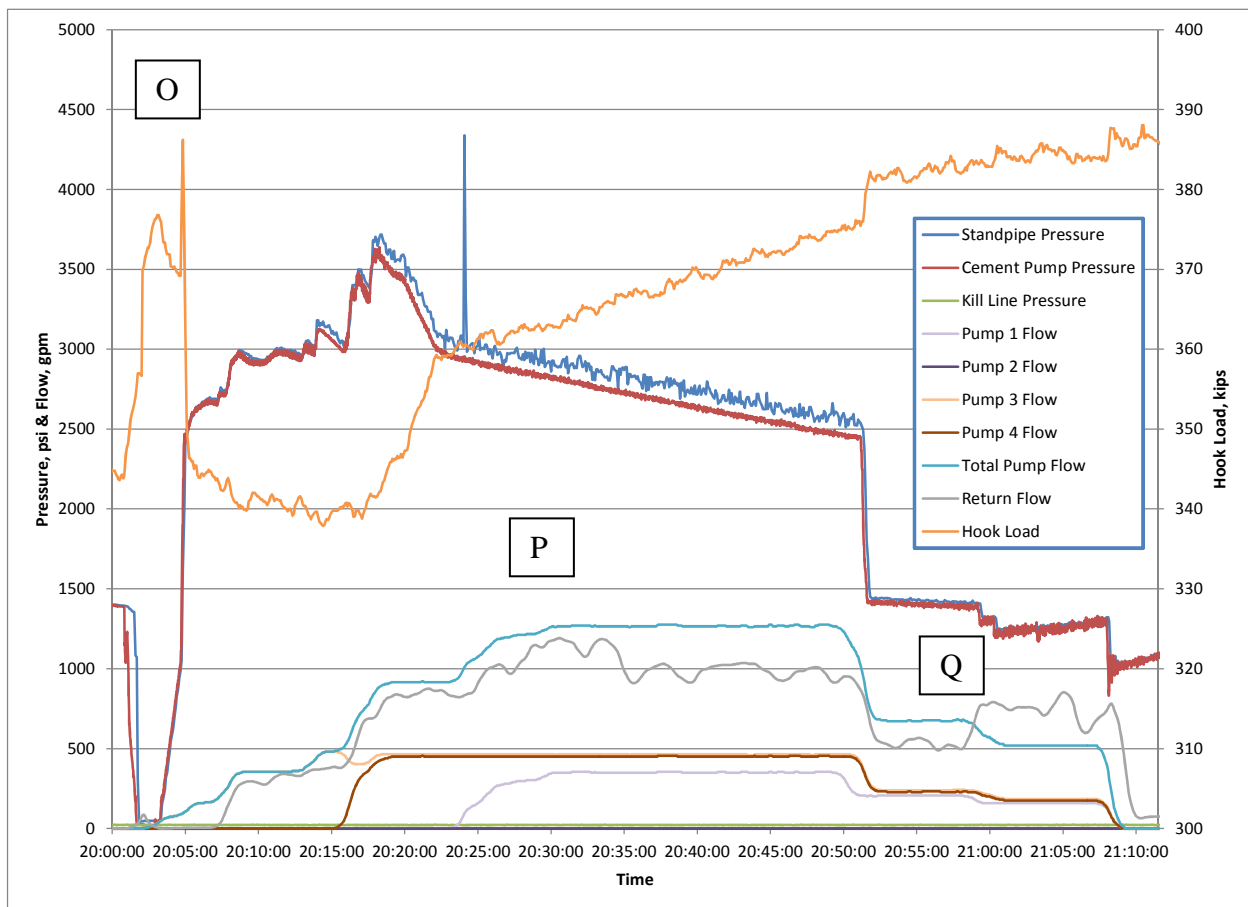


Figure 37: Overview of signals recorded during second seawater displacement

Table 27: Description of events from 20:00 to 21:08

Event	Description	Time
O	Open annular preventer and resume seawater displacement	20:02 to 20:22
P	Activate booster line pump; dump trip tank	20:22 to 20:52
Q	Slow pump rates; dump trip tank, standpipe pressure builds	20:52 to 21:08

4.4.1 Strokes Pumped

Rig pumps #3 and #4 were used to continue the riser displacement through the work string. Shortly thereafter, rig pump #1 was activated to provide additional displacement flow through the booster line. The telemetry data files indicate that 8,103 strokes were pumped on pumps #3 and #4, while 2,255 strokes were pumped on rig pump #1 (see summary tables below). Referring to the mud pump anticipated efficiency in Table 51 (see Appendix A), the anticipated pump volumes were 1,021 and 284 bbl, respectively, for a total volume of 1,305 bbl.

Table 28: Pump output summary, seawater displacement through work string

Time	Pump Strokes (Pumps 3 & 4)	Theoretical Output	Anticipated Output	Anticipated Volume
20:02	6,415	0.13113 bbl/stk	0.126 bbl/stk	808.3 bbl
21:09	14,518	0.13113 bbl/stk	0.126 bbl/stk	1,829 bbl
<i>Interval</i>	<i>8,103</i>	<i>0.13113 bbl/stk</i>	<i>0.126 bbl/stk</i>	<i>1,021 bbl</i>

Table 29: Pump output summary, seawater displacement through booster line

Time	Pump Strokes (Pump 1)	Theoretical Output	Anticipated Output	Anticipated Volume
20:02	0	0.13113 bbl/stk	0.126 bbl/stk	0 bbl
21:09	2,255	0.13113 bbl/stk	0.126 bbl/stk	284.1 bbl
<i>Interval</i>	<i>2,255</i>	<i>0.13113 bbl/stk</i>	<i>0.126 bbl/stk</i>	<i>284.1 bbl</i>

4.4.2 Pit Returns

At approximately 17:10 (a few minutes after the end of the first displacement), the transfer of mud from the active pits to auxiliary pits and the offshore supply vessel ceased. Therefore, by the beginning of the second displacement at 20:02, the well returns could once again be measured directly from the pit volume telemetry. The data recorded over the displacement is plotted in Figure 38, and a tally of the return flows is given in Table 30.

The returns were redirected twice over the pumping interval. Initial returns from 20:02 were taken in pits #9 and #10. The active flow was then directed to pit #7 at 20:33, and finally to pit #6 at 20:48. Following the displacement, excess volume in pits #9 and #10 was transferred to pit #6 from 21:10 to 21:17. This transfer volume is not included in the return tally.

As during the first riser displacement, the apparent return flow was misleading due to trip tank activity (see Figure 38). The initial trip tank volume was 46.5 bbl at the onset of the displacement. The tanks were partially emptied into the flow line from 20:27 to 20:36, but were immediately filled to 46.7 bbl from 20:36 to 20:55¹¹. They were then emptied again at 20:58. The net volume addition to the active system was 42.7 bbl.

The final return volume tally from the pit data is 1,160 bbl. However, in later sections it will be shown that this total also includes 61 bbl of influx volume from the formation, which was flowing during the latter half of the displacement. As such, to obtain the actual pumped volume, the well influx volume must be subtracted from the total to obtain a result of 1,099 bbl.

Comparing with the expected 1,305 bbl based on pump strokes, the calculated volumetric efficiency for the three pumps used is 80.9%. Applying the previously calculated efficiency of 89.0% to rig pumps #3 and #4, the resulting efficiency of pump #1 is 51.9%. This result is very close to the estimated efficiency of 52.2% calculated in Section 4.1.1.3.

¹¹ It is suspected that the trip tank circulation lines were inadvertently left open, or partially open, to the flow line after the tanks were initially emptied. This caused the tanks to fill slowly with return flow over a 20-minute period.

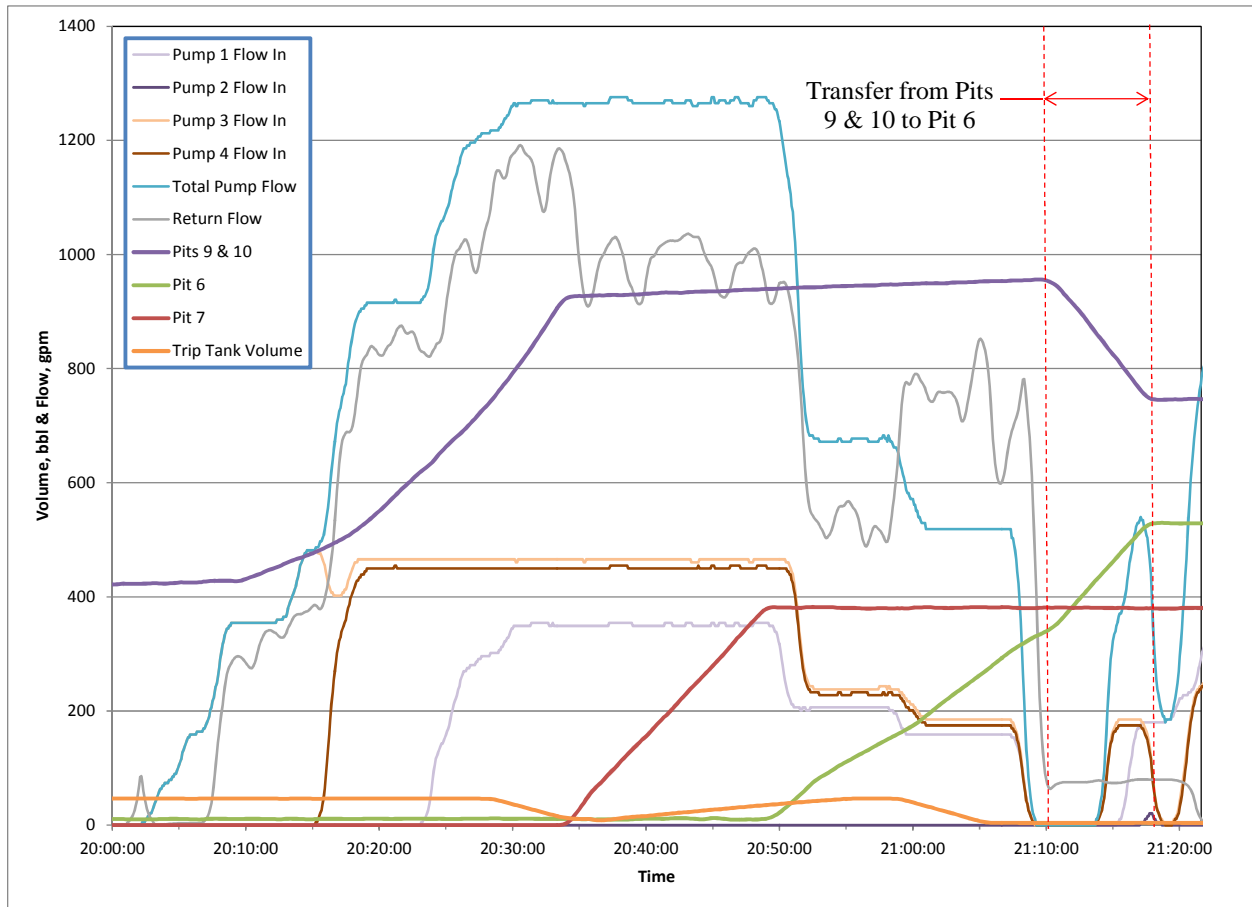


Figure 38: Pit and flow sensor return data during second seawater displacement

Table 30: Pit return volume tally during second seawater displacement

Time	Pit(s)	Volume Gain
20:02 to 20:33	9 & 10	497 bbl
20:33 to 20:48	7	380 bbl
20:48 to 21:10	6	326 bbl
Less Trip Tank Activity		-43 bbl
Total Returns		1160 bbl
Less well influx volume		-61 bbl
Total Pumped Volume		1099 bbl

4.4.3 Riser Flow Out

Integrating the Sperry-Sun flow sensor data over the displacement interval indicates a return volume of 1,155 bbl, compared to the anticipated pump volume of 1,305 bbl. Subtracting the volume from the trip tank activity and well influx gives a result of 1,051 bbl, implying an overall pump volumetric efficiency of 77.4%.

Using the measured pit return volume from Section 4.4.2 as a reference, the corrected flow sensor returns appear to be in error by approximately -4.0%. This error is 3.5% less than that obtained for the spacer displacement (see Section 4.2.3).

Table 31: Pump analysis summary, second seawater displacement

Strokes Pumped (Pumps 1, 3 & 4)	10,358
Return Volume (from flow sensor)	1,051 bbl
Return Volume (from pit returns)	1,099 bbl
Theoretical Pump Output (Pump 3 & 4)	0.13113 bbl/stk
Volumetric Efficiency (based on flow sensor)	77.4%
Volumetric Efficiency (based on pit returns)	80.9%

Simulation results of well flow over the second seawater displacement, using rig #3 and #4 pump stroke data scaled by a volumetric efficiency of 89.0% and pump #1 scaled to 52%, are presented in Figure 39. The measured flow sensor data are indicated in red, while a corrected version of the data in which the flow rate from the trip tank activity is subtracted, is shown in green. The simulated results are generally in good agreement with the corrected measurements, with two exceptions. First, the simulated flow out does not match the corrected data during the first trip tank dump. Second, the simulated flow out does not capture the sudden increase in well flow at the end of the pumping event. As discussed previously, the well was underbalanced and flowing at this time, and the simulation does not model formation inflow.

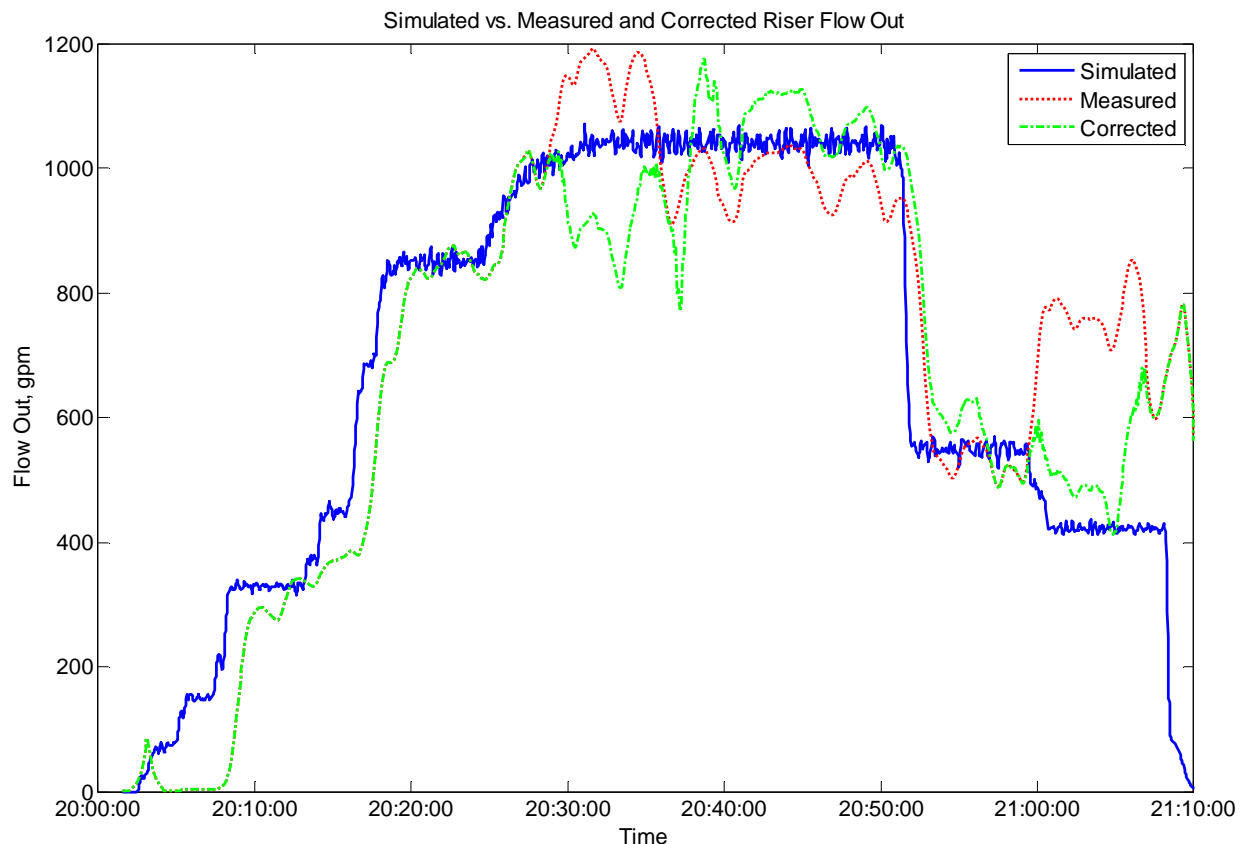


Figure 39: Simulated vs. measured flow out of riser during second seawater displacement

4.4.4 Pressure Response

The pressure response from the same simulation, plotted against the measured standpipe pressure, is presented in Figure 40. The simulation model does not include the bleed-off and associated transients that occur at 20:02, but converges with the measured pressure shortly thereafter.

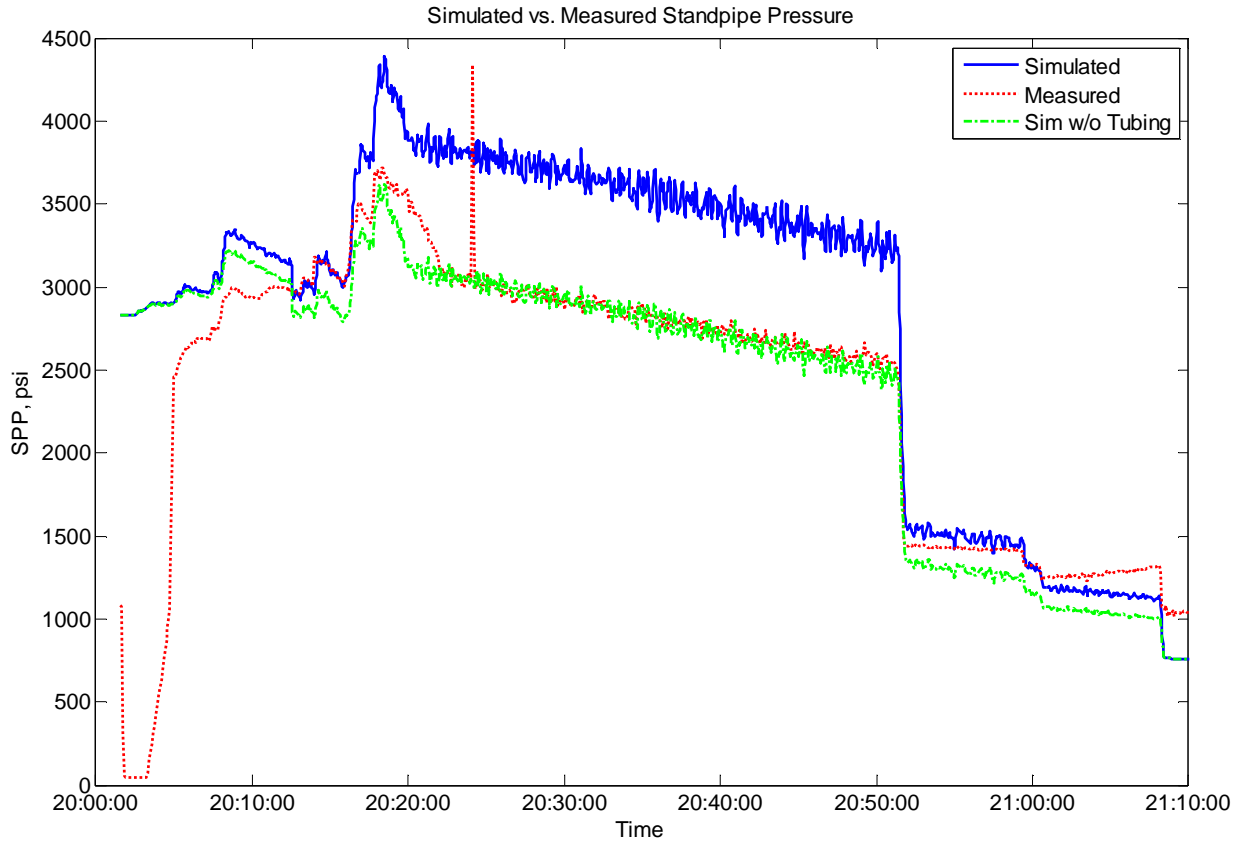


Figure 40: Simulated vs. measured standpipe pressure during second seawater displacement, with tubing washout scenario

The raw simulation results were found to be discrepant with respect to the measured standpipe pressure data during the middle portion of the pumping. A variety of modifications to the model and input flow rates were attempted to try to obtain a match, but only one was found which produced acceptable agreement in both standpipe pressure and flow. This modification is shown in green in Figure 40, and simulates the effect of the removal of a portion of the 3 ½” tubing section from the hydraulic flow path.

The most likely physical phenomenon that could cause such a removal is a washout (i.e. a flow-induced opening in the tubing wall due to high flow velocity) at some point along the tubing length.

A frictional analysis of the work string and annulus flow path reveals that the 3 ½” tubing ID is the dominant source of frictional pressure drop when pumping into the work string. The second most significant source is the annulus formed by the OD of the 5 ½” drill pipe and the production casing ID. All other sections of the flow path provide relatively minor contributions to the total frictional loss. The removal of a portion of the 3 ½” tubing thus has a significant effect on the magnitude of the pressure response during the displacement, but affects neither the flow rates nor the hydrostatic gradients observed during the displacement (because both the work string and the annulus are filled with seawater at this time).

It is also important to note that the flow velocities occurring in the 3 ½” tubing at the time of the presumed washout were quite high. At 20:20, the pump flow rate of approximately 900 gpm (scaled by the reduced volumetric efficiency) would have produced a flow velocity in the tubing in excess of 40 ft/sec. By comparison, piping design standards such as API RP-14E [2] recommend a maximum flow velocity of 15 ft/sec. It is therefore conceivable to experience a washout under these velocity conditions.

Comparing the modified simulation results to the measured standpipe pressure data, the two results begin to diverge slightly starting at about 20:40. This observation may be compared to the simulated bottom-hole EMW results in Figure 41, which indicate that the well became underbalanced to the 13.1 ppg formation at 20:38, and to the 12.6 ppg formation at 20:52. If both formations had been exposed to the well during the negative test activity, the divergent pressure response would match the 13.1 ppg underbalance event.

The results of the analysis indicate that the well may have become underbalanced as early as 20:38, but was certainly underbalanced by 20:52. The well remained underbalanced to the formation from this time through the end of transmission at 21:49.

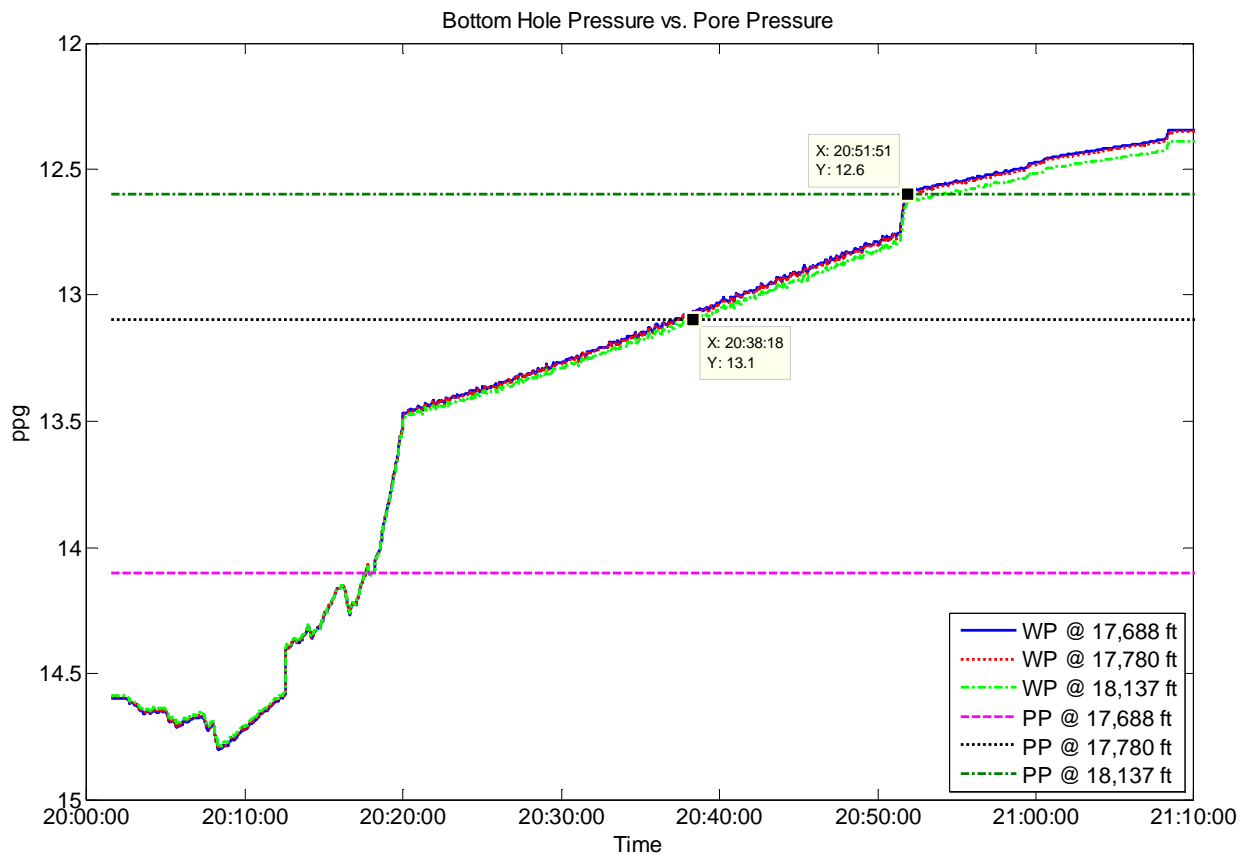


Figure 41: Simulated bottom hole pressures during second seawater displacement, with formation balance points labeled

Simulated liquid boundary positions for the post-negative test seawater displacement are presented in Figure 42. The most significant observation from these results is that the spacer did not reach the top of the riser upon shutting down the pumps for the static sheen test at 21:09. The simulated results place the top of the spacer at a depth of 848 ft, or a volume of 276 bbl, short of the rig floor.

As was noted earlier, the simulation results do not include the effects of well influx. However, a hydrostatic analysis that considered the influx volume (see next section) resulted in an additional volumetric increase of 61 bbl. Incorporating this value into the fluid boundary analysis, the top of spacer is still short by 215 bbl.

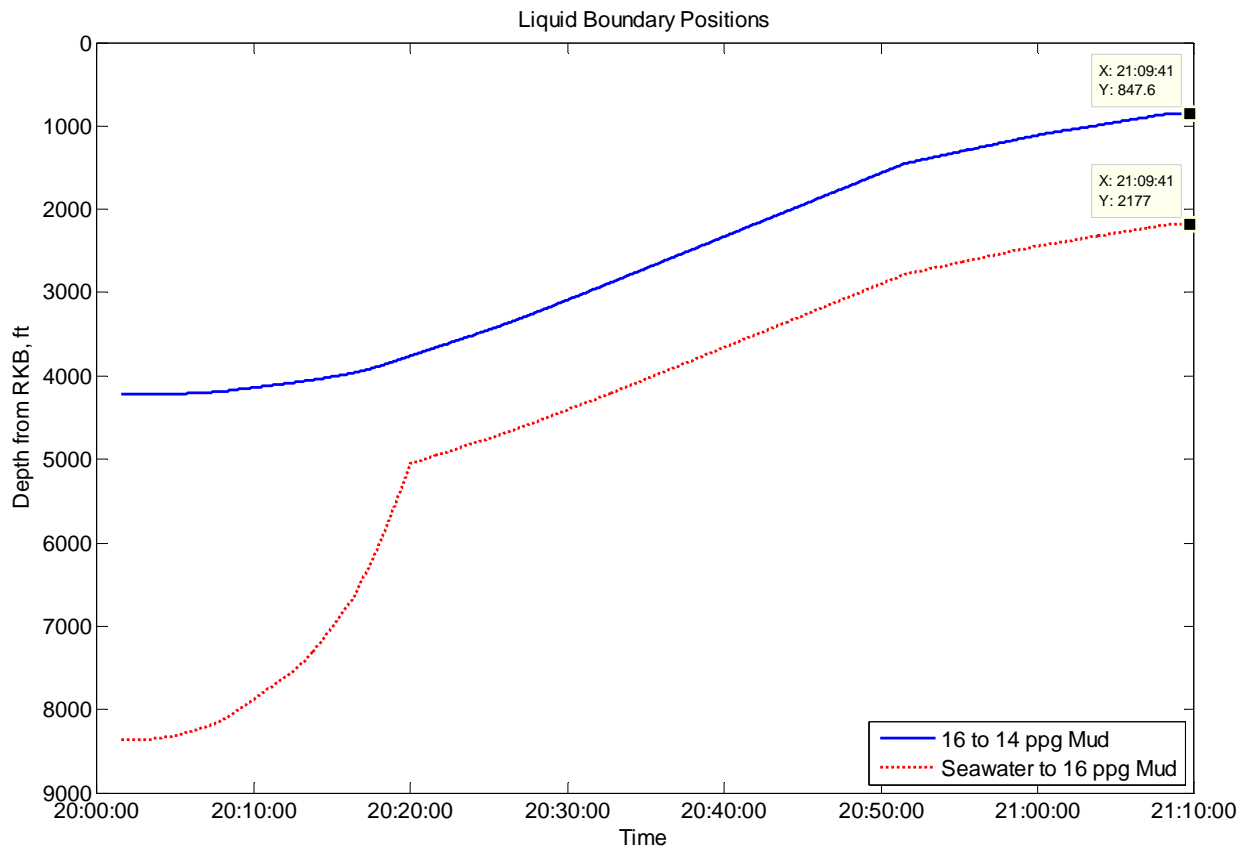


Figure 42: Simulated spacer-to-mud and spacer-to-seawater liquid boundary positions during second seawater displacement

Fluid state diagrams of three points during the seawater displacement are given in Figure 43. The left diagram shows the hydrostatic state at the onset of pumping at 20:02. The middle diagram shows the fluid positions at the balance point with the 12.6 ppg hydrocarbon formation at 20:52 (note that the indicated standpipe pressure is based on a hydrostatic calculation only and does not include pump friction). The right-hand diagram shows the well state at the end of pumping at 21:09 as calculated without hydrocarbon influx from the well. The calculated standpipe pressure of 675 psi was used as a reference case to derive the amount of hydrocarbon influx needed to produce the actual measured pressure of 1,013 psi.

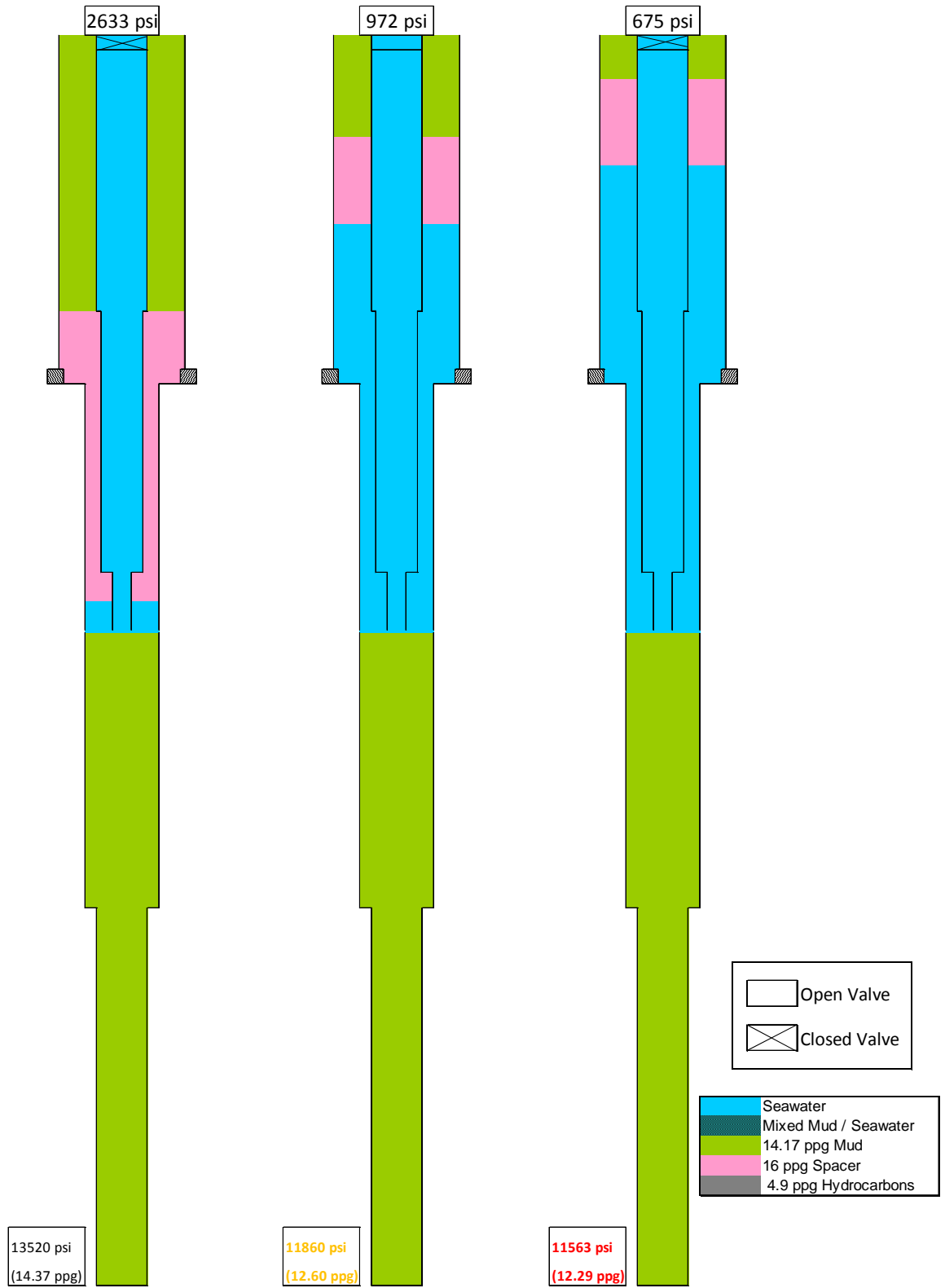


Figure 43: Well fluid states during the post-negative test seawater displacement: 20:02 (left); 20:52 (middle); 21:09 (right, note no well influx)

4.4.5 Estimated Hydrocarbon Influx Volume

Because the well became underbalanced during the seawater displacement, and had been flowing during the negative test, it may be concluded that a portion of the return volume taken during the latter part of the displacement was due to influx from one or both hydrocarbon-bearing formations. A direct indicator of well flow is given in Figure 39, where at approximately 21:05 the flow indicated by the corrected Sperry-Sun flow sensor data is far in excess of the input flow.

By comparing the hydrostatic results at the end of the displacement assuming no well influx to the actual measured pressure readings, an iterative solution for the well state with influx was obtained. The iterated variables were the influx volume and mixed fluid density resulting from the mixing of mud pushed up into the work string-to-casing annulus from the well and seawater pumped in from the work string.

The solution found is presented graphically in Figure 44, left diagram¹². The influx volume was found to be 61 bbl, with 71 bbl of mixed fluid in the lower work string-to-casing annulus. The equivalent density of the mixed fluid was 13.4 ppg. The relatively small amount of seawater in this initial mixture indicates that most of the well flow occurred at the end of the seawater displacement, when the pumps were slowed in anticipation of the static sheen test. The flow sensor data (with trip tank flow correction applied) corroborates this assessment.

4.5 Static Sheen Test

Upon shutting down the pumps at 21:09, a static sheen test was performed. The objective of the sheen test was to examine the return fluid for oil-based contamination in preparation for directing the remaining spacer and seawater returns overboard.

A plot of the signals recorded during the static sheen test (21:09 to 21:13) and subsequent seawater displacement is given in Figure 45 (expanded from Figure 8).

¹² In the diagrams presented herein, hydrocarbons are assigned a constant density of 4.9 ppg, which is an initial density of the single-phase fluid at reservoir conditions. As the influx expanded into the wellbore under reduced pressure and temperature, the actual density decreased. The bottom-hole pressures calculated herein with hydrocarbons in the wellbore are therefore overestimates for the given fluid state. Since the well was underbalanced with hydrocarbons present in the wellbore, precise bottom-hole pressures are inconsequential to the discussion.

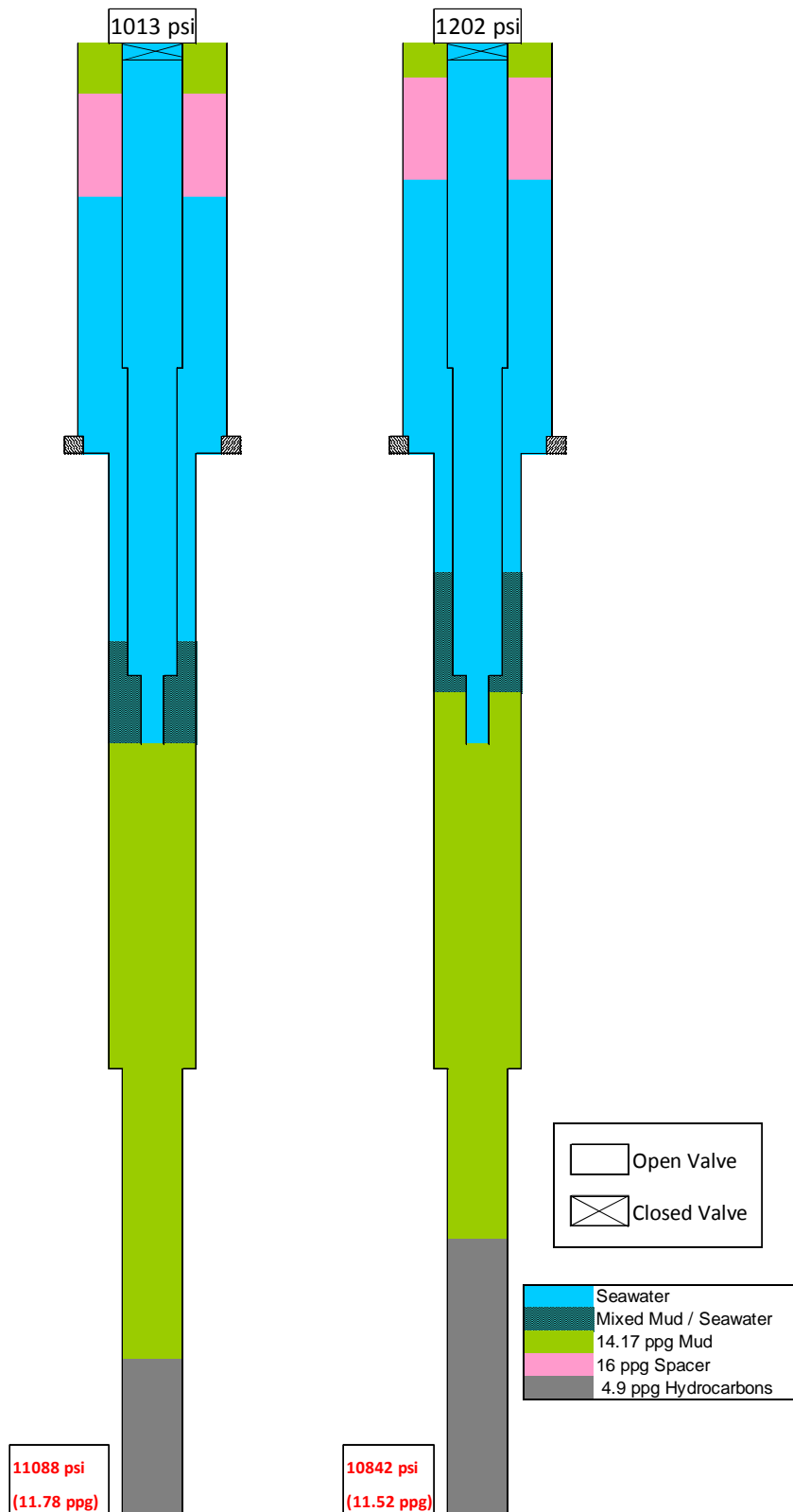


Figure 44: Well state diagrams before and after the static sheen test, with hydrocarbon influx: 21:09 (left); 21:13 (right)

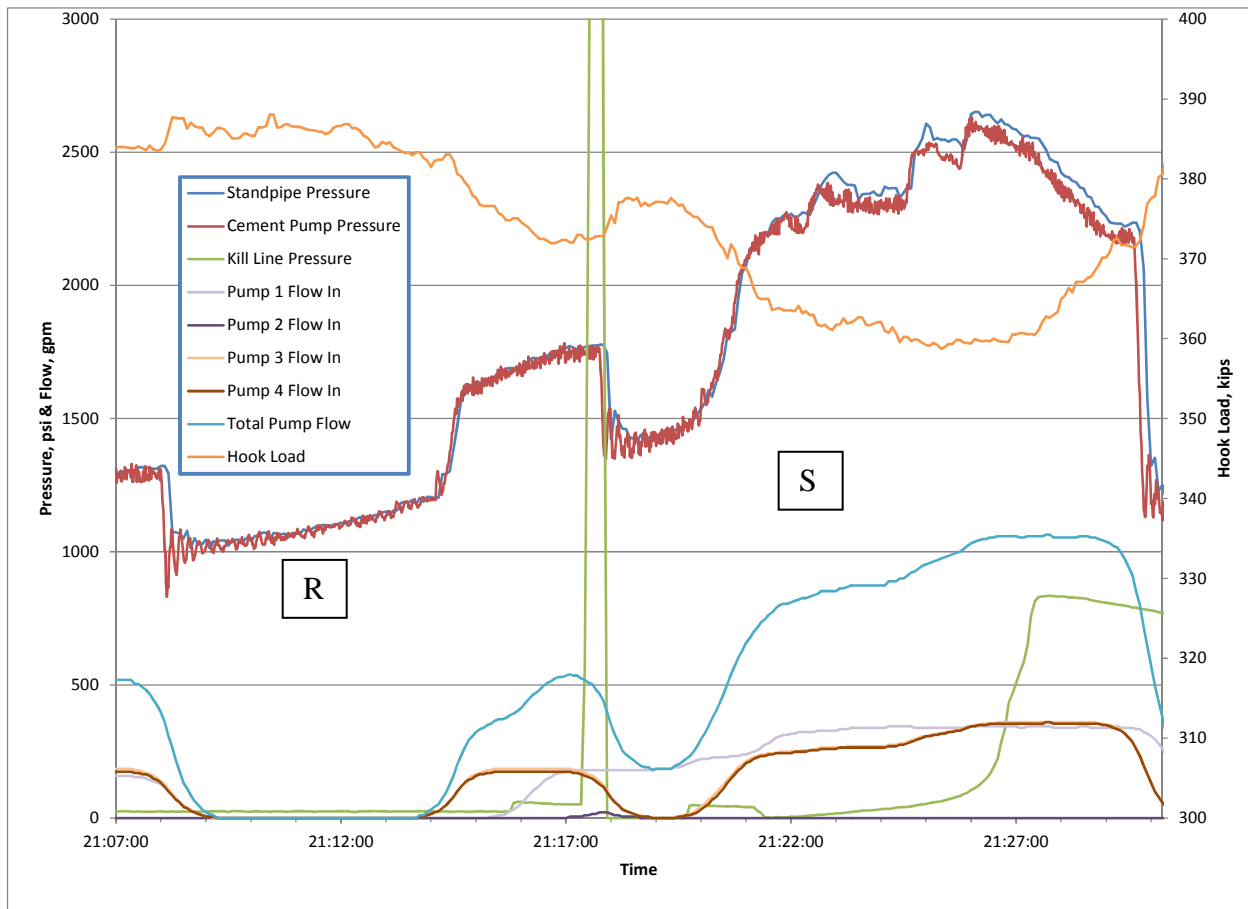


Figure 45: Overview plot of signals recorded during static sheen test and final seawater displacement

Table 32: Description of events from 21:08 to 21:30

Event	Description	Time
R	Static sheen test; standpipe pressure builds	21:08 to 21:13
S	Resume seawater displacement; relief valve blows on pump 2	21:13 to 21:30

4.5.1 Pressure Response

The initial recorded standpipe pressure was 1,013 psi at the beginning of the static sheen test. Over the four-minute test duration, the pressure increased nearly linearly to a final pressure of 1,202 psi just before the pumps were started again.

4.5.2 Estimated Hydrocarbon Influx Volume

Based on the recorded pressure rise, an influx volume was calculated for the static sheen event. Because the pumps were shut down, the well influx pushed pure mud from the lower casing into the work string annulus, making a direct volume estimate possible. The estimated influx over the test is 33 bbl (94 bbl total to this point), and the average well flow rate is approximately 8.25 bpm. The well state solution at the end of the sheen test is shown in Figure 44, right diagram.

4.6 Final Displacement of Seawater After Static Sheen Test

Upon completion of the static sheen test with a reported passing result, well flow returns were directed overboard and displacement of the riser with seawater resumed at 21:13. Directing the returning fluid overboard bypassed the Sperry-Sun flow sensor that provided flow return input to the rig telemetry¹³. As such, with the exception of pump strokes, no valid flow input or output data is available for the remainder of the transmission. The pumps were shut down at 21:30.

See Figure 45 for a plot of signals recorded during the final seawater displacement.

4.6.1 Strokes Pumped

Rig pumps #3 and #4 were used to continue the riser displacement through the work string. Shortly thereafter, rig pump #1 was activated to provide additional flow through the booster line. Rig pump #2 was brought online briefly, but was shut down after only a few strokes due to a blown relief valve (see discussion, next section). The telemetry data files indicate that 1,320 strokes were pumped on pumps #3 and #4, while 777 strokes were pumped on pumps #1 and #2 (see summary tables below). Referring to the mud pump anticipated efficiency in Table 51 (see Appendix A), the anticipated pump volumes were 166 and 98 bbl, respectively, for a total volume of 264 bbl.

Table 33: Pump output summary, seawater displacement through work string

Time	Pump Strokes (Pumps 3 & 4)	Theoretical Output	Anticipated Output	Anticipated Volume
21:13	14,518	0.13113 bbl/stk	0.126 bbl/stk	1,829 bbl
21:30	15,838	0.13113 bbl/stk	0.126 bbl/stk	1,996 bbl
<i>Interval</i>	<i>1,320</i>	<i>0.13113 bbl/stk</i>	<i>0.126 bbl/stk</i>	<i>166.3 bbl</i>

¹³ Although the Sperry-Sun flow sensor was bypassed at this time, data from the Hi-Tec flow sensor was still available to all personnel aboard the rig. See prior discussion in Footnote 4 on page 43.

Table 34: Pump output summary, seawater displacement through auxiliary lines

Time	Pump Strokes (Pump 1)	Theoretical Output	Anticipated Output	Anticipated Volume
21:13	2,255	0.13113 bbl/stk	0.126 bbl/stk	284.1 bbl
21:30	3,032	0.13113 bbl/stk	0.126 bbl/stk	382.0 bbl
<i>Interval</i>	<i>777</i>	<i>0.13113 bbl/stk</i>	<i>0.126 bbl/stk</i>	<i>97.9 bbl</i>

4.6.2 Pressure Response

A simulated pressure response is shown in Figure 46. Here the intent of the simulation is not to replicate the actual measured standpipe pressure, but rather to illustrate the effect of the well influx on the standpipe pressure. As may be observed in the figure, the measured signal diverges considerably from the simulated case, which again does not model the well influx.

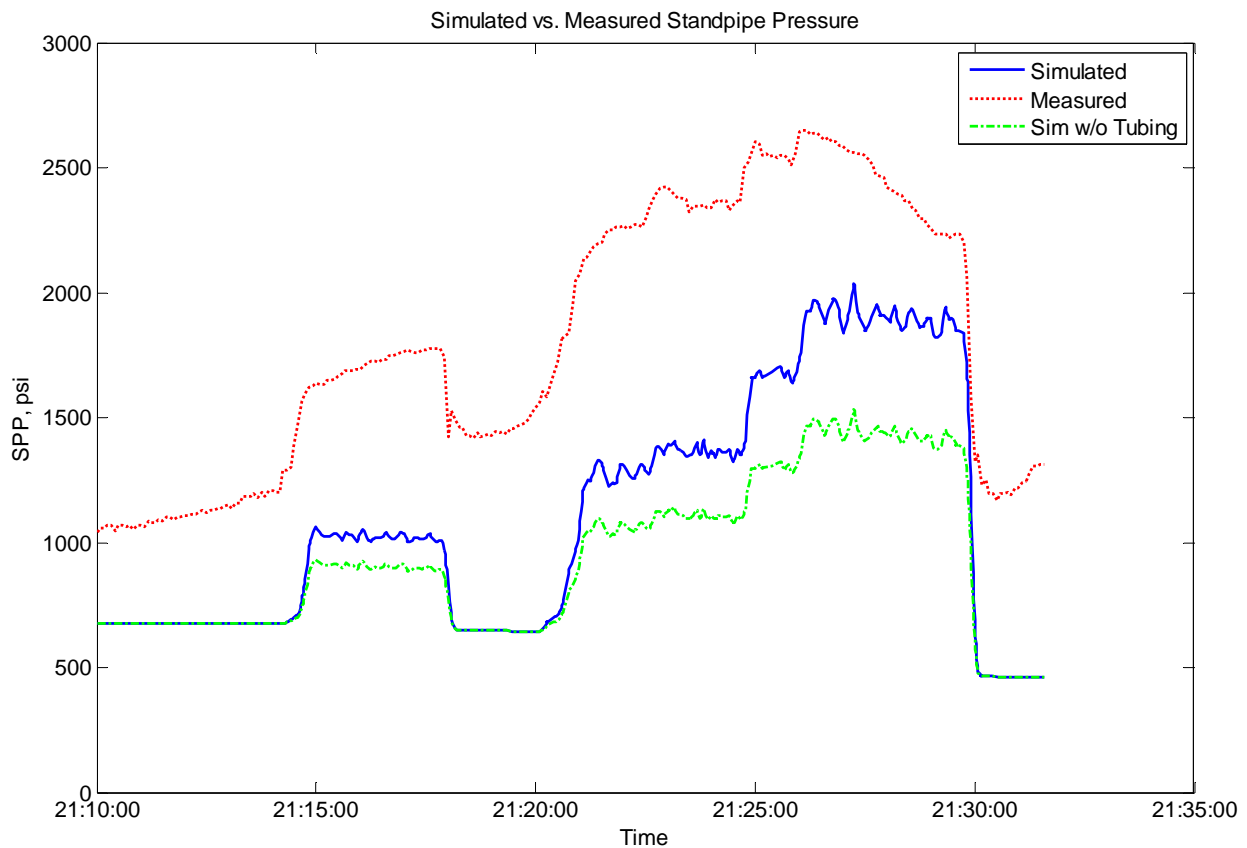


Figure 46: Simulated vs. measured pressure response, second seawater displacement

The divergence implies an increasing influx rate as the displacement progresses. Also notable in the figure is the drop in measured standpipe pressure starting at approximately 21:26. There is no corresponding drop in the simulated response, because the additional influx volume has pushed the spacer to the top of the riser in the measured response, while in the simulated scenario the spacer has not yet reached the surface. The negative pressure gradient in the measured data is an indicator of the removal of spacer weight from the riser.

Referring back to Figure 45, two noteworthy events are present in the kill line signal. First, beginning at about 21:16, a kill line valve appears to have been opened (likely a BOP valve). Shortly thereafter, at 21:17, the measured pressure spikes to over 7,000 psi (not shown in the figure due to the scale). The pressure spike corresponds to the activation of rig pump #2 for a brief period. Immediately after the pressure spike, pumps #2, #3, and #4 were shut down for approximately 2 minutes, after which pumps #3 and #4 were brought back online. This event has been identified, based on information provided by Transocean, as the activation of a relief valve on pump #2, mostly likely due to starting it against a closed surface valve. The pump was deactivated while repairs to the relief valve were made [21].

The second event of interest on the kill line signal occurred starting at approximately 21:22. From this point, the line pressure increased gradually over a four-minute period, then increased rapidly for the next minute, reaching a peak of 833 psi. The pressure then began to decay slowly through the remainder of the final displacement, and continued along the same trend for most of the final 20 minutes of data.

SES interprets the initial pressure rise in the kill line as a partially open surface valve, followed by a full opening just prior to the peak in pressure. Subsequent to this time, the kill line was open and measuring the fluid pressure above the BOP (i.e., in the riser).

4.6.3 Estimated Hydrocarbon Influx Volume

The estimate of hydrocarbon influx during the final seawater displacement is somewhat speculative due to the lack of flow return data, uncertain pump efficiencies, and unknown mixed fluid densities in the work string-to-casing annulus. However, an iterative solution was obtained which matched the observed standpipe pressure immediately following the displacement. This solution is given in Figure 47. It assumes 138 bbl of hydrocarbon influx (232 bbl total gain to this point) and 395 bbl of mixed fluid in the work string-to-casing annulus and lower riser, with an average density of 12.8 ppg.

Note that the calculated kill line pressure for this solution (392 psi) does not match the measured pressure of 767 psi. The measured kill line pressures for this and remaining solutions are consistently higher than the calculated values, although the calculated pressure trend (gradient) initially matches the trend observed in the measurements (see Section 4.7.2 for further discussion). Additional information is necessary to obtain solutions that match both the pressure measurement and volume displacement data.

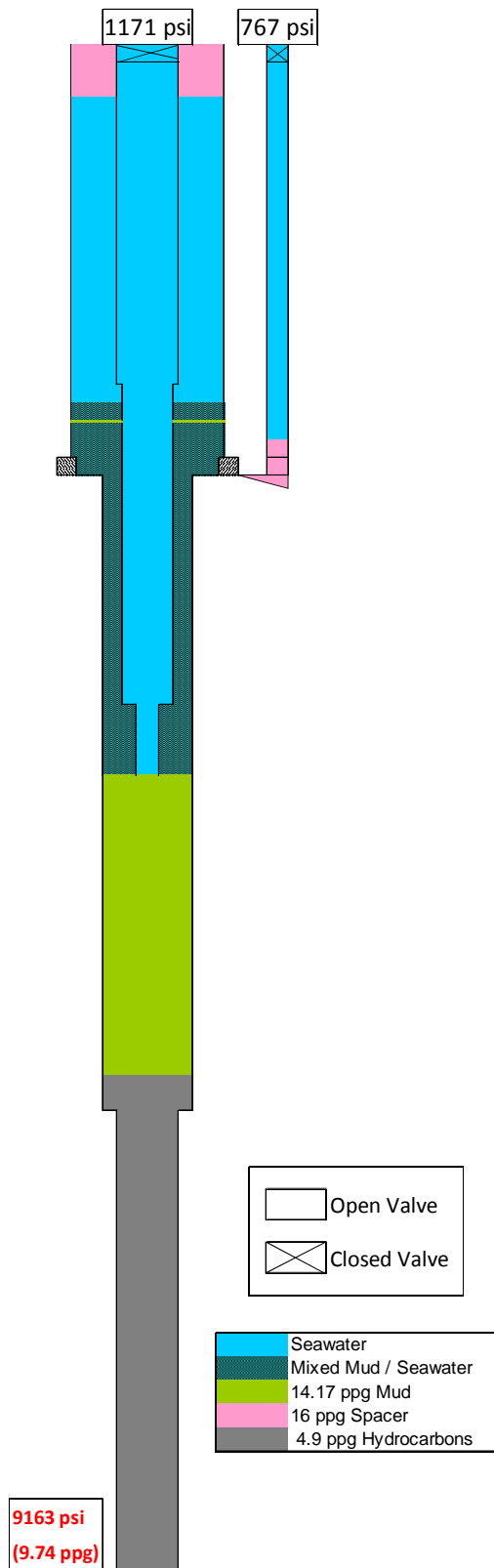


Figure 47: Well state diagram following final seawater displacement, 21:30

4.7 20 Minutes Prior to Explosion

During the final 20-minute period prior to loss of signal, hydrocarbons were actively flowing into the underbalanced well, retarded by the weight, inertia, and friction of the mud and seawater in the casing and riser. The analysis of the following sections attempts to draw conclusions about the rapidly changing hydraulic state of the well during this time.

An overview plot of the signals recorded during the final 20 minutes is given in Figure 48 (expanded from Figure 8), with an accompanying description of the labeled events in Table 36.

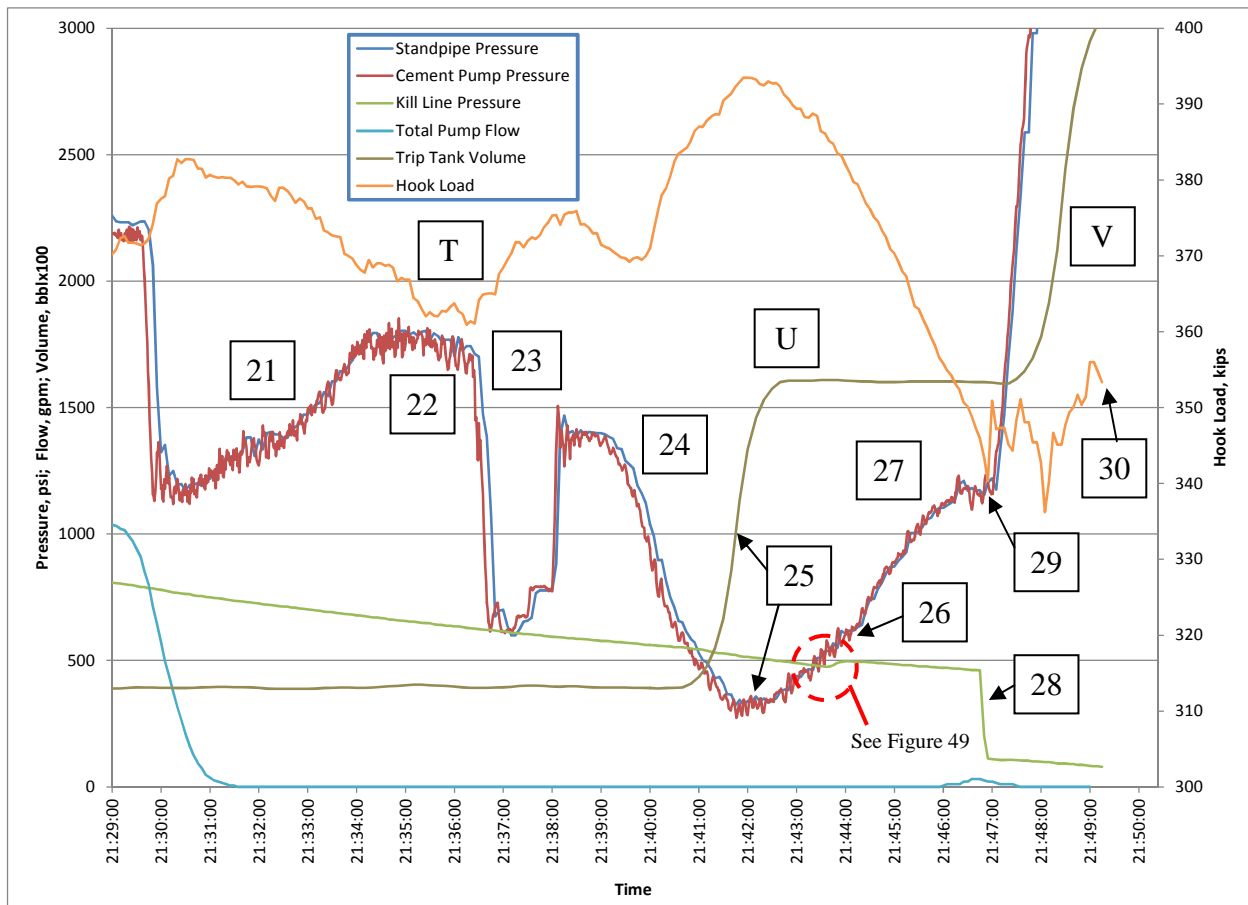


Figure 48: Plot of telemetry signals 20 minutes prior to explosion

Table 35: Description of events from 21:30 to 21:49

Event	Description	Time
T	Observe differential pressure; bleed and shut in work string	21:30 to 21:42
U	Drill floor overflows; well control actions taken	21:42 to 21:46
V	Gas flows onto rig; power loss; end of transmission	21:46 to 21:49

Table 36: Description of events 20 minutes prior to explosion

Event	Description	Time
21	Mud/seawater mix displaced with mud in work string-to-casing annulus	21:30 to 21:34
22	Top of mud reaches BOP; mud continues to fill annulus	21:34 to 21:36
23	Work string bled at surface; mud taken into work string	21:36 to 21:38
24	Hydrocarbons displace mud in work string-to-casing annulus	21:39 to 21:42
25	Hydrocarbons enter riser; flow check performed using trip tank	21:42
26	Annular preventer closed; rig floor overflows; flow diverted to MGS	21:43 to 21:45
27	Flow overwhelms MGS; mud sprays out vent lines	21:45 to 21:46
28	Gas at surface; rapid decompression of riser and well	21:46 to 21:47
29	Variable bore ram (VBR) closed; well temporarily shut in	21:47
30	Loss of signal	21:49

4.7.1 Observed Standpipe, Kill Line, and Trip Tank Signals

From the cessation of pumping at 21:30 to loss of signal at 21:49, the standpipe pressure, kill line pressure, and trip tank volume signals exhibited several different trends, each of which provides key insight as to the state of the well just prior to the explosion. During this time the well state was changing very rapidly, which makes precise numerical determinations difficult. Nevertheless, enough information from the trends themselves can be derived to place the various fluids in the well and riser to within reasonable estimates.

Event 21 (see Figure 48 and Table 36): After completion of pumping, the standpipe pressure dropped to 1,171 psi due to removal of frictional pressure drop from the pumps. After less than a minute of steady pressure, the signal then began to climb, reversing the downward trend exhibited in the final few minutes of the displacement. The pressure continued to increase until 21:34, at which point a peak measurement of 1,803 psi was recorded.

The reversal in pressure gradient between the final minutes of the seawater displacement (while actively pumping) and the subsequent four minutes with the pumps off may be interpreted as follows: During the displacement, the work string-to-casing annulus was being filled with a mixture of mud from the production casing and seawater from the work string. Concurrently, the spacer was being displaced out the top of the riser. The reduction in spacer volume caused a corresponding decrease in the riser hydrostatic pressure, resulting in the observed negative pressure gradients in the standpipe and kill line. Upon cessation of pumping, the seawater flow from the work string halted, but well influx flow did not. Therefore, pure mud began to be pushed up the work string-to-casing annulus. Because of the narrow cross sectional area of the annulus, a large positive pressure gradient was established (that is, the annulus experienced a large hydrostatic pressure increase per unit volume of influx). This positive gradient was larger than the negative gradient established by the removal of spacer; hence the reversal in trend. Note, however, that the kill line signal continued to record the negative spacer gradient during this time (see Figure 48).

Event 22 (see Figure 48 and Table 36): Upon reaching the top of the work string-to-casing annulus at 21:34, the SOBMs flowed into the BOP and riser, which greatly reduced the pressure gradient above the end of the work string due to the sudden increase in cross-sectional area. At this point, the standpipe pressure followed approximately the same negative trend as the kill line pressure.

Event 23 (see Figure 48 and Table 36): At 21:36, the standpipe pressure suddenly dropped to approximately 680 psi. It fluctuated about this value for about 2 minutes, before rapidly increasing to approximately 1400 psi at 21:38. The rapid nature of the changes in the standpipe signature suggest a mechanical intervention at the surface; i.e. a bleed of the work string. This assertion is corroborated by information provided by Transocean [21].

The pressures before and after the work string bleed provide an important clue as to the nature of the fluid state at the end of the work string. The work string was initially filled with seawater. After the bleed, the standpipe pressure was approximately 305 psi lower than the pressure recorded just prior to the intervention. The lower pressure indicates that a fluid heavier than seawater; i.e., 14.17 ppg SOBMs, was drawn into the work string at the time of the bleed. Had a lighter fluid such as hydrocarbons been drawn in, a higher ending pressure would have been recorded; if seawater, no pressure change would have been observed. From this analysis, the conclusion follows that the hydrocarbon influx had not yet reached the bottom of the work string (8,367 ft depth) at this time.

The pressure differential before and after the work string bleed also allows the amount of bleed volume (and hence, the volume of mud drawn into the work string) to be calculated. Based on a differential of 305 psi, SES calculates that 12 bbl of SOBMs were in the work string subsequent to the bleed.

Event 24 (see Figure 48 and Table 36): After remaining stable for about one minute, at 21:39 the standpipe pressure began a rapid decline. SES interprets this to be a key event, as it indicates the time at which the hydrocarbon influx passed the end of the work string. This indicator provides a known hydrocarbon influx volume (501 bbl; equal to the casing volume below the work string), as well as the remaining liquid volume to be expelled prior to the influx reaching the surface (1,809 bbl; consisting of the casing, BOP, and riser annulus volumes).

The decreasing pressure is a reversal of the phenomenon explained in Event 21. Here, the heavy mud in the work string-to-casing annulus was replaced with light hydrocarbons, causing a sharply negative gradient in the annulus that reinforced the negative riser gradient (due to the spacer loss).

Event 25 (see Figure 48 and Table 36): At some point around 21:42, the hydrocarbon influx reached the top of the casing and flowed into the BOP. The standpipe pressure recorded during this time was 325 psi. At this point, the well flow rate was increasing rapidly, and as such, the standpipe pressure measurement contained a significant frictional component (see Section 4.7.4). In fact, the calculated hydrostatic standpipe pressure is a negative value at this point (see next section).

During this period, it is estimated that well control actions began on the rig. The first of these appears to have been a well flow check using the trip tank, which displays a rapid 12 bbl rise¹⁴ at 21:42. Due to the averaging (filtering) applied to the pit volume data, the actual start time and rate of rise cannot be determined precisely¹⁵. Following the rise, the trip tank signal levels out at about 16 bbl, indicating that the trip tank was isolated at this time.

¹⁴ Note that the trip tank volume scaling in Figure 48 is increased by a factor of 100 for clarity.

¹⁵ See Appendix E for further discussion.

Event 26 (see Figure 48 and Table 36): The fluids in the well were unloading rapidly from 21:43 to 21:45. The frictional pressure drop from the high flow caused the standpipe pressure to increase to 885 psi (at 21:45) from the minimum recorded at 21:42.

Well control actions continued during this period, following the initial flow check. The kill line pressure signal provides an indicator of the second action, as shown in Figure 49 (expanded from Figure 48). At 21:43:40, the signal exhibits a brief upward trend, increasing by approximately 20 psi over a 20-second period before continuing on a negative trend similar to previous observations.

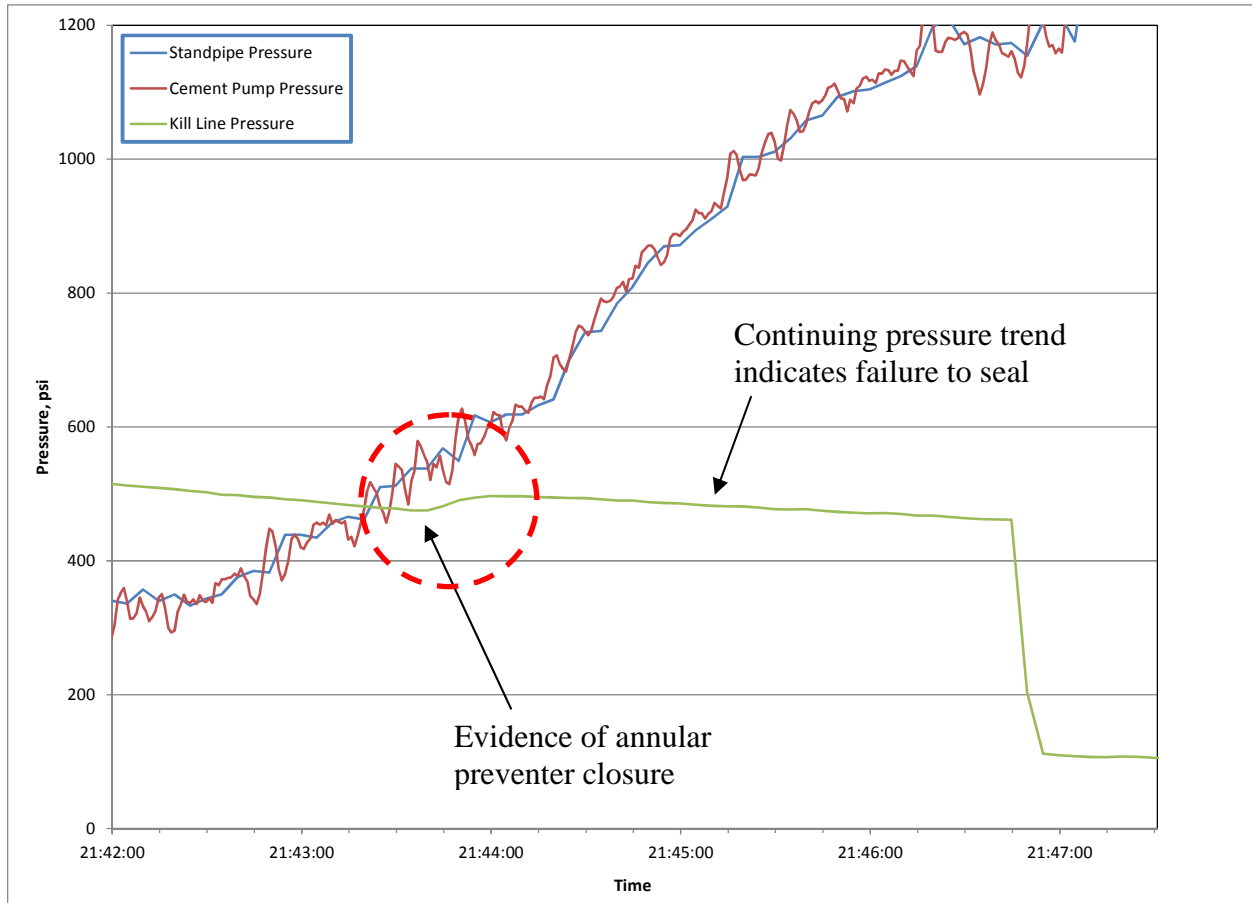


Figure 49: Detail of pressure signals recorded from 21:42 to 21:47

Because the kill line only records pressure activity in the riser above the point at which it enters the BOP, the closure of one or more of the preventers above the entry point would be captured in the signal. Conversely, a closure below the entry point would not be recorded. See Figure 50 for a diagram of the BOP with the two possible kill line entry points circled. The analysis herein assumes that the upper entry point, at a depth of approximately 5,032 ft, was opened to the well during the periods noted in the time interval of interest.

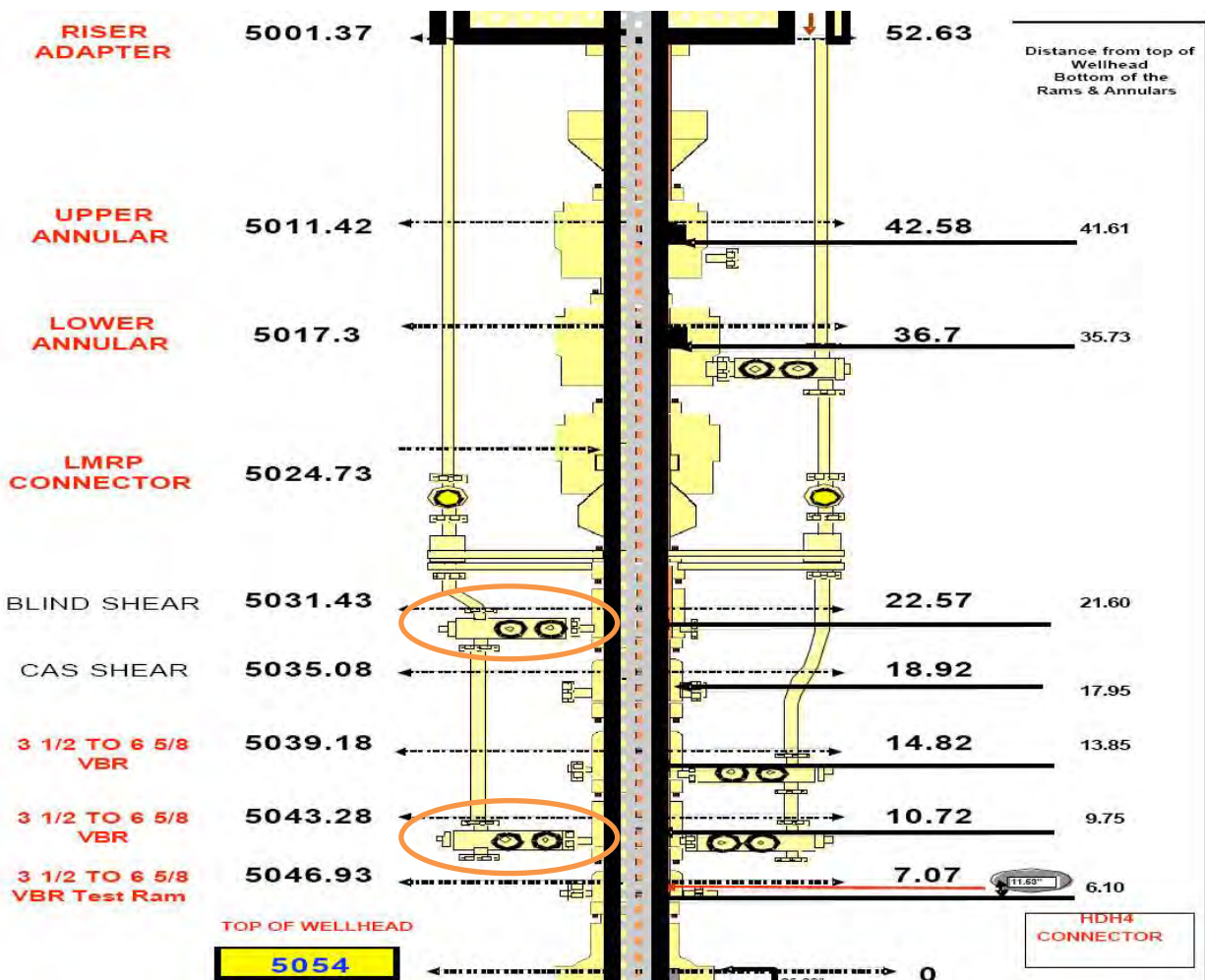


Figure 50: Diagram of BOP showing kill line entry locations (circled). Excerpted from [8].

Because the Transocean well control procedures call for an annular preventer, preferably the upper unit, to be closed as an initial well control step [21], it is surmised that the closure of the upper annular preventer was captured at 21:43:40.

Examining the kill line pressure data at further points in time (21:44 onward), it is seen that the signal continued along a negative pressure gradient similar to the trend recorded earlier. Thus, it is concluded that the closure of the annular preventer failed to seal the well.

Following the annular preventer closure, a third well control action took place: The diverter was closed and surface flows were routed through the mud-gas separator (MGS) system (see Sections 4.7.4 and 4.7.5 for further information) [21].

Event 27 (see Figure 48 and Table 36): During the interval from 21:45 to 21:46, the standpipe pressure continued to increase. At this time, well fluids rapidly filled the MGS system and began flowing out of its various vents (see Sections 4.7.4 and 4.7.5 for further information) [21].

Event 28 (see Figure 48 and Table 36): Between 21:46 and 21:47, the kill line pressure exhibited an extremely rapid decline, from 461 to 112 psi (see Figure 49). One of two possibilities may explain the observed behavior:

1. A mechanical intervention along the kill line by the rig personnel, such as a valve closure or pressure bleed; or
2. A rapid pressure change in the riser.

SES believes that the second option correctly explains the event, for two reasons. First, no witness accounts were provided that address a mechanical intervention at this time. Second, information provided by Transocean indicates that gas (hydrocarbons) had arrived at the rig surface a few minutes prior to a power loss on the rig, with multiple explosions shortly thereafter [21]. Assuming that the loss of the telemetry signal coincides with the loss of rig power, the recorded kill line signal at 21:46 is consistent with a rapid decompression of the riser caused by the last remaining liquid being ejected from the surface equipment and gas emerging at the surface.

Event 29 (see Figure 48 and Table 36): A sudden sharp increase in standpipe pressure took place at 21:47. Over a two-minute period, the pressure increased from 1,125 psi to the final recorded standpipe pressure of 5,706 psi at 21:49:15.

The hook load signal shown in Figure 48 provides information as to the cause of the pressure rise. It may be observed that at all times prior to 21:47, the hook load signal was inversely proportional to the measured standpipe pressure. This is physically intuitive, as pressure end loads on the work string combined with frictional shearing forces on the drill pipe OD apply upward forces on the string, thereby decreasing the hook load measured at the block. This behavior is readily observed at earlier times during the time interval of interest (see Figure 6 through Figure 8).

At 21:47, the inverse relationship between hook load and standpipe pressure ceased. Instead of mirroring the steadily increasing standpipe pressure, the hook load fluctuated within a relatively narrow band of about 335 to 355 kips.

SES interprets this combination of signals as the closure of one or more of the BOP's variable bore rams (VBRs), which successfully (albeit temporarily) shut in the well. The shut-in was indicated by the standpipe pressure rise, while the action of the rams gripping the drill pipe created a mechanical "short circuit". In this condition, loads on the work string were reacted through the BOP, with only residual force variations transmitted to the block; hence, the small fluctuations in hook load.

The kill line pressure signal provides strong evidence that a preventer below the kill line entry point was closed, rather than one above. If the closed preventer were above the entry point, the kill line signal would have followed a trend similar to that of the standpipe pressure, recording a sharp rise as shut-in pressures were reached. Instead, the kill line pressure remained steady at approximately 110 psi, with a slightly decaying trend observed during the final two minutes. This trend is consistent with an expansion of hydrocarbon gas in the riser above.

Indeed, the relative behavior between the standpipe and kill line pressures indicates that the upper kill line entry point at the BOP (see Figure 50) was open rather than the lower point. The only ram below the lower entry point is the test ram. Under standard well control procedures, it is more likely that one or both of the VBRs located at 5,039 and 5,043 ft (see Figure 50) would have been closed instead of the test ram at 21:47.

Event 30 (see Figure 48 and Table 36): At 21:49:15, the telemetry data ends. It is surmised that the rig lost power at this time, with subsequent explosions and fire.

4.7.2 Hydrostatic Calculations

In support of the discussion above, hydrostatic calculations were performed in order to estimate the well state at various points during the final 20 minutes prior to the loss of signal. The cases analyzed are shown schematically in Figure 51 and Figure 52.

The objective in performing the hydrostatic calculations was to maintain consistency in terms of the volume displacements derived from the pressure transients, as discussed in the previous section. Using this approach, calculated standpipe pressures were obtained which were consistent with the measured values. Exact matches were found for the hydrostatic cases at 21:30 and 21:34, but the calculated values were lower than the measurements for the latter two cases (21:39 and 21:42). However, given the flow rates through the well at those times (see next section), frictional pressure drop was present that would cause an increase in standpipe pressure above the hydrostatic case, thus maintaining consistency.

Calculated influx volume and standpipe pressure results are tabulated against the measured standpipe pressures in Table 37, below. See Appendix C for further details.

Table 37: Volume and standpipe pressure results comparison, hydrostatic analysis

Time	Event	Hydrocarbon Influx Volume	Measured Standpipe Pressure	Calculated Standpipe Pressure
21:30	Mud at work string	232 bbl	1,171 psi	1,171 psi
21:34	Mud at casing top	385 bbl	1,803 psi	1,803 psi
21:39	Hydrocarbons at work string	501 bbl	1,390 psi	1,011 psi
21:42	Hydrocarbons at casing top	654 bbl	325 psi	-448 psi

Based on a hydrocarbon saturation pressure of 6,550 psi [10], the hydrocarbon influx began to transition from single-phase liquid to two-phase gas / liquid flow shortly after 21:34, when the hydrocarbon / mud interface was about 1,500 ft below the end of the work string.

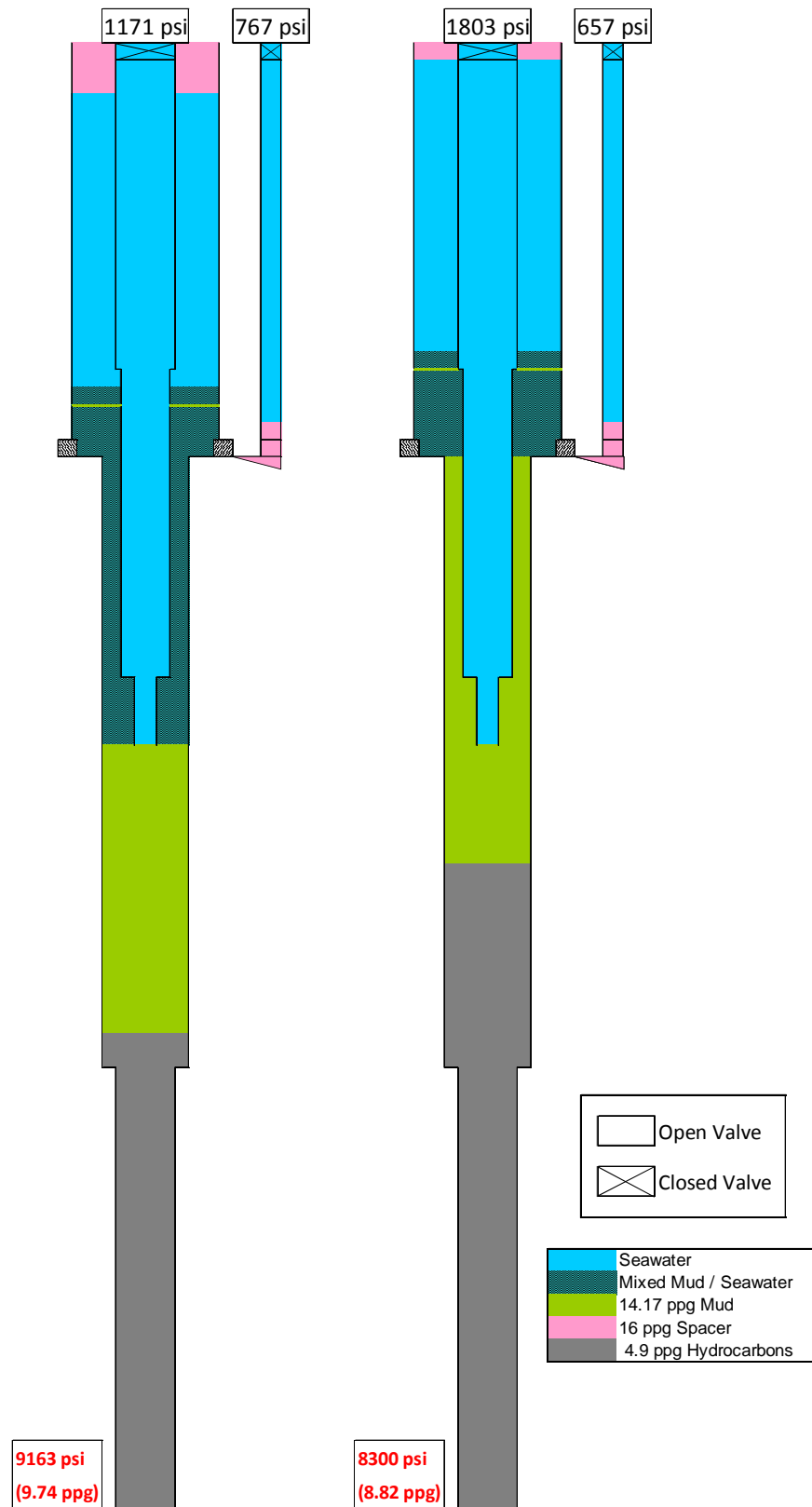


Figure 51: Well state diagrams during final 20 minutes of data: 21:30 (left); 21:34 (right)

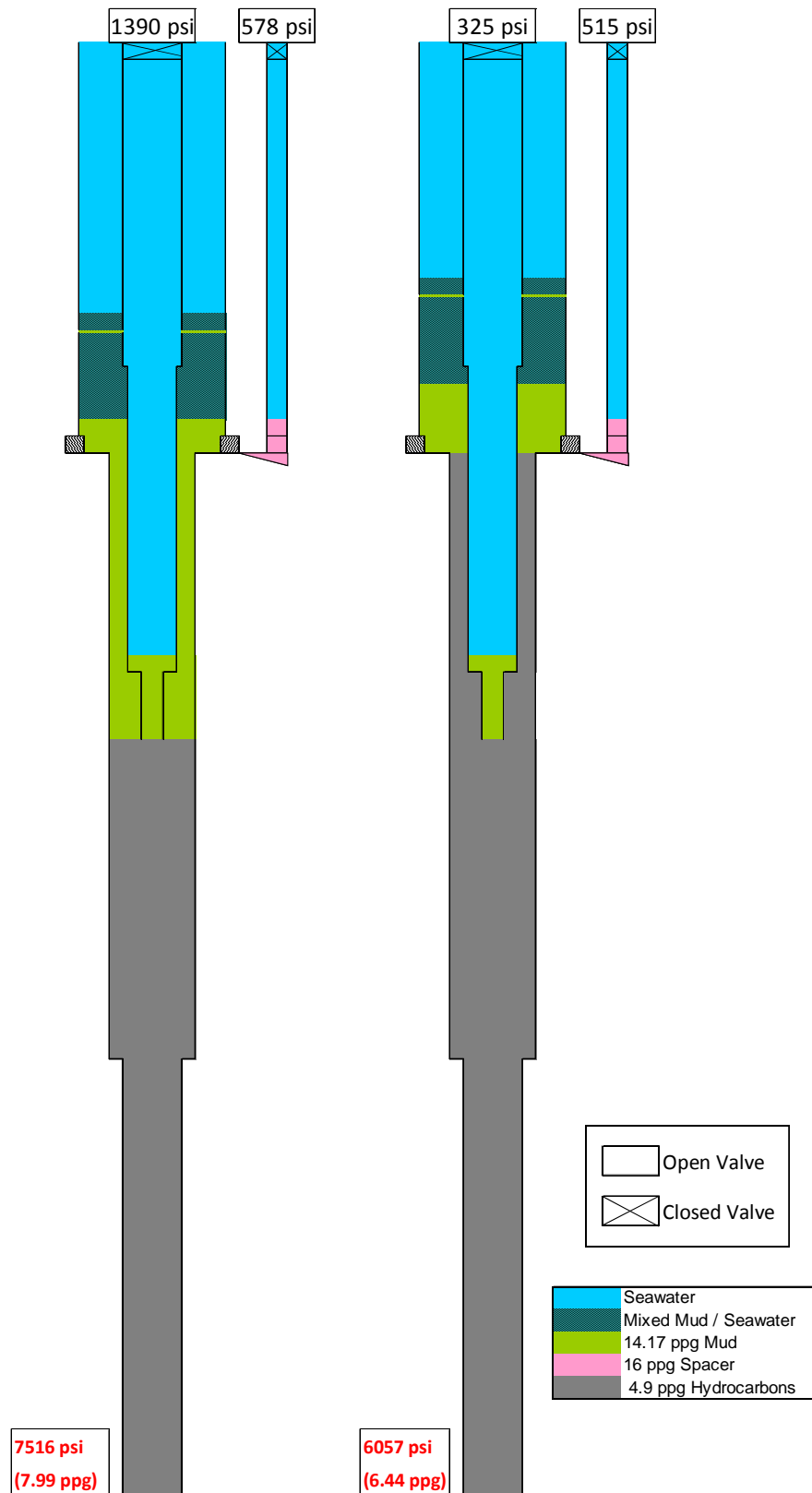


Figure 52: Well state diagrams during final 20 minutes of data: 21:39 (left); 21:42 (right)

Despite the consistency in standpipe pressure, solutions that simultaneously matched the calculated kill line pressure to the measured values were not found. The discrepant values are plotted in Figure 53.

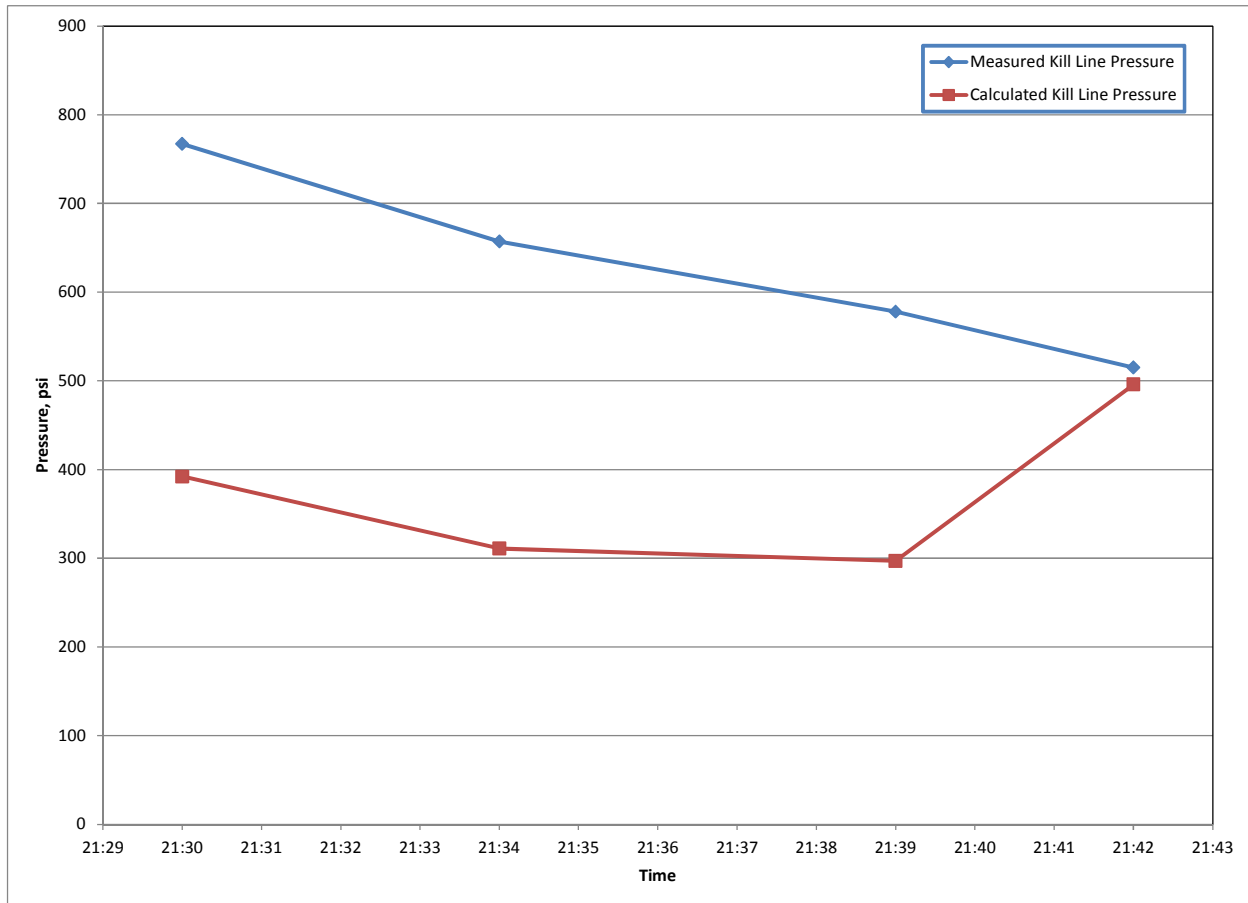


Figure 53: Comparison of measured and calculated kill line pressures

In the first two cases, the kill line pressures are separated by a constant value (~360 psi) and follow the same negative gradient. However, by 21:39 the calculated value approaches zero slope, while the measured value continues along a negative gradient. At 21:42 the calculated result trends to a positive slope, while the measurement gradient remains negative.

Compared to the calculated results, the measured kill line data is consistent with a fluid stack in the riser that is in a less advanced state of displacement; that is, one in which a smaller volume of seawater is present in the riser and the spacer / SOBMs stack is lower in depth. In the scenario

indicated by the calculated values, the last of the spacer exits the riser between 21:34 and 21:39, resulting in the transition from a negative to a positive pressure gradient in the kill line. No such transition exists in the measured data, which indicates that the fluid leaving the riser is heavier than the fluid entering throughout the final recorded minutes.

For this to be possible, the spacer must have remained in the riser for longer than the calculations suggest. However, such a scenario would then result in inconsistencies with respect to the volume displacements over time. To reconcile the inconsistency, the well and / or rig pump flow rates would have to be reduced considerably, which would simply propagate the inconsistency to other areas of the analysis.

Another possible explanation is that mixing occurred between the spacer and seawater. The hydrostatic analysis assumes that the various fluids are cleanly stratified, but in actual operations, some degree of mixing is unavoidable. In the event that a substantial mixed-density interface had developed between the two fluids, the resulting kill line pressures and gradients would more closely match the measurements.

Should more information become available, further work to establish full consistency between well volumes, flow rates, and measured surface pressures would be warranted.

4.7.3 Well Flow Calculations

Building upon the pressure signal observations and hydrostatic analyses performed in the previous two sections, an estimate of the well flow rates over time may be constructed. Prior to this presentation, it is helpful to establish a theoretical basis for the behavior of the hydrocarbon influx as it progressed up the wellbore. The theoretical behavior may then be correlated to the actual well response.

Figure 54 shows an idealized riser model with a run-in work string, forming a simple annular control volume. The riser is initially filled entirely with liquid, which for the simplified analysis is assumed to be seawater. Below the riser is an infinite volume of hydrocarbon gas, assumed to expand under a constant pressure into the riser. For finite gas charges the pressure decreases as the expansion proceeds; therefore, several constant pressure cases are run in the theoretical analysis.

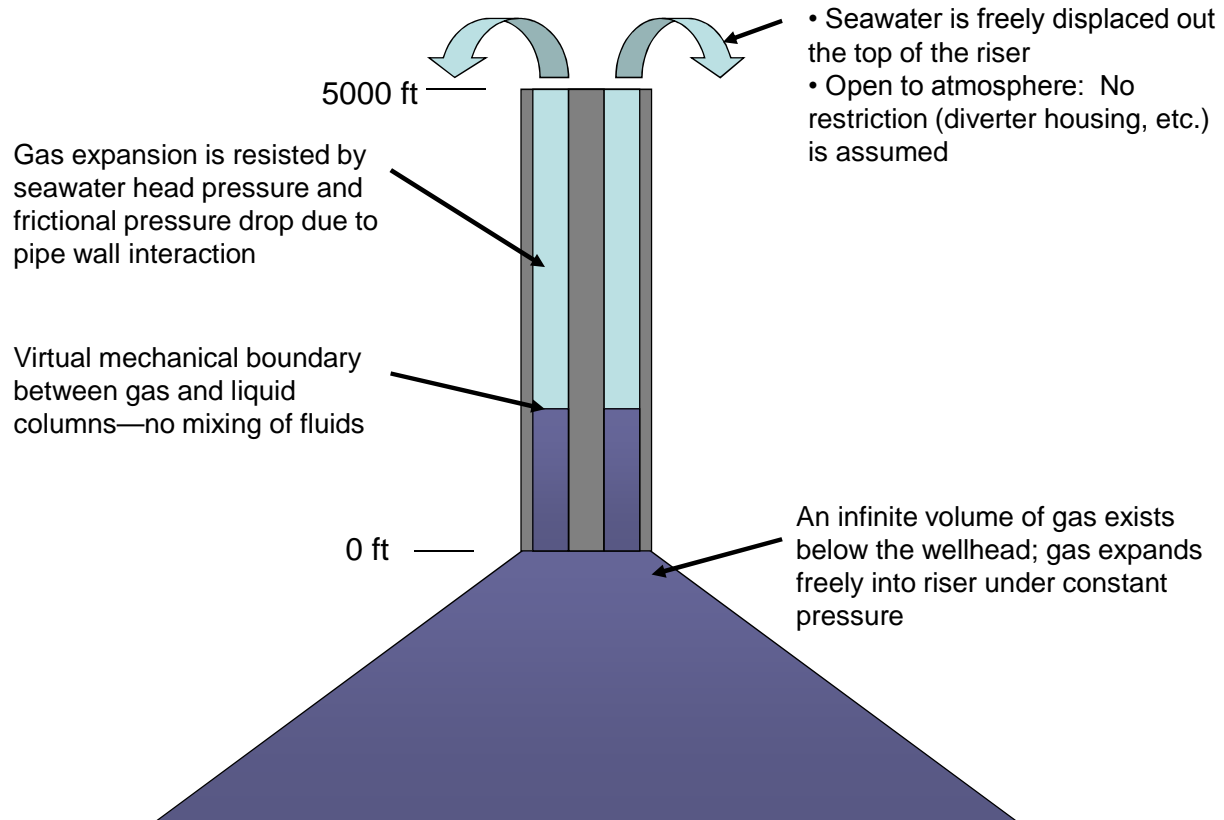


Figure 54: Diagram of theoretical riser model

In the theoretical model, mixing between the gas and liquid is not allowed. The gas expansion is resisted only by the liquid weight, inertia, and shear pressure generated along the riser and drill pipe walls. For purposes of the analysis, inertial effects are neglected.

A free-body diagram of the theoretical liquid column is presented in Figure 55 (equations from [23]).

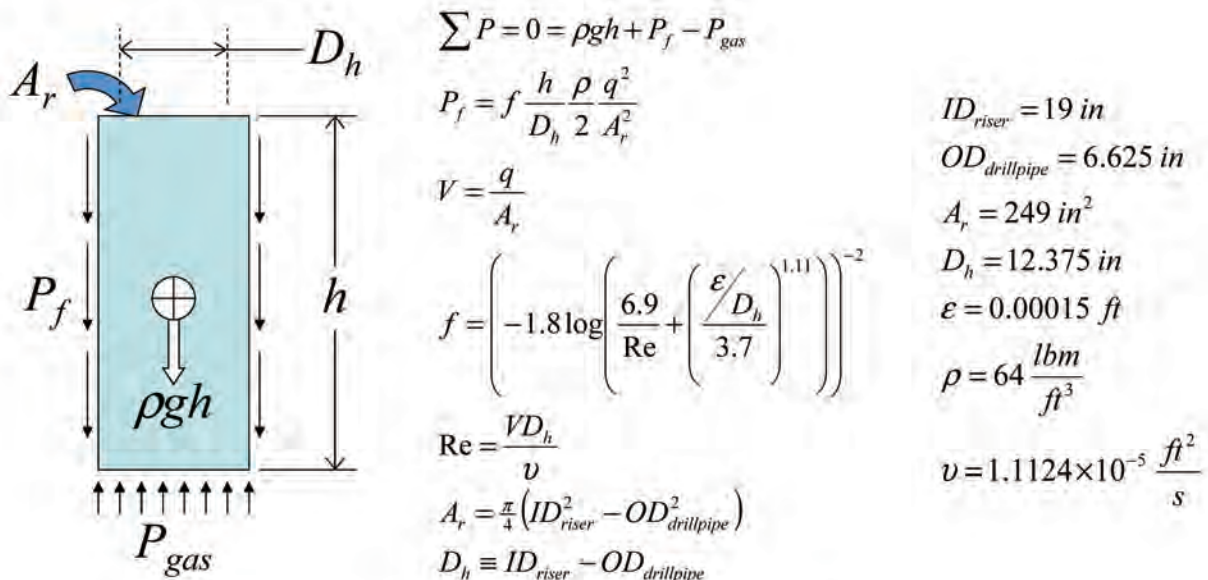


Figure 55: Liquid free-body diagram with relevant equations and values

Because of the assumptions of zero inertial forces, a pure seawater liquid column, an infinite gas volume, and no flow restrictions above or below the riser, the case under study represents a theoretical upper bound in terms of the liquid flow rates (and equivalently, velocities) attained. Correspondingly, the elapsed time required to evacuate the liquid from the riser is a theoretical minimum. In the actual case, the liquid flow rates and velocities will be lower, and the evacuation times higher, however, the general function of flow versus time will exhibit similar behavior.

The results of the theoretical analysis for five separate constant gas pressure cases are presented in Figure 56. As shown, the relationship between the flow velocity and the remaining liquid column height in the riser is roughly exponential in nature.

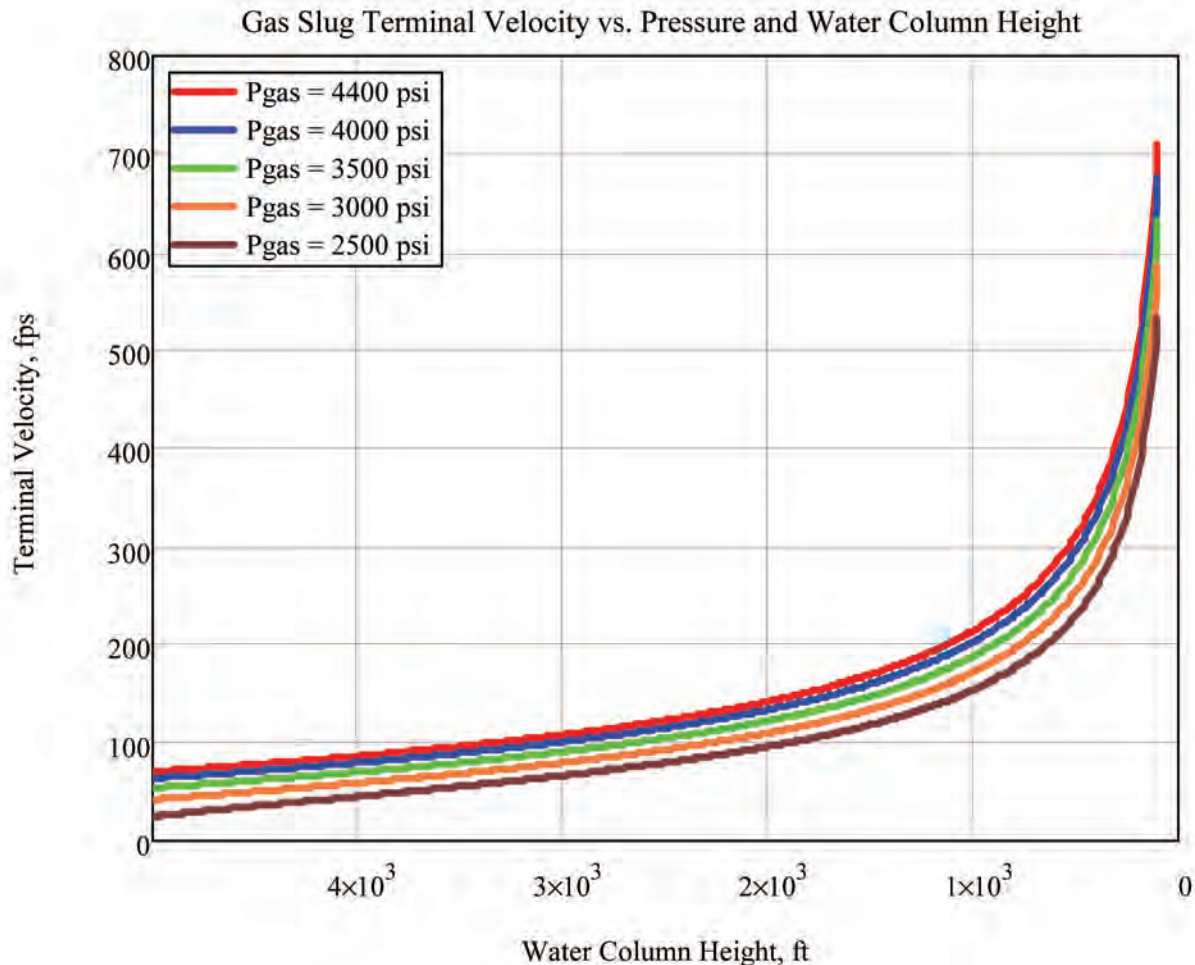


Figure 56: Theoretical gas rise velocity plot

The time required for the gas-to-liquid boundary to traverse the riser length (and hence, the time to evacuate all liquid from the riser) may be obtained by integrating the velocity curves presented above. For the maximum pressure case, the elapsed time is 40 seconds; for the minimum pressure case, 73 seconds.

As mentioned in the previous section, the hydrocarbon boundary crossing the end of the work string at 21:39 is a key event, because it establishes known volumes of hydrocarbon influx and liquid remaining in the riser and wellbore. Further, knowing the time at which the hydrocarbon gas emerged at the surface establishes the time required for the hydrocarbon boundary to traverse through the known volume from the end of the work string to the surface exit point. As will be explained in the following sections, the total volume includes the MGS and associated surface piping volume in addition to the riser, BOP, and casing annulus volumes (because the flow had been directed to the mud-gas separator system at the time). The sum of these is 2,010 bbl.

With the known volume and time duration in hand, and an estimate of the initial flow rate at 21:39, it is possible to fit an exponential flow relationship, similar to the profile explored theoretically, to the data. The initial flow rate estimate may be established from prior volume signatures in the pressure data. Particularly, the analysis of Event 21 (see Figure 48 and Table 36) reveals that mud from the casing annulus below the work string moved to the top of the casing between 21:30 and 21:34. The known volume of this annulus is 153 bbl; therefore, the average flow rate for this period is 38 barrels per minute¹⁶. Assuming a slight flow increase from 21:34 to 21:39, the initial flow rate estimate is 40 barrels per minute¹⁷.

A graph of the exponential flow curve fit, with associated hydrocarbon volume above the work string (equal to the liquid volume gain at the surface) is presented in Figure 57. The initial time is 21:39 and the initial flow rate is 40 bpm.

¹⁶ The flow rate units of barrels per minute, or bbl/min, will be abbreviated to 'bpm' for the remainder of the presentation.

¹⁷ The volume that flowed from the riser from 21:34 to 21:39 cannot be surmised directly from the pressure data. Hydrostatic calculations give an estimate of 116 bbl; however, the flow rate for this volume is only 23 bpm. Since it is unlikely that the flow rate decreased over this period, a slight increase in flow is assumed, which would imply a larger volume gain over this period than suggested by the hydrostatic analysis.

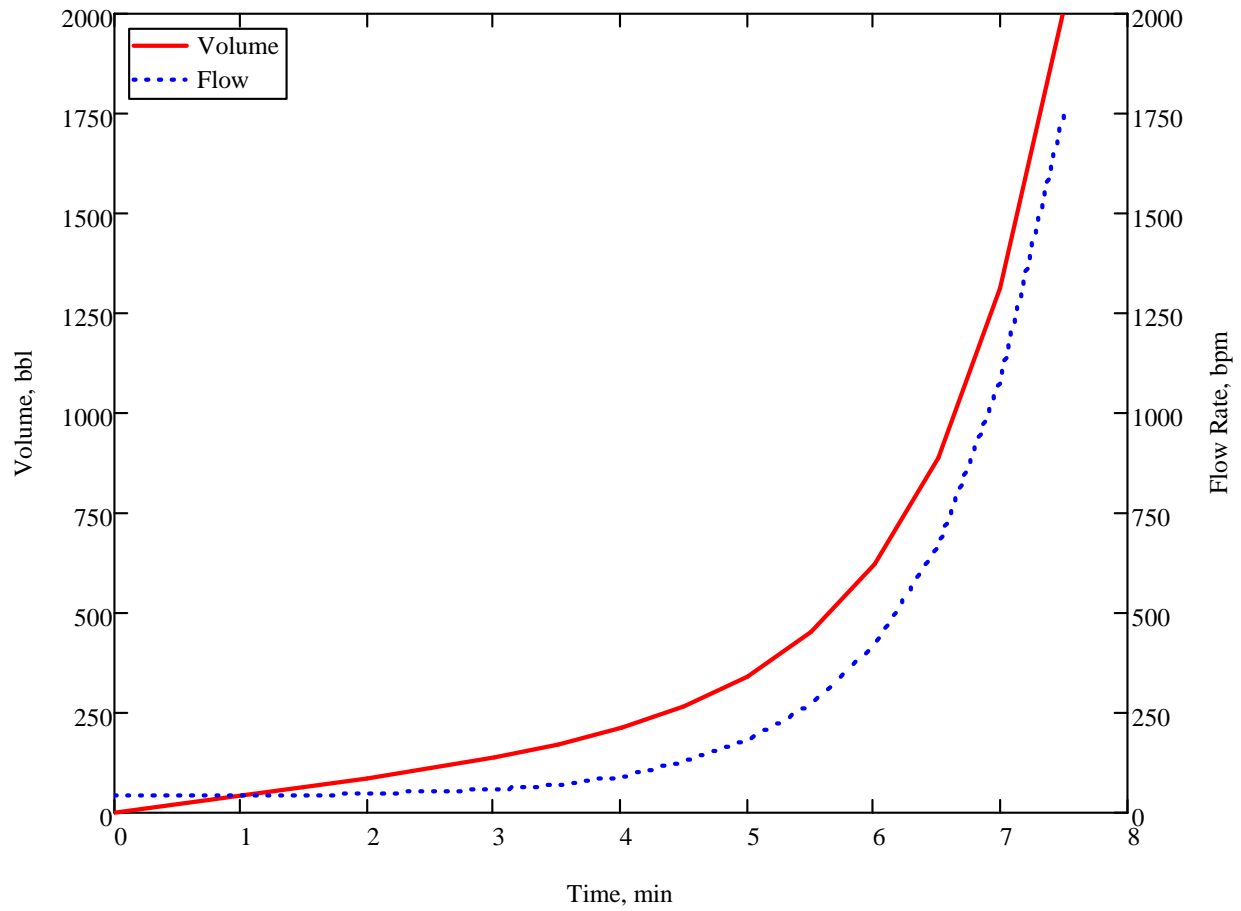


Figure 57: Hydrocarbon volume above work string and surface liquid flow, starting at 21:39

A tabular format summary of the calculated flow rate estimates for the final 20 minutes, including the curve fit results from Figure 57, is presented in Table 38. Also included in the table are volume tallies of hydrocarbons above the work string, and total hydrocarbon volume gain.

Table 38: Tabulated flow and volume gain estimates, final 20 minutes

Time	Surface Liquid Flow Rate	Hydrocarbon Volume Above Work String	Total Hydrocarbon Gain
21:30:00	<35 bpm	0 bbl	232 bbl
21:34:00	38 bpm	0 bbl	385 bbl
21:39:00	40 bpm	0 bbl	501 bbl
21:40:00	43 bpm	42 bbl	543 bbl
21:41:00	47 bpm	86 bbl	597 bbl
21:42:00	59 bpm	138 bbl	639 bbl
21:43:00	92 bpm	211 bbl	712 bbl
21:44:00	180 bpm	339 bbl	840 bbl
21:45:00	422 bpm	621 bbl	1,122 bbl
21:46:00	1,077 bpm	1,316 bbl	1,817 bbl
21:46:30	1,750 bpm	2,009 bbl	2,510 bbl

4.7.4 Frictional Pressure Drop Calculations

The magnitudes of the flow rate estimates in the previous section imply liquid velocities through the wellbore that create significant frictional pressure drops, especially from 21:39 onward. As mentioned previously, the two most significant flow restrictions in the downhole equipment were the 3 ½” tubing ID and the annulus formed by the 5 ½” drill pipe OD to casing ID. With the exception of the bleed that took place from 21:36 to 21:38, the work string remained shut in during the final 20 minutes prior to loss of transmission; hence, no flow passed through the tubing ID. However, all hydrocarbon flow from the well did pass through the work string-to-casing annulus prior to flowing through the riser. As such, this annulus presented the primary frictional flow restriction, first to the mud flowing through it, and then to the multi-phase hydrocarbons that followed.

As mentioned in Section 4.7.2, the standpipe pressures predicted by the hydrostatically-based well state solutions begin to diverge from the measured values between 21:34 and 21:39. For the 40 bpm flow rate estimated during this period, the frictional pressure drop of mud through the casing annulus may be up to 750 psi, depending on the exact values of apparent viscosity and fluid temperature.

From 21:39 to 21:42, the mud flow in the work string-to-casing annulus transitioned to hydrocarbon flow. The hydrocarbons reached saturation pressure just below the work string, indicating that gas breakout occurred as flow through the annulus proceeded. In this state, the density and apparent viscosity of the hydrocarbons were changing rapidly.

An estimate of the frictional pressure drop of the hydrocarbons through the annulus was performed by examining chemical and state analysis data of hydrocarbon samples taken from the well provided by a laboratory report [10]. From the viscosity and density data provided, two bounding cases were selected for frictional pressure drop estimates: 5,000 psi (0.525 gm/cm³; 0.4 cP) and 2,000 psi (0.307 gm/cm³; 0.6 cP), both at 170°F.

Using the above fluid properties combined with the annulus geometry and flow rate estimates from the previous section, curves of frictional pressure drop through the annulus due to hydrocarbon flow were calculated for the bounding cases. These are shown in Figure 58.

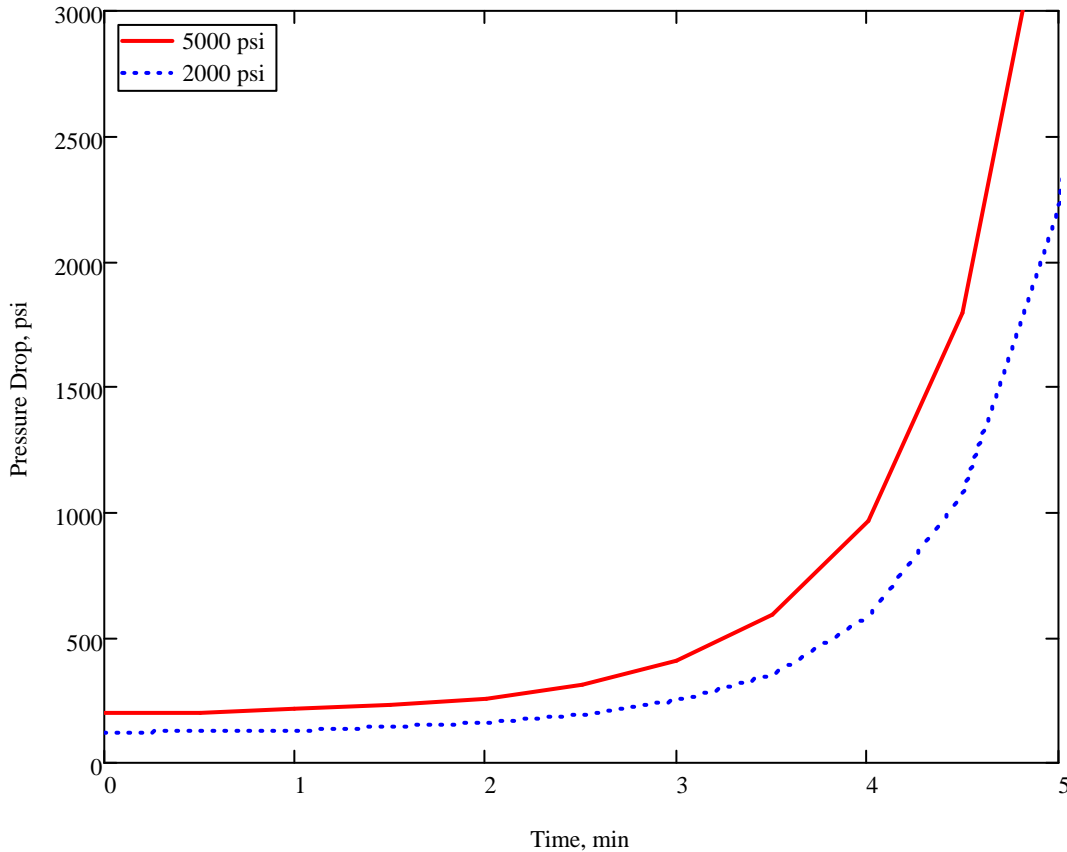


Figure 58: Calculated work string-to-casing annulus pressure drop (starting at 21:39)

The estimates indicate that enough frictional pressure drop was present through the annulus to compensate for the negative hydrostatic pressure at the standpipe, resulting in the positive and increasing standpipe pressure measured from 21:42 to 21:47¹⁸.

¹⁸ The analysis presented in [6] does not attribute the pressure rise from 21:42 to 21:47 in this manner. It is suggested instead that an annular preventer was closed at 21:42 and did not seal completely until 21:47. SES deems the closure of an annular preventer over such a long interval to be less plausible than the simple frictional pressure drop analysis provided herein. This position is reinforced by the observation that if the main restriction were at the annular, the pressure increase should have been recorded at the kill line. However, no such signal was measured.

4.7.5 Flow through Diverter and Mud-Gas Separator System

Subsequent to the closure of the annular preventer at 21:43:40, information provided by Transocean indicates that an additional well control action took place prior to the explosion: The diverter at the top of the riser was closed in response to an overflow of well fluid at the drill floor. Flow through the closed diverter was then routed through the Mud Gas Separator (MGS) system (see Table 36, Event 27).

Knowing the geometry and hydraulic properties of the diverter and flow line [18], an estimate of the flow rate required to produce the observed overflow at the drill floor may be obtained. Overflow occurred when the frictional pressure drop through the flow line and associated piping exceeded the hydrostatic potential in the system. Because of the large line diameters, substantial flow was required to meet this condition.

Calculated frictional and hydrostatic pressures for the diverter, flow line, and gumbo box system are shown in Figure 59 for all three circulated liquids (spacer, mud, and seawater) plotted against the system flow rate. Overflow occurs when the frictional pressure (solid line) exceeds the hydrostatic head (dashed line) for a given fluid.

The fluid type (mud, spacer, or seawater) affects the results only slightly. For 16 ppg spacer, the critical flow is 130 bbl / min; for 14.17 SOBM and seawater, a somewhat higher value of 145 bbl/min is indicated. Calculations indicate that all the spacer had been evacuated from the riser by the time the overflow occurred, making one of the latter two cases more likely.

Note that this calculation is valid for overflow of the diverter housing only. Since additional vertical space existed between the top of the diverter and the drill floor, a higher flow rate would be necessary for the overflow to be observed at the drill floor.

Consulting Table 38, the calculated flow rates from 21:44 to 21:45 are between 180 and 422 bpm. These flow rates are consistent with the conditions described above; therefore, it is estimated that the overflow observed on the drill floor occurred at or near this time. Closure of

the diverter is stated to have occurred within a few seconds of this event, resulting in the remaining riser flows being routed through the MGS system.

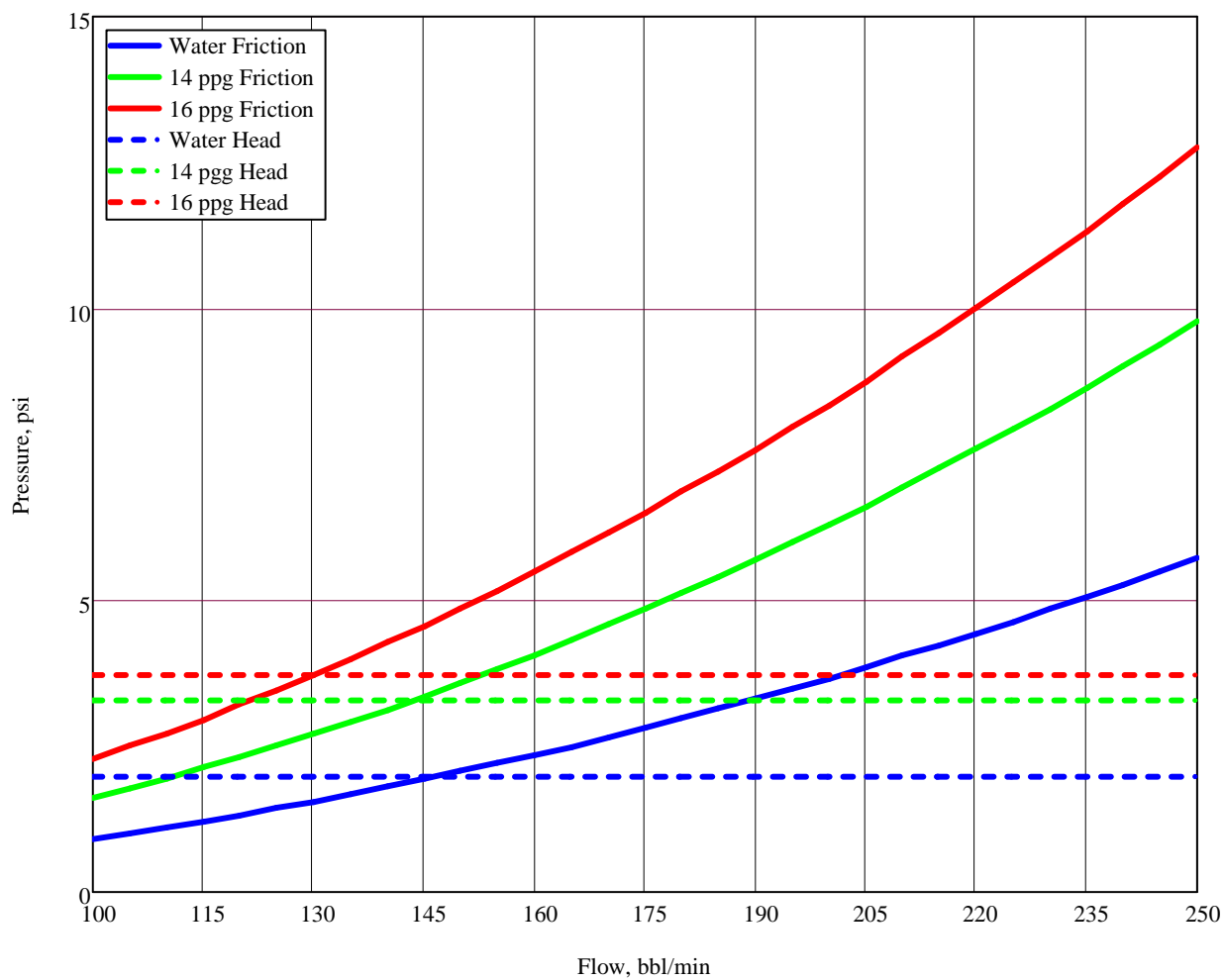


Figure 59: Hydrostatic and frictional pressures in diverter, flow line and gumbo box

The MGS and associated piping are described in [18], [19], and [20]. A simplified model of the MGS is shown at two scales in Figure 60 and Figure 61. The relative elevations of the inlet and outlet lines are represented in the figures, but the total line lengths are not. The height of the MGS is approximately 50 ft, and is shown in the figures for reference. Volumes are shown in Figure 60.

At low flow rates, (gas cut) mud enters the MGS from the diverter through the 14" inlet line. The liquid level in the MGS remains constant at the level of the 10" outlet, which carries the mud to the mud system. The 6" vacuum breaker line allows the 10" outlet line to drain, rather than remaining filled with liquid. Gas exits through the 12" outlet, which extends to the crown (about 200 ft above the MGS). The 6" overboard line has a 15 psig rupture disc to limit pressure in the MGS in the event it overfills.

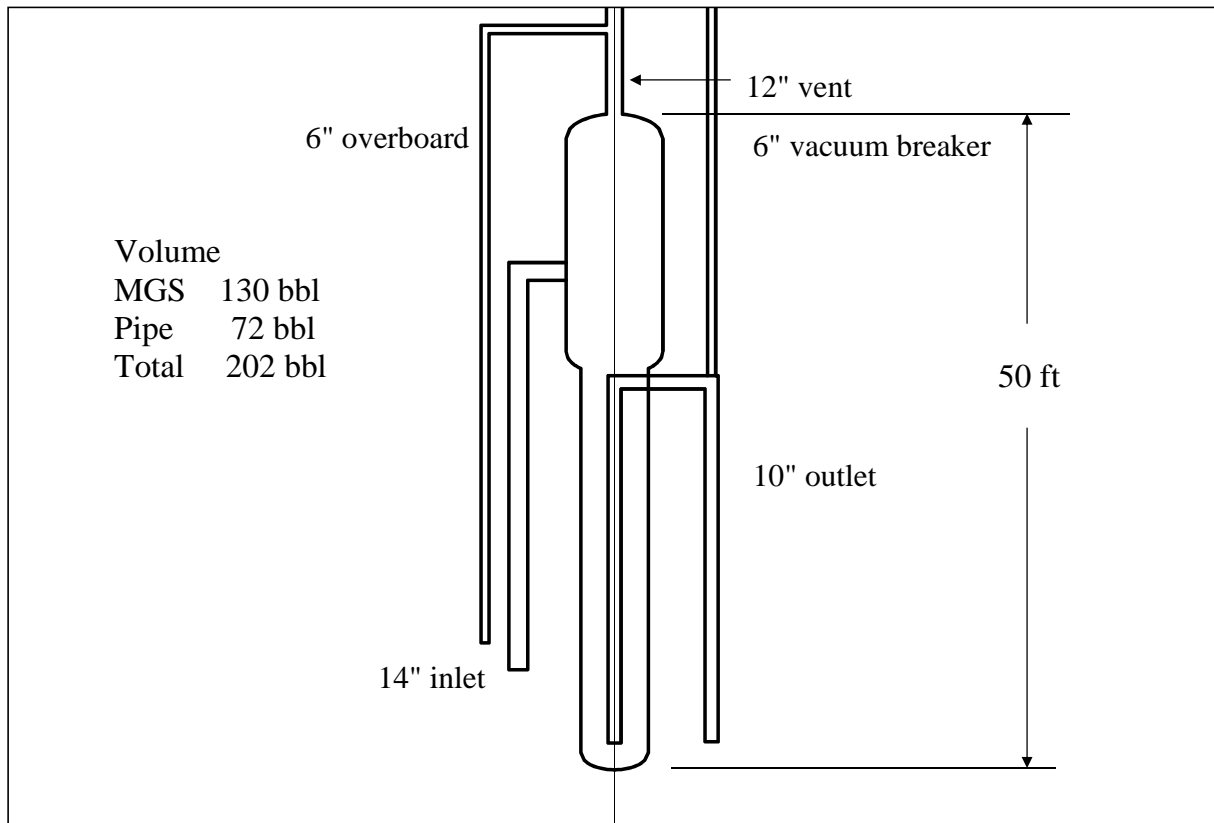


Figure 60: Diagram of mud-gas separator and adjacent piping

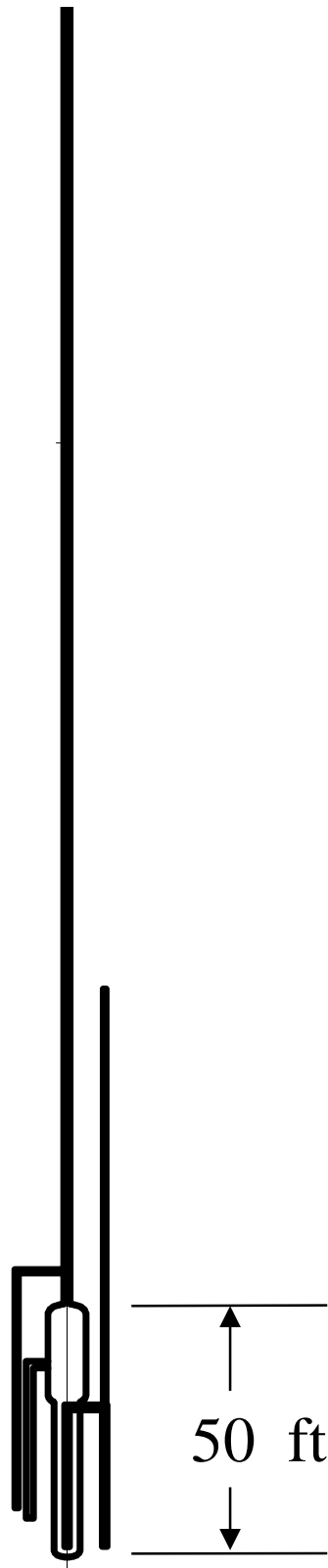


Figure 61: Expanded view of MGS system indicating scale of vent and vacuum breaker lines

For low flow rates, the liquid level in the MGS remains constant at the level of the 10” outlet. As the flow rate increases, the 10” outlet line will remain filled and the liquid level in the MGS will rise. When the liquid level rises inside the 12” to a sufficient distance (about 20 ft) above the 6” overboard line, the 15 psig rupture disc fails and part of the flow exits through the 6” overboard line. As flow rate increases such that the 6” line remains filled, the liquid level in the 12” line and in the 6” vacuum breaker line rises until flow begins out the 6” vacuum breaker line. Further increase in flow rate causes the liquid level to rise in the 12” line until flow begins out the 12” line. Further increases in flow rate are mostly out the 12” line due to the lower frictional pressure drop in the 12” compared to the smaller lines.

Hydraulic calculations were performed, assuming mud flow, to provide quantitative estimates of the flow path out of the various MGS lines. The flow rates such that the 6” overboard line remains full with no flow out the 6” vacuum breaker or the 12” line are given in the table below.

Table 39: Initial flow estimates through MGS

10” outlet line	85 bpm
6” overboard line	26 bpm
Total	111 bpm

The flow rates that fill the 12” line, with flow out the 10” outlet, the 6” overboard and the 6” vacuum breaker are:

Table 40: Flow estimates through MGS, all outlets flowing

10” outlet line	263 bpm
6” overboard line	65 bpm
6” vacuum breaker	98 bpm
Total	426 bpm

The estimated flow rate at 21:45 is 422 bpm; 1,388 bbl of liquid remains in the riser at this time (see Table 38).

If the diverter were closed at 21:44, then liquid flow (as observed from the drill floor) would subside until the MGS was filled, which would require less than one minute. By 21:45, there would be substantial flow out each of the four MGS outlets; the flow would continue until hydrocarbons reached the surface and the liquid in the MGS was expelled.

When the VBR was closed at 21:47, the riser was filled with hydrocarbons. An estimate of the quantity of hydrocarbons in the riser is in Table 41, which is calculated based on the kill line pressure measured at that time, plus the assumption of only hydrocarbons in the riser. Hydrocarbon properties were obtained from [10].

Table 41: Estimate of hydrocarbons in riser

Property	Value	Comment
Annulus Volume	1,649 bbl	Above kill line
Kill line Pressure	500 psi	Shortly before VBR closure
BOP Pressure	2,734 psi	At kill line elevation (5,032 ft)
Standpipe Pressure	1,959 psi	At surface
Density	3 ppg	Average density
Hydrocarbon Mass	207,774 lb _m	Hydrocarbon in riser
Gas	1,128,213 SCF	Equivalent gas volume
Oil	388 STB	Equivalent oil volume

When the liquids were expelled from the riser and MGS, the riser would blow down, discharging hydrocarbons through the MGS outlets, as well as other possible paths, such as the telescoping joint seals and the diverter sealing element. The discharge through each outlet is proportional to the pressure in the MGS and the area of the outlet since the flow is choked. The flow fraction for each of the four outlets is given in the table below.

Table 42: Gas flow distribution through MGS outlets

12" vent line	46%
10" outlet line	31%
6" overboard line	12%
6" vacuum breaker	12%

If the BOP stopped the influx from the well into the riser, then the riser would blow down to ambient pressure. If flow continued, the flow rate could be as much as 70,000 stock tank barrels per day (STB/day) [5]. The associated mass flow rate is presented in Table 43, represented equivalently in various units.

Table 43: Estimated steady state mass flow rate; equivalent representations

70,000 STB/day
203 MMSCF/day
141,264 SCF/min
26,015 lb _m /min

When the hydrocarbon influx displaced the liquids from the riser and MGS, the mass flow rate would ramp up quickly and then decay exponentially. The initial blow down of the riser would be essentially the same whether or not the BOP stopped the influx (via the VBR closure).

4.7.6 Work String Displacement Analysis

In the period preceding closure of the VBR, the accelerating flow created a significant frictional pressure drop in the casing and work string annulus as shown in Figure 58. The work string below the wellhead is assumed filled with seawater and 12 bbl of mud (see Figure 52). With an assumed density of the hydrocarbons of 4 ppg, the effective weight of the work string below the wellhead (see Appendix A) is 73 kips. The upward force on the work string is comprised of the pressure end load and the shear stress on outside of the work string (with no flow through the work string). This upward force is computed to be 38 lb/psi of frictional pressure drop.

The upward load due to frictional pressure drop is shown in Figure 62. The effective weight of the work string below the wellhead is also shown. The axial stiffness of the work string above the wellhead $(AE/L)^{19}$ is 51 kips/ft. At the estimated time of the annular preventer closure at 21:43:40, the graph indicates frictional loading nearly equal to the work string weight. Thus, upward displacement of the work string inside the BOP by one foot or more prior to the closure of the annular preventer was plausible.

¹⁹ The axial stiffness of a long elastic beam or tube may be computed by calculating the ratio of the product of the beam's cross-sectional area (A) and elastic modulus (E) over the length (L). This ratio is referred to as "AE/L".

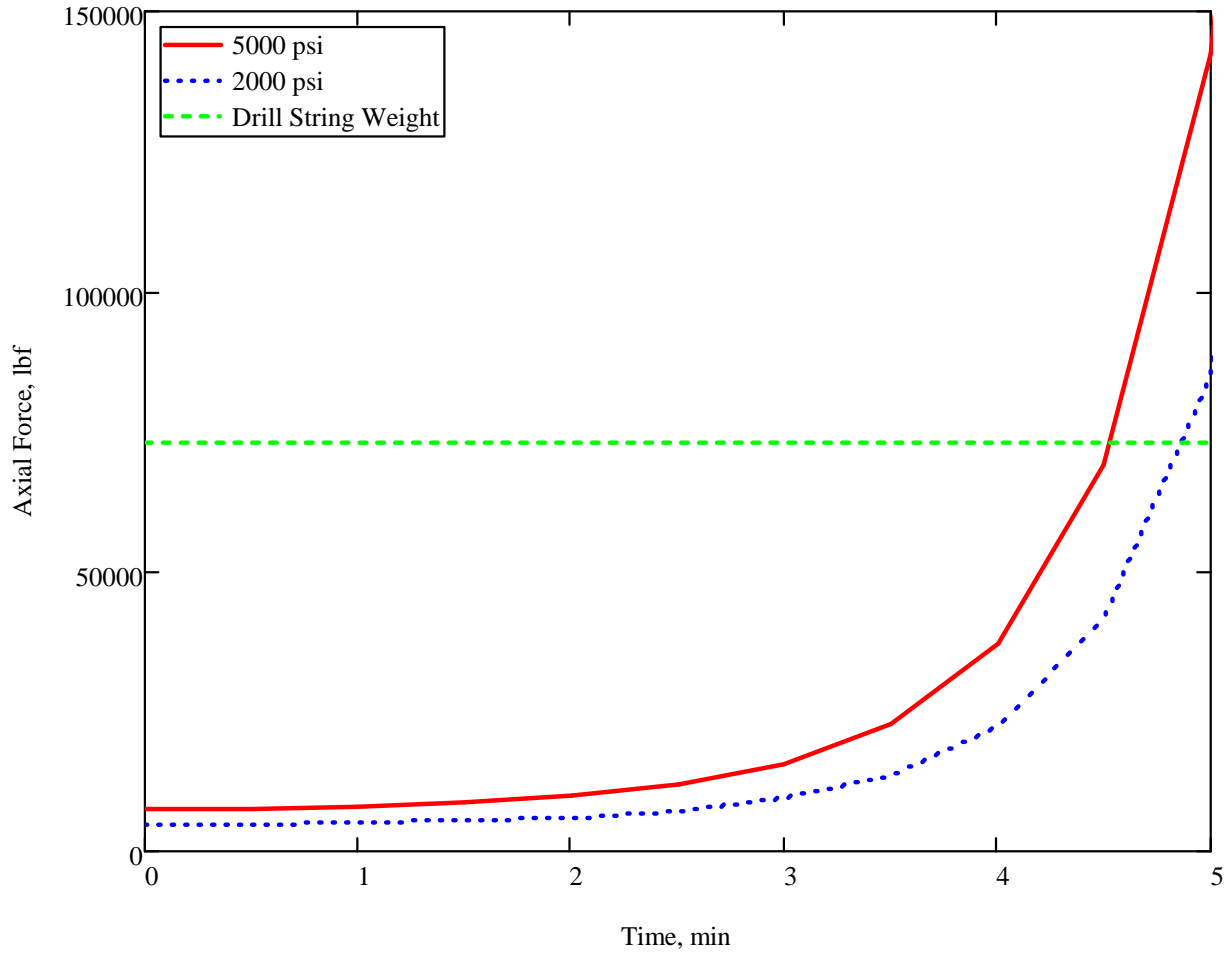


Figure 62: Frictional loading of the work string below the BOP, starting at 21:39

4.7.7 Flow Velocities Around and Through Work String at Selected Times

The flow velocity around and through the work string were deemed to be of interest during the final 20 minutes of transmitted data, as well as for conceivable flow paths occurring after end of transmission. The scenarios of interest are:

1. Flow through the work string-to-casing annulus during closure of the annular (21:43:40);
2. Flow through the annulus just prior to closure of the VBR (21:47:00);
3. Flow through the work string following closure of the VBR, assuming an open flow path through the work string (at some point after end of transmission);
4. Flow through and/or around the work string following further deterioration of the work string (after a prolonged interval following end of transmission).

For flow through the work string-to-casing annulus, the highest velocity is in the annulus between the tool joint of the 5-1/2" drill pipe (7" OD) and the casing (8.625" ID) just below the wellhead; the area of the annulus is 19.9 in². For flow through the work string, the highest velocity is inside the 3-1/2" tubing (2.992" ID); the area is 7.0 in². The average linear flow velocity is the estimated volumetric flow rate divided by the corresponding area.

The volumetric flow rate at the time of the apparent closure of the annular (Scenario 1) is estimated from the transient model shown in Figure 57, since the riser is largely filled with liquid and the flow through the annulus is essentially the same as the surface flow out. For the remaining scenarios, the riser is filled with hydrocarbons and the flow in is based on well performance. Well flow rate estimates as a function of wellhead pressure with flow up the casing, with and without flow through the work string, are reported in [6] (see Figure 3.9, Section 3.4 of Appendix W). The reported flow rates are in stock tank barrels per day (STB/day). The corresponding mass flow rate is calculated using the hydrocarbon properties in [10], with hydrocarbon density estimates based on pressure. The volumetric flow rate is the mass flow rate divided by the density.

Scenario 1: The flow rate just before the apparent closure of the annular is calculated at 21:43:15 (4.25 minutes after 21:39). The calculated flow rate is 4,465 gpm. The hydrocarbon density is approximately 3 ppg, corresponding to 36,043 STB/day or 13,395 lb/min. Flow is around the string (no flow through the work string). The average velocity around a tool joint inside the casing, just below the wellhead, is

$$V = (4,465 \text{ gpm}) / (7.4805 \text{ gal/ft}^3) / (60 \text{ s/min}) / (19.9 \text{ in}^2) / (144 \text{ in}^2/\text{ft}^2) = 72 \text{ ft/sec}$$

Scenario 2: Just prior to VBR closure at 21:47, the riser is filled with hydrocarbons and the flow is around the work string (no flow through the work string). The flow rate (from [6]) is approximately 60,000 STB/day or 22,299 lb/min. With a density of approximately 3 ppg, the volumetric flow rate is 7,433 gpm. The average velocity around a tool joint inside the casing, just below the wellhead, is 120 ft/sec.

Scenario 3: Following closure of the VBR, flow was interrupted as indicated by the rise in standpipe pressure (see Figure 48). With the VBR closed, flow may proceed through the inside of the work string, provided an open flow path is present. In this case, the flow rate (from [6]) is approximately 40,000 STB/day or 14,866 lb/min. The 3-1/2" tubing is at the bottom of the work string, so the pressure inside the tubing is higher than wellhead pressure. The estimated density is approximately 4 ppg, resulting in a volumetric flow rate of 3,716 gpm. The average velocity in the tubing is 170 ft/sec.

Scenario 4: Here we assume that the work string deteriorates such that flow continues both through the work string and around the work string, i.e. a washout or parting occurs in the drill pipe below the wellhead. With the reduced pressure in the riser and the reduced losses in the flow path, the flow rate estimate is 70,000 STB/day or 26,015 lb/min. For a density of 3 ppg, the volumetric flow rate is 8,672 gpm. The average velocity around a 5-1/2" tool joint inside the casing is 140 ft/sec. If all of the flow goes through the inside of a tool joint (4" ID), the average velocity is 220 ft/sec.

5 DISCUSSION

5.1 Key Observations

Several key observations may be drawn from the analysis presented herein, with varying degrees of confidence depending on the presence or lack of corroborating evidence, or accuracy of supporting analysis.

SES places a high degree of confidence in the following observations:

1. From 15:00 onward, rig pump volumetric flow efficiencies are calculated to be significantly lower than previously established values.
2. The Sperry-Sun flow sensor data under-reported the true return flow rates by 4 to 8 percent.
3. During the auxiliary line displacement, spacer displacement, and seawater displacement, pit return volume measurements were obscured due to transfers of mud from the active pits, which occurred at an unknown rate.
4. 421 bbl of 16 ppg spacer were pumped into the well.
5. The spacer was not displaced above the BOP prior to beginning the negative test. Therefore, the annulus below the BOP was partially filled with spacer during the negative test activity.
6. During the negative testing, the well was underbalanced, with potential influx from the pay zone, on three separate occasions.
7. During the second seawater displacement (following the negative test, prior to the static sheen test), it is calculated that the well became underbalanced to the 13.1 ppg formation at 20:38, and to the 12.6 ppg formation at 20:52.
8. A return volume of 1,160 bbl was taken during the second seawater displacement.

9. The spacer was not at the top of the riser upon shutting down the pumps for the static sheen test at 21:09.
10. 33 bbl of hydrocarbon influx were taken into the well during the static sheen test.
11. Approximately 12 bbl of 14.17 ppg mud were drawn into the work string during the bleed from 21:36 to 21:38.
12. By 21:39, 501 bbl of hydrocarbon influx was taken into the well. At this point, the hydrocarbons reached the end of the work string at 8,367 ft depth.
13. It is estimated that an annular preventer was closed on the BOP at 21:43:40, but the closure failed to seal the well.
14. Hydrocarbon gas reached the rig surface (emerging from the mud gas separator vent outlets) at 21:46:40. At this time, the volume gain was 2,510 bbl.
15. A variable bore ram was closed on the BOP at 21:47:00, which temporarily shut in the well.
16. The final recorded data transmission from the *Deepwater Horizon* occurred at 21:49:15.

Other observations that arise from the analysis herein, but which may be subject to revision in light of new data or analysis, are as follows:

1. Some or all of the auxiliary lines (booster, choke, kill) may not have been fully displaced prior to proceeding with the negative test.
2. A theory of volume losses to the wellbore during the seawater displacement prior to the negative test produces analytical results that more closely approximate the recorded measurements. This theory is not conclusive and alternative explanations are conceivable.
3. The well was in balance with the formation twice during the negative testing.
4. During the final negative test, flow through the kill line was blocked by either a gelled spacer plug or a closed valve.
5. Based on a comparison between simulated and measured standpipe pressure and flow data, a washout of a portion of the 3-1/2 inch tubing wall may have occurred during the post-negative test seawater displacement.
6. The return flow taken during the second seawater displacement contained an estimated 61 bbl of influx volume from the underbalanced well.
7. An estimated 138 bbl of well influx was taken during the final seawater displacement (following the static sheen test).

5.2 Comparison of Hypothetical Displacement Scenario to Actual Events

Considering the time interval of interest as a whole compared to the hypothetical displacement procedure presented in Section 3, it is evident that numerous anomalies were present in the well state, along with associated measurements, at many times. Several such events are noted in Table 44. Standpipe and kill line pressures from the hypothetical scenario are repeated from Section 3, with corresponding measured pressures for each event.

Table 44: Pressure responses, hypothetical scenario vs. actual

Event	Standpipe Pressure		Kill Line Pressure	
	<i>Hypothetical</i>	<i>Measured</i>	<i>Hypothetical</i>	<i>Measured</i>
Kill Line Displacement	0 psi	108 psi	1,465 psi	1,440 psi
End of First Displacement	1,570 psi	2,325 psi	1,570 psi	1,185 psi
Open Kill Line to Work String	1,570 psi	1,395 psi	1,570 psi	682 psi
Negative Test (beginning)	0 psi	1,202 psi	0 psi	18 psi
Negative Test (end)	0 psi	1,391 psi	0 psi	25 psi*
Prior to Second Displacement	1,570 psi	~2,600 psi	1,570 psi	22 psi*
End of Second Displacement	500 psi	1,013 psi	500 psi	21 psi*
Final Displacement	0 psi	1,171 psi	0 psi	767 psi

*Lower kill line valve may have been closed or plugged; not measuring well state

From the table it is evident that anomalous pressures were present as early as the end of the first displacement. From that point onward, the standpipe and kill line pressures neither matched the hypothetical values, nor were they equal, as would be expected for a full seawater displacement without formation influx.

An event of particular importance is the opening of the kill line to the work string at 16:57 (see Figure 26 and Table 23, Event 3). The unequal pressures observed at this point were a clear indicator of an incomplete initial displacement. Other anomalous indicators were the pressure buildups to 1,202 and 1,391 psi during the negative test (both of which occurred following a bleed) and the large and unequal standpipe and kill line pressure measurements immediately

following the final displacement at 21:30 (both should have been trending to zero psi at that time).

5.3 Summary of Pump Efficiency Estimates

The performance of the rig pumps was analyzed in detail in Section 4, and the results of the various analyses are presented in Table 45. As indicated, three possible measurements were available during the time interval of interest against which to check the pump volumetric efficiency: The flow sensor, the return volume into the active pits, and the volume drawn from the pits by the pumps. Of these, the last measurement is the most accurate, as it is a direct measurement of the pump volume throughput. The others are indirect, because the fluid must be pumped through the well and return to the surface before being measured, and are therefore subject to losses, thermal and compressibility effects, and other sources of error. The flow sensor is the least accurate indicator, because its output must be integrated in time to obtain a volume estimate.

Table 45: Summary of rig pump volumetric efficiency analyses

Event	Efficiency Based on Flow Sensor	Efficiency Based on Pit Return Volume	Efficiency Based on Pumped Pit Volume
Booster Line Displacement (Pump 1)	52.2%	N/A	N/A
Choke Line Displacement (Pump 2)	74.1%	N/A	N/A
Kill Line Displacement (Pump 2)	76.3%	N/A	N/A
Spacer Displacement (Pumps 3 & 4)	82.3%	N/A	89.0%
First Seawater Displacement (Pumps 3 & 4)	76.5%	N/A	N/A
Second Seawater Displacement (Pumps 1, 3 & 4)	77.4%	80.9%	N/A
Final Seawater Displacement (Pumps 1, 2, 3, & 4)	N/A	N/A	N/A

N/A = Not Available

From Table 45, it is evident that only one pumped pit volume measurement was available during the time interval of interest: the spacer pumped out of pit #5, from which an efficiency of 89% was calculated on rig pumps #3 and #4. Similarly, only one pit return volume measurement is available: the returns taken during the second seawater displacement. The overall efficiency for this event was calculated at 80.9% on pumps #1, #3, and #4. However, if it is assumed that the prior efficiencies calculated for these pumps remained constant relative to earlier estimates, the results are in good agreement, as shown in Table 46.

Table 46: Pump output summary, second seawater displacement

Pump	Strokes	Theoretical Output	Efficiency	Output Volume
3 & 4	8,103	0.13113 bbl/stk	89%	945.7 bbl
1	2,255	0.13113 bbl/stk	52%	153.8 bbl
Total	10,358	0.13113 bbl/stk	80.9%	1,099.5 bbl

The results from the flow sensor, although less reliable, do provide some insight into the performance of pump #2, for which no other measurements are available. If it is assumed that the sensor output error (with respect to the true return volume) remains constant, the actual pump efficiency results for pump #2 are somewhat higher than the values reported in Table 45, yet the resulting volumes are still insufficient to fully displace the choke and kill lines.

In no case during the time interval of interest (from 15:00 onward) was SES able to corroborate the anticipated volumetric efficiency of 96.1% via the measurements available for any of the four rig pumps.

5.4 Hydrocarbon Flow Path

The analyses herein are presented supposing that all hydrocarbon influx occurred through the shoe track and float equipment before proceeding up the inside of the production casing. Nonetheless, it is acknowledged that alternative flow paths were physically possible. The set of possible flow paths include:

1. Flow into the inside of the production casing via the shoe track and float equipment;
2. Flow into the inside of the production casing via a leak in the casing (casing wall or connection failure) above the float equipment but below the work string;
3. Flow into the inside of the production casing (casing wall or connection failure) via a leak above the end of the work string;
4. Flow within the outer production casing annulus via a leak in (or lifting of) the upper seal assembly;
5. Underground flow outside the wellbore.

SES believes that the preponderance of evidence supports the scenario of flow inside the production casing below the work string through the shoe track (flow path 1), per the following rationale:

Flow path 5: This flow path is ruled out because hydrocarbons were observed to be flowing out of the riser and BOP during and after the incident. Note that this observation does not preclude the possibility of underground flow which subsequently returned to the wellbore; however, the net behavior would be consistent with one of the other possible flow paths (1 – 4) in this case.

Flow path 4: Flow path 4 is not consistent with several portions of the measured data set, particularly the record of the final 20 minutes. Had the leak path been through the seal assembly, the fluid inside the production casing would have been undisturbed as the influx progressed. After the final seawater displacement ended at 21:30, a static column of seawater would be present in the work string-to-casing annulus.

Per Table 3, with the drill string and kill line filled with seawater, the difference in pressure between the two lines is zero (or nearly zero, in the event the kill line contained a small amount of mud or spacer). Furthermore, as the hydrocarbon influx displaced mud into the BOP and riser, the kill line and standpipe pressure signals would follow identical (increasing) trends. Referring to Figure 48, it is evident that the standpipe and kill line signals were not zero, not equal, and followed uncorrelated trends over time. The differences in the measured signals must be attributed to flow activity in the work string-to-casing annulus, and hence, influx through the inside of the production casing.

A second argument against flow through the seal assembly is that the heavier column of pure mud in the casing outer annulus would require further displacement of the riser to reach the well's balance point. This is illustrated in Figure 63, which depicts the hypothetical well displacement at the end of the second seawater displacement (the beginning of the static sheen test), with sketches of the outer casing annulus added. If exposure to the formation is assumed through the casing shoe, the well is clearly underbalanced at this stage. However, if the shoe is sealed and exposure is through the casing annulus, the well is still overbalanced. In the case of reduced pump efficiencies presented in Section 4, the overbalance would have been even greater than the hypothetical displacement scenario at this point (21:08). Since the well was demonstrated to be flowing at this time, the theory of flow through the seal assembly is not substantiated.

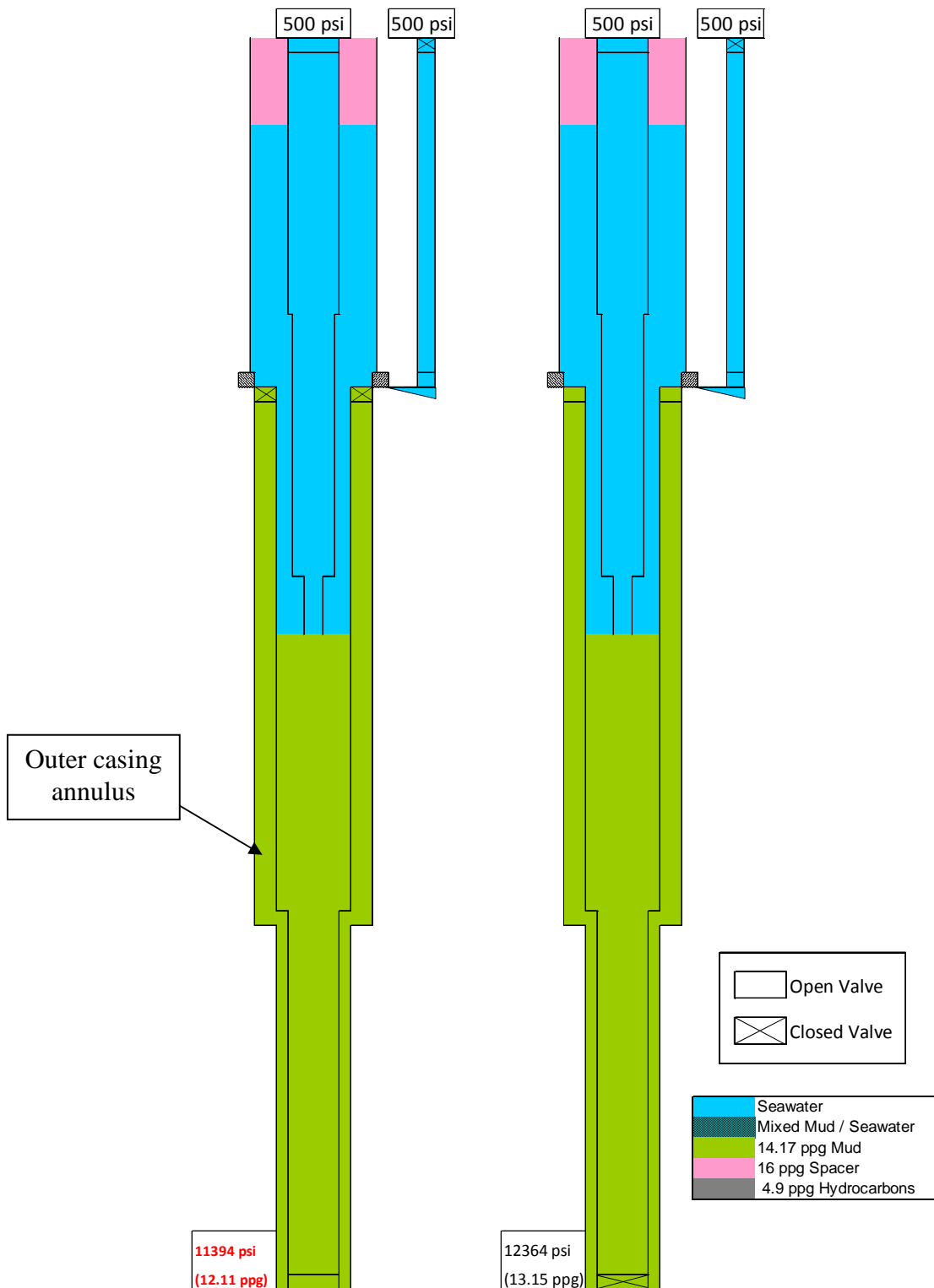


Figure 63: Hypothetical displacement procedure at static sheen test. Formation exposure to production casing only with sealed annulus (left); exposure to open annulus only (right)

Flow path 2 and 3: Both of these flow paths assume a failure of the production casing or one of its connections. This failure mode is less likely than a failure involving the float equipment due to the successful execution of the positive casing test (see Figure 29). In terms of the measured data, an argument similar to that used for flow path 4 may be made for flow path 3, depending on the actual vertical location of the supposed leak path. Flow path 2 would produce pressure responses similar to the actual recorded measurements, and thus is the more likely of the two.

Flow Path 1: SES deems this path to be the most likely, because agreement with the observed measurements can be obtained using this assumption, and the equipment through which the leak would occur (the float collar) was not tested during the positive casing test. Indeed, the success of the positive casing test and failure of the negative test suggests that the leak should be attributed to the primary cement and/or the float collar, as they were not tested by the former activity, but were exercised by the latter.

6 REFERENCES

1. American Petroleum Institute. *Recommended Practice for Field Testing seawater-Based Drilling Fluids*. API Recommended Practice 13B-1, 3rd Ed., December 2003.
2. American Petroleum Institute. *Recommended Practice for Design and Installation of Offshore Process Piping Systems*. API Recommended Practice 14E, 5th Ed., October 1991.
3. American Petroleum Institute. *Rheology and Hydraulics of Oil-Well Fluids*. API Recommended Practice 13D, 6th Ed., May 2010.
4. ASTM International. *Standard Practice for Using Significant Digits in Test Data to Determine Conformance with Specifications*. ASTM E29-08, 2008.
5. BP, PLC. *BP Exploration Project String*. Rig telemetry data time plot, 20 April 2010.
6. BP, PLC. *Deepwater Horizon Accident Investigation Report*. 8 September 2010.
7. BP, PLC. *Washington Briefing: Deepwater Horizon Interim Incident Investigation*. Congressional committee presentation, 24 May 2010.
8. Deepwater Horizon Joint Investigation. "MacondoWellSchematic.796427.pdf". <http://www.deepwaterinvestigation.com/go/doc/3043/796427/>. Accessed 26 July 2010.
9. MI Swaco, LLC. *BP / Deepwater Horizon Rheliant Displacement Procedure, "Macondo" OCS-G 32306*. Undated.
10. Pencor Petroleum Services Division. *Volatile Oil Reservoir Fluid Study*. Report No. 36126-19-5010068508. 30 June 2010.
11. Smith, J.R. *Review of Operational Data Preceding Explosion on Deepwater Horizon in MC 252*. Technical report. 1 July 2010.
12. Transocean Offshore Deepwater Drilling, Inc. "BP - TO11000827.txt". Text-format tabular data file.
13. Transocean Offshore Deepwater Drilling, Inc. "Cement Data 18April 20April2010.las". Text-format tabular data file.
14. Transocean Offshore Deepwater Drilling, Inc. "MC252_001_ST00BP01_APR 15 - Apr 20_ASCII.txt". Text-format tabular data file.
15. Transocean Offshore Deepwater Drilling, Inc. "Slegal0410062412220.pdf". Scanned document of riser dimensions (outside diameter and inside diameter).

16. Transocean Offshore Deepwater Drilling, Inc. "Slegal0410062416350.pdf". Scanned document of drill pipe and casing/connection performance properties, BOP component elevation drawing and well bore/drill string schematic.
17. Transocean Offshore Deepwater Drilling, Inc. "TimeSDLStats 05April20April2010.las". Text-format tabular data file.
18. Transocean Offshore Deepwater Drilling, Inc. "DOC-00011902 Pipe Info For stress". Excel spreadsheet.
19. Transocean Offshore Deepwater Drilling, Inc. "DOC-00003098 Mud Degasser Dwg No.9820138". PDF of drawing.
20. Transocean Offshore Deepwater Drilling, Inc. "DOC-00003099 Mud Degasser Dwg No.9820139". PDF of drawing.
21. Transocean Offshore Deepwater Drilling, Inc. Personal Communications: Transocean Macondo Investigation Team to Stress Engineering Services. 2010.
22. Transocean Offshore Deepwater Drilling, Inc. *Well Control*. Document No.HQS-OPS-HB-01, Issue No. 3, Revision No. 1. Section 5, subsection 3, page 1. March 31, 2009.
23. White, Frank M. *Fluid Mechanics*. 4th ed. McGraw Hill, New York NY 1999.

Appendix A: Analysis Input Parameters

Table 47: Drill Pipe Specifications

Drill Pipe Specifications			
Description	3-1/2" 9.3# Tubing	5-1/2" 21.9 # S-135 HT55	6-5/8" 32.67# S-135 FH
OD (in)	3.5	5.5	6.625
Adjusted OD (in)	3.526	5.606	6.734
ID (in)	2.992	4.778	5.625
Adjusted ID (in)	2.992	4.738	5.586
Displacement (bbl/ft)	0.00338	0.00871	0.01374
Capacity (bbl/ft)	0.00870	0.02181	0.03031

Table 48: Wellbore Fluid Capacities and Volumes

Capacities/Volumes		
Description	Capacity (bbl/ft)	Volume (bbls)
Boost	0.01425	71.26400709
Choke Line	0.01967	99.14808384
Kill Line	0.01967	98.99562852
6-5/8"	0.03031	124.36
5-1/2"	0.02181	75.09
3-1/2"	0.00870	7.14
9-7/8" x 3-1/2"	0.06019	49.42
9-7/8" x 5-1/2"	0.04174	104.01
BOPx 5-1/2 below ann	0.31099	11.53
BOP x 5-1/2 above ann	0.31099	4.95
Riser x 5-1/2"	0.33886	304.30
Riser x 6-5/8"	0.32534	1334.87

Table 49: Wellbore Equipment Depths

Depths (ft)	
RKB to MSL	75
Water Depth	4992
Top of BOP (riser adapter)	5001
Lower Annular	5017
Top of High Pressure Housing	5054
Top of Low Pressure Housing	5057
Mudline depth	5067
Length of 6-5/8" drill pipe	4103
Length of 5-1/2" drill pipe	3443
Length of 3-1/2" tubing stinger	821
Length of boost line	5001
Length of choke (middle entry)	5040
Length of kill line (upper entry)	5032

Table 50: Other Well Specifications

Other Specifications	
ID 21-1/2" Riser (in)	19.50
ID 18-3/4" BOP (in)	18.75
ID 9-7/8" Prod Csg (in)	8.625
ID Boost Line (in)	3.83
ID Kill/Choke Line (in)	4.50
Density of Mud (ppg)	14.17
Density of spacer (ppg)	16.00
Density of seawater (ppg)	8.556

Table 51: Mud Pump Specifications

Mud Pump Specifications - Continental Emsoco Triplex Pumps	
Bore (in)	(3) x 6"
Stroke (in)	15"
Theoretical Output (bbl/stroke)	0.13113
MI-Swaco stated output (bbl/stroke)	0.126
Anticipated Efficiency (%)	96.1%

Appendix B: Time-Domain Hydraulic Models

The simulation results presented herein are based on the output from two independent mathematical hydraulic models of the Macondo wellbore, which were developed at SES. For purposes of the present discussion, the models are designated ‘A’ and ‘B’. The theoretical basis for each is as follows:

- A. Fixed time-step simulation using non-Newtonian fluid viscosities based on the rheological power-law models provided in API RP 13D [2];
- B. Variable time-step simulation using a Newtonian viscosity approximation (plastic viscosities as defined in API RP 13B-1 [1]).

As the rheological properties of the drilling fluids used during the period of interest were not well established, the employment of these separate models provided confidence that differing rheological models (i.e. Newtonian vs. non-Newtonian) would not materially affect the results.

Each model is based on the concept of a series of control volumes, which represent the various segments of the well’s circulating volume. Fixed control volume geometry is employed at each unique hydraulic cross-section within the volume (i.e., a change in cross sectional area or hydraulic diameter requires a new control volume). Flow is assumed incompressible and non-rotational (one-dimensional). Diagrams of the geometric control volumes used in each model are given in Figure 64 and Figure 65. Geometric input parameters are per the tables listed in Appendix A.

In addition, control volumes with varying boundaries are used to segregate multiple fluids (if present) within a geometric segment. For example, spacer and mud flowing in the same drill pipe segment are represented by two variable volumes, with relative capacities defined by the volume of each fluid present within the segment. This modeling decision imposes a “no mixing” constraint between the fluids.

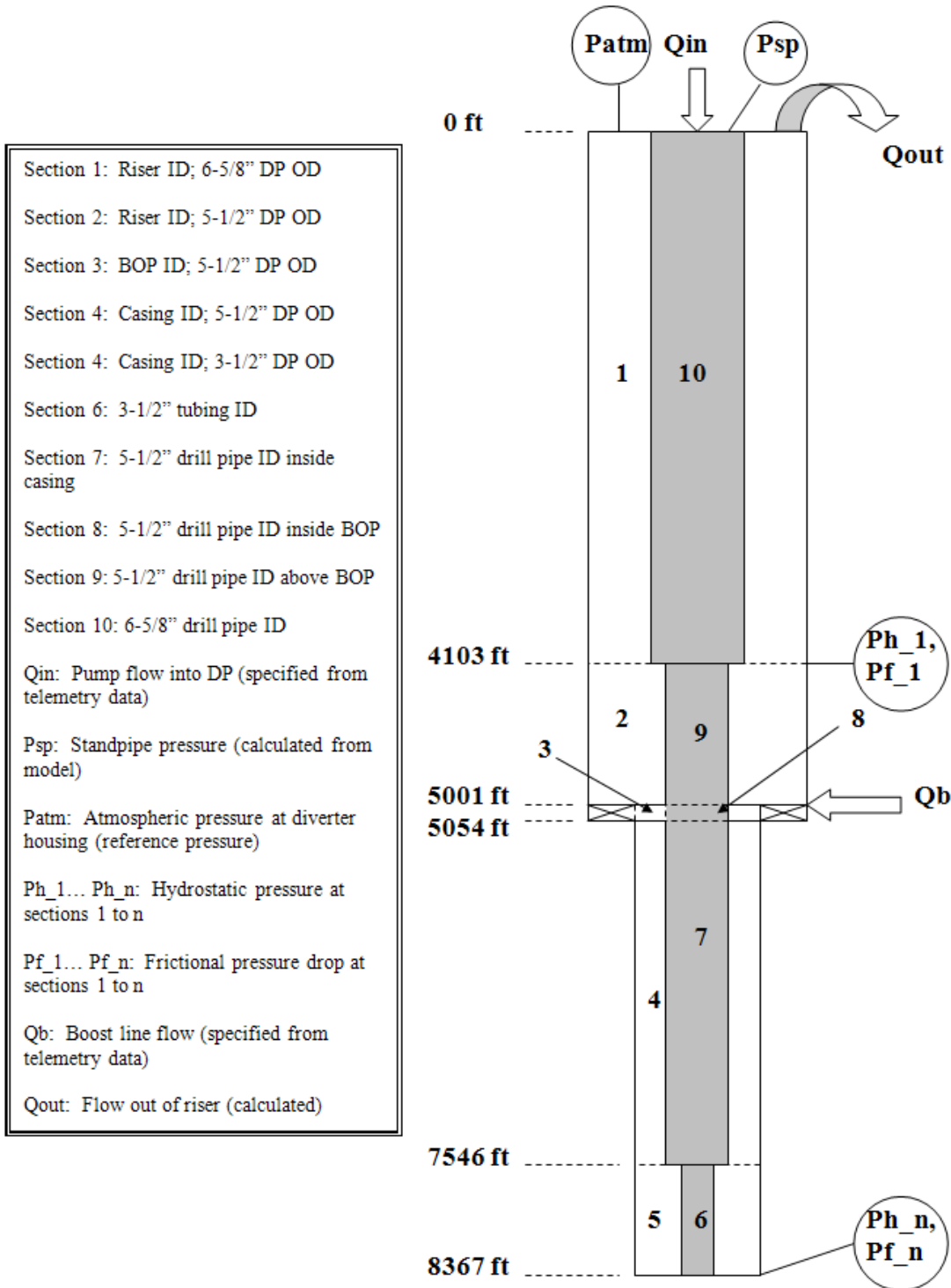


Figure 64: Model A Geometric Diagram and Variable Labeling

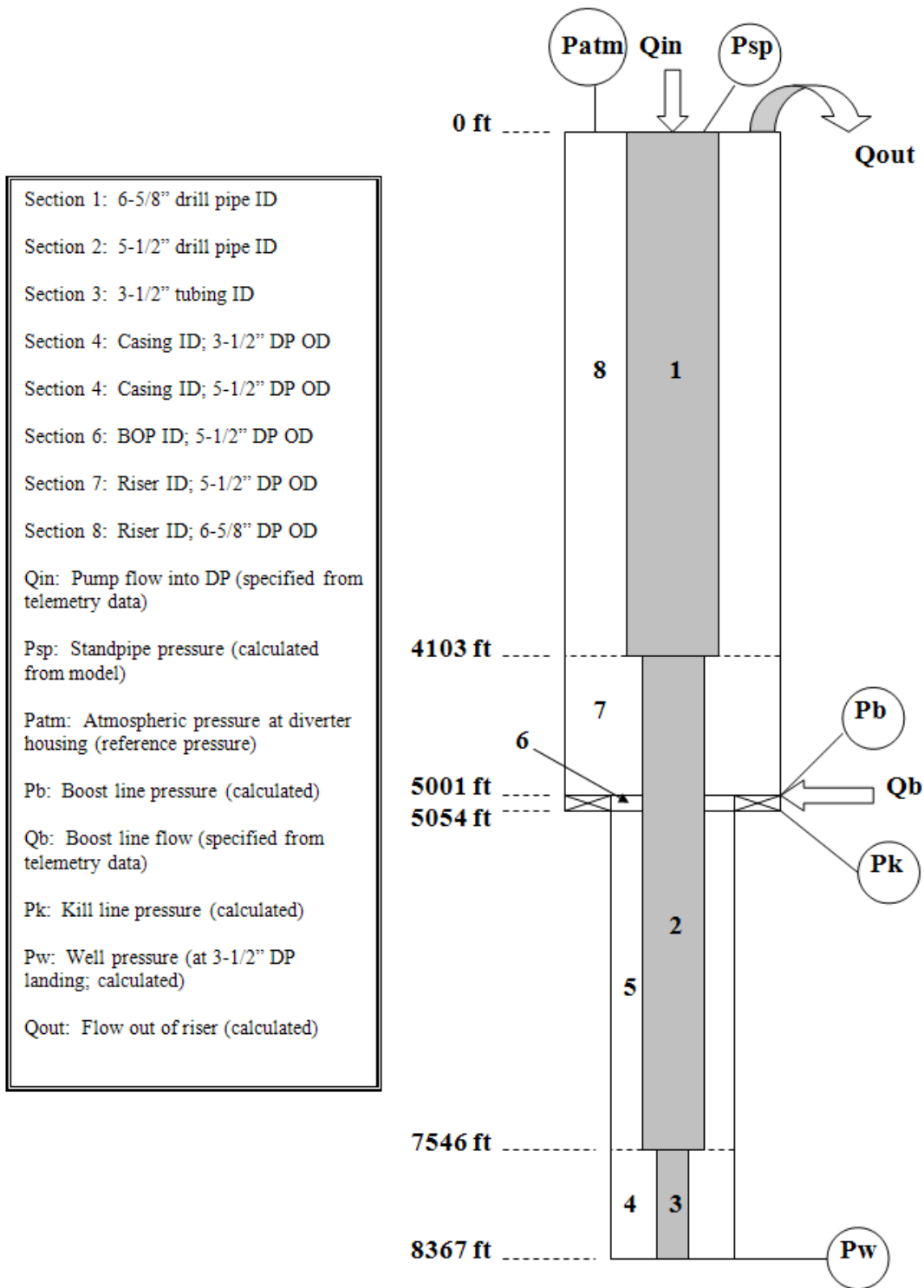


Figure 65: Model B Geometric Diagram and Variable Labeling

As illustrated in Figure 64 and Figure 65, the inputs to the models are prescribed pump flow rates into the work string and booster line. The flow rates are derived from the pump stroke data from the rig telemetry files, modified by appropriate volumetric efficiencies as documented herein.

At each time step, the models calculate the following hydraulic quantities for each control volume segment:

1. Hydrostatic pressure at each distinct elevation;
2. Frictional pressure drop due to flow;
3. Flow velocity;
4. Variable boundary position;
5. Cumulative displaced volume.

Model A also calculates and reports the instantaneous apparent viscosity for each control volume segment, based on the assumed power law.

To achieve a match with the measured data, it was necessary to “tune” each model by varying one or more unknown parameters. In the case of Model A, the coefficients of the power law used to model the non-Newtonian fluid viscosities were varied; in Model B, the pipe wall surface roughness and the initial apparent viscosity of the 14 ppg mud (assumed to be gelled) were varied.

The fluid properties used for the final Model A simulation runs are listed in Table 52. The parameters n and k are the flow index and consistency index, respectively, per [2].

Table 52: Model A fluid properties

Fluid	Density	n (pipe)	k (pipe)	n (annulus)	k (annulus)
Spacer	16 lb _m /gal	0.723	16.340	0.484	30.192
SOBM	14.17 lb _m /gal	0.599	2.420	0.228	31.681
Seawater	8.556 lb _m /gal	1.000	0.010	1.000	0.010

The fluid properties used for the final Model B simulation runs are listed in Table 53. The final pipe surface roughness was 0.002 ft (0.024 inches), a reasonable value for rough pipe.

Table 53: Model B fluid properties

Fluid	Density	Viscosity
Spacer	16 lb _m /gal	324 cP (169 cSt)
SOBM	14.17 lb _m /gal	204 cP (120 cSt)
Seawater	8.556 lb _m /gal	1.07 cP (1.04 cSt)

The apparent viscosity of 204 cP is quite high relative to the published value of 28 cP from mud rheology reports (see [6], Appendix W). This value was found to produce the best match to the recorded data, especially at the beginning of the first displacement where mud was present in the work string-to-casing annulus. Figure 66 compares the model results using the matched value with those obtained using the published value.

After tuning, Model A and Model B produced similar output results, which generally matched the measured data from the rig telemetry files. An example output comparison between the two models is given in Figure 67.

To simulate the displacement of the auxiliary lines (see Section 4.1), separate simpler models were constructed based on the same principles as the main wellbore models.

In general, results from Model B are presented in the main report body figures.

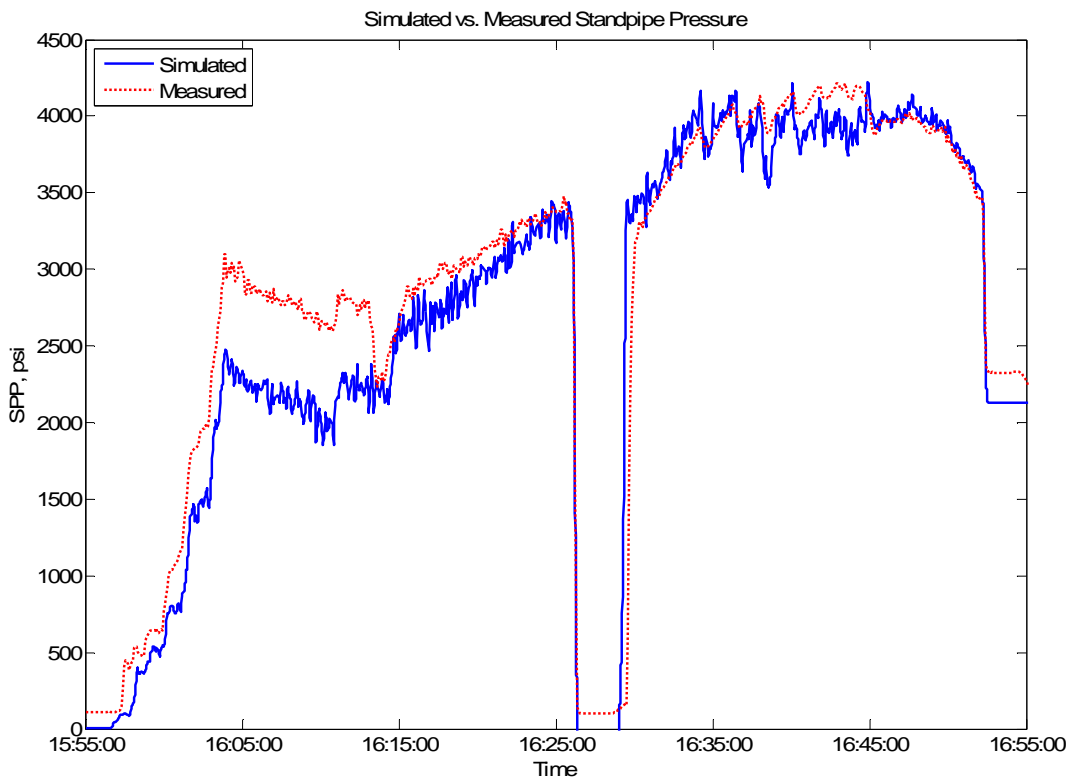
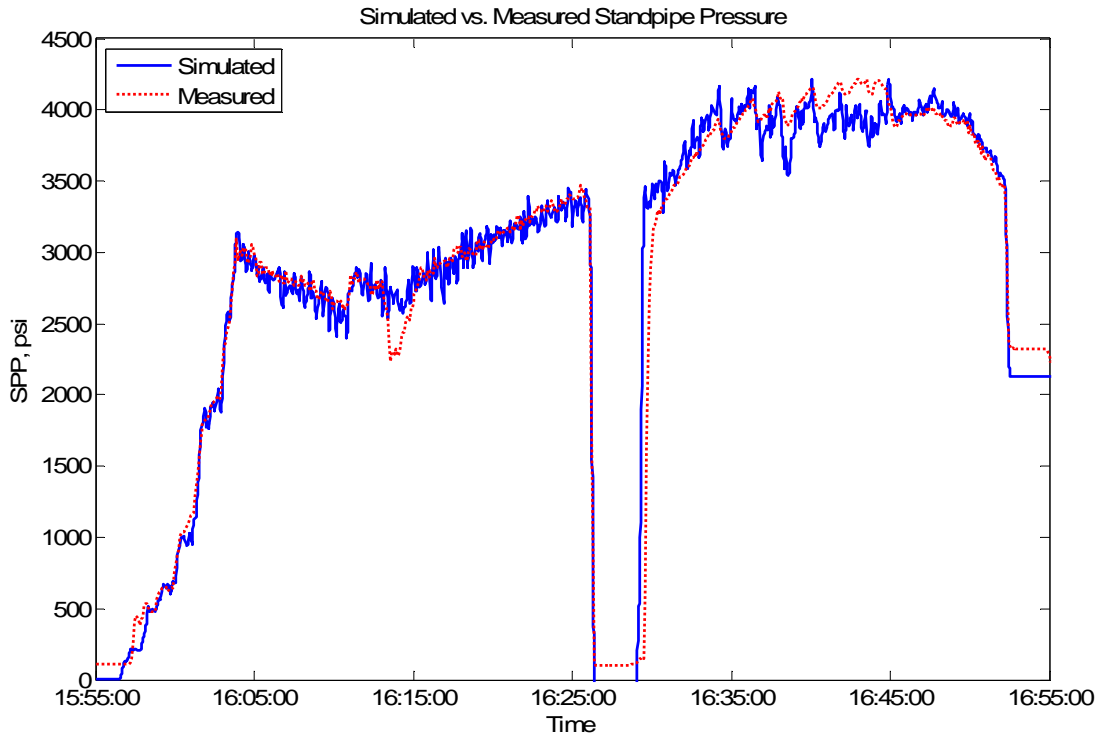


Figure 66: Mud viscosity comparison: 204 cP (top); 28 cP (bottom).

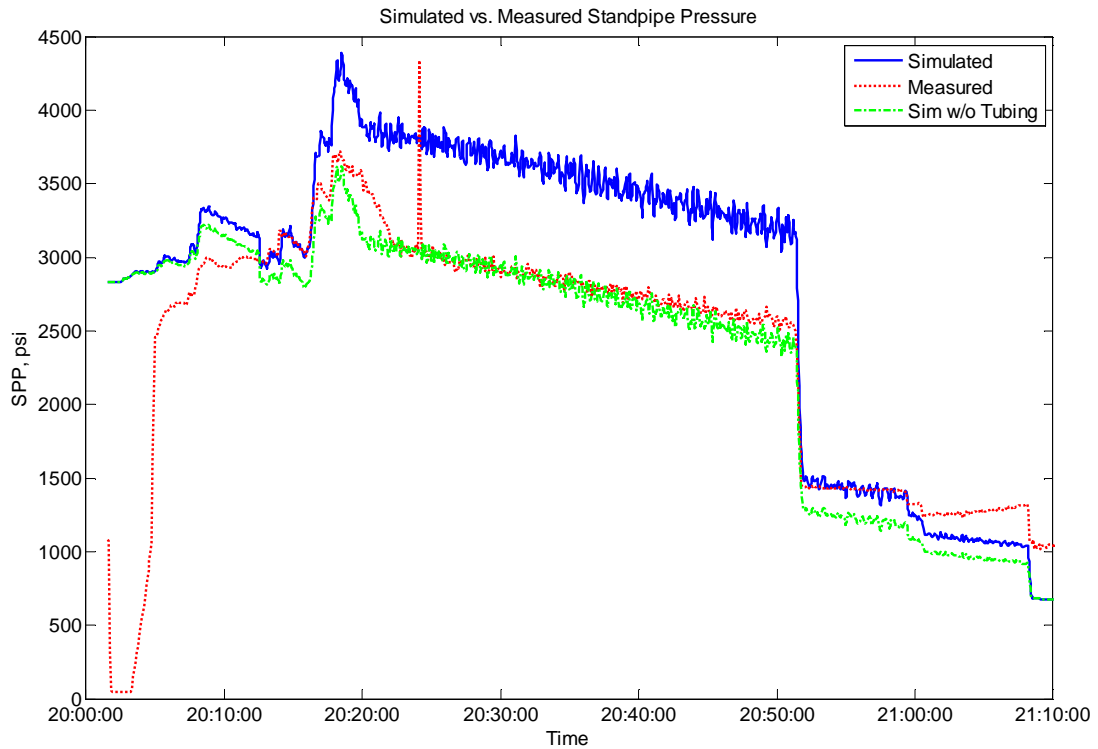
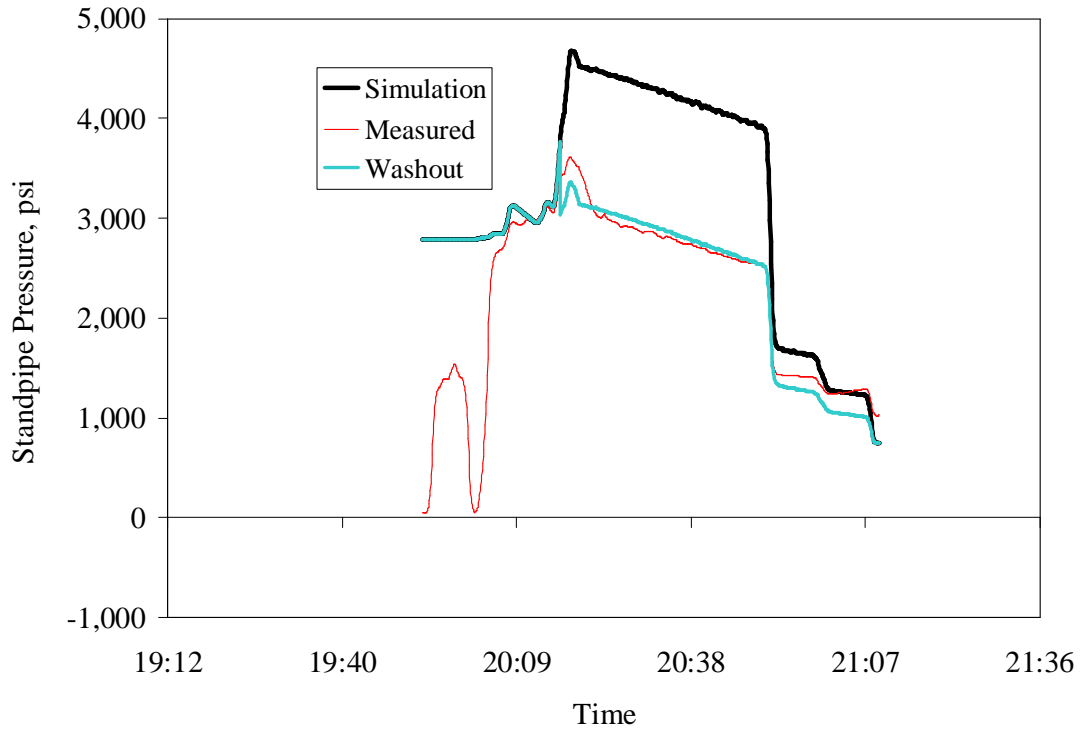
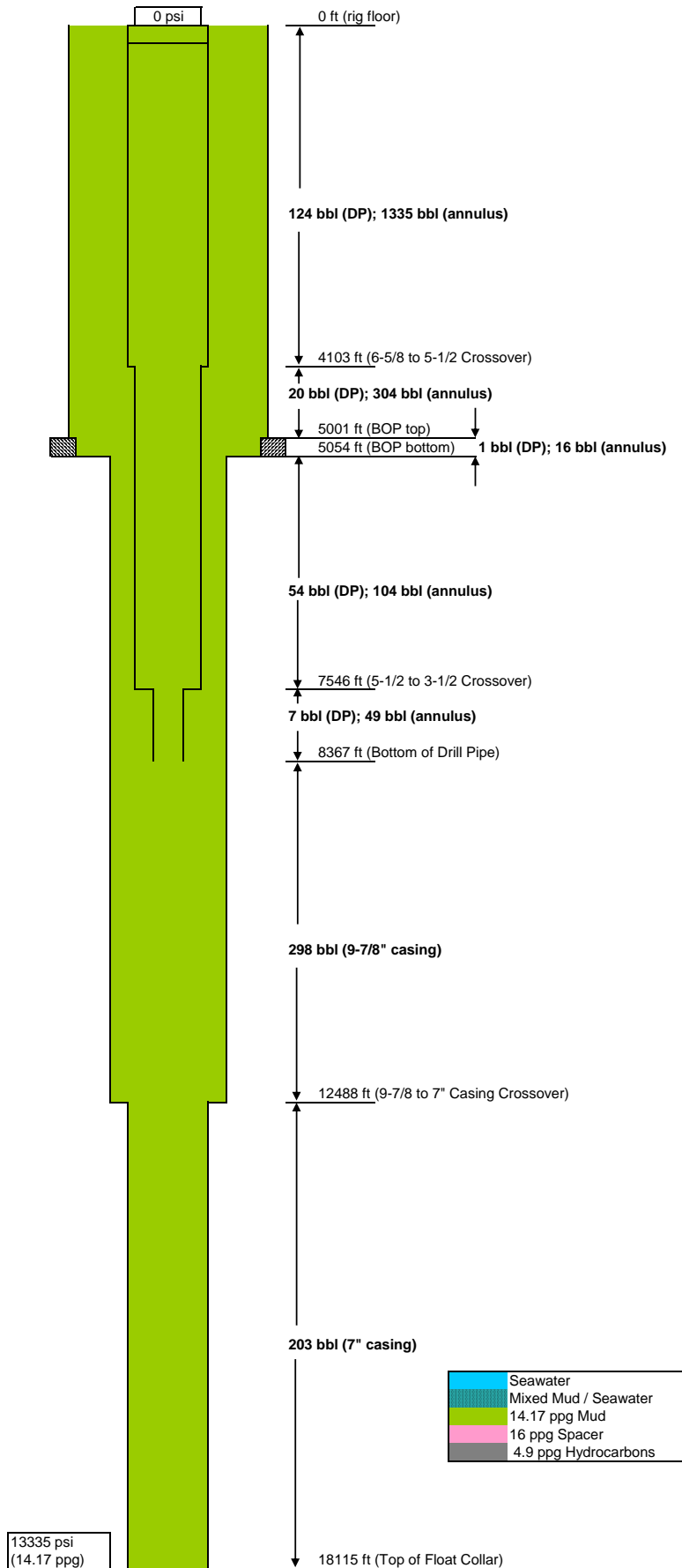


Figure 67: Comparison of simulation outputs: Model A (top); Model B (bottom)

Appendix C: Detailed Charts and Supporting Calculations

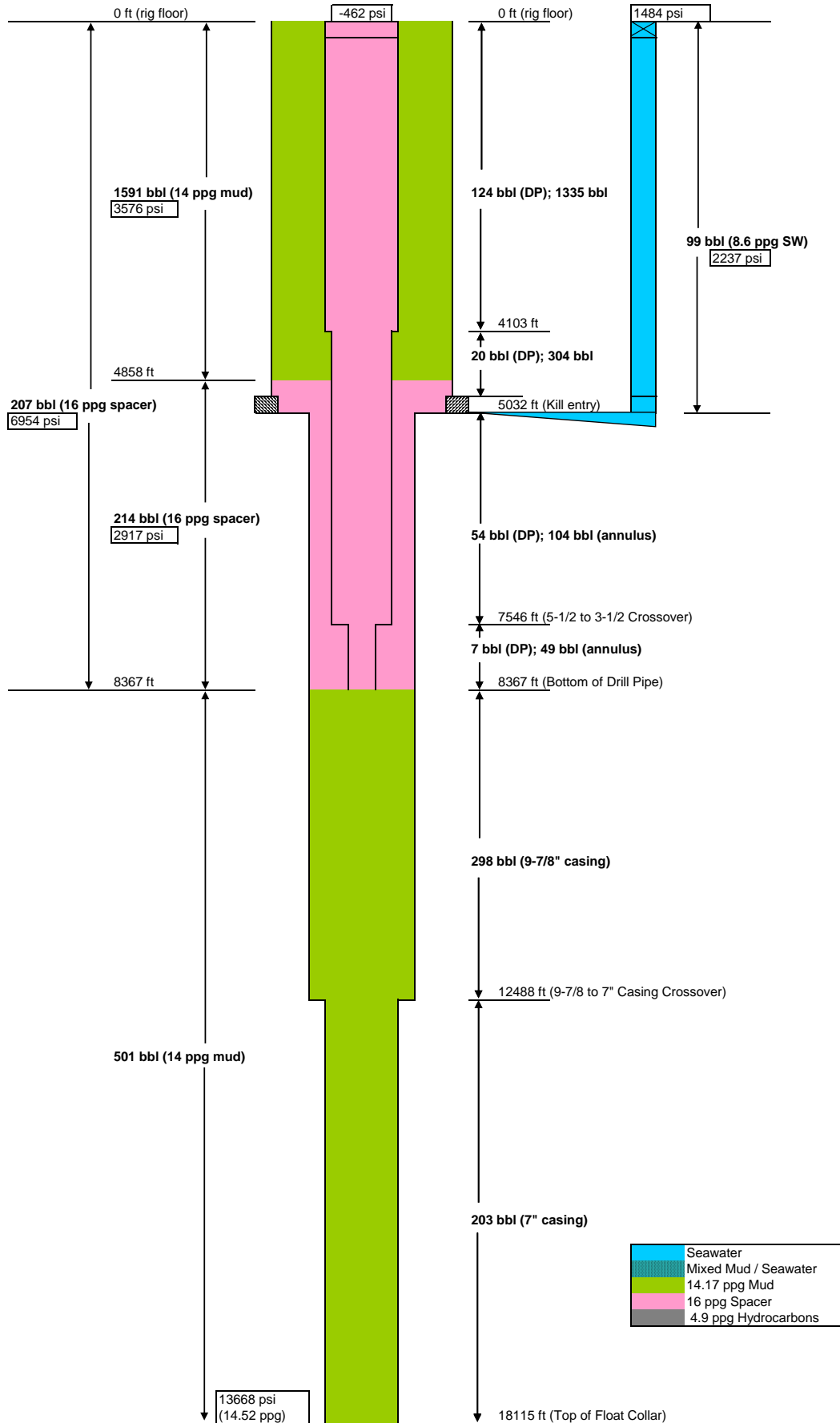
Ideal Pump Schedule Hydrostatics, Pre-Displace #1

1/7/2011



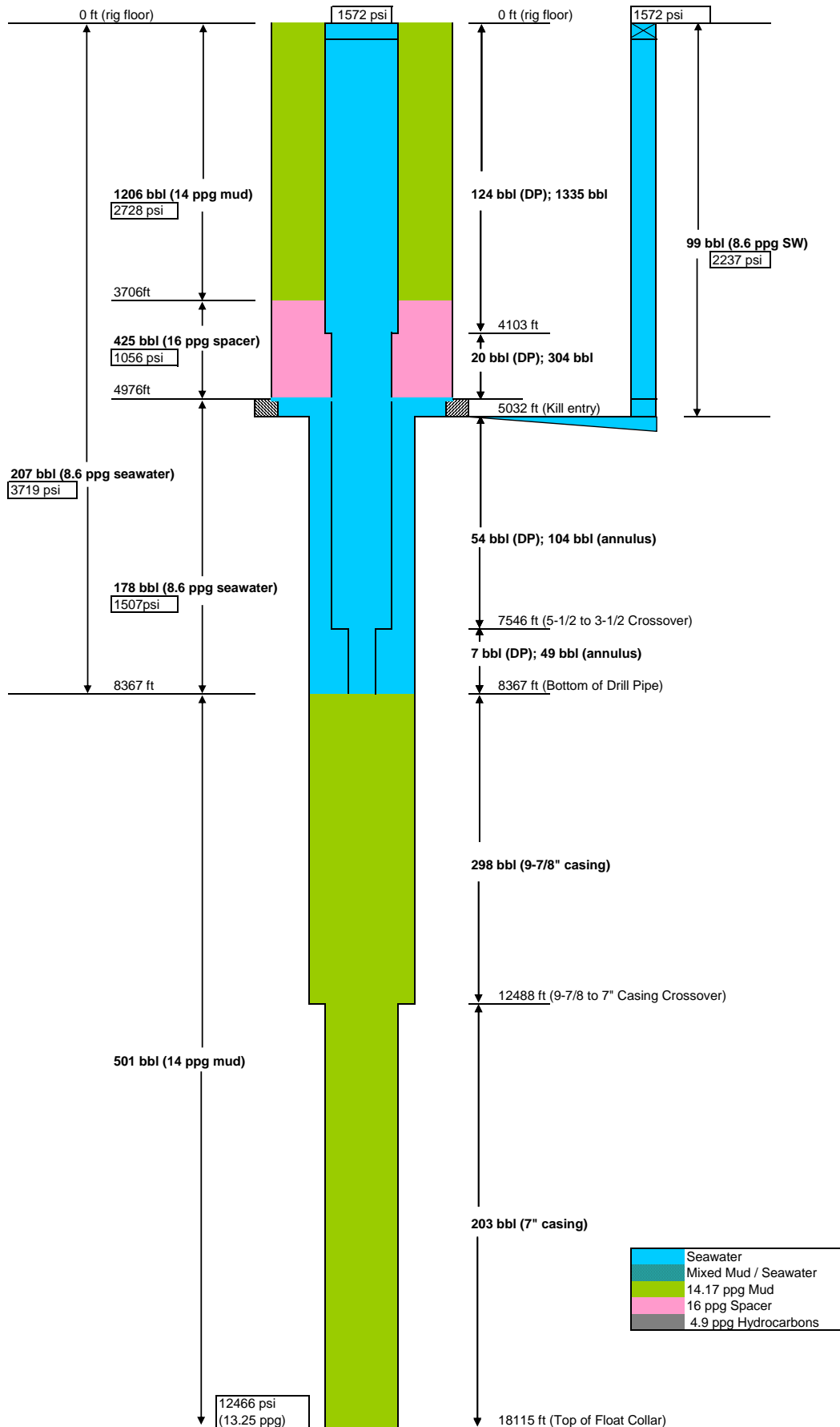
Ideal Pump Schedule, Post Spacer Displace

1/7/2011



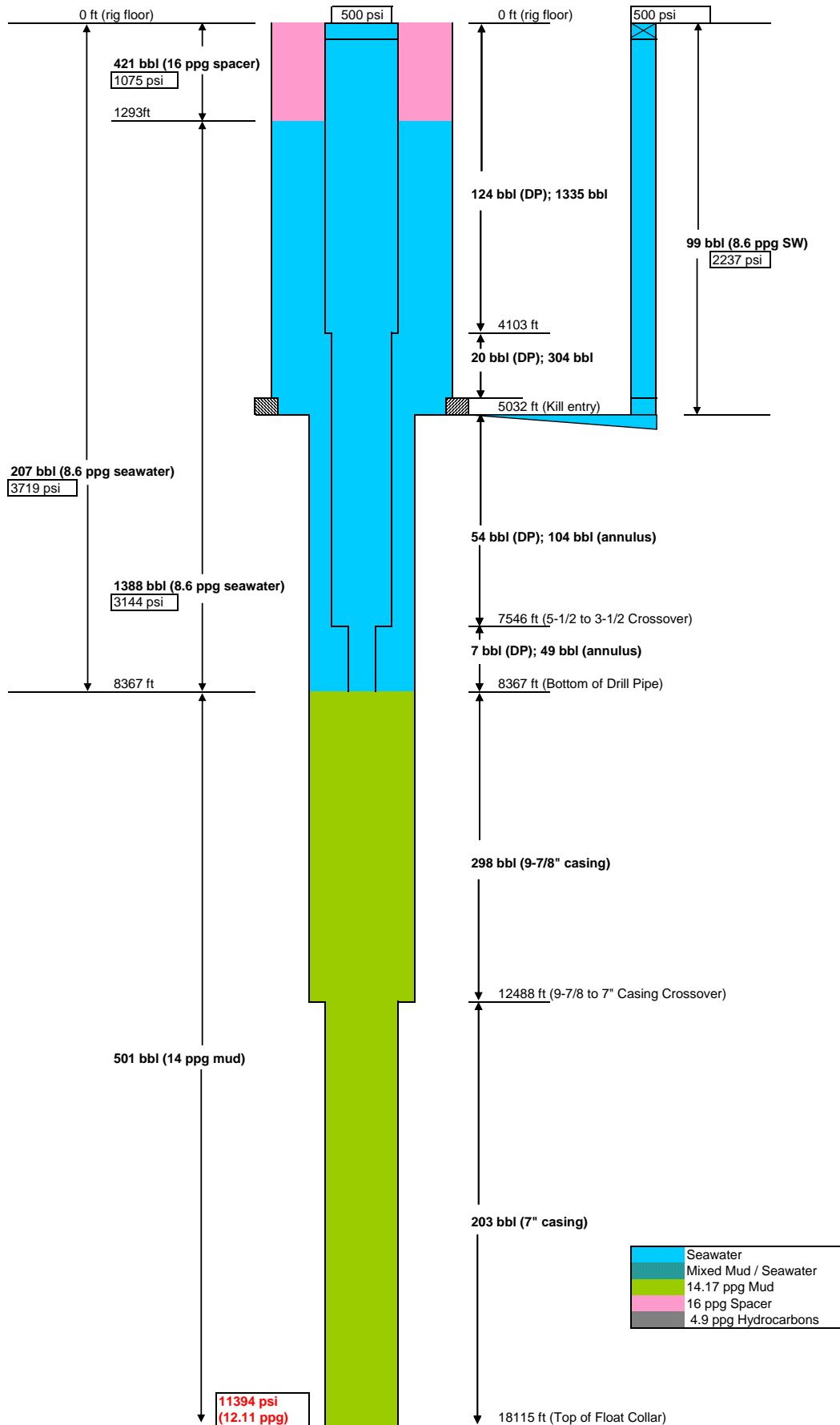
Ideal Pump Schedule, Post Displace #1

1/7/2011



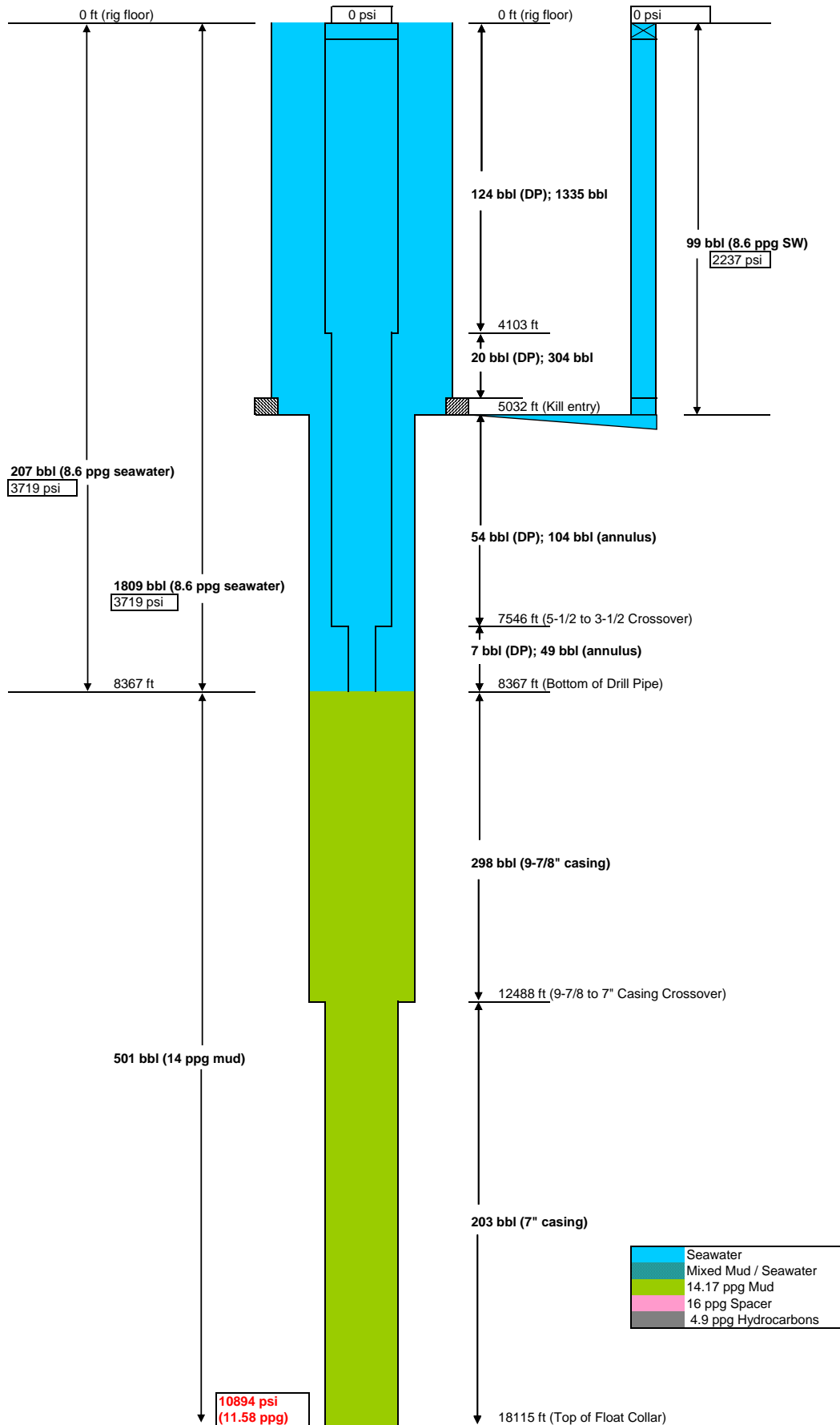
Ideal Pump Schedule, Post-Displace #2

1/7/2011



Ideal Pump Schedule, After Final Displacement

1/7/2011



Macondo Well Hydrostatics, Ideal Displacement Procedure

D. Kluk
12/29/10

Inputs

Fluid Inputs

$\text{bbl} = 42\text{gal}$	Barrel definition	$\rho_{14} := 14.17 \frac{\text{lbm}}{\text{gal}}$	14 ppg mud density
$V_{p_s} := 425\text{bbl}$	Spacer volume pumped	$\rho_{16} := 16 \frac{\text{lbm}}{\text{gal}}$	16 ppg mud density
$V_{p_1} := 385\text{bbl}$	Water pumped during displace #1	$\rho_w := 8.556 \frac{\text{lbm}}{\text{gal}}$	Seawater density
$V_{p_2} := 1210\text{bbl}$	Water pumped during displace #2		
$V_{p_f} := 425\text{bbl}$	Water pumped during final displacement		

Geometry

$V_{dp} := 206.59\text{bbl}$	Drill pipe internal volume	$L_{dp} := 8367\text{ft}$	Drill pipe length
$V_1 := 124.36\text{bbl}$	Drillpipe segment 1 volume (6-1/2" DP)	$L_1 := 4103\text{ft}$	Length of model section 1
$V_2 := 75.09\text{bbl}$	Drillpipe segment 1 volume (6-1/2" DP)	$L_2 := 3443\text{ft}$	Length of model section 1
$V_3 := 7.14\text{bbl}$	Drillpipe segment 1 volume (6-1/2" DP)	$L_3 := 821\text{ft}$	Length of model section 1
$V_4 := 49.42\text{bbl}$	Annulus segment 4 volume (casing, 3-1/2" DP)	$L_4 := 821\text{ft}$	Length of model section 4
$V_5 := 104.01\text{bbl}$	Annulus segment 5 volume (casing, 5-1/2" DP)	$L_5 := 2492\text{ft}$	Length of model section 5
$V_6 := 16.48\text{bbl}$	Annulus segment 6 volume (BOP, 5-1/2" DP)	$L_6 := 53\text{ft}$	Length of model section 6
$V_7 := 304.3\text{bbl}$	Annulus segment 7 volume (riser, 5-1/2" DP)	$L_7 := 898\text{ft}$	Length of model section 7
$V_8 := 1334.87\text{bbl}$	Annulus segment 8 volume (riser, 6-5/8" DP)	$L_8 := 4103\text{ft}$	Length of model section 8
$V_{riser} := 2015.66\text{bbl}$	Total volume in riser, DP, casing, and BOP annulus	$V_{6_ann} := 11.53\text{bbl}$	Volume in BOP below annular
$L_{kill} := 5032\text{ft}$	Length of kill line	$D_{kill} := 4.5\text{in}$	Kill line ID
$L_{csg} := 9748\text{ft}$	Length of casing below drill pipe to float collar	$D_{csg9} := 8.625\text{in}$	ID of 9-5/8" casing
$L_{c7} := 5627\text{ft}$	Length of 7" casing	$D_{csg7} := 6.094\text{in}$	ID of lower 7" casing section
$L_{ann} := 5017\text{ft}$	Depth of annular preventer		

Outputs - Setup Calculations*Cross sectional areas*

$$A_1 := \frac{V_1}{L_1} = 24.505 \text{ in}^2$$

Cross sectional area of model section 4

$$A_2 := \frac{V_2}{L_2} = 17.633 \text{ in}^2$$

Cross sectional area of model section 5

$$A_3 := \frac{V_3}{L_3} = 7.031 \text{ in}^2$$

Cross sectional area of model section 6

$$A_4 := \frac{V_4}{L_4} = 48.668 \text{ in}^2$$

Cross sectional area of model section 4

$$A_5 := \frac{V_5}{L_5} = 33.745 \text{ in}^2$$

Cross sectional area of model section 5

$$A_6 := \frac{V_6}{L_6} = 251.398 \text{ in}^2$$

Cross sectional area of model section 6

$$A_7 := \frac{V_7}{L_7} = 273.972 \text{ in}^2$$

Cross sectional area of model section 7

$$A_8 := \frac{V_8}{L_8} = 263.037 \text{ in}^2$$

Cross sectional area of model section 8

$$A_{\text{csg7}} := \frac{\pi}{4} \cdot D_{\text{csg7}}^2 = 29.167 \text{ in}^2$$

Cross sectional area of 7" casing

$$A_{\text{csg9}} := \frac{\pi}{4} \cdot D_{\text{csg9}}^2 = 58.426 \text{ in}^2$$

Cross sectional area of 9-5/8" casing

$$L_{6_ann} := L_{dp} - L_4 - L_5 - L_{ann} = 37 \cdot \text{ft}$$

Length of segment 6 (BOP) below annular preventer)

$$L_{6_kill} := L_{dp} - L_4 - L_5 - L_{kill} = 22 \cdot \text{ft}$$

Length of segment 6 (BOP) below kill line)

$$L_{\text{annulus}} := L_{dp} - L_{kill} = 3.335 \times 10^3 \cdot \text{ft}$$

Length from kill line to bottom of drill string

Outputs - Timeline Hydrostatic Calculations*Spacer pump, displace #1*

$$V_{\text{spcr7}} := V_{\text{p}_s} - V_6 - V_5 - V_4 - V_{\text{dp}} = 48.5 \cdot \text{bbl}$$

Volume of spacer in model segment 7 after pump

$$h_{14_sp1} := L_8 + L_7 - \left(\frac{V_{\text{spcr7}}}{A_7} \right) = 4.858 \times 10^3 \cdot \text{ft}$$

Height of 14 ppg mud above spacer

$$h_{16_sp1} := L_{\text{dp}} - h_{14_sp1} = 3.509 \times 10^3 \cdot \text{ft}$$

Height of spacer in annulus

$$V_{14_sp1} := V_8 + V_7 - V_{\text{spcr7}} = 1.591 \times 10^3 \cdot \text{bbl}$$

Volume of mud in annulus

$$P_{14_sp1} := \rho_{14} \cdot g \cdot h_{14_sp1} = 3.576 \times 10^3 \cdot \text{psi}$$

Mud head pressure

$$P_{16_sp1} := \rho_{16} \cdot g \cdot h_{16_sp1} = 2.917 \times 10^3 \cdot \text{psi}$$

Spacer head pressure (in annulus)

$$P_{\text{sp_sp1}} := P_{14_sp1} + P_{16_sp1} - \rho_{16} \cdot g \cdot L_{\text{dp}} = -461.814 \cdot \text{psi}$$

Standpipe pressure after spacer pump

$$P_{\text{kill}} := \rho_w \cdot g \cdot L_{\text{kill}} = 2.237 \times 10^3 \cdot \text{psi}$$

Kill line hydrostatic pressure (filled with seawater)

$$P_{\text{k_sp1}} := P_{14_sp1} + \rho_{16} \cdot g \cdot (L_{\text{kill}} - h_{14_sp1}) - P_{\text{kill}} = 1.484 \times 10^3 \cdot \text{psi}$$

Kill line pressure after spacer pump

$$P_{\text{bh_sp1}} := P_{14_sp1} + P_{16_sp1} + \rho_{14} \cdot g \cdot L_{\text{csg}} = 13668 \cdot \text{psi}$$

Bottom hole pressure at this SPP

$$\rho_{\text{bh_sp1}} := \frac{P_{\text{bh_sp1}}}{g \cdot (L_{\text{csg}} + L_{\text{dp}})} = 14.524 \cdot \frac{\text{lbm}}{\text{gal}}$$

Equivalent density at bottom hole

Water pump, displace #1

$$V_{\text{wtr}_7} := V_{\text{p}_1} - V_6 - V_5 - V_4 - V_{\text{dp}} = 8.5 \cdot \text{bbl}$$

Volume of water in model segment 7

$$V_{\text{spcr8}} := V_{\text{p}_s} - (V_7 - V_{\text{wtr}_7}) = 129.2 \cdot \text{bbl}$$

Volume of spacer in model segment 8

$$V_{14_p1} := V_8 - V_{\text{spcr8}} = 1.206 \times 10^3 \cdot \text{bbl}$$

Volume of mud in annulus

$$h_{14_p1} := \frac{V_{14_p1}}{A_8} = 3.706 \times 10^3 \cdot \text{ft}$$

Height of mud

$$h_{16_p1} := \frac{V_{\text{spcr8}}}{A_8} + \frac{V_7 - V_{\text{wtr}_7}}{A_7} = 1.27 \times 10^3 \cdot \text{ft}$$

Height of spacer

$$h_{\text{w}_p1} := L_{\text{dp}} - h_{14_p1} - h_{16_p1} = 3.391 \times 10^3 \cdot \text{ft}$$

Height of water in annulus

$$P_{14_p1} := \rho_{14} \cdot g \cdot h_{14_p1} = 2.728 \times 10^3 \cdot \text{psi}$$

Pressure of mud

$$P_{16_p1} := \rho_{16} \cdot g \cdot h_{16_p1} = 1.056 \times 10^3 \cdot \text{psi}$$

Pressure of spacer

$$P_{\text{w}_p1} := \rho_w \cdot g \cdot h_{\text{w}_p1} = 1.507 \times 10^3 \cdot \text{psi}$$

Pressure of water

$$P_{w_dp} := \rho_w \cdot g \cdot L_{dp} = 3.719 \times 10^3 \text{ psi} \quad \text{Head pressure of water in drill pipe}$$

$$P_{sp_p1} := P_{14_p1} + P_{16_p1} + P_{w_p1} - P_{w_dp} = 1.572 \times 10^3 \text{ psi} \quad \text{Expected standpipe pressure}$$

$$P_{k_p1} := P_{14_p1} + P_{16_p1} + \rho_w \cdot g \cdot (L_{kill} - h_{14_p1} - h_{16_p1}) - P_{kill} = 1.572 \times 10^3 \text{ psi}$$

Expected kill line pressure

$$P_{bh_p1} := P_{sp_p1} + P_{w_dp} + \rho_{14} \cdot g \cdot L_{csg} = 12466 \text{ psi} \quad \text{Bottom hole pressure at this SPP}$$

$$\rho_{bh_p1} := \frac{P_{bh_p1}}{g \cdot (L_{csg} + L_{dp})} = 13.247 \cdot \frac{\text{lbm}}{\text{gal}} \quad \text{Equivalent density at bottom hole}$$

Post-Displace #2

$$V_{14_p2} := V_{14_p1} - V_{p_2} = -4.33 \cdot \text{bbl} \quad \text{14 ppg mud in annulus after displacement}$$

$$V_{16_p2} := V_{p_s} + V_{14_p2} = 420.67 \cdot \text{bbl} \quad \text{Volume of spacer remaining}$$

$$h_{16_p2} := \frac{V_{16_p2}}{A_8} = 1.293 \times 10^3 \cdot \text{ft} \quad \text{Height of remaining spacer}$$

$$P_{16_p2} := \rho_{16} \cdot g \cdot h_{16_p2} = 1.075 \times 10^3 \text{ psi} \quad \text{Head pressure of spacer}$$

$$V_{w_p2} := V_{riser} - V_{16_p2} - V_{dp} = 1.388 \times 10^3 \cdot \text{bbl} \quad \text{Volume of water in annulus}$$

$$h_{w_p2} := L_{dp} - h_{16_p2} = 7.074 \times 10^3 \cdot \text{ft} \quad \text{Height of water in annulus}$$

$$P_{w_p2} := \rho_w \cdot g \cdot h_{w_p2} = 3.144 \times 10^3 \text{ psi} \quad \text{Head pressure of water in annulus}$$

$$P_{sp_p2} := P_{16_p2} + P_{w_p2} - P_{w_dp} = 500.011 \text{ psi} \quad \text{Resulting standpipe pressure}$$

$$P_{k_p2} := P_{16_p2} + \rho_w \cdot g \cdot (L_{kill} - h_{16_p2}) - P_{kill} = 500.011 \text{ psi} \quad \text{Expected kill line pressure}$$

$$P_{bh_p2} := P_{sp_p2} + P_{w_dp} + \rho_{14} \cdot g \cdot L_{csg} = 11394 \text{ psi} \quad \text{Bottom hole pressure at this SPP}$$

$$\rho_{bh_p2} := \frac{P_{bh_p2}}{g \cdot (L_{csg} + L_{dp})} = 12.108 \cdot \frac{\text{lbm}}{\text{gal}} \quad \text{Equivalent density at bottom hole}$$

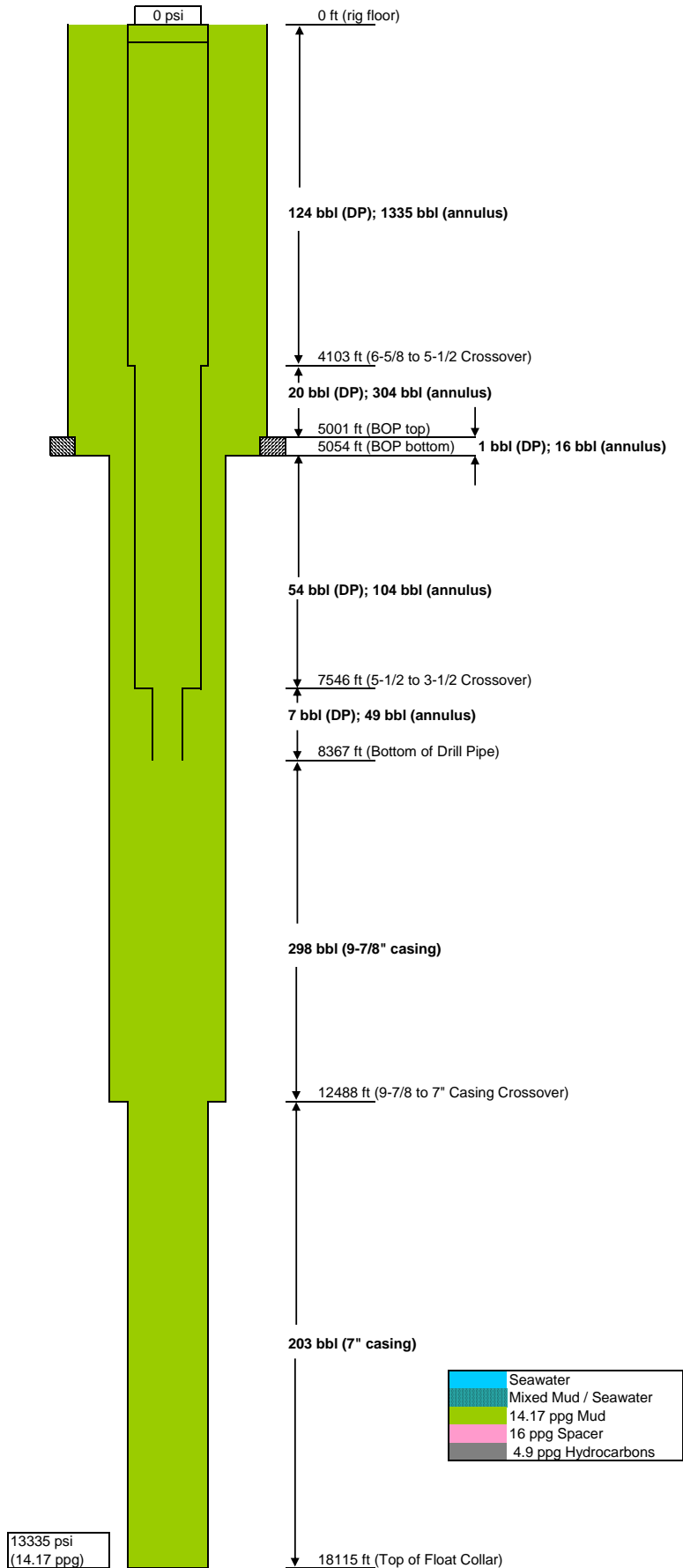
Post final displace

$$P_{bh_end} := P_{w_dp} + \rho_{14} \cdot g \cdot L_{csg} = 10894 \text{ psi} \quad \text{Bottom hole pressure at this SPP}$$

$$\rho_{bh_end} := \frac{P_{bh_end}}{g \cdot (L_{csg} + L_{dp})} = 11.577 \cdot \frac{\text{lbm}}{\text{gal}} \quad \text{Equivalent density at bottom hole}$$

Macondo Well Hydrostatics, Pre-Displace #1, 15:57

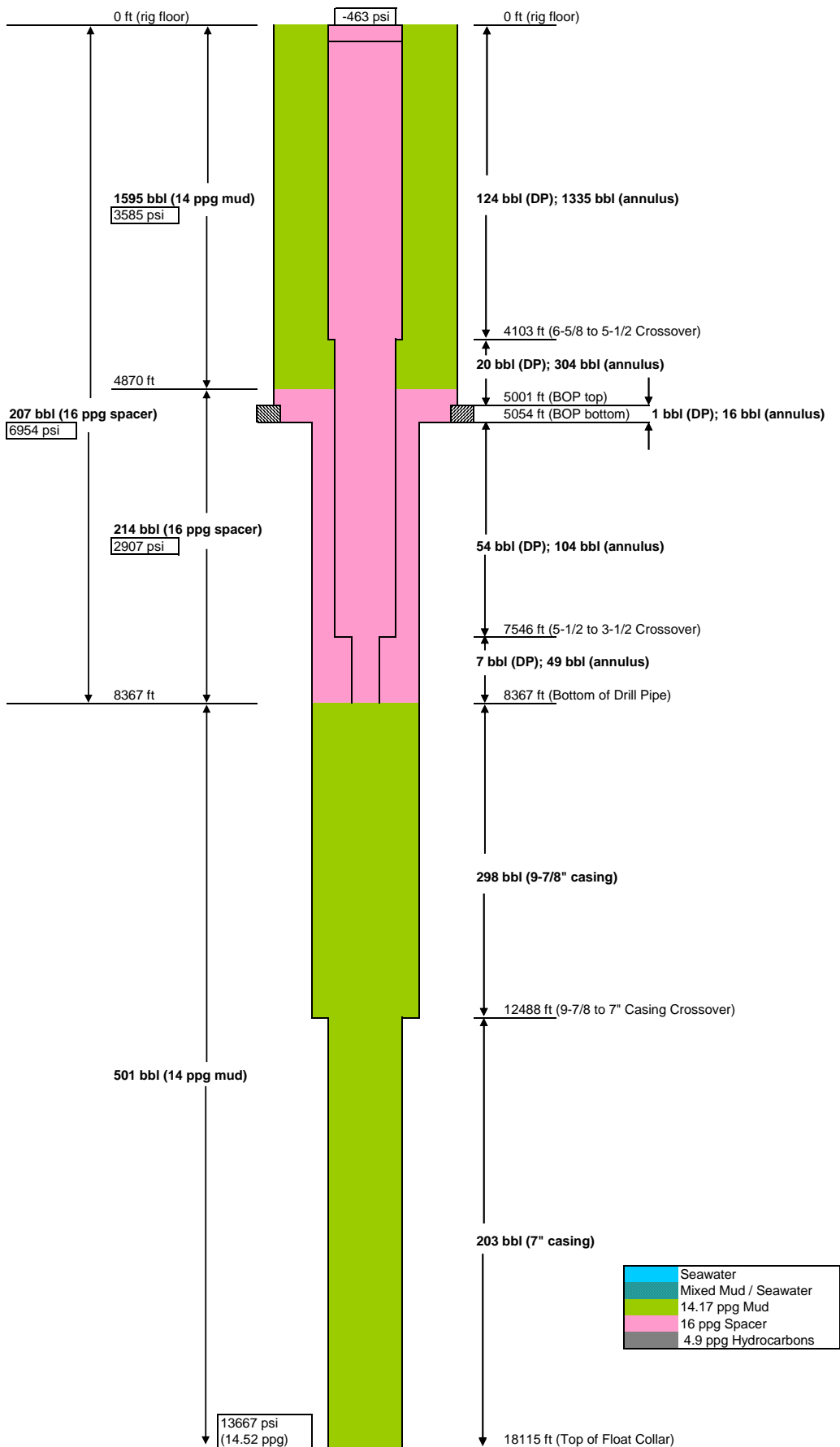
1/7/2011



13335 psi
(14.17 ppg)

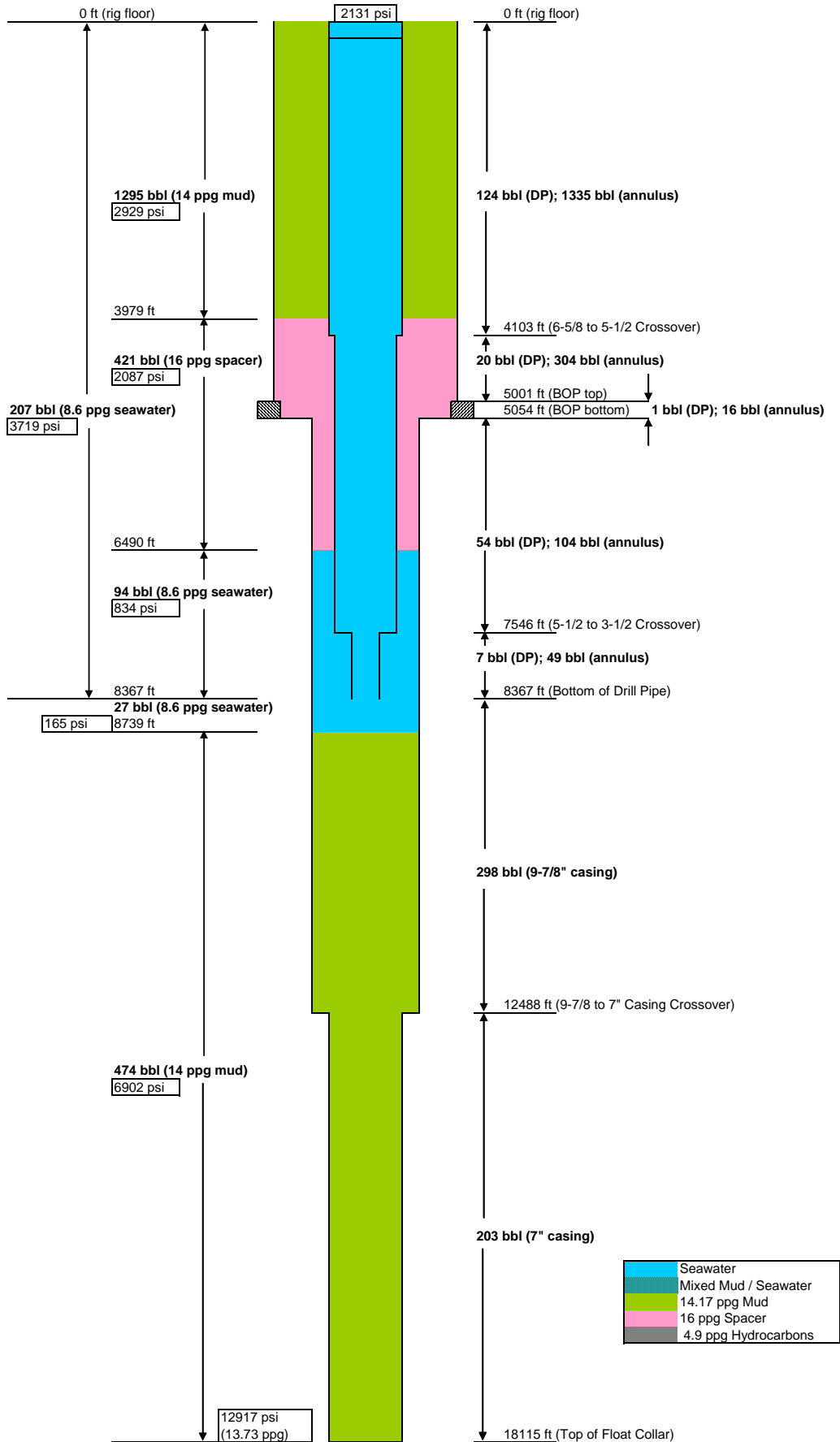
Post Spacer Displace, 16:28

1/7/2011



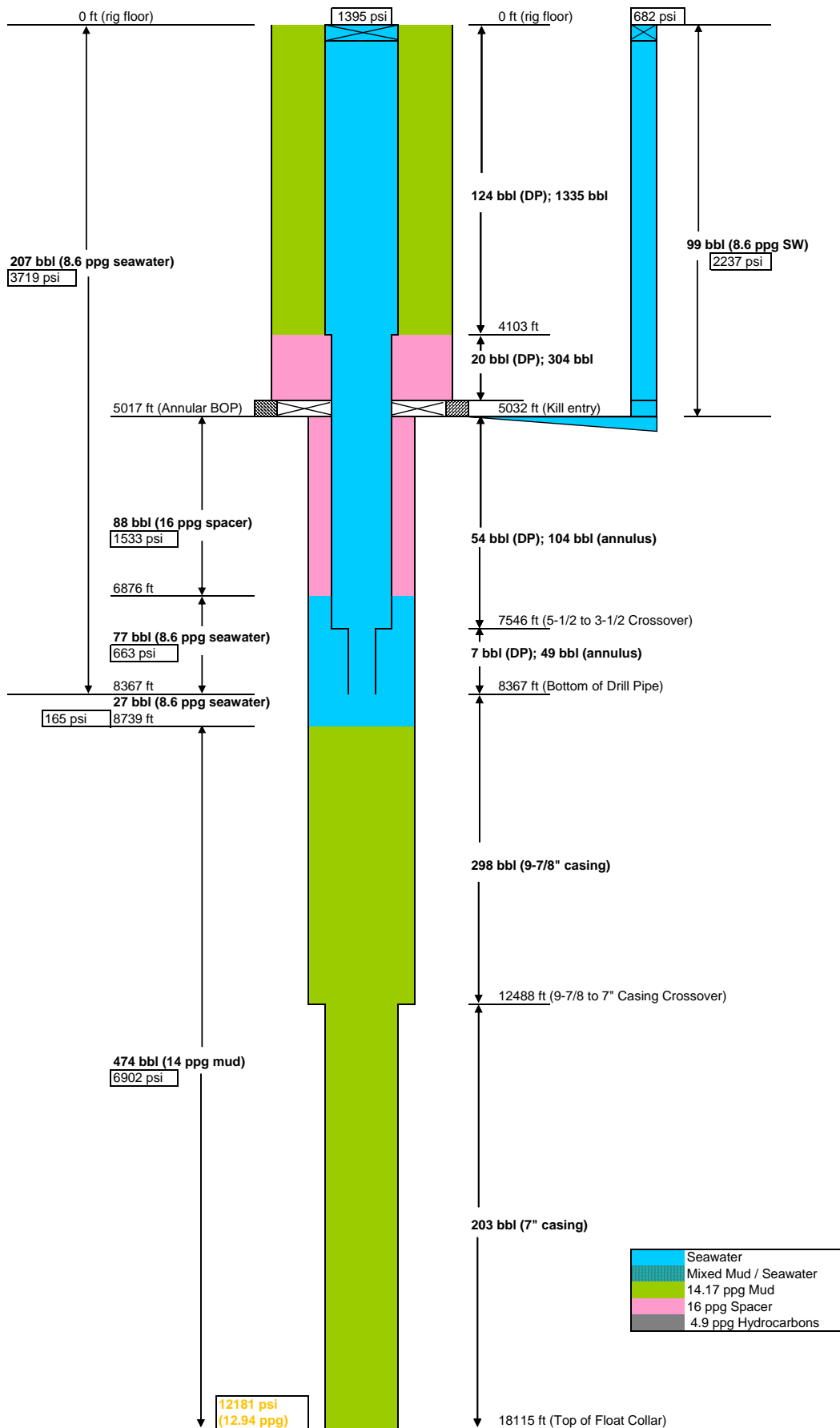
Post Displace #1, 16:54

1/7/2011



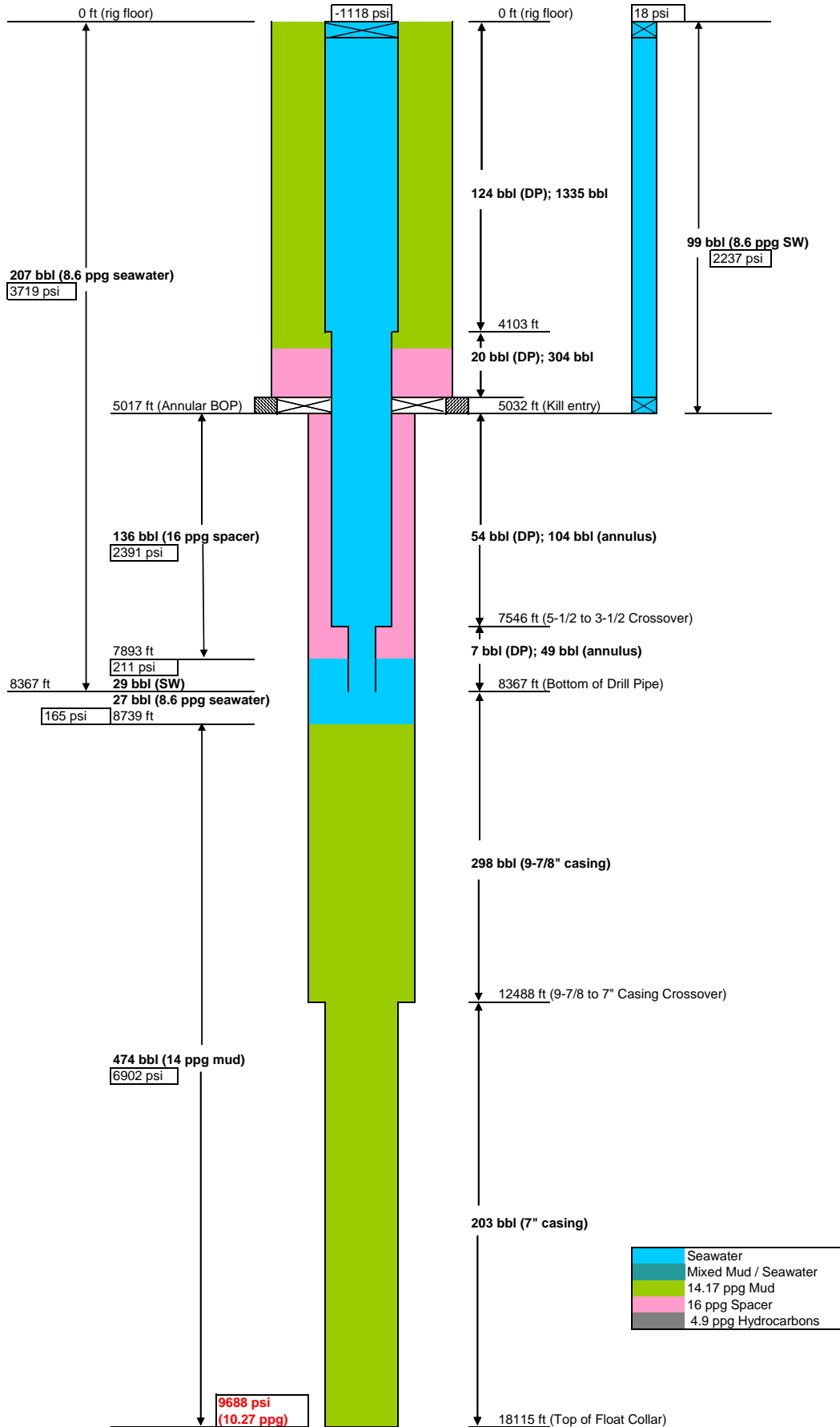
Equalize with Kill Line, 16:58

1/7/2011



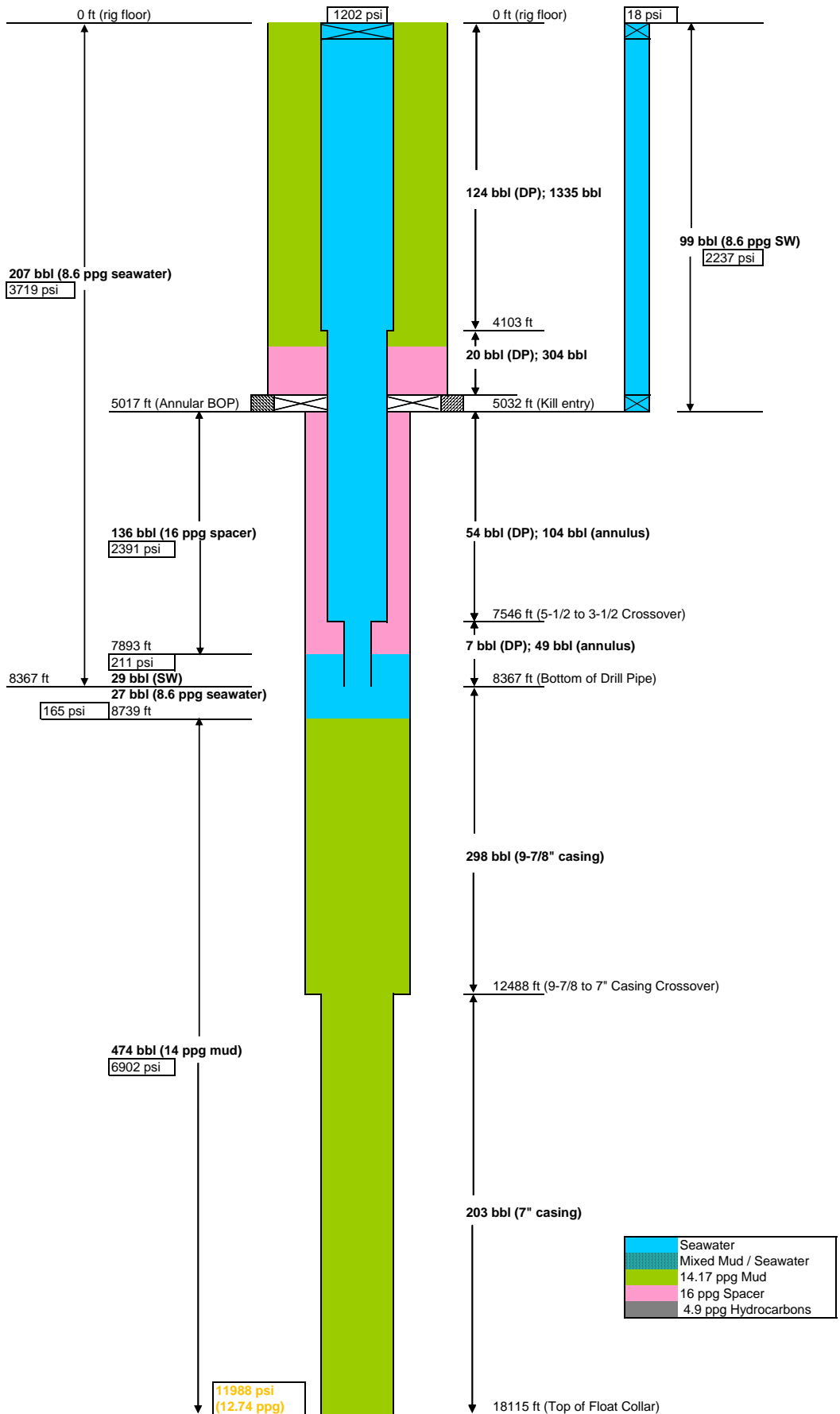
Post-Annular Leakage (calculated), 17:11

1/7/2011



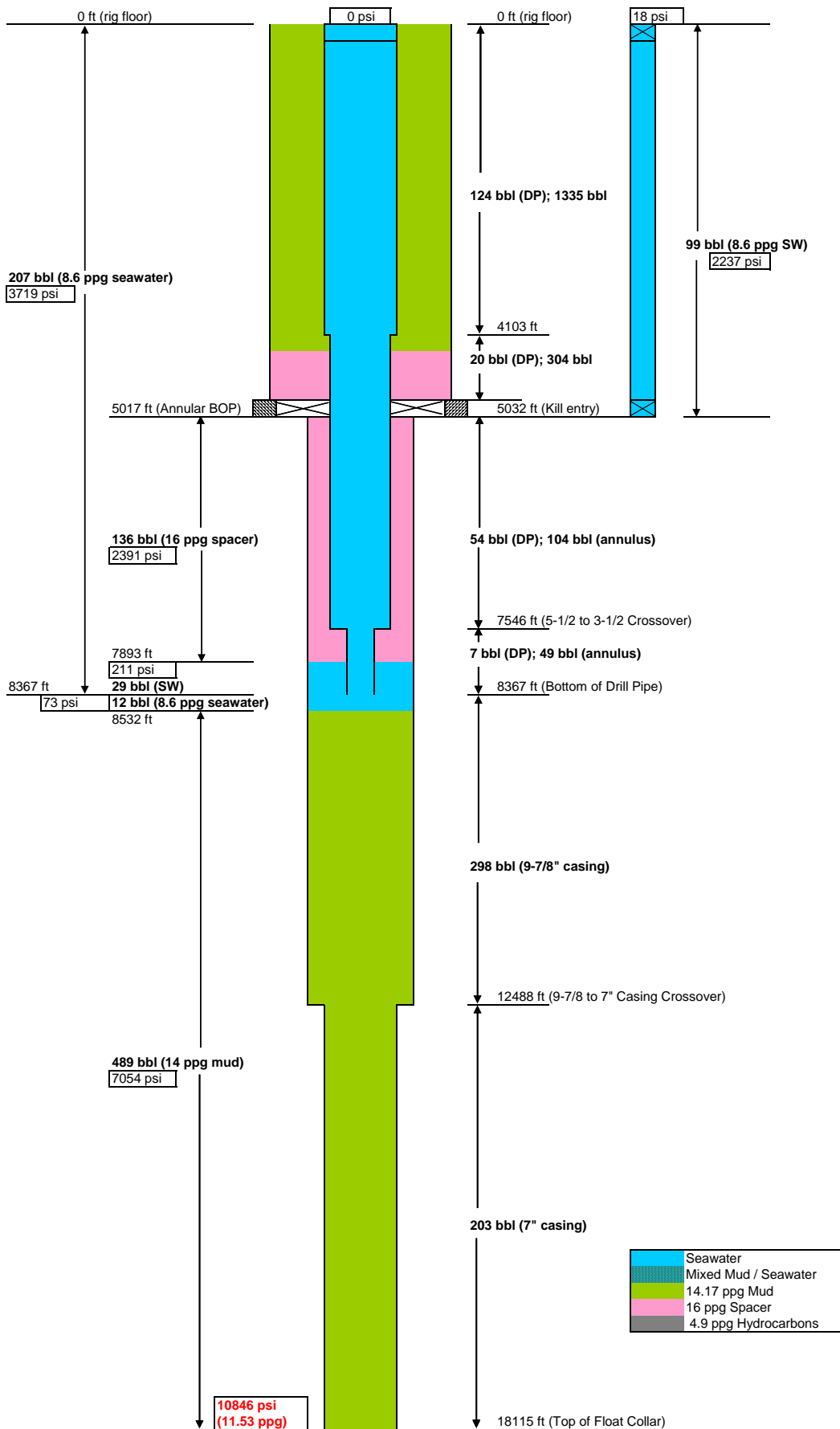
Post-Annular Leakage (actual), 17:26

1/7/2011



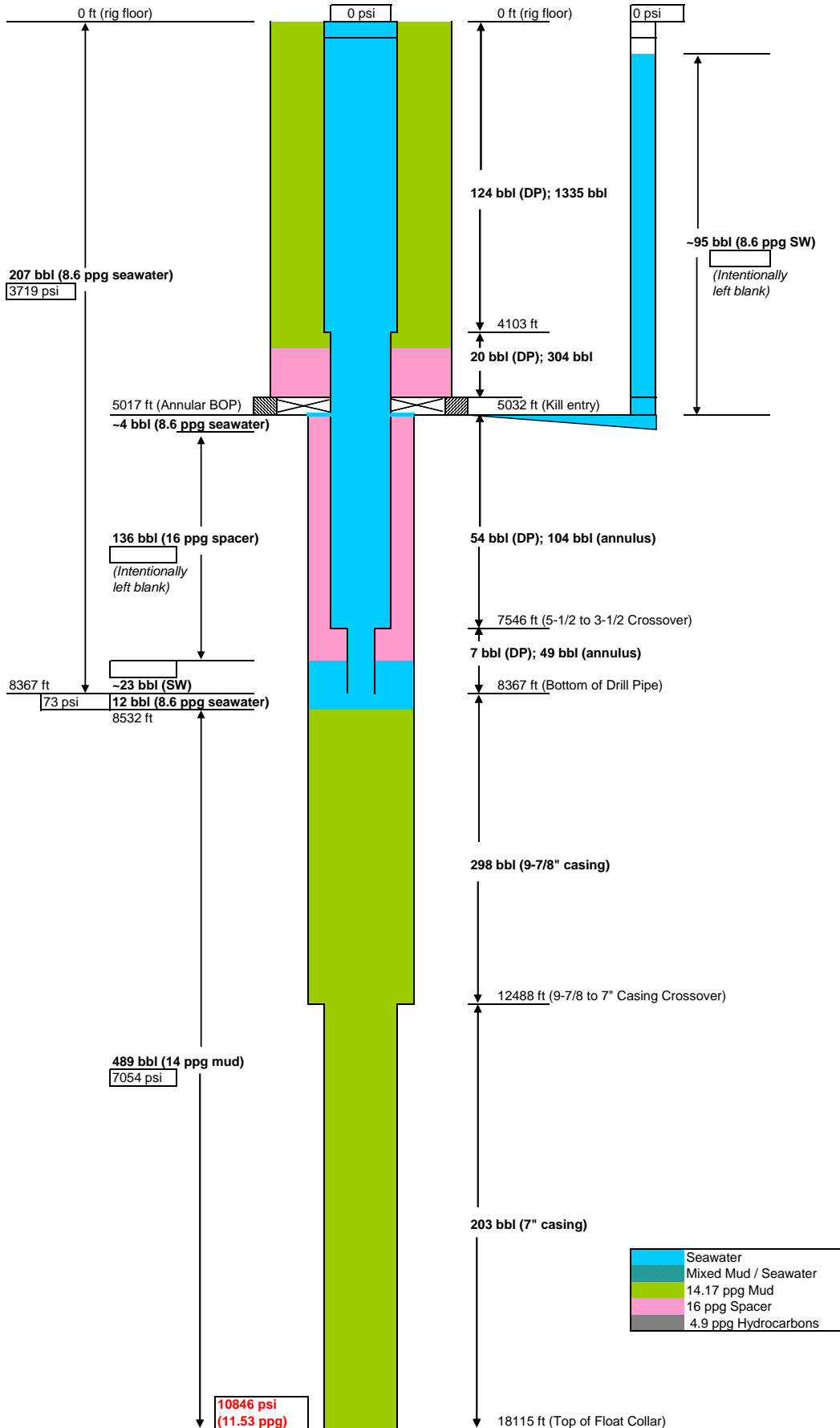
Bleed Standpipe, 17:27

1/7/2011



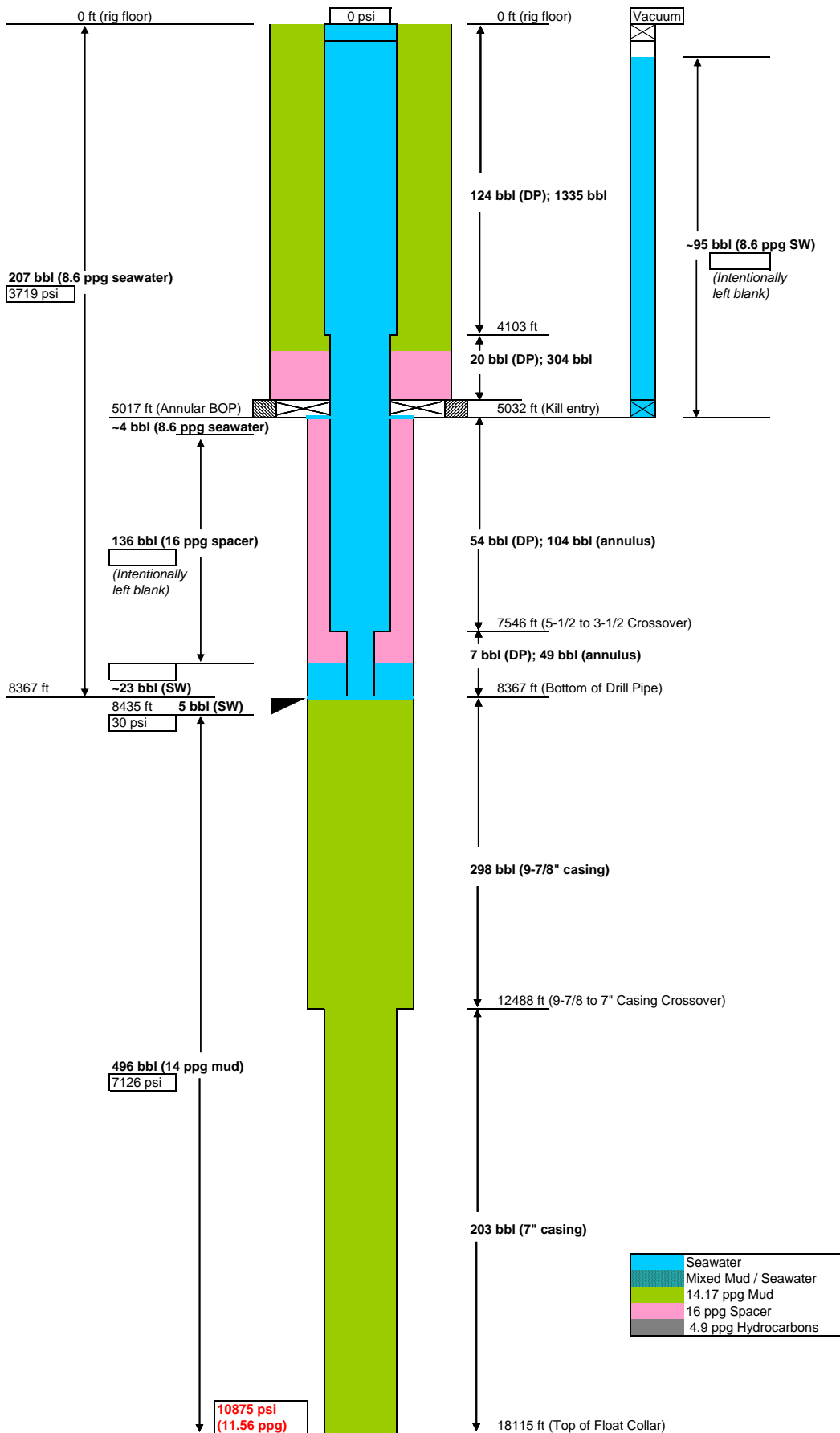
Kill Line U-Tube, 17:33

1/7/2011



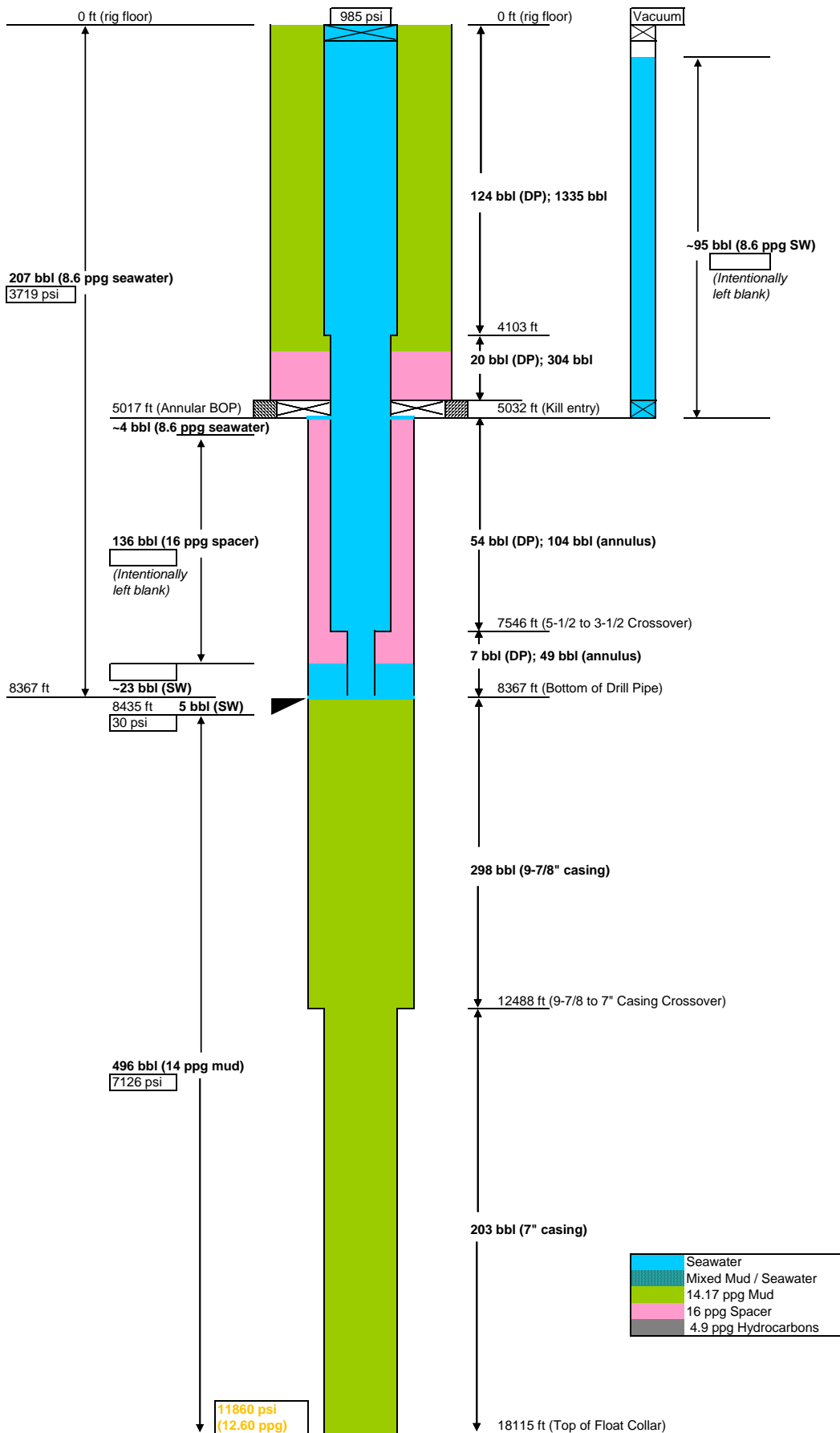
Bleed Standpipe, 17:53

1/7/2011



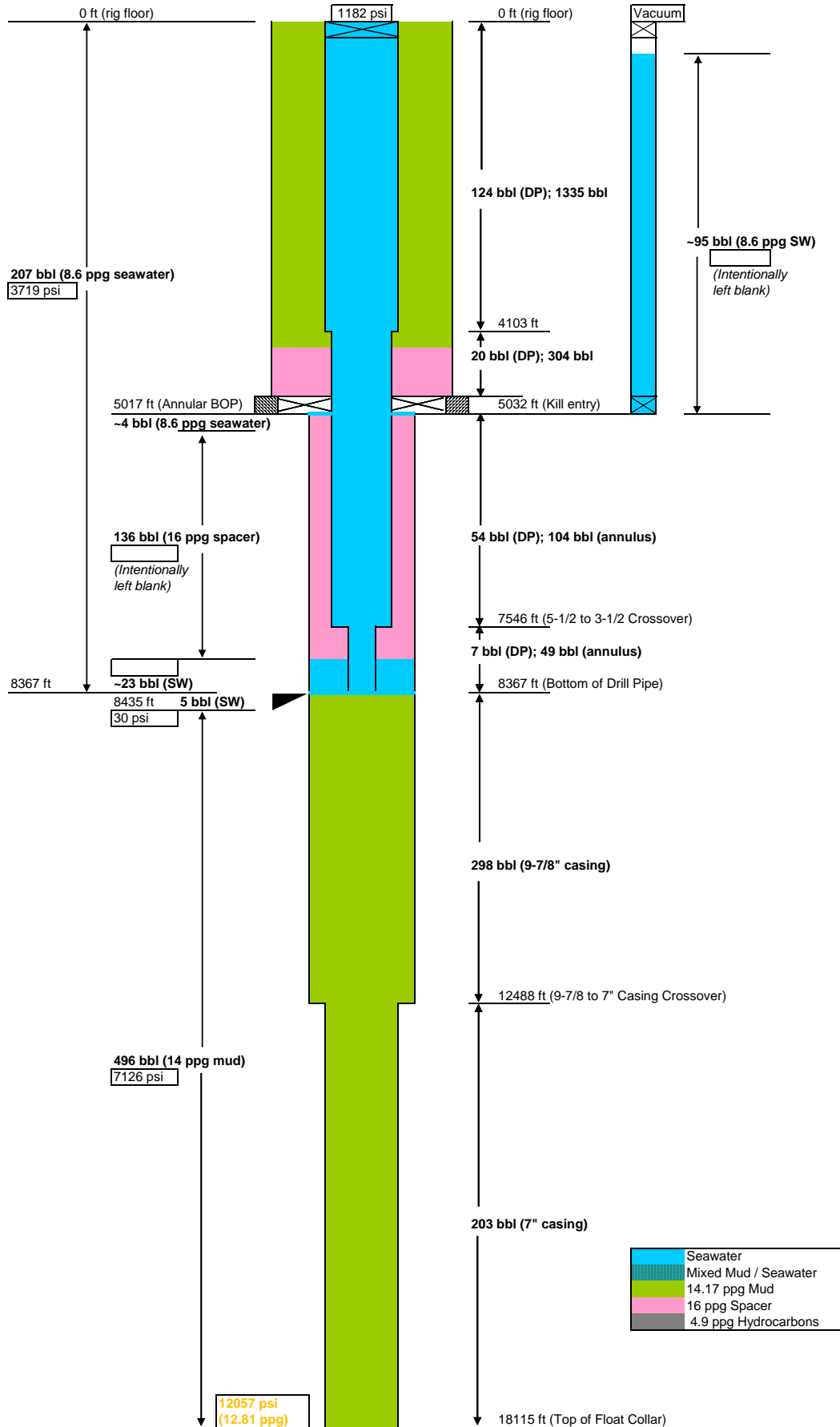
Calculated "Asymptote", 18:31

1/7/2011



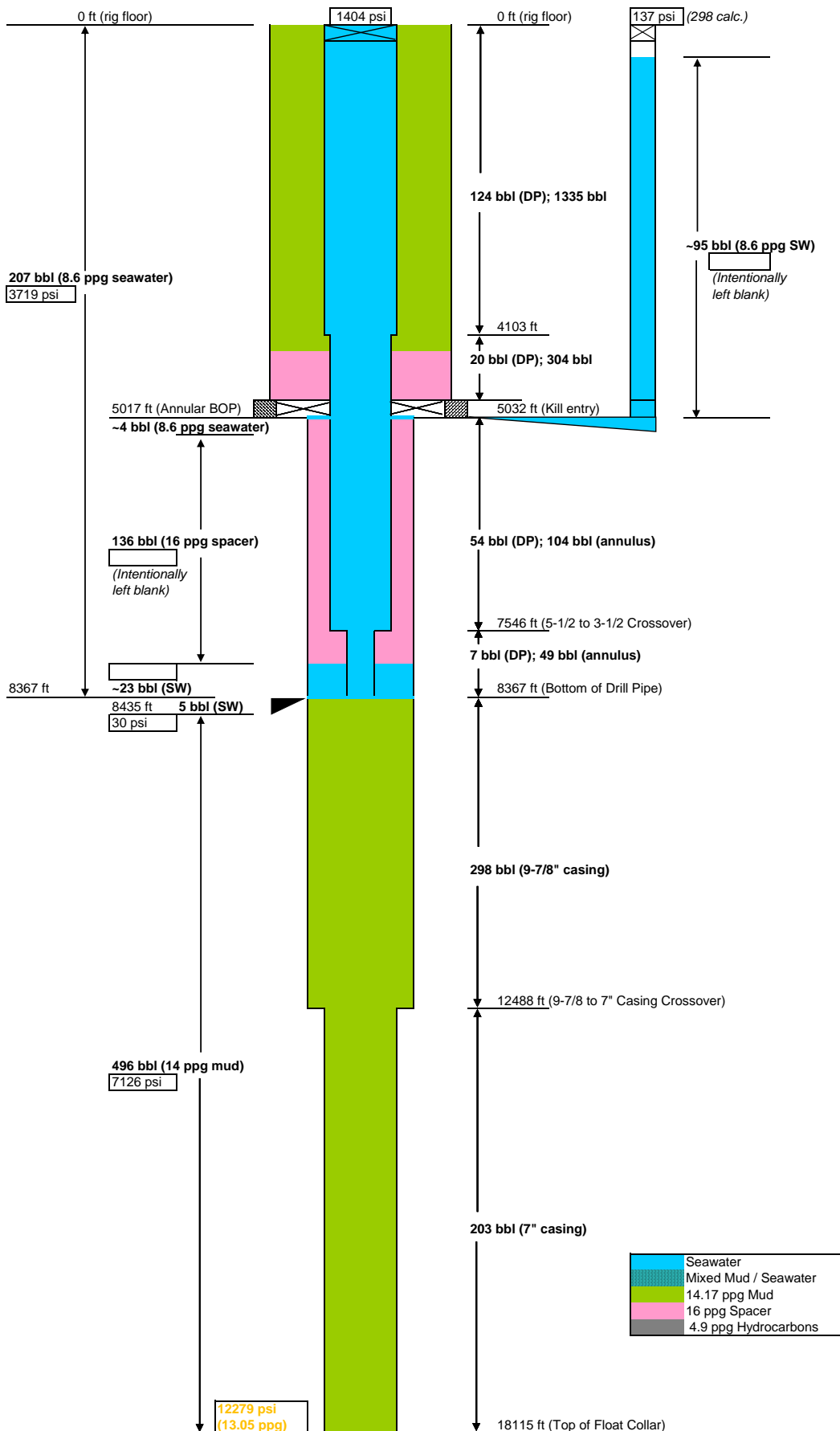
Measured "Asymptote", 18:31

1/7/2011



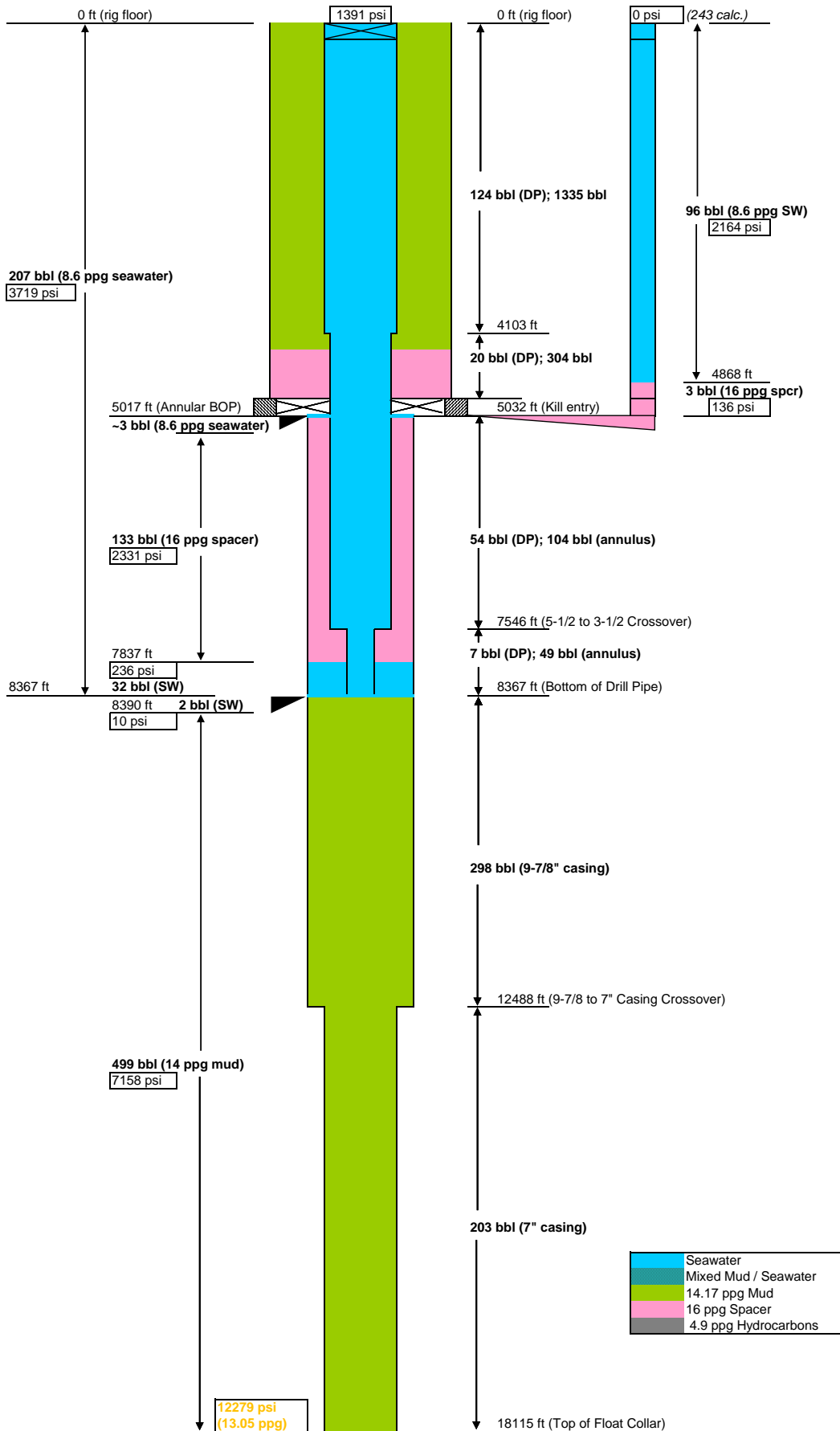
Open Lower Kill Valve, 18:36

1/7/2011



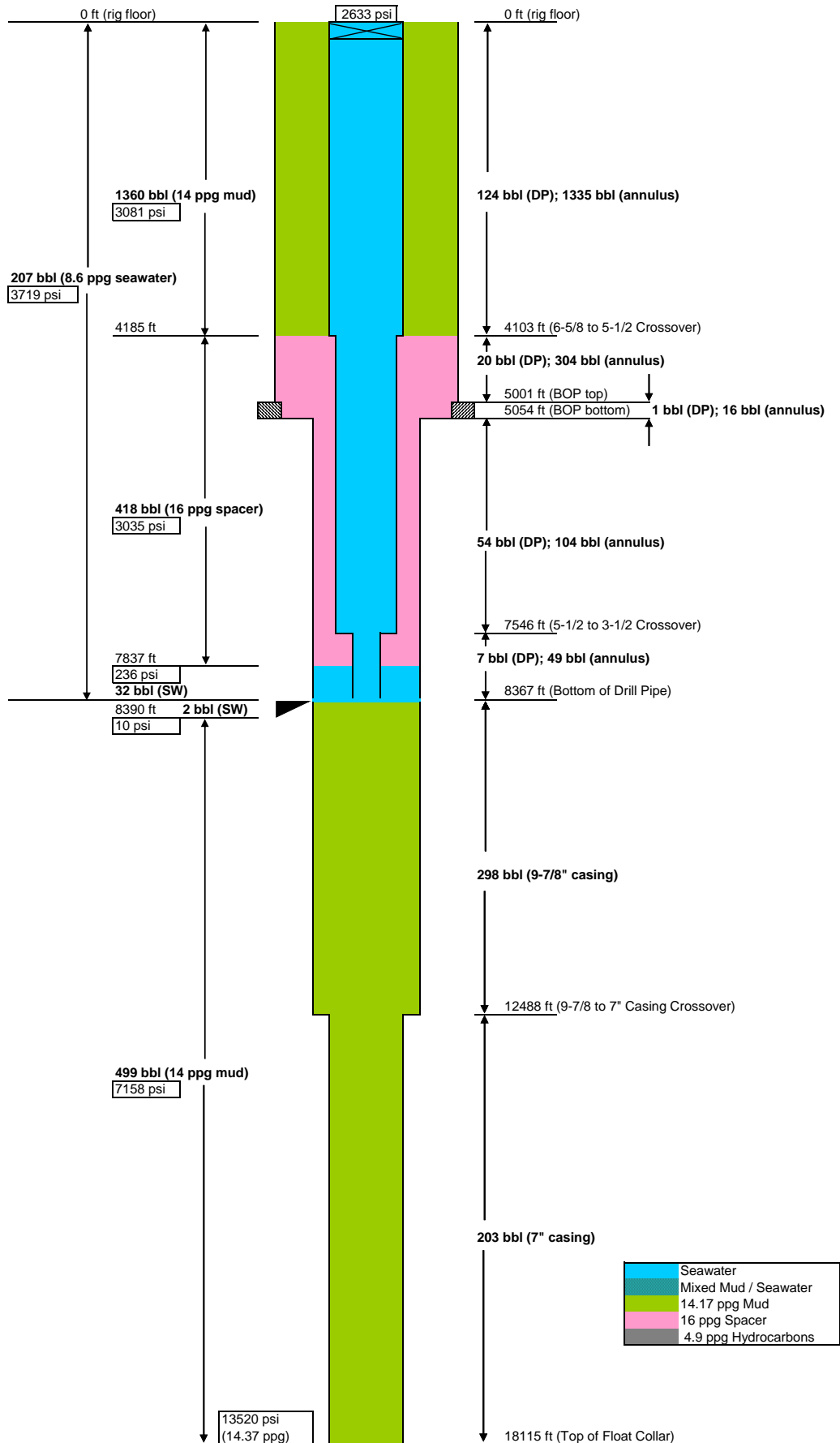
Negative Test, 19:19 - 19:53

1/7/2011



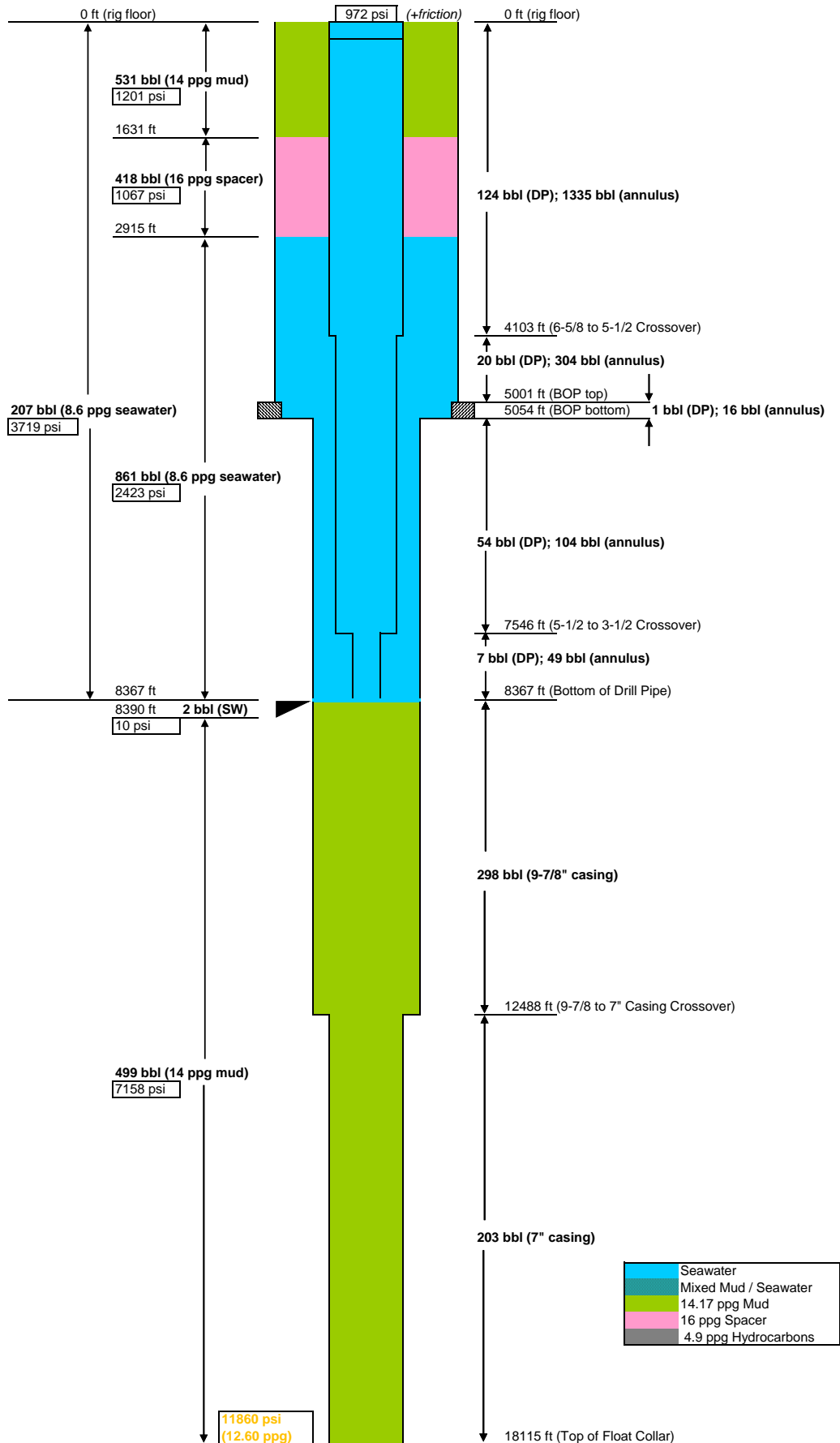
Pre-Displace #2, 20:02

1/7/2011



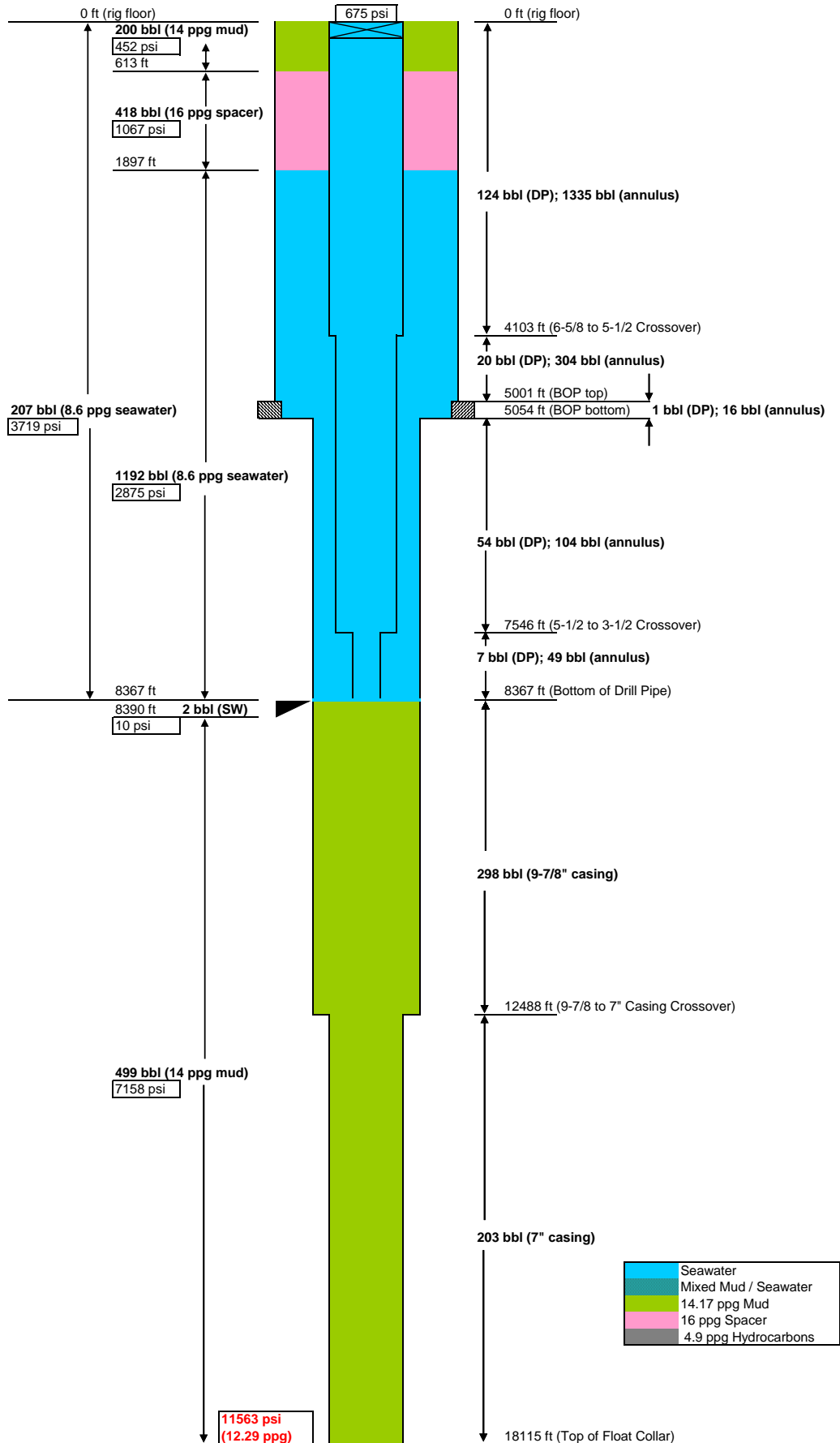
Balance Point, ~20:52

1/7/2011



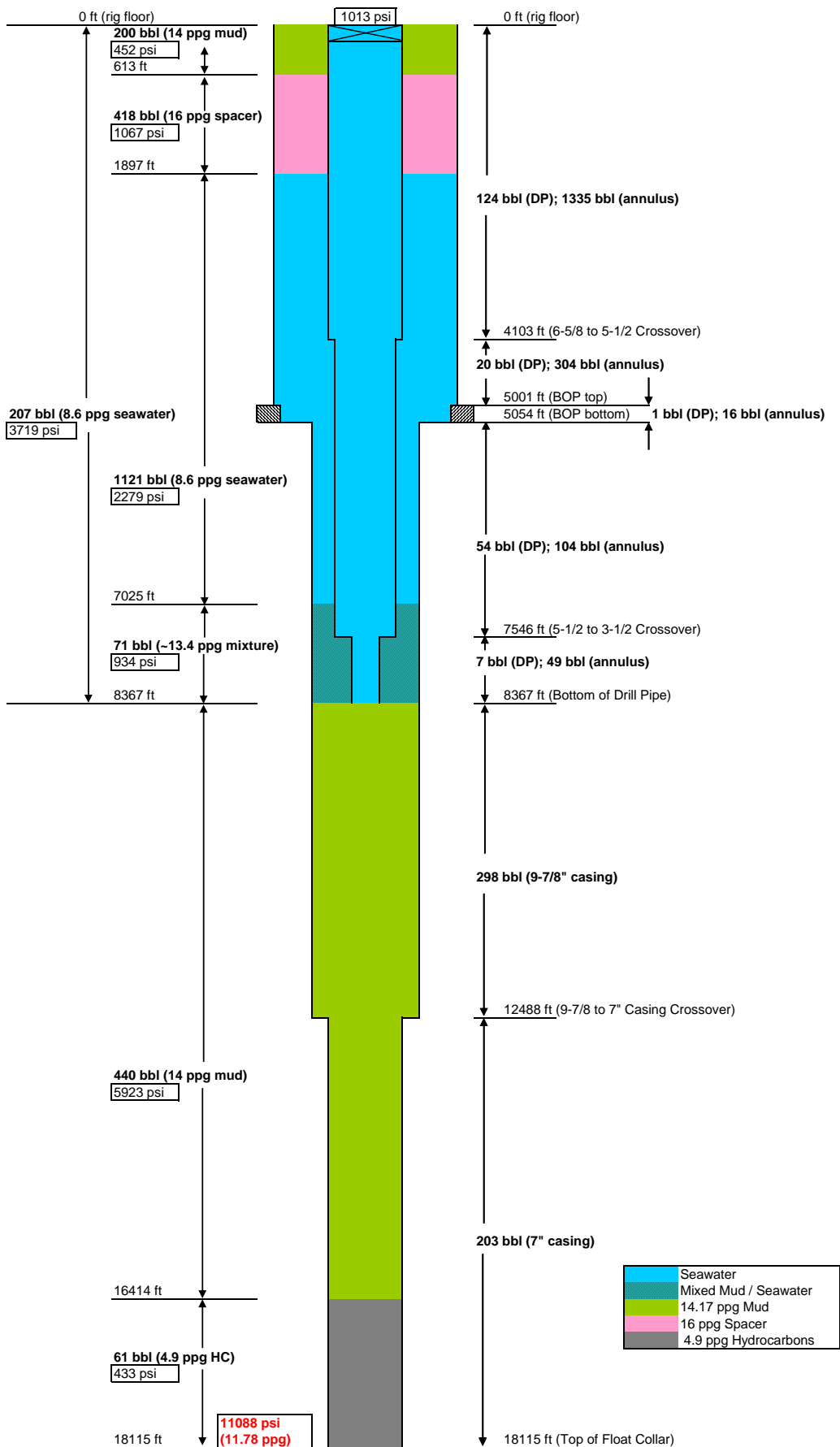
Post-Displace #2 (no influx), 21:09

1/7/2011



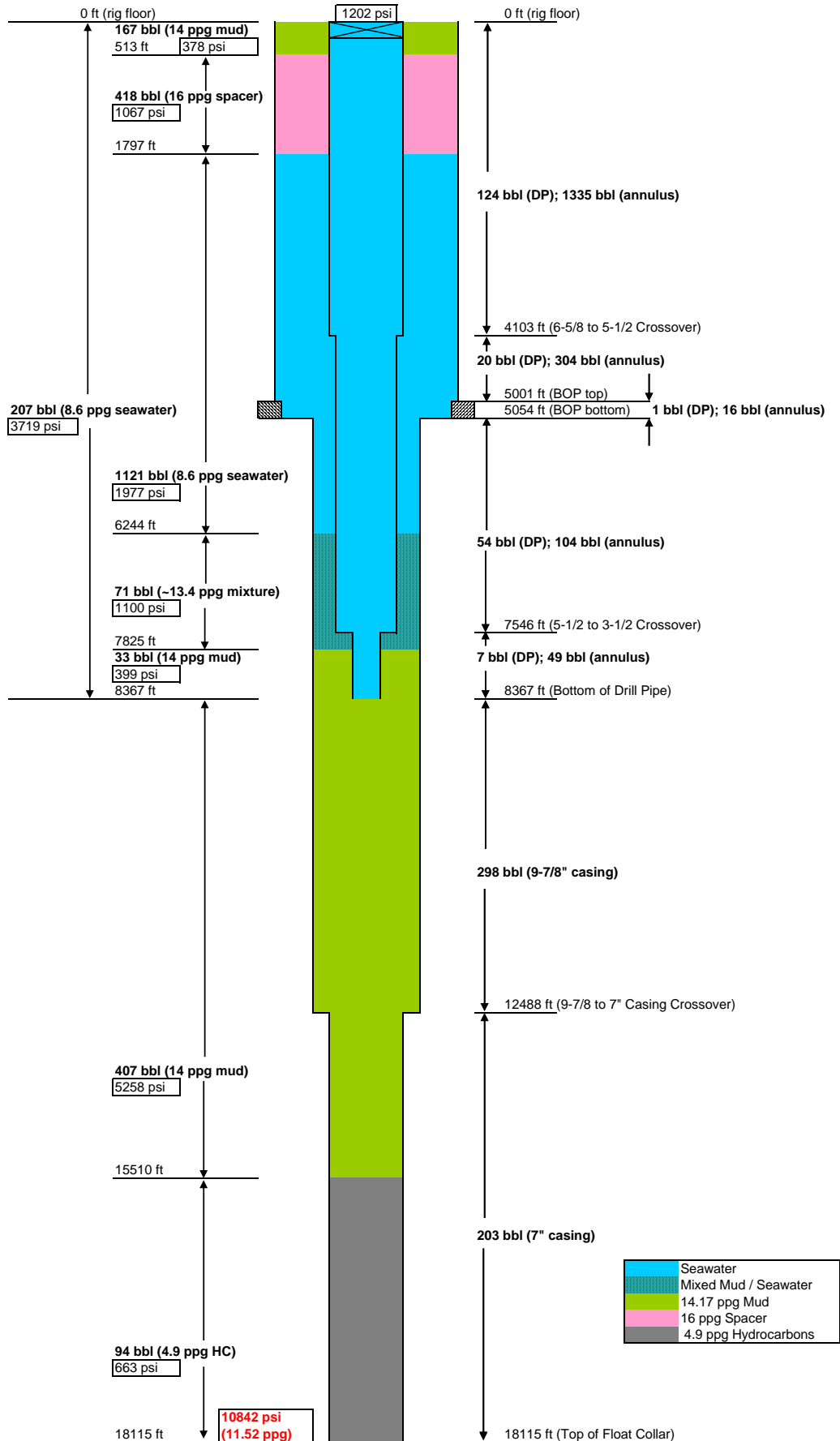
Post-Displace #2 (with influx), 21:09

1/7/2011



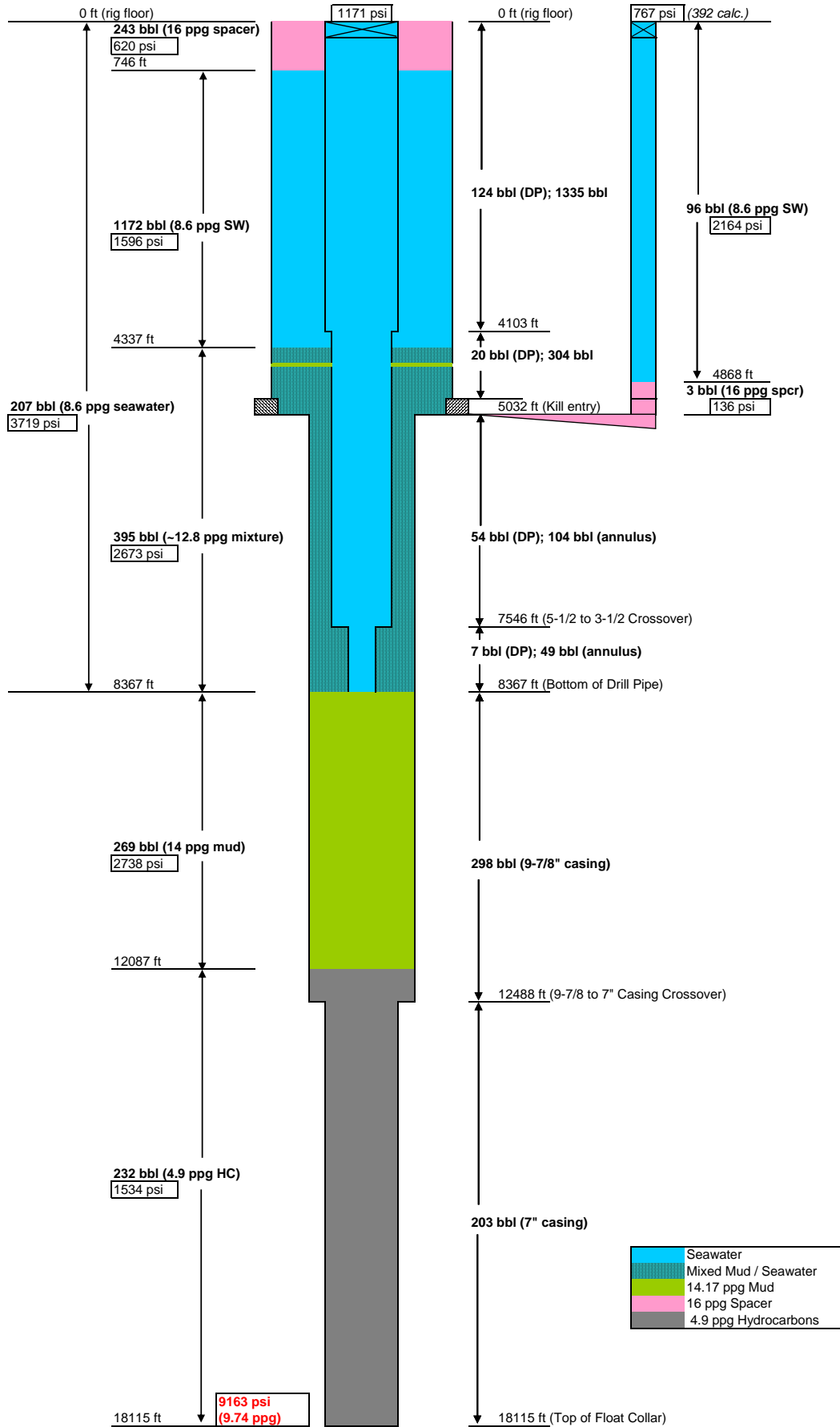
Post-Static Sheen, 21:13

1/7/2011



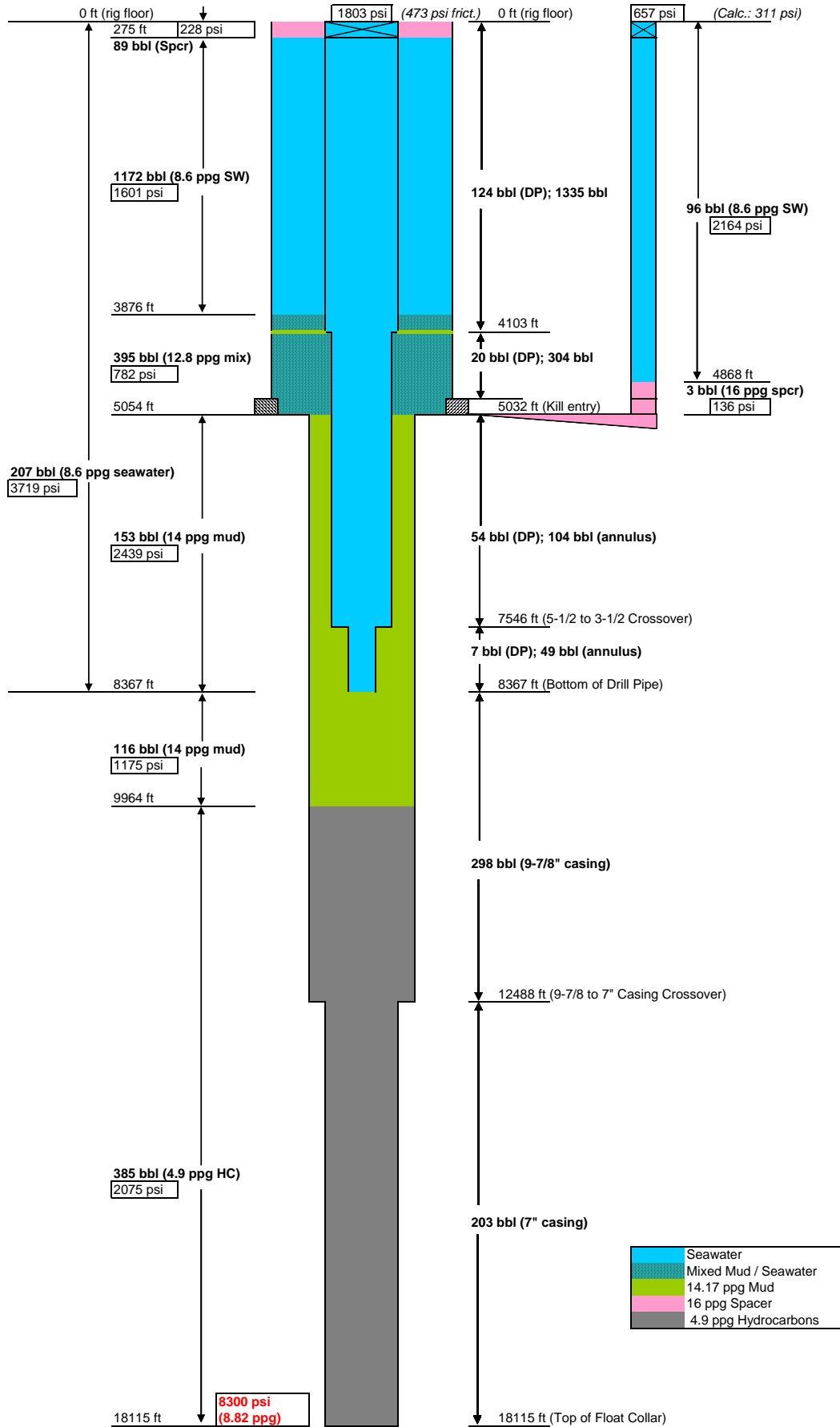
Post-Final Pump, 21:30

1/7/2011



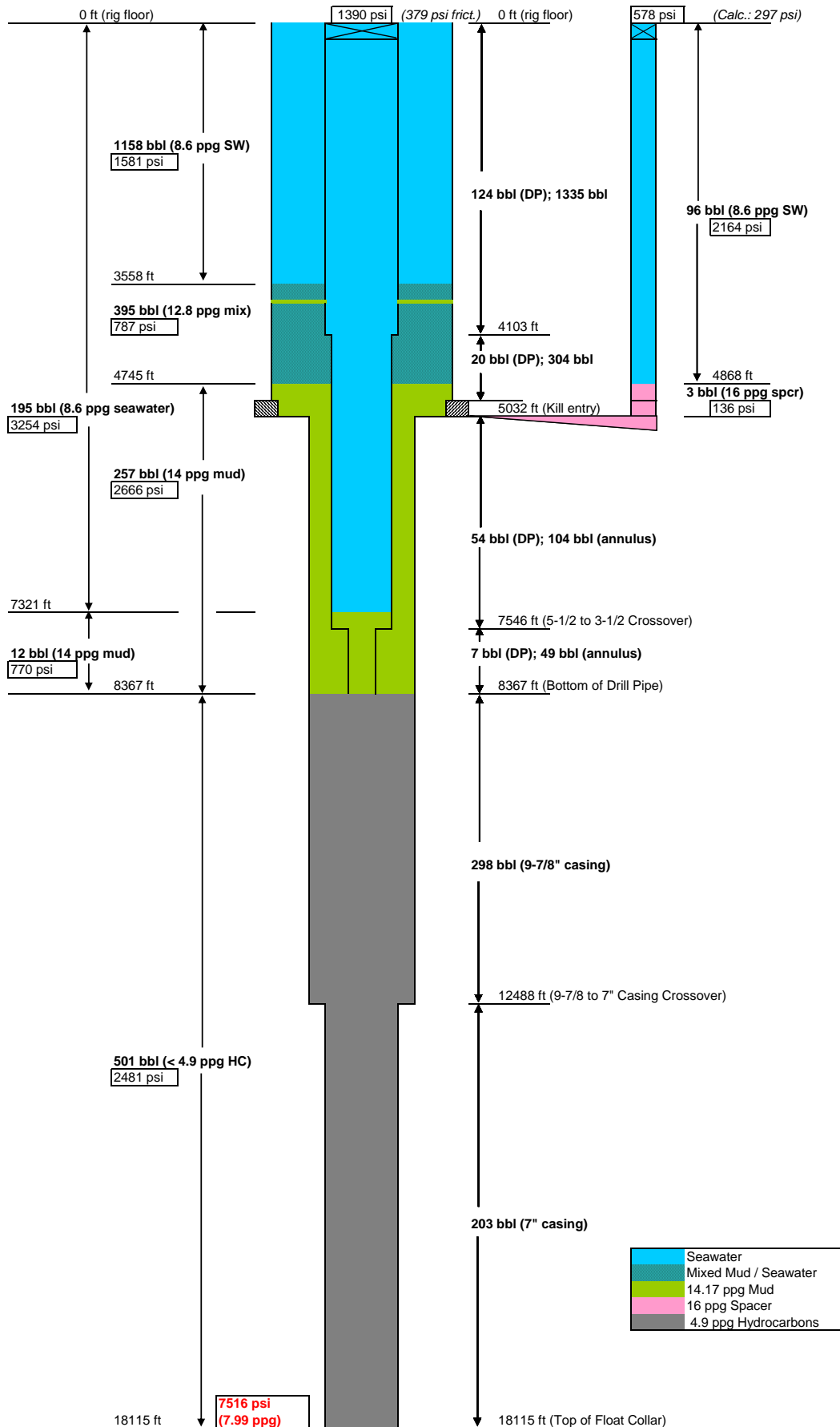
Mud to Riser, 21:34

1/7/2011



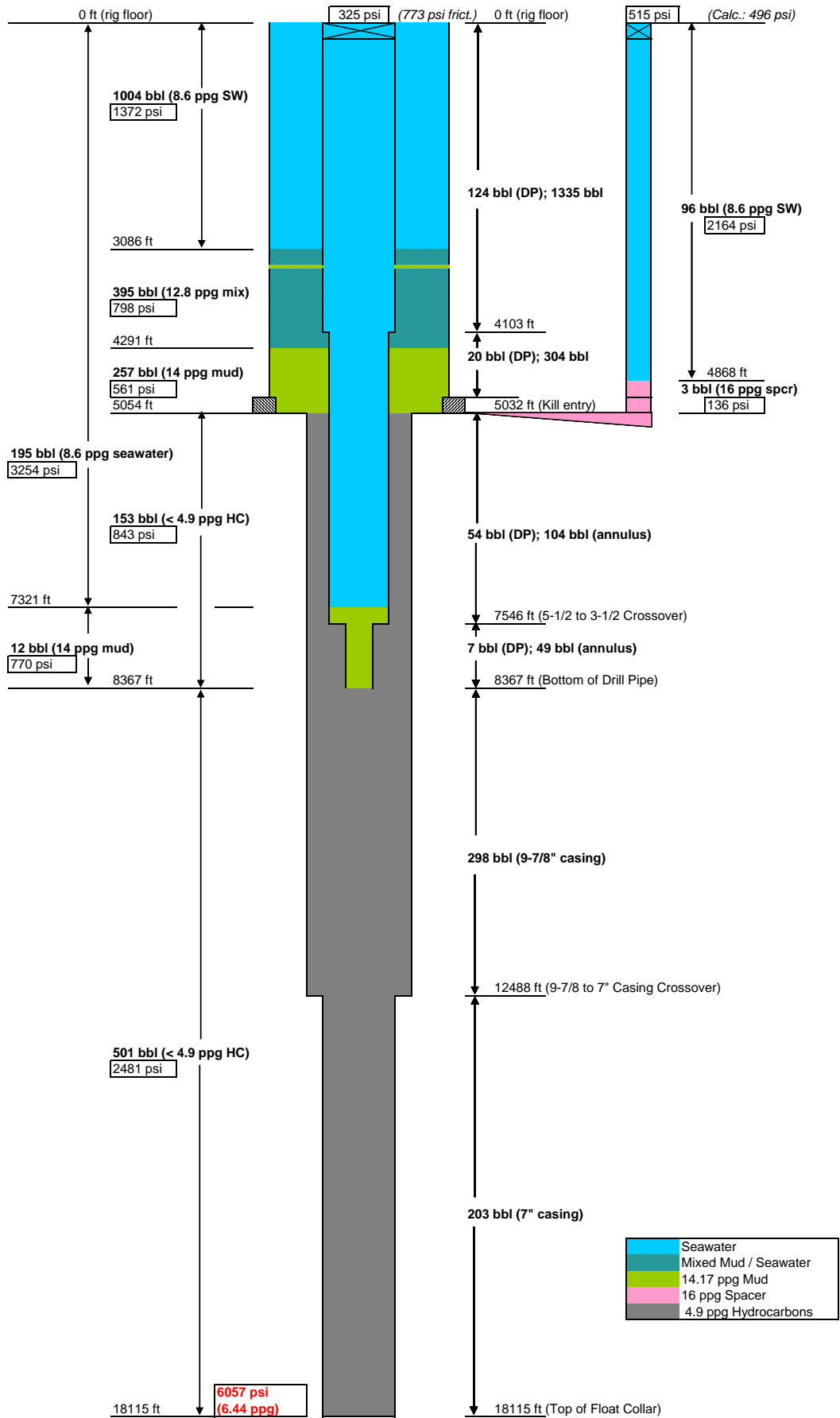
Hydrocarbons to Drill Pipe, 21:39

1/7/2011



Hydrocarbons to Riser, ~21:42

1/7/2011



Macondo Well Negative Test Hydrostatics

Inputs

Fluid Inputs

$\text{bbl} \equiv 42\text{gal}$	Barrel definition	$\rho_{14} := 14.17 \frac{\text{lbm}}{\text{gal}}$	14 ppg mud density
$V_{p_s} := 421\text{bbl}$	Spacer volume pumped	$\rho_{16} := 16 \frac{\text{lbm}}{\text{gal}}$	16 ppg mud density
$V_{p_1} := 327\text{bbl}$	Water pumped during displace #1	$\rho_w := 8.556 \frac{\text{lbm}}{\text{gal}}$	Seawater density
$V_{p_2} := 1160\text{bbl}$	Water pumped during displace #2	$V_{\text{del}} := 26.9\text{bbl}$	Water loss volume
$V_{f_rp} := 153\text{bbl}$	Volume pumped by rig pumps during final pumping	$\rho_{\text{flux}} := 4.9 \frac{\text{lbm}}{\text{gal}}$	Density of hydrocarbon influx (at reservoir, from PVT data)
$V_{f_b} := 51\text{bbl}$	Volume pumped by boost pump during final pumping		

Geometry

$V_{\text{dp}} := 206.59\text{bbl}$	Drill pipe internal volume	$L_{\text{dp}} := 8367\text{ft}$	Drill pipe length
$V_1 := 124.36\text{bbl}$	Drillpipe segment 1 volume (6-5/8" DP)	$L_1 := 4103\text{ft}$	Length of model section 1
$V_2 := 75.09\text{bbl}$	Drillpipe segment 2 volume (5-1/2" DP)	$L_2 := 3443\text{ft}$	Length of model section 2
$V_3 := 7.14\text{bbl}$	Drillpipe segment 3 volume (3-1/2" DP)	$L_3 := 821\text{ft}$	Length of model section 3
$V_4 := 49.42\text{bbl}$	Annulus segment 4 volume (casing, 3-1/2" DP)	$L_4 := 821\text{ft}$	Length of model section 4
$V_5 := 104.01\text{bbl}$	Annulus segment 5 volume (casing, 5-1/2" DP)	$L_5 := 2492\text{ft}$	Length of model section 5
$V_6 := 16.48\text{bbl}$	Annulus segment 6 volume (BOP, 5-1/2" DP)	$L_6 := 53\text{ft}$	Length of model section 6
$V_7 := 304.3\text{bbl}$	Annulus segment 7 volume (riser, 5-1/2" DP)	$L_7 := 898\text{ft}$	Length of model section 7
$V_8 := 1334.87\text{bbl}$	Annulus segment 8 volume (riser, 6-5/8" DP)	$L_8 := 4103\text{ft}$	Length of model section 8
$V_{\text{riser}} := 2015.66\text{bbl}$	Total volume in riser, DP, casing, and BOP annulus	$V_{6_ann} := 11.53\text{bbl}$	Volume in BOP below annular
$L_{\text{kill}} := 5032\text{ft}$	Length of kill line	$D_{\text{kill}} := 4.5\text{in}$	Kill line ID
$L_{\text{csg}} := 9748\text{ft}$	Length of casing below drill pipe to float collar	$D_{\text{csg9}} := 8.625\text{in}$	ID of 9-5/8" casing
$L_{\text{c7}} := 5627\text{ft}$	Length of 7" casing	$D_{\text{csg7}} := 6.094\text{in}$	ID of lower 7" casing section
$L_{\text{ann}} := 5017\text{ft}$	Depth of annular preventer		

$PP_{well} := 12.603 \frac{lbm}{gal}$	Lower zone pore pressure (EMW)	$PP_{well2} := 13.1 \frac{lbm}{gal}$	Upper zone pore pressure (EMW)
$P_{sp_init} := 2131psi$	Initial standpipe pressure	$P_{kill} := 682psi$	Kill line pressure during U-tube (16:58)
$P_{sp_ut} := 1395psi$	Standpipe pressure during U-tube (16:58)	$\Delta V_{bleed} := 25bbl$	Volume bled prior to u-tube (16:54)
$P_{sp_new} := 1202psi$	Recorded SPP after annular leakage (17:26)	$\Delta V_{ann} := 65bbl$	Total leakage volume through annular (17:11)
$V_{bl_dp} := 15bbl$	Volume bled from drillpipe (bleed #2) - (17:27)	$V_{bl_dp2} := 7bbl$	Volume bled from drillpipe (bleed #3) - (17:53)
$P_{sp_asy} := 1182psi$	Pressure "asymptote" (SPP was headed here before kill line opening) - (18:31)	$P_{sp_neg} := 1404psi$	Pressure on standpipe when kill line opened just prior to negative test (18:40)
$V_{k_bleed} := 0.2bbl$	Volume bleed from kill line when opened for negative test (19:15)	$P_{sp_ng2} := 1391psi$	Final SPP during negative test (19:20)
$P_{sp_d2a} := 1013psi$	Measured standpipe pressure at end of displacement #2 (21:09)	$P_{sp_fp} := 1202psi$	Measured SPP just prior to final pumping (21:13)
$P_{ssp} := 1171psi$	Standpipe pressure after final pumping (21:30)	$P_{k_ssp} := 764psi$	Kill line pressure after final pumping (21:30)
$P_{peak} := 1803psi$	Peak SPP after final pumping (21:34)	$P_{k_pk} := 657psi$	Kill line pressure during peak standpipe pressure (21:34)
$\Delta P_{sp} := 305psi$	Approximate pressure delta observed after final SP bleed (21:38)		
$P_{turn} := 1390psi$	Standpipe pressure just before rapid drop (21:39)	$P_{k_tn} := 578psi$	Kill line pressure at onset of rapid drop in standpipe pressure (21:39)

Outputs - Setup Calculations*Cross sectional areas*

$$A_1 := \frac{V_1}{L_1} = 24.505 \text{ in}^2$$

Cross sectional area of model section 1

$$A_2 := \frac{V_2}{L_2} = 17.633 \text{ in}^2$$

Cross sectional area of model section 2

$$A_3 := \frac{V_3}{L_3} = 7.031 \text{ in}^2$$

Cross sectional area of model section 3

$$A_4 := \frac{V_4}{L_4} = 48.668 \text{ in}^2$$

Cross sectional area of model section 4

$$A_5 := \frac{V_5}{L_5} = 33.745 \text{ in}^2$$

Cross sectional area of model section 5

$$A_6 := \frac{V_6}{L_6} = 251.398 \text{ in}^2$$

Cross sectional area of model section 6

$$A_7 := \frac{V_7}{L_7} = 273.972 \text{ in}^2$$

Cross sectional area of model section 7

$$A_8 := \frac{V_8}{L_8} = 263.037 \text{ in}^2$$

Cross sectional area of model section 8

$$A_{\text{csg7}} := \frac{\pi}{4} \cdot D_{\text{csg7}}^2 = 29.167 \text{ in}^2$$

Cross sectional area of 7" casing

$$A_{\text{csg9}} := \frac{\pi}{4} \cdot D_{\text{csg9}}^2 = 58.426 \text{ in}^2$$

Cross sectional area of 9-5/8" casing

$$L_{6_ann} := L_{dp} - L_4 - L_5 - L_{ann} = 37 \cdot \text{ft}$$

Length of segment 6 (BOP) below annular preventer)

$$L_{6_kill} := L_{dp} - L_4 - L_5 - L_{kill} = 22 \cdot \text{ft}$$

Length of segment 6 (BOP) below kill line)

$$L_{\text{annulus}} := L_{dp} - L_{kill} = 3.335 \times 10^3 \cdot \text{ft}$$

Length from kill line to bottom of drill string

Outputs - Timeline Hydrostatic Calculations*Spacer pump, displace #1 (16:28)*

$$V_{\text{spcr7}} := V_{\text{p_s}} - V_6 - V_5 - V_4 - V_{\text{dp}} = 44.5 \cdot \text{bbl}$$

Volume of spacer in model segment 7 after pump

$$h_{14_sp1} := L_8 + L_7 - \left(\frac{V_{\text{spcr7}}}{A_7} \right) = 4.87 \times 10^3 \cdot \text{ft}$$

Height of 14 ppg mud above spacer

$$h_{16_sp1} := L_{\text{dp}} - h_{14_sp1} = 3.497 \times 10^3 \cdot \text{ft}$$

Height of spacer in annulus

$$V_{14_sp1} := V_8 + V_7 - V_{\text{spcr7}} = 1.595 \times 10^3 \cdot \text{bbl}$$

Volume of mud in annulus

$$P_{14_sp1} := \rho_{14} \cdot g \cdot h_{14_sp1} = 3.585 \times 10^3 \cdot \text{psi}$$

Mud head pressure

$$P_{16_sp1} := \rho_{16} \cdot g \cdot h_{16_sp1} = 2.907 \times 10^3 \cdot \text{psi}$$

Spacer head pressure (in annulus)

$$P_{\text{sp_sp1}} := P_{14_sp1} + P_{16_sp1} - \rho_{16} \cdot g \cdot L_{\text{dp}} = -462.936 \cdot \text{psi}$$

Standpipe pressure after spacer pump

$$P_{\text{bh_sp1}} := P_{14_sp1} + P_{16_sp1} + \rho_{14} \cdot g \cdot L_{\text{csg}} = 13667 \cdot \text{psi}$$

Bottom hole pressure at this SPP

$$\rho_{\text{bh_sp1}} := \frac{P_{\text{bh_sp1}}}{g \cdot (L_{\text{csg}} + L_{\text{dp}})} = 14.523 \cdot \frac{\text{lbm}}{\text{gal}}$$

Equivalent density at bottom hole

Pore pressure balance with seawater in drillpipe and water loss to casing

$$P_{\text{pp_well}} := PP_{\text{well}} \cdot g \cdot (L_{\text{dp}} + L_{\text{csg}}) = 11860 \cdot \text{psi}$$

Pressure at bottom of well due to 12.6 ppg formation

$$P_{\text{pp_well2}} := PP_{\text{well2}} \cdot g \cdot (L_{\text{dp}} + L_{\text{csg}}) = 1.233 \times 10^4 \cdot \text{psi}$$

Pressure at bottom of well due to 13.1 ppg formation

$$P_{\text{sp_126}} := P_{\text{pp_well}} - (\rho_{\text{w}} \cdot g \cdot L_{\text{dp}} + \rho_{14} \cdot g \cdot L_{\text{csg}}) = 965.513 \cdot \text{psi}$$

Theoretical SPP with seawater in DP, mud in remainder of casing, exposure to 12.6 ppg

$$P_{\text{sp_131}} := P_{\text{pp_well2}} - (\rho_{\text{w}} \cdot g \cdot L_{\text{dp}} + \rho_{14} \cdot g \cdot L_{\text{csg}}) = 1.433 \times 10^3 \cdot \text{psi}$$

Theoretical SPP with seawater in DP, mud in remainder of casing, exposure to 13.1 ppg

$$h_{\text{w_ex}} := \frac{V_{\text{del}}}{A_{\text{csg9}}} = 372.241 \cdot \text{ft}$$

Extra height of water in casing below drillpipe

$$h_{\text{c_14}} := L_{\text{csg}} - h_{\text{w_ex}} = 9.376 \times 10^3 \cdot \text{ft}$$

New height of 14 ppg mud in casing below drillpipe

$$P_{\text{w_ex}} := \rho_{\text{w}} \cdot g \cdot h_{\text{w_ex}} = 165.449 \cdot \text{psi}$$

Hydrostatic pressure of water below drillpipe

$$P_{14_ex} := \rho_{14} \cdot g \cdot h_{\text{c_14}} = 6.902 \times 10^3 \cdot \text{psi}$$

Hydrostatic pressure of mud below drillpipe

$$P_{\text{c_loss}} := P_{\text{w_ex}} + P_{14_ex} = 7.067 \times 10^3 \cdot \text{psi}$$

Hydrostatic pressure in casing below drillpipe

Water pump, displace #1 (16:54)

$P_{w_dp} := \rho_w \cdot g \cdot L_{dp} = 3.719 \times 10^3 \text{ psi}$	Head pressure of water in drill pipe
$P_{an_init} := P_{sp_init} + P_{w_dp} = 5.85 \times 10^3 \text{ psi}$	Pressure in annulus
$V_{w_al} := V_{p_1} - V_{dp} - V_{del} = 93.51 \cdot \text{bbl}$	Water volume in annulus
$h_{w_al} := \frac{V_{w_al} - V_4}{A_5} + L_4 = 1.877 \times 10^3 \cdot \text{ft}$	Water height in annulus
$V_{s81} := V_{p_s} - (V_5 + V_4 - V_{w_al}) - V_6 - V_7 = 40.3 \cdot \text{bbl}$	Spacer volume in model segment 8
$h_{s_al} := (L_4 + L_5 - h_{w_al}) + L_6 + L_7 + \frac{V_{s81}}{A_8} = 2.511 \times 10^3 \cdot \text{ft}$	Spacer height
$h_{m_al} := L_{dp} - h_{w_al} - h_{s_al} = 3.979 \times 10^3 \cdot \text{ft}$	14 ppg mud height
$V_{m_al} := h_{m_al} \cdot A_8 = 1.295 \times 10^3 \cdot \text{bbl}$	Volume of mud in riser
$P_{w_al} := \rho_w \cdot g \cdot h_{w_al} = 834.427 \text{ psi}$	Water head pressure in annulus
$P_{s_al} := \rho_{16} \cdot g \cdot h_{s_al} = 2.087 \times 10^3 \text{ psi}$	Spacer head pressure
$P_{m_al} := \rho_{14} \cdot g \cdot h_{m_al} = 2.929 \times 10^3 \text{ psi}$	Mud head pressure
$P_{w_al} + P_{s_al} + P_{m_al} - P_{w_dp} = 2.131 \times 10^3 \text{ psi}$	Check SPP
$P_{bh_al} := P_{sp_init} + P_{w_dp} + P_{c_loss} = 12917 \text{ psi}$	Bottom hole pressure
$\rho_{eq_al} := \frac{P_{bh_al}}{g \cdot (L_{dp} + L_{csg})} = 13.726 \cdot \frac{\text{lbm}}{\text{gal}}$	Equivalent density at bottom hole

U-tube (Equalize) Event (16:58)

$$P_{k_s} := \rho_w \cdot g \cdot L_{kill} = 2.237 \times 10^3 \text{ psi} \quad \text{Head pressure in kill line (filled with seawater)}$$

$$P_{an_ut} := P_{sp_ut} + P_{w_dp} - P_{k_s} - P_{kill} = 2.195 \times 10^3 \text{ psi} \quad \text{Pressure in annulus below kill line}$$

$$h_{s_b} := \frac{P_{an_ut} - \rho_w \cdot g \cdot (L_{annulus})}{g \cdot (\rho_{16} - \rho_w)} = 1844 \cdot \text{ft} \quad \text{Height of spacer below kill line after closure}$$

$$h_{w_b} := L_{annulus} - h_{s_b} = 1.491 \times 10^3 \cdot \text{ft} \quad \text{Height of water below kill line after closure}$$

$$V_{s_b} := V_{6_ann} + (h_{s_b} - L_{6_kill}) \cdot A_5 = 87.568 \cdot \text{bbl} \quad \text{Volume of spacer below annular}$$

$$V_{w_b} := V_{6_ann} + V_5 + V_4 - V_{s_b} = 77.392 \cdot \text{bbl} \quad \text{Volume of water below annular}$$

$$P_{w_b} := \rho_w \cdot g \cdot h_{w_b} = 662.79 \text{ psi} \quad \text{Pressure of water column below kill line}$$

$$P_{s_b} := \rho_{16} \cdot g \cdot h_{s_b} = 1.533 \times 10^3 \text{ psi} \quad \text{Pressure of spacer column below kill line}$$

$$P_{spp} := P_{kill} + P_{k_s} + P_{s_b} + P_{w_b} - P_{w_dp} = 1.395 \times 10^3 \text{ psi} \quad \text{Standpipe pressure (check)}$$

$$P_{bh2} := P_{spp} + P_{w_dp} + P_{c_loss} = 12181 \text{ psi} \quad \text{Bottom hole pressure at this SPP}$$

$$\rho_{bh2} := \frac{P_{bh2}}{g \cdot (L_{csg} + L_{dp})} = 12.944 \cdot \frac{\text{lbm}}{\text{gal}} \quad \text{Equivalent density at bottom hole}$$

Bleed Drill Pipe after U-Tube (16:59)

$$P_{sp_k0} := P_{spp} - P_{kill} = 713 \text{ psi} \quad \text{SPP when kill line goes to zero pressure}$$

$$P_{bh3} := P_{sp_k0} + P_{w_dp} + P_{c_loss} = 11499 \text{ psi} \quad \text{Bottom hole pressure at this SPP}$$

$$\rho_{bh3} := \frac{P_{bh3}}{g \cdot (L_{csg} + L_{dp})} = 12.219 \cdot \frac{\text{lbm}}{\text{gal}} \quad \text{Equivalent density at bottom hole}$$

Calculated Hydrostatics after Annular Leakage and SPP decay (17:26)

$$V_{s_new} := V_{s_b} + \Delta V_{ann} - (V_{w_a1} - V_{w_b}) = 136.45 \cdot \text{bbl} \quad \text{New volume of spacer below annular after leakage}$$

$$V_{b_ann} := V_{6_ann} + V_5 + V_4 = 164.96 \cdot \text{bbl} \quad \text{Total volume of annulus below annular}$$

$$V_{w_new} := V_{b_ann} - V_{s_new} = 28.51 \cdot \text{bbl} \quad \text{New volume of water in annulus after leakage}$$

$$h_{w_new} := \frac{V_{w_new}}{A_4} = 473.628 \cdot \text{ft} \quad \text{Height of new water column}$$

$$h_{s_new} := L_{dp} - h_{w_new} - L_{ann} = 2.876 \times 10^3 \cdot \text{ft} \quad \text{Height of new spacer column}$$

$$P_{s_new} := \rho_{16} \cdot g \cdot h_{s_new} = 2.391 \times 10^3 \text{ psi} \quad \text{Head pressure of spacer column after leakage}$$

$$P_{w_new} := \rho_w \cdot g \cdot h_{w_new} = 210.512 \text{ psi} \quad \text{Head pressure of water column after leakage}$$

$$P_{sp_calc} := P_{s_new} + P_{w_new} - P_{w_dp} = -1.118 \times 10^3 \text{ psi} \quad \text{Calculated standpipe pressure after leakage}$$

$$P_{bh4} := P_{sp_calc} + P_{w_dp} + P_{c_loss} = 9668 \text{ psi} \quad \text{Bottom hole pressure at this SPP}$$

$$\rho_{bh4} := \frac{P_{bh4}}{g \cdot (L_{csg} + L_{dp})} = 10.274 \cdot \frac{\text{lbm}}{\text{gal}} \quad \text{Equivalent density at bottom hole}$$

"Actual" Hydrostatics after Annular Leakage and SPP decay (17:26)

$$P_{bh_act} := P_{sp_new} + P_{w_dp} + P_{c_loss} = 11988 \text{ psi}$$

$$\rho_{bh_act} := \frac{P_{bh_act}}{g \cdot (L_{csg} + L_{dp})} = 12.739 \cdot \frac{\text{lbm}}{\text{gal}}$$

Bleed off 1200 psi standpipe pressure (17:27)

$$h_{w_en} := h_{w_ex} - \frac{V_{bl_dp}}{A_{csg9}} = 164.672 \cdot \text{ft} \quad \text{New height of water in casing below drillpipe after bleed}$$

$$h_{c_14n} := L_{csg} - h_{w_en} = 9.583 \times 10^3 \cdot \text{ft} \quad \text{New height of 14 ppg mud in casing below drillpipe}$$

$$P_{w_en} := \rho_w \cdot g \cdot h_{w_en} = 73.191 \text{ psi} \quad \text{Hydrostatic pressure of water below drillpipe}$$

$$P_{14_en} := \rho_{14} \cdot g \cdot h_{c_14n} = 7.054 \times 10^3 \text{ psi} \quad \text{Hydrostatic pressure of mud below drillpipe}$$

$$P_{c_in} := P_{w_en} + P_{14_en} = 7.128 \times 10^3 \text{ psi} \quad \text{Hydrostatic pressure in casing below drillpipe}$$

$$P_{bh5} := P_{w_dp} + P_{c_in} = 10846 \text{ psi} \quad \text{Bottom hole pressure at this SPP}$$

$$\rho_{bh5} := \frac{P_{bh5}}{g \cdot (L_{csg} + L_{dp})} = 11.526 \cdot \frac{\text{lbm}}{\text{gal}} \quad \text{Equivalent density at bottom hole}$$

Bleed off 750 psi standpipe pressure after buildup (17:53)

$$h_{w_en2} := h_{w_en} - \frac{V_{bl_dp2}}{A_{csg9}} = 67.806 \cdot \text{ft}$$

New height of water in casing below drillpipe after bleed

$$h_{c_14n2} := L_{csg} - h_{w_en2} = 9.68 \times 10^3 \cdot \text{ft}$$

New height of 14 ppg mud in casing below drillpipe

$$P_{w_en2} := \rho_w \cdot g \cdot h_{w_en2} = 30.138 \text{ psi}$$

Hydrostatic pressure of water below drillpipe

$$P_{14_en2} := \rho_{14} \cdot g \cdot h_{c_14n2} = 7.126 \times 10^3 \text{ psi}$$

Hydrostatic pressure of mud below drillpipe

$$P_{c_ln2} := P_{w_en2} + P_{14_en2} = 7.156 \times 10^3 \text{ psi}$$

Hydrostatic pressure in casing below drillpipe

$$P_{bh6} := P_{w_dp} + P_{c_ln2} = 10875 \text{ psi}$$

Bottom hole pressure at this SPP

$$\rho_{bh6} := \frac{P_{bh6}}{g \cdot (L_{csg} + L_{dp})} = 11.556 \cdot \frac{\text{lbm}}{\text{gal}}$$

Equivalent density at bottom hole

Calculated pressure "asymptote" prior to opening kill valve (18:31)

$$P_{sp_a_calc} := P_{pp_well} - P_{c_ln2} - P_{w_dp} = 985.288 \text{ psi}$$

Calculated pressure asymptote

$$P_{bh_a} := P_{sp_asy} + P_{w_dp} + P_{c_ln2} = 12057 \text{ psi}$$

Downhole pressure based on actual reading

$$\rho_{bh_a} := \frac{P_{bh_a}}{g \cdot (L_{csg} + L_{dp})} = 12.812 \cdot \frac{\text{lbm}}{\text{gal}}$$

Equivalent density at bottom hole, based on actual

Open lower kill valve before negative test (18:36)

$$P_{s_bk} := P_{s_new} - \rho_{16} \cdot g \cdot (L_{kill} - L_{ann}) = 2.378 \times 10^3 \text{ psi}$$

Head pressure of spacer in annulus below kill line

$$PP_{add} := P_{w_dp} + P_{sp_neg} - P_{s_bk} - P_{w_new} - P_{k_s} = 297.504 \text{ psi}$$

Gain in formation pressure to cause observed pressure response

$$P_{bh_neg} := P_{sp_neg} + P_{w_dp} + P_{c_ln2} = 12279 \text{ psi}$$

Bottom hole pressure at this SPP

$$\rho_{bh_neg} := \frac{P_{bh_neg}}{g \cdot (L_{csg} + L_{dp})} = 13.048 \cdot \frac{\text{lbm}}{\text{gal}}$$

Equivalent density at bottom hole

Negative Test after kill line bleed (19:15 - 19:54)

$$P_{c_ng2} := P_{bh_neg} - P_{sp_ng2} - P_{w_dp} = 7.169 \times 10^3 \text{ psi}$$

Casing pressure required for SPP at increased pore pressure

$$h_{w_ng2} := \frac{P_{c_ng2} - \rho_{14} \cdot g \cdot L_{csg}}{g \cdot (\rho_w - \rho_{14})} = 23.23 \cdot \text{ft}$$

New height of water in casing below drillpipe after bleed

$$h_{c_14ng2} := L_{csg} - h_{w_ng2} = 9.725 \times 10^3 \cdot \text{ft}$$

New height of 14 ppg mud in casing below drillpipe

$$P_{w_ng2} := \rho_w \cdot g \cdot h_{w_ng2} = 10.325 \text{ psi}$$

Hydrostatic pressure of water below drillpipe

$$P_{14_ng2} := \rho_{14} \cdot g \cdot h_{c_14ng2} = 7.158 \times 10^3 \text{ psi}$$

Hydrostatic pressure of mud below drillpipe

$$\Delta V_{neg} := (h_{w_en2} - h_{w_ng2}) \cdot A_{csg9} = 3.221 \cdot \text{bbl}$$

Volume gain required for new casing pressure (also equal to volume of spacer drawn into kill line)

$$\Delta h_{k2} := \frac{\Delta V_{neg}}{\frac{\pi}{4} \cdot D_{kill}^2} = 163.755 \cdot \text{ft}$$

Extra height of 16 ppg spacer in kill line

$$h_{w_k2} := L_{kill} - \Delta h_{k2} = 4.868 \times 10^3 \cdot \text{ft}$$

Height of water in kill line

$$P_{w_k2} := \rho_w \cdot g \cdot h_{w_k2} = 2.164 \times 10^3 \text{ psi}$$

Water head pressure in kill line

$$P_{s_k2} := \rho_{16} \cdot g \cdot \Delta h_{k2} = 136.108 \text{ psi}$$

Spacer head pressure in kill line

$$P_{k_s2} := P_{w_k2} + P_{s_k2} = 2.3 \times 10^3 \text{ psi}$$

Resulting kill line head pressure

$$V_{w_ng2} := V_{w_new} + \Delta V_{neg} + V_{k_bleed} = 31.931 \cdot \text{bbl}$$

New water volume in casing annulus, accounting for stated bleed volume out kill line

$$V_{s_ng2} := V_{s_new} - \Delta V_{neg} = 133.229 \cdot \text{bbl}$$

New spacer volume in casing annulus

$$h_{wa_ng2} := \frac{V_{w_ng2}}{A_4} = 530.465 \cdot \text{ft}$$

New water height

$$h_{s_ng2} := L_{dp} - L_{kill} - h_{wa_ng2} = 2.805 \times 10^3 \cdot \text{ft}$$

New spacer height

$$P_{wa_ng2} := \rho_w \cdot g \cdot h_{wa_ng2} = 235.775 \text{ psi}$$

Water head pressure

$$P_{s_ng2} := \rho_{16} \cdot g \cdot h_{s_ng2} = 2.331 \times 10^3 \text{ psi}$$

Spacer head pressure

$$P_{sp_ng2c} := P_{k_s2} + P_{s_ng2} + P_{wa_ng2} - P_{w_dp} = 1.148 \times 10^3 \text{ psi}$$

Check of SPP

$$\Delta P := P_{sp_ng2} - P_{sp_ng2c} = 243.158 \text{ psi}$$

Delta between calculated and measured SPP (equal to expected kill line pressure)

Open Annular Prior to Displace #2 (20:02)

$$V_{s_a} := V_{p_s} - V_{s_new} - \Delta V_{neg} = 281.329 \cdot \text{bbl} \quad \text{Volume of spacer above annular}$$

$$h_{s_a} := L_{ann} - (L_8 + L_7) + \frac{V_{s_a} - (V_6 - V_{6_ann})}{A_7} = 831.603 \cdot \text{ft} \quad \text{Height of spacer above annular}$$

$$h_{s_b2} := h_{s_a} + L_{dp} - h_{wa_ng2} - L_{ann} = 3.651 \times 10^3 \cdot \text{ft} \quad \text{Total spacer height}$$

$$P_{s_b2} := \rho_{16} \cdot g \cdot h_{s_b2} = 3.035 \times 10^3 \text{ psi} \quad \text{Spacer head pressure}$$

$$h_{14_b2} := L_{dp} - h_{wa_ng2} - h_{s_b2} = 4.185 \times 10^3 \cdot \text{ft} \quad \text{14 ppg mud height}$$

$$P_{14_b2} := \rho_{14} \cdot g \cdot h_{14_b2} = 3.081 \times 10^3 \text{ psi} \quad \text{Mud head pressure}$$

$$V_{14_b2} := V_8 + (h_{14_b2} - L_8) \cdot A_7 - \Delta V_{neg} = 1.36 \times 10^3 \cdot \text{bbl} \quad \text{Mud volume in riser}$$

$$V_{s_b2} := V_{p_s} - \Delta V_{neg} = 417.779 \cdot \text{bbl} \quad \text{Total spacer volume (minus volume in kill line)}$$

$$P_{sp_b2} := P_{14_b2} + P_{s_b2} + P_{wa_ng2} - P_{w_dp} = 2.633 \times 10^3 \text{ psi} \quad \text{SPP prior to pumping}$$

$$P_{bh_b2} := P_{sp_b2} + P_{w_dp} + P_{c_ng2} = 13520 \text{ psi} \quad \text{Bottom hole pressure at this SPP}$$

$$\rho_{bh_b2} := \frac{P_{bh_b2}}{g \cdot (L_{csg} + L_{dp})} = 14.367 \cdot \frac{\text{lbm}}{\text{gal}} \quad \text{Equivalent density at bottom hole}$$

Well balance point to 12.6 ppg (during displace #2, ~20:52)

$$P_{sp_b} := P_{pp_well} - P_{c_ng2} - P_{w_dp} = 972.288 \text{ psi}$$

Hydrostatic standpipe pressure at balance
(measured pressure is greater due to friction)

$$h_{s_8} := \frac{V_{s_b2}}{A_g} = 1.284 \times 10^3 \cdot \text{ft}$$

Height of spacer while in upper part of riser

$$P_8 := P_{sp_b} + P_{w_dp} - \rho_w \cdot g \cdot (L_4 + L_5 + L_6 + L_7) = 2.796 \times 10^3 \text{ psi}$$

Head pressure in upper part of riser

$$P_{s_8} := \rho_{16} \cdot g \cdot h_{s_8} = 1.067 \times 10^3 \text{ psi}$$

Spacer contribution to upper riser head pressure

$$\rho_u := \frac{(P_8 - P_{s_8})}{g \cdot (L_8 - h_{s_8})} = 11.805 \cdot \frac{\text{lbm}}{\text{gal}}$$

Equivalent ppg of remainder (for ratio of 14 ppg to water)

$$h_{14} := (L_8 - h_{s_8}) \cdot \frac{\rho_u - \rho_w}{\rho_{14} - \rho_w} = 1631 \cdot \text{ft}$$

Height of 14 ppg mud remaining

$$h_w := L_8 - h_{s_8} - h_{14} = 1.188 \times 10^3 \cdot \text{ft}$$

Height of water in upper part of riser

$$P_{14_b} := \rho_{14} \cdot g \cdot h_{14} = 1.201 \times 10^3 \text{ psi}$$

Head pressure of 14 ppg mud

$$V_{14_b} := h_{14} \cdot A_g = 530.69 \cdot \text{bbl}$$

Volume of 14 ppg mud

$$P_{wtr_b} := \rho_w \cdot g \cdot (h_w + L_7 + L_6 + L_5 + L_4) = 2.423 \times 10^3 \text{ psi}$$

Head pressure of water in annulus

$$V_{wtr_b} := h_w \cdot A_g + V_7 + V_6 + V_5 + V_4 = 860.611 \cdot \text{bbl}$$

Volume of water in annulus

Post-Displace, with no well influx (20:09)

$$V_{14_d2} := V_{14_b2} - V_{p_2} = 199.57 \cdot \text{bbl}$$

14 ppg mud in annulus after displacement

$$h_{14_d2} := \frac{V_{14_d2}}{A_g} = 613.42 \cdot \text{ft}$$

Height of 14 ppg mud

$$P_{14_d2} := \rho_{14} \cdot g \cdot h_{14_d2} = 451.541 \text{ psi}$$

Head pressure of mud in annulus

$$V_{w_d2} := V_{riser} - V_{14_d2} - V_{s_b2} - V_{dp} = 1.192 \times 10^3 \cdot \text{bbl}$$

Volume of water in annulus

$$h_{w_d2} := L_{dp} - h_{14_d2} - h_{s_8} = 6.469 \times 10^3 \cdot \text{ft}$$

Height of water in annulus

$$P_{w_d2} := \rho_w \cdot g \cdot h_{w_d2} = 2.875 \times 10^3 \text{ psi}$$

Head pressure of water in annulus

$$P_{sp_d2} := P_{14_d2} + P_{s_8} + P_{w_d2} - P_{w_dp} = 675.47 \text{ psi}$$

Resulting standpipe pressure

$$P_{bh_d2} := P_{sp_d2} + P_{w_dp} + P_{c_ng2} = 11563 \text{ psi}$$

Bottom hole pressure at this SPP

$$\rho_{bh_d2} := \frac{P_{bh_d2}}{g \cdot (L_{csg} + L_{dp})} = 12.288 \cdot \frac{\text{lbm}}{\text{gal}}$$

Equivalent density at bottom hole

Post-Displace, with well influx (21:09)

$$\rho_{\text{mix}} := 13.4 \frac{\text{lbm}}{\text{gal}}$$

Assumed density of initial mud/water mixture
(from gradient estimates)

$$P_{\text{ann_d2}} := P_{\text{sp_d2a}} + P_{\text{w_dp}} = 4.732 \times 10^3 \text{ psi}$$

Head pressure in annulus to get measured SPP

$$\rho_{\text{ann}} := \frac{P_{\text{ann_d2}} - P_{\text{s_8}} - P_{14_d2}}{g \cdot (L_{\text{dp}} - h_{\text{s_8}} - h_{14_d2})} = 9.56 \frac{\text{lbm}}{\text{gal}}$$

Equivalent ppg of water and mud in annulus (not including spacer)

$$h_{\text{mx_1}} := (L_{\text{dp}} - h_{\text{s_8}} - h_{14_d2}) \cdot \frac{\rho_{\text{ann}} - \rho_{\text{w}}}{\rho_{\text{mix}} - \rho_{\text{w}}} = 1.341 \times 10^3 \text{ ft}$$

Height of mud/water mix in lower casing annulus

$$h_{\text{w_d2a}} := L_{\text{dp}} - h_{\text{s_8}} - h_{14_d2} - h_{\text{mx_1}} = 5.128 \times 10^3 \text{ ft}$$

Total height of water in annulus

$$P_{\text{w_a}} := \rho_{\text{w}} \cdot g \cdot h_{\text{w_d2a}} = 2.279 \times 10^3 \text{ psi}$$

Head pressure of water in annulus

$$\Delta V := (h_{\text{mx_1}} - L_4) \cdot A_5 + V_4 = 71.138 \cdot \text{bbl}$$

Mix volume required to produce measured hydrostatic state

$$V_{\text{w}} := V_{\text{riser}} - V_{\text{dp}} - V_{14_d2} - V_{\text{s_b2}} - \Delta V = 1.121 \times 10^3 \cdot \text{bbl}$$

Water volume

$$\Delta V_{14} := \Delta V \cdot \frac{\rho_{\text{mix}} - \rho_{\text{w}}}{\rho_{14} - \rho_{\text{w}}} = 61.381 \cdot \text{bbl}$$

Mud volume in mixture (equivalent to influx volume from well)

$$P_{\text{mx_1}} := \rho_{\text{mix}} \cdot g \cdot h_{\text{mx_1}} = 933.712 \text{ psi}$$

Head pressure of mixture in lower casing annulus

$$h_{\text{flux}} := \frac{\Delta V_{14}}{A_{\text{csg7}}} = 1.701 \times 10^3 \text{ ft}$$

Height of well influx

$$P_{\text{flux}} := \rho_{\text{flux}} \cdot g \cdot h_{\text{flux}} = 433.094 \text{ psi}$$

Head pressure of well influx

$$P_{14\text{c}} := \rho_{14} \cdot g \cdot (L_{\text{csg}} - h_{\text{flux}}) = 5.923 \times 10^3 \text{ psi}$$

Head pressure of mud in casing below drillpipe

$$P_{\text{bh_d2a}} := P_{\text{ann_d2}} + P_{14\text{c}} + P_{\text{flux}} = 11088 \text{ psi}$$

Bottom hole pressure

$$\rho_{\text{eq_d2a}} := \frac{P_{\text{bh_d2a}}}{g \cdot (L_{\text{csg}} + L_{\text{dp}})} = 11.783 \frac{\text{lbm}}{\text{gal}}$$

Equivalent ppg at bottom hole

$$V_{\text{flux}} := \Delta V_{14} = 61.381 \cdot \text{bbl}$$

Influx total at this time

Post-static sheen, with well influx (21:13)

$\Delta V_{ss} := 32.6 \text{ bbl}$	Volume change due to influx (set to match SPP)
$\Delta h_u := \frac{\Delta V_{ss}}{A_8} = 100.203 \cdot \text{ft}$	Height change at upper riser due to flow out
$\Delta h_l := \frac{\Delta V_{ss}}{A_4} = 541.574 \cdot \text{ft}$	Height change in lower casing annulus due to HC influx
$V_{14_l_fp} := \Delta V_{14} + \Delta V_{ss} = 93.981 \cdot \text{bbl}$	Total influx volume required to produce measured hydrostatic state (equal to 14 ppg mud volume in lower casing annulus)
$V_{14_u_fp} := V_{14_d2} - \Delta V_{ss} = 166.97 \cdot \text{bbl}$	Volume of 14 ppg mud in upper riser
$h_{14_u_fp} := h_{14_d2} - \Delta h_u = 513.217 \cdot \text{ft}$	New height of mud in upper riser
$P_{14_l_fp} := \rho_{14} \cdot g \cdot \Delta h_l = 398.655 \text{ psi}$	Head pressure of 14 ppg mud in lower casing annulus
$P_{14_u_fp} := P_{14_d2} - \rho_{14} \cdot g \cdot \Delta h_u = 377.781 \text{ psi}$	Head pressure of 14 ppg mud in riser annulus
$V_{w_pss8} := V_8 - V_{14_u_fp} - V_{s_b2} = 750.121 \cdot \text{bbl}$	Volume of water in model section 8
$V_{w_pss5} := V_w - V_{w_pss8} - V_7 - V_6 = 49.682 \cdot \text{bbl}$	Volume of water in model section 5
$h_{w_pss} := \frac{V_{w_pss8}}{A_8} + L_7 + L_6 + \frac{V_{w_pss5}}{A_5} = 4.447 \times 10^3 \cdot \text{ft}$	Height of water
$P_{w_pss} := \rho_w \cdot g \cdot h_{w_pss} = 1.977 \times 10^3 \text{ psi}$	Head pressure of water
$V_{m_pss4} := \Delta V - (V_5 - V_{w_pss5}) = 16.81 \cdot \text{bbl}$	Volume of mixture in model section 4
$h_{m_pss} := \frac{V_5 - V_{w_pss5}}{A_5} + \frac{V_{m_pss4}}{A_4} = 1.581 \times 10^3 \cdot \text{ft}$	Height of mixture
$P_{m_pss} := \rho_{\text{mix}} \cdot g \cdot h_{m_pss} = 1.1 \times 10^3 \text{ psi}$	Pressure of mixture
$P_{14_u_fp} + P_{s_8} + P_{w_pss} + P_{m_pss} + P_{14_l_fp} - P_{w_dp} = 1.202 \times 10^3 \text{ psi}$	Hydrostatic SPP (must match)
$h_{\text{flux_fp}} := \frac{V_{14_l_fp}}{A_{\text{csg7}}} = 2.605 \times 10^3 \cdot \text{ft}$	Height of well influx
$P_{\text{flux_fp}} := \rho_{\text{flux}} \cdot g \cdot h_{\text{flux_fp}} = 663.116 \text{ psi}$	Head pressure of well influx
$P_{14c_fp} := \rho_{14} \cdot g \cdot (L_{\text{csg}} - h_{\text{flux_fp}}) = 5.258 \times 10^3 \text{ psi}$	Head pressure of mud in casing below drillpipe
$P_{\text{bh_fp}} := P_{\text{sp_fp}} + P_{w_dp} + \rho_{14} \cdot g \cdot (L_{\text{csg}} - h_{\text{flux_fp}}) + P_{\text{flux_fp}} = 10842 \text{ psi}$	Bottom hole pressure

$$\rho_{eq_d2b} := \frac{P_{bh_fp}}{g \cdot (L_{csg} + L_{dp})} = 11.521 \cdot \frac{\text{lbm}}{\text{gal}}$$

Equivalent ppg at bottom hole

$$V_{influx} := \Delta V_{14} + \Delta V_{ss} = 93.981 \cdot \text{bbl}$$

Influx total at this time

After static sheen pumping, with well influx (21:30)

$$V_{wss} \equiv 138 \cdot \text{bbl}$$

Assumed influx volume during post static sheen pumping

$$P_{ann} := P_{w_dp} + P_{ssp} = 4.89 \times 10^3 \text{ psi}$$

Required head pressure in annulus

$$V_{tss} := V_{f_rp} + V_{wss} = 291 \cdot \text{bbl}$$

Volume of mixed mud and seawater (from pumping plus well influx) pumped through annulus

$$V_{14} := V_{14_u_fp} - V_{tss} - V_{f_b} = -175.03 \cdot \text{bbl}$$

Volume of 14 ppg mud remaining in upper riser after pumping (if value is negative, all mud is gone)

$$h_{14ss} := \begin{cases} \frac{V_{14}}{A_8} & \text{if } V_{14} > 0 \text{ bbl} \\ (0 \text{ ft}) & \text{otherwise} \end{cases} = 0 \cdot \text{ft}$$

Height of mud in riser

$$P_{14ss} := \rho_{14} \cdot g \cdot h_{14ss} = 0 \text{ psi}$$

Pressure of mud in riser

$$V_{16} := \begin{cases} V_{s_b2} + V_{14} & \text{if } V_{14} < 0 \\ V_{s_b2} & \text{otherwise} \end{cases} = 242.749 \cdot \text{bbl}$$

Volume of spacer remaining in upper riser (if mud is gone add the negative volume)

$$h_{16} := \frac{V_{16}}{A_8} = 746.139 \cdot \text{ft}$$

Height of spacer in riser

$$P_{16} := \rho_{16} \cdot g \cdot h_{16} = 620.167 \text{ psi}$$

Pressure of spacer in riser

$$V_{7_w} := V_{16} + V_w + V_{f_b} - V_8 = 79.462 \cdot \text{bbl}$$

Volume of water in section 7

$$h_{7_w} := \frac{V_{7_w}}{A_7} = 234.496 \cdot \text{ft}$$

Height of water in section 7

$$h_{w_ssp} := L_8 + h_{7_w} - h_{16} = 3.591 \times 10^3 \cdot \text{ft}$$

Total height of water

$$P_{w_ssp} := \rho_w \cdot g \cdot h_{w_ssp} = 1.596 \times 10^3 \text{ psi}$$

Water head pressure

$$\rho_{rsr} := \frac{P_{k_ssp} + P_{k_s2} - P_{16} - P_{14ss} - P_{w_ssp}}{g \cdot (L_{kill} - h_{16} - h_{14ss} - h_{w_ssp})} = 23.49 \cdot \frac{\text{lbm}}{\text{gal}}$$

Equivalent density of mixed fluid above kill line

$$\rho_r := \frac{P_{ann} - P_{16} - P_{14ss} - P_{w_ssp}}{g \cdot (L_{dp} - h_{16} - h_{14ss} - h_{w_ssp})} = 12.772 \cdot \frac{\text{lbm}}{\text{gal}}$$

Equivalent density of mixed fluid above drill pipe

$V_{\text{mix}} := V_{\text{riser}} - V_{\text{dp}} - V_{\text{w}} - V_{\text{f}_b} - V_{16} = 394.738 \cdot \text{bbl}$	Volume of mixture
$h_{\text{mix}} := L_{\text{dp}} - h_{16} - h_{14\text{ss}} - h_{\text{w_ssp}} = 4.03 \times 10^3 \cdot \text{ft}$	Height of mixture
$P_{\text{mix}} := \rho_{\text{r}} \cdot g \cdot h_{\text{mix}} = 2.673 \times 10^3 \text{ psi}$	Head pressure of mixture
$P_{\text{mix}_a} := \rho_{\text{r}} \cdot g \cdot (h_{\text{mix}} - L_5 - L_4) = 475.378 \text{ psi}$	Pressure of mixture above casing
$P_{\text{k_calc}} := P_{\text{mix}_a} + P_{\text{w_ssp}} + P_{16} - P_{\text{k}_s2} = 391.902 \text{ psi}$	Calculated kill line pressure
$V_{\text{hc}} := V_{\text{wss}} + V_{\text{flux}} = 231.981 \cdot \text{bbl}$	Influx volume at this point
$V_{\text{csg7}} := A_{\text{csg7}} \cdot L_{\text{c7}} = 202.998 \cdot \text{bbl}$	Volume of lower casing segment
$h_{\text{hc}} := \frac{V_{\text{hc}} - V_{\text{csg7}}}{A_{\text{csg9}}} + L_{\text{c7}} = 6.028 \times 10^3 \cdot \text{ft}$	Height of influx
$P_{\text{hc}} := \rho_{\text{flux}} \cdot g \cdot h_{\text{hc}} = 1.534 \times 10^3 \text{ psi}$	Head pressure of influx
$P_{\text{csg}} := \rho_{14} \cdot g \cdot (L_{\text{csg}} - h_{\text{hc}}) = 2.738 \times 10^3 \text{ psi}$	Head pressure of remainder of mud in casing
$P_{\text{bh}} := P_{\text{hc}} + P_{\text{csg}} + P_{\text{ann}} = 9.163 \times 10^3 \text{ psi}$	Bottom hole pressure
$\rho_{\text{eq}} := \frac{P_{\text{bh}}}{g \cdot (L_{\text{dp}} + L_{\text{csg}})} = 9.737 \cdot \frac{\text{lbm}}{\text{gal}}$	Equivalent ppg at bottom hole

$V_{\text{mud}} := V_4 + V_5 = 153.43 \cdot \text{bbl}$	Casing volume (filled with mud)
$V_{16\text{m}} := V_{16} - V_{\text{mud}} = 89.319 \cdot \text{bbl}$	Spacer volume remaining
$h_{16\text{m}} := \frac{V_{16\text{m}}}{A_8} = 274.54 \cdot \text{ft}$	Spacer height
$P_{16\text{m}} := \rho_{16} \cdot g \cdot h_{16\text{m}} = 228.189 \cdot \text{psi}$	Spacer head pressure
$h_{\text{w}_8} := \frac{V_{\text{w}} + V_{\text{f}_b}}{A_8} = 3.601 \times 10^3 \cdot \text{ft}$	Water height
$P_{\text{w}_8} := \rho_{\text{w}} \cdot g \cdot h_{\text{w}_8} = 1.601 \times 10^3 \cdot \text{psi}$	Water head pressure
$P_{\text{mud}} := \rho_{14} \cdot g \cdot (L_4 + L_5) = 2.439 \times 10^3 \cdot \text{psi}$	Mud head pressure
$h_{\text{mx}} := L_{\text{dp}} - h_{16\text{m}} - h_{\text{w}_8} - L_5 - L_4 = 1.178 \times 10^3 \cdot \text{ft}$	Mixture height
$P_{\text{mx}} := \rho_{\text{r}} \cdot g \cdot h_{\text{mx}} = 781.802 \cdot \text{psi}$	Mixture head pressure
$V_{\text{hc_tc}} := V_{\text{hc}} + V_{\text{mud}} = 385.411 \cdot \text{bbl}$	Volume of hydrocarbon influx at this point
$V_{\text{csg}} := A_{\text{csg}9} \cdot (L_{\text{csg}} - L_{\text{c}7}) + V_{\text{csg}7} = 500.802 \cdot \text{bbl}$	Total casing volume below drill pipe
$V_{14_bdp} := V_{\text{csg}} - V_{\text{hc_tc}} = 115.391 \cdot \text{bbl}$	Volume of mud remaining below drill pipe
$h_{\text{hc_tc}} := \frac{V_{\text{hc_tc}} - V_{\text{csg}7}}{A_{\text{csg}9}} + L_{\text{c}7} = 8.151 \times 10^3 \cdot \text{ft}$	Height of hydrocarbon influx in casing
$P_{\text{hc_tc}} := \rho_{\text{flux}} \cdot g \cdot h_{\text{hc_tc}} = 2.075 \times 10^3 \cdot \text{psi}$	Head pressure of HC influx
$P_{\text{c_tc}} := \rho_{14} \cdot g \cdot (L_{\text{csg}} - h_{\text{hc_tc}}) = 1.175 \times 10^3 \cdot \text{psi}$	Head pressure of remainder of mud in casing
$P_{\text{sp_tc}} := P_{16\text{m}} + P_{\text{w}_8} + P_{\text{mx}} + P_{\text{mud}} - P_{\text{w_dp}} = 1.33 \times 10^3 \cdot \text{psi}$	Calculated SPP
$P_{\text{k_tc}} := P_{16\text{m}} + P_{\text{w}_8} + P_{\text{mx}} - P_{\text{k_s}2} = 310.68 \cdot \text{psi}$	Calculated kill line pressure
$P_{\text{bh_tc}} := P_{\text{hc_tc}} + P_{\text{c_tc}} + P_{\text{mud}} + P_{\text{mx}} + P_{\text{w}_8} + P_{16\text{m}} = 8.3 \times 10^3 \cdot \text{psi}$	Bottom hole pressure
$\rho_{\text{eq_tc}} := \frac{P_{\text{bh_tc}}}{g \cdot (L_{\text{dp}} + L_{\text{csg}})} = 8.82 \cdot \frac{\text{lbm}}{\text{gal}}$	Equivalent ppg at bottom hole

HC to bottom of drillpipe (21:39)

$$h_{14_dp} := \frac{P_{w_dp} + \Delta P_{sp} - \rho_w \cdot g \cdot L_{dp}}{g \cdot (\rho_{14} - \rho_w)} = 1.046 \times 10^3 \cdot \text{ft} \quad \text{Height of mud drawn up the drill pipe}$$

$$P_{14_dp} := \rho_{14} \cdot g \cdot h_{14_dp} = 769.834 \text{ psi} \quad \text{Pressure of mud drawn up the drill pipe}$$

$$P_{w_bdp} := \rho_w \cdot g \cdot (L_{dp} - h_{14_dp}) = 3.254 \times 10^3 \text{ psi} \quad \text{Pressure of remaining water in drill pipe}$$

$$h_{14_2} := h_{14_dp} - L_3 = 224.823 \cdot \text{ft} \quad \text{Height of mud in model section 2}$$

$$V_{14_dp} := h_{14_2} \cdot A_2 + V_3 = 12.043 \cdot \text{bbl} \quad \text{Volume of mud drawn up the drill pipe}$$

$$V_{14_ex} := V_{14_bdp} - V_{14_dp} = 103.348 \cdot \text{bbl} \quad \text{Volume of mud above the casing}$$

$$h_{14_ex} := \frac{V_{14_ex} - V_6}{A_7} + L_6 = 309.351 \cdot \text{ft} \quad \text{Height of mud above the casing}$$

$$P_{14_bdp} := P_{mud} + \rho_{14} \cdot g \cdot h_{14_ex} = 2.666 \times 10^3 \text{ psi} \quad \text{Total mud pressure (in annulus)}$$

$$V_{14_tot} := V_{14_ex} + V_5 + V_4 = 256.778 \cdot \text{bbl} \quad \text{Total mud volume (in annulus)}$$

$$V_{mix7} := V_7 + V_6 - V_{14_ex} = 217.432 \cdot \text{bbl} \quad \text{Volume of mixture in model section 7}$$

$$h_{m_bdp} := \frac{V_{mix7}}{A_7} + \frac{V_{mix} - V_{mix7}}{A_8} = 1.187 \times 10^3 \cdot \text{ft} \quad \text{Total mixture height}$$

$$P_{m_bdp} := \rho_r \cdot g \cdot h_{m_bdp} = 787.296 \text{ psi} \quad \text{Mixture head pressure}$$

$$h_{w_bdp} := L_{dp} - L_4 - L_5 - h_{14_ex} - h_{m_bdp} = 3.558 \times 10^3 \cdot \text{ft} \quad \text{Height of water remaining in riser}$$

$$V_{w_bdp} := h_{w_bdp} \cdot A_8 = 1.158 \times 10^3 \cdot \text{bbl} \quad \text{Volume of water in riser}$$

$$P_{wa_bdp} := \rho_w \cdot g \cdot h_{w_bdp} = 1.581 \times 10^3 \text{ psi} \quad \text{Water head pressure}$$

$$P_{hc_bdp} := \rho_{flux} \cdot g \cdot L_{csg} = 2.481 \times 10^3 \text{ psi} \quad \text{Head pressure of hydrocarbon in casing}$$

$$P_{sp_bdp} := P_{wa_bdp} + P_{m_bdp} + P_{14_bdp} - P_{14_dp} - P_{w_bdp} = 1.011 \times 10^3 \text{ psi} \quad \text{Calculated SPP}$$

$$P_{k_bdp} := P_{wa_bdp} + P_{m_bdp} + \rho_{14} \cdot g \cdot h_{14_ex} - P_{k_s2} = 296.547 \text{ psi} \quad \text{Calculated kill line pressure}$$

$$P_{bh_bdp} := P_{hc_bdp} + P_{14_bdp} + P_{m_bdp} + P_{wa_bdp} = 7.516 \times 10^3 \text{ psi} \quad \text{Bottom hole pressure}$$

$$\rho_{eq_bdp} := \frac{P_{bh_bdp}}{g \cdot (L_{dp} + L_{csg})} = 7.987 \cdot \frac{\text{lbm}}{\text{gal}} \quad \text{Equivalent ppg at bottom hole}$$

HC to riser (~21:42)

$$V_{w_hcr} := V_8 + V_7 + V_6 - V_{14_tot} - V_{mix} = 1.004 \times 10^3 \cdot \text{bbl} \quad \text{Volume of water remaining}$$

$$h_{w_hcr} := \frac{V_{w_hcr}}{A_8} = 3.086 \times 10^3 \cdot \text{ft} \quad \text{Height of water remaining}$$

$$P_{w_hcr} := \rho_w \cdot g \cdot h_{w_hcr} = 1.372 \times 10^3 \text{ psi} \quad \text{Pressure of water}$$

$$V_{m_8hcr} := V_8 - V_{w_hcr} = 330.736 \cdot \text{bbl} \quad \text{Volume of mixture in model section 8}$$

$$h_{m_hcr} := \frac{V_{m_8hcr}}{A_8} + \frac{V_{mix} - V_{m_8hcr}}{A_7} = 1.205 \times 10^3 \cdot \text{ft} \quad \text{Height of mixture}$$

$$P_{m_hcr} := \rho_r \cdot g \cdot h_{m_hcr} = 799.783 \text{ psi} \quad \text{Head pressure of mixture}$$

$$h_{14_hcr} := \frac{V_{14_tot} - V_6}{A_7} + L_6 = 762.128 \cdot \text{ft} \quad \text{Height of mud}$$

$$P_{14_hcr} := \rho_{14} \cdot g \cdot h_{14_hcr} = 561.005 \text{ psi} \quad \text{Head pressure of mud}$$

$$P_{hca_hcr} := \rho_{flux} \cdot g \cdot (L_4 + L_5) = 843.309 \text{ psi} \quad \text{Head pressure of hydrocarbons in DP annulus}$$

$$P_{sp_hcr} := P_{w_hcr} + P_{m_hcr} + P_{14_hcr} + P_{hca_hcr} - P_{14_dp} - P_{w_bdp} = -447.951 \text{ psi} \quad \text{Calculated SPP}$$

$$P_{k_hcr} := P_{w_hcr} + P_{m_hcr} + P_{14_hcr} - P_{k_s} = 496.039 \text{ psi} \quad \text{Calculated kill line pressure}$$

$$P_{bh_hcr} := P_{hc_bdp} + P_{hca_hcr} + P_{14_hcr} + P_{m_hcr} + P_{w_hcr} = 6.057 \times 10^3 \text{ psi} \quad \text{Bottom hole pressure}$$

$$\rho_{eq_hcr} := \frac{P_{bh_hcr}}{g \cdot (L_{dp} + L_{csg})} = 6.437 \cdot \frac{\text{lbm}}{\text{gal}} \quad \text{Equivalent ppg at bottom hole}$$

Kill Line Gradient Calculations

$$\Delta P_k := P_{k_ssp} - P_{k_pk} = 107 \text{ psi}$$

$$\Delta V_{\text{flux}} := V_4 + V_5 = 153.43 \cdot \text{bbl}$$

$$\rho_{\text{kg_pk}} := \frac{\rho_{16} \cdot g \cdot \frac{\Delta V_{\text{flux}}}{A_8} - \Delta P_k}{g \cdot \frac{\Delta V_{\text{flux}}}{A_7}} = 12.116 \cdot \frac{\text{lbm}}{\text{gal}}$$

Drop in kill line pressure measured from 21:30 to 21:34

Gain from well during this period

Equivalent density of fluid entering riser, assuming spacer is displaced out the top

$$\Delta P_{k2} := P_{k_pk} - P_{k_tn} = 79 \text{ psi}$$

$$\Delta V_{f2} := 160 \text{ bbl}$$

$$\rho_{\text{kg_tn}} := \frac{\rho_{16} \cdot g \cdot \frac{\Delta V_{f2}}{A_8} - \Delta P_{k2}}{g \cdot \frac{\Delta V_{f2}}{A_7}} = 13.444 \cdot \frac{\text{lbm}}{\text{gal}}$$

Drop in kill line pressure measured from 21:34 to 21:39

Gain from well during this period

Equivalent density of fluid entering riser, assuming spacer is displaced out the top

Macondo Terminal Velocity Calculations

D. Kluk
6/22/10

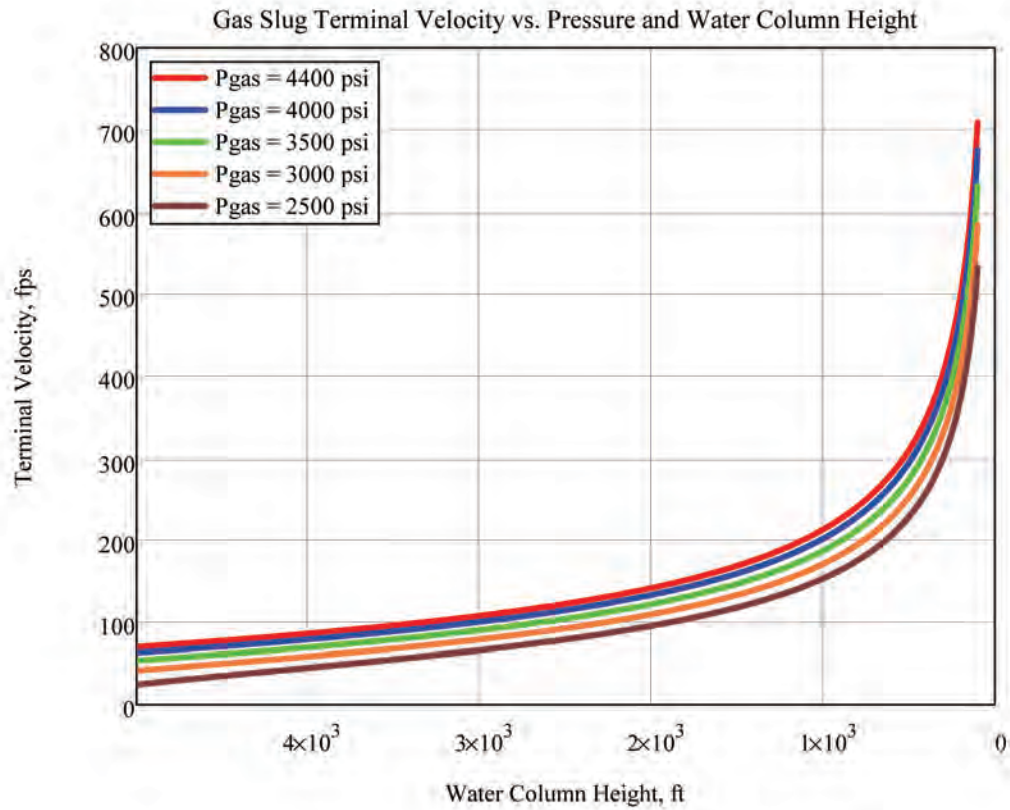
Equations from *Fluid Mechanics*, White, 4th Ed., 1999

Inputs

$V := 1 \frac{\text{ft}}{\text{sec}}, 2 \frac{\text{ft}}{\text{sec}} \dots 300 \frac{\text{ft}}{\text{sec}}$	Range variable, flow velocity	$h := 100\text{ft}, 110\text{ft} \dots 5000\text{ft}$	Range variable, riser water column height
$\rho := 64 \frac{\text{lbm}}{\text{ft}^3}$	Density of seawater	$\nu := 1.1124 \cdot 10^{-5} \frac{\text{ft}^2}{\text{sec}}$	Kinematic viscosity, seawater
$D_h := 12.375\text{in}$	Hydraulic diameter (Annulus, 19" OD, 6.625" ID)	$A := 249\text{in}^2$	Annulus area
$\epsilon := 0.00015\text{ft}$	Pipe surface roughness	$P_{\text{gas}} := 4400\text{psi}$	Gas pressure (assume constant)
$\text{bbl} := 42\text{gal}$	Barrel definition		

Outputs

$\text{Re}(V) := \frac{V \cdot D_h}{\nu}$	Compute Reynolds number as a function of velocity
$f(V) := \frac{1}{\left[-1.8 \cdot \log \left[\frac{6.9}{\text{Re}(V)} + \left(\frac{\epsilon}{D_h} \right)^{1.11} \right] \right]^2}$	Compute friction coefficient as a function of velocity
$P_{\text{eq}}(V, h, P_{\text{gas}}) := f(V) \cdot \frac{h}{D_h} \cdot \frac{\rho}{2} \cdot V^2 + \rho \cdot g \cdot h - P_{\text{gas}}$	Set up pressure balance between frictional pressure and head pressure against gas pressure
$\text{vel} := 80 \frac{\text{ft}}{\text{sec}}$	Guess value for root solver
$v_{4400}(h) := \text{root}(P_{\text{eq}}(\text{vel}, h, 4400\text{psi}), \text{vel})$	Solve for the root of the pressure balance equation for various pressures; plot below
$v_{4000}(h) := \text{root}(P_{\text{eq}}(\text{vel}, h, 4000\text{psi}), \text{vel})$	
$v_{3500}(h) := \text{root}(P_{\text{eq}}(\text{vel}, h, 3500\text{psi}), \text{vel})$	
$v_{3000}(h) := \text{root}(P_{\text{eq}}(\text{vel}, h, 3000\text{psi}), \text{vel})$	
$v_{2500}(h) := \text{root}(P_{\text{eq}}(\text{vel}, h, 2500\text{psi}), \text{vel})$	



$$t_{4400} := \int_{0\text{ft}}^{5000\text{ft}} \frac{1}{v_{4400}(x)} dx = 40.298 \cdot \text{sec}$$

Integrate velocity function to find time to reach top of riser for high and low pressure cases

$$t_{2500} := \int_{0\text{ft}}^{5000\text{ft}} \frac{1}{v_{2500}(x)} dx = 72.617 \cdot \text{sec}$$

Macondo Well Flow Line Overflow Calculations

D. Kluk
10/19/10

Loss equations and K values from *Fluid Mechanics*, White, 4th Ed., 1999. Geometric data from e-mail "FW: ID of the 350 mm (14 inch) Diverter Lines", R. Smith, 10/19/10.

Inputs

$\rho_w := 8.556 \frac{\text{lbm}}{\text{gal}}$	Seawater density	$\nu_w := 0.01044 \text{ stokes}$	Seawater kinematic viscosity
$\rho_{14} := 14.17 \frac{\text{lbm}}{\text{gal}}$	14 ppg mud density	$\nu_{14} := 0.167 \text{ stokes}$	14ppg mud kinematic viscosity
$\rho_{16} := 16 \frac{\text{lbm}}{\text{gal}}$	16 ppg mud density	$\nu_{16} := 1.69 \text{ stokes}$	16ppg mud kinematic viscosity
$ID_1 := 17.25 \text{ in}$	ID of 450 mm flow line	$K_{gv} := 0.05$	K value for 14" gate valve
$ID_2 := 13 \text{ in}$	ID of 350 mm gumbo divert	$K_{45} := 0.15$	K value for 45° elbow (18")
$L_{1a} := 2297 \text{ mm}$	First flowline section length	$K_{90} := 0.12$	K value for 90° elbow (14")
$L_{1b} := 2268 \text{ mm}$	Second flowline section length	$\epsilon := 0.001 \text{ ft}$	Pipe surface roughness
$L_{1e} := 27 \text{ in}$	Flowline elbow length	$\text{grade} := \frac{1}{60}$	Slope of flow lines
$L_{2l} := 1205 \text{ mm}$	Total plan length of all divert lines	$\text{drop}_2 := 1270 \text{ mm}$	Elevation change in divert lines
$L_{2w} := 3050 \text{ mm}$	Total plan width of all divert lines	$N_{2e} := 6$	Number of elbows in divert line
$\text{bbl} := 42 \text{ gal}$	Barrel definition	$Q := 100 \frac{\text{bbl}}{\text{min}}, 105 \frac{\text{bbl}}{\text{min}} \dots 250 \frac{\text{bbl}}{\text{min}}$	Flow variable

Outputs*Geometry and K factors*

$$A_1 := \frac{\pi}{4} \cdot ID_1^2 = 233.705 \text{ in}^2$$

Cross sectional area of 18" flow line

$$A_2 := \frac{\pi}{4} \cdot ID_2^2 = 132.732 \text{ in}^2$$

Cross sectional area of 14" divert line

$$L_1 := L_{1a} + L_{1b} + L_{1e} = 17.227 \cdot \text{ft}$$

Total length of flow line

$$L_2 := 2 \cdot L_{2l} + L_{2w} + \text{drop}_2 = 22.08 \cdot \text{ft}$$

Total length of divert line

$$\text{drop}_1 := L_1 \cdot \text{grade} = 3.445 \text{ in}$$

Drop from diverter outlet to gumbo box inlet

$$\text{drop} := \text{drop}_1 + \text{drop}_2 = 53.445 \text{ in}$$

Total drop from diverter outlet to gumbo box outlet

$$K_2 := N_{2e} \cdot K_{90} + K_{gv} = 0.77$$

Total K factor for divert line

Hydrostatics

$$\text{head}_w := \rho_w \cdot g \cdot \text{drop} = 1.98 \text{ psi}$$

Water head

$$\text{head}_{14} := \rho_{14} \cdot g \cdot \text{drop} = 3.278 \text{ psi}$$

14 ppg mud head

$$\text{head}_{16} := \rho_{16} \cdot g \cdot \text{drop} = 3.702 \text{ psi}$$

Spacer head

Reynolds number, friction, and frictional pressure functions

$$\text{Re}(Q, A, d, \nu) := \frac{Q \cdot d}{A \cdot \nu}$$

$$f(\text{Re}, \varepsilon, d) := \frac{1}{\left[-1.8 \log \left[\frac{6.9}{\text{Re}} + \left(\frac{\varepsilon}{d} \right)^{1.11} \right] \right]^2}$$

$$P_f(f, L, d, K_1, \rho, A, Q) := \frac{\rho \cdot Q^2}{2 \cdot A^2} \cdot \left(\frac{f \cdot L}{d} + K_1 \right)$$

Friction factors for given flow

$$f_{1_w}(Q) := f(\text{Re}(Q, A_1, ID_1, \nu_w), \varepsilon, ID_1)$$

Friction factor for water through flow line

$$f_{1_14}(Q) := f(\text{Re}(Q, A_1, ID_1, \nu_{14}), \varepsilon, ID_1)$$

Friction factor for 14 ppg mud through flow line

$$f_{1_16}(Q) := f(\text{Re}(Q, A_1, ID_1, \nu_{16}), \varepsilon, ID_1)$$

Friction factor for 16 ppg spacer through flow line

$$f_{2_w}(Q) := f(\text{Re}(Q, A_2, ID_2, \nu_w), \varepsilon, ID_2)$$

Friction factor for water through divert line

$$f_{2_14}(Q) := f(\text{Re}(Q, A_2, ID_2, \nu_{14}), \varepsilon, ID_2)$$

Friction factor for 14 ppg mud through divert line

$$f_{2_16}(Q) := f(\text{Re}(Q, A_2, ID_2, \nu_{16}), \varepsilon, ID_2)$$

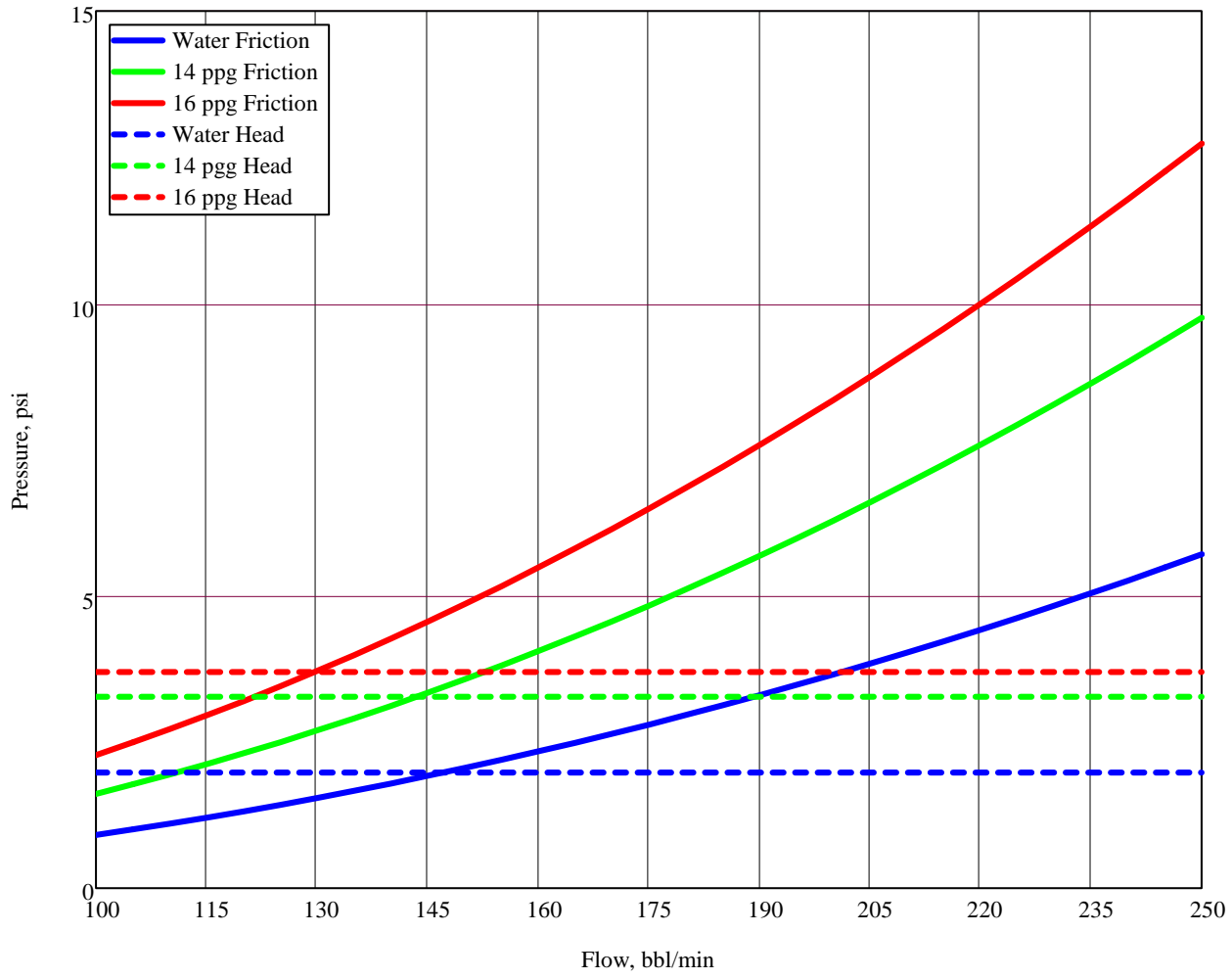
Friction factor for 16 ppg spacer through divert line

Hydrostatic and frictional pressure drops for given flow, all segments and fluids

$$P_{f_w}(Q) := P_f(f_{1_w}(Q), L_1, ID_1, K_{45}, \rho_w, A_1, Q) + P_f(f_{2_w}(Q), L_2, ID_2, K_2, \rho_w, A_2, Q)$$

$$P_{f_14}(Q) := P_f(f_{1_14}(Q), L_1, ID_1, K_{45}, \rho_{14}, A_1, Q) + P_f(f_{2_14}(Q), L_2, ID_2, K_2, \rho_{14}, A_2, Q)$$

$$P_{f_16}(Q) := P_f(f_{1_16}(Q), L_1, ID_1, K_{45}, \rho_{16}, A_1, Q) + P_f(f_{2_16}(Q), L_2, ID_2, K_2, \rho_{16}, A_2, Q)$$



Macondo Hydrocarbon Viscosity and Flow Calculations

D. Kluk
11/26/10

Viscosity and density data from Pencor Report 36126-19-5010068508, 6/30/10.

Inputs

$\text{bbl} := 42\text{gal}$	Barrel definition	$\text{OD}_5 := 5.606\text{in}$	5-1/2" DP nominal OD
$\rho_{\text{hc5}} := 0.525 \frac{\text{gm}}{\text{cm}^3}$	Hydrocarbon density @ 5000 psi	$\text{OD}_3 := 3.526\text{in}$	3-1/2" DP nominal OD
$\mu_{\text{hc5}} := 0.004\text{poise}$	Hydrocarbon viscosity @ 5000 psi	$\text{ID}_{\text{csg}} := 8.625\text{in}$	Casing ID (9-5/8" casing)
$\rho_{\text{hc2}} := 0.307 \frac{\text{gm}}{\text{cm}^3}$	Hydrocarbon density @ 2000 psi	$L_4 := 821\text{ft}$	Length of model section 4
$\mu_{\text{hc2}} := 0.007\text{poise}$	Hydrocarbon viscosity @ 2000 psi	$L_5 := 2492\text{ft}$	Length of model section 5
$\varepsilon := 0.0016\text{ft}$	Assumed pipe roughness	$\text{vol} := (1808 + 202)\text{bbl}$	Annulus volume from bottom of DP to top of riser
$Q := 10 \frac{\text{bbl}}{\text{min}}, 20 \frac{\text{bbl}}{\text{min}} \dots 300 \frac{\text{bbl}}{\text{min}}$	Flow variable	$t := 0\text{min}, 0.5\text{min} \dots 7.5\text{min}$	Time for HC to flow from bottom of DP to top of riser
$Q_{\text{init}} := 40 \frac{\text{bbl}}{\text{min}}$	Estimated initial flow rate when HC reaches bottom of DP		

Outputs

$$D_{h_4} := ID_{csg} - OD_3 = 5.099 \text{ in}$$

Hydraulic diameter of section 4 annulus

$$A_4 := \frac{\pi}{4} \cdot (ID_{csg}^2 - OD_3^2) = 48.662 \text{ in}^2$$

Cross sectional area of section 4 annulus

$$D_{h_5} := ID_{csg} - OD_5 = 3.019 \text{ in}$$

Hydraulic diameter of section 5 annulus

$$A_5 := \frac{\pi}{4} \cdot (ID_{csg}^2 - OD_5^2) = 33.743 \text{ in}^2$$

Cross sectional area of section 5 annulus

$$\nu_{hc5} := \frac{\mu_{hc5}}{\rho_{hc5}} = 7.619 \times 10^{-3} \text{ stokes}$$

Kinematic viscosity of hydrocarbon @ 5000 psi

$$\nu_{hc2} := \frac{\mu_{hc2}}{\rho_{hc2}} = 0.023 \text{ stokes}$$

Kinematic viscosity of hydrocarbon @ 2000 psi

$$\text{Re}(Q, A, d, \nu) := \frac{Q \cdot d}{A \cdot \nu}$$

Reynolds number function

$$f(\text{Re}, \epsilon, d) := \frac{1}{\left[-1.8 \log \left[\frac{6.9}{\text{Re}} + \left(\frac{\epsilon}{3.7} \right)^{1.11} \right] \right]^2}$$

Friction factor function

$$P_f(f, L, d, \rho, A, Q) := \frac{f \cdot L \cdot \rho \cdot Q^2}{2 \cdot d \cdot A^2}$$

Frictional pressure drop function

$$f_4(Q) := f(\text{Re}(Q, A_4, D_{h_4}, \nu_{hc5}), \epsilon, D_{h_4})$$

Friction factor through 3.5" DP x 9-7/8 casing

$$f_5(Q) := f\left(\text{Re}(Q, A_5, D_{h_5}, \nu_{hc5}), \frac{\epsilon}{10}, D_{h_5}\right)$$

Friction factor through 5.5" DP x 9-7/8 casing

$$P_{f4}(Q) := P_f(f_4(Q), L_4, D_{h_4}, \rho_{hc5}, A_4, Q)$$

Pressure drop across 3.5" DP x 9-7/8 casing

$$P_{f5}(Q) := P_f(f_5(Q), L_5, D_{h_5}, \rho_{hc5}, A_5, Q)$$

Pressure drop across 5.5" DP x 9-7/8 casing

$$\Delta P(Q) := P_{f4}(Q) + P_{f5}(Q)$$

Total frictional pressure drop, 5000 psi

$$f_{4_2}(Q) := f(\text{Re}(Q, A_4, D_{h_4}, \nu_{hc2}), \epsilon, D_{h_4})$$

Friction factor through 3.5" DP x 9-7/8 casing

$$f_{5_2}(Q) := f\left(\text{Re}(Q, A_5, D_{h_5}, \nu_{hc2}), \frac{\epsilon}{10}, D_{h_5}\right)$$

Friction factor through 5.5" DP x 9-7/8 casing

$$P_{f4_2}(Q) := P_f(f_{4_2}(Q), L_4, D_{h_4}, \rho_{hc2}, A_4, Q)$$

Pressure drop across 3.5" DP x 9-7/8 casing

$$P_{f5_2}(Q) := P_f(f_{5_2}(Q), L_5, D_{h_5}, \rho_{hc2}, A_5, Q)$$

Pressure drop across 5.5" DP x 9-7/8 casing

$$\Delta P_2(Q) := P_{f4_2}(Q) + P_{f5_2}(Q)$$

Total frictional pressure drop, 2000 psi

$$A_v := \frac{\text{vol} - Q_{\text{init}} \cdot 7.5 \text{min}}{e^{7.5 \cdot \text{min}}} = 0.945774 \cdot \frac{\text{bbl}}{\text{min}}$$

Coefficient for exponential flow function

$$Q_{hc}(t) := A_v \cdot e^{\frac{t}{\text{min}}} + Q_{\text{init}}$$

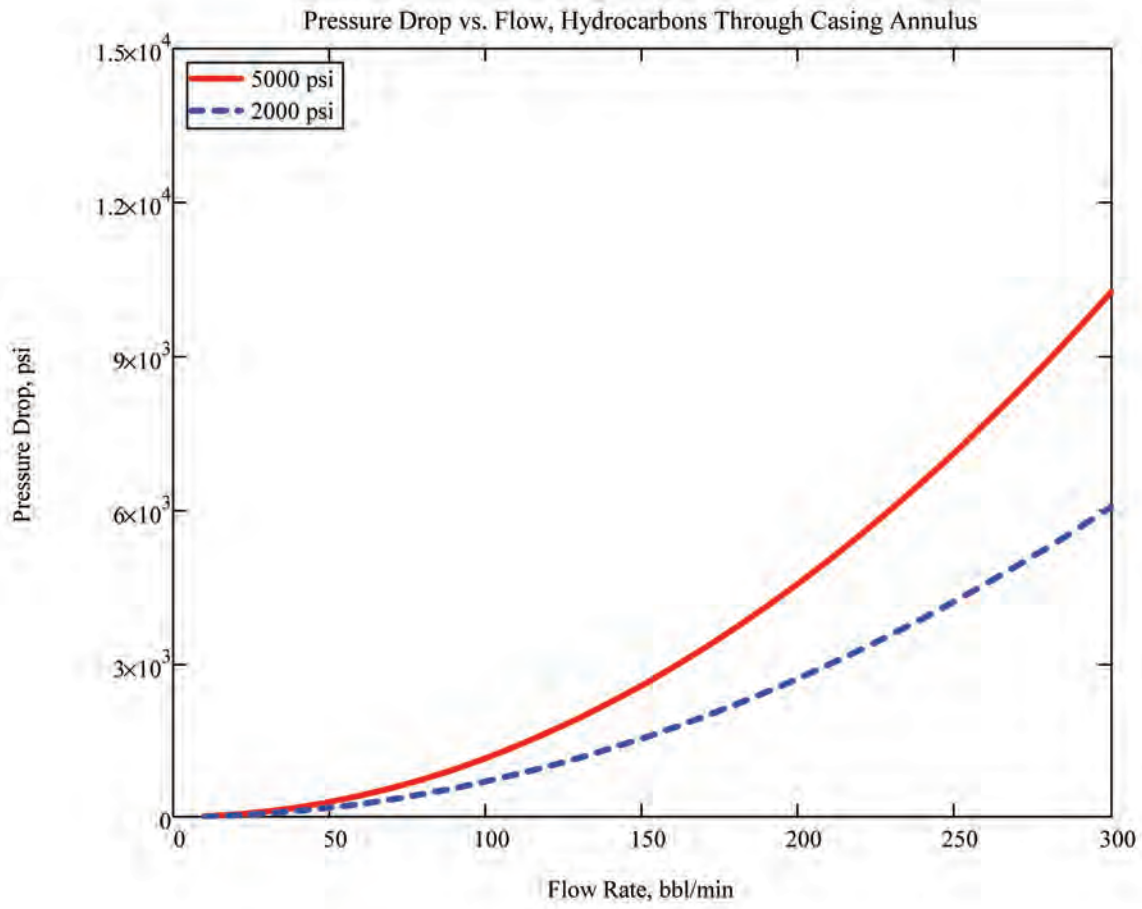
Flow function (assume exponential curve) starting at 21:39

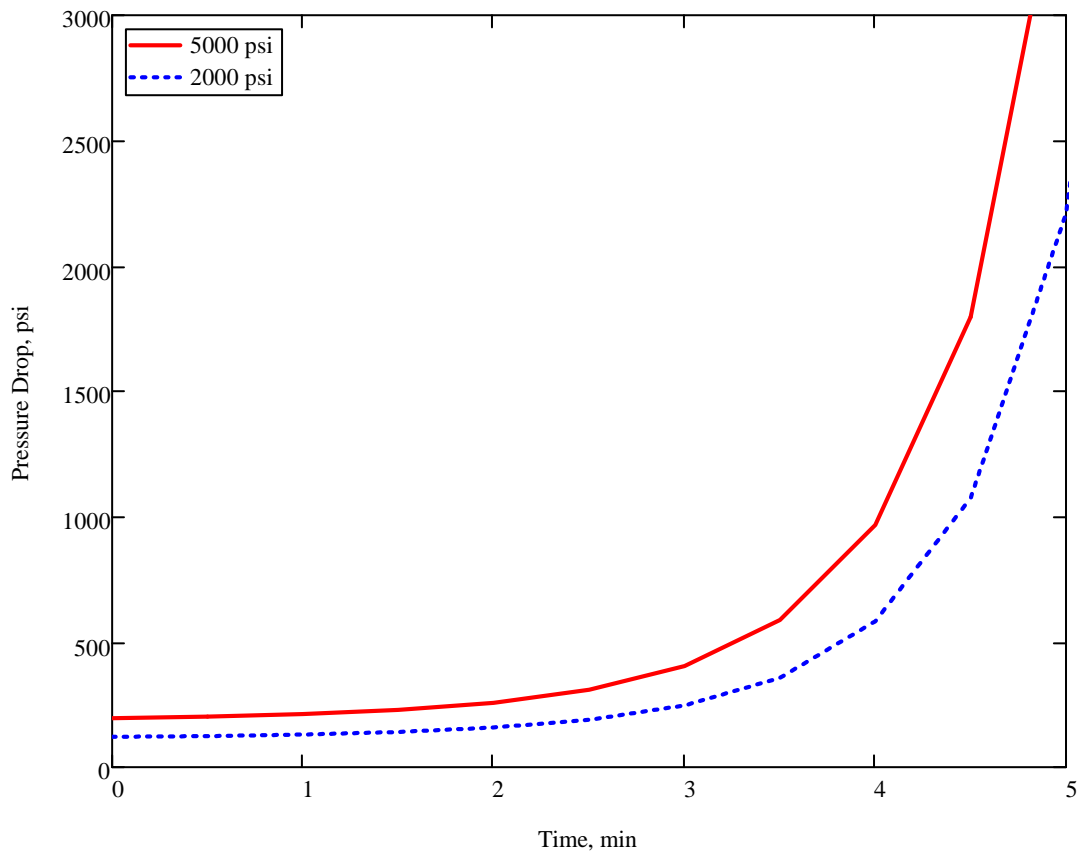
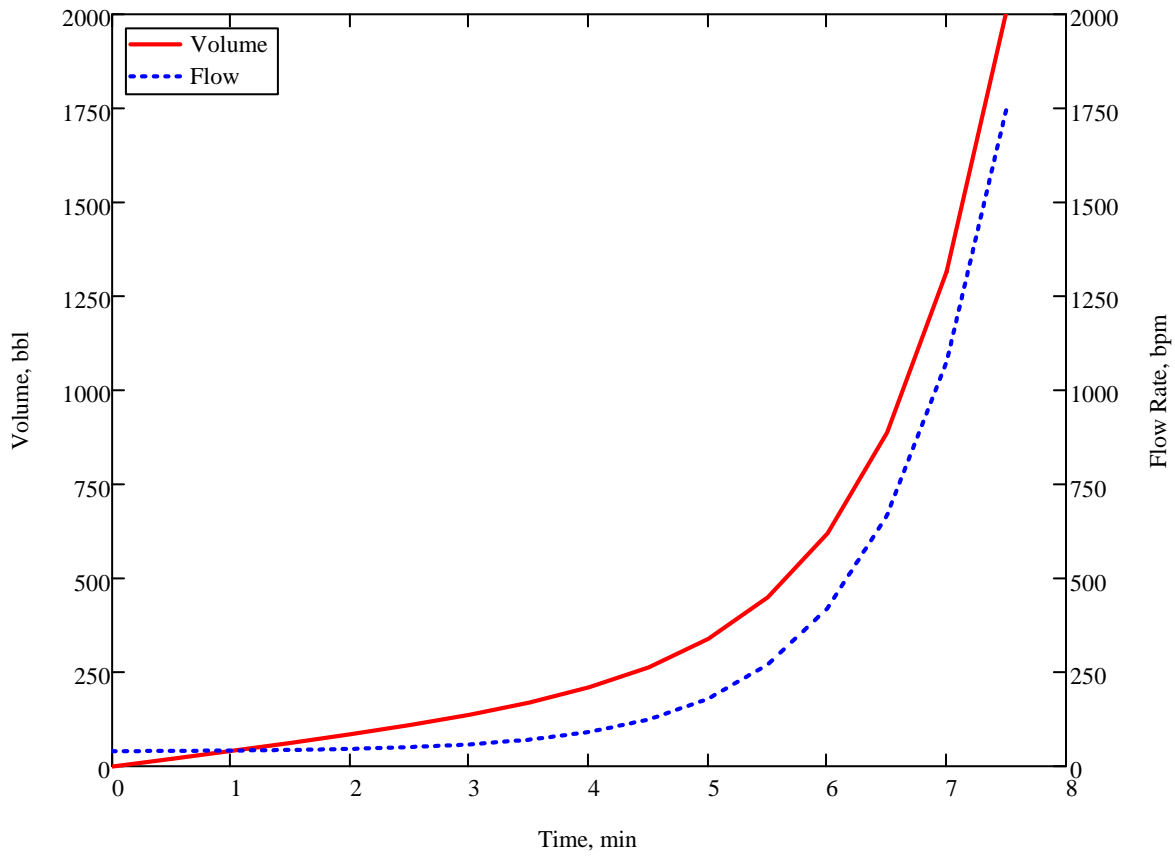
$$\text{vol}_f(t) := \int_{0 \text{min}}^t Q_{hc}(t) dt$$

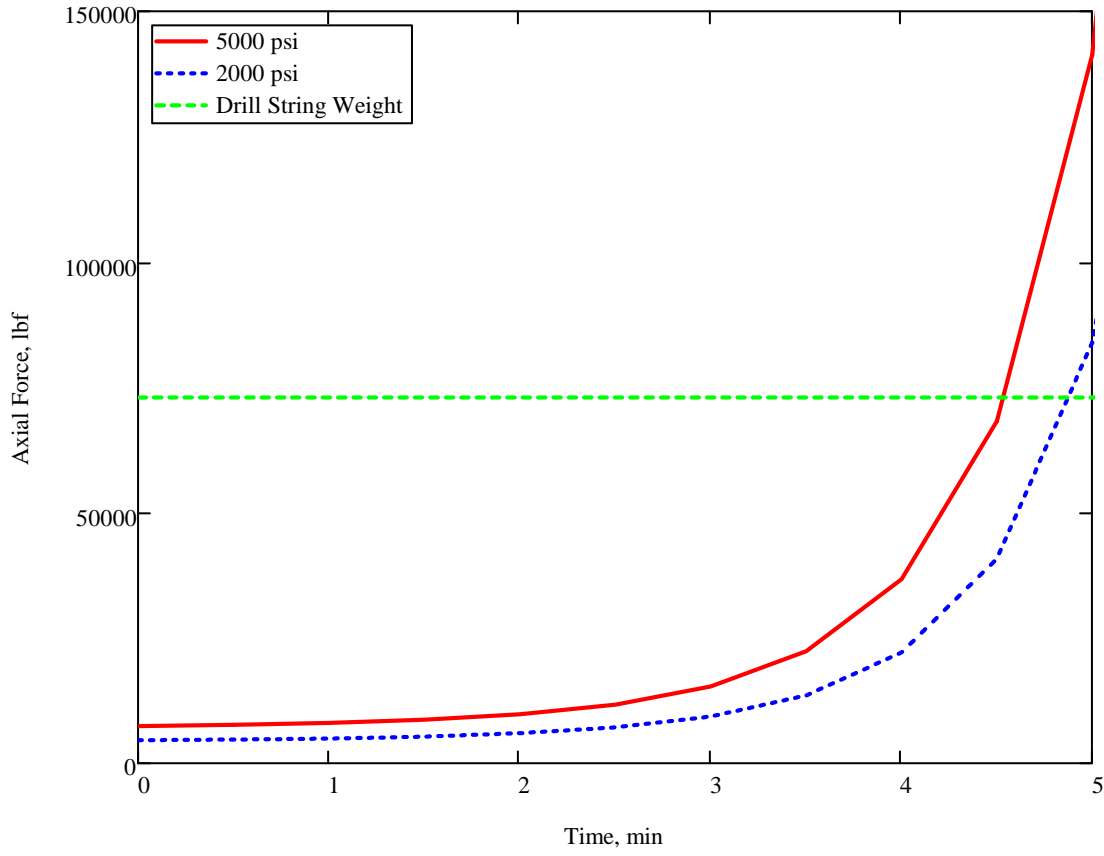
Integrate flow function to obtain volume

$$\text{vol}_f(7.5 \text{min}) = 2.009 \times 10^3 \cdot \text{bbl}$$

Check gain at 7.5 minutes (21:46:30)







Appendix D: MI-Swaco Rheliant Displacement Procedure



BP / Deepwater Horizon
Rheliant Displacement Procedure
"Macondo" OCS-G 32306

1. Before displacing to seawater, conduct a THINK DRILL with all.
2. *Remember it's very important that we must avoid trapping SBM in pits, pumps, lines and hole. We will displace SBM from all four mud pumps, both stand pipes, choke, kill, boost lines, casing and riser.*
3. Pump excess volume to Bankston, and have boat on starboard with mud hose on her.
4. Line up on sea chest.
5. Build 425 bbl **WBM spacer** in pit # 5, and use Duo Vis to thicken up.
6. Capacities:
Choke 100 bbls/794 strokes; Kill 100 bbls/794 strokes;
Boost 73 bbls/579 strokes; Drill pipe 196 bbls/1555 strokes;
Casing/Riser w/drill pipe annular 1817 bbls/14,420 stks.
Total displaced volume for hole and drill string, 2012 bbls/15,968 strokes
Pump Output 0.126 bbls/stk.

Displacement

1. Line up for all SBM returns to go to the pits and bypass sandtraps. Function test dump valve. As we displace, pump SBM to Bankston.
2. Displace choke, kill, and boost lines, and close lower valves after each. Zero stroke counter. (Note: when displacing choke line, over displace 8 bbls (63 strokes) for surface lines).
3. Pump 425 bbl **WBM spacer** from **pit # 5** down drill pipe followed by seawater.
4. Pump 775 bbls or 6150 stks. Spacer should be above the upper annular.
5. Close annular and conduct negative test. After successful negative test, open bag.
6. Continue displacement up the riser until spacer is 500ft past BOP stack (950 bbls 7540 strokes). We can boost riser.
7. Do not shut down until displacement is complete.
8. When WBM spacer returns at 15,968 stks, over-displace until interface is incorporated. When interface is incorporated, Compliance Engineer will take sample for Static Sheen test and ROC and shut down pumps. Switch to overboard discharge.
9. If static sheen is an apparent pass, discharge remaining spacer and seawater down overboard line. Mud Engineer will advise.

NOTE: Good communication will be necessary to accomplish a successful displacement. If you are not sure, stop and ask.

Appendix E: Comparison of Input Data Sets

As discussed in Section 1.3, it became apparent during the SES review that the comprehensive set of pit volume [12] and rig telemetry data [14] were processed using a digital filter of some type. This assertion was confirmed when supplementary data sets [13] and [17] containing selected signals with less aggressive (or no) filtering became available later in the investigation.

When plotted against one another, the filtered and unfiltered signals are in good agreement when their behavior changes very slowly in time, but stark differences are present when the signals change rapidly. Examples of this disparity are shown in Figure 68 and Figure 69.

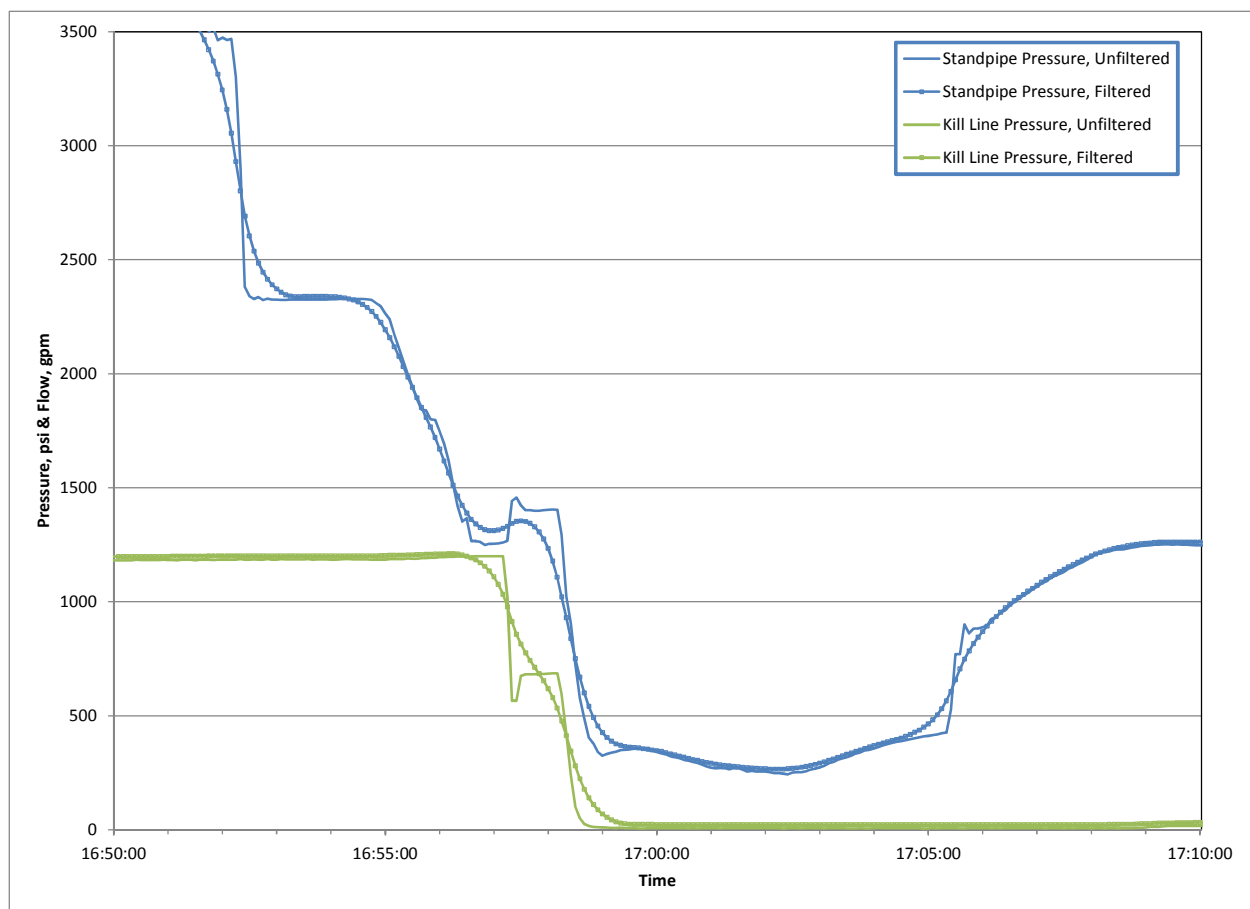


Figure 68: Comparison of filtered and unfiltered data sets, example 1

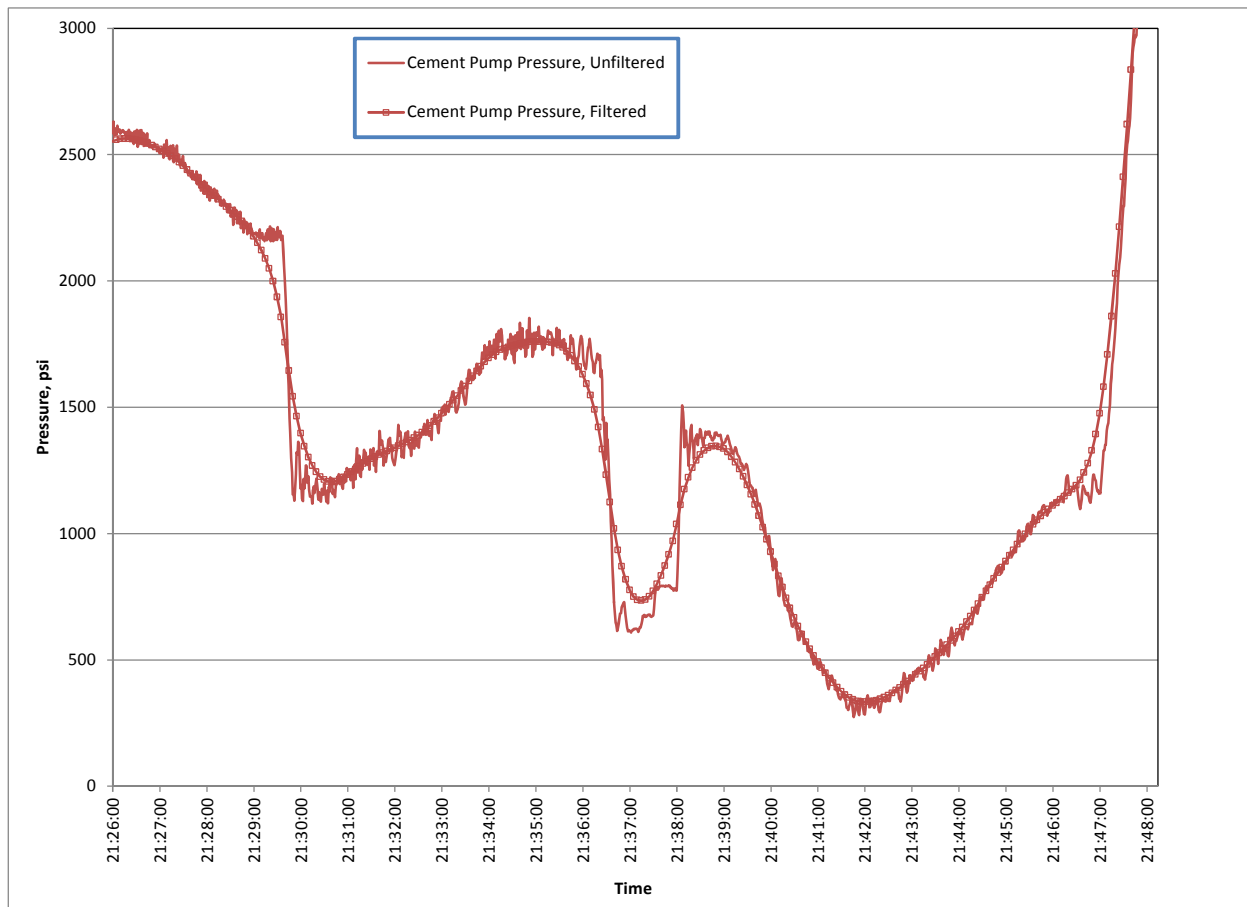


Figure 69: Comparison of filtered and unfiltered data sets, example 2

It is apparent that calculations and analysis results derived from the filtered data are prone to significant errors when rapidly changing events are examined. For example, an accurate calculation of the hydrostatic well state at 16:57 – 16:58 (see Figure 68 and discussion in Event 3, Section 4.3.2) is not possible using the filtered data, given the distortions present in the signals during this interval.

Unfortunately, because the supplementary data sets contain only selected telemetry signals, it was necessary to rely on the original filtered data for many of the discussions and analyses presented herein. Many plots and figures contain data from both sets. The data set employed herein for each signal is summarized in Table 54, below.

Table 54: Characteristics of reported telemetry signals

Signal	Reference	Sampling Interval	Apparent Filtering?
Hook Load	[17]	5 seconds	No
Standpipe Pressure (SPP2)	[17]	5 seconds	No
Kill Line Pressure (SPP1)	[17]	5 seconds	No
Cement Pump Pressure	[13]	1 second	No
Pump Strokes & Flow	[14]	5 seconds	Yes
Return Flow (Flow Sensor)	[14]	5 seconds	Yes
Pit Volumes (all)	[12]	10 seconds	Yes

Appendix H BOP Modifications

APPENDIX H BOP Modifications

The investigation team reviewed the 20 modifications or improvements made to the *Deepwater Horizon* blowout preventer (BOP) stack and control system that occurred from the time the rig was commissioned in 2001 until the date of the incident. For nine of these, Transocean Management of Change (MOC) documentation was located, including two of the nine MOC modifications or improvements that were requested by BP. The supporting formal documentation for the other 11 modifications was lost with the rig. In general, the modifications were to improve BOP operation and reliability while maintaining the same functionality; in some cases, functionality was improved. It was found that none of these modifications adversely impaired the operation of the BOP stack at the time of the incident.

The modifications are listed in chronological order.

1. Replace subsea pod flow meters with improved flow meters—MOC SS-004

Performed by Cameron (Completed Jan. 1, 2003)

The Ultrasonic flow meters for the BOP stack's hydraulic system control fluid fitted on each of the subsea pods were replaced with three high-shock, vane-type flow meters.¹ These flow meters measure the flow (in gallons) of control fluid and verify proper functioning. The ultrasonic flow meter types use sound wave propagation to determine the flow, whereas vane-type flow meters use rotation of an internal vane.

Conclusion: This modification installed more reliable and more accurate high-shock, vane-type flow meters.

2. Change retrievable pod to a non-retrievable pod—MOC SS-005

Performed by Cameron (Completed Jan. 1, 2003)

This change required a modification of the control system software, and removal of hoses and piping connections, as well as oil-filled control cables. Although retrievable pods can be removed more readily for repairs, they require additional hydraulic hose and piping connections and can create additional leak points. Retrievable pods also create unnecessary failure points within the electrical system, as there are many additional pressure cables installed from the pods to the riser control box and the riser mounted junction box.²

Conclusion: This modification simplified and improved the reliability of the subsea pods by eliminating hose connections, piping and cables, and reducing the number of possible failure points.

3. Remove lower marine riser package (LMRP) failsafe panels, convert failsafe valves to more reliable spring-loaded operation —MOC MD-0029A

Performed by the Deepwater Horizon crew (Approved on Aug. 3, 2004; work was completed with the removal of the LMRP failsafe panels on June 10, 2005)

The LMRP failsafe panels control the gate valves connected to the annular BOP on the LMRP and include all associated accumulators, hoses and piping. The failsafe assist circuit supplies closing pressure to assist the spring closure of the valves in the event no close pressure is available from the pods. By removing the LMRP failsafe panels, the modification removed hoses, piping and the additional accumulators, reducing the number of possible leak failure points. This modification also was conducted on the BOP failsafe panel in February 2005.

Conclusion: This modification simplified the valve operating system and improved reliability by removing connection points in the system.³

4. Install new rigid conduit manifold and remove riser-mounted junction box in two phases—MOC MD-0029B

Performed by Cameron and the Deepwater Horizon crew (Approved Aug. 6, 2004; work completed in October 2004)

Transocean installed a new, modified rigid conduit manifold and removed unnecessary equipment and circuits.⁴ The original package used pilot-operated check valves that must have pilot pressure to open for the accumulator supply to pass through to BOP functions, while the new package used a pod valve that springs to the block position if pod supply is lost.

Conclusion: The new rigid conduit manifold system used components with higher reliability and simplified the system while accomplishing the same functions as the original design.

5. Install Cameron control software modification—MOC MD-054

Performed by Cameron (Approved Dec. 16, 2007; work completed June 10, 2009)

New central control unit software was installed to correct erroneous coil faults and function-lock problems.⁵

Conclusion: The software modification for the central control unit was designed to allow proper functioning.

6. Change G pin x H box and flex joint modification—MOC SS-021

Installed by the Deepwater Horizon subsea crew (Approved Sept. 8, 2008; installed Sept. 9, 2008)

The existing flex joint on top of the BOP stack required a complete overhaul. The rig received a spare flex joint to use in operations while their unit was being overhauled, the replacement had a riser connector with a different tensile rating. A special riser joint (crossover) was required to adapt between the spare flex joint's G-rated riser connector and the *Deepwater Horizon* H-rated riser system.⁶

Conclusion: This modification was a maintenance requirement. The rig's flex joint was sent in for a routine complete overhaul, and a spare flex joint was used in its absence. This spare flex joint had a G-rated riser connector at the top connection where the *Deepwater Horizon* flex joint was designed to connect to an H-rated riser. A crossover was employed to adapt the replacement flex joint to the rig's riser. The G-rated riser is designed to withstand 3,000,000 lb. of tension, while the H-rated riser is rated for 3,500,000 lb. For the operations and water depth at the Macondo well location, it was determined that the lower 3,000,000-lb. riser rating was more than sufficient.⁶

7. Replace auto-shear valve—MOC SS-027

Performed by the Deepwater Horizon crew (Completed Aug. 3, 2009)

The original auto-shear valve had a history of leaks. Cameron redesigned the original auto-shear valve with an improved version, and made the old valve obsolete.⁷

Conclusion: The modification solved the issue of leaks on the old-style auto-shear valve and upgraded the valve according to OEM recommendations.

8. Convert BOP lower pipe rams to inverted test rams—MOC SS-010

Performed by Cameron (Completed Dec. 13, 2004)

At the request of BP, the lower pipe rams were converted to inverted test rams.⁸ The test rams allow pressure testing on most stack components above the test rams to full working pressure without

having to run a test plug into the well.⁹

Conclusion: The conversion saved time for running and retrieving the test plug while still allowing pressure testing of all the components above the test rams, with the exception of the shear rams. The modification removed one wellbore sealing ram from the stack because the test rams can only seal pressure from the top side and not pressure coming from the wellbore. With this modification, the BOP still met industry and regulatory requirements.

9. Install annular stripper packer—MOC SS-016

Performed by the Deepwater Horizon crew (Approved July 29, 2006; stripping packer installed in the lower annular June 5, 2006¹⁰)

At BP's request, an 18-3/4-in. annular stripping element, capable of stripping 6-5/8-in. drill pipe through the closed annular, was installed in the lower annular. The pressure limit for the annular is 5,000 psi when the stripping element is installed, as opposed to the 10,000-psi rating of the standard element. The element in the upper annular remained rated to 10,000 psi.

Conclusion: The lower annular element was changed to a stripping element because the Cameron standard element (as installed in the upper annular) had more difficulty stripping 6-5/8-in. drill pipe due to the large diameter tool joint and interference with the annular element's metal insert fingers. As the BP well plan included the use of 6-5/8-in. drill pipe for the Macondo well, and required the capability to strip the pipe during well operations, BP requested that a stripping element be installed in the lower annular. The Cameron stripping element is not tested in accordance with API Specification 16A and has a maximum pressure rating of 5,000 psi.

10. ST Lock modification, replacement of overhauling nut—Cameron Product Alert 4078¹¹

Performed by the Deepwater Horizon crew (Completed Oct. 28, 2002¹²)

The overhauling nuts were replaced by the *Deepwater Horizon* crew in accordance with the Cameron product alert.

Conclusion: Per Cameron, this modification eliminated previous ST Lock issues and improved operation.

11. Replace selected SPM valves with upgraded valves¹³

Performed by the Deepwater Horizon crew (Completed November 2001)

Conclusion: This modification from standard Cameron valves to Cameron premium valves improved operation and reliability.

12. Install Gilmore high-interflow shuttle valves¹⁴

Performed by the Deepwater Horizon crew (Completed Nov. 9, 2003)

Conclusion: This modification improved operation by replacing the 1-1/2-in. shuttle valve for the casing shear rams with an improved design.

13. Install orifices in regulators to stop oscillating—OPT-ADV-435-003¹⁵

Performed by the Deepwater Horizon crew (Completed May 11, 2004)

In accordance with a Transocean operations advisory, orifices were installed in regulators. The orifices create a slight flow restriction that dampens the pilot pressure pulses and thus stops oscillation of the regulator. There was a software change required with this modification related to new conduit valve package installation.¹⁶

Conclusion: This modification improved operation and reliability.

14. Pod SEM, software upgrade by Cameron¹⁷

Performed by Cameron (Completed May 27, 2004)

Pod software upgrade.

Conclusion: This modification improved operation.

15. Add second pod select function for double redundancy¹⁸

Performed by Cameron and the Deepwater Horizon crew (Completed November 2004)

A second pod select solenoid was added to provide double redundancy to each control pod. An existing pod select switch was used.

Conclusion: This modification improved operation and reliability.

16. Remotely operated vehicle (ROV) intervention panel was modified to consolidate blind shear ram close and ST Locks as one function, and pipe ram close and ST Locks as one function

Performed by the Deepwater Horizon crew (Completed approximately 2004)

Conclusion: This modification improved the ROV intervention panel allowing the ROV to operate the blind shear rams and associated ST Locks through a single ROV stab. The pipe rams were similarly modified. The modification allowed for faster and more efficient ROV intervention when required.

17. Blanked off unused pod functions on pod¹⁹

Performed by Cameron and the Deepwater Horizon crew (Completed February 2005)

Installation of a new conduit manifold package and removal of the BOP failsafe assist panel valve circuits, as described in item No. 3 above, left some pod functions unused. The functions were removed, and the manifold was sealed with blank flanges to avoid possible failure points.

Conclusion: This modification improved operation and avoided failure points.

18. Replaced pilot regulator with a more reliable unit.²⁰

Performed by the Deepwater Horizon crew (Completed Nov. 27, 2005)

Replaced the original problematic pod pilot regulators with a more robust and reliable regulator that could handle the required pilot system functionality.

Conclusion: This modification improved operation and reliability.

19. Upgrade software to add alarm if button on control panel is stuck²¹

Performed by Cameron (Completed February 2006)

The control panel software was modified to sound an alarm at the control panels if any button stays pushed more than 15 seconds, in accordance with a Transocean advisory. If a button were stuck in the pushed position, the panel would lock up.

Conclusion: This modification improved operation.

20. Automatic mode function (AMF) modification and replacement of pie connectors²²

Performed by Cameron and the Deepwater Horizon crew (Completed January 2007)

The AMF modification kit and new pie connectors were installed on pod No. 3 by Cameron at its facility. Cameron assisted with the change out of the pie connectors and installation of the AMF modification kit on the other two pods.

Conclusion: This modification improved operation.

Engineering Bulletins, Product Advisories and Product Alerts

A total of 314 items were found by checking Cameron and Transocean files for engineering bulletins, product advisories and product alerts covering BOP stack equipment. Of the 314 items, 73 had been completed on the *Deepwater Horizon* equipment, 113 did not apply to the *Deepwater Horizon*, 127 were for information purposes only, and one was post-incident. While the status of one advisory could not be determined; it was found that this advisory did not affect the BOP operation on April 20, 2010.

- Manufacturer/Technical Bulletin CIS-01-C11 was issued in 2001 and concerned ROV pump flow rates and how they interacted with the subsea ROV interface shuttle valves. No records of the testing could be found.

The following table cites a number of documents or alerts and contains some misspelled words. These misspellings are a result of those contained in these documents.

Alert Number	Alert Status	Alert Issue Date	Work Description/Alert Description
1A-PRODUCT-ADVISORY-INDEX	Information	May 21, 2003	1A-PRODUCT-ADVISORY-INDEX
Cameron Information Sheets Index April 7Rev01	Information	April 7, 2003	Cameron Information Sheets Index April 7Rev01
CIS-01-C01	Completed	October 26, 2001	INSTALLATION OF HIGH SHOCK FLOWMETERS AND UPGRADES TO STM A & B.
CIS-01-C02	Completed	February 26, 2002	PBOF Connector/Cable Design Features
CIS-01-C03	Completed	August 28, 2002	Premium Valves for Drilling Control Systems
CIS-01-C04	Did not apply	October 26, 2001	Pilot Operated Check Valve, 1 ½" Upgrade
CIS-01-C05RevA01	Completed	May 21, 2002	Solenoid Valve (3/2Way) Valve Upgrade
CIS-01-C06	Complete	October 26, 2001	Solenoid Valve (3/2Way) Cable Upgrade
CIS-01-C07	Information	October 26, 2001	Event Logger: Features & Upgrades
CIS-01-C08	Information	October 26, 2001	Standard Shuttle Valve in Cameron Control Systems Mark III
CIS-01-C09	Information	January 15, 2002	Drilling Control System Troubleshooting Guide
CIS-01-C10	Information	October 26, 2001	Unbalanced Shuttle Valve in Cameron Control Systems

Alert Number	Alert Status	Alert Issue Date	Work Description/Alert Description
CIS-01-C11	Undetermined	October 26, 2001	Pressure Biased Shuttle Valve for ROV Functions in Cameron Control Systems
CIS-01-C12	Completed	October 26, 2001	High Drag Shuttle Valve in Cameron Control Systems Mark III Upgrade
CIS-04-001	Information	N/A	18-3/4" Annular Stripper Packer for Cameron 18-3/4" - 10,000 psi Annular BOP
CIS-04-002	Information	N/A	In-Service Condition of Cameron D/DI Annular Blowout Preventer Packing Element Subassemblies
CIS-04-003	Information	N/A	18-3/4"-5000 psi Low Temperature Annular Packing Element Subassembly for the Cameron 18-3/4"-5,000 psi D/DL Annular BOP
CIS-96-002	Completed	November 13, 2003	Proper Storage of Cameron Elastomer Products This is done on rig
EB 001 D	Did not apply	March 27, 2003	Cameron Drilling EB Index EB001D
EB 004 M	Did not apply	November 22, 2002	Cameron Marine Drilling and Production Engr. Index EB004M
EB 007 H	Did not apply	June 12, 2000	Cameron Choke Engineering Bulletins EB007h 1A Index
EB 015 W	Information	September 11, 1981	on wellhead equipment year (1981)
EB 046 D	Information	February 7, 1966	FIELD REPLACEMENT OF 'SS - BOP BONNET BOLTS (CAPSTAN SCREW) 1966
EB 050 D	Did not apply	February 7, 1966	Installation of Blind Rams in SS BOP While Pipe is in Hole eb050d
EB 079 C	Did not apply	January 10, 1966	Cameron 2 In. High Pressure Shear Relief Valves
EB 096 W	Information	February 9, 1988	on 1/4 check valves Year (1988)
EB 10717	Did not apply	October 24, 1973	Standard Test Stump
EB 10717	Information	October 24, 1973	Standard Test Stump Not approved for distribution
EB 10733	Information	February 25, 1976	H-4 Connector Cam Ring and Dogs
EB 10734	Information	March 31, 1976	H-4 AX/VX Gasket Retainer Screws
EB 119 D	Did not apply	September 29, 1977	PLASTIC PACKING. INSTRUCTIONS FOR 'F' PREVENTER GLANDS
EB 124 D	Did not apply	February 7, 1966	F' BLOWOUT PREVENTER SH@T REMOVAL TOOLS
EB 126 W	Completed	February 15, 1966	Storage and aging of rubber goods This is done on rig
EB 136 D	Did not apply	February 21, 1966	OPERATOR HOOti-UP FOR 'F' PREVENTER
EB 154 C	Did not apply	October 1, 1966	Cameron Type B Reset Relief Valve eb154c
EB 160 D	Did not apply	March 10, 1982	SKEWED FACE VERSUS FLAT FACE RAM PACKERS FOR 'U'BOPs
EB 167 C	Did not apply	July 15, 1977	Cameron Type B Reset Relief Valve eb167c
EB 191 D	Did not apply	July 25, 1966	'U' BOP SIDE OUTLET AVAILABILITY
EB 195 D	Information	January 10, 1966	USE OF RAM PACKERS IN RAMS OF DIFFERENT SIZES

Appendix H BOP Modifications

Alert Number	Alert Status	Alert Issue Date	Work Description/Alert Descrip
EB 196 D	Did not apply	January 10, 1966	Hydraulic Control System of the U BOP Preventer eb196d
EB 197 D	Did not apply	July 1, 1991	RAM Change Procedure for U BOP Preventer eb197d
EB 198 D	Did not apply	September 22, 1980	U BOP Installation eb 198d
EB 200 D	Did not apply	September 12, 1991	Servicing U BOPS For Storage and Moving eb200d
EB 201 D	Did not apply	January 10, 1966	Overhaul of U BOP Preventor eb201d
EB 202 D	Did not apply	January 10, 1966	Cold Weather Operation of the U BOP Preventer eb202d
EB 205 D	Information	January 10, 1966	on use of check valves to lock rams in position (1966)
EB 209 D Rev G2	Did not apply	September 8, 2003	Cup Tester
EB 212 C	Did not apply	November 8, 1978	Cameron Shear Relief Valve eb212c
EB 213 C	Did not apply	January 10, 1966	Cameron Type B Reset Relief Valve eb213c
EB 214 C	Did not apply	January 10, 1966	Cameron Weight Indicator Design and Engr. Data eb214c
EB 215 C	Did not apply	January 10, 1966	Cameron Weight Indicators Principal of Operations eb215c
EB 216 C	Did not apply	January 10, 1966	Cameron Weight Indicators Assembly and Calibration eb216c
EB 217 C	Did not apply	January 10, 1966	Cameron types E and F Weight Indicators Installation eb217c
EB 218 C	Did not apply	January 10, 1966	Cameron Weight Indicators Maintenance eb218c
EB 219 C	Did not apply	January 10, 1966	Cameron Special Low Range Type C Weight Indicator eb219c
EB 220 C	Did not apply	January 10, 1966	Cameron Pressure Gauges Engr.Data n Perform. Characteristics Principle of Oper.eb220c
EB 221 C	Did not apply	January 10, 1966	Cameron Pressure Gauges Field Installation and Service eb221c
EB 222 C	Did not apply	January 10, 1966	Cameron Pressure Gauges Assy, Calibration, n Service eb222c
EB 223 C	Did not apply	January 10, 1966	Cameron Pressure Gauge Required Information for Ordering eb223c
EB 224 C	Did not apply	January 10, 1966	Cameron Pressure Gauges Assembled eb224c
EB 226 C	Did not apply	May 24, 1965	Cameron Directions for Recalibration of Cameron Type C Weight Indicators eb226c
EB 229 C	Did not apply	May 25, 1965	Cameron Type B Reset Relief Valves eb229c
EB 230 C	Did not apply	May 25, 1965	Cameron Shear Relief Valves eb230c
EB 240 D	Information	July 30, 1969	THE MODEL 60 COLLET CONNECTOR
EB 241M	Information	August 13, 1986	THE PIN CONNECTOR
EB 352 H	Did not apply	February 15, 1982	Indroduction - chokes
EB 364 C	Did not apply	December 7, 1966	Cameron Piston Stem Seal For Type B Reset Relief Valves eb364c
EB 404 D	Did not apply	July 1, 1991	CAMERON MODEL III SHEAR RAMS

Alert Number	Alert Status	Alert Issue Date	Work Description/Alert Description
EB 418 H	Did not apply	November 2, 1981	Cameron Choke Engineering Bulletins EB418h Cameron Remote Manual Drilling Choke Control Sys.
EB 430 H	Did not apply	November 2, 1981	Cameron Choke Engineering Bulletins EB430h Cameron Remote Reading Pressure Gage Sys.
EB 442 M	Information	September 1, 1971	OPERATION AND MAINTENANCE OF THE CAMERON COLLET CONNECTOR, MODEL 70
EB 461 H	Did not apply	November 2, 1981	Cameron Choke Engineering Bulletins EB461h Cameron Modified Semi-Automatic Drlg Choke Control Console
EB 464 D	Did not apply	November 11, 1972	FIELD TESTING FOR ACCEPTANCE OF CAMERON 'SS' BOP
EB 465 D	Did not apply	November 11, 1972	FIELD TESTING FOR ACCEPTANCE OF CAMERON 'QRC' BOP,
EB 480 H	Did not apply	November 2, 1981	OPERATING INSTRUCTIONS FOR MODIFIED SEMI-AUTOMATIC CHOKE CONTROL CONSOLE
EB 484 H	Did not apply	November 2, 1981	Cameron Choke Engineering Bulletins EB484h Cameron Type J-2 Transmitter
EB 494 H	Did not apply	November 2, 1981	Cameron Choke Engineering Bulletins EB494h Testing Procedure fo Pneumatic Comparator 40066
EB 495 D	Information	July 5, 1991	MARINE BOP STACK WEIGHT. SET TEST' TOOLS FOR LOWER RISER PACKAGE
EB 503 D	Information	February 20, 1990	Lower Riser Package Emergency Recovery Tool (ERT)
EB 506 H	Did not apply	May 20, 1982	MODIFICATION REQUERMENTS TO REMOUNT CONTROL CONSOLE FOR 5000 PSI DRILLING CHOKES
EB 521 D	Did not apply	March 2, 1978	DESIGN AND EN.GINEERING DATA CAMERON S/QRC SNUBBING BLOWOUT PREVENTERS 4-1/16" - IOM & 75M PSI WP, 3-1/16" - 20M.PSI WP
EB 527 D	Information	June 30, 1978	STRIPPING RECOMMENDATIONS -- CAMERON D ANNULAR BOP
EB 532 D	Did not apply	September 5, 1978	DUAL STRING CENTRALIZING RAM "U type"
EB 533 D	Did not apply	September 15, 1978	DUAL STRING CENTRALIZING RAM OPERATION AND MAINTENANCE
EB 537 D	Information	October 24, 1991	Camerron Hydraulic bonnet bolt and Hydraulic Bolt Tensioner
EB 538 D	Did not apply	April 25, 1979	SHEARING BLIND RAMS -- OPERATION, CARE, AND MAINTENANCE
EB 539 D	Did not apply	June 8, 1979	Correct Installation of Lip Seals and Bearing Rings on U BOP Operating Pistons eb539d
EB 542 C	Did not apply	August 14, 1979	Cameron Type D Pressure Gauge eb542c
EB 545 D	Did not apply	October 12, 1979	11In. and 13 -5.8 In - 15M U BOP Bore Type Bonnet Seals

Appendix H BOP Modifications

Alert Number	Alert Status	Alert Issue Date	Work Description/Alert Description
EB 549 H	Did not apply	February 15, 1982	MODIFICATION RRQUIREMENT FOR AIR PURGING WATHERRPROOF PUMP STROKE COUNTER IN EXISTING CHOKE CONTROL CONSOLES
EB 550 D	Information	April 10, 1980	LOW TEMPERATURE OPERATION OF THE CAMERON D ANNULAR BOP
EB 552 D	Information	October 31, 1991	RECOMMENDATIONS FOR FIELD, TESTING OF THE CAMERON 'D' ANNULAR BLOWOUT PREVENTER
EB 555 D	Did not apply	August 19, 1982	VARIABLE BORE RAM -- ENGINEERING DATA
EB 557 H	Did not apply	July 31, 1981	Cameron Choke Engineering Bulletins EB557h Drilling Control Console
EB 561 W	Information	December 13, 1988	on cadmium plating of nuts and bolts (1988)
EB 571 D	Did not apply	August 18, 1986	LARGE BORE SHEAR BONNETS
EB 575 D	Did not apply	September 9, 1981	New Wedgelocks for Cameron U II BOP Preventers eb575d
EB 580 D	Information	March 26, 1982	OPERATION AND USE OF SHUII-LE VALVE WITH S/QRC SNUBBING BLOWOUT PREVENTERS
EB 586 D	Did not apply	November 10, 1982	Marine BOP Stack Weight Set Test Tools for Lower Riser Pkg.Sedco709 eb586m
EB 587 D	Did not apply	November 10, 1982	Marine BOP Stack Weight Set Tet Tools for Lower Riser Pkg.Sedco710 eb587m
EB 598 H	Did not apply	December 5, 1996	Cameron Choke Engineering Bulletins EB598h The Cameron Drilling Choke
EB 599 C	Did not apply	February 29, 1984	CANERON I-1/2" POD VALVE WITH QUICK DUMP 309538-01, -02 CAMERON I/ 4" DUMP VALVE 309542-01
EB 601 D	Information	June 15, 1991	CANERON COLLET CONNECTOR - SELF-LOCKING DESIGN
EB 603 D	Information	July 26, 1984	SAFE OPERATION OF THE CAMERON HYDRAULIC BONNET BOLT TENSIONER
EB 604 C	Did not apply	August 15, 1984	Cameron Instructions for Installation Hdlg and Care of Burton Underwater Connectors and Cables eb604c
EB 608 W	Information	October 19, 1984	installation of BOP Plug Type Tester in "FMTB" Bowl Preparation (1984)
EB 612 D	Did not apply	June 21, 1985	Type A Lip Seals Update for D and DL Annular BOP Preventers eb612d
EB 617 H	Did not apply	April 9, 1985	Cameron Choke Engineering Bulletins EB617h Cameron Constant Standpipe Pressure Console
EB 628 H	Did not apply	November 14, 1985	Cameron Choke Engineering Bulletins EB628h Positive Seal Test of Cameron Drilling Choke
EB 633 C	Did not apply	February 7, 1986	Cameron Emergency Acoustic BOP Control System Operating Characteristics eb633c
EB 637 D	Information	May 5, 1989	ST-LOCK SEQUENCING VALVE FOR T BOP

Alert Number	Alert Status	Alert Issue Date	Work Description/Alert Description
EB 641 D	Information	July 18, 1986	STRIPPING (SNUBBING) PROCEDURE THROUGH CAMERON RAM-TYPE BLOWOUT PREVENTERS
EB 648 D	Information	October 18, 2001	H2S SHEARING BLIND RAMS
EB 649 C	Information	May 14, 1990	System Flushing Procedures (1990)
EB 650 C	Information	June 19, 1990	RECOMMENDED PR4CTICES FOR INSTALLATION AND OPERATION OF BOP AND WORKOVER CONTROL HOSE BUNDLES
EB 667 W	Did not apply	October 25, 1988	RECOMMEND OPERATING PROCEDURES FOR THE CASTLE NUT TIEDOWN SCREW
EB 670 D	Information	August 25, 1988	Periodic Inspection of Unified inch Screw Threads
EB 679 D	Information	July 16, 1990	Does not Apply (1990)
EB 686 C	Information	May 17, 1990	SEQUENCING OF FAILSAFE GATE VALVES ON SUBSEA BLOWOUT PREVENTER STACKS
EB 687 C	Completed	July 23, 1999	CONTINUOUS LATCH PRESSURE CONTROL MODEL WC* COLLET CONNECTORS
EB 691 D	Information	September 13, 1990	SHEARING LIMITATIONS DUE TO INCREASED PIPE STRENGTH
EB 699 D	Information	February 8, 1992	"D" SEAL -- "D" SHAPED SEAL USED AS AN OPTIONAL REPLACEMENT FOR THE STANDARD LIP SEAL IN ANNULAR BOPs
EB 700 D	Did not apply	September 14, 1999	CAMERON DS SHEARING BLIND RAMS – OPERATION, CARE, AND MAINTENANCE
EB 701 D	Information	July 1, 1991	Recommended Torque for Grade B-7 Cap Screws (1991)
EB 702 D	Information	June 21, 2007	Shearing Capabilities of Cameron Shear Rams (2007)
EB 707 C	Information	December 9, 1991	FAIL CLOSE AND FAIL OPEN CONTROLS FOR GATE VALVES
EB 715 H	Did not apply	September 17, 1992	Cameron Choke Engineering Bulletins eb715h Cameron Type J-2 and J-2 Transmitters
EB 722 C	Information	September 15, 1989	BOP Fluid (1989)
EB 725 C	Information	February 15, 1993	PILOT LINE QUICK-DISCONNECT COUPLINGS FOR DRILLING EQUIPMENT
EB 729 C	Information	March 22, 1993	INSPECTION AND SERVICING MODULAR BOP CONTROL POD STINGERS AND RECEPTACLES
EB 747 W	Information	August 19, 1993	INSTALLATION AND RETRIEVAL PROCEDURE FOR NcEVOY 6" TYPE 'D' VALVE ARRROVAL PLUG
EB 767 W	Information	October 15, 1993	Modafied tubing head adaptors
EB 783 D	Information	November 29, 1993	LOW TEMPERATURE TESTING OF VARIABLE BORE RAMS (VBRs)
EB 798 D	Information	July 21, 1994	GENERAL INFORMATION FOR CAMERON RAM BOPs

Appendix H BOP Modifications

Alert Number	Alert Status	Alert Issue Date	Work Description/Alert Description
EB 806 W	Information	October 1, 1994	Installation and Operation Procedure for High Pressure Injection and Bleeder fittings
EB 807 W	Information	October 1, 1994	Installation Procedure for Type MS-1 Secondary seals.
EB 809 W	Information	October 1, 1994	HV-SHP TUBING HEAD ADAPTERS AND TUBING NIPPLES
EB 810 W	Information	October 1, 1994	B.O.P. TESTER/BOWL PROTECTOR RUNNING & RETRIEVAL TOOL RUNNING PROCEDURE AND MAINTENANCE
EB 814 W	Information	October 20, 1995	Valve Removal Tool MI11338 Operating Instructions
EB 820 C	Information	January 31, 1995	DIRECTIONAL VALVE, HYDRAULIC PUMPS, P/ N304004-01
EB 823 W	Information	May 11, 1995	PLASTIC PACKING INJECTION PORTS
EB 831 M	Completed	December 4, 1995	STROKE LIMIT - MODEL 70 & HC COLLET CONNECTORS
EB 833D	Information	January 23, 1996	HIGH TEMPERATURE BOP ELASTOMERS
EB 841 W	Information	January 1, 1997	PROCEDURE FOR CHECKING I/4" NPT BURIED CHECK VALVES AND CORRECTIVE ACTION WERE FOUND NECESSARY (1997)
EB 842 M-B1	Completed	April 22, 2002	Surface Treatment for Collet Segments and Actuator Rings and Secondary Locking Recommendations for Cameron Collet Connectors
EB 843 W	Did not apply	April 17, 1997	MAXIMUM TEMPERATURE RATING OF K-2 AND K-6 SLIP AND SEAL ASSEMBLIES
EB 848 M, rev. B1	Did not apply	January 30, 1998	Potential High Separating Forces for Collet Connectors Operated in Deep Water. Connectors
EB 849 H	Did not apply	June 9, 1998	Cameron Choke Engineering Bulletins EB849h Cameron H2 Choke Bean and Seat Make-up
EB 851 D, Rev. C1	Information	December 2, 2002	Bonnet Bolt Torque for Seal Carrier BOP Bonnets: U, UL/UM & TL
EB 852 D	Information	October 30, 1998	Shear Ram Product Line
EB 854 D	Information	February 12, 1999	TL BOP Operating Cylinder to Bonnet Seal Updated part
EB 855 D	Information	May 20, 1999	Sequence Valve On-Site Inspection Procedure
EB 856 D	Information	June 12, 2000	Long-Term Storage of T & TL BOPs Equipped with "ST" and "Ram" Locks
EB 857 C	Information	July 10, 1999	1/4" Double Retractable Connector seal placement
EB 858 C	Information	August 30, 1999	Welding On The Stack With MUX PODs Installed
EB 859 D (Rev. D1)	Information	August 23, 2003	Variable Bore Ram & Flexpacker – Sealing & Hangoff
EB 861 C WForm	Information	September 27, 1999	Ceramic Seal Plates Cameron Pod p/n 112391-01, 112392-01, 112386-02, & 656222-12

Alert Number	Alert Status	Alert Issue Date	Work Description/Alert Description
EB 862 D	Did not apply	April 3, 2000	SHEARING CAPABILITY OF THE CAMERON 7-1/16" – 10,000 PSI 'DSI' SHEAR RAMS
EB 864 D	Information	December 10, 1999	Recommended Flange Bolt Torques
EB 865 C	Information	December 10, 1999	Deadman/AMF System Surface Testing
EB 868 D	Information	June 6, 2000	LONG-TERM STORAGE OF D & DL ANNULAR BOPs
EB 869 C	Did not apply	September 29, 2000	Cameron Existing Diverter Packer Circuits Rev. A01 eb869c
EB 870 D Rev. B1	Information	January 21, 2003	BOP Control System Recommendations for the Efficient Operation of Cameron BOP's Equipped with "ST" or "RamLock" Operating Systems.
EB 874 D with Form	Completed	September 4, 2001	18-3/4" 15M TL BOP Super Shear Ram Bonnets - with close bonnet supply in center of end Cap (External porting)
EB 875 D	Information	September 4, 2001	18 3/4" 15M TL BOP Super Shear Ram Retainer Pins
EB 876 D	Did not apply	September 4, 2001	18-3/4" 10M TL BOP DVS Shear Ram Top Seals
EB 882 D	Did not apply	March 8, 2002	Choke and Kill Manifold Systems – API 16C, Clarification of Material Class
EB 885 D (Rev. A01)	Did not apply	September 8, 2002	Cameron 18 3/4" 15M PSI UII Blowout Preventer Upgrades to Bonnet bolts for Proof Tests
EB 886 D Rev 01	Information	May 27, 2003	Preventive Maintenance of BOP's
EB 890 D	Did not apply	May 5, 2004	Periodic Inspection and Air Purging
EB 891 D	Information	September 9, 2004	AMF/Dead Battery Replacement
EB 893 D	Information	September 27, 2005	Low Temperature and Ambient Temperature Testing of Shearing Rams
EB A950001	Information	July 5, 1995	18-3/4" BOP Gasket – Temperature and Pressure Ratings With IP-0001
EB A960007	Information	November 21, 1996	Lubrication of Subsea H-4 Connectors
EB H022	Completed	March 17, 1992	18-3/4" Studed Top 10 & 15K H-4 Connectors, Model E & ExF Dog window modification
EB H032202	Information	March 28, 2003	VX-2, Vgx-2, & VT-2 (2nd) Generation of Wellhead Gaskets for Vetco Connectors
EB H970002	Information	November 15, 1997	Socket Head Cap Screw Usage in Maine Environments
EB H990750	Completed	May 10, 1999	H-4 Wellhead Connector Excluder ring for Hydrate or Shallow Flow Silt Contamination; Supersedes Engineering Bulletin EBH-960002. 16-3/4", 18-3/4", and super HD Connectors
ER 2768	Completed	November 28, 2000	Deadman Battery Longevity (Life) Test
FSA A033322	Information	April 11, 2007	H-4 Test Stump Handling & Lifting Hole Thread Protectors
FSA A070008	Information	March 29, 2004	VX-2 Gaskets
H051195Hydrates	Completed	June 30, 2005	H-4 Wellhead connector hydrate protection recommendations
HQS_HSE_AL_80	Information	May 8, 2006	HQS_HSE_AL_80_BOP_Test_Tool_Failure
HQS_OPS_ADV_405_003	Completed	March 10, 2008	Cameron Type Collet Connectors

Appendix H BOP Modifications

Alert Number	Alert Status	Alert Issue Date	Work Description/Alert Description
HQS_OPS_ADV_405_004_Rev_1	Completed	January 29, 2009	(Revised) Enhancement for Corrosion Resistance in Super HD H-4 Connectors.
HQS_OPS_ADV_435_026_Single_point_failureRev2	Completed	June 2, 2005	Elimination of Critical Solenoid Valve Single Point Failures
HQS_OPS_ADV_435_029soft_shift	Did not apply	July 19, 2006	Oceaneering Rigid Conduit Manifold Soft Shift Assembly
HQS_OPS_ADV_435_030_rev1_Mux_Connectors	Completed	August 2, 2006	MUX Umbilical Connector and Cable Standard
HQS_OPS_ADV_BOPR_010	Information	February 24, 2009	Cameron ST Lock Problems
HQS_OPS_EAL_209_002	Did not apply	September 25, 2008	Water Ingress Into the Azimuth Bearing, Seal , Gear Oiling HQS_OPS_EAL_209_002
HQS_OPS_EAL_BOPR_005	Information	November 11, 2009	Reduced Fatigue Life Of Packer For BOP Ram
HQS-HSE-AL-080	Completed	May 8, 2006	BOP TEST TOOL FAILURE
HQS-OPS-ADV-07	Information	August 1, 2009	FUNCTION TESTS FOR SUBSEA BOP (Advisory: The following changes will be made to the Well Control Manual to clarify the requirements for BOP function tests on subsea BOPs:)
HQS-OPS-ADV-401-005	Completed	January 12, 2005	HQS-OPS-ADV-401-005 - Cameron Super Shear Rams - Read advisory and ensure the mandatory action items listed below are completed.
HQS-OPS-ADV-401-006	Completed	May 2, 2005	HQS-OPS-ADV-401-006 Rev. 1 - Cameron Rams with ST-Locks - NOTE: There has been a change to Mandatory Action Item 4. The original action item 4 has been replaced by Action Items 4a and 4b. Please follow-up accordingly. Copy/Paste the following link to your browser to access this Advisory: http://edocs.houston.deepwater.com/eDocs/eDocs.nsf/FRAC?ReadForm&Rev=1&Ref=HQS-OPS-ADV-401-006
HQS-OPS-ADV-405-002	Completed	February 19, 2005	Cameron 18 3/4" 10K Collet Connectors
HQS-OPS-ADV-405-003	Information	March 10, 2008	Cameron Type Collet Connectors
HQS-OPS-ADV-413-003	Completed	June 2, 2005	HQS-OPS-ADV-413-003 - Implementation of "Stuck Button" Alarm on Cameron BOP Control Systems. Copy/Paste link to your browser to access this bulletin: http://edocs.houston.deepwater.com/eDocs/eDocs.nsf/FRAC?ReadForm&Rev=1&Ref=HQS-OPS-ADV-413-003
HQS-OPS-ADV-434-001	Completed	September 27, 2004	Read advisory HQS-OPS-ADV-434-001 - "BOP Fluid Concentration Error" and communicate same to all sub-sea engineers

Alert Number	Alert Status	Alert Issue Date	Work Description/Alert Description
HQS-OPS-ADV-435-028	Completed	June 13, 2006	HQS-OPS-ADV-435-028 - Subsea Transducer Modules (STM) and Subsea Transducer/Battery Modules (STBM) - Read Advisory and follow the actions below. Copy / paste the following link to your browser to access this Advisory. http://edocs.houston.deepwater.com/edocs/edocs.nsf/Frac?ReadForm&Rev=1&Ref=HQS-OPS-ADV-435-028
HQS-OPS-ADV-976-007	Completed	November 19, 2004	HQS-OPS-ADV-976-007 - Cameron BOP Control System - Solenoid Vent - Read Advisory and follow the actions below.
HQS-OPS-ADV-BOPR-010	Information	February 24, 2009	Cameron ST Lock Problems
HQS-OPS-EAL-401-04	Completed	August 6, 2007	HQS-OPS-EAL-401-04 - Cameron - Inspection of Cameron Shear Ram Blocks- Read this Advisory and follow the actions below. Copy/ Paste the following link to your browser access this Advisory. http://edocs.houston.deepwater.com/edocs/edocs.nsf/RAC?ReadForm&Rev=1&Ref=HQS-OPS-EAL-401-04
HQS-OPS-EAL-413-01-Rev1	Completed	December 3, 2003	HQS-OPS-EAL-413-01 BOP CONTROL PANEL Read Alert HQS-OPS-EAL-413-01 and complete action items on page 3 of this work order. The Maintenance Supervisor (or other management-designated person in charge of rig maintenance) must copy this Work Order to a Local Work Order against the affected equipment. When the Local Work Order is completed, its number must be recorded in the notes section of this original Work Order. Both work orders are then closed out with comments. NOTE: You should receive this alert via the normal document distribution channels.
HQS-OPS-EAL-422-04	Did not apply	N/A	HMF Riser Auxiliary Line Test Fixture HQS-OPS-EAL-422-04
HQS-OPS-EAL-444-001	Information	October 22, 2009	MUX Connector Failures operating procedures
HQS-OPS-EAL-480-001 Rev. 1	Did not apply	February 24, 2009	Lower Flex Joint Kick-Out Subs
HQS-OPS-EAL-BOPR-005	Completed	November 11, 2009	Reduced Fatigue Life Of Packer For BOP Ram
HQS-OPS-TIB-400-OH-01	Information	November 4, 2003	CAMERON D & DL ANNULAR TYPE BOP'S OVERHAUL SCOPE OF WORK
HQS-OPS-TIB-401-OH-01	Did not apply	November 4, 2003	Cameron Type U BOPS Overhaul HQS-OPS-TIB-401-OH-01
HQS-OPS-TIB-401-OH-02	Did not apply	November 4, 2003	Cameron U2 BOPS Scope of Work HQS-OPS-TIB-401-OH-02
HQS-OPS-TIB-401-OH-03	Information	November 4, 2003	CAMERON "TL" RAM TYPE BOP'S WITH 3 FUNCTION HYDRAULIC LOCKS
HQS-OPS-TIB-401-OH-04-Rev-1	Did not apply	October 26, 2004	CAMERON TYPE "T" RAM TYPE BOP'S WITH ST LOCKS MAJOR OVERHAUL / SCOPE OF WORK

Appendix H BOP Modifications

Alert Number	Alert Status	Alert Issue Date	Work Description/Alert Description
HQS-OPS-TIB-405-01	Information	June 6, 2005	Preventing Internal Corrosion of Vetco H4 and Cameron Model 70 Connectors
HQS-OPS-TIB-405-OH-02	Information	November 4, 2003	CAMERON HC COLLET CONNECTORS MAJOR OVERHAUL / SCOPE OF WORK
HQS-OPS-TIB-405-OH-03	Information	November 4, 2003	CAMERON MODEL 70 CONNECTORS MAJOR OVERHAUL / SCOPE OF WORK
HQS-OPS-TIB-405-OH-04	Completed	November 4, 2003	VETCO H4 CONNECTORS MAJOR OVERHAUL / SCOPE OF WORK
HQS-OPS-TIB-415-01	Information	May 11, 2005	Accumulator Bank Safety
HQS-OPS-TIB-435-01Rev1	Information	July 19, 2004	INSTRUCTIONS FOR REBUILDING CAMERON CONTROLS SOLENOID VALVE
HQS-OPS-TIB-435-02	Information	September 3, 2003	Cameron Solenoid Internal Pressure Test
HQS-OPS-TIB-BOPU-001	Information	October 1, 2009	BOP Control System Ball Valve Failures
HQS-OPS-TIB-BOTS-001	Information	May 15, 2009	Blow Out Preventer (BOP) Test Stumps
HQS-SS-2001-002	Information	August 28, 2001	Subsea BOP MUX Training Requirements
HQS-SS-ADV -2003-04	Information	March 8, 2003	NEW LAPTOP FOR SUBSEA ENGINEER TO MONITOR CAMERON EQUIPMENT Do not Know if the Proper software was loaded
HQS-SS-ADV-2001-001	Did not apply	June 25, 2002	The Cameron HC Collet Connector's actuator piston for certain rigs that were manufactured in Beziers do not have optimal coating applied to the Actuator Piston.
HQS-SS-ADV-2001-004	Did not apply	October 17, 2001	Subsea Equipment Survey
HQS-SS-ADV-2001-010	Completed	October 15, 2001	Cathodic Protection for Mark II Pods
HQS-SS-ADV-2001-011	Completed	October 15, 2001	HQS-SS-ADV-2001-011 REPLACE SEAT MATERIAL IN NEEDLE VALVE FOR CAMERON CONTROL SYSTEM FOR 1/2" & 1-1/2" NEEDLE VALVES
HQS-SS-ADV-2001-012	Information	October 15, 2001	Heat in BOP Control Panels
HQS-SS-ADV-2001-013	Information	October 17, 2001	Event Logger Software
HQS-SS-ADV-2002-001	Completed	February 11, 2002	Cameron Pressure Vessel Modifications of Test & Purge Ports: SEM, STM, STBM, RCB, RMJ, SXM & Inclinator
HQS-SS-ADV-2002-002	Did not apply	January 14, 2002	Cameron: Pressure Transducers
HQS-SS-ADV-2002-003	Did not apply	January 24, 2002	Cameron: BOP Control Fluid Mixing System Requirements
HQS-SS-ADV-2002-004	Information	January 24, 2002	Ordering MUX Cables
HQS-SS-ADV-2002-006	Completed	April 18, 2002	Shuttle Valve Approval
HQS-SS-ADV-2002-007	Completed	April 5, 2002	MUX Panel Power Down / Power Up Indications
HQS-SS-ADV-2002-008	Completed	May 1, 2002	Cameron PODs - 3/4" Slide Valve Spring Replacement
HQS-SS-ADV-2002-010	Completed	May 3, 2002	Cameron Control Pod SEM Shroud Removal
HQS-SS-ADV-2002-011	Completed	June 3, 2002	Cameron Control Pod 5K Slide Valves to be upgraded to Premium Type
HQS-SS-ADV-2002-012	Completed	June 11, 2002	Cameron Mark I & Mark II Pod Cylinder Tie Rod Replacements

Alert Number	Alert Status	Alert Issue Date	Work Description/Alert Description
HQS-SS-ADV-2002-014	Information	June 24, 2002	Use of Cameron FPR Reporting for Cameron Controls Equipment
HQS-SS-ADV-2002-019	Did not apply	September 10, 2002	Cameron MUX Controls – Self-Audit
HQS-SS-ADV-2003-001	Completed	January 22, 2003	E-Connector
HQS-SS-ADV-2003-002	Completed	January 14, 2003	Pressure Balanced Oil Filled Cables (PBOF)
HQS-SS-ADV-2003-003	Information	March 7, 2003	Cameron Mux Controls System Modem Specifications
HQS-SS-ADV-2003-005	Completed	March 28, 2003	Corrosion Resistant Seal Plates For Cameron Pod Valves
HQS-SS-ADV-2003-008	Completed	May 20, 2003	Cameron MUX Controls – PLC's
HQS-SS-ADV-2003-009	Completed	May 28, 2003	PEP digital out Boards.
HQS-SS-ADV-2003-010_R1	Completed	August 24, 2004	Gilmore HP Style Shuttle Valve Upgrade
HQS-SS-ADV-2003-011	Completed	June 30, 2003	Cameron Autoshear System Reaction Spring
HQS-SS-ADV-2003-04	Completed	March 8, 2003	Software changes on the Cameron Mux System
MEMO-26-Sep-02	Information	September 26, 2002	on Cameron Controls, describes their policies for dealing with component obsolescence
OPT-ADV-435-003	Completed	July 24, 2003	Cameron Regulator Upgrade - Orifice Addition
OPT-ADV-435-012	Did not apply	August 19, 2003	Cameron Controls Monitoring of OLM's
OPT-ADV-435-021	Completed	August 5, 2003	Cameron MUX 24V DC System Protection & Coordination
OPT-ADV-435-022	Completed	August 27, 2003	Cameron Controls Mark I & Mark II, STM and STBM Modifications
OPT-EAL-415-01	Information	June 8, 2001	BOP Accumulator Units / HPU To inform TSF personnel of three cases of pump relief valves being incorrectly installed.
OPT-EAL-415-02	Information	April 3, 2003	BOP Accumulator units.To inform Transocean personnel of the potential for serious or fatal injury, while working on BOP accumulator units.
OPT-EAL-435-01	Information	October 23, 2001	SUBSEA BOP CONTROLS
OPT-EAL-435-02	Did not apply	May 1, 2002	Equipment Alert-Equipment Hydraulic Piloted BOP Control Systems OPT-EAL-435-02
OPT-EAL-435-03	Completed	December 9, 2002	Cameron MUX Pod
OPT-EAL-444-01	Information	August 16, 2001	MUX Cables and Pod Hoses
OPT-EAL-447-01	Did not apply	May 18, 2000	To inform TSF personnel of a Bop control system and ST lock Incident caused by incorrect design of the hydraulic system
OPT-EAL-994-01	Information	October 22, 2001	BOP Control Fluids & Mix Water To inform TSF Subsea Engineers, and Rig Management of the importance of following the BOP FLUIDCARE instructions provided by Houghton Offshore.
OPT-EAL-994-02	Information	April 1, 2002	BOP Fluid Contamination To inform TSF personnel of BOP Fluid Contamination problems and the actions necessary to minimize contamination.

Appendix H BOP Modifications

Alert Number	Alert Status	Alert Issue Date	Work Description/Alert Description
PA #006024	Completed	May 1, 2002	CAMERON CONTROLS SERVICE ET REP. NEEDED FRO NEXT RIG MOVE TO COMPLY WITH TSF BULLETIN PA-6024 INSTALLING TRANSFORMERS, SEM WORK, INSTALLING SOFTWARE, ETC.
PA #006044	Did not apply	May 1, 2002	Cooling Kits for Driller's Control Panels
PA #006104	Information	March 13, 2002	ST-Lock Brake Hub – Transocean Sedco Forex Discrepant Parts
PA #006124	Completed	March 14, 2002	ST-Lock Overhauling Nut P/N 644682-03 Excess Thread Wear
PA #10030	Did not apply	September 2, 2005	CAMERON BOP RAMS Top Seals all types
PA #1005	Did not apply	February 14, 2000	Cameron 18 3/4" 5/10,000 psi TL BOP Variable Bore Ram Assembly 3 1/2" to 7 5/8"
PA #12022	Completed	October 30, 2001	Atlas Cylinder Tie Rods in Cameron Control Pods
PA #1204	Completed	June 21, 2000	Bearing Overhauling Nut, ST-Lock – Bearing upgrade
PA #1602	Completed	August 30, 2000	Shuttle Valves for Drilling Multiplex BOP Control Systems
PA #18020	Completed	September 11, 2000	Complete Covers were installed over Pushbuttons LMRP & WELLHEAD CONNECTOR FUNCTION LOCKOUT
PA #1802036	Completed	January 14, 1998	Deepwater Connectors
PA #1802058	Information	April 2, 1999	PRODUCT ADVISORY: 1802058 18 3/4" NOMINAL WEAR BUSHING POTENTIAL TO BLOCK BOP RAM CAVITY
PA #18040	Completed	October 4, 2000	Drilling Multiplex BOP Control System Mark II Control Pod Subsea Electronic Module Power Supplies
PA #1814034	Did not apply	August 12, 1997	The Cameron Drilling Choke PA-1814034
PA #1816038	Completed	August 20, 1999	Drilling Multiplex BOP Control System Subsea Electronics Module (SEM)
PA #1816058	Did not apply	August 19, 1998	Cameron Gate Valve Lubrication Practices and Fittings PA-1816058
PA #1816096	Did not apply	August 28, 1998	18 3/4" 15K UII Blowout Preventer Re-manufacture
PA #1818038	Information	November 16, 1999	Possible Removal Difficulties of AX Gaskets with Elastomer Seal Rings
PA #1820038	Completed	October 18, 1999	1/2" Unbalanced Shuttle Valve
PA #20	Information	April 12, 1985	Hydraulic Bonnet Bolts Tensioners for Cameron BOP Hydraulic Bonnet Bolts
PA #20060 (Revised)	Completed	October 30, 2001	Atlas Cylinder Nuts with kit part numbers
PA #20080	Did not apply	October 31, 2000	Cathodic Protection of Cylinders Pod Cylinders pa-20080
PA #20200	Did not apply	August 28, 2001	Relief Valve Change Out PA-20200
PA #22020	Completed	November 2, 2000	Model 70 Collet, Mini Collets, LMRP Jacking System, Transponder/Transducer Arms

Alert Number	Alert Status	Alert Issue Date	Work Description/Alert Description
PA #35	Did not apply	November 26, 1990	Cameron Falsified API Compliance Documents (1990)
PA #38	Information	April 30, 1991	Info Subsea actuated gate valves design problems.
PA #4070	Did not apply	September 2, 2005	Shuttle Valve Cap screws
PA #4078	Information	February 24, 2009	ST Locks
PA #44	Information	October 7, 1996	Stinging open ball check valve
PA #6020	Completed	March 9, 2000	TL Super Shear Ram Recommended Operating Practice
PA #6040	Completed	March 13, 2000	ST-Lock Operating and Preventer Maintenance, ST-Locks with ball bearing assemblies
PA #606	Completed	April 4, 2000	Sequence Valve for ST-Lock Elastomer Failure
PA #8164	Completed	April 2, 2002	Super Shear Retainer Pin Part Number 2724258-02
Ram-01-03	Completed	January 1, 2003	Ram assembly – Optional Wear Pads
S&T-Index	Information	February 1, 2002	Index of Cameron Specifications & Test Documents Issued to TSF
SA-008048	Did not apply	April 5, 2004	Trap point in Tubing Hanger
SA-014086	Did not apply	July 2, 2004	7-1/16" Nominal Type C Tubing Spools and Tubing Hangers
SA-16070	Did not apply	August 29, 2005	Cameron Hydraulic Riser Running Tools SA_16070Cameron&Quote
SA-2072	Did not apply	January 11, 2006	18 3/4" 15,000 TL BOP with RamLock
SA-2092	Completed	January 11, 2006	SA-2092 - 18 3/4" 15,000 TL BOP Super Shear - Read Bulletin and follow the actions below. Copy / paste the following link to your browser to access this Bulletin. http://edocs.houston.deepwater.com/edocs/eDocs.nsf/FRAC?ReadForm&Rev=1&Ref=SA-2092
SA-2520	Did not apply	January 5, 2006	18 3/4" 5,000/10,000 TL BOP with RamLock
SA-6028	Did not apply	June 1, 2004	Cameron RD Riser Running Tool SA-6028
Tech_Hazard_Alert1	Information	October 20, 2000	Floating Rig DST: Damage to Ram BOP Seals From Internal Pressure Less Than Ambient Seawater Hydrostatic
TO10065	Information	July 23, 2009	Blue Mux Cable And Yellow Mux Cable Connector Issues
X -9VBat	Information	February 10, 2003	Cameron-X-9VBat
X_234102_01Rev2	Completed	September 14, 2005	Handling Procedure for SEM Pie Connectors and Solenoid Cable Connectors

Appendix H BOP Modifications

Alert Number	Alert Status	Alert Issue Date	Work Description/Alert Description
X-065438-39	Completed	August 23, 2000	Cameron Handling Procedure: Dry Mateable Subsea Connections Seacon MSS Series
X-201678-01	Information	September 28, 2000	Water Based Hydraulic Fluid Purchaser's Guide, defining functional requirements for water based fluids
X-201679-01	Information	September 28, 2000	Water Based Hydraulic Fluid User's Guide, for fluid handling practices, & fluid cleanliness

1. Change Proposal, Proposal No.: SS 004, *Deepwater Horizon*, Flowmeters & Software, Nov. 10, 2002, TRN-USCG_MMS-00042069.
2. Change Proposal, Proposal No.: SS 005, *Deepwater Horizon*, Non-retrievable pods, Nov. 13, 2002, TRN-USCG_MMS-00042086.
3. Change Proposal, Proposal No.: MD-0029, *Deepwater Horizon*, LMRP failsafe panel removal, August 28, 2004; Change Proposal, Proposal No.: MD-0029, BOC MOC for Horizon, Jan. 5, 2004.
4. Change Proposal, Proposal No.: MD-0029, *Deepwater Horizon*, BOP MOC for Horizon, Jan. 5, 2004.
5. Change Proposal, Proposal No.: MD-054, *Deepwater Horizon*, Cameron Control Software, March 5, 2007.
6. Change Proposal, Proposal No.: SS-021, *Deepwater Horizon*, "G" Pin x "H" Box Modification, Aug. 27, 2008.
7. Change Proposal, Proposal No.: SS-027 *Deepwater Horizon*, Installation of New Auto Sheer Valve, Aug. 8, 2009.
8. Letter from Christopher Young, Transocean Holdings, Inc. to Jeff Sturseth, BP America Production Company, dated Oct. 11, 2004, TRN-MDL-00105868.
9. Change Proposal, Proposal No.: SS-10, *Deepwater Horizon*, BOP Test Rams, Nov. 21, 2004.
10. Change Proposal, Proposal No.: SS-016, *Horizon*, 18 3/4" Annular Stripper Packer, March 9, 2006.
11. Cameron Product Advisory #4078, ST-Locks, Feb. 24, 2009, CAM-CIV-0003093.
12. DAR Consolidation Report, entry for Oct. 29, 2002, TRN-MDL-00302302, 11; Cameron Product Advisory #006124, ST-Lock Overhauling Nut P/N 644682-03 Excess Thread Wear, March 14, 2002.
13. Repetitive Work Order, 8701-001749-000 (C), November 2001; Repetitive Work Order, 8701-001753-000 (C); Repetitive Work Order, 8701-001757-000 (C). Cameron Information Sheet CS-01-C03, Reference, Oct. 26, 2001.
14. Minor Work Order, 8703-006557 (C), November 2003.
15. Operational & Maintenance Advisory, Cameron Regulator Upgrade—Orifice Addition, July 24, 2003.
16. Subsea DAR Consolidation Report, entry for May 11, 2004, TRN-MDL-00302302, 43.
17. Transocean Routine Work Order, 8704-002880-000 (C), June 2004.
18. Routine Work Order, 8704-003355-000, June 2004; Cameron Purchase Order, P602587, June 22, 2004.
19. Routine Work Order, 8704-002881-000, June 2004; Cameron Purchase Order, P626479, July 14, 2005.
20. Routine Work Order, 8705-003777-000, November 2005.
21. Operational & Maintenance Advisory, HQS-OPS-ADV-413-003, Implementation of "Stuck Button" Alarm on Cameron BOP Control Systems, June 2, 2005; Routine Work Order, 8705-003343-000, November 2005; Cameron Purchase Order, P770353, July 12, 2005.
22. Routine Work Order, 8706-002608-0000, August 2007; Transocean Routine Work Order, 8706-001242-000, December 2006; Cameron Purchase Order, P926729, Oct. 12, 2006; Cameron Purchase Order, P961088, Nov. 14, 2006; Cameron Engineering Bulletin, EB 891 D, AMF/Deadman Battery Replacement, Sept. 8, 2004.

Appendix I

BOP Maintenance History

The *Deepwater Horizon* had 752 planned maintenance “jobs” for the well-control system and related components that came due during the 365 days prior to the incident; 748 of these tasks were completed. Four of these maintenance tasks were overdue on the day of the incident. None of these overdue maintenance tasks adversely impacted the operation of the BOP or well-control equipment on April 20, 2010.

The *Deepwater Horizon* BOP stack is displayed in *Figure 1*; the diagram is color coded, showing the individual BOP stack components and their maintenance status at the time of the incident. *Table 1* notes the next required maintenance deadline.

Overdue Maintenance Tasks

Maintenance Task 1—Ram Non-Destructive Test Preventative Maintenance

- **Scope of Preventative Maintenance Task:** Ram BOP non-destructive testing on the operating piston end, ram blocks, bonnet studs and BOP body threads.
- **RMS Tag Numbers:** WCS BOPR 001, WCS BOPR 002 and WCS BOPR 003

A non-destructive test (NDT) of the BOP stack’s 18-3/4-in. middle single, lower double and upper double rams (closing and sealing components) was scheduled for Jan. 12, 2010.¹ This NDT covers inspection of the bonnet studs and nuts, operating piston end, ram blocks and BOP body threads. This preventative maintenance task is conducted every 365 days.

Transocean’s computerized maintenance management system, RMS-2, showed that this test was last completed on Jan. 12, 2009, by a third-party company, and that there were no discrepancies noted.² As the BOP stack was in operation at the time that this maintenance task came due, rig management was informed and a decision was made to defer this maintenance until completion of the Macondo well. Regularly scheduled pressure tests were conducted every 14 days to validate the functionality of the BOP rams.³ All of these tests were successful. Therefore, this outstanding maintenance task had no adverse impact on the functioning of the rams. The critical BOP ram cavity gap measurements, signature test data and pressure testing can be found in *Table 2*.

Maintenance Task 2—LMRP Connector Service

- **Scope of Preventative Maintenance Task:** Pressure testing the hydraulic operating chamber and hydraulic gasket retainer circuit. Perform a deck test procedure, including measuring indicator rod travel from latch to unlatch.
- **RMS Tag Number:** WCS CONN 001

A connector-service test (SPM05-Connector Service) for the BOP stack lower marine riser package connector was scheduled for March 30, 2010.⁴ This preventative maintenance task is conducted every 180 days and can be performed only when the BOP stack is on the surface. As the BOP stack was below the surface when this task became due, rig management was informed and a decision was made to defer the test until completion of the Macondo well. Regularly scheduled pressure tests were conducted every 14 days to validate the functionality of the well-control equipment.⁵ All of these tests were successful. Therefore, this outstanding maintenance task had no effect on the outcome of the incident.

Maintenance Task 3—BOP Choke Control Unit

- **Scope of Preventative Maintenance Task:** Conduct an operational check of the choke control unit to ensure it functions as designed.
- **RMS Tag Number:** WCS CTRU 005

A surface BOP stack choke control inspection and service check (SPM 01 CTRU-Service), which is performed at seven-day intervals, was last completed on April 9, 2010. It was scheduled again for April 16, 2010, but may not have been completed due to operations.⁶ The choke control unit was available, but not utilized during the well-control operations. As this equipment was not in operation at the time of the incident, this outstanding maintenance task had no effect on the outcome of the incident.

Maintenance Task 4—BOP Surface Choke and Kill Pipe Work

- **Scope of Preventive Maintenance Task:** Visually inspect all high-pressure choke and kill piping from the manifold to the hose connections.
- **RMS Tag Number:** WCS PIPE 002

A visual inspection of all high-pressure choke and kill piping (SPM 01 PIPE-BOP Choke and Kill-Checks) from the manifold to the hose connections, which is performed at 30-day intervals, was last completed on March 19, 2010, and another was scheduled for April 19, 2010.⁷ This task was one day overdue at the time of the incident. The BOP surface choke and kill pipe work had been inspected and used with no issues prior to the time of the incident. This outstanding maintenance task had no effect on the outcome of the incident.

Appendix I BOP Maintenance History

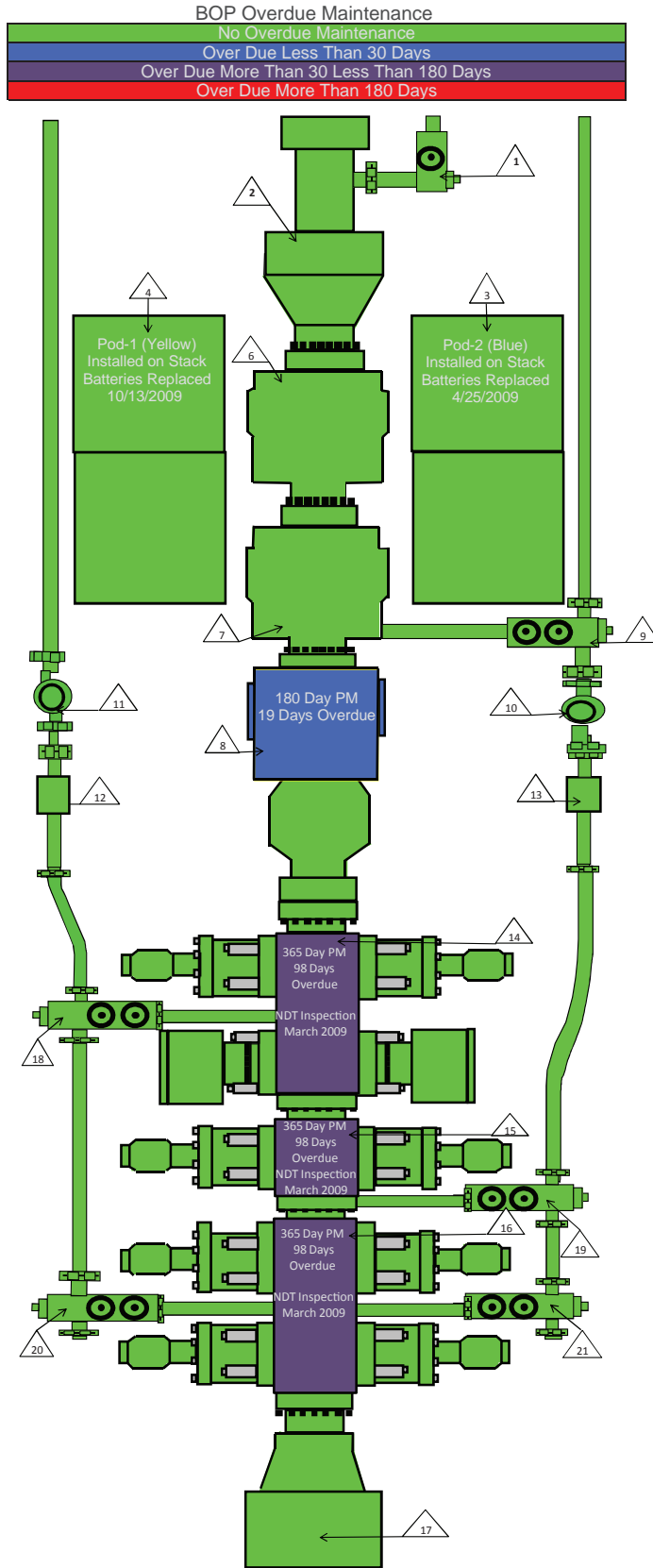


Figure 1

(1) RISER BOOST VALVE		
Job Description	PM Interval	Due Date
365-Day Annular	365 Day	October 7, 2011
1,095-Day Annular	1,095 Day	January 13, 2011
1,825-Day Annular NDT	1,825 Day	June 7, 2012
(2) RISER FLEX JOINT		
Job Description	PM Interval	Due date
365-Day Flex Joint/Riser Adapter	365 Day	July 2, 2010
1,825-Day Flex Joint/Riser Adapter NDT	1,825 Day	April 28, 2011
(3) CONTROL POD 1 (BLUE)		
Job Description	PM Interval	Due date
SPM02-BOP Control Pod-Service	360 Day	July 11, 2010
SPM03-BOP Control Pod-Service	720 Day	January 8, 2011
SPM04-BOP Control Pod-Overhaul	1,800 Day	September 20, 2012
(4) CONTROL POD 2 (YELLOW)		
Job Description	PM Interval	Due date
SPM02-BOP Control Pod-Service	360 Day	January 8, 2011
SPM03-BOP Control Pod-Service	720 Day	December 23, 2011
SPM04-BOP Control Pod-Overhaul	1,800 Day	September 20, 2012
(5) CONTROL POD 3 (WHITE)		
Job Description	PM Interval	Due date
SPM02-BOP Control Pod-Service	360 Day	January 8, 2011
SPM03-BOP Control Pod-Service	720 Day	July 11, 2010
SPM04-BOP Control Pod-Overhaul	1,800 Day	May 28, 2012
(6) UPPER ANNULAR		
Job Description	PM Interval	Due date
365-Day Annular	365 Day	January 6, 2011
1,095-Day Annular	1,095 Day	September 12, 2012
1,825-Day Annular NDT	1,825 Day	June 4, 2012
(7) LOWER ANNULAR		
Job Description	PM Interval	Due date
365-Day Annular	365 Day	July 21, 2010
1,095-Day Annular	1,095 Day	January 12, 2011
1,825-Day Annular NDT	1,825 Day	June 5, 2012
(8) LMRP CONNECTOR		
Job Description	PM Interval	Due date
SPM01-Connector-Service	14 Day	April 9, 2010
SPM03-Connector-Service	180 Day	June 30, 2010
SPM05-Connector-Service	180 Day	March 30, 2010
SPM06-Connector-Overhaul	1,800 Day	April 30, 2010
(9) INNER & OUTER BLEED VALVE		
Job Description	PM Interval	Due Date
365-Day Annular	365 Day	January 7, 2011
1,095-Day Annular	1,095 Day	January 12, 2011
1,825-Day Annular NDT	1,825 day	January 13, 2014
(10) CHOKE ISOLATION VALVE		
Job Description	PM Interval	Due Date
365-Day Annular	365 Day	January 1, 2011

Table 1 BOP Modifications

Appendix I BOP Maintenance History

(11) KILL ISOLATION VALVE		
Job Description	PM Interval	Due Date
365-Day Annular	365 Day	January 1, 2011
(12) KILL MINI COLLET CONNECTOR		
Job Description	PM Interval	Due Date
365-Day Annular	365 Day	July 2, 2010
1,095-Day Annular	1,095 Day	April 7, 2012
(13) CHOKE MINI COLLET CONNECTOR		
Job Description	PM Interval	Due Date
365-Day Annular	365 Day	July 2, 2010
1,095-Day Annular	1,095 Day	April 7, 2012
(14) UPPER DOUBLE RAMS		
Job Description	PM Interval	Due date
365-Day Ram BOP NDT	365 Day	January 12, 2010
1,825-Day Ram BOP NDT	1,825 Day	May 26, 2012
(15) MIDDLE SINGLE RAMS		
Job Description	PM Interval	Due date
365-Day Ram BOP NDT	365 Day	January 12, 2010
1,825-Day Ram BOP NDT	1,825 Day	May 26, 2012
(16) LOWER DOUBLE RAMS		
Job Description	PM Interval	Due date
365-Day Ram BOP NDT	365 Day	January 12, 2010
1,825-Day Ram BOP NDT	1,825 Day	May 26, 2012
(17) WELLHEAD CONNECTOR		
Job Description	PM Interval	Due date
180-Day Connector	180 Day	June 27, 2010
1,825-Day Connector NDT	180 Day	January 12, 2014
(18) UPPER KILL VALVES		
Job Description	PM Interval	Due Date
365-Day Annular	365 Day	January 8, 2011
1,095-Day Annular	1,095 Day	January 12, 2011
1,825-Day Annular NDT	1,825 day	January 13, 2014
(19) UPPER CHOKE VALVES		
Job Description	PM Interval	Due Date
365-Day Annular	365 Day	January 8, 2011
1,095-Day Annular	1,095 Day	January 12, 2011
1,825-Day Annular NDT	1,825 day	January 13, 2014
(20) LOWER KILL VALVES		
Job Description	PM Interval	Due Date
365-Day Annular	365 Day	January 8, 2011
1,095-Day Annular	1,095 Day	January 12, 2011
1,825-Day Annular NDT	1,825 Day	January 13, 2014
(21) LOWER CHOKE VALVES		
Job Description	PM Interval	Due Date
365-Day Annular	365 Day	January 8, 2011
1,095-Day Annular	1,095 Day	January 12, 2011
1,825-Day Annular NDT	1,825 Day	January 13, 2014

Table 1 BOP Modifications (cont.)

BOP Ram Gap Measurements, Signature Tests, and Pressure Tests

Blind Shear	31-Aug-09	Upper Rams	31-Aug-09
Top Port Gap Measurement	0.031	Top Port Gap Measurement	0.025
Side Port Gap Measurement	0.014	Side Port Gap Measurement	0.012
Top Stbd Gap Measurement	0.029	Top Stbd Gap Measurement	0.026
Side Stbd Gap Measurement	0.013	Side Stbd Gap Measurement	0.013
Signature Test	70 psi/80 psi	Signature Test	70 psi/80 psi
Pressure Test	1-Feb-10	Pressure Test	1-Feb-10
Middle Rams	31-Aug-09	Lower Rams	31-Aug-09
Top Port Gap Measurement	0.029	Top Port Gap Measurement	0.025
Side Port Gap Measurement	0.012	Side Port Gap Measurement	0.008
Top Stbd Gap Measurement	0.016	Top Stbd Gap Measurement	0.01
Side Stbd Gap Measurement	0.03	Side Stbd Gap Measurement	0.033
Signature Test	70 psi/80 psi	Signature Test	60 psi/90 psi
Pressure Test	1-Feb-10	Pressure Test	1-Feb-10
Casing Shear	NA		
Pressure Test	1-Feb-10		
▶ BOP Gap measurements were verified by Deepwater Horizon Maintenance Crew during Interviews			

Table 2

Appendix I BOP Maintenance History

1. Rig Management System, as of April 20, 2010.
2. Certificate of Test Bonnet Bolts, March 2009, TRN-TBD-00001634.
3. Daily Activity Consolidation Report, April 24, 2002–Feb. 17, 2010.
4. Rig Management System, as of April 20, 2010.
5. Daily Activity Consolidation Report, June 3, 2010.
6. Rig Management System, as of April 20, 2010.
7. *Ibid.*

Appendix J BOP Testing

The blowout preventer (BOP) stack was pressure and function tested numerous times over the course of the Macondo well, including on the day of the incident. See *Table 1*. From this evidence, the investigation team concluded that the BOP stack was fully operational and that there were no defects that would have impacted the ability of the BOP to function.

Function and pressure testing are performed on the BOP stack and control system on the rig prior to lowering the BOP to the ocean floor and continue while the BOP Stack is deployed subsea to confirm the integrity of the rig's well-control system. Routine pressure and function tests were performed on the *Deepwater Horizon* subsea BOP equipment in compliance with Transocean's internal policies and regulatory requirements. The BOP passed all pressure and function testing while conducting operations on the Macondo well.

Testing Requirements

BOP testing requirements are stated in the Code of Federal Regulations – Title 30: Mineral Resources. The purpose of the tests is to ensure the BOP system and system components are pressure tight and fit for purpose.¹

Function Testing

The purpose of function testing is to ensure the subsea well-control equipment is operational. A complete function test is performed on the BOP stack from both control pods prior to lowering it to the ocean floor. This is done to ensure the equipment is operating properly and that there are no problems. After the BOP stack is in operation, it is function tested weekly.²

Method of Function Testing

- **Surface function test (prior to running the BOP stack)**
Operate all functions on the BOP stack from both control pods and record gallon counts to verify that there was a complete operation of the tested function. Visually verify that there are no leaks in the system. Verify there are no system faults.
- **Subsea function test**
Operate all functions on the BOP stack from one of the control pods (alternating pods and control panels) and record gallon counts to verify that there was a complete operation of the tested function. Verify that there are no leaks in the system. Verify that there are no system faults. There are a number of functions that are not tested when the BOP stack is deployed on bottom due to the risk of disconnect from the well or damage to equipment that may require retrieval of the BOP stack to correct.³

Pressure Testing

The purpose of pressure testing is to verify that the well-control equipment is operating and leak-free, as well as to verify the integrity of casing and the well. A complete pressure test is performed on the BOP stack to full working pressure prior to lowering it to the ocean floor. This is done to ensure the equipment is operating properly and is leak-free. After the BOP stack is deployed, it is pressure tested at a minimum of every 14 days. During some critical well operations, it is not possible to test the BOP stack. When this occurs, a request is submitted to the Bureau of Ocean Energy Management, Regulation and Enforcement (BOEMRE), formerly the Minerals Management Services (MMS), asking for a BOP test extension. See *Table 1*.⁴

Recording Pressure Tests

Chart Recorder Method

Shut-in test pressures are recorded on circular chart recorders. The BOP stack is pressurized, followed by a waiting period (stabilization period) until stable pressures are obtained. Then a five-minute hold period (no pressure increase or decrease) is required as proof of integrity. Reasonably stable pressures must be greater than or equal to the required test pressure and allow for temperature-related pressure variations.

Digital Testing

In July 2008, BP introduced digital testing on the *Deepwater Horizon* for BOP stack pressure tests. BP developed a digital method for pressure testing that decreased the time required to test the BOP stack, which they called “Anatomization.” In 2008, BP submitted a request, and MMS approved this digital testing method.⁵

Test Conducted	Test Date	References
Function Test Both Pods (Surface Pre-run)	February 5, 2010	Daily Drilling Report, February 5, 2010, TRN-HCJ-00076220.
Pressure Test BOP (Surface Pre-run)	February 6, 2010	Daily Drilling Report, February 6, 2010, BP-HZN-CEC019063.
Function Test Diverter	February 9, 2010	Daily Drilling Report, February 9, 2010, BP-HZN-BLY00101577.
Pressure Test BOP	February 9, 2010	Daily Drilling Report, February 9, 2010, BP-HZN-BLY00101577.
Pressure Test BOP	February 10, 2010	Daily Drilling Report, February 10, 2010, TRN-HCJ-00076236.
Function Test BOP	February 10, 2010	Daily Drilling Report, February 10, 2010, TRN-HCJ-00076236.
Well Casing Integrity Test	February 10, 2010	Daily Drilling Report, February 10, 2010, TRN-HCJ-00076236.
Pressure Test Upper Annular	February 12, 200	Daily Drilling Report, February 12, 2010, TRN-TBD-00000162.
Function Test BOP	February 17, 2010	Daily Drilling Report, February 17, 2010, TRN-HCJ-00076240.
Function Test Diverter	February 17, 2010	Daily Drilling Report, February 17, 2010, TRN-HCJ-00076240.
Pressure Test BOP	February 24, 2010	Daily Drilling Report, February 24, 2010, BP-HZN-CEC019196.
Pressure Test BOP	February 25, 2010	Daily Drilling Report, February 25, 2010, BP-HZN-CEC019202.
Function Test BOP	February 25, 2010	Daily Drilling Report, February 25, 2010, BP-HZN-CEC019202.
Function Test Diverter	February 25, 2010	Daily Drilling Report, February 25, 2010, BP-HZN-CEC019202.
Casing Integrity Test	March 1, 2010	Daily Drilling Report, March 1, 2010, BP-HZN-BLY00047076.
Function Test BOP	March 4, 2010	Daily Drilling Report, March 4, 2010, TRN-HCJ-00076264.
Function Test Diverter	March 4, 2010	Daily Drilling Report, March 4, 2010, TRN-HCJ-00076264.
MMS BOP Test Extension	March 12, 2010	Daily Drilling Report, March 12, 2010, BP-HZN-CEC019117.
MMS BOP Test Extension	March 13, 2010	Daily Drilling Report, March 13, 2010, TRN-TBD-00000191.
Pressure Test BOP	March 15, 2010	Daily Drilling Report, March 15, 2010, TRN-MDL-00011448.
Function Test BOP	March 15, 2010	Daily Drilling Report, March 15, 2010, TRN-MDL-00011448.

Table 1 Identifies All Tests Performed on the BOP Prior to and During the Macondo Well

Appendix J BOP Testing

Test Conducted	Test Date	References
Function Test Shear Rams	March 21, 2010	Daily Drilling Report, March 21, 2010, TRN-MDL-00026217.
Pressure Test Shear Rams	March 21, 2010	Daily Drilling Report, March 21, 2010, TRN-MDL-00026217.
Function Test BOP	March 22, 2010	Daily Drilling Report, March 22, 2010, BP-HZN-CEC019186.
Pressure Test Shear Rams	March 26, 2010	Daily Drilling Report, March 26, 2010, BP-HZN-CEC19211.
Function Test Shear Rams	March 26, 2010	Daily Drilling Report, March 26, 2010, BP-HZN-CEC19211.
Casing Integrity Test	March 26, 2010	Daily Drilling Report, March 26, 2010, BP-HZN-CEC19211.
Function Test BOP	March 27, 2010	Daily Drilling Report, March 27, 2010, BP-HZN-CEC019217.
Pressure Test BOP	March 27, 2010	Daily Drilling Report, March 27, 2010, BP-HZN-CEC019217.
Test Diverter	March 31, 2010	Daily Drilling Report, March 31, 2010, BP-HZN-CEC019232.
Pressure Test Shear Rams	April 1, 2010	Daily Drilling Report, April 1, 2010, BP-HZN-2179MDL00336968.
Casing Integrity Test	April 1, 2010	Daily Drilling Report, April 1, 2010, BP-HZN-2179MDL00336968.
Function Test BOP	April 3, 2010	Daily Drilling Report, April 3, 2010, TRN-TBD-00000212.
Function Test Diverter	April 3, 2010	Daily Drilling Report, April 3, 2010, TRN-TBD-00000212.
Pressure Test Shear Rams	April 8, 2010	Daily Drilling Report, April 8, 2010, BP-HZN-2179MDL00333539.
Pressure Test BOP	April 9, 2010	Daily Drilling Report, April 9, 2010, BP-HZN-2179MDL00333544.
Pressure Test BOP	April 10, 2010	Daily Drilling Report, April 10, 2010, BP-HZN-2179MDL00333548.
Function Test BOP	April 10, 2010	Daily Drilling Report, April 10, 2010, BP-HZN-2179MDL00333548.
Function Test Diverter	April 10, 2010	Daily Drilling Report, April 10, 2010, BP-HZN-2179MDL00333548.
Function Test BOP	April 17, 2010	Daily Drilling Report, April 17, 2010, BP-HZN-2179MDL00333577.
Function Test Diverter	April 17, 2010	Daily Drilling Report, April 17, 2010, BP-HZN-2179MDL00333577.
Function Test Shear Rams	April 17, 2010	Daily Drilling Report, April 17, 2010, BP-HZN-2179MDL00333577.
Function Test Diverter	April 19, 2010	Daily Drilling Report, April 19, 2010, BP-HZN-CEC011567.
Casing Integrity Test	April 20, 2010	Daily Drilling Report, April 20, 2010, BP-HZN-2179MDL00333592.
Pressure Test Shear Rams	April 20, 2010	Daily Drilling Report, April 20, 2010, BP-HZN-2179MDL00333592.

1. IADC Deepwater Control Guidelines 3.7.2.1, TRN-TBD-00003062; 30 C.F.R. 250, 446-451; Transocean Well Control Manual.
2. *Ibid.*
3. POD Function Test, April 8, 2010, TRN-TBD-00006091; 30. C.F.R.
4. *Deepwater Horizon* Yellow Pod Function Test, April 8, 2010. TRN-TBD-00006090.
5. BP, Digital Interpretation of Subsea BOP tests, 2008, TRN-TBD-00008133.

Appendix K BOP Leaks

Appendix K BOP Leaks

There were five minor leaks in the *Deepwater Horizon* BOP control system: three were identified after the BOP stack was latched to the wellhead in February 2010, and two were identified during the post-incident intervention by the remotely operated vehicle (ROV). None of these leaks caused or contributed to the April 20 incident, and they did not adversely impact the functionality or redundancy of the BOP control system to perform as designed in a well control event. The five leaks were as follows:

Identified Pre-Incident

- Leak on the open-side function of the test ram BOP
- Leak on accumulator surge bottle on the upper annular BOP
- Leak on the lower annular BOP close function

Identified Post-Incident

- Leak on a hose fitting to the lock function on the ST Lock circuit
- Leak on blind shear ram ST Lock sequence valve to ST Lock chamber

The leaks were small in volume and, in some cases, regardless of volume, they would not have adversely impacted the closure of the well-control components.^A Functioning of the well-control components relied on the hydraulic supply from the rig via a hydraulic conduit line, and from surface and subsea accumulator storage bottles. Low-volume leaks did not impede functionality because any fluid lost was recharged by the rigid conduit line being supplied by the Cameron Surface Control System, which included 45 40-gallon accumulators that were continuously replenished to a stored pressure of 5,000 psi.¹ In the event the hydraulic conduit line was severed or destroyed, eight 80-gallon accumulator bottles on the BOP stack would have fed hydraulic fluid to function the BOP.²

Importantly, the ST Lock circuit leak on the blind shear ram sequence valve to ST Lock lock chamber confirms that the blind shear ram functioned. The blind shear ram BOP must be approximately 90% closed for the sequence valve to open and allow fluid to pass through to the ST Lock locking chamber. Thus, the presence of a leak on the lock system of the ST Lock circuit confirmed that the blind shear ram on this bonnet was activated and closed at least 90%.³

Test Ram Open-Side Function

The test ram was the lowermost ram and was used during function and pressure testing of the BOP stack. It was not used during well control and would not have had any impact on the incident.⁴

The Transocean subsea team reported the small volume test ram leak to BP as reflected in the Feb. 23, 2010, BP operations report.⁵ This report identified a leak on the yellow pod, and the rig crew switched to the blue pod to allow further investigation. The leak was confirmed to be on the open circuit to the test ram, and the leak was isolated by placing the test ram open circuit in the neutral, or “vent,” position.⁶ See *Figure 1*.

Upper Annular Close Circuit

On Feb. 19, 2010, a Transocean senior subsea supervisor identified a leak in the upper annular close circuit.⁷ During the post-incident intervention, the upper annular close circuit leak was identified on the hose fitting that connects the 10-gallon accumulator surge bottle to the close function of the upper annular BOP.⁸ The leak was detectable but very small. At 1,500 psi, the leak rate was determined to be approximately 0.1 gallons per minute (gpm).⁹

This leak would not have adversely affected the response time and sealing capability of the upper annular due to the large hydraulic supply that was continuously provided by the hydraulic conduit line being supplied by the Cameron Surface Control System that includes 45 40-gallon accumulators which were continuously replenished to a stored pressure of 5,000 psi.¹⁰

^A The BP investigation report identified a sixth possible leak but concluded that it would not have impacted performance. The Transocean investigation team does not agree that the evidence supports such a leak, but agrees that such a leak would not have impacted functionality.

Leak on Lower Annular

The *Deepwater Horizon* BOP stack had two annular BOPs: an upper annular and a lower annular. Each annular serves as a back-up for the other. The upper annular was rated to 10,000 psi.¹¹ In 2006, at the request of BP, the lower annular was outfitted with a stripping annular sealing element rated at 5,000 psi.¹² This stripping annular sealing element allowed the stripping of large 6-5/8-in. tool joints while pressure was contained by the closed annular.

The *Deepwater Horizon* senior subsea engineer noted a lower annular close function leak, confirming, however, that it was very small and that the annular BOP would still close when needed.¹³ The flow rate of the leak was confirmed to be similar to the leak on the upper annular at 0.1 gpm. The leak appeared as a “tick,” or a brief flickering indication, on the hydraulic fluid flow gauge located on the BOP control panel.¹⁴ The flow indication appeared only when the lower annular preventer was in the closed position, and the *Deepwater Horizon* subsea team did not identify any fluid leaking externally from the system.¹⁵ This leak would not have adversely affected the response time and sealing capability of the lower annular due to the large hydraulic supply that was continuously provided by the hydraulic conduit line being supplied by the *Deepwater Horizon* Cameron Surface Control System, including 45 40-gallon accumulators that were continuously replenished to a stored pressure of 5,000 psi.¹⁶

Lock Function on ST Lock Circuit

The ST Lock was hydraulically actuated and closed behind the tail rod of the ram operating piston to prevent the ram from opening even if close/lock pressure was lost.¹⁷ There were eight ST Locks on the *Deepwater Horizon* BOP stack, one lock on each side of the pressure containing rams. See Figure 1. A shuttle valve connected the eight ST Locks to their respective ram bonnets (one lock per bonnet). Each ram bonnet contained the operating piston and connecting rod used to activate the rams.¹⁸

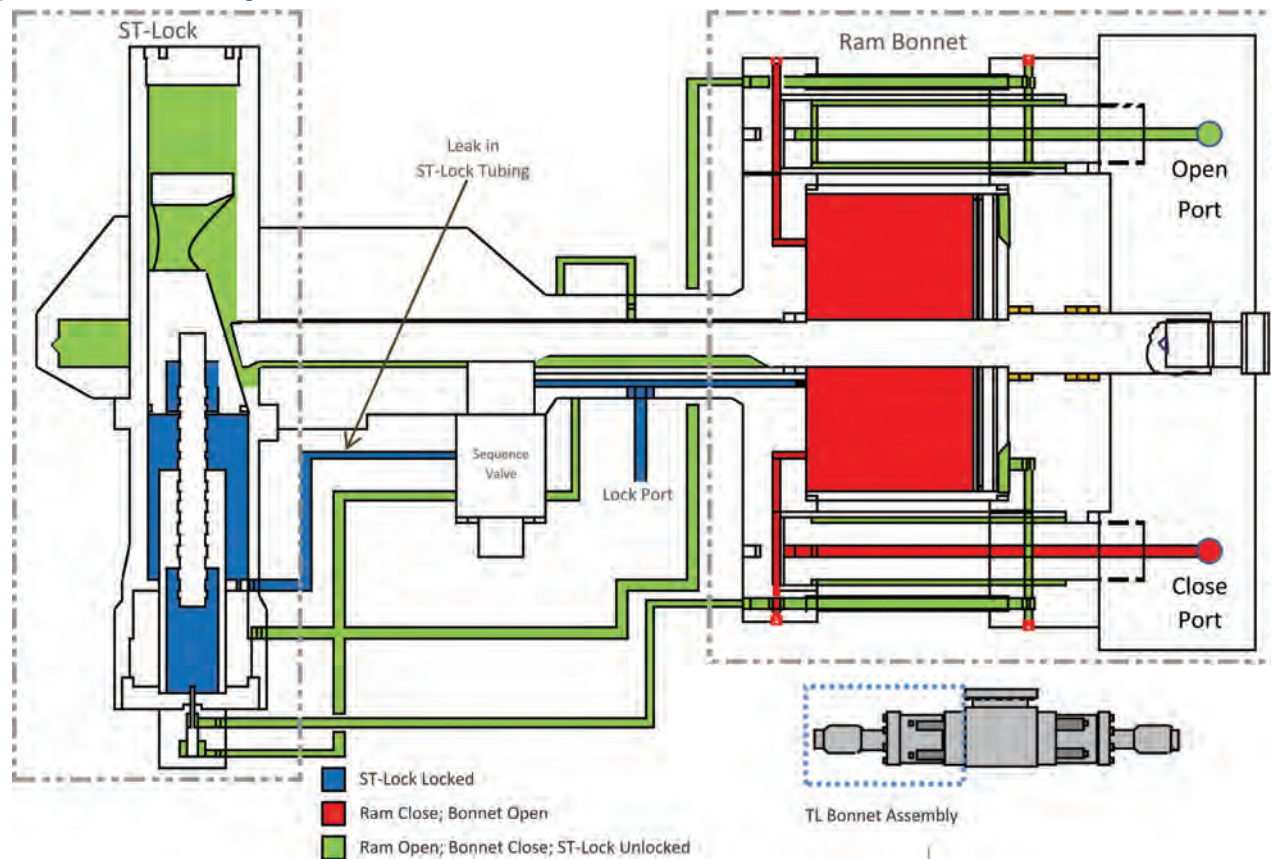


Figure 1 Leak in Sequence Valve Tubing on Shear Ram ST-Lock

Some of the specific firing and locking functions were plumbed (connected) together as a single function. In other words, whenever the remotely operated vehicle (ROV), automatic mode function (AMF) or auto-shear functions were fired on the pipe ram or shear ram circuits, the ST Lock locking function also was activated or pressurized.

During the post-incident response efforts, when the ROV functioned the pipe ram on the ROV intervention panel, a leak was noted on the lock function of the ST Lock circuit for the BOPs.¹⁹ The intervention team used an ROV to re-tighten the hose fitting to correct this leak.²⁰

Based on the ROV video, this leak was small and would not have prevented actuation of the pipe or shear rams. This leak in the ST Lock circuit would not have reduced the available hydraulic power provided by the BOP stack accumulators enough to prevent the blind shear rams from shearing the drill pipe and sealing the wellbore. Actuation of the AMF or auto-shear emergency modes would have properly operated the blind shear rams.²¹

Blind Shear Ram ST Lock Sequence Valve to ST Lock Chamber

A leak in the tubing connection that runs from the blind shear ram ST Lock sequence valve to the ST Lock chamber was identified on April 26, 2010, at 7:15 a.m.²² The BOP ram must be approximately 90% closed for the ST Lock sequence valve to open, allowing fluid to pass through to the ST Lock locking function, creating the conditions for a leak in this location. The existence of this leak confirms that the shear ram on this bonnet was closed. Further, based on the ROV video, this leak was small and would not have prevented the ST Lock function from operating.

1. Cameron Controls, Data Books, RBS 8D – Multiplex BOP Control System, Vol. 1, Reading & Bates Falcon *Deepwater Horizon* Project, October 2000, § 3, 254, 257-258, TRN-HCEC-00003804.
2. WEST Engineering Services, Accumulator Sizing Calculations, *Deepwater Horizon*, Feb. 11, 2011, Figure 2.
3. *Ibid.*
4. George Coltrin e-mail to Darrell Boudreaux, et al., Oct. 19, 2004, BP-HZN-BLY00056058.
5. Daily Operations Report, February 23, 2010, BP-HZN-MBI 135226.
6. Owen McWhorter e-mail to James Kent, June 25, 2010.
7. *Deepwater Horizon* SubSea Supervisor e-mail to *Deepwater Horizon* OIM, et al., Feb. 19, 2010.
8. Boa Sub C Log, May 1, 2010, at 11:15 a.m.
9. *Deepwater Horizon* SubSea Supervisor e-mail to *Deepwater Horizon* OIM, et al., Feb. 19, 2010.
10. Cameron Controls, Data RBS8-D – Multiplex BOP Control System, Vol. 1, Reading & Bates Falcon *Deepwater Horizon* Project, October 2000, § 3, 254, 257-258.
11. *Deepwater Horizon* TL BOP Stack Operation and Maintenance Manual, Initial Release, Rev. A, September 2000, Drawing No. SD034221, 14, Item 302.
12. Change Proposal, Proposal No.: SS-016, March 9, 2006.
13. ModuSpec USA, Rig Condition Assessment Report, *Deepwater Horizon*, Prepared for Transocean USA, Inc., April 1–12, 2010, 52.
14. Testimony of Mark Hay, Hearing before the *Deepwater Horizon* Joint Investigation Team, Aug. 25, 2010:246:10–247:17.
15. *Ibid.*
16. Cameron Controls, BKS RBS8-D, Multiplex BOP Control System Vol. 1, Reading & Bates Falcon *Deepwater Horizon* Project, October 2000, § 3, 254, 257-258.
17. Cameron Drilling Products, Stack Section, TL Blowout Preventer, ST-Locks, 2000, 1–6.
18. Cameron Drilling Products, Stack Section, TL Blowout Preventer, ST-Locks, 2000, 1-6; Vastar Resources, Inc. and R&B Falcon Drilling Co., Exhibit B-2 of Drilling Contract RBS-8D, Semisubmersible Drilling Unit, Contract No. 980249, Dec. 9, 1998, 32, 33.
19. Boa Sub C Log, April 25, 2010 at 8:16 p.m.
20. Boa Sub C Log, April 26, 2010 between 12:02 a.m. and 3:48 a.m.
21. *Deepwater Horizon* Accident Investigation Report, Sept. 8, 2010.
22. Boa Sub C Log, April 26, 2010 at 7:15 a.m.

Appendix L Drill Pipe in the BOP

The location of the drill pipe in the *Deepwater Horizon* BOP stack at the time of the incident has been established. It has been confirmed by comparing the measured height between the five ram preventers and the two annular preventers in the BOP stack to the measured length of recovered drill pipe sections, and by the distinctive markings or damage to the drill pipe.

When the recovered drill pipe lengths and locations were examined they confirmed that, at the time of the incident:

- The flow-washed drill pipe tool joint was in the upper annular;
- The upper and middle variable bore pipe rams were closed; and
- The blind shear rams cut the drill pipe.¹

The sections of drill pipe recovered from the *Deepwater Horizon* BOP stack and the recovered marine riser section from above the BOP stack were photographed, cleaned, inspected, re-photographed, and the lengths measured by the Det Norske Veritas (DNV) at the NASA Michoud Assembly Facility (Michoud) in New Orleans.² The sections were then laid out and placed in order for comparison.³ See *Figure 6 and Table 1*.

A. Drill Pipe Section “AA”: Upper Annular to Blind Shear Rams

Drill pipe section AA consists of three pieces of drill pipe that were located in the BOP stack between the upper annular and the blind shear rams. These three drill pipe sections are identified below as “AA-1,” “AA-2” and “AA-3.” The total measured length of these drill pipe sections is 234 in. The dimension from the bottom of the upper annular element to the middle of the blind shear rams in the BOP stack is 234 in., confirming the tool joint was partially in the upper annular when the drill pipe was cut by the blind shear rams. Refer to A and AA in *Figure 6 and Table 1*.

The top of drill pipe (section AA) includes the flow-washed tool joint that was eroded in the upper annular. The bottom of section AA was cut by the blind shear rams. The bottom of section AA was found resting upon the top of the upper annular element indicating it was ejected upward through the upper annular by the well flow. This section of drill pipe was fixed in place in the marine riser where the riser folded over and “kinked” as the *Deepwater Horizon* sank 36 hours after the first explosion. Refer to *Figures 1 and 2*.

During the intervention operations, on June 2, 2010, a band saw cut partially through the riser before becoming stuck. The lower portion of drill pipe section AA was cut by the saw creating AA-3. Sections AA-1 and AA-2 remained as one piece, captured in the riser kink.

Subsequently, on June 3, 2010, a subsea shearing device (scissor) cut the riser and drill pipe creating sections AA-1 and AA-2. See *Figures 2, 3, and 4 below*.

Drill Pipe Section AA-1: Tool Joint Connection Shoulder (at Flow-wash End) to the Riser Scissor Cut

Section AA-1 is 111.5 in. long from the tool joint connection shoulder to the sheared bottom.^A It was captured in the riser “kink” and then removed from the recovered riser at Michoud on Jan. 20, 2011.⁴ See *Figures 1, 2 and 3*.⁵

Drill Pipe section AA-2: Riser Scissor Cut to Saw Cut Section

Section AA-2 is 7.5 in. long and was created when the scissor cut through the drill pipe above the saw cut. When cut, section AA-2 dropped and landed on top of the upper annular element. It was recovered later from above the upper annular element in the BOP stack onboard the *Q4000* on Sept. 6, 2010.⁶ Section AA-2 has a shear-cut top and a saw-cut bottom.⁷

A When the drill pipe was removed from the recovered riser section at Michoud in January 2011, it was found that section AA-1 had broken in two parts at the riser “kink” approximately 30 in. from the bottom where the riser was sheared. The measured length of 111.5 in. includes both parts of section AA-1 recovered from the riser section.

Drill Pipe Section AA-3: Section Recovered From Above the Upper Annular in the LMRP

Section AA-3 is 109 in. long and was created when the band saw cut through the drill pipe. When cut, section AA-3 dropped and landed on top of the upper annular element. It was recovered later from above the upper annular in the BOP stack on board the *Q4000* on Sept. 6, 2010.⁸ Section AA-3 has a saw-cut top and a sheared and deformed bottom.⁹

Dimension XX: Start of the Flow-wash Damage to the Tool Joint Connection Shoulder

Dimension XX is the distance above the AA-1 tool joint connection shoulder to where the flow-wash damage starts on section EE-3. This distance is 6 in. above the tool joint connection shoulder. This distance is the length of drill pipe between the bottom of the upper annular and the center of the blind shear rams. See *Figure 1*.

B. Drill Pipe Section BB: Blind Shear Rams to the Casing Shear Rams

The length of the drill pipe section recovered from below the blind shear rams resting on the casing shear rams is 42 in. and identified as drill pipe section BB.¹⁰ This section was later removed from the BOP on board the *Q4000* on Sept. 6, 2010.¹¹ The distance between the center of the blind shear rams to the center of the casing shear rams in the BOP is 43.5 in. See *Figure 6 and Table 1*. This confirms drill pipe section BB was cut by the blind shear rams and the casing shear rams.

C. Drill Pipe Section CC: Casing Shear Rams to the Lower Pipe Rams (Test Rams)

The length of the drill pipe section recovered from below the casing shear rams and above the test rams is 142 in. and identified as drill pipe section CC. This section was removed from the BOP at Michoud on Dec. 16, 2010.¹² The dimension from the center of the casing shear rams to the center of the lower test rams in the BOP is 142 in., confirming the drill pipe was cut by the casing shear rams and was positioned in the upper variable bore rams, middle variable bore rams and test rams. See *Figure 6 and Table 1*. The bottom of section CC ends at the center of the lower test rams, where it was washed away. There are clear and obvious flow-wash areas on section CC where the upper variable bore rams and middle variable bore rams were closed on the drill pipe.¹³

D. Drill Pipe Dimension DD: Upper Annular to the Lower Pipe Rams (Test Rams)

Dimension DD is 418 in., representing the total length of drill pipe sections AA, BB, and CC, as shown in *Table 1*. The dimension from the bottom of the upper annular element to the center of the lower test rams in the BOP is 420 in. See *Figure 6 and Table 1*. This confirms the location of the drill pipe at the time of the incident.

E. Drill Pipe Section EE: Drill Pipe Tool Joint in the Recovered Riser to Drill Pipe Section A Tool Joint

The measured length of the drill pipe sections for dimension EE is 551 in. This represents the total length of drill pipe sections EE-1, EE-2, and EE-3, as shown in *Table 1*. The nominal length of a joint of 5.5-in. S-135 drill pipe is 552 in. (46 ft.) with a variance of plus or minus 6 in.^B See *Figure 6 and Table 1*. The location of the tool joints that were fixed in place by the riser kink confirms the location of the drill pipe inside the BOP at the time of the incident.

^B S-135 is a designation of the material strength and properties of drill pipe.

Section EE was captured in the marine riser in a kink above the BOP when the riser folded over as the *Deepwater Horizon* sank 36 hours after the first explosion. On June 3, 2010, a scissor tool was used to cut the riser and drill pipe.¹⁴ As a result, EE-1 was created above the scissor cut, and EE-2 was created below the scissor cut.

Drill Pipe Section EE-1: Upper Section of Drill Pipe Recovered from the Riser Joint Above the BOP Stack

Drill pipe section EE-1 is 388 in. long and is continuous from top to bottom with both ends scissor cut. See *Figures 2 and 3*. Section EE-1 is measured from the drill pipe tool joint connection shoulder, located in the upper end of the riser, to the bottom scissor-cut end. Section EE-1 was removed from the recovered riser section at Michoud on Jan. 20, 2011.¹⁵ Section EE-1 has a tool joint connection on top, a scissor cut on bottom, is bent 30 in from the bottom at the riser kink, and is bent (“corkscrewed”) and flattened in the section above the riser kink.¹⁶

Drill Pipe Section EE-2: Section of Drill Pipe Recovered from Inside the Deepwater Horizon BOP Upper Annular BOP

Section EE-2 is 136 in. long and is bent in a long sweeping bend. It has a scissor-cut top and a flow-washed and deformed bottom that aligns with the flow-washed top of drill pipe section A.¹⁷ See *Figures 1, 2 and 5*.

Drill pipe sections AA-1 and EE-2 were created when the *Deepwater Horizon* lost power and started to drift off location, parting the drill pipe at its weakened section. Approximately 30 minutes later, the travelling block fell, dropping approximately 5,000 ft. of drill pipe onto the partially closed annular element.¹⁸ The bottom of the drill pipe, section EE-2, landed on top of the upper annular element.

When the riser flange was removed from the top of the BOP stack on July 11, 2010, section EE-2 was visible with hydrocarbon flow coming out of the top.¹⁹ During drill pipe fishing operations, the upper section of the BOP stack was inspected with a bore-scope camera on Aug. 26, 2010. The upper annular element was closed and section EE-2 was in the opening of the element.²⁰ An attempt was made to recover section EE-2 from the top of the BOP stack. When the fishing tool touched the top of section EE-2, it dropped down through the upper annular element, stopping at the scissor-cut top where the pipe is flattened and wider.²¹ Section EE-2 was later recovered out of the *Deepwater Horizon* upper annular element at Michoud on Nov. 24, 2010.

Drill Pipe Section EE-3: Tool Joint Connection Shoulder to Top of Flow-washed Drill Pipe

Drill pipe section EE-3 measures 17.5–20.5 in. and is connected to the top of drill pipe section AA at the tool joint.²² For comparison, the height of a Cameron DL Annular element is 18 in., confirming the annular was closed on this section of pipe and tool joint. Section EE-3 was removed from the recovered riser section at Michoud on Jan. 20, 2011. See *Figures 1 and 2*.

F. Dimension XX - Start of the Flow-wash Damage to the Tool Joint Connection Shoulder

Dimension XX is part of drill pipe section EE-3 and is referenced to identify the distance from the tool joint connection to where the flow-wash damage starts, 6 in. above the tool joint connection shoulder. See *Figure 1*.

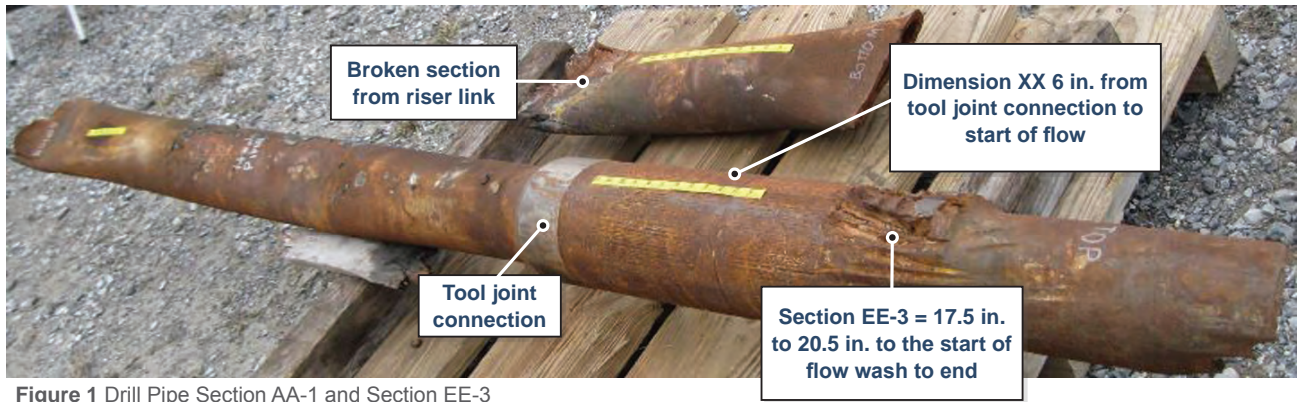


Figure 1 Drill Pipe Section AA-1 and Section EE-3

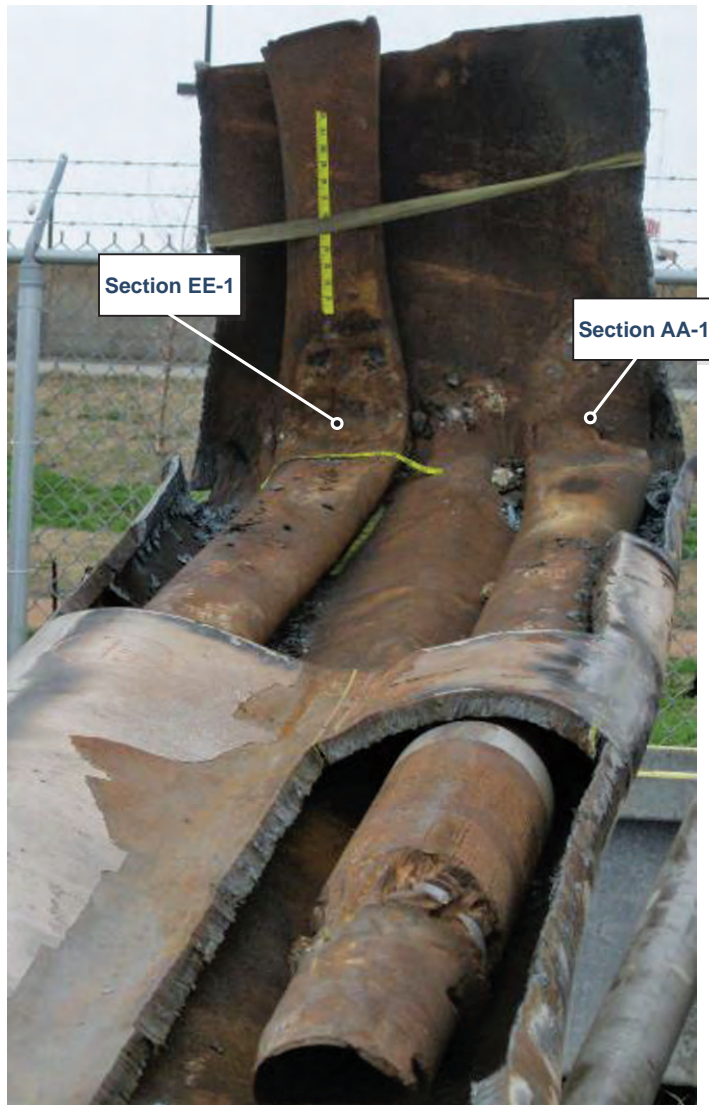


Figure 2 Drill Pipe in the Recovered Riser Section at the Kink End with the Drill Pipe Sections EE-1, AA-1 (with EE-3 Attached)

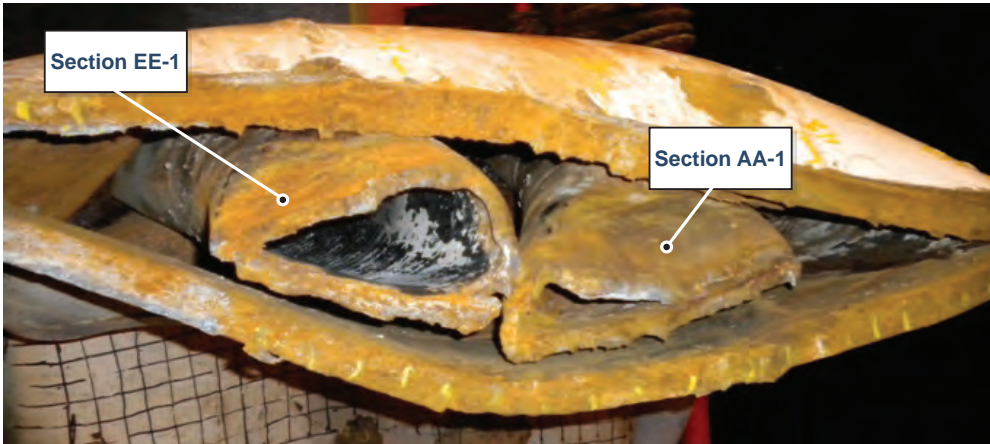


Figure 3 Sheared Section of the Recovered Riser at the Lower Kink End with the Drill Pipe Sections EE-1 and AA-1

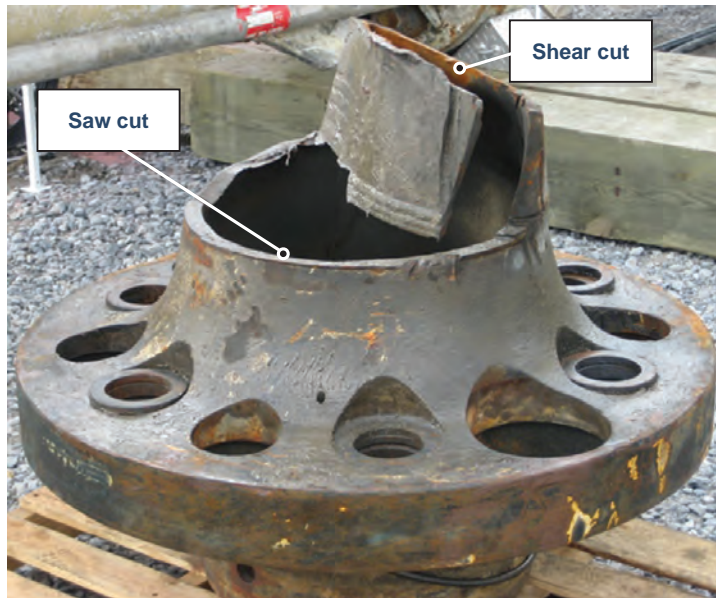


Figure 4 Riser Flange from Above the *Deepwater Horizon* BOP with the Partial Saw Cut and the Final Shear Cut

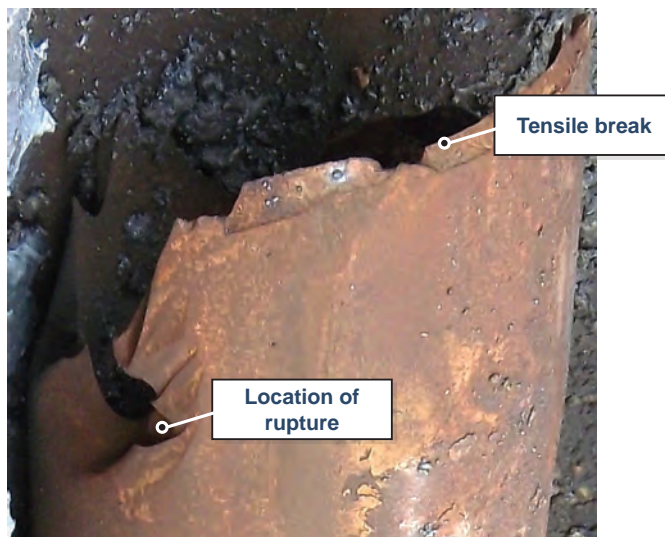


Figure 7 Failed End of Drill Pipe – Top of Section EE-3 Showing Location of the Rupture and the Tensile Break

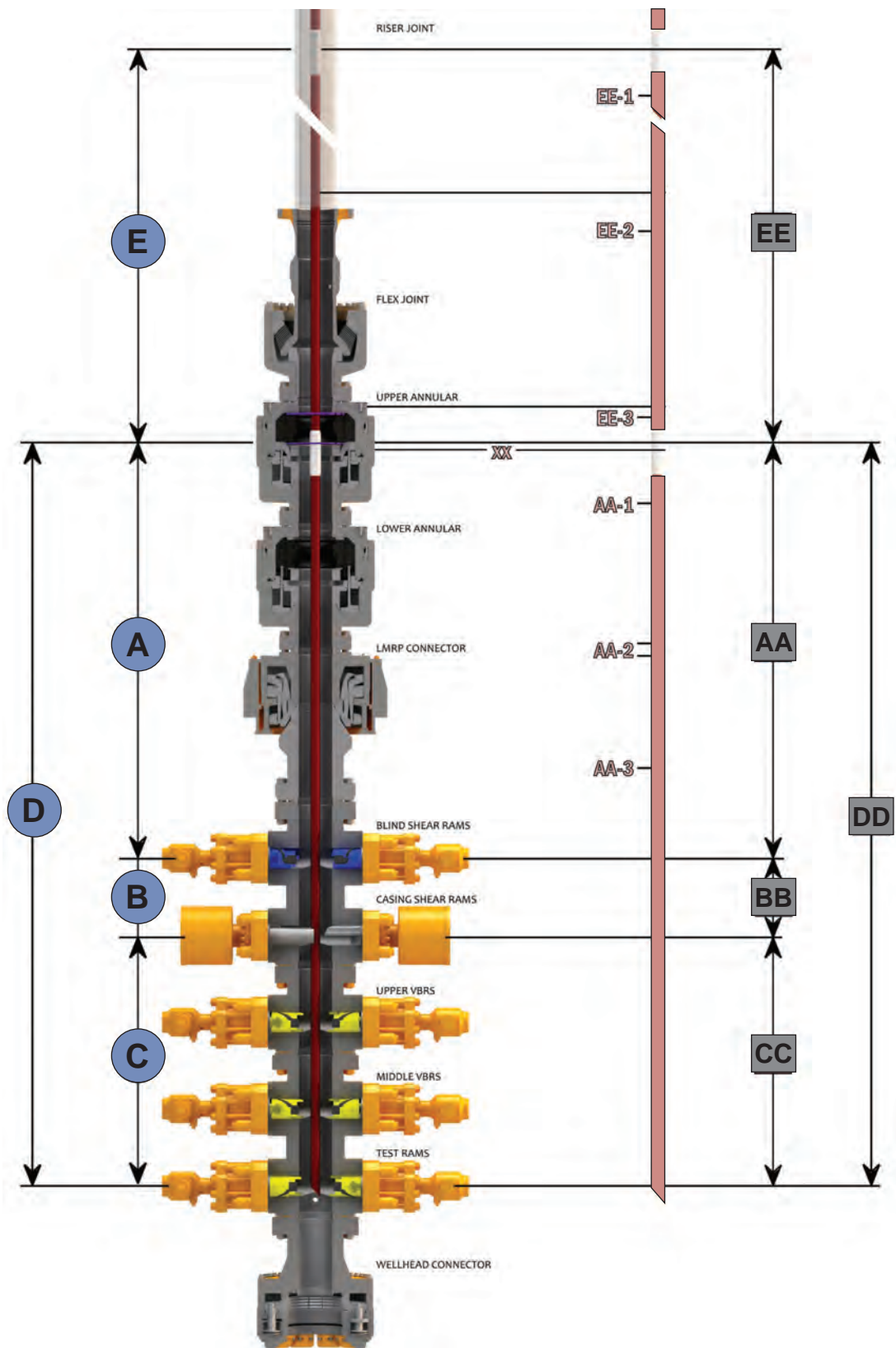


Figure 6 DWH BOP with the Drill Pipe in the Position at the Time of the Incident

Appendix L Drill Pipe in the BOP

#	Description	Length (inches)
A	Bottom of upper annular element to the center of the blind shear ram	234
XX	Start of the flow-wash damage to the tool joint connection break	6
AA-1	Tool joint connection break at flow-wash end to the riser shear cut	111.5
AA-2	Riser shear cut to saw cut section	7.5
AA-3	Section recovered from inside the upper annular in the <i>Deepwater Horizon</i> LMRP	109
AA	Total length of drill pipe section	234
B	Center of the blind shear ram to center of casing shear ram	43.5
BB	Section recovered from below the BSR and above the CSR	42
C	Center of the casing shear ram to the center of the lower test rams	142
CC	Section recovered from below the CSR that extends to the lower test rams	142
D	Bottom of upper annular element to the center of the lower test rams	420
XX	Tool joint connection to the start of the flow-wash damage on the tool joint	6
AA-1	Upper tool Joint connection break at flow-wash end to riser shear cut	111.5
AA-2	Riser shear cut to saw cut section	7.5
AA-3	Section recovered from inside the upper annular in the <i>Deepwater Horizon</i> LMRP	109
BB	Section recovered from below the BSR and above the CSR	42
CC	Section recovered from below the CSR that extends to the lower test rams	142
DD	Total length of drill pipe section (AA + BB + CC)	418
E	Nominal length of the <i>Deepwater Horizon</i> S-135 Drill Pipe = (+/- 6 inches)	552
EE-1	Upper section recovered from the riser joint above the BOP	388
EE-2	Section recovered from inside the upper annular in the <i>Deepwater Horizon</i> LMRP	136
EE-3	Flow-washed tool joint connection to failed end	27
EE	Total length of upper drill pipe section	551

Table 1

1. DNV, Forensic Examination of *Deepwater Horizon* Blowout Preventer, March 20, 2011.
2. *Ibid.*
3. *Ibid.*
4. Riser Drill Pipe Dimension Sketch, Sept. 15, 2010, Revised by Geoff Boughton, Dec. 4, 2010.
5. DNV Metallurgical Examination and testing of Drill Pipe, Feb. 3, 2011.
6. *Ibid.*
7. DNV, Forensic Examination of *Deepwater Horizon* Blowout Preventer, March 20, 2011.
8. DNV Metallurgical Examination and testing of Drill Pipe, Feb. 3, 2011.
9. The inspection of this section indicates it was sheared by the blind shear rams. DNV, Forensic Examination of *Deepwater Horizon* Blowout Preventer, March 20, 2011.
10. DNV, Forensic Examination of *Deepwater Horizon* Blowout Preventer, March 20, 2011.
11. DNV Metallurgical Examination and testing of Drill Pipe, Feb. 3, 2011.
12. *Ibid.*
13. DNV, Forensic Examination of *Deepwater Horizon* Blowout Preventer, March 20, 2011.
14. Transocean operations report from BP ERC, June 3, 2010.
15. DNV, Forensic Examination of *Deepwater Horizon* Blowout Preventer, March 20, 2011; DNV Metallurgical Examination and Testing of Drill Pipe, Feb. 3, 2011.
16. DNV, Forensic Examination of *Deepwater Horizon* Blowout Preventer, March 20, 2011.
17. *Ibid.*
18. *Ibid.*
19. DNV, Forensic Examination of *Deepwater Horizon* Blowout Preventer, March 20, 2011.
20. *Ibid.*
21. *Ibid.*
22. *Ibid.*

Appendix M
Structural Analysis of the Macondo
#252 Work String



Structural Analysis of the Macondo #252 Work String

SES Document No.: 1101190-ST-RP-0003

Prepared for:
Transocean Offshore Deepwater Drilling, Inc.

REV	DATE	DESCRIPTION	ORIGINATOR	REVIEWER	APPROVER
B	26-May-11	Issued for Client Review	DLG	DJK/BL	
A	23-May-11	Issued for Internal Review	DLG	N/A	N/A

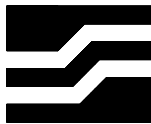
Structural Analysis of the Macondo #252 Work String

SES DOCUMENT NO.: 1101190-ST-RP-0003

Prepared By: David L. Garrett
David L. Garrett, Ph.D.
Principal

Reviewed By: Daniel Kluk
Daniel Kluk
Associate

Bisen Lin
Bisen Lin
Senior Analyst



Stress Engineering Services, Inc.
13800 Westfair East Drive
Houston, Texas 77041-1101
281-955-2900 / www.stress.com

MAY 2011

EXECUTIVE SUMMARY

Transocean Offshore Deepwater Drilling, Inc., (Transocean) retained Stress Engineering Services, Inc. (SES) to provide technical assistance in their investigation of the blowout that occurred April 20, 2010. Hydraulic analysis, reported elsewhere, indicates that well flow after 21:39 CDT could result in a net upward force in the work string at the level of the Blowout Preventer (BOP). Transocean requested that SES provide structural modeling of the work string and calculations that may help in understanding the behavior of the work string. Structural modeling, assumptions and results of calculations are presented here.

A record of the lengths of individual components in the work string (called a tally) was not available. Therefore, the structural model is somewhat idealized since individual component lengths and the vertical position of the top tool joint, were not available. The component lengths used in the hydraulics analysis were used in the structural model. Pipe joint lengths for each size were assumed equal. The average length used is close to the nominal length of the pipe joint. The structural modeling results are representative and are suitable for understanding the behavior of the work string under various loading conditions.

Load cases were selected based on estimates of effective compression in the pipe near the BOP. Calculations were performed for effective compression up to 150 kips. Two configurations were analyzed in sequence: (1) all BOP elements in the BOP stack are open, and (2) a simulation of closure of the upper annular and the upper variable bore ram (VBR). At the beginning of the simulation, one 5-1/2" tool joint is in the BOP. Vertical displacement of the tool joint, contact loads between the work string and the riser, BOP and casing, and stresses in the work string are of interest.

The work string deforms into a helical configuration in contact with the inside of the riser, the BOP and the casing. Only a portion of the 6-5/8" (upper section of the work string) deforms into a helical configuration; the amount depends on the force applied.

The calculated vertical displacement of the tool joint in the BOP is less than seven feet. Temperature effects, which were not included, would serve to reduce the vertical displacement.

Calculated contact loads between the work string and the inside of the BOP are less than 10 kips. This is the force that would be required to move the pipe away from the wall of the BOP. Calculated stress in the work string is less than yield for all cases.

DNV's forensic investigation indicated that the tool joint in the BOP was partially in the upper annular when the pipe was sheared. In the idealized structural model, the tool joint in the BOP does not reach the elevation of the upper annular due to the applied hydraulic loads. However, the discrepancy in elevation is within the error of the idealized model.

LIMITATIONS OF THIS REPORT

The scope of this report is limited to the matters expressly covered. This report is prepared for the sole benefit of Transocean Offshore Deepwater Drilling, Inc. (“Transocean”). In preparing this report, Stress Engineering Services, Inc. (SES) has relied on information provided by Transocean. Stress Engineering Services, Inc. (SES) has made no independent investigation as to the accuracy or completeness of such information and has assumed that such information was accurate and complete. Further, Stress Engineering Services, Inc. (SES) is not able to direct or control the operation or maintenance of client’s equipment or processes.

All recommendations, findings and conclusions stated in this report are based upon facts and circumstances, as they existed at the time that this report was prepared. A change in any fact or circumstance upon which this report is based may adversely affect the recommendations, findings, and conclusions expressed in this report.

NO IMPLIED WARRANTY OF MERCHANTABILITY OR FITNESS FOR A PARTICULAR PURPOSE SHALL APPLY. STRESS ENGINEERING SERVICES, INC. MAKES NO REPRESENTATION OR WARRANTY THAT THE IMPLEMENTATION OR USE OF THE RECOMMENDATIONS, FINDINGS, OR CONCLUSIONS OF THIS REPORT WILL RESULT IN COMPLIANCE WITH APPLICABLE LAWS OR PERFECT RESULTS.

TABLE OF CONTENTS

	<u>Page No.</u>
EXECUTIVE SUMMARY	III
LIMITATIONS OF THIS REPORT	V
1 INTRODUCTION.....	1
2 WORK STRING MODEL	3
3 LOADING	6
4 RESULTS FOR DRAG LOAD CASES.....	7
5 RESULTS FOR VBR LOAD CASES	11
6 CALCULATED STRESS.....	14

APPENDICES

	<u>Page No.</u>
Appendix A: Work String Model	16
Appendix B: Beam Model	20
Appendix C: Discussion of Loads	25
Appendix D: Modeling a Helix.....	32

LIST OF TABLES

	<u>Page No.</u>
Table 1: Selected Load Cases	6
Table 2: Maximum Calculated Axial Plus Bending Stress for Load Cases	14

LIST OF FIGURES

	<u>Page No.</u>
Figure 1: Diagram of Macondo #252, April 20, 2010	4
Figure 2: Initial configuration of pipe near BOP	5
Figure 3: Effective Tension for Five Drag Load Cases	7
Figure 4: Deformed Shape of 5-1/2" Drill Pipe.....	8
Figure 5: Deformed Shape of 5-1/2" Drill Pipe near the BOP	8
Figure 6: Upward Displacement for a Range of Drag Loads	9
Figure 7: Tool Joint Contact Loads for a Range of Drag Loads.....	10
Figure 8: Effective Tension for Four VBR Load Cases	11
Figure 9: Shape with Annular and VBR Closed.....	12
Figure 10: Shape between Annular and VBR.....	12
Figure 11: Contact Load between Annular and VBR.....	13

1 INTRODUCTION

Transocean Offshore Deepwater Drilling, Inc., (Transocean) retained Stress Engineering Services, Inc. (SES) to provide technical assistance in their investigation of the blowout that occurred April 20, 2010. Hydraulic analysis, reported elsewhere, indicates that well flow after 21:39 CDT could result in a net upward force in the work string at the level of the Blowout Preventer (BOP). Transocean requested that SES provide structural modeling of the work string and calculations that may help in understanding the behavior of the work string. Structural modeling, assumptions and results of calculations are presented here.

A record of the lengths of individual components in the work string (called a tally) was not available. Therefore, the structural model is somewhat idealized since individual component lengths and the vertical position of the top tool joint, were not available. The component lengths used in the hydraulics analysis were used in the structural model. Pipe joint lengths for each size were assumed equal. The average length used is close to the nominal length of the pipe joint. The structural modeling results are representative and are suitable for understanding the behavior of the work string under various loading conditions.

Load cases were selected based on estimates of effective compression in the pipe near the BOP. Calculations were performed for effective compression up to 150 kips. Two configurations were analyzed in sequence: (1) all BOP elements in the BOP stack are open, and (2) a simulation of closure of the upper annular and the upper variable bore ram (VBR). At the beginning of the simulation, one 5-1/2" tool joint is in the BOP. Vertical displacement of the tool joint, contact loads between the work string and the riser, BOP and casing, and stresses in the work string are of interest.

Numerical modeling of the work string is described in Appendix A. Structural calculations are performed with RAMS, SES' proprietary software [1]. A simplified beam model of the pipe between the annular and the VBR is described in Appendix B, together with results for the selected load cases. The beam model is similar to that described in the DNV report [3]. Calculations for the load cases are described in Appendix C. Modeling an ideal helix is

presented in Appendix D. Comparisons to numerical modeling and equations that may be useful in associated analytical calculations are presented.

2 WORK STRING MODEL

The work string configuration used for structural analysis is the same as that used for hydraulic analysis [2]. A diagram of the well is in Figure 1, taken from [2]. A record of the lengths of individual components in the work string (called a tally) was not available. The component lengths used in the hydraulics analysis were used in the structural model. Pipe joint lengths for each size were assumed equal.

With these assumptions, the center of the 5-1/2" tool joint in the BOP is at 5,021 ft RKB. Two 5-1/2" drill pipe joints span the BOP (joints 20 and 21 below the 6-5/8"). The vertical location of the tool joint is uncertain, due to uncertainty in joint lengths and uncertainty regarding the vertical position of the top of the model. The model assumes a 6-5/8" tool joint at the drill floor. The tool joint would more likely be a few feet above the drill floor so slips can be set on the pipe. The initial configuration of the work string near the BOP is illustrated in Figure 2. In the figure, the horizontal scale is amplified by a factor of 10. Locations of the elements of the BOP are shown.

Details of the RAMS model are in Appendix A.

A model of only the portion of the work string between the upper annular and the upper VBR was also developed. The configuration is similar to that shown in Figure 127 of [3]. The model does not include the effects of the work string above the upper annular or below the upper VBR. Details of the model are in Appendix B.

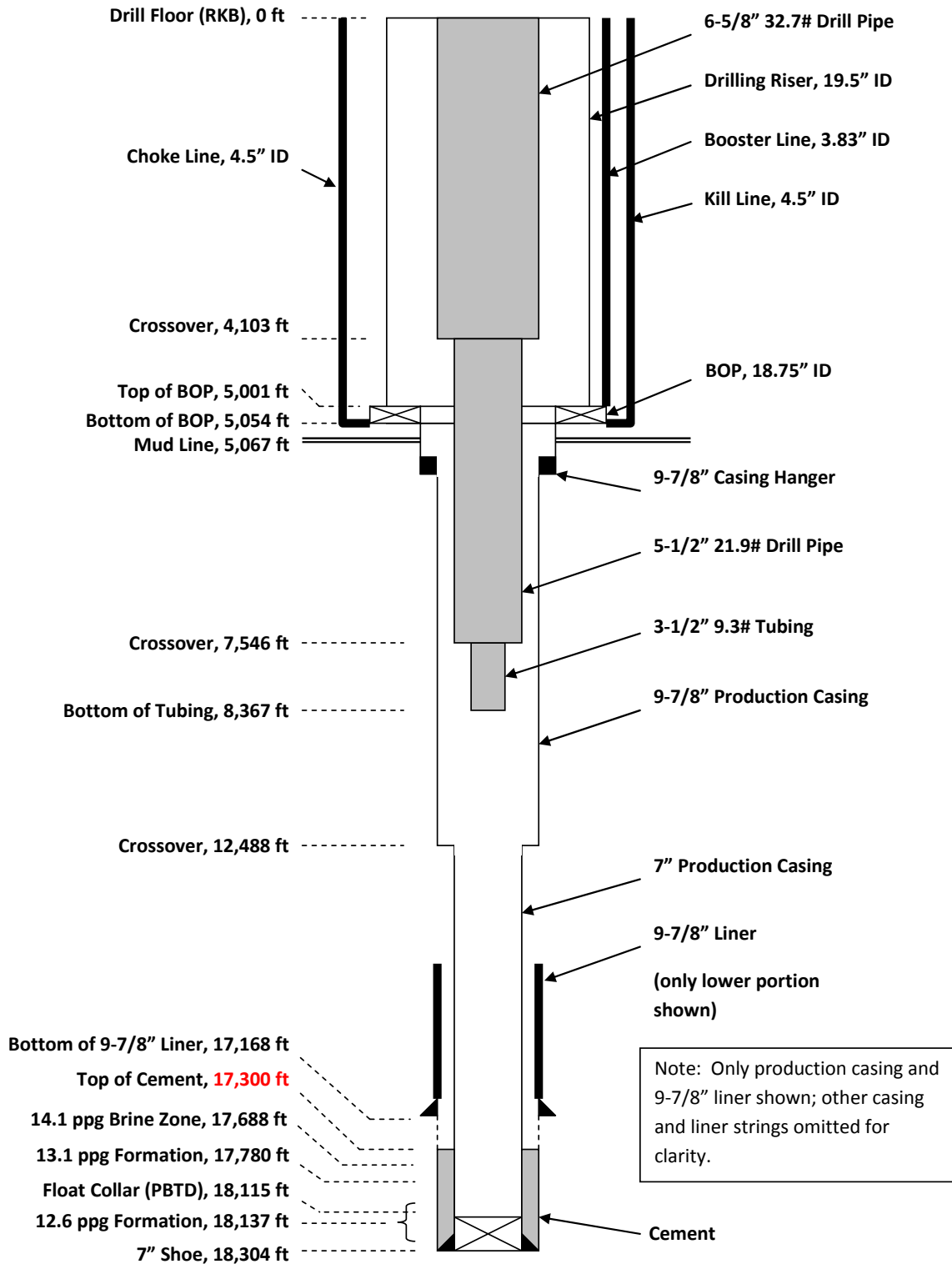


Figure 1: Diagram of Macondo #252, April 20, 2010

Initial configuration

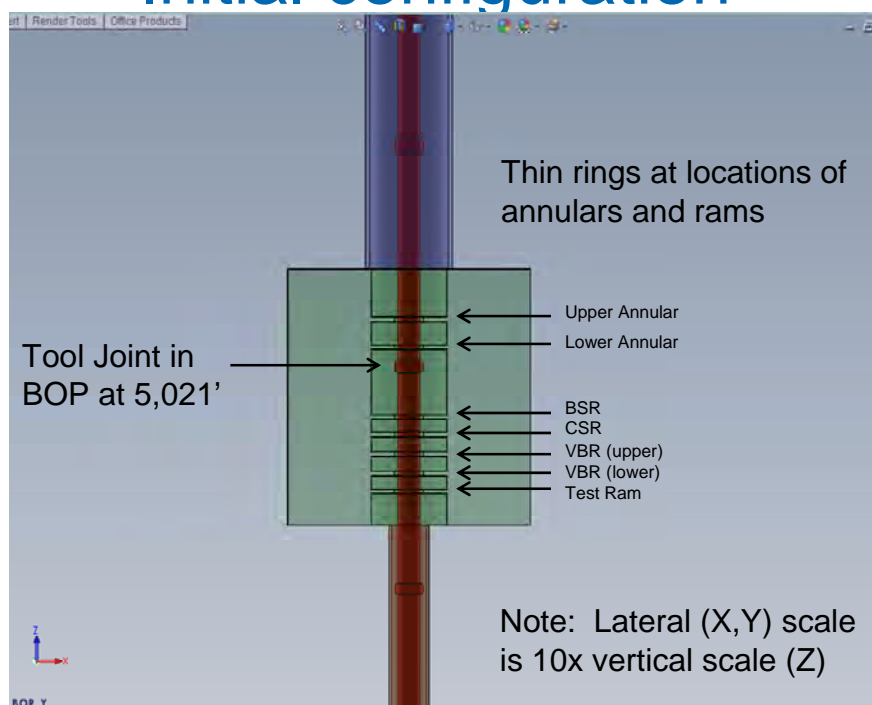


Figure 2: Initial configuration of pipe near BOP

3 LOADING

Prior to closure of the variable bore ram (VBR), flow up the annulus between the work string and the casing produced an upward force on the work string that may have exceeded the weight of the work string below the VBR (see 4.7.6 of [2]). The flow rate, and consequently the upward force, was increasing rapidly. The net upward force would cause the tool joint in the BOP to move up.

When the annular closed, it did not stop the flow and flow rate continued to increase until the VBR was closed [2]. Flow stopped when the VBR closed. The pressure below the VBR increased as the well approached shut in conditions. At the same time, the pressure above the VBR was dropping due to expansion of the hydrocarbons in the riser.

Two sets of load cases were selected: (1) drag loading prior to closure of the VBR, and (2) loading due to the pressure differential across the VBR after closure of the VBR. The load cases are described by the level of compression in the work string at the BOP. The selected load cases are listed in Table 1.

Table 1: Selected Load Cases

Case	Compression at BOP, kips				
Drag	30	60	90	120	150
VBR	NA	60	90	120	150

Details of the load cases, including associated calculations, are in Appendix C. The range of load cases is intended to bound loads that may have occurred.

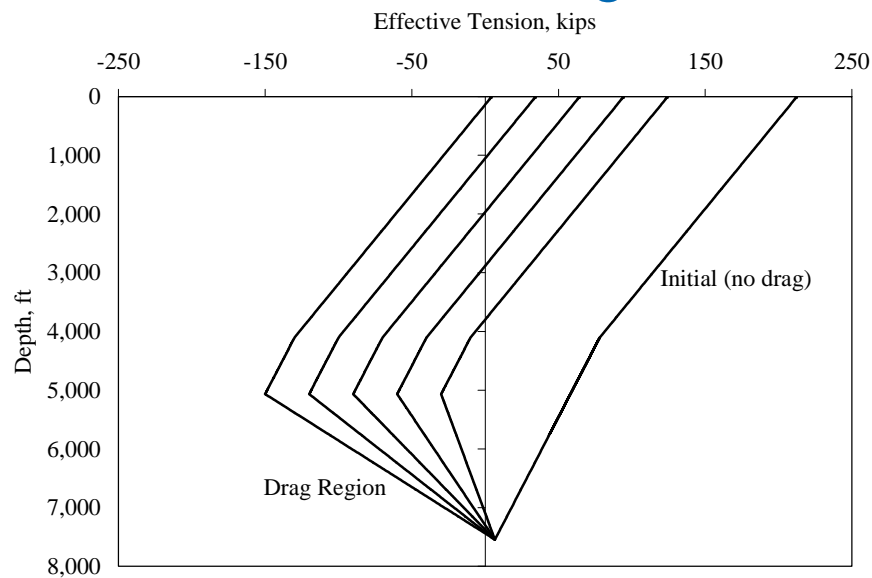
Drag loads were applied to the RAMS model, starting with 30 kips and increased to the maximum of 150 kips. To simulate closing the annular, the center of the tool joint in the BOP was moved to the centerline of the BOP. To simulate closing the VBR, a point below the tool joint was moved to the centerline of the BOP. The distance between the two points was selected to represent the distance between the upper annular and the upper VBR (27.3 ft). The load was then decreased from the maximum of 150 kips to the minimum of 60 kips.

The VBR loads were also applied to the reduced model in Appendix B.

4 RESULTS FOR DRAG LOAD CASES

The effective tension distributions for the five drag load cases are in Figure 3 (and Appendix C).

Effective tension for drag load cases

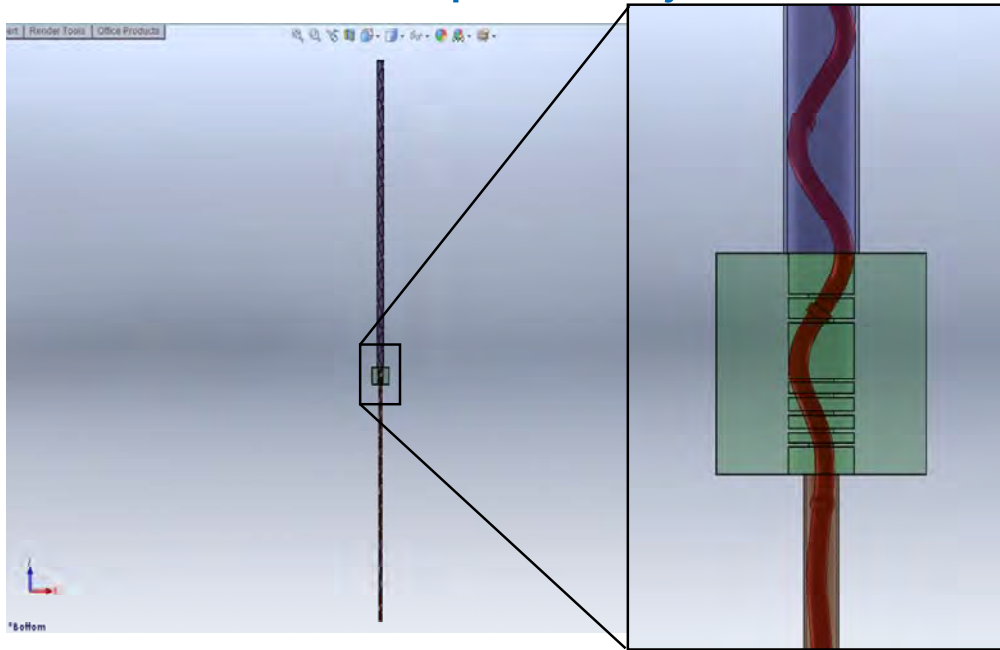


Pipe below the neutral point (effective tension = 0) will contact the wall and form a helix

Figure 3: Effective Tension for Five Drag Load Cases

The maximum compression (negative tension) occurs at the first tool joint below the BOP. The pipe that is in compression will contact the wall (of the production casing, the BOP, or the riser) and form a helix. All of the 5-1/2" drill pipe is in compression for all cases. Varying amounts of the 6-5/8" drill pipe are in compression. The deformed shape of 36 joints of the 5-1/2" is illustrated in Figure 4. A closer look near the BOP is in Figure 5. The pitch of the helix is close to the height of the BOP (53 ft).

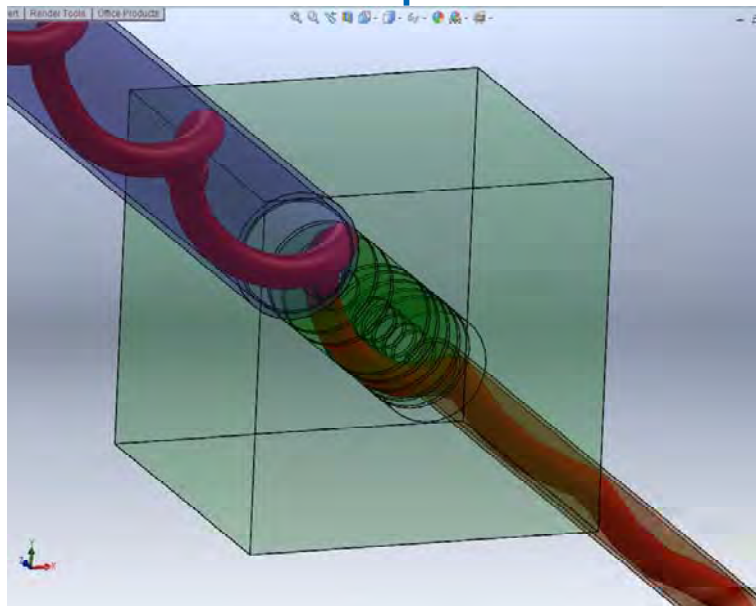
Deformed shape – 36 joints of 5-1/2”



Drag load case 120 kips at BOP

Figure 4: Deformed Shape of 5-1/2” Drill Pipe

Deformed shape near BOP



Drag load case 120 kips at BOP

Figure 5: Deformed Shape of 5-1/2” Drill Pipe near the BOP

Drag loads on the work string cause the pipe to displace upward. Calculated upward displacements for a range of loads are in Figure 6. Tool joint contact forces are in Figure 7. If the annular closed on a tool joint, then the tool joint was probably a few feet below the annular prior to 21:39. The pipe was in contact with the inside of the BOP, riser and casing. Closing the annular would result in a horizontal force on the annular. If the tool joint restricted further upward motion, the pipe above the annular would retain the helical shape just prior to closure. The pipe below the annular would continue to have increasing compression and be in contact with the wall.

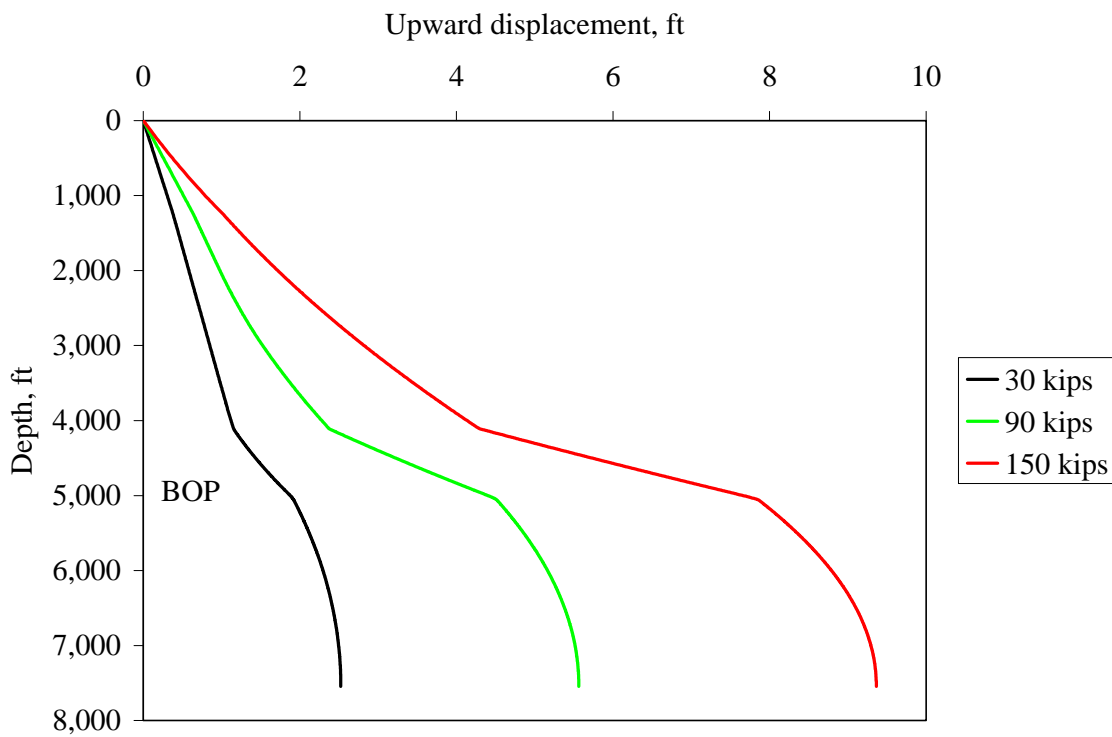


Figure 6: Upward Displacement for a Range of Drag Loads

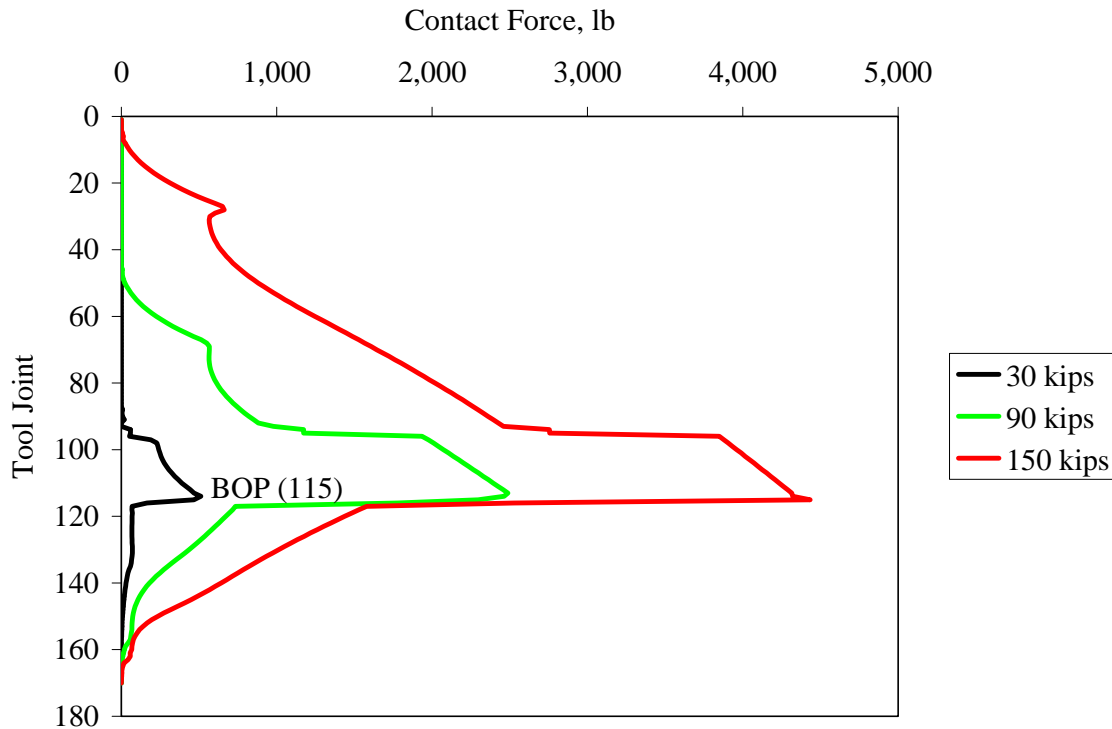
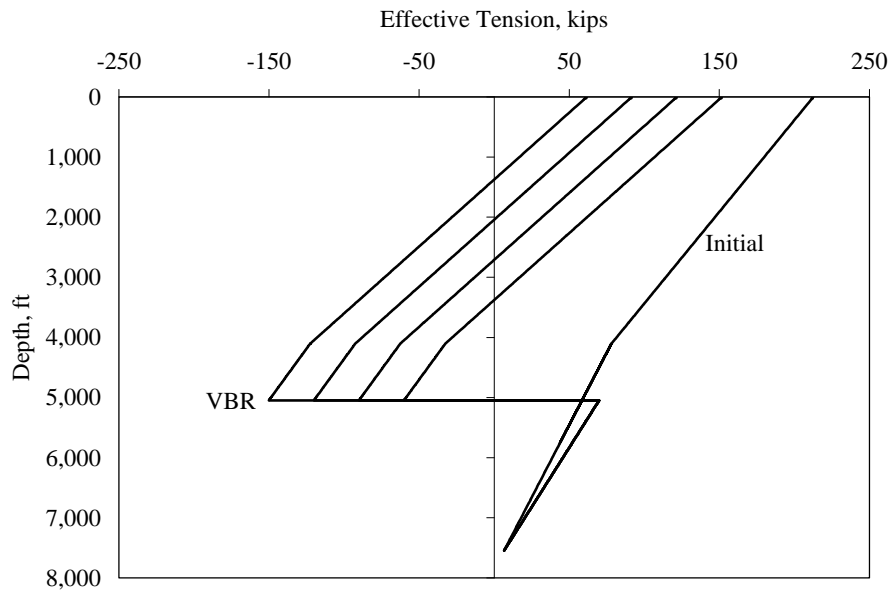


Figure 7: Tool Joint Contact Loads for a Range of Drag Loads

5 RESULTS FOR VBR LOAD CASES

The effective tension distributions for the four VBR load cases are in Figure 8 (and in Appendix C). The pipe below the VBR hangs under its own weight. The jump due to pressure drop across the VBR is apparent. The maximum compression occurs at the VBR.

Effective tension for VBR load cases

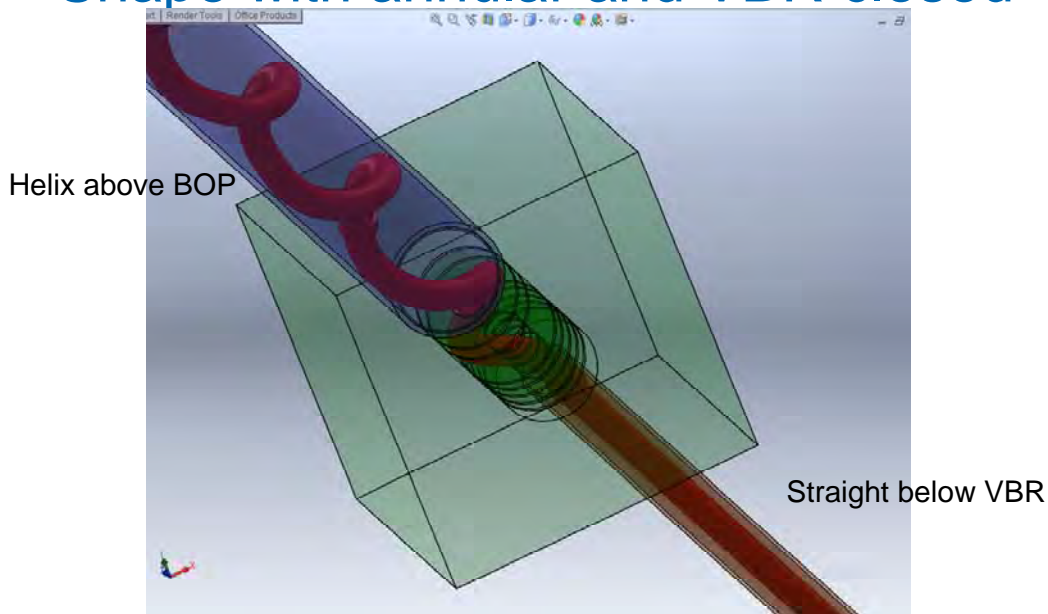


Assumes 2 ppg above VBR and 5 ppg below VBR

Figure 8: Effective Tension for Four VBR Load Cases

The pipe above the annular has a helical shape and the pipe below the VBR is straight as illustrated in Figure 9. The configuration between the annular and VBR (the two constraints) is illustrated in Figure 10. In the model, the elevation of the tool joint did not reach the upper annular, indicating that the assumed initial position of the tool joint is off by a few feet. The pipe between the annular and the VBR is essentially planar and is in contact with the BOP. The idealized case in Appendix D also indicates that the pipe would be planar between the supports (i.e. the upper annular and the upper VBR) and would be in contact between the supports.

Shape with annular and VBR closed



Load case 120 kips compression at VBR

Figure 9: Shape with Annular and VBR Closed

Configuration near BOP

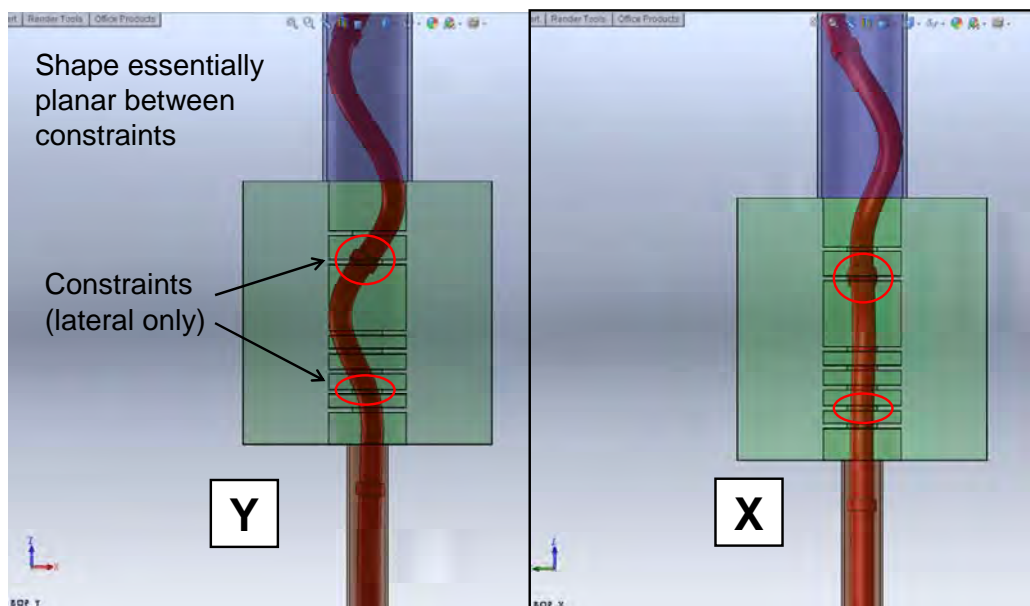


Figure 10: Shape between Annular and VBR

The wall contact force on the pipe between the annular and the VBR is shown in Figure 11. The load calculated using the reduced model in Appendix B is also in Figure 11 for comparison. The contact load from the full work string model is lower than the contact load from the reduced model in Appendix B (labeled “Beam” in the figure). The load is lower due to the influence of the pipe below the VBR, because the casing tends to centralize the drill pipe.

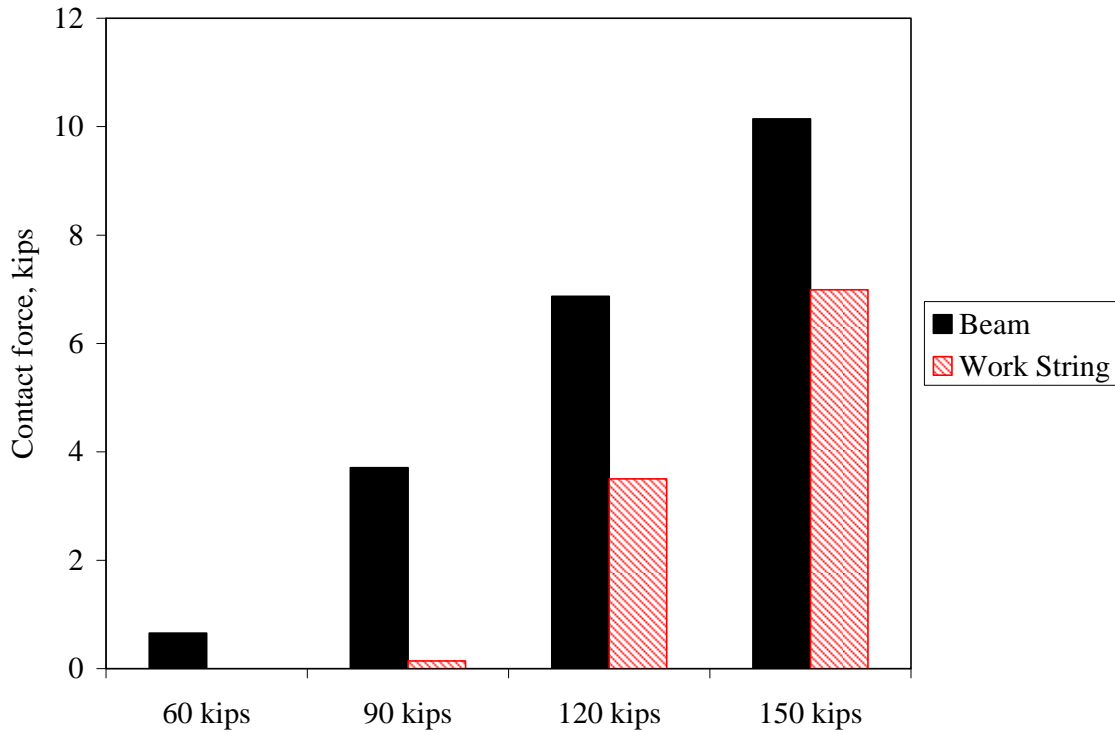


Figure 11: Contact Load between Annular and VBR

6 CALCULATED STRESS

The maximum calculated axial plus bending stress for the load cases is in Table 2.

Table 2: Maximum Calculated Axial Plus Bending Stress for Load Cases

Case	Axial + Bending Stress, ksi			
	30 kips	90 kips	120 kips	150 kips
Drag	21	62	84	105
VBR	NA	74	88	108

The maximum stress is in the 5-1/2" drill pipe in the BOP. The specified minimum yield stress is 135 ksi. A difference in internal pressure and external pressure would increase the von Mises stress. To increase the von Mises stress to yield, a difference in internal pressure and external pressure of 10,000 psi, which is greater than difference in internal pressure and external pressure that may have occurred, would be required to yield the pipe. The calculated stress for all cases is below yield.

REFERENCES

1. Garrett, D. L., **Coupled Analysis of Floating Production Systems**, Ocean Engineering 32 (2005), p. 802-816.
2. **Hydraulic Analysis of Macondo #252 Well Prior to Incident of April 20, 2011**, Stress Engineering Services Document No. 1101190-ST-RP-0002, Rev. 1, April 27, 2011.
3. **FORENSIC EXAMINATION OF DEEPWATER HORIZON BLOWOUT PREVENTER**, Vol. 1, Det Norske Veritas Report No. EP030842, March 20, 2011.

Appendix A: Work String Model

The work string is comprised of three segments as listed in Table A.1.

Table A.1: Work String Length

Segment	Length, ft
6-5/8"	4,103
5-1/2"	3,443
3-1/2"	821
Total	8,367

The 3-1/2" tubing was not included in the detailed structural model, but was represented by its weight acting at the bottom of the 5-1/2" drill pipe. Drill pipe joints were modeled as equal length segments. The number of joints in the model is in Table A.2.

Table A.2: Pipe joints in the model

Segment	Length	# joints
6-5/8"	4,103	94
5-1/2"	3,443	75
Total	7,546	169

Structural properties of the drill pipe (DP) and of the tool joint (TJ) for each size are listed in Table A.3.

Table A.3: Structural Properties of Pipe and Tool Joint

Component	6-5/8" DP	6-5/8" TJ	5-1/2" DP	5-1/2" TJ
Pipe OD, in.	6.625	8.250	5.500	7.000
Pipe wall thickness, t, in.	0.500	1.750	0.361	1.500
Pipe ID, in.	5.625	4.750	4.778	4.000
External area, A_o , in ²	34.472	53.456	23.758	38.485
Internal area, A_i , in ²	24.850	17.721	17.930	12.566
Steel area, A , in ²	9.621	35.736	5.828	25.918
Axial stiffness, AE, lb	2.8863E+08	1.0721E+09	1.7485E+08	7.7754E+08
Bending stiffness EI, lb-ft ²	9.4622E+06	4.2168E+07	4.0281E+06	2.1936E+07

For gravity loading, the weight of the pipe, the volume inside the pipe and the volume displaced by the pipe are needed. The weight per unit length of a joint of pipe is assumed constant along the length; the weights used are averaged over a joint. The weights and volumes are in Table A.4.

Table A.4: Pipe Weight and Volume

Segment	Length	Weight, lb/ft	Volume, gal/ft	
			Internal	External
6-5/8"	4,103	37.71	1.273	1.85
5-1/2"	3,443	23.9	0.916	1.282
3-1/2"	821	9.3	0.3652	0.5072

To model a tool joint, one element for each the pin and box was used. The element length is 5% of the joint length and the element stiffness varies linearly over the element from the tool joint stiffness to the pipe stiffness. The remaining 90% of the length has uniform properties. Ten equal length elements were used for 34 joints of the 5-1/2", 18 elements were used for the two joints that span the BOP, and eight elements were used for the lower 39 joints. This gives a total of 738 elements to model the 5-1/2".

A similar model was developed for the 6-5/8". The lower 65 joints were modeled using 5% of the length for pin and box, with four equal length elements for the uniform segment. Fewer elements were used for the upper portion of the 6-5/8". The total number of elements in the 6-5/8" model is 450.

Pipe contact with the inside of the riser, BOP or casing was modeled using distributed quadratic springs (see Appendix D). The hole diameter in the model is in Table A.5. The riser inside diameter is 19.5", the BOP inside diameter is 18.75", and the casing inside diameter is 8.625". Changes in diameter were assumed to vary linearly over ten feet.

Table A.5: Hole Diameter in the Model

Depth, ft	Hole ID, in
0	19.500
4,991	19.500
5,001	18.750
5,044	18.750
5,054	8.625
10,000	8.625

Model parameters were determined as described in Appendix D. The spring stiffness used is the same and the initial contact radius is reduced by 0.015 ft as in Appendix D.

Tool joints contact the hole first due to their larger diameter. Contact was modeled by a single quadratic spring in the center of the tool joint. The spring is equivalent to a one foot length of the distributed springs.

The 3-1/2” tubing was modeled as a vertical force at the bottom of the 5-1/2”. Assuming the tubing is filled with seawater and seawater is in the annulus, the calculated force (weight of tubing) is 6,638 lb. In the initial condition, the work string and annulus are assumed filled with seawater.

The top of the work string is pinned. The vertical location is 0 ft RKB.

Appendix B: Beam Model

Modeling the pipe between the annular and the VBR as a beam can provide useful information. The effects of pipe above the annular and below the VBR are ignored. The pipe is assumed uniform with properties of the 5-1/2” pipe (tool joints are not modeled). The model is assumed weightless. The model length is 27.3 ft (see Figure 127 of [3]).

The model results presented here assumed the ends of the beam are pinned. One end is axially restrained and a vertical load is applied at the other end. If the axial load is less than the Euler buckling load, then the idealized model is straight. For higher loads, the beam will deflect and contact the inside of the BOP. Contact is modeled using the same distributed quadratic springs as used in the work string model.

The calculated Euler buckling loads for various boundary conditions are listed in Table B.1. A pinned boundary condition provides no rotational restraint. A clamped boundary condition allows no rotational displacement. The estimated critical load in the DNV report [3] is 113,568 lb, which is close to the clamped-pinned case.

Table B.1: Euler Buckling Load for a Range of Cases

Case	Euler Buckling Load, lb
pinned-pinned	53,343
clamped-pinned	108,820
clamped-clamped	213,363

The total contact force acting on the inside of the BOP is shown in Figure B.1 for a range of loads. For comparison, the loads calculated from the work string model are also shown. The maximum calculated stress is shown in Figure B.2.

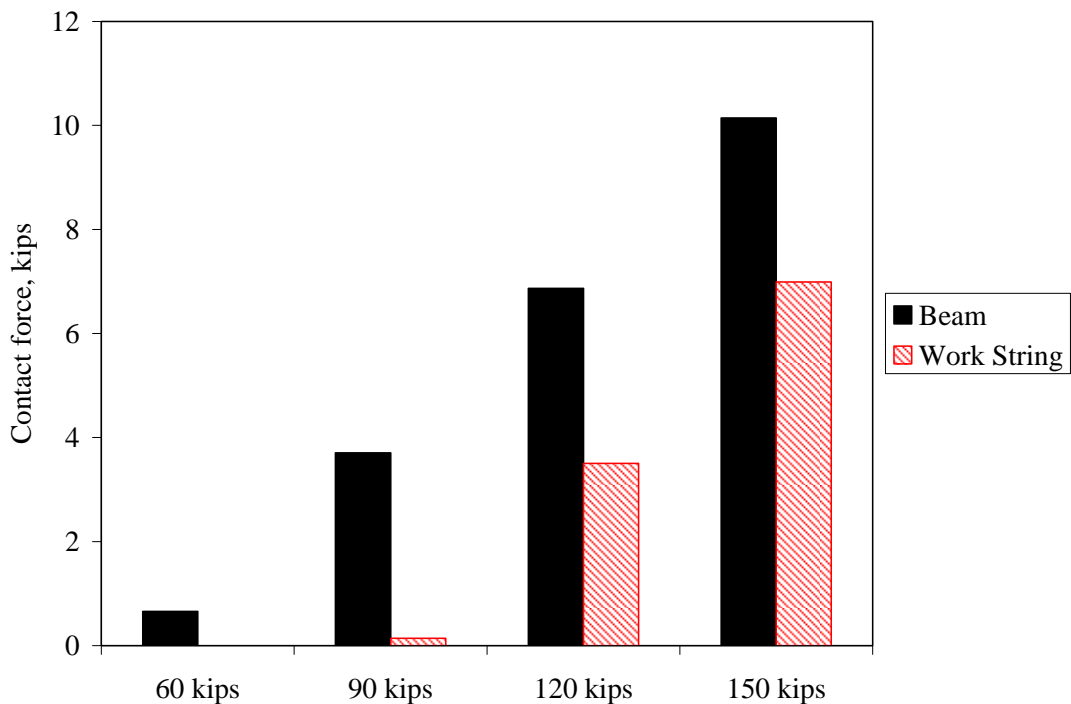


Figure B.1: Contact Force on BOP for A Range Of Loads

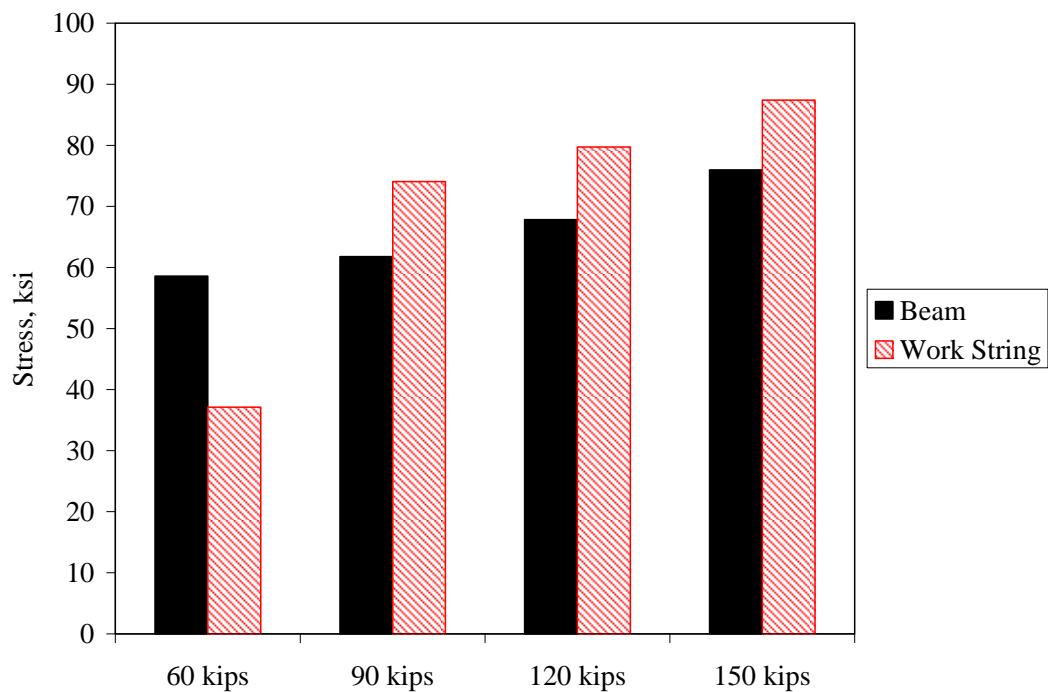


Figure B.2: Maximum Stress for a Range of Loads

The calculated contact force from the beam model is higher than the contact force from the work string model.

Additional comparisons were made to the model in Appendix D (an ideal helical model). The model in Appendix D is 20 times the length of the beam model. A 27.3 ft portion of the model in Appendix D was constrained by moving the nodes to the centerline. A comparison of the distributed contact load is in Figure B.3 and a comparison of stress is in Figure B.4.

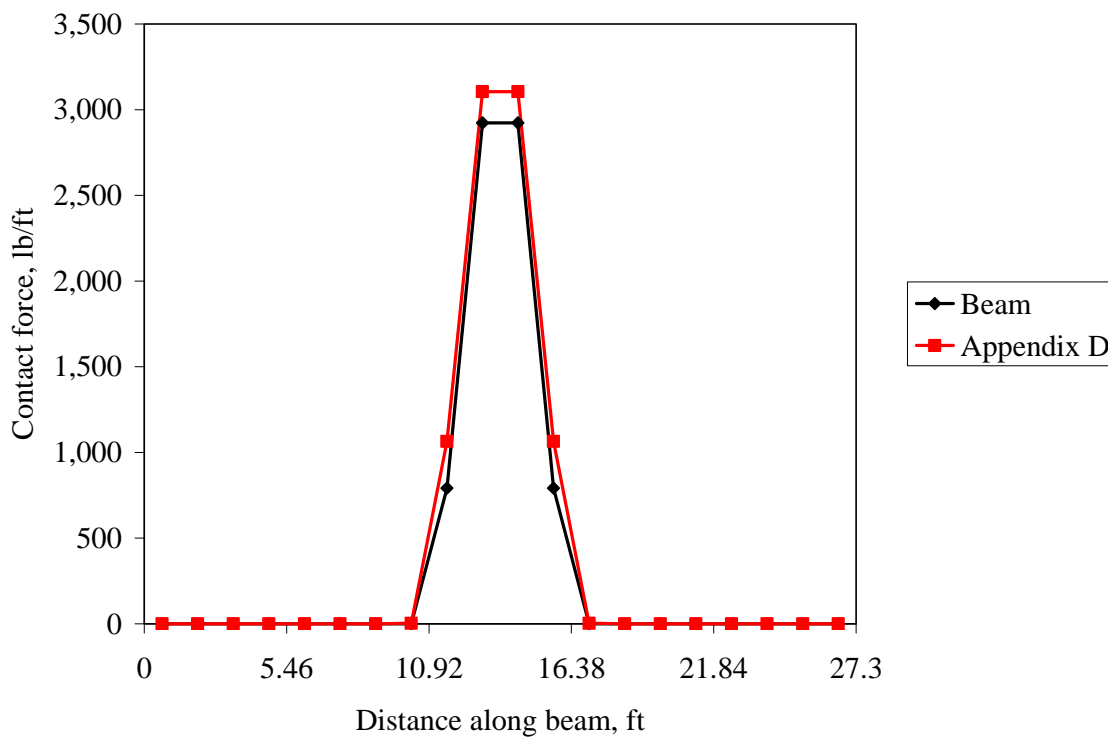


Figure B.3: Comparison of Contact Loads for F=150 kips

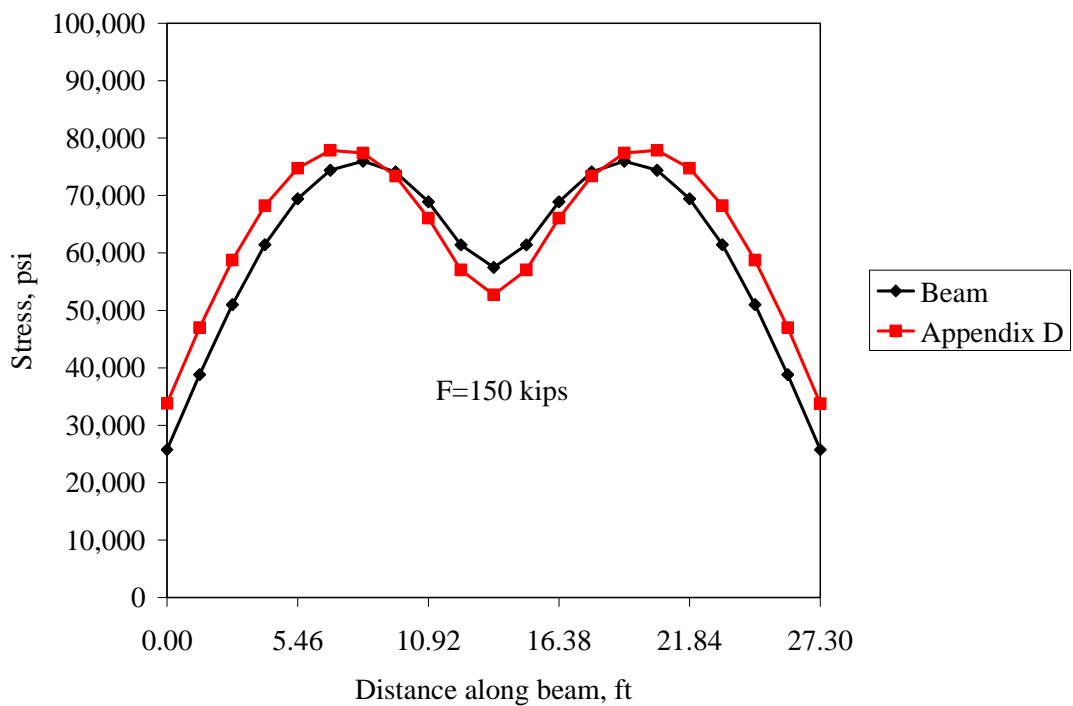


Figure B.4: Comparison of Stress for F=150 kips

Appendix C: Discussion of Loads

Loads on the work string can come from drag loads due to flow up the annulus or from a pressure differential across a closed BOP ram. The high flow rate conditions prior to closure of the variable bore ram could produce frictional pressure losses in the annulus between the drill pipe and the casing. The resulting vertical load on the work string can exceed the weight of the work string below the BOP. The resulting compressive load in the work string can lead to helical buckling and upward displacement of the work string. Closing the variable bore ram could stop the flow, resulting in a pressure increase below the ram as the well reaches a shut in condition. Calculations associated with load estimates are presented here.

Consider a segment of pipe suspended in casing as illustrated in Figure C.1. The pipe is closed at the top and is open at the bottom. The initial condition is static. The force, F , required to support the pipe is equal to the weight of the pipe plus the weight of the fluid in the pipe less the weight of the fluid displaced by the pipe. The pressures inside and outside the pipe at the top may be different if the fluid in the pipe and the fluid in the annulus have different densities. The force, F , is called the effective tension. The weight of the pipe plus the weight of the fluid in the pipe less the weight of the fluid displaced by the pipe is called the effective weight of the pipe.

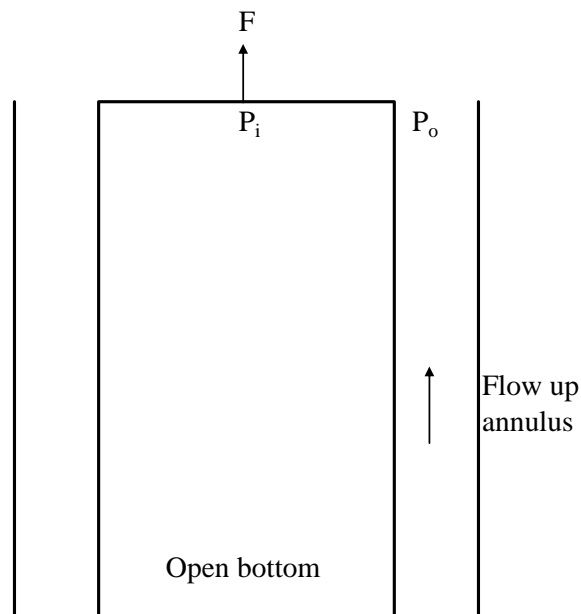


Figure C.1: Pipe Suspended in Casing

The first case we consider is such that there is flow up the annulus and the pressure outside the pipe at the top is constant. Flow up the annulus results in a frictional pressure drop in the annulus. The change in the force to support the pipe consists of two components: (1) the pressure end load, and (2) friction on the pipe due to the flow. The changes in force and pressure are;

$\Delta P_{friction}$	is the frictional pressure drop
ΔP_o	is the change in back pressure
$\Delta P_i = \Delta P_{friction} + \Delta P_o$	is the change in internal pressure
$\Delta F = -\Delta P_{friction} \left(\frac{\pi d^2}{4} + \frac{\pi(D^2 - d^2)}{4} \frac{d}{D+d} \right)$	is the change in force
d	is the diameter of the pipe
D	is the inside diameter of the casing

The first term in the expression for change in force is the pressure end load and the second term is friction on the pipe. In the second term, the assumption is made that the average shear stress on the surface area of the annulus is applied to the surface area of the pipe. If the density of the fluid in the annulus changes, there is an additional component of change in force due to change in effective weight of the pipe.

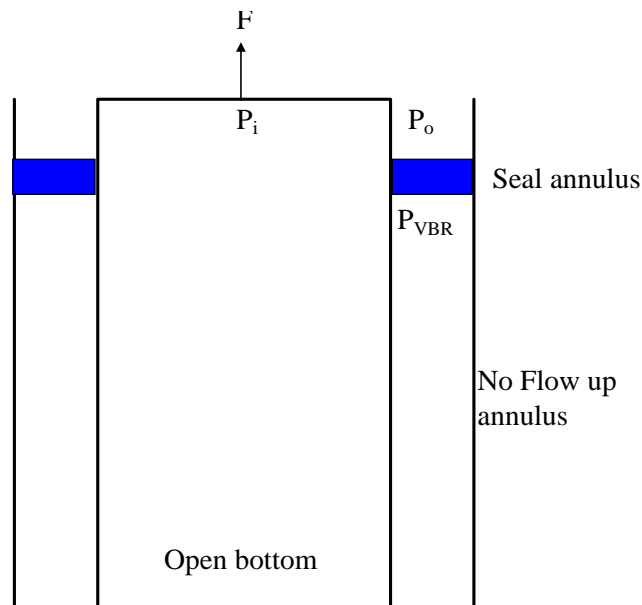


Figure C.2: Pipe Suspended in Casing with Annular Seal

The second case assumes a seal in the annulus, so there is no flow in the annulus as shown in Figure C.2. Prior to closure of the seal, the pressure below the seal and the pressure above the seal are equal. The changes in force and pressure are;

$$\begin{aligned} P_o & \text{ is the pressure above the seal} \\ P_{VBR} & \text{ is the pressure below the seal} \\ \Delta P_{VBR} = P_{VBR} - P_o & \text{ is the pressure drop across the seal} \\ \Delta F = -\Delta P_{VBR} \left(\frac{\pi d^2}{4} \right) & \text{ is the change in force} \\ d & \text{ is the pipe diameter} \end{aligned}$$

The load is equivalent to a vertical force applied at the location of the seal. The seal is assumed frictionless and does not provide vertical restraint.

When the change in force exceeds the effective weight, the pipe is in effective compression. We can use these formulae to estimate the pressure drop to produce a given net effective compression.

For the drag loading case, we assume that the frictional pressure drop occurs in the drill pipe/casing annulus below 5,067 ft MD (the first tool joint below the BOP). The effective weight of the work string below 5,067 ft is 73 kips, which assumes water inside the work string and 4 ppg hydrocarbon in the annulus. The 5-1/2" drill pipe diameter was modified to an equivalent diameter to account for the tool joints in the pressure drop calculations.

For the VBR loading case, the effective weight of the work string below the VBR is 70 kips, which assumes water in the work string and 5 ppg hydrocarbon in the annulus. We use the nominal pipe diameter for the area calculation since the VBR is assumed to close on the pipe (not on a tool joint).

The dimensions used for calculation of pressure drop are in Table C.1. The resulting calculated pressure drop for a range in net compression at the BOP is in Figure C.3.

Table C.1: Pressure Drop Calculation Parameters

d	5.500	in
Adjusted d	5.606	in
D	8.625	in
Drag	38.0	lb/psi
VBR	23.76	lb/psi

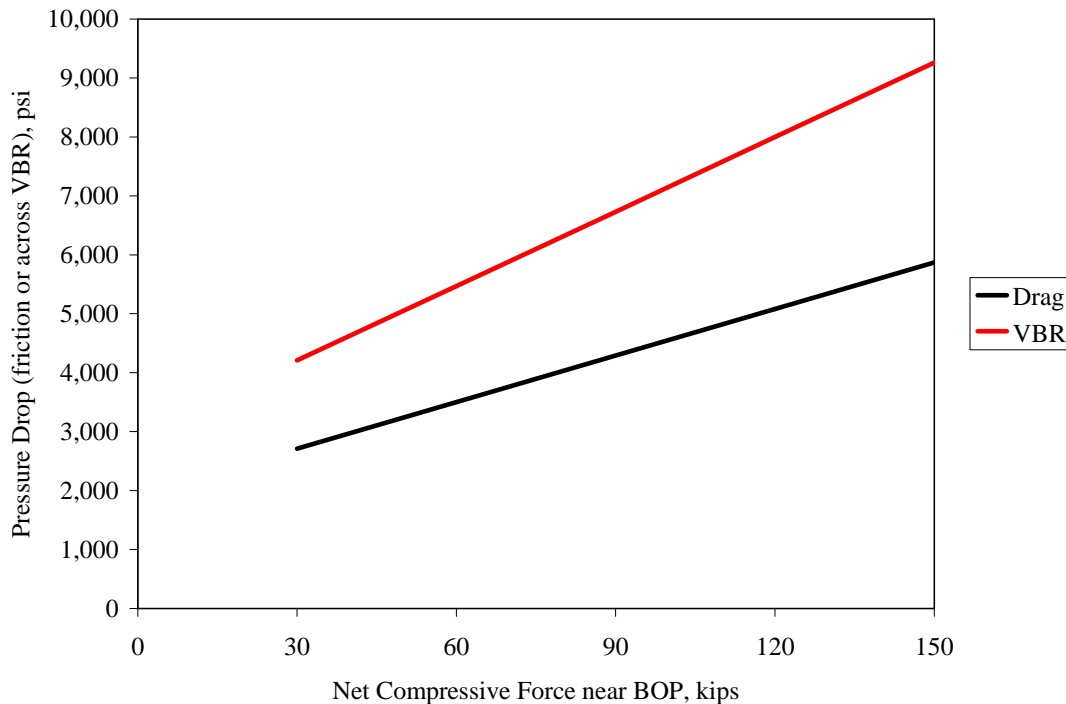


Figure C.3: Pressure Drop as a Function of net Compressive Force

When the VBR is closed, the pressure below the VBR increases and the pressure above the VBR will decrease as the hydrocarbons expand in the riser. In the shut in condition, the pressure below the VBR is 8,000 – 8,500 psi. With an assumed hydrocarbon density of 2 ppg above the VBR, the pressure above the VBR is 500 psi. Thus, the pressure drop across the VBR is about 8,000 psi, which corresponds to a net compression of about 120 kips. For structural analysis, loads from 60 kips to 150 kips were used. A vertical load was applied to the model at 5,049 ft MD.

For the drag loading case, we apply a uniformly distributed force from 5,067 ft to 7,546 ft (bottom of the 5-1/2” drill pipe). For structural analysis, loads from 30 kips to 150 kips were used.

The effective tension distributions for the selected load cases are in Figures C.4 and C.5.

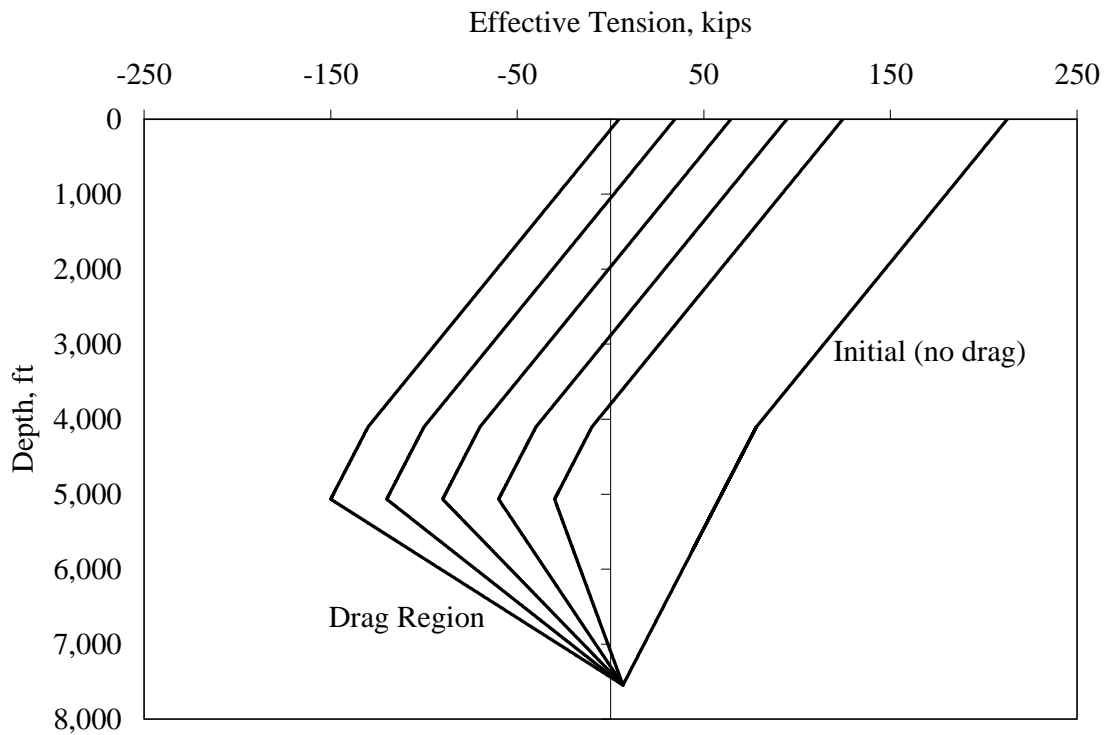


Figure C.4: Effective Tension Distribution for Drag Load Cases

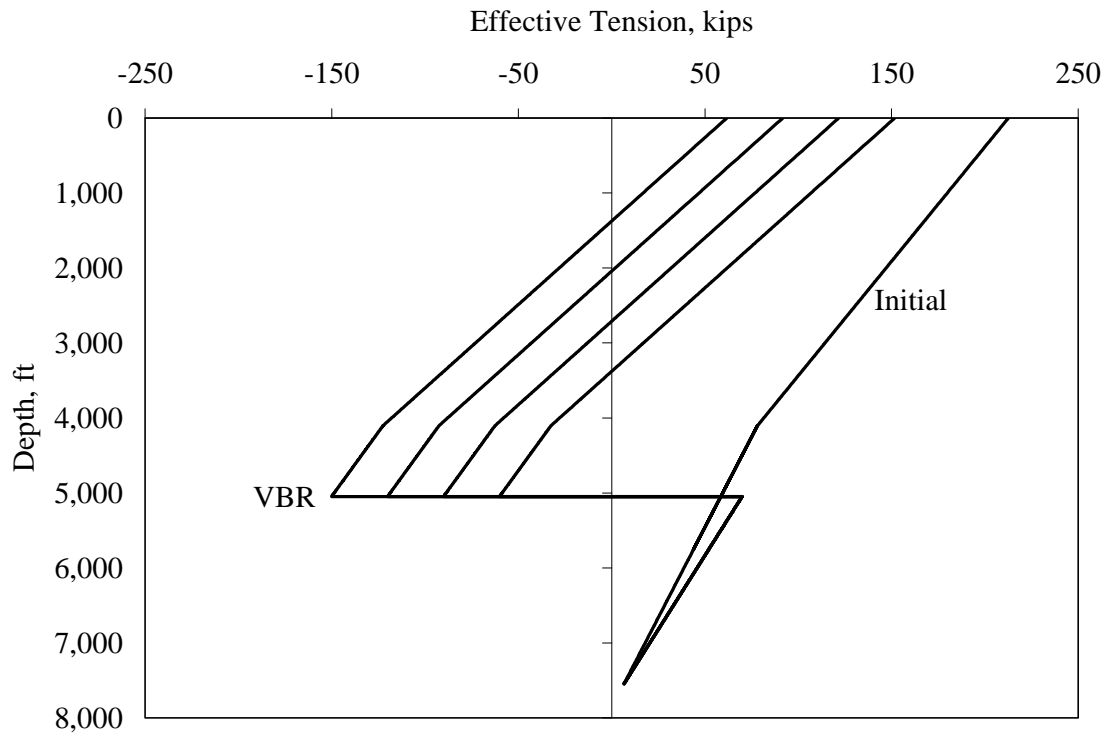


Figure C.5: Effective Tension Distribution for VBR Load Cases

Appendix D: Modeling a Helix

The equations for the centerline coordinates of a helix are

$$X = r \cos\left(\frac{2\pi s}{p}\right)$$

$$Y = r \sin\left(\frac{2\pi s}{p}\right)$$

$$Z = s \sqrt{1 - \left(\frac{2\pi r}{p}\right)^2}$$

where

r is the radius of the helix

p is the pitch of the helix

s is the distance along the centerline

For a uniform, weightless pipe inside a cylindrical hole, the equilibrium configuration can be determined analytically. The equations are

$$r = \frac{D - d}{2} \quad \text{is the radius of the helix}$$

$$p = \sqrt{\frac{8\pi^2 EI}{F}} \quad \text{is the pitch of the helix}$$

$$M = \frac{Fr}{2} \quad \text{is the bending moment}$$

$$N = \frac{F^2 r}{4EI} \quad \text{is the wall contact force per unit length}$$

D is the diameter of the hole

d is the diameter of the pipe

EI is the bending stiffness of the pipe

F is the compressive force along the axis of the hole

We compare the analytical solution to results from an equivalent numerical model analyzed in RAMS. The analytical formulation may also be used as a check against the numerical results presented in the main body of the report.

For numerical modeling, we use 5-1/2" drill pipe inside an 18-3/4" hole. We assume uniform properties and assume the pipe is weightless to fit the analytical model. One end is pinned and the other is fixed laterally ($X=Y=0$) and a compressive force in the Z direction is applied. The

model length is $20 \times 27.3 = 546$ ft to provide sufficient length for developing the helical form away from the ends.

Radial restraint is provided by distributed quadratic springs. The radial force is given by

$$N = \begin{cases} K(r - r_0)^2 & r > r_0 \\ 0 & r < r_0 \end{cases}$$

r is the radial displacement of the pipe

r_0 is the initial contact with the spring

Model parameters are summarized in Table D.1.

D	18.75	in.
d	5.5	in.
EI	4.028E+06	lb-ft ²
Length	546	ft
K	1.00E+07	lb/ft/ft ²
r_0	0.537	ft
Ideal r	0.552	ft

The initial contact with the radial spring is 0.015 ft less than the ideal radius.

The model was analyzed for loads over the range of 30 kips to 150 kips.

The X displacement for a range of loads is in Figure D.1. There is a transition from the pinned end to first contact with the wall of the hole. The middle portion of the model is helical. The pitch of the helix decreases with increasing load. The calculated stress is in Figure D.2. The transition at each end is apparent. The middle, helical portion has constant stress.

The pitch, radial displacement, contact load and stress in the middle 50% of the model length are compared to the analytical solution in Figures D.3 – D.6. The error in pitch length, which does not depend on the radial displacement, is much less than 1%. The pitch ranges from 103 ft to 46 ft. The model radial displacement varies slightly with load due to the radial spring constraint.

The slight discrepancy in radial displacement results in a corresponding discrepancy in contact load and stress since the contact load and the bending moment are proportional to the radial displacement. Agreement between the numerical model and the analytical solution is very good.

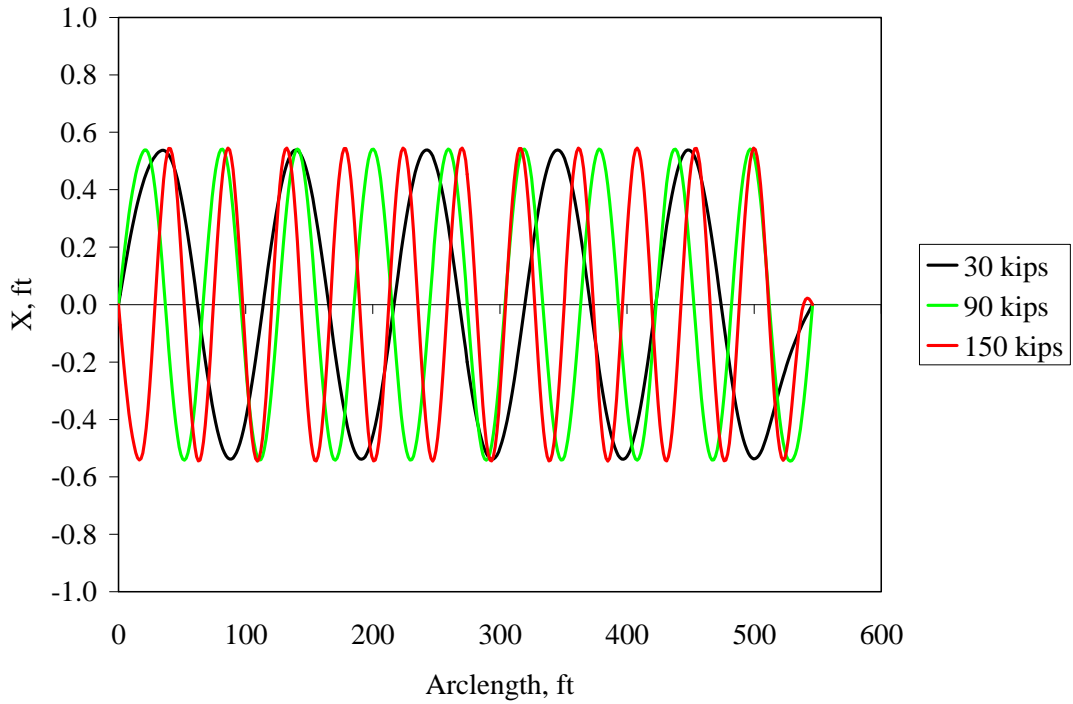


Figure D.1: X Displacement for a Range of Loads

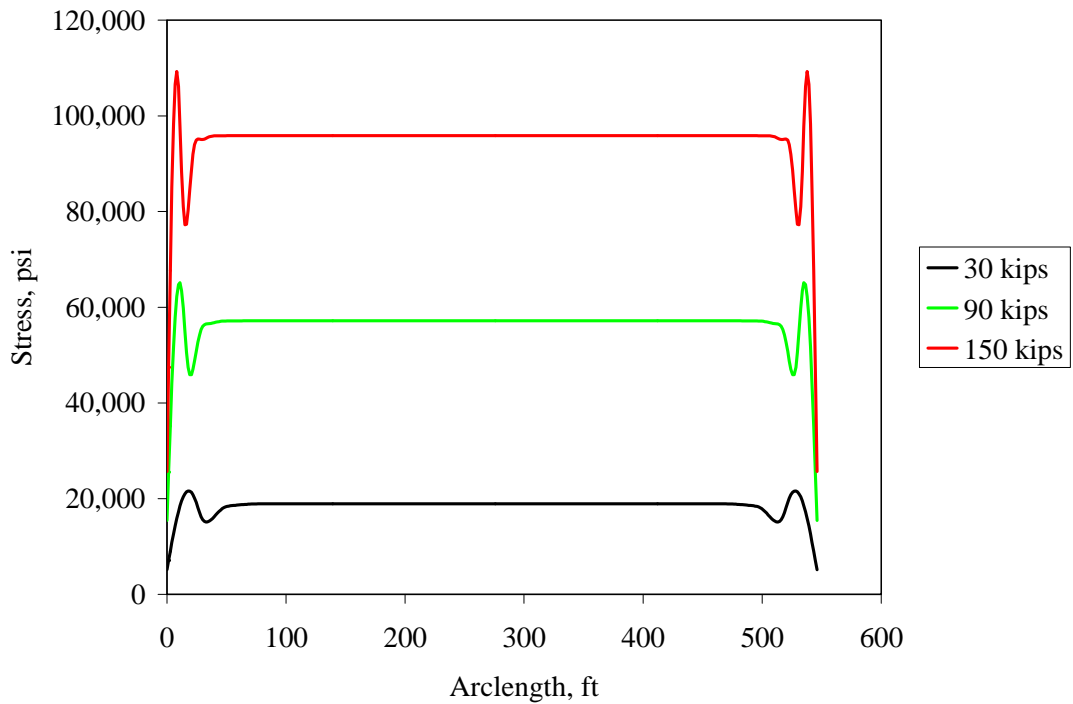


Figure D.2: Axial Plus Bending Stress for a Range of Loads

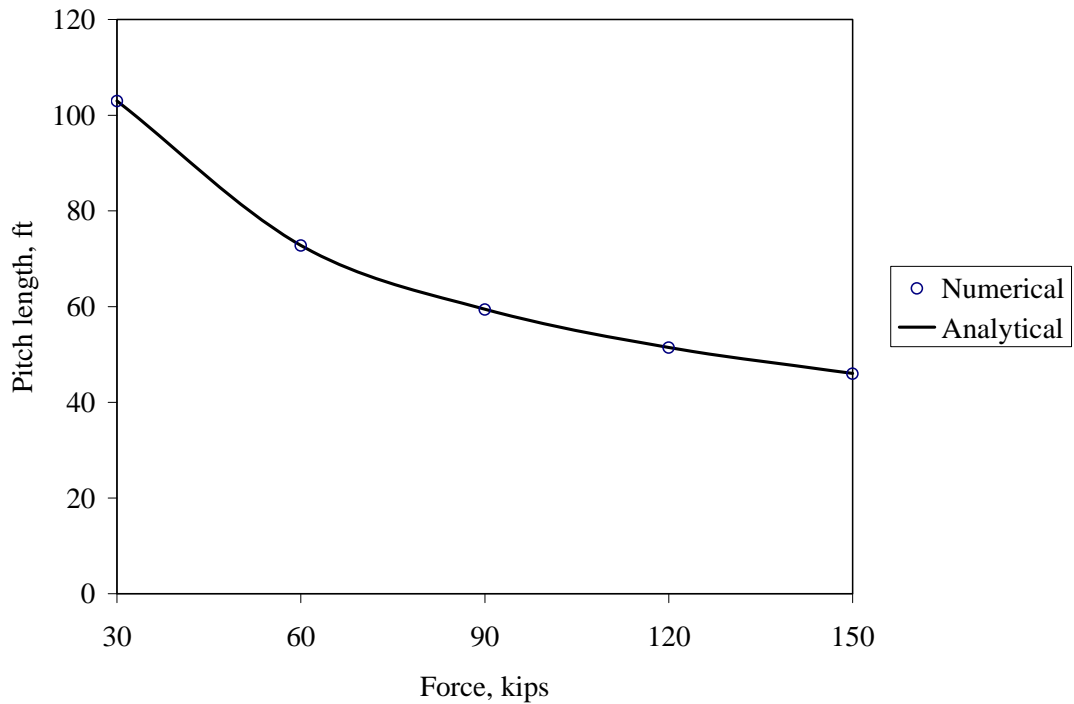


Figure D.3: Comparison of Numerical to Analytical Pitch Length

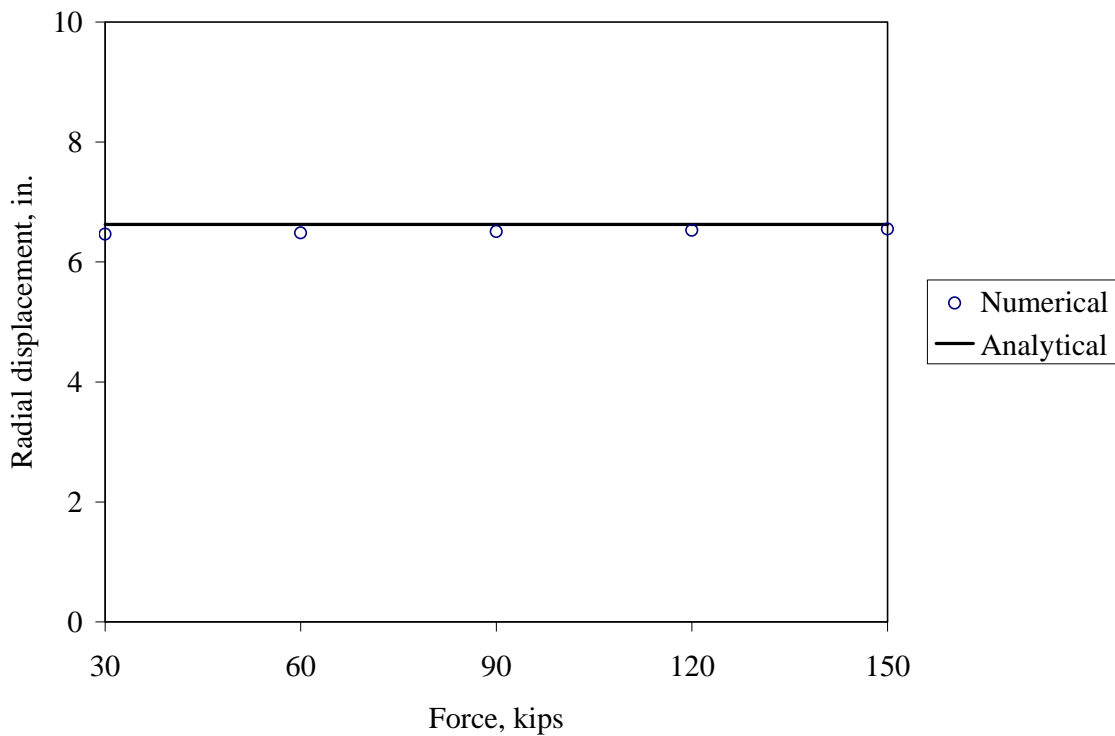


Figure D.4: Comparison of Numerical to Analytical Radial Displacement

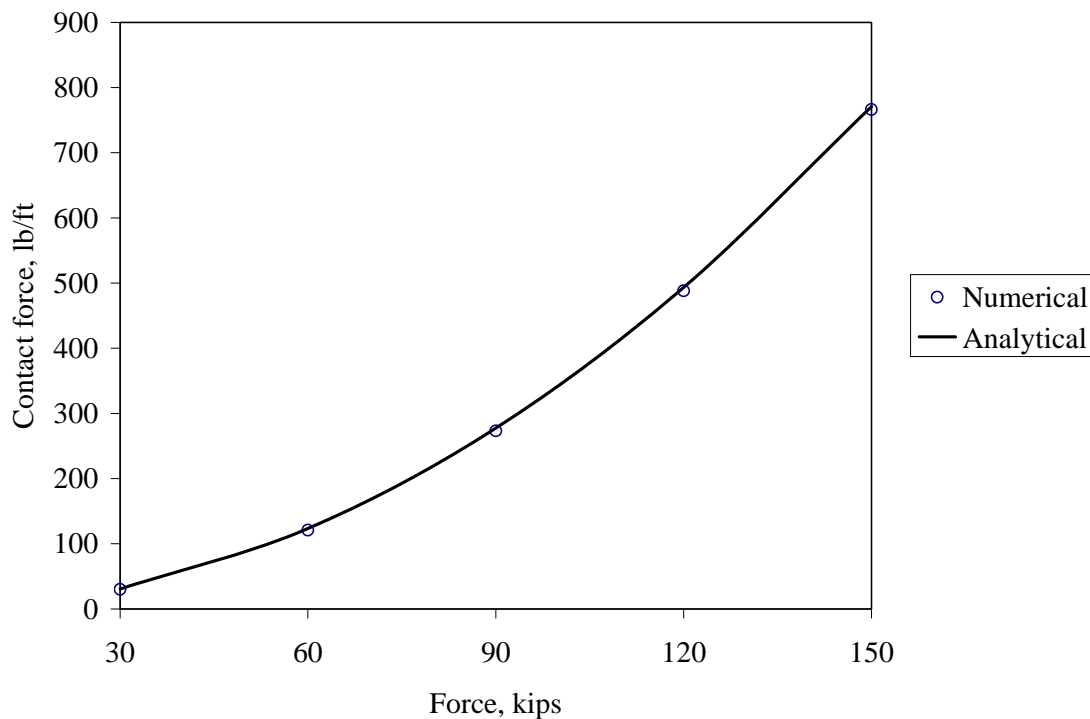


Figure D.5: Comparison of Numerical to Analytical Contact Force

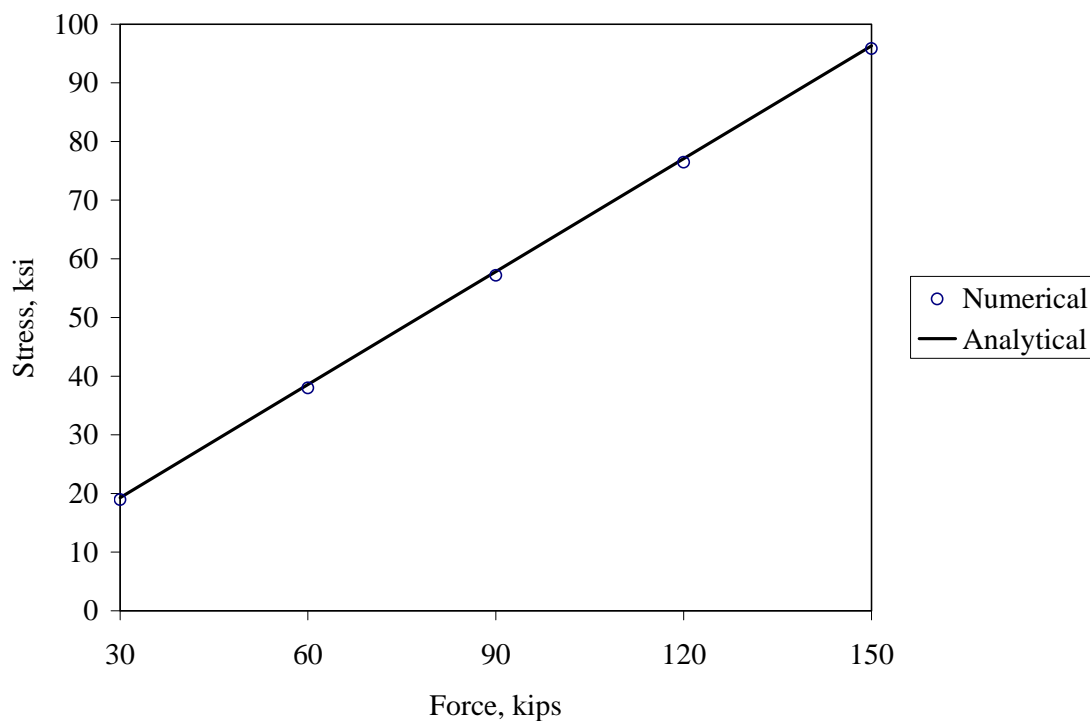


Figure D.6: Comparison of Numerical to Analytical Axial plus Bending Stress

Another Test Case

To examine a somewhat idealized case of closure of the annular and of the variable bore ram, two nodes, separated by 27.3 ft, in the middle of the model, were constrained to the centerline ($X=Y=0$). Only the case for $F=150$ kips is presented.

A plan view (X-Y) of the portion of the model between the constrained nodes is in Figure D.7. Prior to setting the constraints, the model is in a helix (as evident by the circular shape). After setting the constraints, the model is planar between the constrained nodes.

Contact loads before and after setting the constraints are in Figure D.8. The contact loads for the helix are constant. After setting the constraints, the model deflects and contacts the wall of the hole. The maximum contact load is much higher than the contact load for the helical configuration.

Axial plus bending stress before and after setting the constraints are in Figure D.9. Stress is constant for the helix. After setting the constraints, the maximum stress is lower.

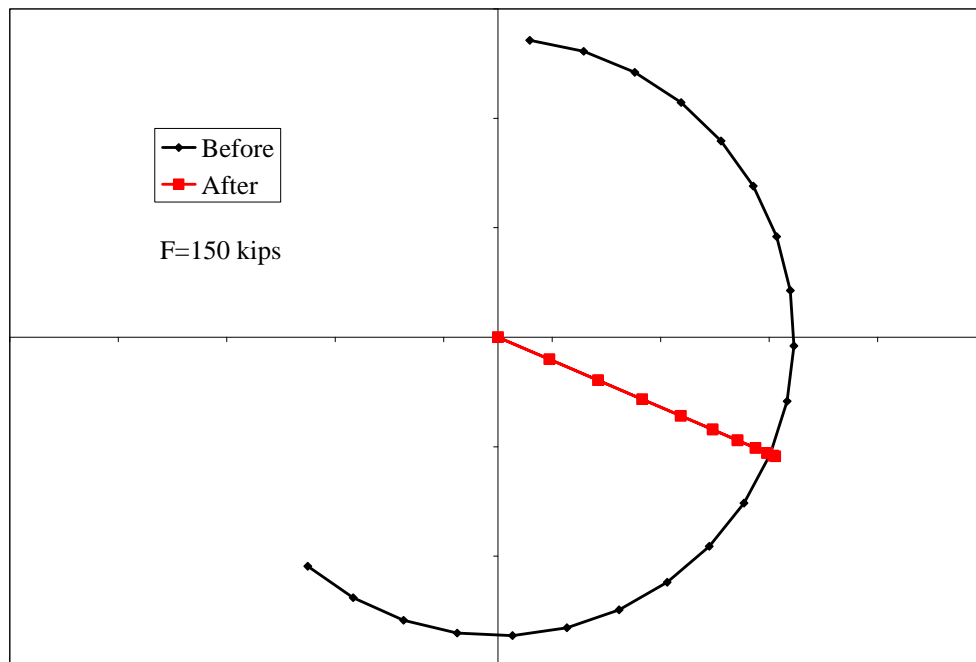


Figure D.7: Plan View (X-Y) Before and After Setting Constraints

Displacements along Axis of Helix

When a compressive force F is applied, the distance between the ends is reduced. The length of the pipe, measured along the axis of the pipe, is reduced by compressive strain. The distance between the ends, measured along the axis of the hole, is reduced due to the helical shape. The change in distance between the ends is

$$\Delta = \Delta_{axial} + \Delta_{helix} \quad \text{is the total change in distance between the ends}$$

$$\Delta_{axial} = \frac{FL}{AE} \alpha \approx \frac{FL}{AE} \quad \text{is the change due to axial compression in the pipe}$$

$$\Delta_{helix} = (1 - \alpha)L \approx \frac{Fr^2L}{4EI} \quad \text{is the change due to the helical shape}$$

$$\Delta \approx \Delta_{axial} \left(1 + \frac{r^2}{4} \frac{AE}{EI} \right) \quad \text{is the total change in distance}$$

L is the undeformed length of pipe

AE is the axial stiffness of the pipe

EI is the bending stiffness of the pipe

r is the radius of the helix

F is the compressive applied load

$$\alpha = \frac{dZ}{ds} = \sqrt{1 - \left(\frac{2\pi r}{p} \right)^2} \quad \text{is approximately 1 for cases considered here}$$

From the fourth equation, the displacement is the axial compression times a constant. For the parameters in this example (5-1/2" pipe in an 18-3/4" hole), the constant is 4.3. Most of the displacement along the axis of the hole is due to the helical shape.

The formulae presented are for a weightless pipe. For a pipe in a vertical hole, the displacement due to the helical shape changes due to variation in the compressive load

$$\Delta_{helix} = \begin{cases} F^2 \frac{r^2}{8EIw} & F < wL \\ \left(F^2 - (F - wL)^2 \right) \frac{r^2}{8EIw} & F > wL \end{cases}$$

w is the weight of the pipe per unit length

Appendix N AMF Testing

The Automatic Mode Function (AMF) is an optional feature of the subsea control system designed to automatically close the blind shear rams (BSRs) in the blowout preventer (BOP) stack in the event of an unplanned separation of the drilling riser from the BOP. The AMF option was offered by Cameron and purchased by Transocean for the *Deepwater Horizon* BOP stack.¹ The AMF monitors the connectivity to the BOP stack from the surface control system and initiates a sequence of functions if electrical power, electronic communication between pods, and hydraulic supply from surface are lost.

BOP Control System Components²

The following components are associated with BOP control and AMF functionality:

- **Surface Control Panels:** Driller's control panel located on the drill floor and toolpusher's control panel located in the central control room³
- **Central Control Unit (CCU):** Main electronic hub and interface point to both surface and subsea controls⁴
- **Hydraulic Unit:** High-pressure pumps and surface accumulators to maintain a supply of operating fluid at the pressures and volumes necessary to function the BOPs⁵
- **Yellow and Blue Pods:** The yellow and blue pods house subsea controls on the BOP stack, including the subsea electronic modules (SEMs), subsea transducer modules (STMs), hydraulic pressure regulators, solenoid pilot valves, hydraulic accumulators and hydraulic valves. The yellow and blue pods operate functions on the BOP stack in response to commands from the surface control system with the exception of the AMF system.⁶
- **Subsea Electronic Modules:** Two subsea electronic modules (SEM A and SEM B) are located in each pod for a total of four SEMs on the BOP stack.⁷ The SEMs consist of programmable logic controllers (PLC), power supply units, AMF controllers, batteries, fuse boards and communication boards. When functions are activated from the surface controls, a signal is sent to the SEMs to energize the respective solenoid valves, which then route the pressurized hydraulic fluid to a particular BOP function. Each solenoid valve has two operating coils — one coil is connected to SEM A and the other coil is connected to SEM B — allowing either or both SEMs to operate the valve. In normal subsea operation, both SEM A and SEM B in each pod receive a signal from the surface control system and activate their respective coil in the solenoid simultaneously.
- **Automatic Mode Function:** The AMF is designed to secure the wellbore during a loss of electrical power, electronic communication between pods and hydraulic supply from surface. The system consists of electrical circuitry housed in the SEMs and uses existing hardware (including solenoids, valves and pressurized hydraulic fluid) to function the BOP.⁸ Each AMF card works independently, and any or all of them can initiate the function of the high-pressure shear circuit.⁹

Components of the AMF system include:

- AMF processor board (one per SEM, two per pod and four in the BOP system).¹⁰
- Dedicated 9-volt (V) DC battery pack per AMF card (one per SEM, two per pod and four in the BOP system).¹¹
- 27V DC battery pack shared for both SEM A and B (one per pod and two in BOP system).¹²
- Dedicated subsea hydraulic accumulators to operate the functions commanded by the AMF system.¹³
- A custom software file added to the PLC in each of the SEMs that defines the hydraulic activation sequence and timing instructions.¹⁴
- A bi-stable "latching" relay in each AMF card. Once the relay is latched in either the arm or disarm mode, it will remain in that mode whether it is powered or not.

AMF System Activation

During normal drilling operations, when the BOP stack is latched on the wellhead, the AMF system is armed and will remain in the armed state.¹⁵ The following conditions must be met before the AMF will activate:

- **The AMF must be armed.** The AMF is armed at surface by a single-button activation from the surface control panel. All four AMF processor cards are armed by this signal. A photo taken during a ModuSpec survey on April 10, 2010, shows that the AMF system was in the armed mode.¹⁶ When the AMF is armed, the voltage reading at the control system event logger is approximately 0V.¹⁷
- **Communication and electrical power loss from the surface control system.** If one pod loses power from the surface, the two AMF cards in that pod are powered from two 9V battery packs, one dedicated to each card. Each AMF card monitors the condition of the other pod to verify that it is still operating normally and has power from the CCU. In the event of a power loss from the surface control system, the AMF processor will send a signal to pressure transducers in the pod to check the status. The pressure transducers are powered by the 27V battery pack.
- **Surface hydraulic supply pressure loss.** Each AMF card checks the status of the pressure transducers in the subsea transducer module. The pressures monitored are the seawater hydrostatic and surface hydraulic fluid pressures from the rigid conduit supply manifold. When the pressure reading from the rigid conduit manifold drops to 400 psi or less above the hydrostatic pressure reading, the AMF processor will initiate and verify the status of the other requirements. If power and communications loss signals are present, the AMF processor card will activate the sequence.

Once the AMF conditions are confirmed by the processor, the AMF card provides power to the SEM PLC using the 9V battery pack. The AMF controller indicates to the PLC that the AMF card is in an active state. Immediately after startup, the SEM PLC detects the AMF active state and initiates the AMF sequence by firing the solenoids in the pre-programmed sequence.¹⁸

The AMF sequence of functions for the *Deepwater Horizon* pods was custom-programmed into the SEMs. The Cameron recommendation for any AMF sequence is that no more than six solenoids be activated at any one time to reduce power consumption.¹⁹

The following was the sequence for the *Deepwater Horizon*:

- 0-second LMRP stinger extend
- 0-second stack stinger extend
- 5-second LMRP stinger seals energize
- 5-second stack stinger seals energize
- 7-second deactivate LMRP stinger extend
- 7-second deactivate stack stinger extend
- 7-second high-pressure shear ram close
- 37-second deactivate high-pressure shear ram close

AMF Batteries

Each Cameron AMF system uses non-rechargeable battery packs that power the SEM PLC, solenoid driver card, solenoids, AMF card and STM for the AMF sequence.²⁰ The battery type used by Cameron for this application has a flat discharge curve, which means that the battery supplies constant output voltage until it reaches the end of life. See *Figure 1*. Due to this characteristic there is no practical way to predict the battery life simply by measuring the voltage.²¹

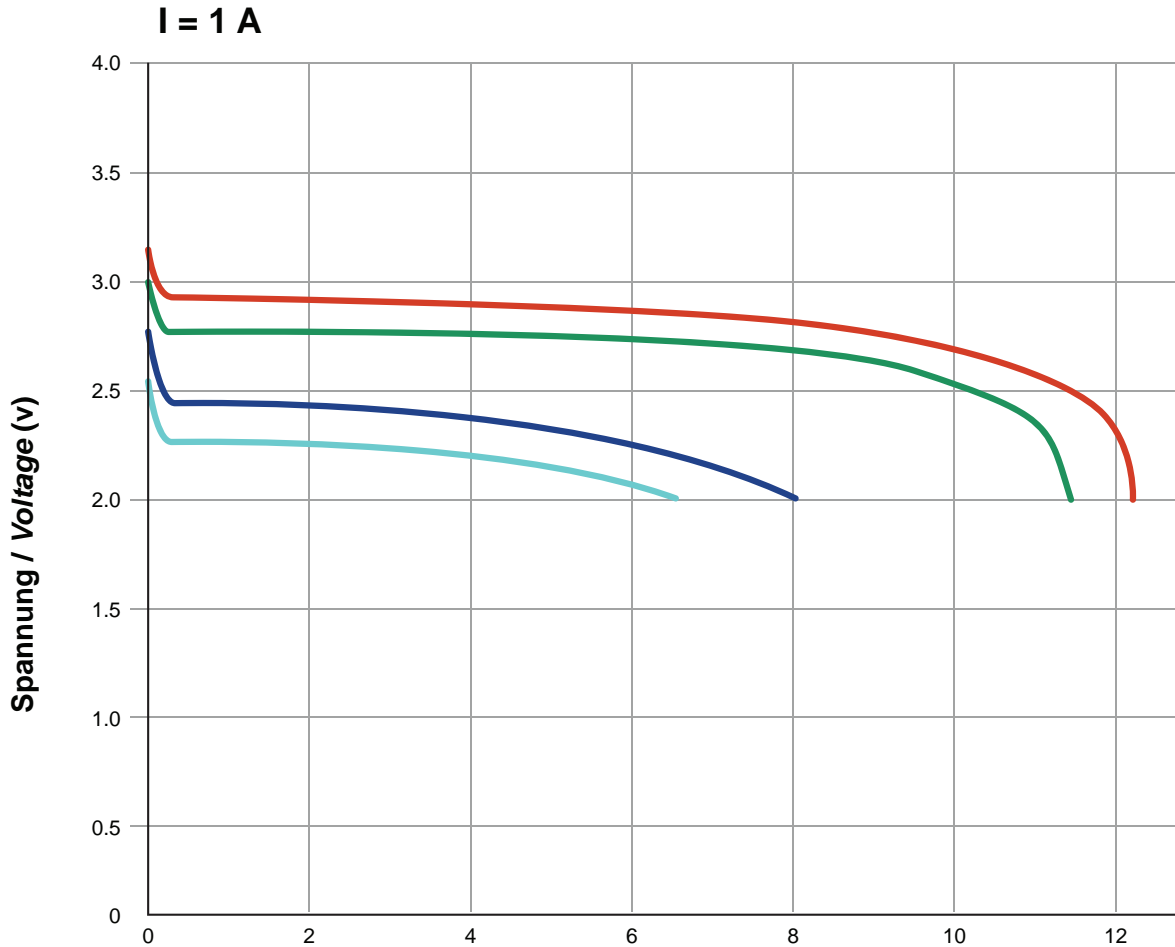


Figure 1 Representative Discharge Curve of SAFT Li MgO₂ Type AMF Battery²²

Cameron recommends replacing the batteries after one year of operation or 33 AMF actuations, or within five years of shelf life.²³ The *Deepwater Horizon* pod batteries were last changed on the following dates:²⁴

- Pod No. 1 (blue pod) on April 25, 2009
- Pod No. 2 (yellow pod) on Oct. 13, 2009
- Pod No. 3 (spare pod) on Nov. 4, 2007

Cameron completed the overhaul of the *Deepwater Horizon* spare pod SEM in 2010, and it arrived on the rig after the BOP stack was lowered to the wellhead in February 2010. The AMF system in the SEM had new batteries installed and was factory-acceptance tested prior to shipment.

During a routine rig condition assessment on the *Deepwater Horizon* in April 2010, ModuSpec confirmed that all batteries in the SEMs were new.²⁵

Software and AMF Function Testing

Tests using AMF cards and an SEM from a functionally identical Cameron BOP stack were performed to check various fault conditions and how these may relate to the Macondo incident. During the pod interventions, battery readings were taken showing that the yellow pod batteries were at an acceptable voltage level. However, the blue pod battery readings recorded during the intervention indicated that two out of the three batteries had low readings. The batteries that supply the AMF system have four potential failure modes. These conditions are:

Condition 1

<i>Battery</i>	<i>Condition</i>
9V (2)	Both have low voltage and insufficient power to operate the AMF cards.
27V	Sufficient power to (1) operate the solenoids and STM, and (2) disarm AMF card.
Result	The AMF will not activate and power the PLCs. The 27V battery will not be connected to power the STM or operate the solenoids. Inspection will show two low 9V batteries and one good 27V battery.

Condition 2

<i>Battery</i>	<i>Condition</i>
9V (2)	Both have sufficient voltage and power to operate the AMF cards.
27V	Insufficient power or low charge to (1) operate the solenoids and STM, or (2) disarm AMF card.
Result	The PLC drains the 9V batteries until they are depleted, as the AMF card cannot receive a 24V signal to disarm from the 27V battery. Inspection will show two low 9V batteries and one good 27V battery.

Condition 3

<i>Battery</i>	<i>Condition</i>
9V (2)	One with insufficient energy to boot and power the PLC. The other has sufficient energy to boot and power the PLC.
27V	Sufficient power to (1) operate the solenoids and STM, and (2) disarm AMF card.
Result	Both PLCs will start up, but only the SEM with the good 9V battery will fully complete the AMF sequence and disarm that AMF card. The SEM powered by the insufficient 9V battery will not be able to complete its sequence, and will try continually to boot up the PLC, draining both the 27V and remaining 9V battery of energy.

Condition 4

<i>Battery</i>	<i>Condition</i>
9V (2)	Both with insufficient energy to boot and power the PLC.
27V	Sufficient power to (1) operate the solenoids and STM, and (2) disarm AMF card.
Result	The SEMs powered by the insufficient 9V battery will not be able to complete their sequence, and will try continually to boot up the PLC, draining the 27V and both remaining 9V batteries of energy.

During the tests it was noted that the condition of the 9V battery packs is important to a successful completion of the AMF cycle. In the event that the 9V battery pack has insufficient power, the PLC will not successfully complete its startup. The 9V battery pack will be drained by continuous startup attempts of the PLC. In this condition the PLC will not supply a 24V disarm signal to the AMF card, leaving the 27V batteries draining while connected to and powering the STM.

During testing it was also found that AMF cards will start their activation sequence again, if not disarmed. The time to restarting the sequence is 3 minutes 43 seconds for the *Deepwater Horizon* AMF.

Based on the battery voltages found in the pods during the intervention process and the subsequent testing at

Michoud, the investigation team concluded that the yellow pod AMF cards both fired and completed the AMF sequence. The investigation team concluded that the low voltage on the blue pod SEM B 9V battery pack is caused by the scenario described above as Condition 3. One AMF card correctly fired the AMF sequence, and the second AMF card could not boot and power its associated PLC, therefore continually cycling and draining one 9V and the common 27V battery in the pod.

Post-Incident Investigation

Pod Intervention – Yellow Pod Condition

The yellow pod was pulled to the surface for the first time 15 days after the incident. The yellow pod functions were tested by Cameron using a Portable Electronic Test Unit (PETU). The pod functioned as designed with the following notations:²⁶

- No indication of Solenoid No. 103 firing on SEM A or B. This valve was replaced during the rig move in February 2010.²⁷
- Upper annular regulator increase, Solenoid 3A would not function on SEM A or B.²⁸
- Lower outer choke close on SEM B would not function.²⁹
- The yellow pod batteries were tested and found to be at acceptable voltage levels.³⁰

Battery readings:

- 9V SEM A Battery: 8.85V³¹
- 9V SEM B Battery: 8.85V³²
- 27V Pod Battery: 26V³³
- Solenoid 103 was replaced with a spare.
- The yellow pod AMF system was tested and functioned as expected following the Cameron AMF test procedure.

When the yellow pod was pulled the second time on July 23, 2010, the following conditions were noted:

- Extend stack stinger – observed leak from 1/4-in. pod valve.³⁴
- Replaced lower annular close valve due to slide not going into vent, 1 1/2-in. pod valve.³⁵

The yellow pod AMF system was tested by DNV at Michoud.

- *Test No. 1:* AMF system test with the spare solenoid 103 installed in the pod. The AMF functioned as expected.
- *Test No. 2:* The original solenoid 103 was then re-installed on the yellow pod. The AMF system in the pod was tested with SEM A and SEM B active (normal operation). The AMF functioned, and solenoid 103 functioned (at 43 seconds) after a 22-second delay from the expected activation time.³⁶
- *Tests Nos. 3 and 4:* The AMF system in the yellow pod was tested two additional times with SEM A and SEM B active. Solenoid 103 functioned (at 21 seconds) as expected at the correct activation time.³⁷

Pod Intervention – Blue Pod Condition

During the post-incident intervention on the BOP stack, the blue pod was pulled to surface 74 days after the incident and the following items were noted:³⁸

- BOP manifold regulator was leaking.
- Using a PETU, it was noted the blue pod AMF did not activate on the AMF battery power when functioned. Once the external power was re-supplied via the PETU, the PLC completed the AMF sequence.

Battery readings:³⁹

- 9V SEM A battery: 8.78V
- 9V SEM B battery: 0.142V
- 27V pod battery: 7.61V

During the DNV investigation at Michoud, NASA engineers measured the following for the blue pod batteries:

- 9V SEM A battery: 8.91V
- 9V SEM B battery: 8.68V
- 27V pod battery: 1.04V

The investigation team concluded that the NASA engineers recorded the correct voltage readings. The low voltage readings taken while the POD was on the *Discoverer Enterprise* for the 9V SEM B battery pack likely reflect an error in measuring the voltage difference across the wrong pins in the PIE connector, and reading the difference in voltage between the 9V SEM A battery pack and the 9V SEM B battery pack. After the AMF test of the blue pod by DNV, the blue pod SEM B AMF card did not reset after power was re-applied with the PETU. In addition, after power was re-applied with the PETU, the blue pod completed the AMF sequence, indicating that SEM B had a weak 9V battery.

The investigation team concluded that the 27V and the SEM B 9V battery packs were drained due to continual cycling of the AMF, trying to boot the PLC in the SEM, as evidenced by the dead 27V battery and SEM B not resetting upon testing at Michoud. The Cameron technician verified that solenoid 103 fired after external power was reapplied to the SEMs during surface testing after the incident. The intervention tests on surface showed that the AMF electrical circuitry and components were functional and that the solenoids did not function initially during the intervention tests on surface because the 27V and SEM B 9V battery had insufficient battery capacity. This conclusion is based on the battery voltages and subsequent testing on a similar Cameron AMF system.

The SEM B 9V battery did not have sufficient power to boot the AMF processor, resulting in a continuing “re-boot” cycle approximately every three minutes. In addition, it has been determined the AMF cards have a “low voltage drop out” feature that prevents the 9V battery from powering the PLC when voltage is less than 5V. The 27V battery powers the STM on and off as the AMF “re-boot” cycle continues. This allows the 9V battery to rest and regenerate; however, the higher voltage reading is not indicative of the remaining power. The investigation team has demonstrated this phenomenon in the lab where a 9V battery was drained to 0V at 32°F (approximate temperature at operating water depth), and voltage increased dramatically when returned to room temperature only to go back down to near 0V when tested under load. This indicates voltage alone is not a valid indicator of the battery condition.

When the AMF card is armed, the 27V battery powers the STM. While the SEM B 9V battery did not have sufficient power to boot the SEM PLC, the 27V battery would power the STM during the “re-boot” cycle of approximately 3 minutes. This continued until the 9V battery voltage dropped to less than 5V. During the period that the SEM B 9V battery remained at a voltage less than 5V, the 27V battery would continue to power the STM for several seconds while the AMF card determined whether the AMF conditions were met. The resulting condition would have drained the remaining power in the 27V battery until the blue pod was retrieved 74 days after the incident and tested.

Table 1 shows the relative difference of the in-service time for two new batteries powering the AMF card and two STM transducers. Cameron rates both the 27V battery and the SEM 9V battery for 42 amp-hr. The AMF card requires 2 mA of power while in the armed state. Each STM transducer provides a current output proportional to the pressure reading of 4 mA to 20 mA. At these current drain rates, a full 42 amp-hr. battery will provide 875 days of service life powering the AMF card, but only 43 days of service life powering two STM transducers.

	Amp-hr.	Rate of Discharge – Amps	Hours of Service	Days of Service
27V B powering 2 sensors	42	0.040	1,050	43.75
9V B powering AMF card	42	0.002	21,000	875.00

Table 1

Appendix N AMF Testing

1. American Petroleum Institute, Specification for Control Systems for Drilling Well Control Equipment and Control Systems for Diverter Equipment, 16D, Second Edition, July 2004, § 5.9.3.
2. Cameron Controls, RBS 8D – Multiplex BOP Control System, R & B Falcon–*Deepwater Horizon*, Basic Operation Manual for Standard Systems–3rd Generation, Vol. 1, June 2000, § 1.3, 7; Cameron Controls, Data Books, RBS 8D – Multiplex BOP Control System, Reading & Bates Falcon–*Deepwater Horizon* Project, October 2000, 9, TRN-HCEC-00003804.
3. Cameron Controls, RBS 8D – Multiplex BOP Control System, Vol. 1, 9, TRN-HCEC-00003804; Cameron Controls, RBS 8D – Multiplex BOP Control System, R & B Falcon–*Deepwater Horizon*, Basic Operation Manual for Standard Systems–3rd Generation, Vol. 1, June 2000, TRN-HCEC-0003804.
4. Cameron Controls, RBS 8D – Multiplex BOP Control System, Vol. II, 33-39, TRN-MDL-00042810.
5. Cameron Controls, Data Books, RBS 8D – Multiplex BOP Control System, Reading & Bates Falcon–*Deepwater Horizon* Project, October 2000, 249-290, TRN-HCEC-00003804; Cameron Controls, RBS 8D – Multiplex BOP Control System, TRN-HCEC-0003804.
6. Cameron Controls, RBS 8D – Multiplex BOP Control System, §1.19.1, 50 & 51 of 79. TRN-HCEC-0003804.
7. *Ibid.*
8. Cameron Controls, Data Books, RBS 8D–Multiplex BOP Control System, Vol. 4, Reading & Bates Falcon *Deepwater Horizon* Project, June 2000, 258, TRN-HCEC-00007060; Cameron Controls, Deck Test Procedure for Mark-II Control Pod, Cameron P/N 2020708-21, *Deepwater Horizon*, May 11, 2010, §1.1, 25, CAM-CIV-0002990.
9. Multiplex BOP Cntrl Sys-Valves-Regulators, Vol. 1, TRN-HCEC-0003804; Cameron Controls, Data Books, RBS 8D-Multiplex BOP Control System, Vol. 4, June 2000, TRN-HCEC-00007060; Cameron Controls, Data Books, RBS 8D-Multiplex BOP Control System, Vol. 4, June 2000, TRN-HCEC-00007060.
10. Cameron Controls, Data Books, RBS 8D–Multiplex BOP Control System, Vol. 4, Reading & Bates Falcon *Deepwater Horizon* Project, June 2000, 237, 258, TRN-HCEC-00007060; Cameron Controls, Deck Test Procedure for Mark-II Control Pod, Cameron P/N 2020708-21, *Deepwater Horizon*, May 11, 2010, CAM-CIV-0002990.
11. Cameron Controls, Data Books, RBS 8D–Multiplex BOP Control System, Vol. 4, June 2000, TRN-HCEC-00007060.
12. *Ibid.*
13. Cameron Controls, Data Books, RBS 8D–Multiplex BOP Control System, Vol. 1, October 2000, TRN-HCEC-00003804.
14. *Deepwater Horizon* Shutdown AMF Shutdown Sequence Definition File, May 11, 2000, CAM-CIV-0002990; Cameron Controls, Deck Test Procedure for Mark-II Control Pod, Cameron P/N 2020708-21, May 11, 2010, CAM-CIV-0002990.
15. Owen McWhorter e-mail message to Michael Fry, Feb. 19, 2010, TRN-MDL-00310861.
16. Rig Condition Assessment Report, April 1–14, 2010, TRN-MDL-00038591, 649.
17. Owen McWhorter e-mail message to Michael Fry, Feb.19, 2010, TRN-MDL-00310861.
18. *Deepwater Horizon* Shutdown AMF Sequence Definition File, May 11, 2000. The AMF sequence is encoded in an ASCII-file in the SEM PLC's memory.
19. Cameron Controls, Deck Test Procedure for Mark-II Control Pod, Cameron P/N 2020708-21, May 11, 2010, CAM-CIV-0002990.
20. FRiWO Lithium–MnO₂ Type M 20 Battery Spec Sheet; Cameron Engineering Bulletin EB891D, AMF/Deadman Battery Replacement, Sept. 8, 2004.
21. Friwo, Product Specification, Lithium-MnO₂ Type M 20, Nov. 2, 2009.
22. *Ibid.*
23. Cameron Engineering Bulletin EB891D, AMF/Deadman Battery Replacement, Rev. 01, Sept. 8, 2004.
24. Subsea Workbook, February 2010; Owen McWhorter e-mail message to James Kent, Feb. 23, 2010.
25. Rig Condition Assessment Report, April 1–14, 2010, TRN-MDL-00038591, 649.
26. Daily Report Sheet, Subsea Pod Intervention, Horizon/BP, May 5, 2010, CAM_CIV_0012191.
27. Daily Report Sheet, Subsea Pod Intervention, Horizon/BP, May 5, 2010, CAM_CIV_0012191, 03.

28. Daily Report Sheet, Subsea Pod Intervention, Horizon/BP, May 5, 2010, CAM_CIV_0012191, 95.
29. Daily Report Sheet, Subsea Pod Intervention, Horizon/BP, May 5, 2010, CAM_CIV_0012191, 99.
30. *Ibid.*
31. Daily Report Sheet, Subsea Pod Intervention, Horizon/BP, May 5, 2010, CAM_CIV_0012191, 94.
32. *Ibid.*
33. *Ibid.*
34. Evidence Chain of Custody Receipt, Yellow Pod from *Deepwater Horizon* BOP Stack on MC 252 Well, July 25, 2010, 3.
35. Yellow Pod Deck Test Log, July 25, 2010.
36. DNV, Forensic Examination of *Deepwater Horizon* Blowout Preventer, March 20, 2011.
37. *Ibid.*
38. Daily Report Sheet, Subsea Blue Pod Intervention, June 28, 2010.
39. Daily Report Sheet, Subsea Blue Pod Intervention, June 28, 2010, 03.

Appendix O

Analysis of Solenoid 103

The *Deepwater Horizon* blowout preventer (BOP) stack was supplied with a Cameron Mark II MUX control system. The system had two subsea MUX pods (called the “blue” and “yellow” pods) to control the BOP functions. Each pod had one subsea electronic module (SEM) with two redundant electronic control systems (SEM A and SEM B). To control hydraulic valves and regulators, the SEMs were connected by individual cables to 87 dual-coil solenoids in each pod. Each solenoid had two coils for redundancy, one was controlled and powered by SEM A, and the other was controlled and powered by SEM B. In normal subsea operation of the pods, both SEM A and SEM B applied power to one of the solenoid coils in the dual solenoid when the function is activated. These solenoids controlled 1/4-in. hydraulic pilot valves that (when activated) controlled hydraulic supply valves and regulators in each pod to operate the BOP functions.

Yellow pod solenoid 103 (when activated) supplied hydraulic pilot pressure to the high pressure (HP) shear circuit control valve mounted on the lower BOP stack. The HP shear circuit caused the blind shear rams to close, the ST Locks to lock, and inner failsafe valves to close. Solenoid 103 was powered and activated by the surface BOP control system or by the automatic mode function (AMF) system mounted in each SEM.¹ In normal system operation, when the AMF system was placed into the “arm” mode from a surface control panel, all four AMF processor boards received the signal to arm and stayed in the armed mode until given a “disarm” signal.

Yellow Pod Solenoid 103

February 2010

In the course of routine maintenance to the pods during the *Deepwater Horizon* move to Macondo, several solenoids were replaced on the yellow pod. At that time, solenoid 103 was replaced with a rebuilt spare and function tested prior to lowering the BOP stack to the wellhead. No problems were noted with the yellow pod solenoid 103 while the BOP stack was deployed on the Macondo well.

Testing on the Q4000

May 5, 2010

Fifteen days after the incident, as part of the response to secure the well, the yellow pod was lifted off the *Deepwater Horizon* BOP stack and pulled to surface by an ROV intervention vessel. The pod was transferred immediately to the *Q4000* to prepare the pod to operate the BOP functions.^A The yellow pod AMF battery voltages were checked by a Cameron service technician and found to be at acceptable levels — 8.85 volts (V) for both 9V SEM batteries and 26V for the 27V pod battery.²

May 6, 2010

During the first function test of the AMF system on board the *Q4000*, yellow pod solenoid 103 was tested on the surface by Cameron following Cameron’s AMF test procedure and using an electromagnetic pin technique to determine whether the coil(s) were activated. With one AMF armed and activated per test, there was no indication of solenoid 103 activating.^{3, B} A test was then performed using the Cameron portable electronic test unit (PETU) activating one SEM per test; again, there was no indication of solenoid 103 activating.

The team sent offshore to prepare the yellow pod to again operate the *Deepwater Horizon* BOP had very limited access to the pod, as it was considered evidence. No access was allowed into the subsea electronic module, and no checking or manipulation was allowed of the components or electrical connections.

A The *Q4000* is a dynamically positioned offshore intervention vessel.

B Cameron AMF system consists of one AMF electronic processor board and 9V battery pack for SEM A and SEM B (two per pod) and one 27V battery pack shared by both SEM A and SEM B AMF processor boards (one per pod).

May 8, 2010

With no further testing performed and in preparation to re-run the yellow pod, solenoid 103 was removed from the pod and replaced with a spare solenoid. At that time it was noted that the plug end connection of solenoid 103 was different than the plug end on the replacement spare that was to be installed.⁴ Solenoid 103 was then locked in an evidence box and taken into custody by the U.S. Coast Guard and MMS. The replacement solenoid 103 was successfully function tested by activation of the PETU.⁵

May 12, 2010

The yellow pod AMF system was tested and functioned as expected following the Cameron AMF test procedure.⁶

May 19, 2010

The yellow pod was lowered to the *Deepwater Horizon* BOP stack and latched in place.⁷ The yellow pod was used to operate functions remotely on the *Deepwater Horizon* BOP stack from the *Q4000* for 114 days (May 19–Sept. 10, 2010) when the BOP stack was loaded on a barge to be sent ashore.

Testing at NASA's Michoud Assembly Facility

Feb. 25, 2011

Nearly eight months after removal from the yellow pod on board the *Q4000*, solenoid 103 was bench tested by DNV at NASA's Michoud Assembly Facility (Michoud) in New Orleans using Cameron's test criteria. Solenoid 103 passed all of the tests performed.⁸

March 2, 2011

Solenoid 103 was re-installed in the yellow pod by the DNV at Michoud in preparation to test the AMF system in the blue and yellow pods.⁹

March 3, 2011

Solenoid 103 was tested using the Cameron PETU. When functioned on SEM A only or SEM B only, there was no indication of solenoid 103 fully activating.¹⁰

During the activations of the solenoid, no electrical faults were found with the PETU.¹¹

When solenoid 103 was activated with SEM A or SEM B, the meter on the PETU for monitoring electrical current was indicating current flow, as expected during normal operation.¹²

Solenoid 103 was again removed from the pod and replaced with the same spare that was installed May 8, 2010, on the *Q4000*. The AMF system in the yellow pod was tested with the spare solenoid and functioned as expected.

Solenoid 103 was then re-installed on the yellow pod. The AMF system in the pod was tested with SEM A and SEM B active (normal operation). Solenoid 103 functioned (at 43 seconds) after a 22-second delay from the expected activation time.¹³

The AMF system in the yellow pod was tested two additional times with SEM A and SEM B active. Solenoid 103 functioned (at 21 seconds) as expected at the correct activation time.¹⁴

Note: Each time the AMF was activated in the yellow and blue pods by DNV at Michoud, both the SEM A and SEM B AMF systems were armed and functioned in tandem.

March 4, 2011

The DNV and the investigation Technical Working Group decided that additional tests were required to re-confirm the results.

The group decided both solenoid coils in solenoid 103 should be activated from the Cameron PETU to simulate the normal control system operation when the BOP is subsea.

The No. 1 PETU that was connected to the yellow pod was configured to operate only

SEM A or SEM B. The No. 2 PETU that was connected to the blue pod was configured to operate both SEM A and SEM B at the same time.

The No. 2 PETU was connected to the yellow pod and power supplied to SEM A and SEM B. Hydraulic pilot pressure of 3,000 psi was supplied to the solenoids.

Solenoid 103 was activated three times by PETU No. 2 with both SEM A and SEM B, then with only SEM A or SEM B, and functioned as expected each time.¹⁵

The No. 1 PETU was connected to the yellow pod and power supplied to SEM A. Hydraulic pilot pressure of 3,000 psi was supplied to the solenoids.

Solenoid 103 was activated six times by PETU No. 1 with only SEM A or SEM B. Solenoid 103 functioned as expected on the first activation of SEM A, but did not function again on SEM B or SEM A.¹⁶

The No. 2 PETU was connected to the yellow pod and power supplied to both SEM A and SEM B. The plug end connection of solenoid 103 was pulled from the SEM PIE receptacle.

Solenoid 103 was activated on both SEM A and SEM B. Voltage readings were taken at the PIE receptacle for SEM A and SEM B and were in the correct range per Cameron's specification.¹⁷

The No. 1 PETU was connected to the yellow pod and power supplied to both SEM A and SEM B.

Solenoid 103 was activated on both SEM A and SEM B. Voltage readings were taken at the PIE receptacle for SEM A and SEM B and were in the correct range per Cameron's specification.¹⁸

The No. 2 PETU was connected to the yellow pod and power supplied to both SEM A and SEM B. The plug end connection of solenoid 103 was plugged in to the SEM PIE receptacle. 3,000 psi pilot pressure was supplied to the solenoids.

Solenoid 103 was activated three times by PETU No. 2 with only SEM A or SEM B, then with both SEM A and SEM B, and functioned as expected each time.¹⁹

Solenoid "E-cable" and Plug

Questions were raised by a Cameron service technician's comments written in the Cameron service report on the *Q4000* about the plug end of the solenoid cable.²⁰ These comments caused DNV at Michoud to investigate. The plug on solenoid 103 was not the same as the spare replacement solenoid installed on the yellow pod. Photos and measurements were taken to compare the two versions.²¹

The Transocean investigation team further researched the solenoid cable plug issue by contacting the manufacturer of the cable and plug system directly. The cable and plug on solenoid 103 were the later revision for improved performance that was released by the manufacturer in 2009. All solenoid cable and plug assemblies purchased from 2009 forward would be this revision, whether supplied directly to Transocean by the manufacturer, or from the manufacturer through Cameron.²²

Additional Inspection of Solenoid 103

After review of the test results of solenoid 103 from Michoud and history from the *Q4000*, it appeared there could be a mechanical issue requiring more electrical current to “pull in” (actuate) the solenoid armature that operates the hydraulic pilot valve. Requests were submitted to DNV by the BOP investigation Technical Working Group to perform additional testing and to disassemble the solenoid for inspection.

May 2011

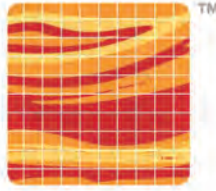
DNV and NASA engineers performed additional inspections and tests of Solenoid 103.

- Solenoid 103 was bench tested by NASA engineers. When power was applied to coil A or B, the solenoid functioned correctly. When power was applied to both coil A and B, solenoid 103 did not function.
- Solenoid 103 was installed in the Yellow Pod and successfully functioned with the PETU three times.
- Solenoid 103 was removed from the Yellow Pod and the wiring was inspected. It was found that one of the coils in the solenoid was wired in reverse polarity to the other coil.

Appendix O Analysis of Solenoid 103

1. See Appendix N.
2. Daily Report Sheet, Subsea Pod Intervention, May 5, 2010, CAM_CIV_0012191.
3. Daily Report Sheet, Subsea Pod Intervention, May 5, 2010, CAM_CIV_0012191.
4. Daily Report Sheet, Subsea Pod Intervention, May 5, 2010, CAM_CIV_0012191.
5. *Ibid.*
6. *Ibid.*
7. *Ibid.*
8. DNV, Forensic Examination of *Deepwater Horizon* Blowout Preventer, March 20, 2011.
9. *Ibid.*
10. *Ibid.*
11. *Ibid.*
12. *Ibid.*
13. DNV, Forensic Examination of *Deepwater Horizon* Blowout Preventer, March 20, 2011.
14. *Ibid.*
15. DNV, Forensic Examination of *Deepwater Horizon* Blowout Preventer, March 20, 2011.
16. *Ibid.*
17. *Ibid.*
18. *Ibid.*
19. *Ibid.*
20. Daily Report Sheet, Subsea Pod Intervention, May 5, 2010, CAM_CIV_0012191.
21. DNV, Forensic Examination of *Deepwater Horizon* Blowout Preventer, March 20, 2011.
22. *Ibid.*

Appendix P
Deepwater Horizon Investigation:
Gas Dispersion Studies



PROSPECT

a Hallin company

A Superior Energy Services Company

Commercial in Confidence

This Report is for Transocean. It should not be disclosed to other parties without the consent of Prospect

Report for:



Document Title:

**Deepwater Horizon Investigation
Gas dispersion studies**

Document Number:

102H006-004R-D

Revision	Date	Description	Originated By	Checked By	Approved By	Client
D	31 Mar 11	Amended labels on Figures 16 & 17	GM	DY	AEG	
C	08 Mar 11	Added labels to Figures 31 - 34	GM	SAH	AEG	
B	04 Feb 11	Revised to include latest result	SAH	GM	AEG	
Draft	29 Jan 11	Draft text	-	-	-	
A	15 Dec 10	Initial issue	SAH	GM	AEG	

CONTENTS

SUMMARY	3
1 BACKGROUND	4
2 TECHNICAL APPROACH	6
3 INFORMATION REGARDING THE EVENT	12
4 DISCUSSION OF THE CFD PREDICTIONS	23
5 CONCLUSIONS	43
REFERENCES	45
FIGURES	46
APPENDICES	
APPENDIX A RESULTS FOR CASE A	
APPENDIX B RESULTS FOR CASE B	
APPENDIX C RESULTS FOR CASE C	

SUMMARY

Transocean is conducting an internal investigation into the explosion that occurred on the Deepwater Horizon, following a release of hydrocarbon gas onto the drilling rig during operations on well MC252. As part of their internal investigation, Transocean has contracted Prospect to perform a sequence of advanced analyses to develop an insight into the explosive event with regard to where the gas is most likely to have been.

This document presents Prospect's findings to date for the gas dispersion phase of the work. Based upon information provided to Prospect by Transocean, the cases presented are considered to represent the most realistic scenarios.

I BACKGROUND

I.1 Introduction

Transocean is conducting an internal investigation into the explosion that occurred on the Deepwater Horizon, following a release of hydrocarbon gas onto the drilling rig during operations on well MC252. This explosion led to the loss of eleven members of the crew and complete loss of the rig.

Transocean's internal investigation is divided into two parts, the first of which is concerned with understanding the likely events leading up to the release of the hydrocarbons onto the rig. The second part of the investigation is dedicated to developing an insight into the explosive event itself and is concerned with where the gas is most likely to have been. Transocean has contracted Prospect to perform a sequence of advanced analyses to support the second part of the investigation.

The objective of the proposed analyses is to support Transocean's investigation by helping find answers to the following questions:

- 1 Where and how did the gas enter the rig hull structure?
- 2 What was the likely position and size of the gas cloud?

This document presents Prospect's findings to date for the gas dispersion phase of the work.

I.2 Sequence of events

The stages of analysis required to support this investigation mirror the sequence of events that led up to the explosive event experienced by the Deepwater Horizon. This sequence of events is summarised in Figure 1 below.

In order to identify the likely sequence of events that led to the explosion onboard the rig it will be necessary to accurately model each of the stages within the sequence. The scope of this document includes the prediction of the background ventilation pattern for the wind conditions on the night of the event and the subsequent discharge and dispersion pattern of flammable gas following the loss of control of the well. The prediction of the dynamics of the explosion event(s) following the ignition of the flammable gas cloud is not within the scope of this document.

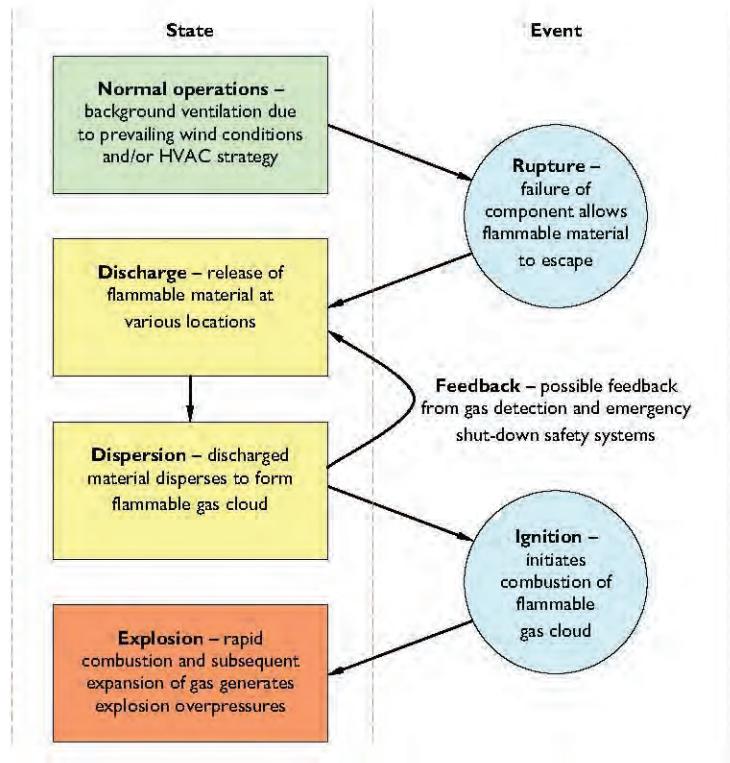


Figure 1 Sequence of relevant events leading to the explosion

2 TECHNICAL APPROACH

2.1 Background ventilation

Under normal operating conditions before the loss of control of the well the background ventilation pattern through the rig will have been determined entirely by the wind conditions and the HVAC strategy in place at the time of the incident and the geometry of the rig. Prospect has assumed that the wind conditions and HVAC strategy remained steady in the period before the loss of the well.

Prospect has used the three-dimensional steady-state unstructured CFD approach to predict the background ventilation pattern around the complex geometry of the rig and within selected internal spaces.

Prospect selected the FLUENT 12.1 CFD code by ANSYS for the background ventilation analysis. The key points for this selection were:

- Realistic representation of geometry;
- Implementation of the atmospheric boundary layer;
- Realistic representation of resistance to flow due to small-scale congestion.

2.1.1 Capturing a realistic representation of the geometry

Although much of the geometry of the platform was rectangular which may have been captured using the simple structured hex-mesh approach shown in Figure 2 below, there were a large number of geometrical features that could not have been easily captured by this type of mesh. Prospect exploited the flexibility of the CFD code to allow a combination of structured hex-meshing, and where necessary, unstructured tetra-meshing (as shown in Figure 3) to capture the complex geometrical details of the rig.

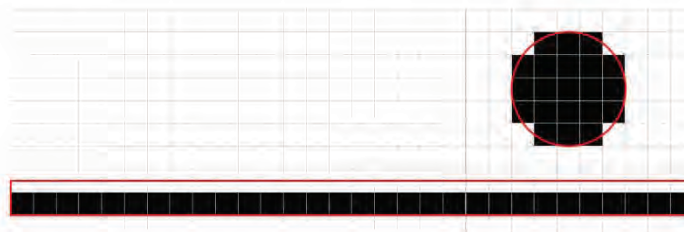


Figure 2 Approximation of non-rectangular geometry with a structured hex-mesh



Figure 3 Non-rectangular geometry with an unstructured tetra-mesh

The CFD model geometry was constructed in accordance with the as-built drawings that were made available by Transocean [1]. The CFD model of the rig is shown in Figure 31 to Figure 40 at the end of this report.

2.1.2 Implementation of the atmospheric boundary layer

Within the atmospheric boundary layer the wind speed is observed to decrease in the region close to the surface of the sea due to the effects of friction. Given a long-enough fetch where the surface roughness remains constant, the atmospheric boundary layer will reach an equilibrium whereby the momentum required to overcome the surface shear stresses exactly balances the momentum supplied from higher layers, such that the mean vertical profiles of wind speed and turbulence remain constant.

Prospect has used the Deaves and Harris model [2] for the mean vertical profiles of wind speed, turbulence kinetic energy and the rate of dissipation of turbulence kinetic energy. The model was implemented using the user-defined function (UDF) capability of the CFD code. This implementation of the model requires the following three inputs to be specified:

- Wind speed specified at 10m above sea level [m/s];
- Wind direction, defined as the direction from which the wind is blowing measured clockwise from the bow [°];
- Latitude of the site [28°].

The vertical profiles for wind speed and turbulence were imposed at the windward boundary of the CFD model. Turbulence effects were modelled using the two-equation realizable $k\varepsilon$ closure.

2.1.3 Incorporating a realistic representation of resistance to flow due to small-scale congestion

Although it is possible to embed the geometry of the small-scale congestion within the CFD mesh, the cell count of the CFD mesh will soon become excessive, especially as the details become smaller, as shown for a simple pipe bundle in Figure 4 below, which prohibits this as a sensible approach.

A more pragmatic alternative approach is to employ the *Approximation of Cylindrical Elements* (ACE) method [3] where the geometry of the platform is divided into the primary geometry, which will include all details larger than some cut-off dimension, and the secondary geometry, which will include all details smaller than that cut-off dimension, such as pipework. Whilst all of the primary geometry will be captured explicitly within the CFD mesh as normal, the smaller-scale secondary geometry will instead be represented in terms of a resistance to the flow distributed across the appropriate cells within the CFD mesh.

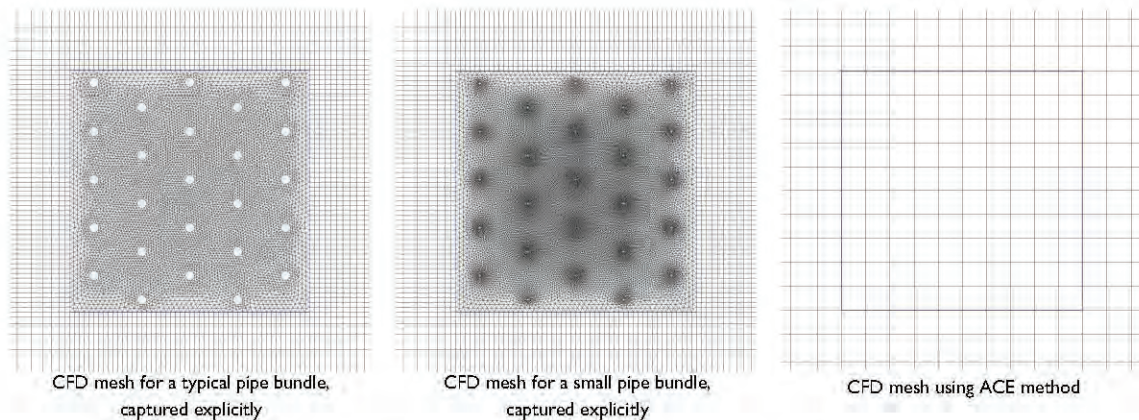


Figure 4 Capturing small scale congestion within the CFD mesh

Prospect has implemented the ACE method using the UDF capability of the CFD code. A view of the CFD model showing the primary geometry of the platform (in grey) and the ACE approximation for the small-scale congestion around the platform and within the moonpool (using a yellow-red scale) is given in Figure 41 to Figure 44 at the end of this report.

2.2 Discharge

Due to the high momentum of the jet in the near-field region close to a high pressure rupture, Prospect has assumed the geometry of the discharge jet will not have been significantly influenced by the background ventilation pattern, but will, instead, have tended to become circular in cross-section as ambient air is entrained.

Prospect has applied the laws of conservation for mass and momentum to determine analytically the flow conditions at the end of the near-field region, which was chosen to occur where the mean velocity within the discharge jet had fallen to around thirty percent of the local speed of sound, such that high speed compressibility effects could be ignored.

Whilst Prospect acknowledges that the CFD approach could have been used to predict the flow in this near-field region, this would have required a more refined mesh in the near-field which would have significantly increased the computational requirements unnecessarily.

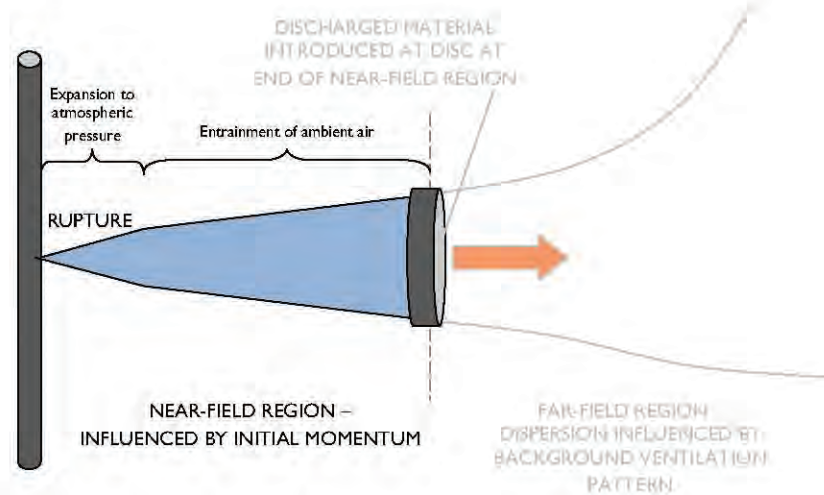


Figure 5 Near-field and far-field for a jet emerging from a rupture

2.3 Dispersion

Downstream of the near-field region, Prospect has used the three-dimensional unstructured CFD approach to predict the dispersion pattern for the release of hydrocarbon gas around and within the rig. Since it is the behaviour of the build-up of hydrocarbon gas in the period following the loss of control of the well that is of interest, a transient CFD analysis was undertaken.

For each case considered a set of circular discs were included within the CFD mesh that coincided with the end of the near-region for each release location. The area of each disc matched the area calculated at the end of the near-field region at the maximum flow rate. A mixture of hydrocarbon gas and ambient air was released in the appropriate direction from the release face on the downstream side of the disc. A corresponding amount of ambient air was withdrawn from the upstream face of the disc to account for the flow entrained into the discharge jet in the near-field.

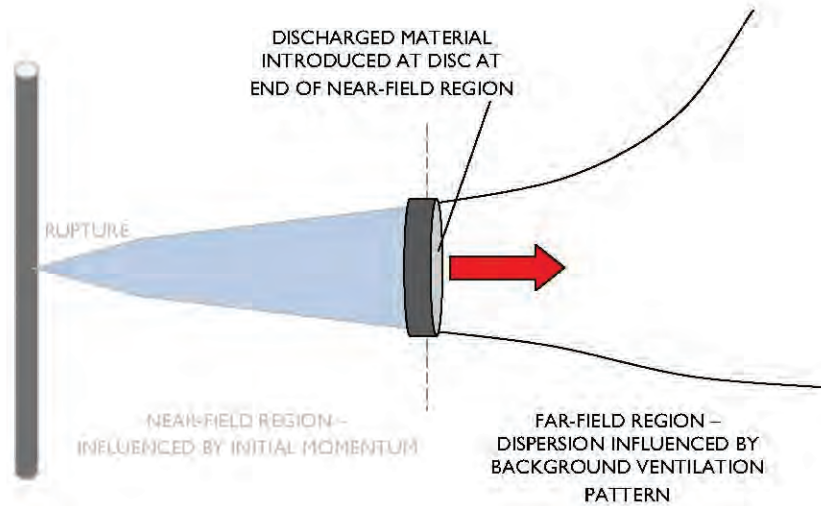


Figure 6 Far-field dispersion for a jet emerging from a rupture

Prospect has used the same FLUENT 12.1 CFD code for the dispersion analysis. In addition to the key points considered for the background ventilation analysis (Section 2.1), the key point for this selection was:

- Ability to refine the mesh along path of the dispersing plume of gas.

2.3.1 Refinement of the CFD mesh along the path of the dispersing jet

In order to improve the accuracy of a CFD prediction it is necessary to refine the mesh in the regions of interest. In the case of this dispersion analysis, it is necessary to refine the mesh along the path of the dispersing hydrocarbon gas. The dispersion pattern for the released gas will generally not follow one of the principal coordinate directions. With a structured orthogonal hex-mesh the released gas may soon stray into regions of large cells within the mesh, thus limiting the accuracy of any analysis, as shown in Figure 7 below.

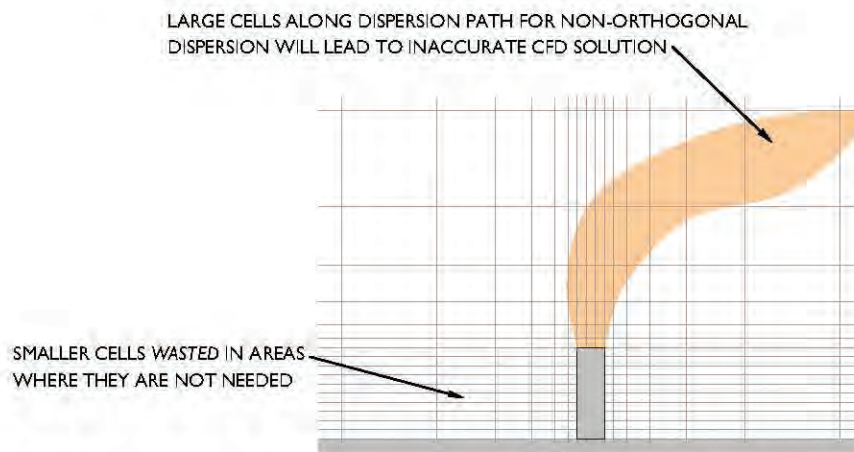


Figure 7 Dispersion pattern on a structured orthogonal hex-mesh

Using the flexible unstructured meshing capability of the CFD code, a refined mesh was achieved along the path of the released gas using mesh adaption during the solution process, as illustrated in Figure 8 below.

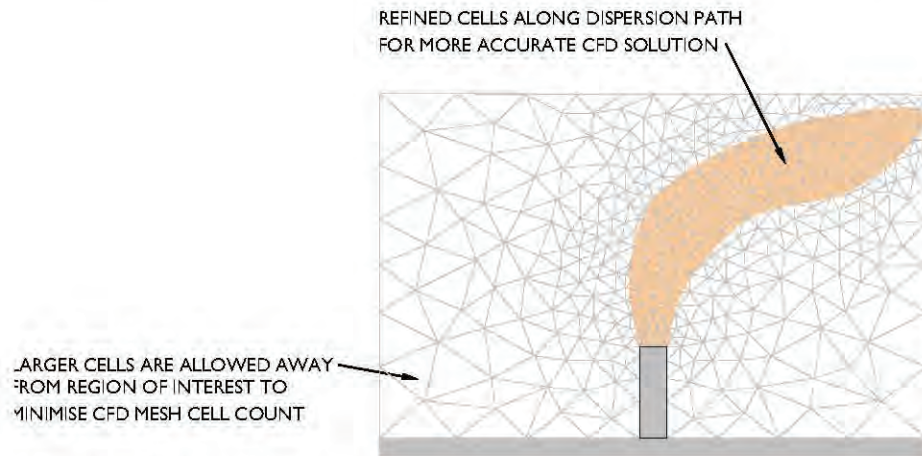


Figure 8 Dispersion pattern on an unstructured tetra-mesh, refined along path of released gas

Rather than monitor the extent of the jet at each time-step and adapt the mesh during the transient simulation, which would have prolonged the time required for each dispersion simulation, Prospect employed the following two-stage approach:

- Undertake a steady-state dispersion simulation to refine the mesh along the path of each jet at the maximum release rate;
- Using this refined mesh, undertake the transient dispersion analysis, as required.

With this approach, the CFD mesh could remain fixed throughout the transient analysis.

3 INFORMATION REGARDING THE EVENT

3.1 Incident wind conditions

Transocean has advised that at the time of the incident there was a slight breeze of around three knots ($\approx 1.5\text{m/s}$) blowing from the southwest [4]. Since the vessel was on a southeast bearing [4], the wind was blowing from starboard to port (see Figure 9).



Figure 9 Wind direction at the time of the incident

3.2 Mechanical ventilation systems in operation at the time of the incident

A number of mechanical ventilation systems were installed, with each system serving specific internal spaces within the rig. The location of each ventilation fan is shown graphically in Figure 31 to Figure 34.

Generally, the internal spaces included within the CFD model were maintained under pressure by an imbalance in the supply and extract ventilation rates to the space. Where the space was maintained under a positive pressure by supplying air at a higher rate than it was extracted from the space, the supplied air will have escaped through doorways and gaps in the structure to neighbouring spaces within the rig. Likewise, if the space was maintained at a negative pressure by extracting air at a higher rate than it was supplied from the space, air will have been drawn into the space through doorways and gaps from neighbouring spaces.

Rather than attempt to model the air infiltration between spaces within the rig, Prospect has neglected the imbalance between the rate at which air was supplied and extracted. Instead, in order to ensure a flow balance within each space, either the supply rate or the extract rate was specified, according to Table 1 below. The ventilation rates were imposed by introducing a momentum source within the appropriate ventilation duct to yield the correct flow rate.

Table 1 Assumed ventilation rates to internal spaces within the CFD model

Internal space	Fan	Description	Flow rate [m ³ /hr]
Shale shaker house	SF-55	Shale shaker house supply 1	24 000
	SF-56	Shale shaker house supply 2	24 000
	EF-57	<i>Shale shaker house exhaust 1</i>	<i>30 000</i>
	EF-58	<i>Shale shaker house exhaust 2</i>	<i>30 000</i>
Engine room 1	SF-01	Engine room 1 supply	118 950
	EF-07	<i>Engine room 1 extract</i>	<i>52 000</i>
Engine room 2	SF-02	Engine room 2 supply	101 107
	EF-08	<i>Engine room 2 extract</i>	<i>34 157</i>
Engine room 3	SF-03	Engine room 3 supply	101 107
	EF-09	<i>Engine room 3 extract</i>	<i>34 157</i>
Engine room 4	SF-04	Engine room 4 supply	101 107
	EF-10	<i>Engine room 4 extract</i>	<i>34 157</i>
Engine room 5	SF-05	Engine room 5 supply	101 107
	EF-11	<i>Engine room 5 extract</i>	<i>34 157</i>
Engine room 6	SF-06	Engine room 6 supply	118 950
	EF-12	<i>Engine room 6 extract</i>	<i>52 000</i>
Mud pump room	SF-18	Mud pump room supply fan (port)	52 708
	SF-19	Mud pump room supply fan (starboard)	52 708
	EF-20	Mud pit room exhaust fan (port)	43 104
	EF-21	<i>Mud pit room exhaust fan (starboard)</i>	<i>43 104</i>
HVAC rooms	SF-72	AHU room 5	3 700
	SF-73	AHU room 6	3 700
Sack storage room	SF-26	Common space supply (starboard)	51 643
	EF-27	<i>Common space exhaust (starboard)</i>	<i>50 520</i>
Mud tank room	SF-13	Mud pit room supply fan A	21 411
	SF-14	Mud pit room supply fan B	21 411
	EF-15	Mud pit room exhaust fan A	25 190
	EF-16	<i>Mud pit room exhaust fan B</i>	<i>25 190</i>
	EF-17	<i>Mud pit tank extractor exhaust fan</i>	<i>8 496</i>
Cement room	SF-22	Cement room supply	35 021
	EF-23	Cement room exhaust	25 437

Table 1 Assumed ventilation rates to internal spaces within the CFD model

Internal space	Fan	Description	Flow rate [m ³ /hr]
Port transformer room	SF-30	Transformer room supply (port)	50 705
	<i>EF-32</i>	<i>Transformer room exhaust (port)</i>	<i>43 949</i>
Starboard transformer room	SF-31	Transformer room supply (starboard)	50 705
	<i>EF-33</i>	<i>Transformer room exhaust (starboard)</i>	<i>43 949</i>

To ensure a flow balance within each internal space, the fans in italics were not activated within the CFD model.

In addition to the ventilation systems to the internal spaces described in Table 1, the supply fans listed in Table 2 and the extract fans listed in Table 3 were also included within the CFD model.

Table 2 Additional supply fans included within the CFD model

Supply fan ID	Description	Flow rate [m ³ /hr]
SF-24	Common space supply (port)	20 930
SF-34	Column supply (port forward 1)	18 070
SF-35	Column supply (port forward 2)	3 460
SF-36	Column supply (starboard forward 1)	18 070
SF-37	Column supply (starboard forward 2)	3 460
SF-38	Column supply (port aft 1)	18 070
SF-39	Column supply (port aft 2)	5 150
SF-40	Column supply (starboard aft 1)	18 070
SF-41	Column supply (starboard aft 2)	5 150
SF-63	Mud lab supply fan	1 820

Table 3 Additional extract fans included within the CFD model

Supply fan ID	Description	Flow rate [m ³ /hr]
EF-25	Common space exhaust (port)	14 139
EF-42	Column exhaust (port forward 1)	17 400
EF-43	Column exhaust (port forward 2)	3 250
EF-44	Column exhaust (starboard forward 1)	17 400
EF-45	Column exhaust (starboard forward 2)	3 250
EF-46	Column exhaust (port aft 1)	17 400
EF-47	Column exhaust (port aft 2)	4 950
EF-48	Column exhaust (starboard aft 1)	17 400
EF-49	Column exhaust (starboard aft 2)	4 950
EF-59	FO room exhaust (port)	10 435
EF-60	FO room exhaust (starboard)	10 435
EF-61	Welding shop exhaust	4 460

3.3 Engines in operation at the time of the incident

Transocean has advised that at the time of the incident only two engines were operational, engine 3 and engine 6. It was assumed that both engines consumed air directly from the surrounding engine room at a rate of 5.28 m³/s under 35 % load [5], which was subsequently rejected at the engine exhausts.

3.4 Composition and properties of the hydrocarbon gas emerging from the riser

The composition assumed for the hydrocarbon gas as it emerged from the riser is summarised in Table 4 below [6].

Table 4 Assumed composition of hydrocarbon gas

Component	Volume fraction
Nitrogen	0.49 %
Carbon Dioxide	1.00 %
Hydrogen Sulfide	0.00 %
Methane	73.70 %
Ethane	6.89 %
Propane	4.69 %
Iso-Butane	0.94 %
N-Butane	2.08 %
Iso-Pentane	0.80 %
N-Pentane	0.94 %
Hexanes	1.17 %
Heptanes	1.66 %
Octanes	1.41 %
Nonanes	0.98 %
Decanes	0.80 %
Undecanes	0.51 %
Dodecanes	0.38 %
Tridecanes	0.29 %
Tetradecanes	0.21 %
Pentadecanes	0.16 %
Hexadecanes	0.13 %
Heptadecanes	0.10 %
Octadecanes	0.10 %
Nonadecanes	0.08 %
Eicosanes	0.49 %

The properties of this gas mixture are summarised in Table 5 below.

Table 5 Properties of assumed hydrocarbon gas

Property	Value
Molecular weight	31.4 kg/kmol
Lower flammable limit (LFL)	2.6 % by volume
Stoichiometric concentration	5.5 % by volume
Upper flammable limit (UFL)	13.1 % by volume

The released gas could have burned only if the local concentration was within the flammable range between the lower flammable limit (LFL) and the upper flammable limit (UFL). If the local concentration was below the LFL there would have been insufficient fuel to sustain combustion (fuel-lean). Likewise, if the local concentration was above the UFL, there would have been insufficient oxygen to sustain combustion (fuel-rich).

Furthermore, whilst it is possible for a flammable gas mixture to ignite at the LFL concentration, ignition may prove difficult, even in the presence of a suitable source of ignition. Ignition, however, becomes more probable as the stoichiometric concentration is approached, as shown in Figure 10 below.

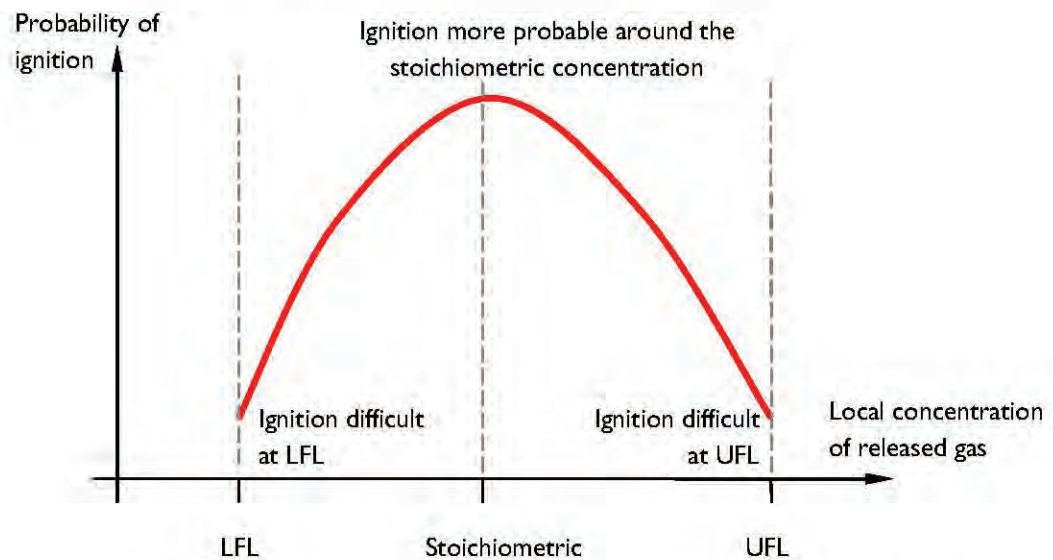


Figure 10 Probability of ignition across the flammability range for hydrocarbon gas

3.4.1 Transient profile for rate of gas release from riser

A preliminary analysis of the dynamics of hydrocarbon within the riser was performed by Stress Engineering Services [7], which provided an estimate of the rate at which hydrocarbon gas may have been released from the riser following the loss of control of the well.

According to this analysis, hydrocarbon gas most likely reached a peak within a short time of the initial arrival of gas and then decayed to a more steady rate after a few minutes. As an initial estimate, Prospect was asked to consider a peak release of 600 MMscfd after 60 s, as shown by the green curve in Figure 11 below. The steady rate of release was estimated to be 203 MMscfd [7], as shown by the red curve.

In the event that the BOP had closed, the release of hydrocarbons would have been restricted to the inventory already within the riser, which was estimated to be 1.128 MMscf [7]. With the additional assumption that the riser inventory would have escaped within eight minutes of the initial release, the decay curve was calculated to be that shown by the green curve, with the area under the curve corresponding to the riser inventory.

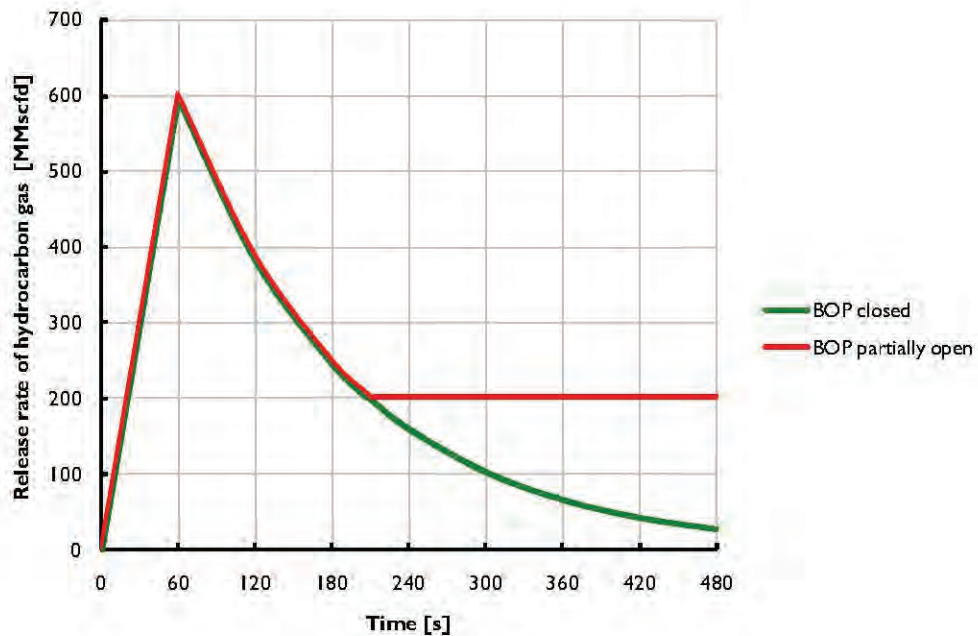


Figure 11 Transient profile for the rate of gas release from the riser

Since both the peak release rate and the time taken to reach this peak remain uncertain, Prospect has considered a number of cases to assess the sensitivity of the gas dispersion pattern to the precise release profile. Preliminary sensitivity studies demonstrated that the predicted arrival time of the LFL envelope at ventilation intakes across the aft deck of the vessel was sensitive to the rate of increase of the mass release profile until the peak flow was reached, rather than to the magnitude of the peak.

To address this, three alternative profiles are considered within this report, as summarised in Figure 12 below. From the initial profile (shown in red), Profile A with a peak of 500 MMscfd, Profile B with a peak of 400 MMscfd and Profile C with a peak of 300 MMscfd were constructed, with the initial rise time adjusted to maintain an area of 1.128MMscf under the curve (inventory of riser in the event of the closed BOP) whilst retaining the same decay curve.

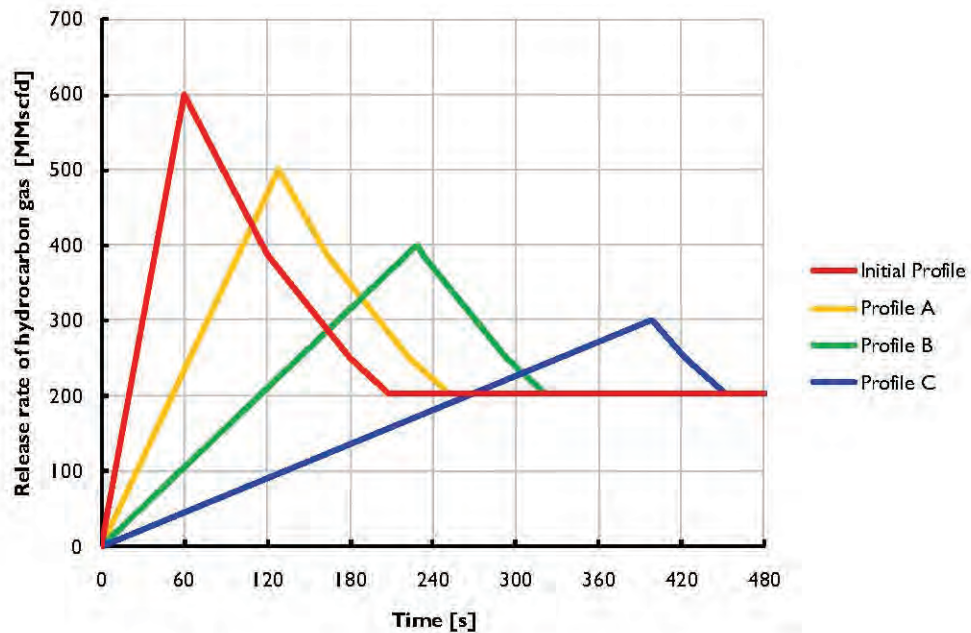


Figure 12 Release profiles considered for this study

3.5 Release locations

In discussions with Transocean, a number of rupture locations were identified within the riser system and the mud-gas separator (MGS) system further downstream. Each of the rupture locations is shown graphically in Figure 45 to Figure 51 at the end of this report.

3.5.1 Riser system

The first possible failure may have occurred at the slip joint in the moonpool. It is plausible that the packer seal failed, which could have resulted in a rupture around the circumference of the seal. For the purpose of this study, the release was assumed to be a strip up to $\frac{1}{2}$ -inch wide around the circumference of the telescopic joint, with an area of 0.024 m^2 . The direction of this release was assumed to be upward, towards the underside of the rotary table.

3.5.2 Diverter

The second possible failure may have occurred at the diverter mounted just below the drill floor. It is possible that the packer of the diverter and its ability to seal against the drill pipe was impaired by the escaping fluid following the loss of well control. It was assumed that any failure to seal would result in an upward discharge of fluids. A discussion of the degree of damage to the seal is presented in Section 3.5.4.1.

3.5.3 MGS system

The MGS system is shown schematically in **Error! Reference source not found.** below. It is understood that hydrocarbon gas may have been entering the mud-gas separator at the time of the incident via the 14 inch diverter from the riser. Assuming the separator remained intact during the initial stages of the gas release, there are two routes from which the gas may have emerged.

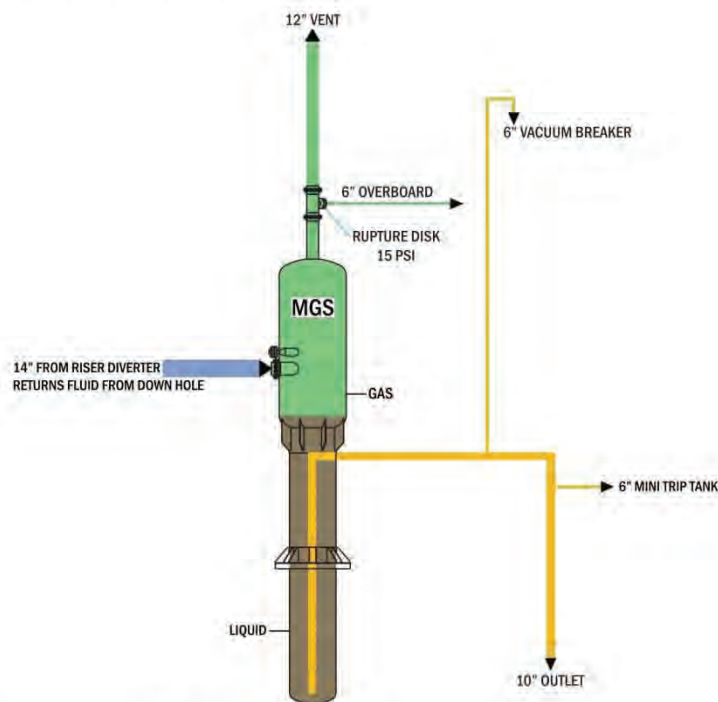


Figure 13 Mud-gas separator (MGS) system

The gas takeoff is a twelve-inch line which rises to the top of the drilling derrick and terminates pointing towards port and downward at approximately thirty degrees below horizontal. There is also a six-inch relief line from this takeoff which runs towards starboard and terminates horizontally to starboard at the edge of the vessel. The relief line is isolated by a bursting disk rated at 15 psi - it was assumed that this burst disk was ruptured by the escaping mud during the loss of control of the well, immediately prior to the first release of gas from the riser.

The liquid takeoff is a ten-inch line which leads to the gumbo-box within the shale shaker house, which has an open top with an area of 5.39 m². There are two additional six-inch lines from this takeoff: a vacuum breaker line

which rises up the starboard aft leg of the drilling derrick to a height of EL+67 m and terminates with a gooseneck pointing downward, and a line to the mini trip tank located on the starboard side of the drill floor which has an open top with an area of 0.43 m².

3.5.4 Estimation of damage

It was assumed that the damage to the rotary table and slip joint, and the burst disk to the six-inch starboard relief line from the MGS gas takeoff, had been caused by the escaping mud during the loss of control of the well, immediately prior to the first release of gas from the riser. Whilst the area of each exit from the MGS system was known, the release area at the rotary table and the slip joint was more uncertain since this was the result of damage caused by the escaping mud.

3.5.4.1 Rotary table

Transocean has advised that during the aftermath of the explosion a vertical flame, around one-hundred feet in length, was observed rising from the centre of the drill floor [8]. Assuming that this flame was emerging from the damaged bush at the rotary table and using the following empirical relationship relating the length of a vertical flame, L, to the energy release rate, Q [9]:

$$L = 2.76Q^{0.452}$$

the mass flow rate of hydrocarbon gas escaping at this location was of the order of 6 kg/s, which is around 7% of the estimated steady rate of release of 203 MMscfd [7]. Upon this basis, the rupture area of the partially damaged rotary table was assumed to be 0.013 m².

3.5.4.2 Slip joint

If the packer seal at the slip joint had failed entirely there would have been a 1/2-inch gap around the 24 inch riser, with a corresponding rupture area of 0.024 m². This represents only a small fraction (around one-eighth) of the total rupture area summed across the rotary table and the offtakes from the MGS system. As a consequence, if the packer seal was only partially damaged the increase in the flow escaping from the other release locations to conform to the same total release rate would have been marginal.

Prospect has undertaken several CFD cases to assess the sensitivity of the gas dispersion to the degree of damage at the packer seal. It was found that the sensitivity of the dispersion pattern across the aft deck of the vessel to this degree of damage was not significant. For the cases presented in this report, Prospect has assumed that the packer seal at the slip joint had failed entirely.

3.5.5 Summary of assumed rupture areas

In summary, the rupture area assumed at each release location for this study is presented in Table 6 below. The total rupture area is 0.217 m².

Table 6 Summary of the assumed area for each release location

Release location	Description	Area [m²]
Slip joint	½ inch gap around circumference of 24 inch riser	0.024
Rotary table	Assuming 100ft flame	0.013
Gumbo box	10 inch line	0.051
Vacuum breaker	6 inch line	0.018
Mini trip tank	6 inch line	0.018
MGS outlet	12 inch line	0.073
MGS starboard relief	6 inch line	0.018

4 DISCUSSION OF THE CFD PREDICTIONS

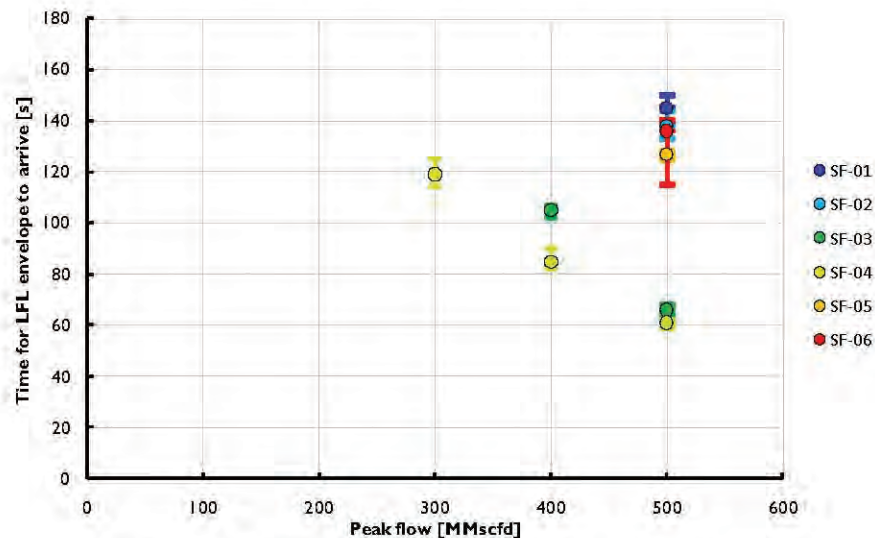
Prospect has undertaken many CFD simulations to assess the sensitivity of the gas dispersion pattern to a number of uncertain parameters including the mass release profile, the degree of damage to the packer seal at the slip joint and the wind speed and direction. For each case, the profile for the release rate of hydrocarbon gas given in Figure 12 was divided on an area-weighted basis using the areas summarised in Table 6. Based upon their best evidence and witness statements, Transocean advised Prospect to simulate the dispersion of the released gas for the first three minutes after the arrival of hydrocarbon gas at the rig.

Prospect has undertaken an analysis of the CFD predictions, from which a number of trends are identified and discussed in Section 4.1. Following this, Prospect has selected three cases for further discussion, presented in Section 4.2, which are thought to represent the most realistic scenarios from the CFD cases considered.

4.1 Trends from CFD study

4.1.1 Sensitivity to mass release profile

The trend for the predicted arrival time of flammable gas at each of the supply fan intakes to the engine rooms for the mass release profiles considered is shown in Figure 14 below. It is apparent that the arrival time is sensitive to the rate of increase of the mass release profile before the peak flow was reached.

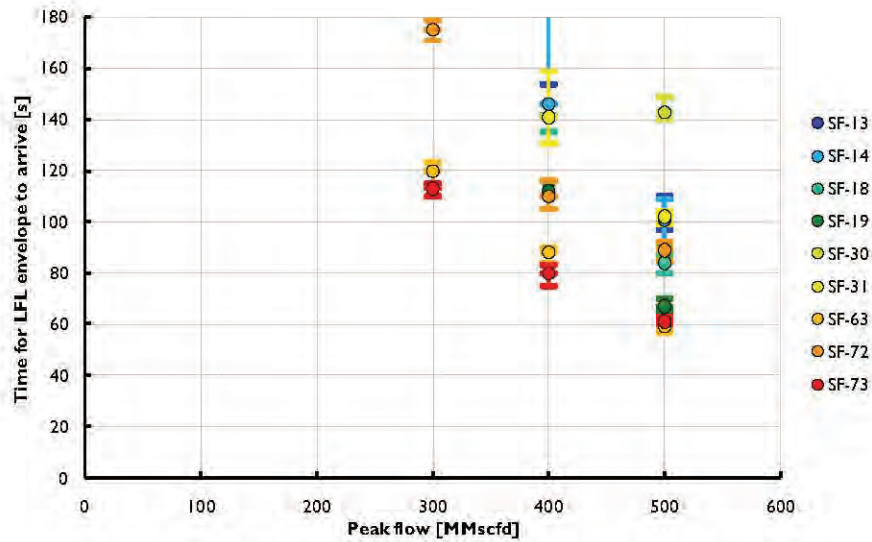


Lower bound of error bar corresponds to predicted arrival time of 90% LFL

Upper bound of error bar corresponds to predicted arrival time of 110% LFL

Figure 14 Trend for the arrival time of the LFL envelope at the engine room intakes

Similarly, it is apparent from Figure 15 that the predicted arrival time at the ventilation intakes across the midship section of the aft deck of the vessel is also sensitive to the rate of increase of the mass release profile before the peak flow was reached.



Lower bound of error bar corresponds to predicted arrival time of 90% LFL
Upper bound of error bar corresponds to predicted arrival time of 110% LFL

Figure 15 Trend for the arrival time of the LFL envelope at midship intakes

4.1.2 Sensitivity to wind speed

The trend for the predicted arrival time of flammable gas at each supply fan intake, assuming the mass release Profile A (with a peak flow of 500 MMscfd), is shown in Figure 16 and Figure 17 below.

For the intakes within the central region of the main deck, including SF-03, SF-04, SF-18, SF-19, SF-63, SF-72 and SF-73, it is apparent that the dispersion of the flammable gas of released gas is dominated by the momentum of the released gas as it emerges from the shale shaker ventilation system, such that the predicted arrival time for the LFL envelope remains relatively insensitive to the wind speed.

For the intakes located along the port deck it is apparent that the dispersion pattern is further influenced by the wind which carries the released gas downwind from the central region of the main deck. The predicted arrival time of the LFL envelope at, for example SF-01 and SF-02, is therefore delayed at the lighter wind (for example at the lighter wind speed the arrival of flammable gas at SF-02 occurs after 180s, hence this intake does not appear in Figure 16).

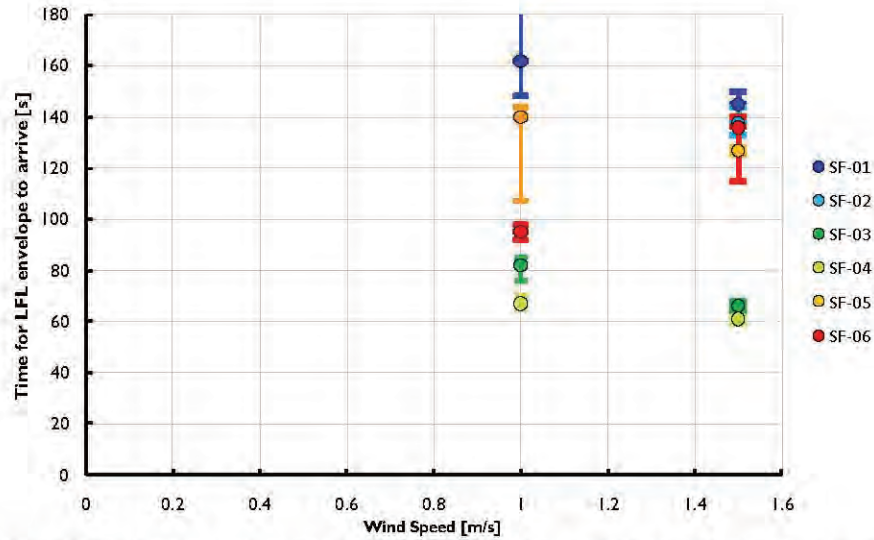


Figure 16 Trend for the arrival time of the LFL envelope at the engine room intakes (assuming release Profile A)

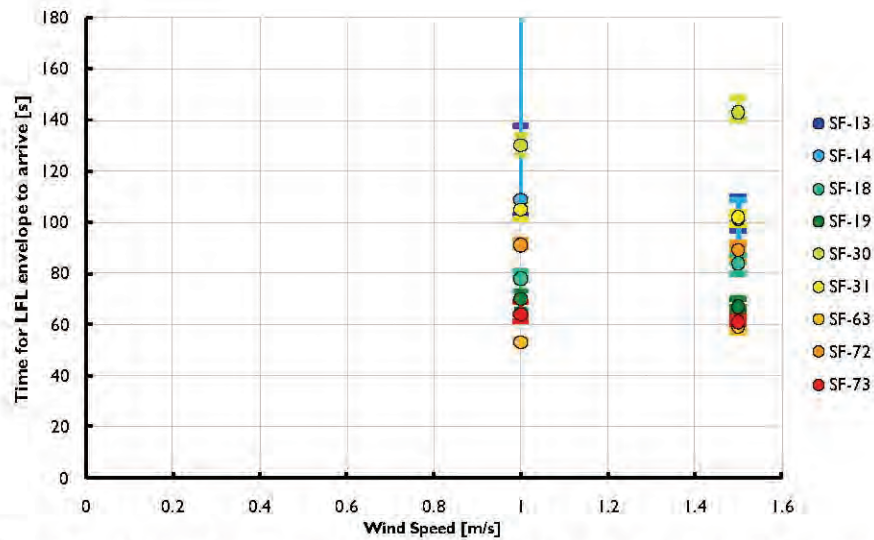


Figure 17 Trend for the arrival time of the LFL envelope at other intakes (assuming release Profile A)

For the intakes located along the starboard deck, the dispersion pattern is significantly influenced by the recirculating eddies in the boundary layer downstream of the leading edge shown in Figure 18 below. It is apparent that the progress of gas against the wind towards the starboard intakes, specifically SF-05 and SF-06, is critically dependent upon the wind speed due to the action of turbulent dispersion and counter-flow within the recirculating eddies. Since the wind speed is likely to vary at low wind speeds, such as that reported during the

incident, it is not possible to draw firm conclusions regarding the exact timing of the arrival of the LFL envelope at the starboard ventilation intakes, or the amount of flammable gas ingested into engine rooms 5 and 6.

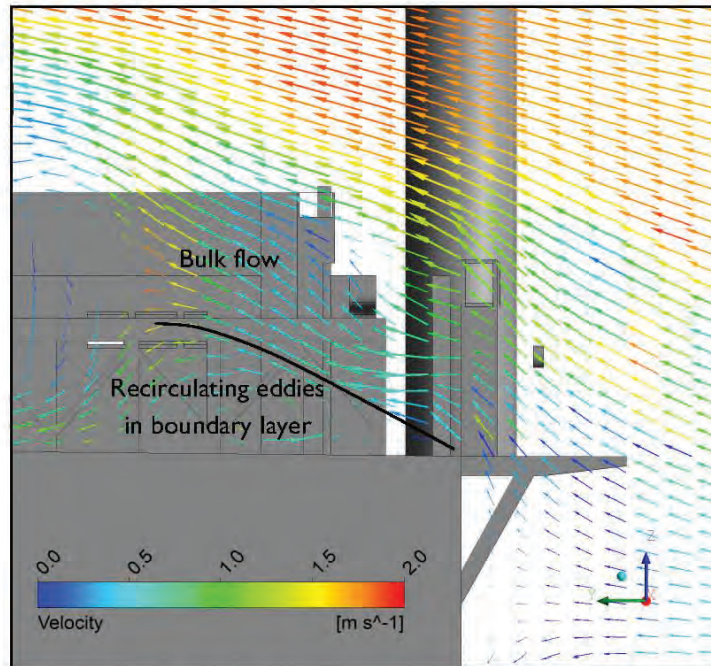


Figure 18 Velocity vector plot showing separation of flow at the starboard edge of the main deck (looking towards bow)

4.2 Presentation of specific cases

Prospect has selected the three cases in Table 7 for further discussion in this report, which are thought to represent the most realistic scenarios from the CFD cases considered.

Table 7 Summary of cases presented

Case	Release profile	Wind speed	Wind direction
Case A	Profile A	1.5 m/s	From starboard
Case B	Profile B	1.5 m/s	From starboard
Case C	Profile C	1.5 m/s	From starboard

4.2.1 Case A

The results for Case A are presented in Appendix A at the end of this report.

4.2.1.1 General observations

The largest release is directed portward from the MGS outlet at the top of the derrick. The associated plume is predicted to remain clear of the rig, away from the main deck and the ventilation intakes to internal spaces. Likewise, the plume of hydrocarbon gas from the MGS starboard relief is predicted to remain clear of the starboard side of the rig.

The release from the gumbo box is predicted to fill the shale shaker house with a flammable gas mixture within 10 s to 20 s. After this point, the environment within the shale shaker house becomes fuel rich. After around 20 s, the flammable gas is predicted to emerge from the exhausts (EF-57 and EF-58) to form an expanding cloud of flammable gas which is predicted to disperse over the starboard aft deck of the vessel. The plume of hydrocarbon gas from the vacuum breaker is predicted to augment the cloud emerging from the shale shaker exhaust ventilation system in the region around the starboard aft leg of the derrick.

The release from the mini trip tank at the drill floor is predicted to fill the drawworks house with a flammable gas mixture, which is predicted to disperse over the drill floor and around the BOP house with the wind.

The release directed upward from the rotary table and the associated plume of hydrocarbon gas is predicted to rise away from the rig, away from the main deck and the ventilation intakes to internal spaces.

The release from the slip joint is predicted to fill much of the moonpool with a flammable gas mixture. After around 60 s, flammable gas is predicted to escape from the forward openings to the moonpool and disperse over the forward deck.

4.2.1.2 Ingestion of hydrocarbon gas at ventilation intakes

The predicted time history for the concentration of hydrocarbon gas averaged across each engine room ventilation intake is provided in Figure 19 below. From this graph the LFL envelope is predicted to arrive at SF-03 and SF-04, the ventilation intakes to engine rooms 3 and 4 located along the centreline of the vessel, after around 60 s, with the stoichiometric envelope arriving after around 100 s to 120 s.

The increase in concentration of hydrocarbon gas at SF-01 and SF-02, the intakes to engine rooms 1 and 2 located at the port/leeward edge of the vessel, is more gradual, with the LFL envelope predicted to arrive after around 140 s. The stoichiometric envelope is not predicted to reach these intakes within the three minute duration of the CFD simulation.

The concentration of hydrocarbon gas at SF-05 and SF-06, the intakes to engine rooms 5 and 6 located at the starboard/windward edge of the vessel, is predicted to reach the LFL threshold at around 120 s for this case. Further to the discussion in Section 4.1. regarding the sensitivity of the dispersion pattern at these intakes to the mass flow profile and the wind speed, this arrival time should be treated with caution. The concentration of hydrocarbon is predicted to remain below the stoichiometric concentration for this case.

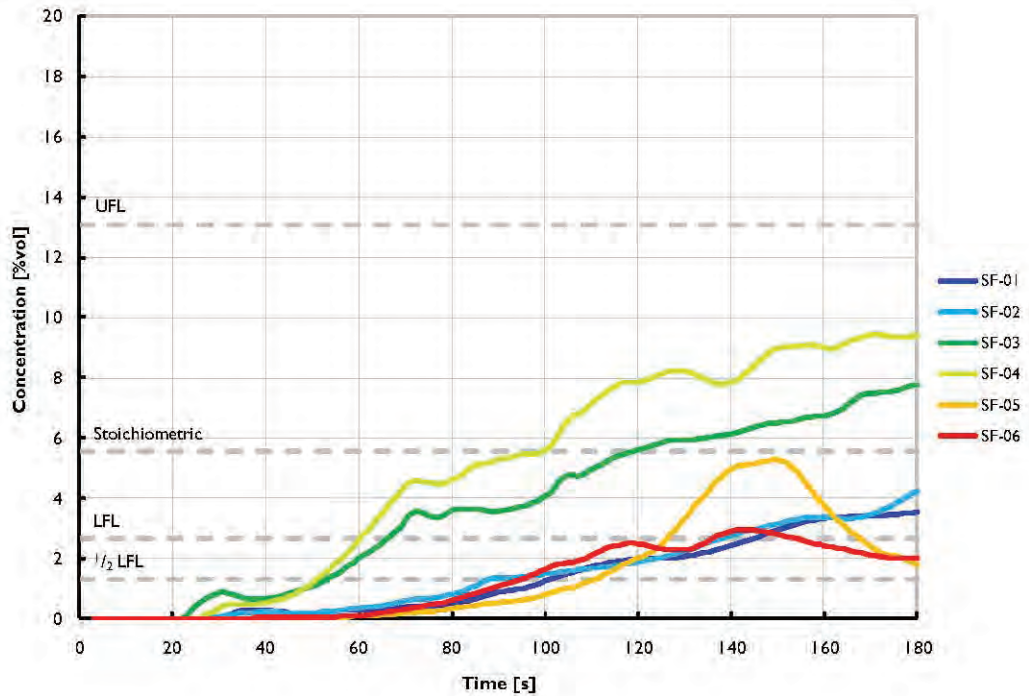


Figure 19 Predicted time history for the concentration of hydrocarbon gas at each of the engine room ventilation intakes – Case A

The predicted time history for the concentration of hydrocarbon gas averaged across each ventilation intake across the central region of the main deck is provided in Figure 20 below. From this graph the LFL envelope is predicted to arrive at each of the nine ventilation intakes, generally in the period from 60 s to around 100 s after the start of the release, but with a delay upon arrival at SF30, the intake to the port transformer room.

The stoichiometric envelope is predicted to arrive at SF-63 and SF-73, the intakes to the mud lab and the starboard HVAC room respectively, after around 80 s. It is apparent from the graph that at SF-63 and SF73 the concentration is predicted to be higher than at the other ventilation intakes in the central region of the aft deck. Indeed, the concentration of gas at SF-63 is predicted to exceed the UFL after around 90 s. In the case of SF-63, this is due to the location of the intake which was under the vacuum breaker release point on the starboard aft leg of the derrick, in the region where the associated plume is predicted to descend and impinge on the deck. In the case of SF-73, this is also due to the location of the intake which was the aftmost ventilation stack on the starboard side of the riser conveyor, in the centre of the aft deck, directly in the predicted path of the dispersing cloud emerging from the shale shaker exhausts vents.

The stoichiometric envelope is also predicted to arrive at SF-18 and SF-19, the intakes to the mud pump rooms, SF-31, the intake to the starboard transformer room, and SF72, the intake to the port HVAC room, after around 110 s to 130 s.

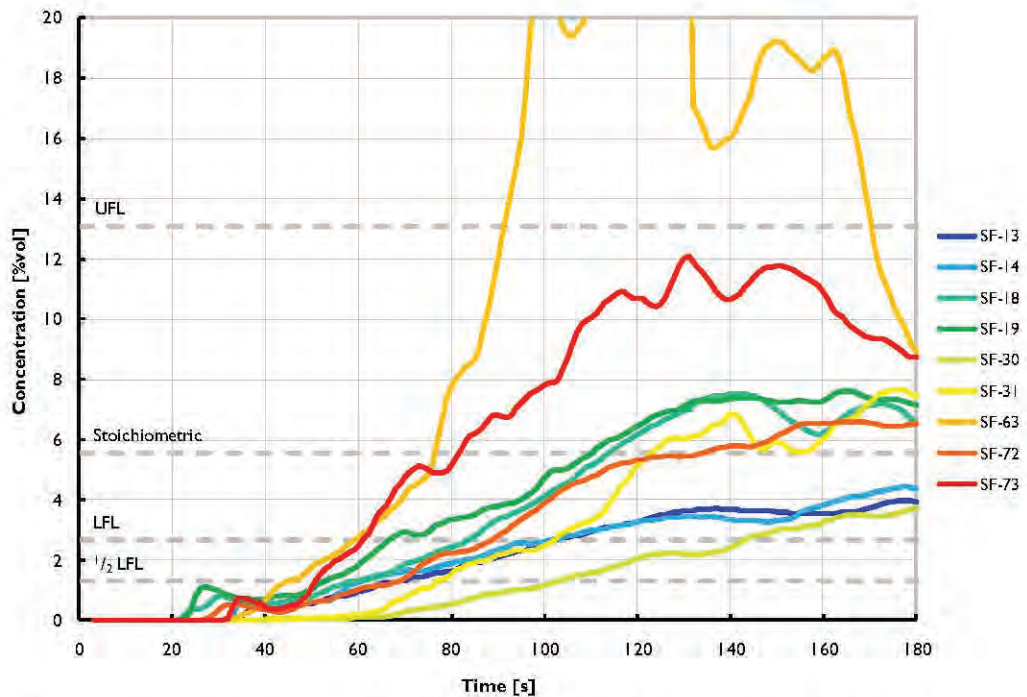


Figure 20 Predicted time history for the concentration of hydrocarbon gas at the ventilation intakes in the central region of the aft deck – Case A

The predicted time history for the concentration of hydrocarbon gas averaged across the remaining ventilation intakes is provided in Figure 21 below.

It is apparent from the graph that at SF-22, the intake to the cement house, the concentration is predicted to be higher than at the other remaining ventilation intakes. This is due to the location of the intake which was near to and directly starboard of the shale shaker exhaust vents. The LFL envelope is predicted to arrive at SF-22 after around 40 s, with the stoichiometric envelope arriving after around 55 s and the UFL envelope arriving after 90 s.

The LFL envelope is predicted to arrive at SF-39, the ventilation intake to the port aft column, after around 140 s. The concentration of hydrocarbon gas at the remaining intakes is predicted to remain below the LFL for the three minute duration of the CFD simulation.

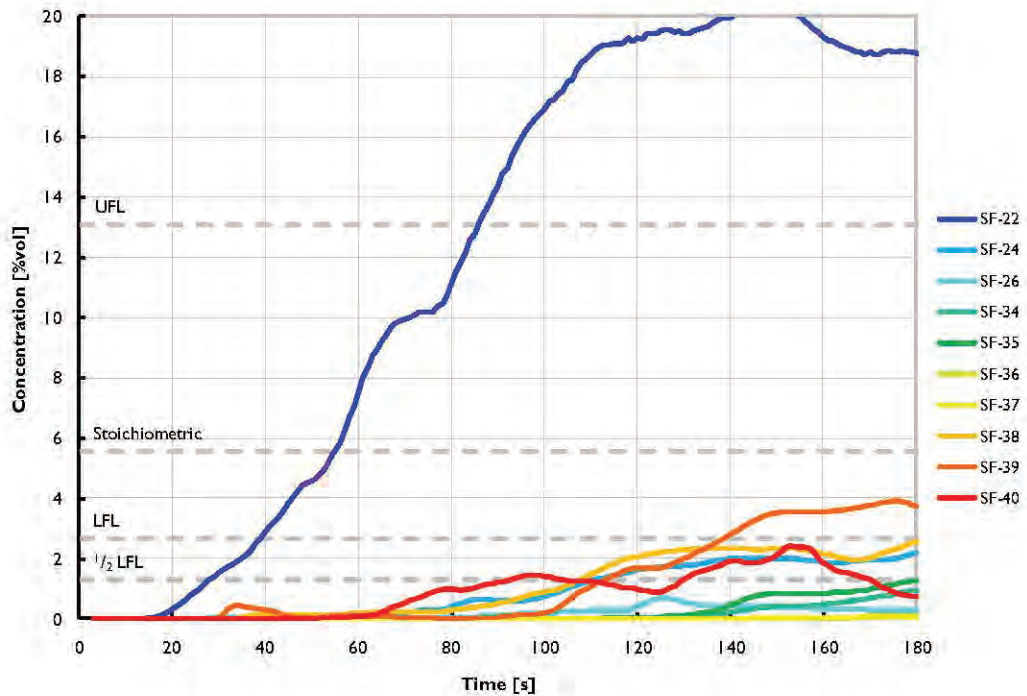


Figure 21 Predicted time history for the concentration of hydrocarbon gas at the remaining ventilation intakes – Case A

The predicted arrival time for the $1/2$ LFL, LFL and stoichiometric envelopes at the intakes to the internal spaces for Case A are summarised in Table 8 below.

Table 8 Predicted arrival times at selected intakes for Case A

Internal space	½ LFL	LFL	Stoichiometric
Intake to engine room 1 (SF-01)	102 s	145 s	---
Intake to engine room 2 (SF-02)	89 s	138 s	---
Intake to engine room 3 (SF-03)	54 s	66 s	119 s
Intake to engine room 4 (SF-04)	52 s	61 s	100 s
Intake to engine room 5 (SF-05)	111 s	127 s	---
Intake to engine room 6 (SF-06)	96 s	136 s	---
Intake to mud tank room (SF-13)	70 s	102 s	---
Intake to mud tank room (SF-14)	62 s	101 s	---
Intake to mud pump room (SF-18)	61 s	84 s	114 s
Intake to mud pump room (SF-19)	54 s	67 s	111 s
Intake to cement room (SF-22)	29 s	39 s	55 s
Intake to sack storage room (SF-26)	---	---	---
Intake to port transformer room (SF-30)	104 s	143 s	---
Intake to starboard transformer room (SF-31)	78 s	102 s	123 s
Intake to mud lab (SF-63)	45 s	59 s	77 s
Intake to HVAC rooms (SF-72)	69 s	89 s	134 s
Intake to HVAC rooms (SF-73)	51 s	61 s	82 s

‘---’ denotes that the envelope has not arrived within the three minute duration of the CFD simulation.

4.2.1.3 Ingestion of hydrocarbon gas at engine intakes

The predicted time history for the concentration of hydrocarbon gas at each engine air intake is provided in Figure 22 below. From this graph the concentration of gas at the intakes to engines 3 and 4 is predicted to reach the ½ LFL after 70 s and the LFL after around 90 s.

The concentration of gas at the intakes to engines 5 and 6 is predicted to reach the ½ LFL after 100 s to 110 s and the LFL after 120 s to 130 s. The arrival of the flammable gas at the intakes to engines 1 and 2 is delayed - the concentration is predicted to reach the ½ LFL after around 120 s and the LFL after around 150 s.

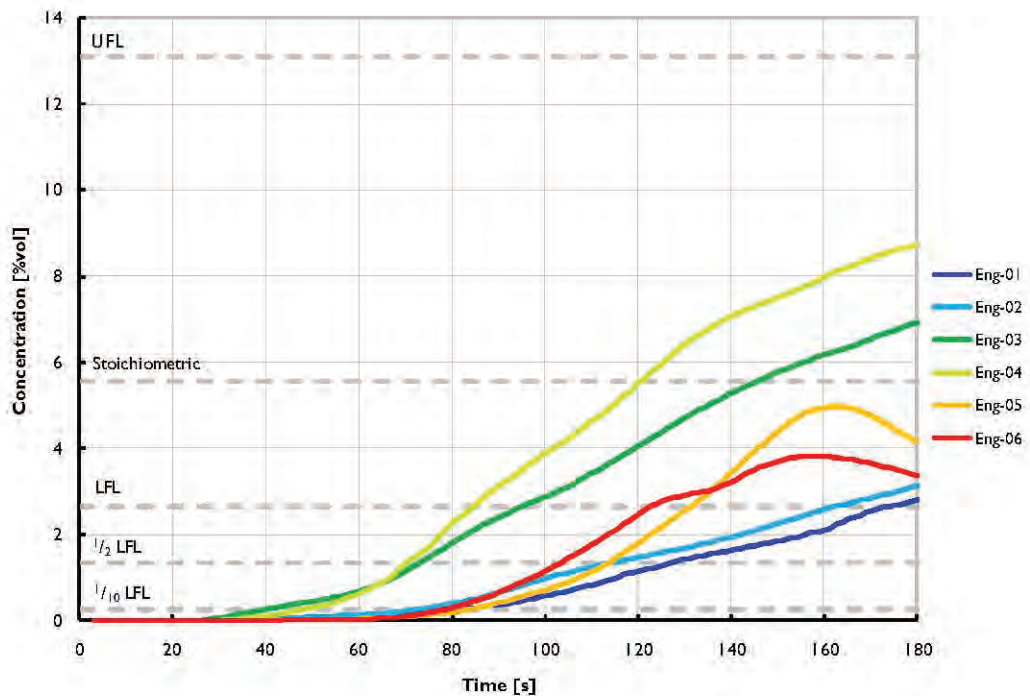


Figure 22 Predicted time history for the concentration of hydrocarbon gas at the engine air intakes – Case A

4.2.2 Case B

The results for Case B are presented in Appendix B at the end of this report.

4.2.2.1 General observations

The plume from the MGS outlet at the top of the derrick is predicted to remain clear of the rig, away from the main deck and the ventilation intakes to internal spaces. Likewise, the plume of hydrocarbon gas from the MGS starboard relief is predicted to remain clear of the starboard side of the rig.

The release from the gumbo box is predicted to fill the shale shaker house with a flammable gas mixture within 20 s to 30 s. After around 50 s, the environment within the shale shaker house becomes fuel rich. After approximately 20 s, the flammable gas is predicted to emerge from the exhausts (EF-57 and EF-58) to form an expanding cloud of flammable gas which is predicted to disperse over the starboard aft deck of the vessel. After around 60 s the plume of hydrocarbon gas from the vacuum breaker is predicted to augment the cloud emerging from the shale shaker exhaust ventilation system at deck level in the region around the starboard aft leg of the derrick.

The release from the mini trip tank at the drill floor is predicted to fill the drawworks house with a flammable gas mixture, which is predicted to disperse over the drill floor and around the BOP house with the wind.

The release directed upward from the rotary table and the associated plume of hydrocarbon gas is predicted to rise away from the rig, away from the main deck and the ventilation intakes to internal spaces.

The release from the slip joint is predicted to fill much of the lower section of the moonpool with a flammable gas mixture, although the BOP house is predicted to remain largely free from flammable gas for the three minute duration of the CFD simulation. After around 80 s, flammable gas is predicted to escape from the forward openings to the moonpool and disperse over the forward deck.

4.2.2.2 Ingestion of hydrocarbon gas at ventilation intakes

The predicted time history for the concentration of hydrocarbon gas averaged across each engine room ventilation intake is provided in Figure 23 below. From this graph the LFL envelope is predicted to arrive at SF-03 and SF-04, the ventilation intakes to engine rooms 3 and 4 located along the centreline of the vessel, after around 80 s to 100 s. The stoichiometric envelope is predicted to arrive at SF-04 after around 140 s but is not predicted to arrive at SF-03 during the three minute duration of the CFD simulation.

The concentration of hydrocarbon gas at the remaining engine room intakes is predicted to remain below the LFL throughout the three minutes of the CFD simulation.

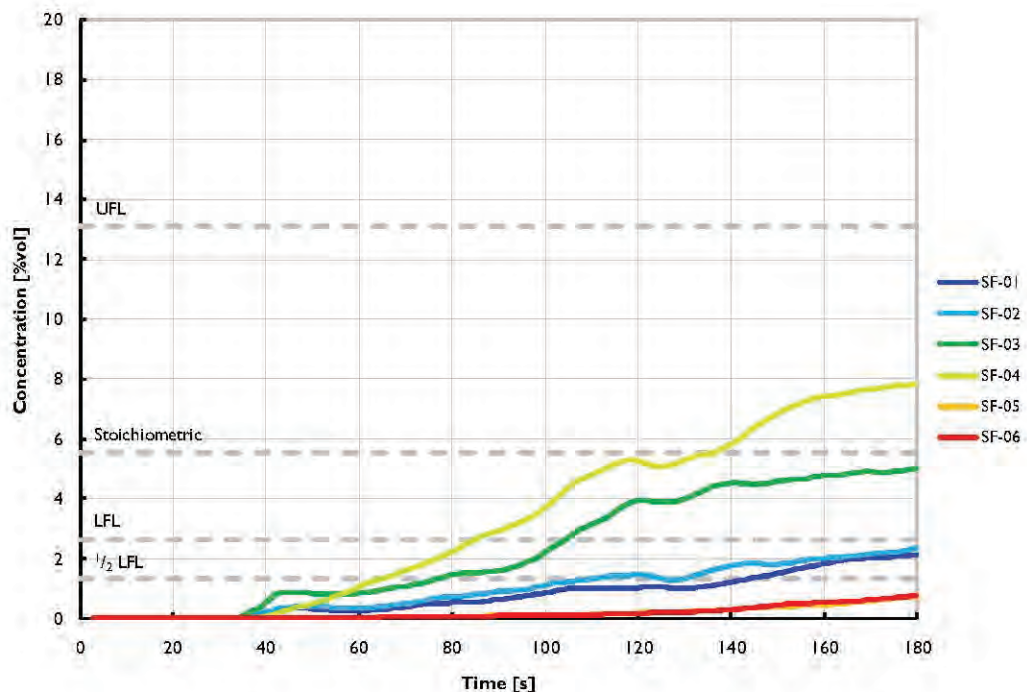


Figure 23 Predicted time history for the concentration of hydrocarbon gas at each of the engine room ventilation intakes – Case B

The predicted time history for the concentration of hydrocarbon gas averaged across each ventilation intake across the central region of the main deck is provided in Figure 24 below.

As for Case-A, the concentration at SF-63 and SF-73 is predicted to be higher than at the other ventilation intakes in the central region of the aft deck due to their respective locations: SF-63 directly under the vacuum breaker release point on the starboard aft leg of the derrick, and SF-73 which was the aftmost ventilation stack on the starboard side of the riser conveyor, in the centre of the aft deck, directly in the predicted path of the dispersing cloud emerging from the shale shaker exhausts vents. The LFL envelope is predicted to arrive after around 80 s with the stoichiometric envelope arriving after around 110 s. The UFL envelope is predicted to arrive at SF-63 after around 130s.

The LFL envelope is predicted to arrive at SF-19 and SF-72, the starboard intake to the mud pump room and the intake to the port HVAC room respectively, after around 110 s. The stoichiometric envelope is predicted to arrive at SF-72 after around 160 s, but is not predicted to arrive at SF-19 within the three minute CFD simulation.

The concentration of hydrocarbon gas at the other ventilation intakes is predicted to approach or arrive at the LFL after 140 s, but will remain below the stoichiometric concentration throughout the three minutes of the CFD simulation.

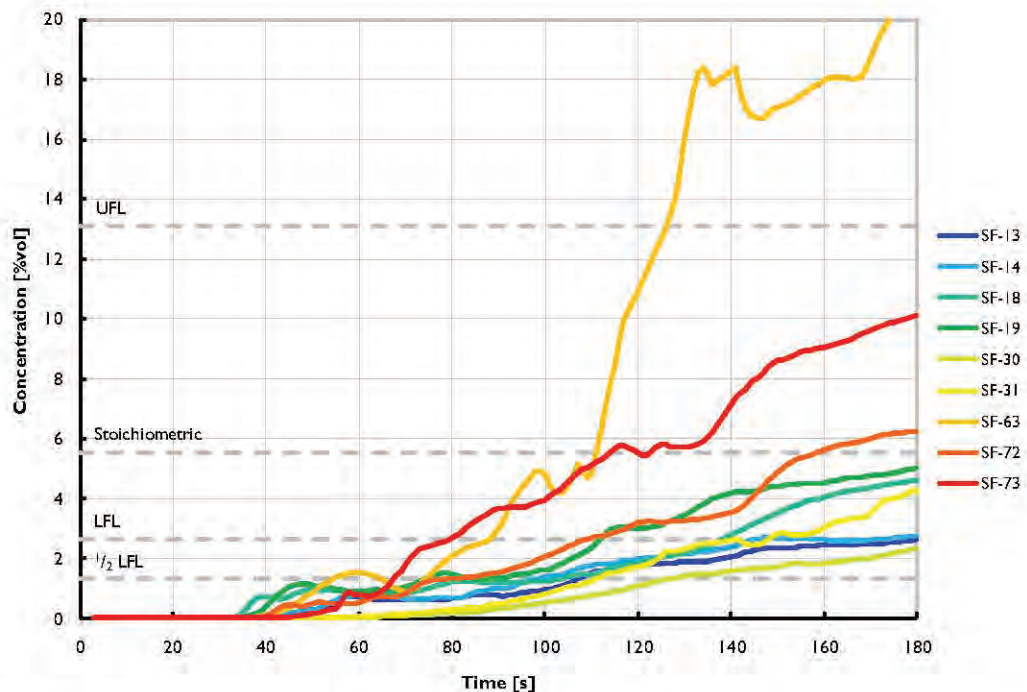


Figure 24 Predicted time history for the concentration of hydrocarbon gas at the ventilation intakes in the central region of the aft deck – Case B

The predicted time history for the concentration of hydrocarbon gas averaged across the remaining ventilation intakes is provided in Figure 25 below.

As for Case-A, the concentration at SF-22 is predicted to be higher than at the other remaining ventilation intakes due to its location near to and directly starboard of the shale shaker exhaust vents. The LFL envelope is predicted to arrive after around 60 s, with the stoichiometric envelope arriving after around 100 s and the UFL envelope arriving after 150s.

The concentration of hydrocarbon gas is predicted to remain below the LFL at the remaining ventilation intakes for the three minute duration of the CFD simulation.

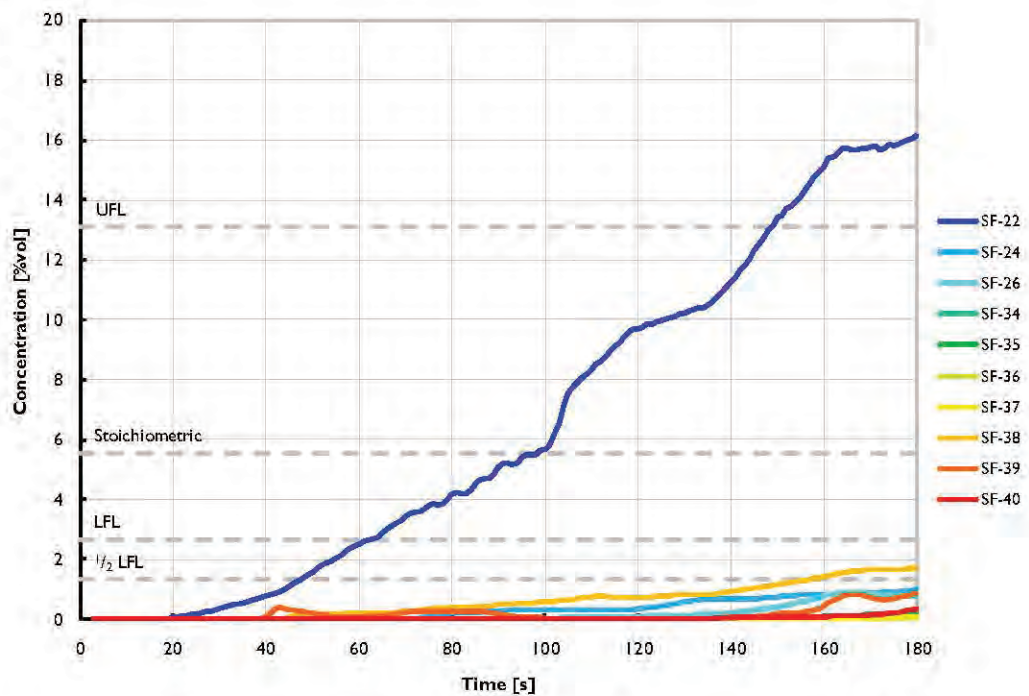


Figure 25 Predicted time history for the concentration of hydrocarbon gas at the remaining ventilation intakes – Case B

The predicted arrival time at the intakes to the internal spaces for Case B are summarised in Table 9 below.

Table 9 Predicted arrival times at selected intakes for Case B

Internal space	½ LFL	LFL	Stoichiometric
Intake to engine room 1 (SF-01)	144 s	---	---
Intake to engine room 2 (SF-02)	111 s	---	---
Intake to engine room 3 (SF-03)	77 s	105 s	---
Intake to engine room 4 (SF-04)	65 s	85 s	141 s
Intake to engine room 5 (SF-05)	---	---	---
Intake to engine room 6 (SF-06)	---	---	---
Intake to mud tank room (SF-13)	108 s	---	---
Intake to mud tank room (SF-14)	100 s	146 s	---
Intake to mud pump room (SF-18)	104 s	141 s	---
Intake to mud pump room (SF-19)	75 s	112 s	---
Intake to cement room (SF-22)	48 s	63 s	99 s
Intake to sack storage room (SF-26)	---	---	---
Intake to port transformer room (SF-30)	127 s	---	---
Intake to starboard transformer room (SF-31)	111 s	141 s	---
Intake to mud lab (SF-63)	55 s	88 s	112 s
Intake to HVAC rooms (SF-72)	80 s	110 s	159 s
Intake to HVAC rooms (SF-73)	68 s	80 s	114 s

‘---’ denotes that the envelope has not arrived within the three minute duration of the CFD simulation.

4.2.2.3 Ingestion of hydrocarbon gas at engine intakes

The predicted time history for the concentration of hydrocarbon gas at each engine air intake is provided in Figure 26 below. From this graph the concentration of gas at the intake to engine 4 is predicted to reach the ½ LFL after 90 s and the LFL after around 110 s. Similarly, the concentration at the intake to engine 3 is predicted to reach the ½ LFL after 100 s and the LFL after around 130 s.

The arrival of the flammable gas at the intakes to engines 1 and 2 is delayed. The ½ LFL envelope is predicted to reach the intake to engine 2 after 120 s and engine 1 after 160 s. The concentration is not predicted to reach the LFL at either intake within the three minute duration of the CFD simulation.

The concentration of gas at the intakes to engines 5 and 6 is predicted to remain well below the ½ LFL throughout the three minutes of the CFD simulation.

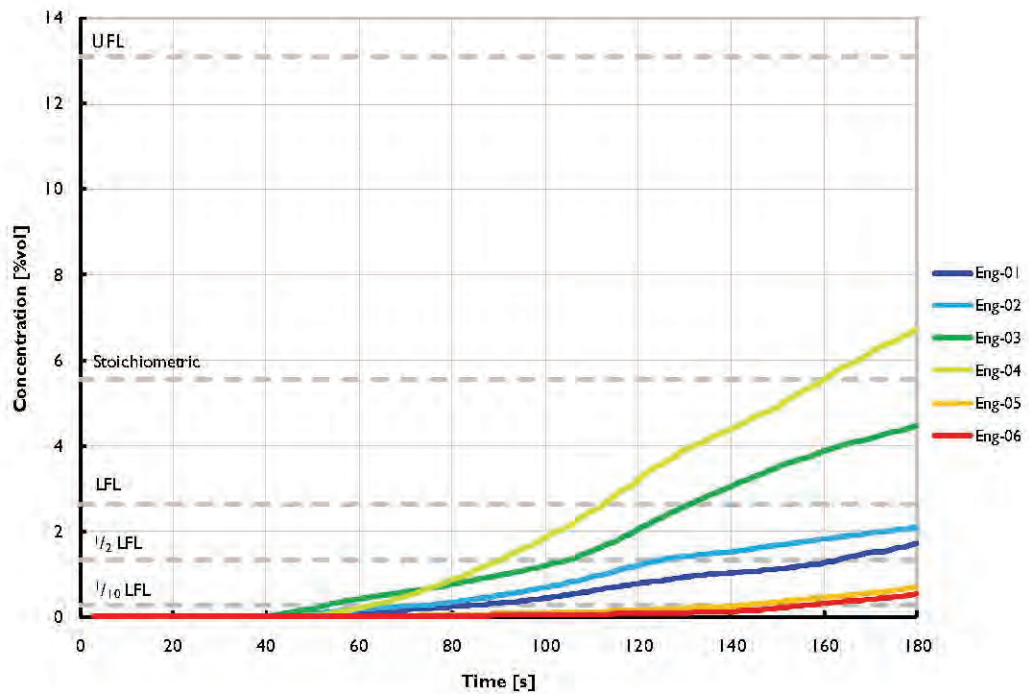


Figure 26 Predicted time history for the concentration of hydrocarbon gas at the engine air intakes – Case B

4.2.3 Case C

The results for Case C are presented in Appendix C at the end of this report.

4.2.3.1 General observations

The plume from the MGS outlet at the top of the derrick is predicted to remain clear of the rig, away from the main deck and the ventilation intakes to internal spaces. Likewise, the plume of hydrocarbon gas from the MGS starboard relief is predicted to remain clear of the starboard side of the rig.

The release from the gumbo box is predicted to fill the shale shaker house with a flammable gas mixture within 30 s to 40 s. After around 80 s, the environment within the shale shaker house becomes fuel rich. After approximately 30 s, the flammable gas is predicted to emerge from the exhausts (EF-57 and EF-58) to form an expanding cloud of flammable gas which is predicted to disperse over the starboard aft deck of the vessel. After around two minutes the plume of hydrocarbon gas from the vacuum breaker is predicted to augment the cloud emerging from the shale shaker exhaust ventilation system at deck level in the region around the starboard aft leg of the derrick.

The release from the mini trip tank at the drill floor is predicted to fill the drawworks house with a flammable gas mixture, which is predicted to disperse over the drill floor with the wind.

The release directed upward from the rotary table and the associated plume of hydrocarbon gas is predicted to rise away from the rig, away from the main deck and the ventilation intakes to internal spaces.

The release from the slip joint is predicted to fill much of the lower section of the moonpool with a flammable gas mixture after two to three minutes, although the BOP house is predicted to remain largely free from flammable gas for the three minute duration of the CFD simulation. After around two minutes, flammable gas is predicted to escape from the forward openings to the moonpool and disperse over the forward deck.

4.2.3.2 Ingestion of hydrocarbon gas at ventilation intakes

The predicted time history for the concentration of hydrocarbon gas averaged across each engine room ventilation intake is provided in Figure 27 below. From this graph the concentration of hydrocarbon gas at SF-04, the ventilation intake to engine room 4, is predicted to reach the LFL after around 120 s, but is not predicted to reach the stoichiometric concentration within the three minute duration of the CFD simulation.

The concentration of hydrocarbon gas at the remaining engine room intakes is predicted to remain below the LFL throughout the three minutes of the CFD simulation.

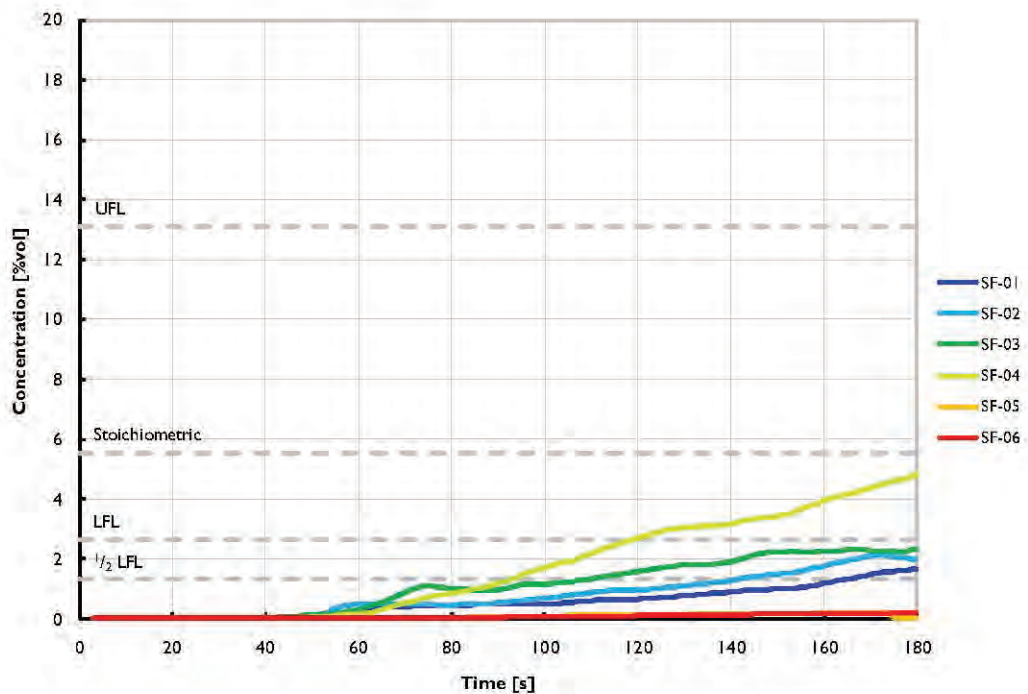


Figure 27 Predicted time history for the concentration of hydrocarbon gas at each of the engine room ventilation intakes – Case C

The predicted time history for the concentration of hydrocarbon gas averaged across each ventilation intake across the central region of the main deck is provided in Figure 28 below.

As for Case-A and Case-B, the concentration at SF-63 and SF-73 is predicted to be higher than at the other ventilation intakes in the central region of the aft deck due to their respective locations. The LFL envelope is predicted to arrive after around 110 s to 120 s. The stoichiometric envelope is predicted to arrive at SF-63 after around 140 s and at SF-73 after around 170 s.

The LFL envelope is predicted to arrive at SF-72, the intake to the port HVAC room, after around 175 s.

The concentration of hydrocarbon gas at the other ventilation intakes is predicted to remain below the LFL throughout the three minutes of the CFD simulation.

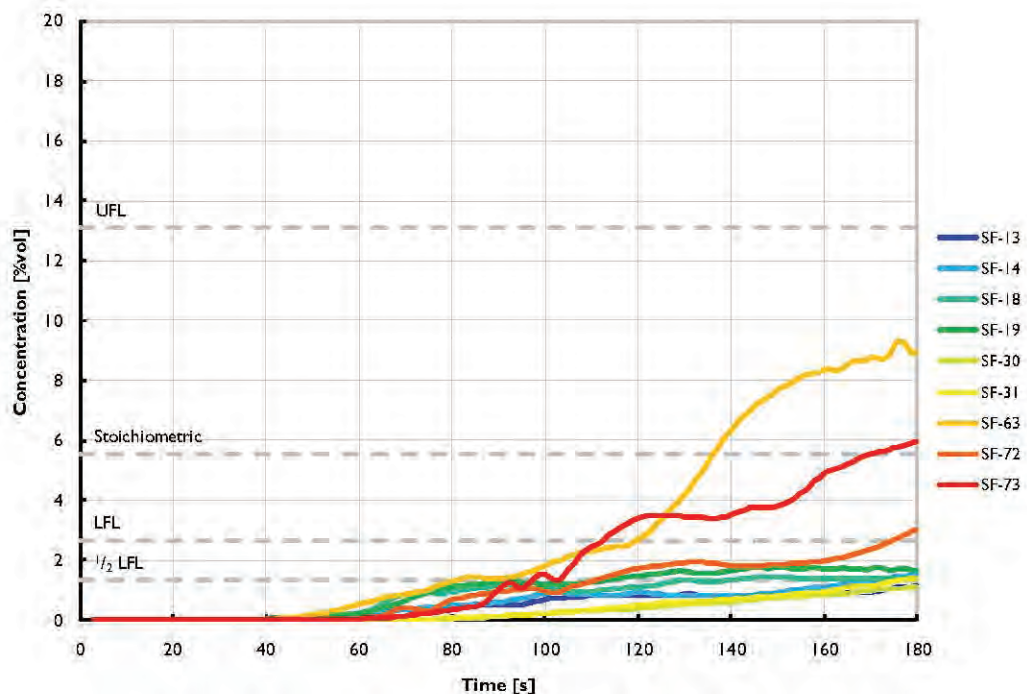


Figure 28 Predicted time history for the concentration of hydrocarbon gas at the ventilation intakes in the central region of the aft deck – Case C

The predicted time history for the concentration of hydrocarbon gas averaged across the remaining ventilation intakes is provided in Figure 29 below.

As for Case-A and Case-B, the concentration at SF-22 is predicted to be higher than at the other remaining ventilation intakes due to its location. The LFL envelope is predicted to arrive after around 110 s, with the stoichiometric envelope arriving after a around 180 s.

The concentration of hydrocarbon gas is predicted to remain below the $\frac{1}{2}$ LFL at the remaining ventilation intakes for the three minute duration of the CFD simulation.

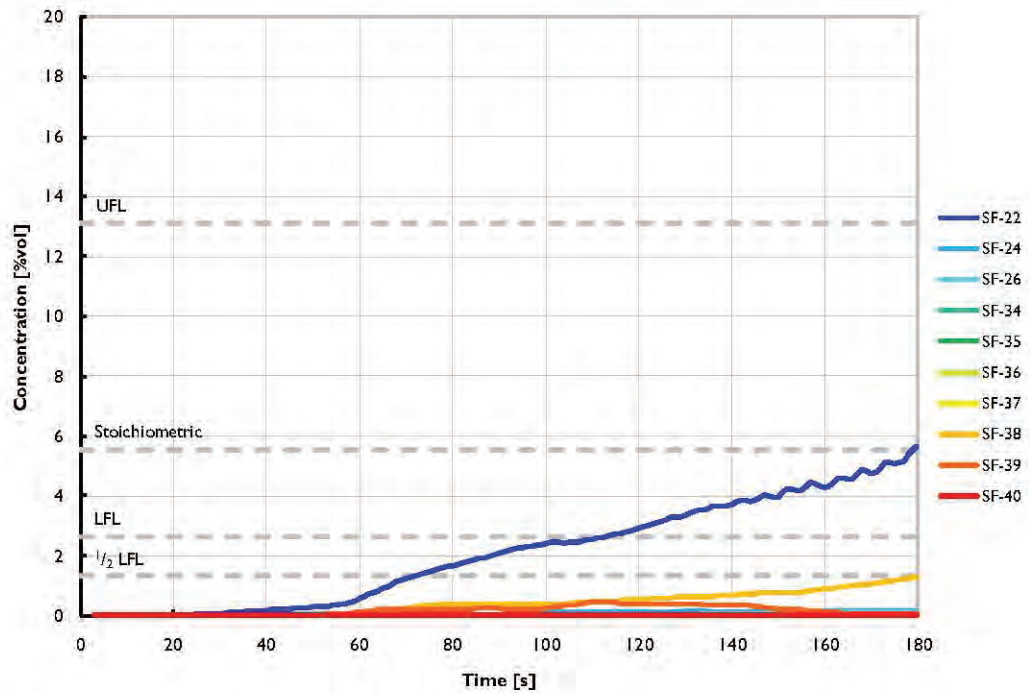


Figure 29 Predicted time history for the concentration of hydrocarbon gas at the remaining ventilation intakes – Case C

The predicted arrival time at the intakes to the internal spaces for Case C are summarised in Table 10 below.

Table 10 Predicted arrival times at selected intakes for Case C

Internal space	½ LFL	LFL	Stoichiometric
Intake to engine room 1 (SF-01)	165 s	---	---
Intake to engine room 2 (SF-02)	142 s	---	---
Intake to engine room 3 (SF-03)	110 s	---	---
Intake to engine room 4 (SF-04)	94 s	119 s	---
Intake to engine room 5 (SF-05)	---	---	---
Intake to engine room 6 (SF-06)	---	---	---
Intake to mud tank room (SF-13)	---	---	---
Intake to mud tank room (SF-14)	173 s	---	---
Intake to mud pump room (SF-18)	129 s	---	---
Intake to mud pump room (SF-19)	113 s	---	---
Intake to cement room (SF-22)	72 s	114 s	179 s
Intake to sack storage room (SF-26)	---	---	---
Intake to port transformer room (SF-30)	---	---	---
Intake to starboard transformer room (SF-31)	177 s	---	---
Intake to mud lab (SF-63)	81 s	120 s	137 s
Intake to HVAC rooms (SF-72)	112 s	175 s	---
Intake to HVAC rooms (SF-73)	98 s	113 s	170 s

‘---’ denotes that the envelope has not arrived within the three minute duration of the CFD simulation.

4.2.3.3 Ingestion of hydrocarbon gas at engine intakes

The predicted time history for the concentration of hydrocarbon gas at each engine air intake is provided in Figure 30 below. From this graph the concentration of gas at the intake to engine 4 is predicted to reach the ½ LFL after 120 s and the LFL after around 150 s.

The ½ LFL envelope is predicted to reach the intake to engine 3 after 140 s and engine 2 after 160 s. The concentration is not predicted to reach the LFL at either intake within the three minute duration of the CFD simulation. The concentration of gas at the intake to engine 1 is predicted to remain below the ½ LFL throughout the simulation.

The concentration of gas at the intakes to engines 5 and 6 is predicted to remain below the 1/10 LFL throughout the three minutes of the CFD simulation.

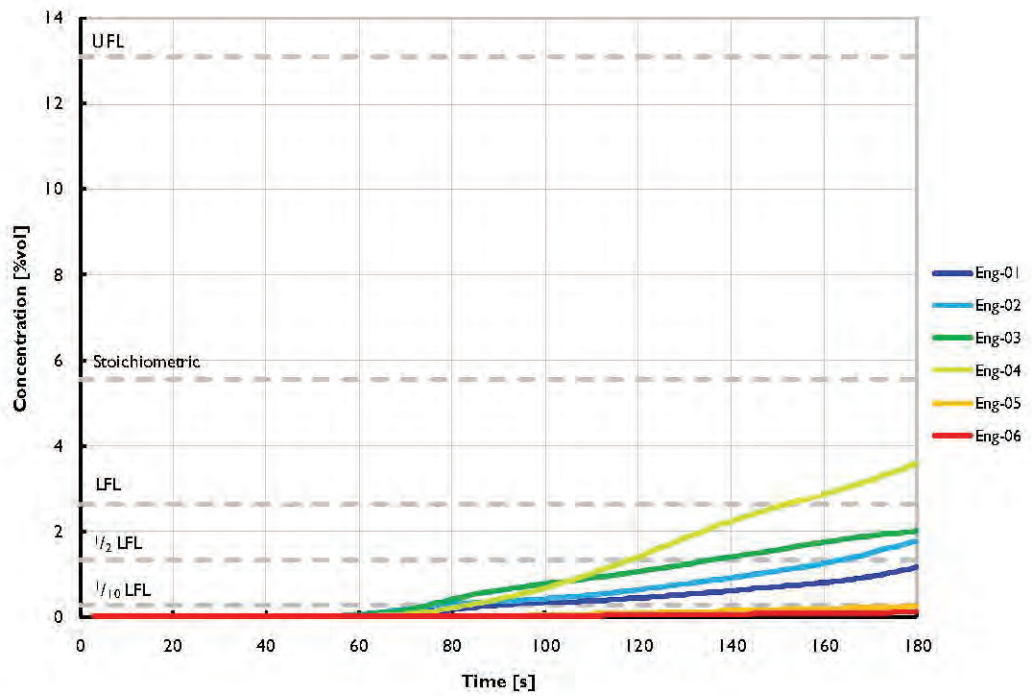


Figure 30 Predicted time history for the concentration of hydrocarbon gas at the engine air intakes – Case C

5 CONCLUSIONS

Based upon the assumption that the total release rate of hydrocarbon gas as given in Figure 12 can be divided on an area-weighted basis using the areas summarised in Table 6, the following conclusions can be inferred from the CFD analysis:

- Although the largest release area and, therefore, associated release is at the MGS outlet at the top of the derrick, the direction of release would have been portward, such that the associated plume of hydrocarbon gas is likely to have remained clear of the rig, away from the aft deck and the supply fan intakes.
- It is likely that gas released from the six inch MGS relief line and at the packer seal at the rotary table would have remained clear of the rig, away from the aft deck and the supply fan intakes.
- The bulk of the flammable gas dispersing across the aft deck of the vessel is likely to have emerged from the open-top gumbo box within the shale shaker house and spilled onto the aft deck via EF-57 and EF-58.
- It is likely that flammable gas was ingested into engine room 4 if the rate of release had equalled or exceeded that for Case C (with a peak of 300 MMscfd).
- It is likely that flammable gas was ingested into engine rooms 3 and 4 if the rate of release had equalled or exceeded that for Case B (with a peak of 400 MMscfd).
- It is likely that the arrival time at the intakes to engine rooms 3 and 4 will have depended mainly upon the initial rate of increase of the release of flammable gas.
- It is likely that flammable gas was ingested into engine rooms 1, 2, 3 and 4 if the rate of release had equalled or exceeded that for Case A (with a peak of 500 MMscfd).
- The arrival time at the intake to engine room 1 and engine room 2 will have depended upon the initial rate of increase of the release rate of flammable gas following the arrival of flammable gas, and the wind speed and direction.
- Flammable gas may have been ingested at the intakes to engine room 5 and engine room 6, however, with such sensitivity to the wind speed and direction, it is not possible to draw any firm conclusions.

- It is likely that flammable gas was ingested into the supply ventilation intakes to the cement room (SF-22), the mud lab (SF-63) and the HVAC rooms (SF-72 and SF-73) if the rate of release had equalled or exceeded that for Case C (with a peak of 300 MMscfd).
- It is likely that flammable gas was also ingested into the supply ventilation intakes to the mud tank room (SF-14), the mud pump rooms (SF-18 and SF-19) and the starboard transformer room (SF-31) if the rate of release had equalled or exceeded that for Case B (with a peak of 400 MMscfd).
- It is likely that flammable gas was also ingested into the supply ventilation intake to the port transformer room (SF-30) if the rate of release had equalled or exceeded that for Case A (with a peak of 500 MMscfd).
- It is likely that the concentration of hydrocarbon gas ingested into the air intakes of engines 3 and 4 approached or exceeded the LFL.

REFERENCES

- 1 Drawing register for Deepwater Horizon (Rig No 6087), received from Transocean, 28th July 2010.
- 2 *A mathematical model of the structure of strong winds*, Deaves D.M. and Harris R.I, CIRIA Report 76, London, 1978.
- 3 Improved modelling of sub-grid pipework within a CFD flow simulation; Ely A.C., MSc Thesis, University of Leeds 2004.
- 4 *Deepwater Horizon Current Report*, 20 April 2010 at 17:30.
- 5 *E-mail regarding engine intake flow rate*, from Transocean to Prospect, dated 11th November 2010.
- 6 *Volatile Oil Reservoir Fluid Study for BP, OCS-G-32306 Well No. 1 ST00 BP01*, Report No: 36126-19-5010068508, Core Lab Reservoir Optimization, 30th June 2010.
- 7 *Macondo hydraulics update*, Stress Engineering Services Inc., October 7th 2010.
- 8 *E-mail regarding gas dispersion cases*, from Transocean to Prospect, dated 1st December 2010.
- 9 *Guide for pressure-relieving and depressuring systems*, API-RP-521, 1997.

FIGURES

- Figure 1 Sequence of relevant events leading to the explosion
- Figure 2 Approximation of non-rectangular geometry with a structured hex-mesh
- Figure 3 Non-rectangular geometry with an unstructured tetra-mesh
- Figure 4 Capturing small scale congestion within the CFD mesh
- Figure 5 Near-field and far-field for a jet emerging from a rupture
- Figure 6 Far-field dispersion for a jet emerging from a rupture
- Figure 7 Dispersion pattern on a structured orthogonal hex-mesh
- Figure 8 Dispersion pattern on an unstructured tetra-mesh, refined along path of released gas
- Figure 9 Wind direction at the time of the incident
- Figure 10 Probability of ignition across the flammability range for hydrocarbon gas
- Figure 11 Transient profile for the rate of gas release from the riser
- Figure 12 Release profiles considered for this study
- Figure 13 Mud-gas separator (MGS) system
- Figure 14 Trend for the arrival time of the LFL envelope at the engine room intakes
- Figure 15 Trend for the arrival time of the LFL envelope at midship intakes
- Figure 16 Trend for the arrival time of the LFL envelope at the engine room intakes (assuming release Profile A)
- Figure 17 Trend for the arrival time of the LFL envelope at other intakes (assuming release Profile A)
- Figure 18 Velocity vector plot showing separation of flow at the starboard edge of the main deck (looking towards bow)
- Figure 19 Predicted time history for the concentration of hydrocarbon gas at each of the engine room ventilation intakes – Case A
- Figure 20 Predicted time history for the concentration of hydrocarbon gas at the ventilation intakes in the central region of the aft deck – Case A
- Figure 21 Predicted time history for the concentration of hydrocarbon gas at the remaining ventilation intakes – Case A
- Figure 22 Predicted time history for the concentration of hydrocarbon gas at the engine air intakes – Case A
- Figure 23 Predicted time history for the concentration of hydrocarbon gas at each of the engine room ventilation intakes – Case B
- Figure 24 Predicted time history for the concentration of hydrocarbon gas at the ventilation intakes in the central region of the aft deck – Case B
- Figure 25 Predicted time history for the concentration of hydrocarbon gas at the remaining ventilation intakes – Case B
- Figure 26 Predicted time history for the concentration of hydrocarbon gas at the engine air intakes – Case B
- Figure 27 Predicted time history for the concentration of hydrocarbon gas at each of the engine room ventilation intakes – Case C
- Figure 28 Predicted time history for the concentration of hydrocarbon gas at the ventilation intakes in the central region of the aft deck – Case C
- Figure 29 Predicted time history for the concentration of hydrocarbon gas at the remaining ventilation intakes – Case C

- Figure 30 Predicted time history for the concentration of hydrocarbon gas at the engine air intakes – Case C
- Figure 31 Isometric view of CFD model, looking towards the port bow
- Figure 32 Isometric view of CFD model, looking towards the port aft quarter
- Figure 33 Isometric view of CFD model, looking towards the starboard aft quarter
- Figure 34 Isometric view of CFD model, looking towards the starboard bow
- Figure 35 Isometric view of moonpool, looking towards the port bow
- Figure 36 Isometric view of shale shaker house, looking towards the starboard aft quarter
- Figure 37 Isometric view of engine rooms, looking towards the port bow
- Figure 38 Isometric view of mud-pump rooms, looking towards the starboard aft quarter
- Figure 39 Isometric view of HVAC, sack storage, warehouse, cement and mud tank rooms
- Figure 40 Isometric view of transformer rooms, looking towards the starboard aft quarter
- Figure 41 Isometric view of CFD model showing ACE congestion, looking towards the port bow
- Figure 42 Isometric view of CFD model showing ACE congestion, looking towards the port aft quarter
- Figure 43 Isometric view of CFD model showing ACE congestion, looking towards the port bow
- Figure 44 Isometric view of CFD model, showing ACE congestion, looking towards the port aft quarter
- Figure 45 Release point at slip joint below moonpool, looking starboard through BOP house
- Figure 46 Release point at rotary table at drill floor, looking towards the port bow
- Figure 47 Open top of gumbobox within shale shaker house, looking towards the starboard aft
- Figure 48 Release point at vacuum breaker, on starboard aft leg of drilling derrick
- Figure 49 MGS outlet at top of drilling derrick, looking towards the port bow
- Figure 50 MGS starboard relief line, looking towards the port bow
- Figure 51 Mini trip tank, looking into the drawworks towards the starboard bow

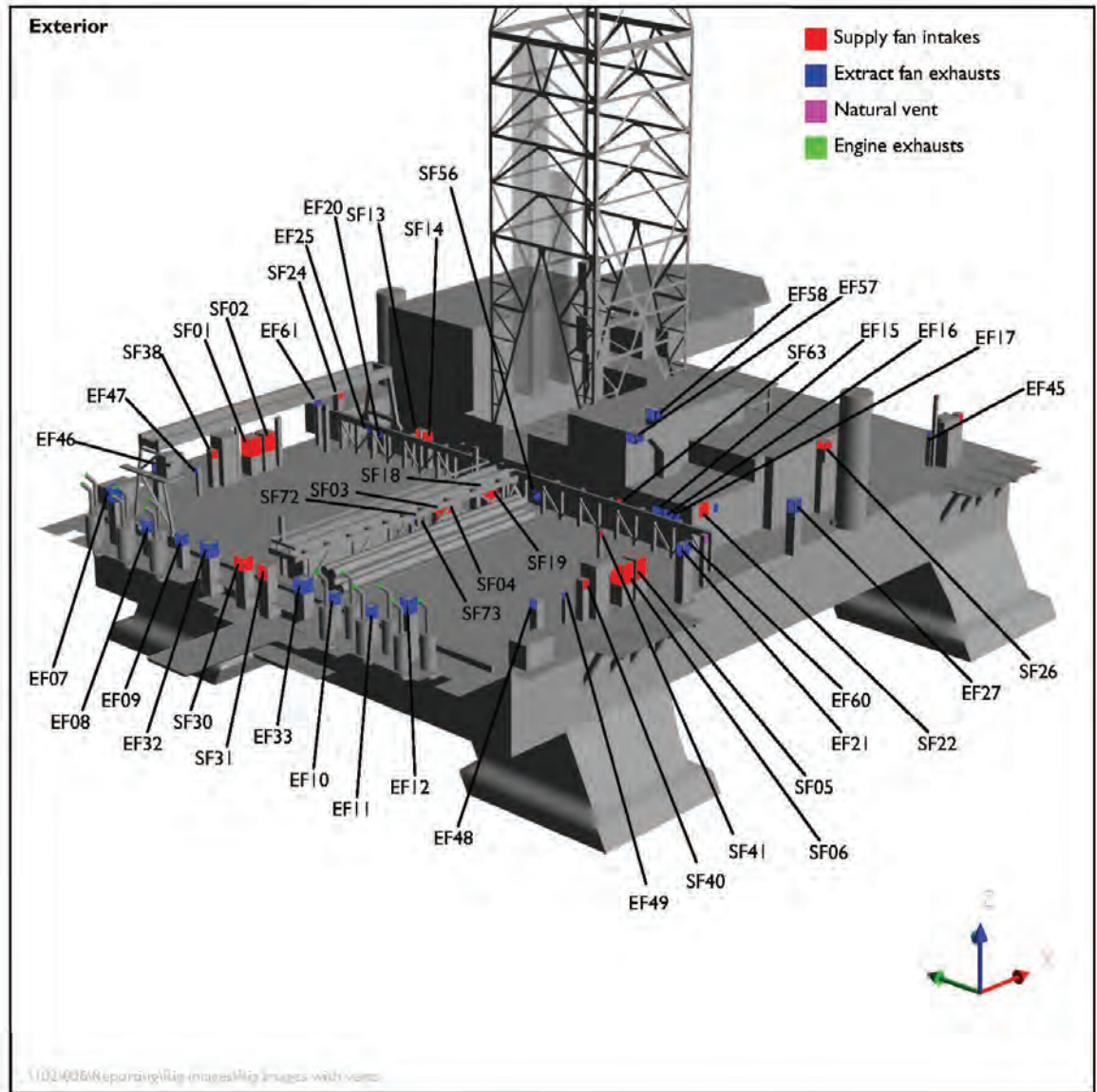


Figure 31 Isometric view of CFD model, looking towards the port bow

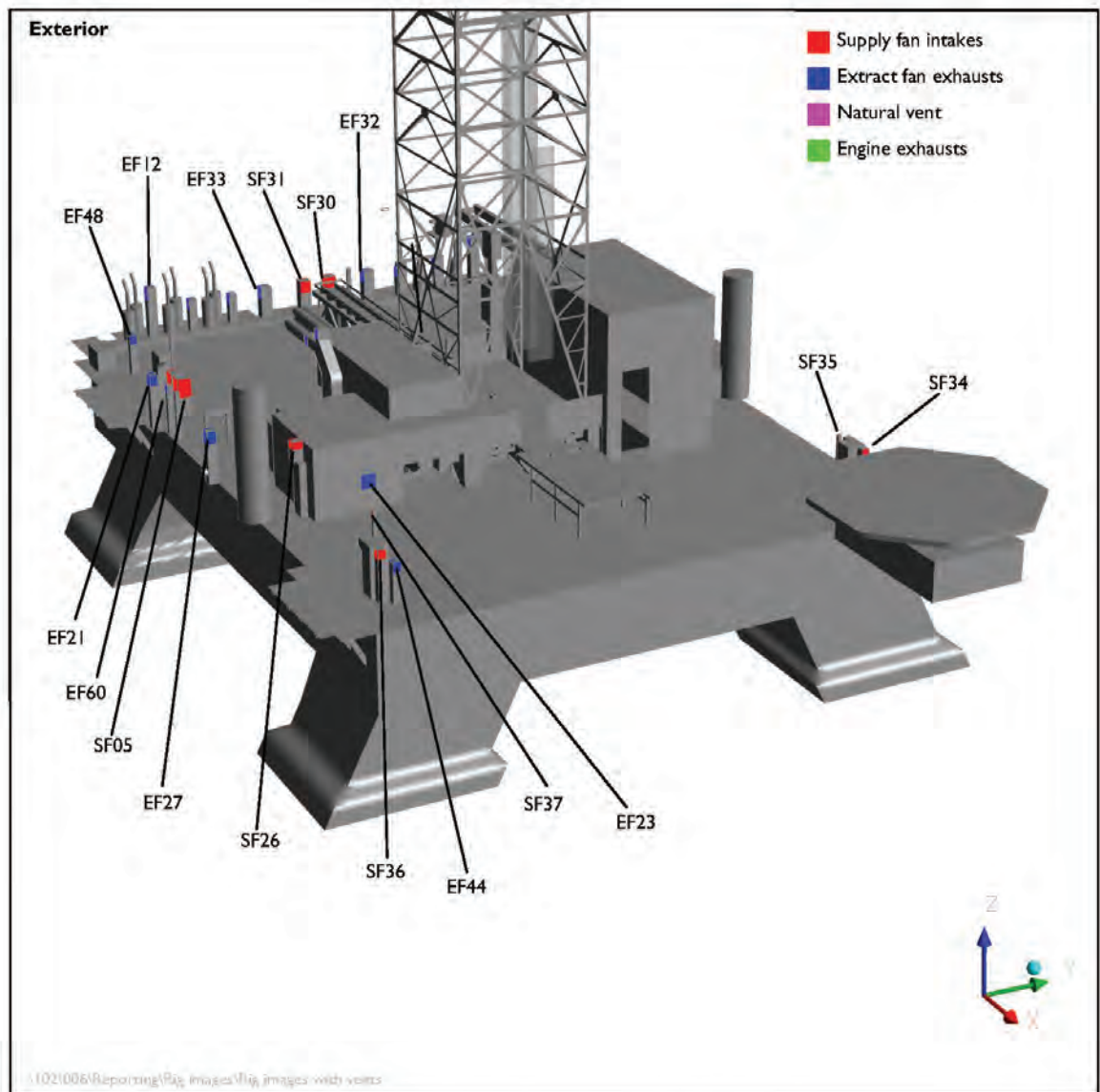


Figure 32 Isometric view of CFD model, looking towards the port aft quarter

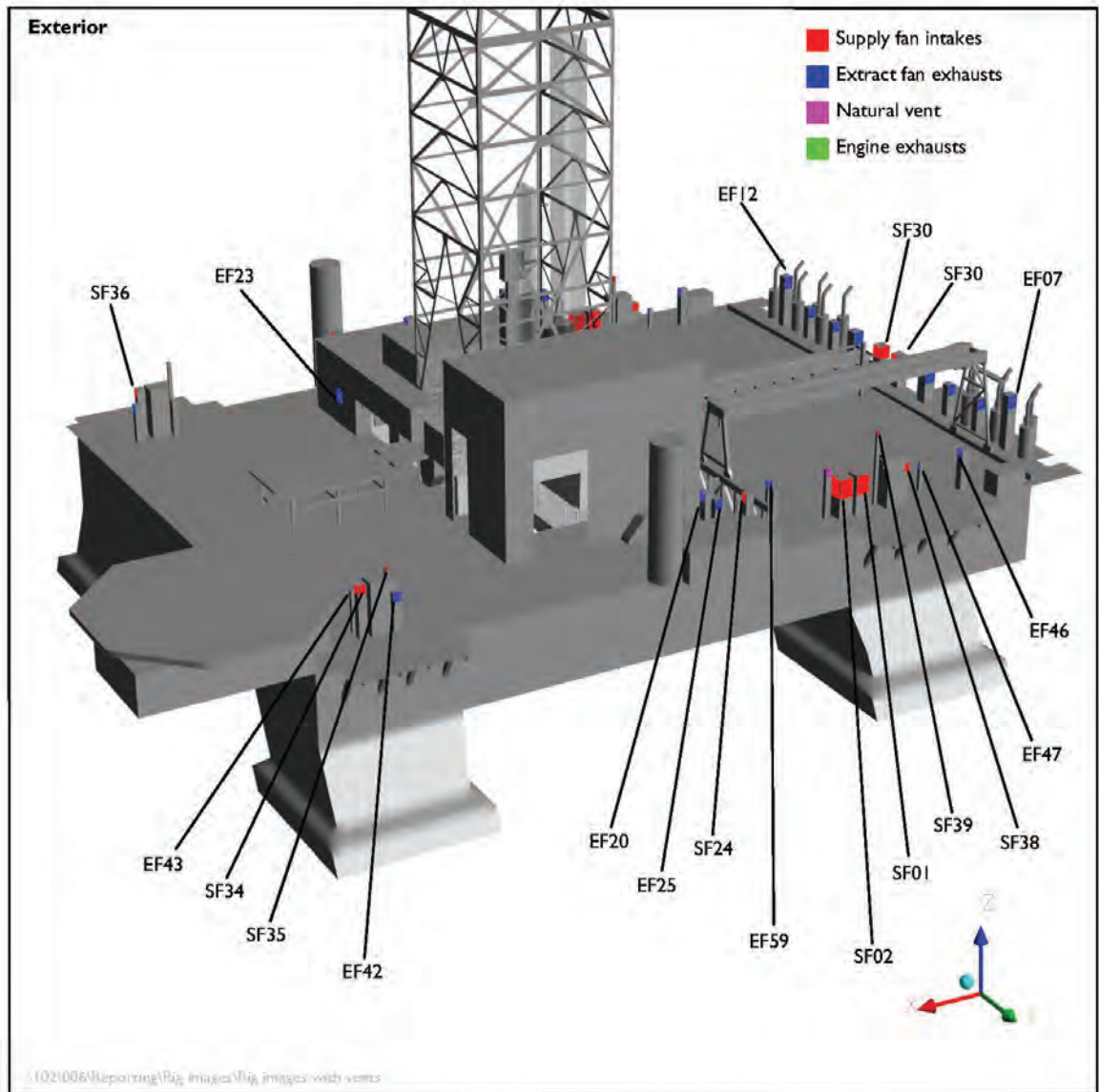


Figure 33 Isometric view of CFD model, looking towards the starboard aft quarter

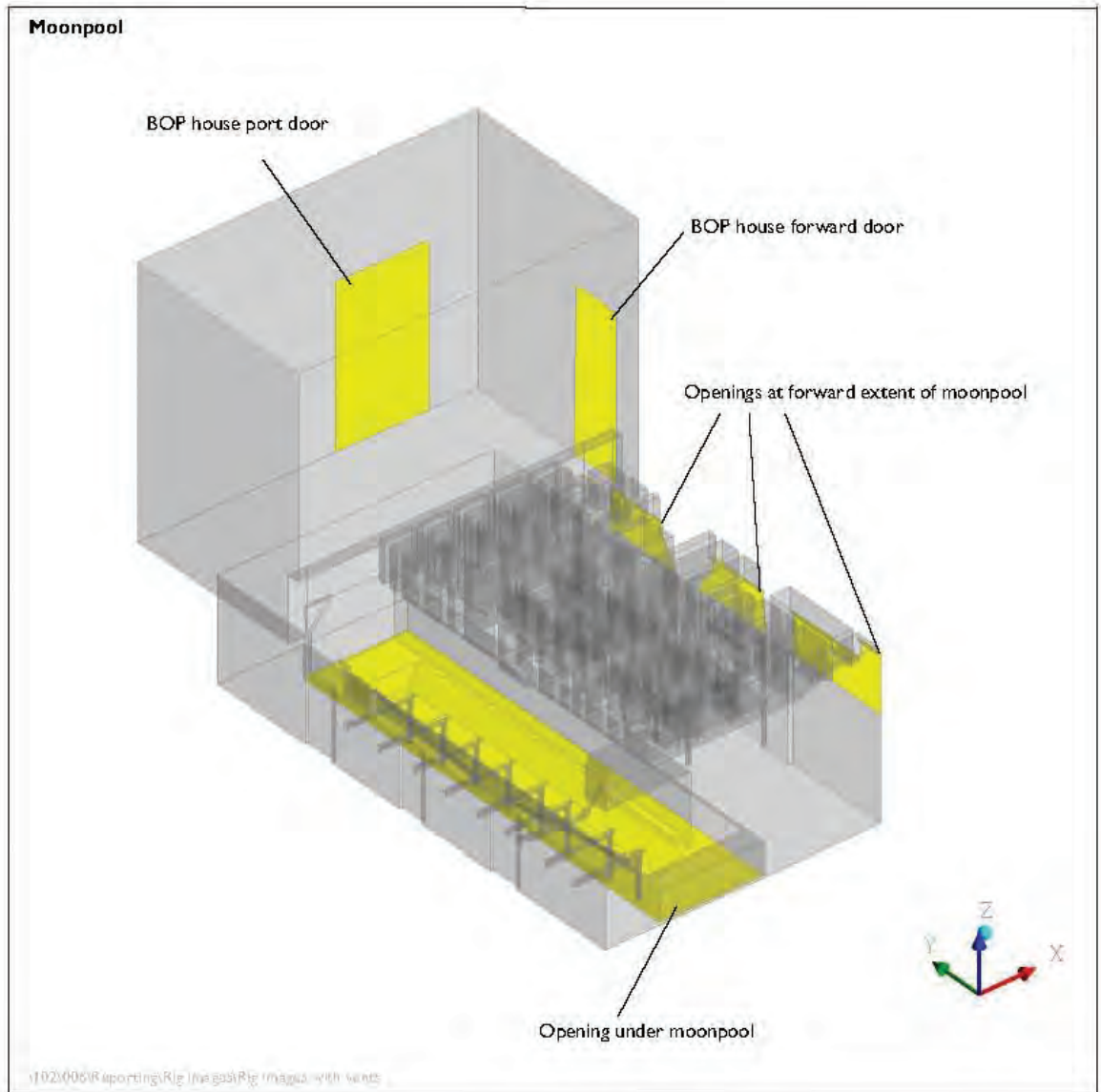


Figure 35 Isometric view of moonpool, looking towards the port bow

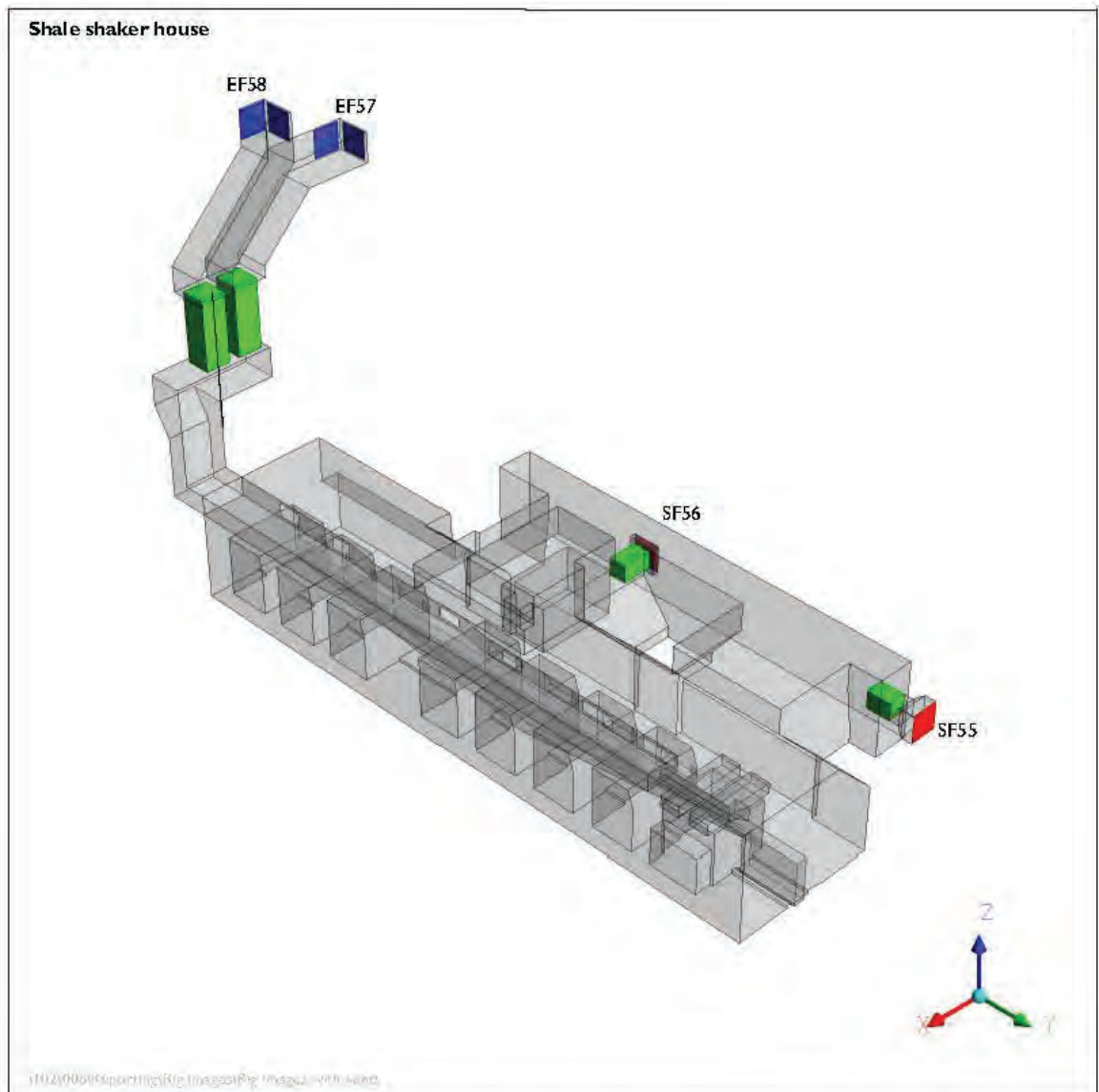


Figure 36 Isometric view of shale shaker house, looking towards the starboard aft quarter

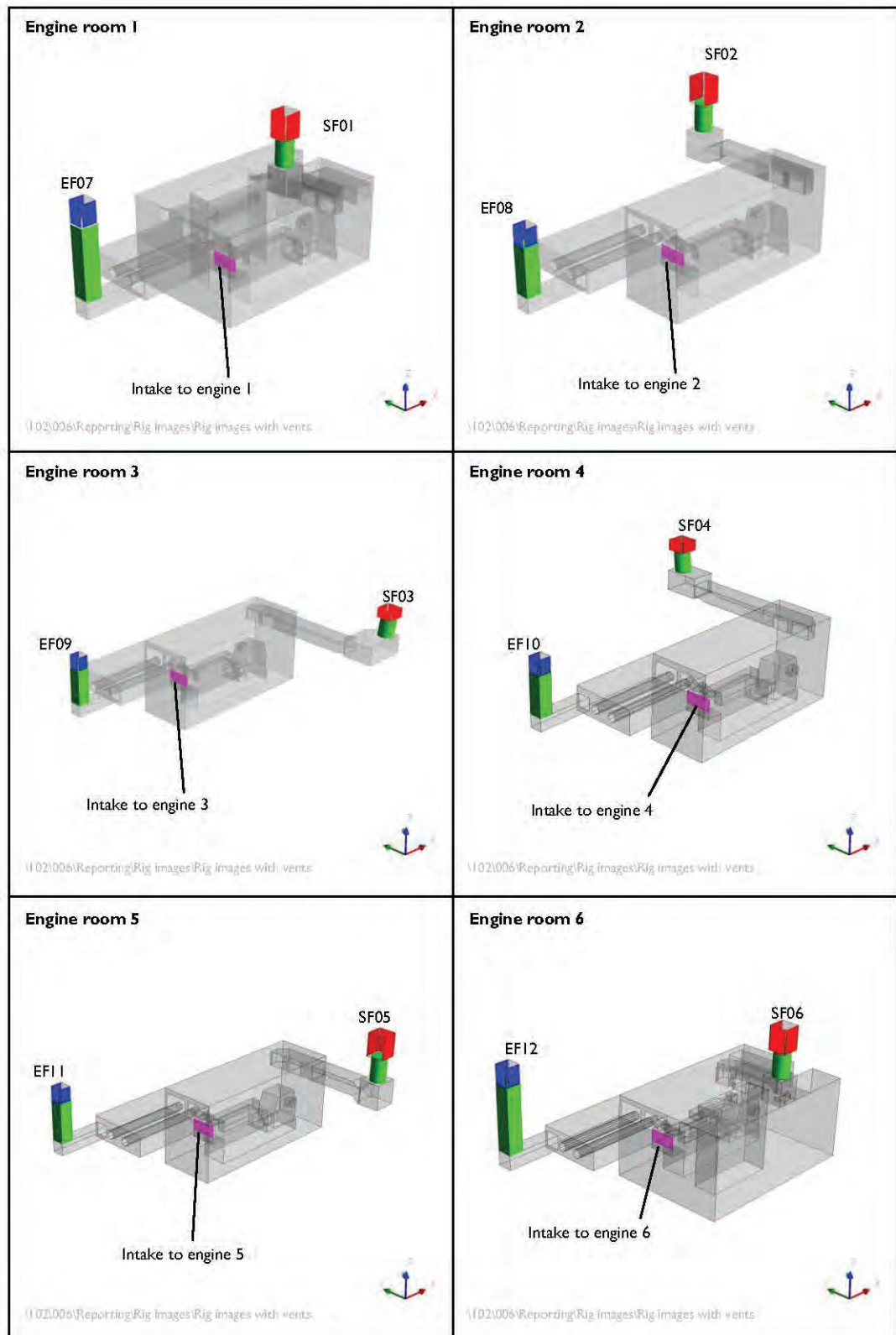


Figure 37 Isometric view of engine rooms, looking towards the port bow

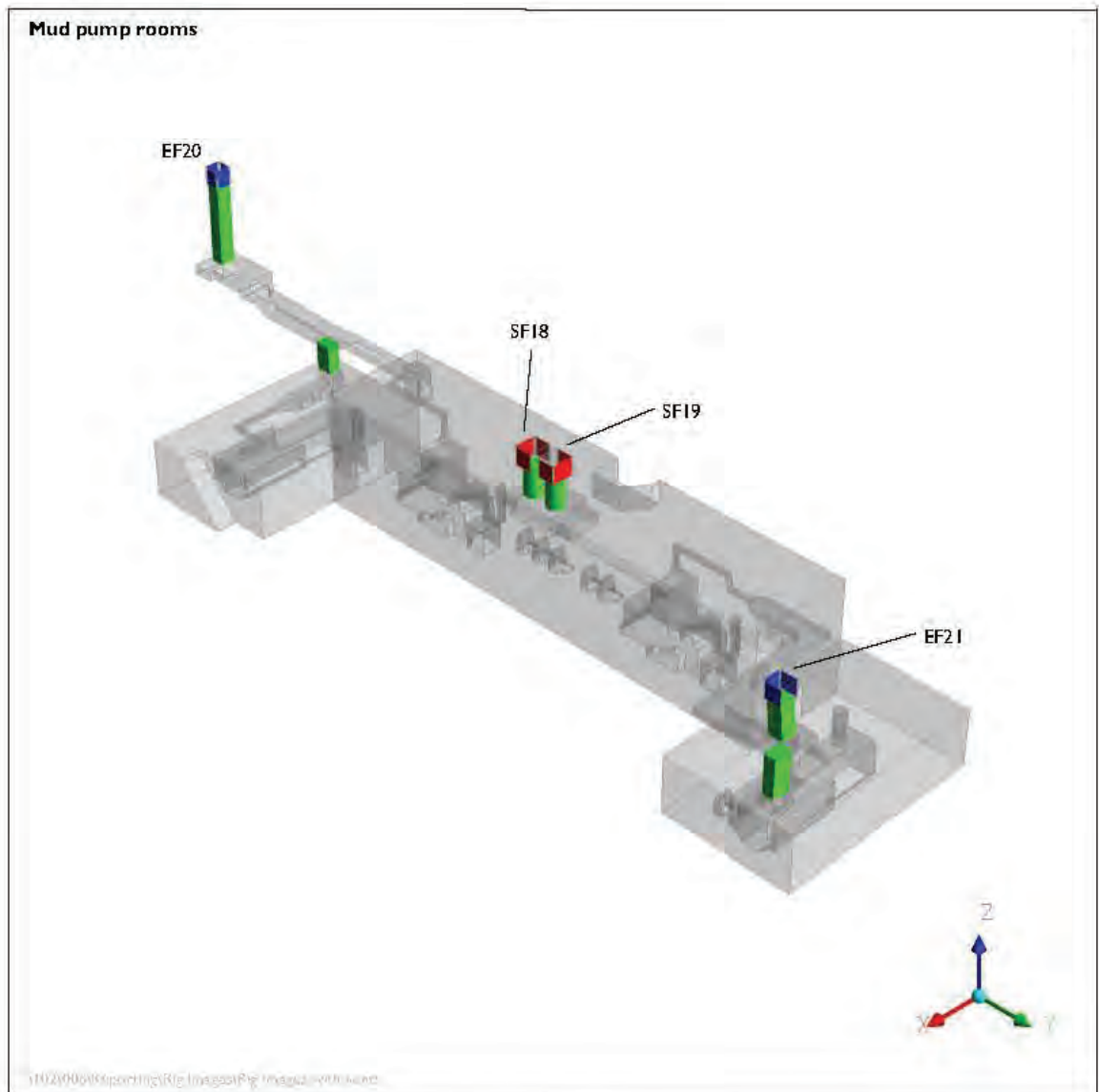


Figure 38 Isometric view of mud-pump rooms, looking towards the starboard aft quarter

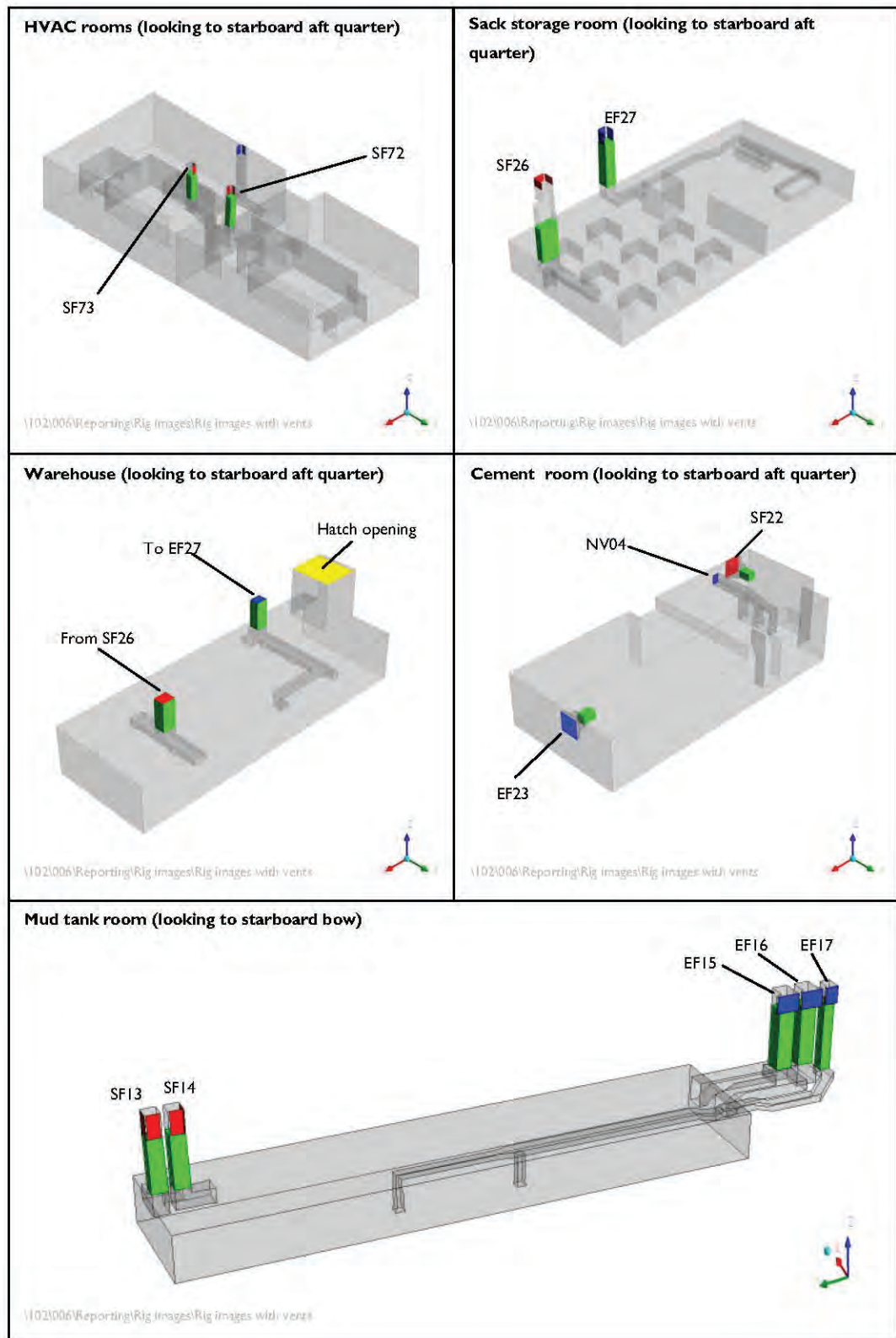


Figure 39 Isometric view of HVAC, sack storage, warehouse, cement and mud tank rooms

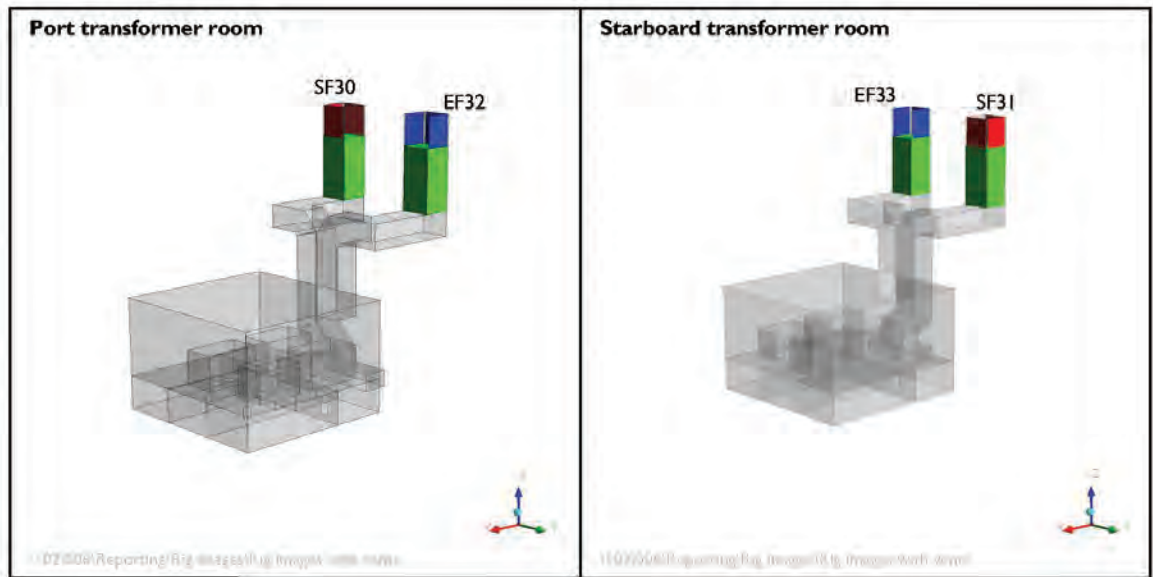


Figure 40 Isometric view of transformer rooms, looking towards the starboard aft quarter

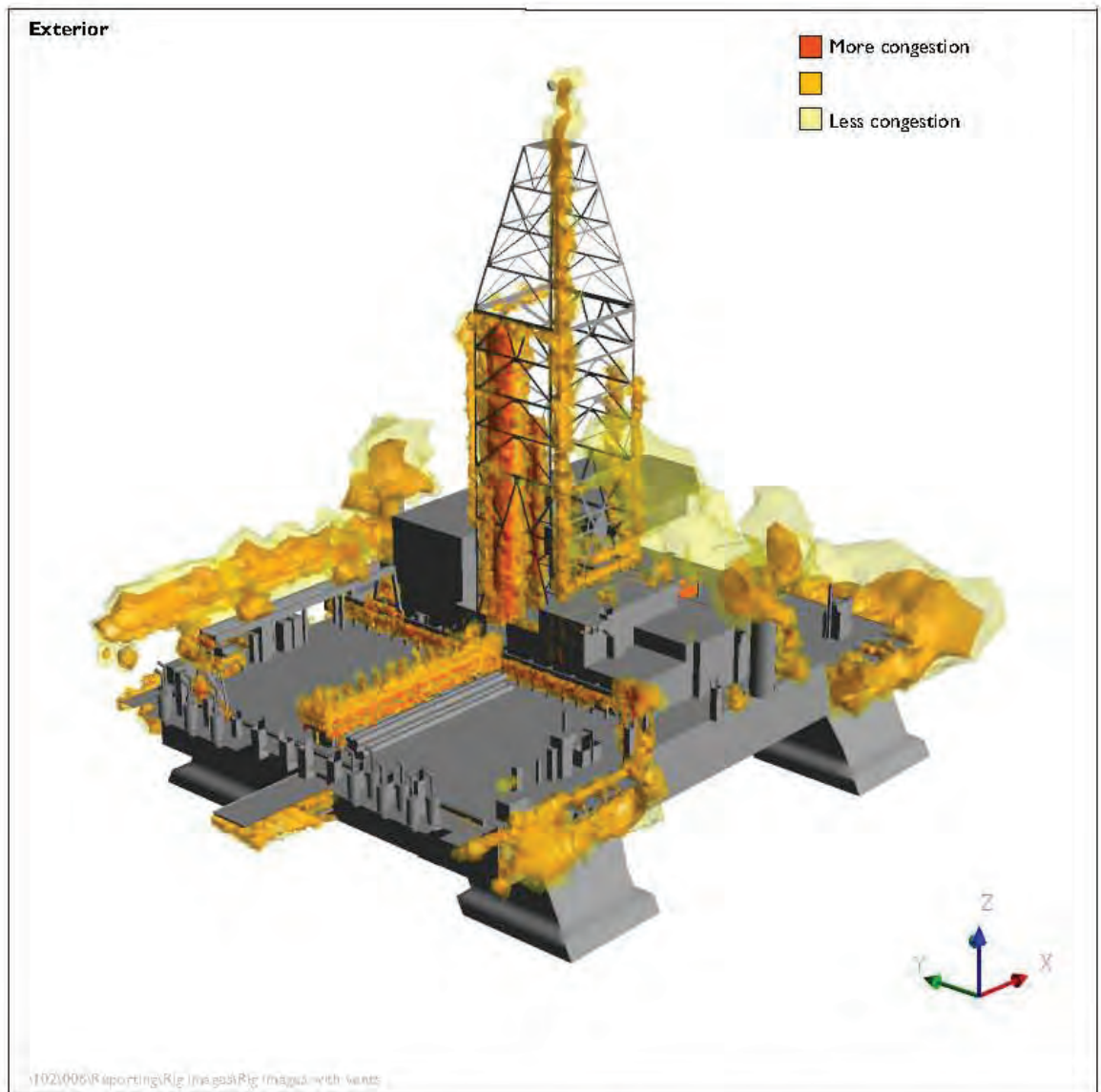


Figure 41 Isometric view of CFD model showing ACE congestion, looking towards the port bow

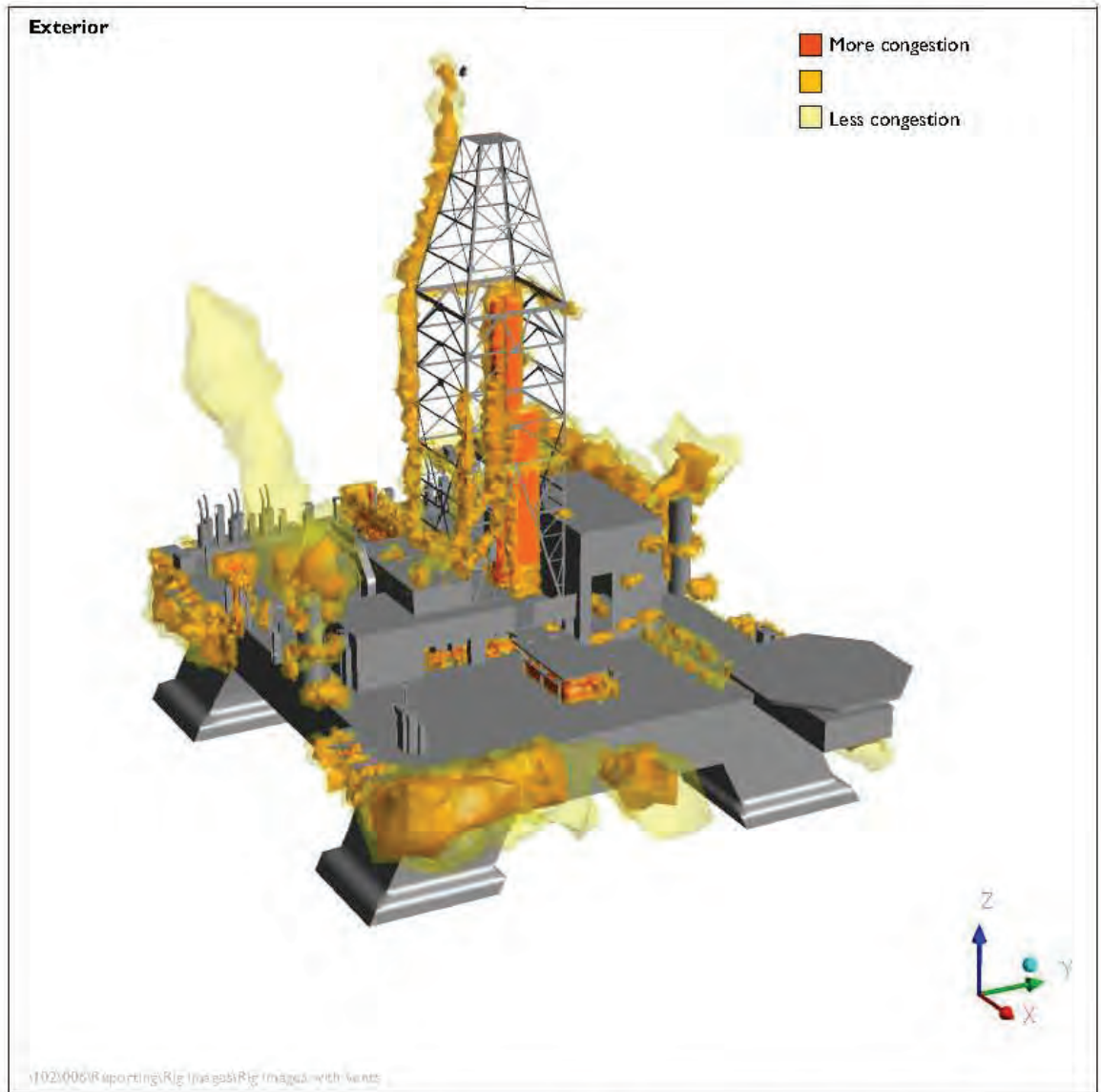


Figure 42 Isometric view of CFD model showing ACE congestion, looking towards the port aft quarter

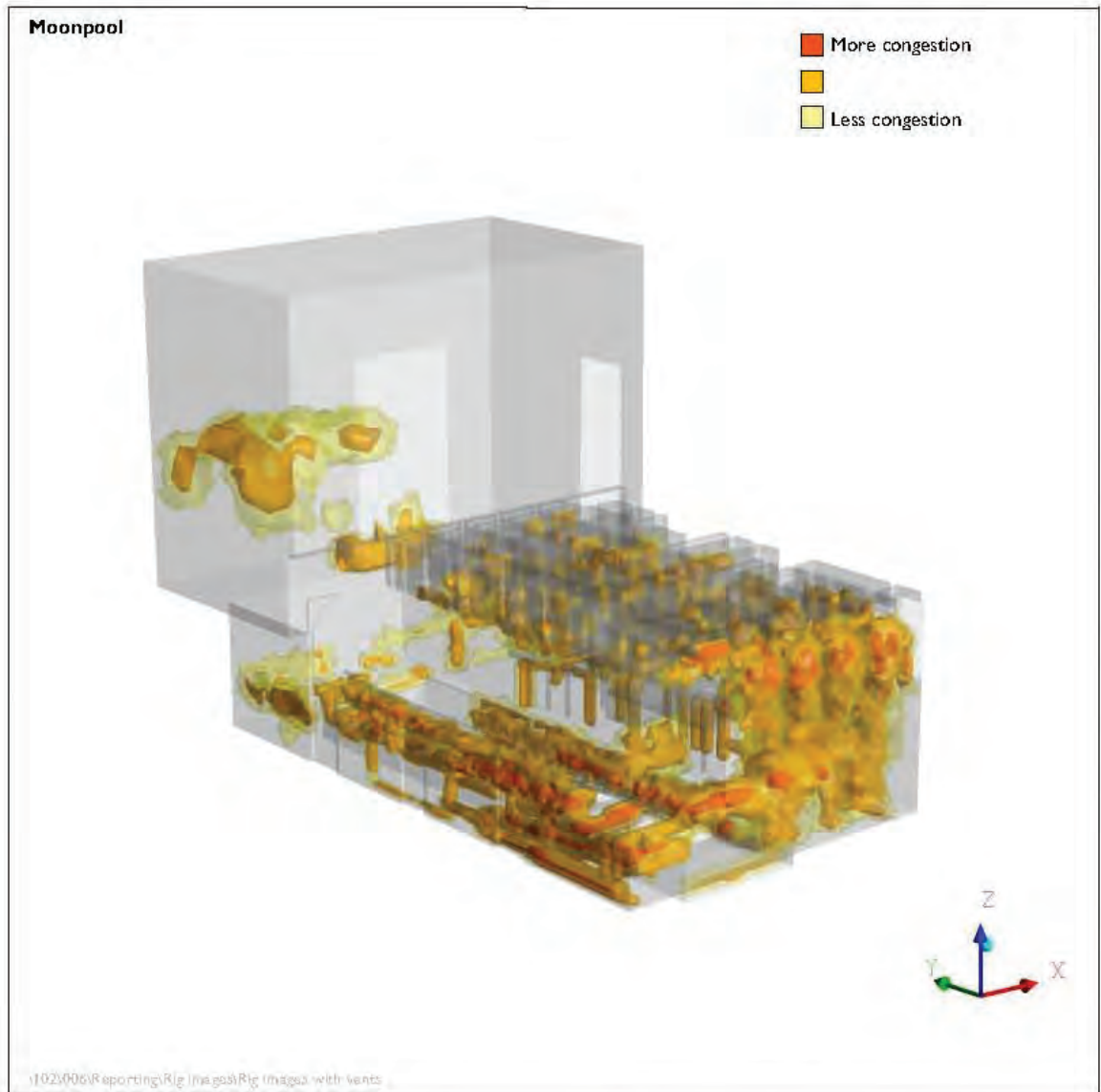


Figure 43 Isometric view of CFD model showing ACE congestion, looking towards the port bow

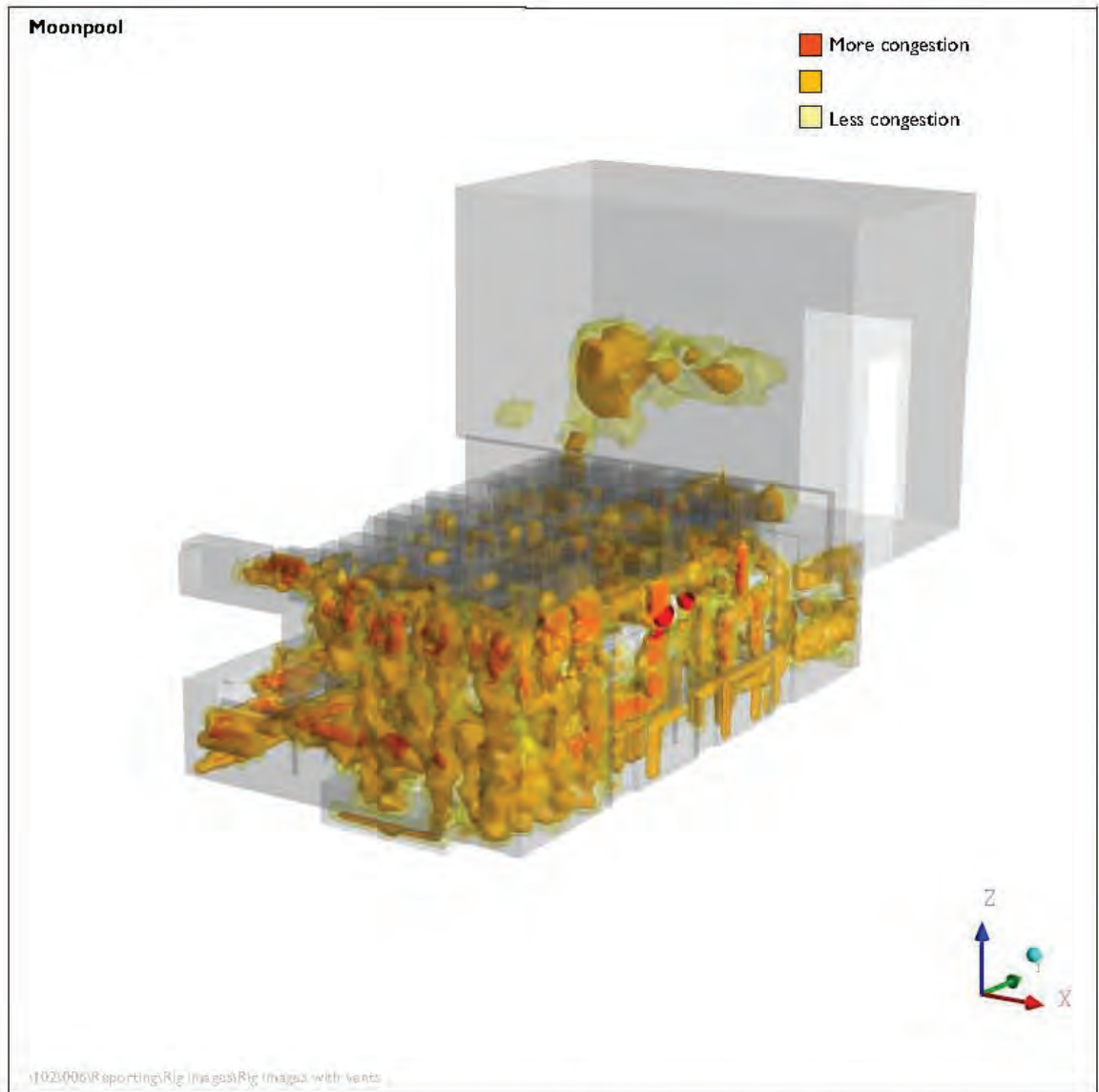


Figure 44 Isometric view of CFD model, showing ACE congestion, looking towards the port aft quarter

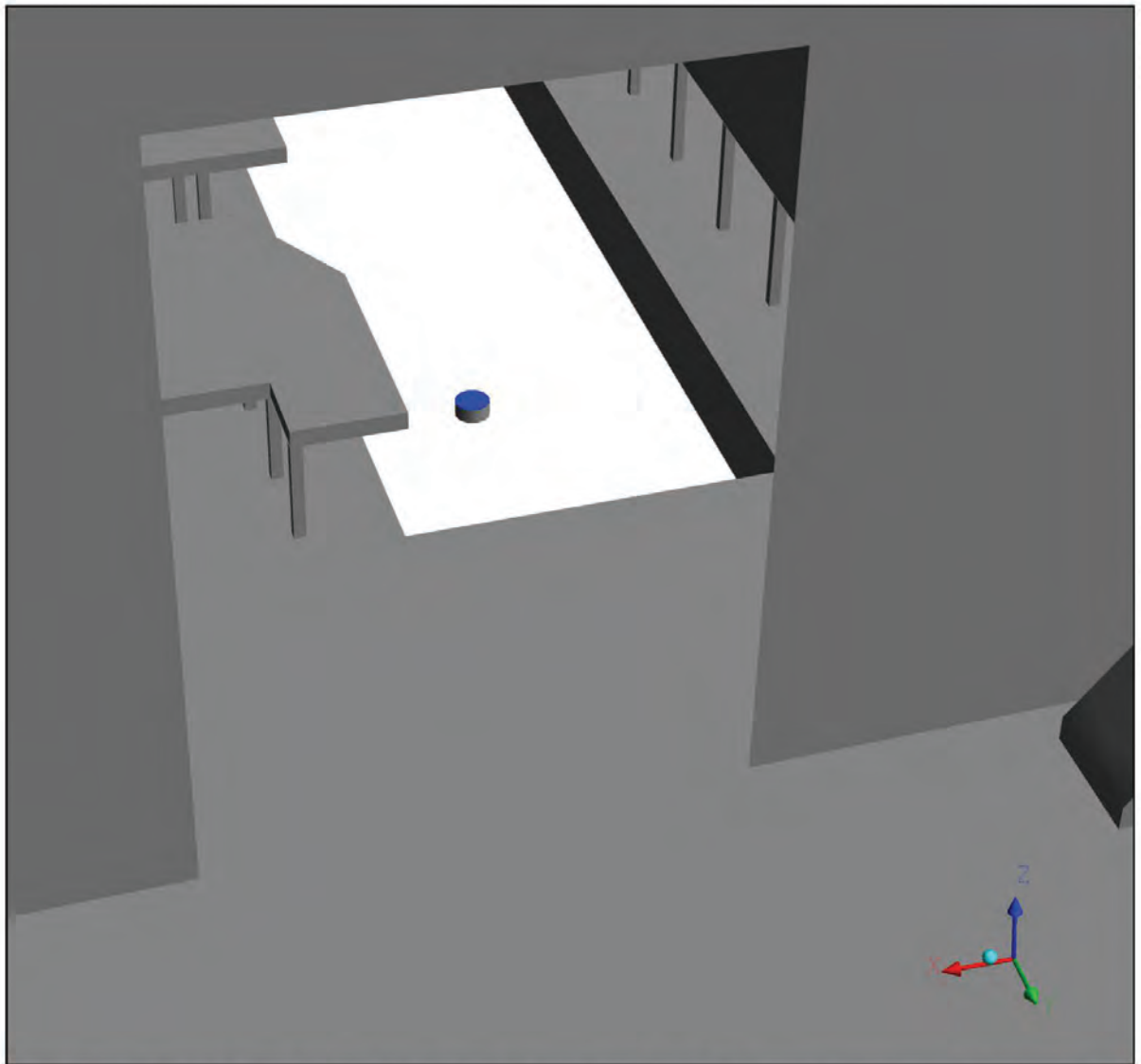


Figure 45 Release point at slip joint below moonpool, looking starboard through BOP house

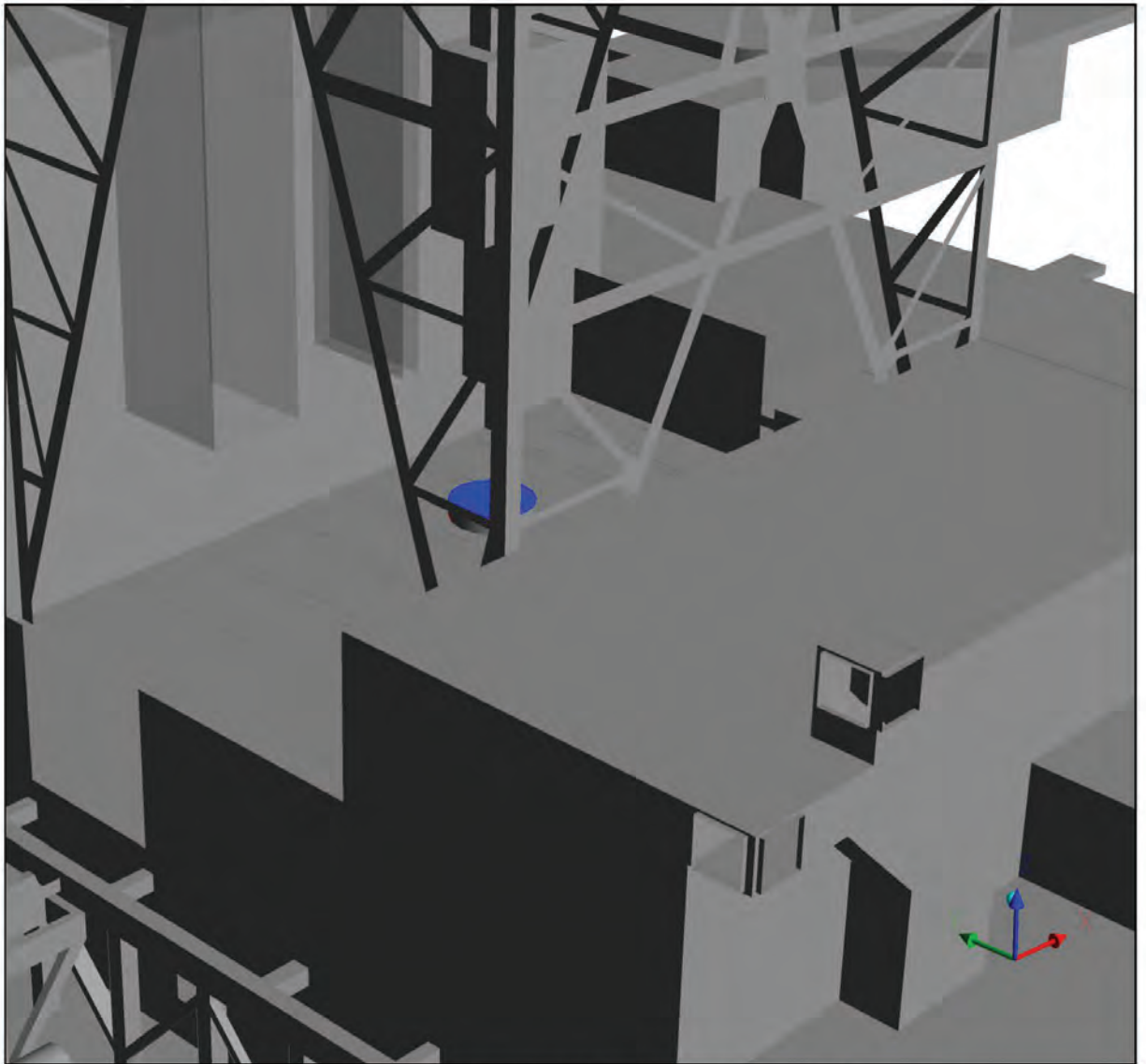


Figure 46 Release point at rotary table at drill floor, looking towards the port bow

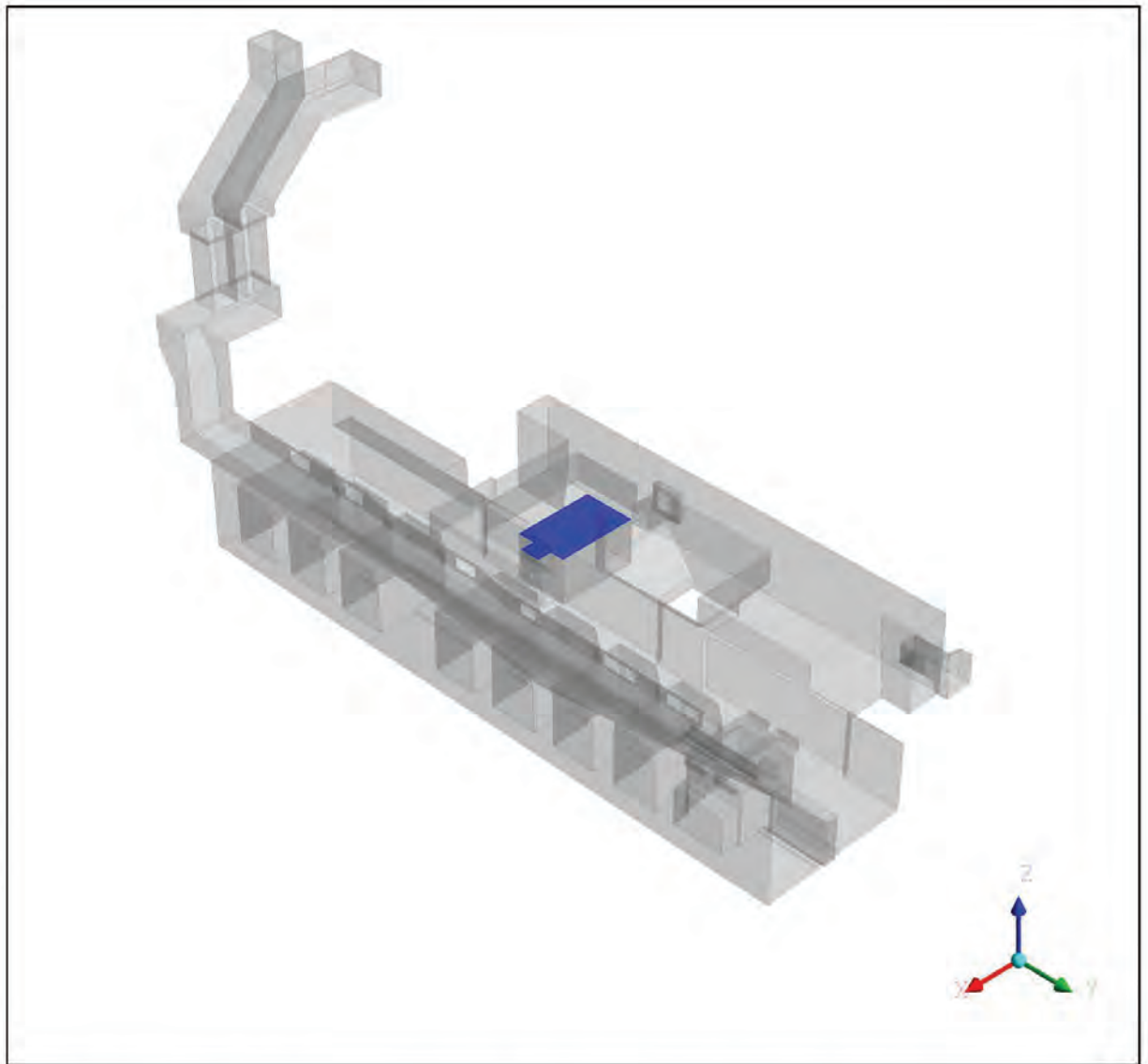


Figure 47 Open top of gumbobox within shale shaker house, looking towards the starboard aft

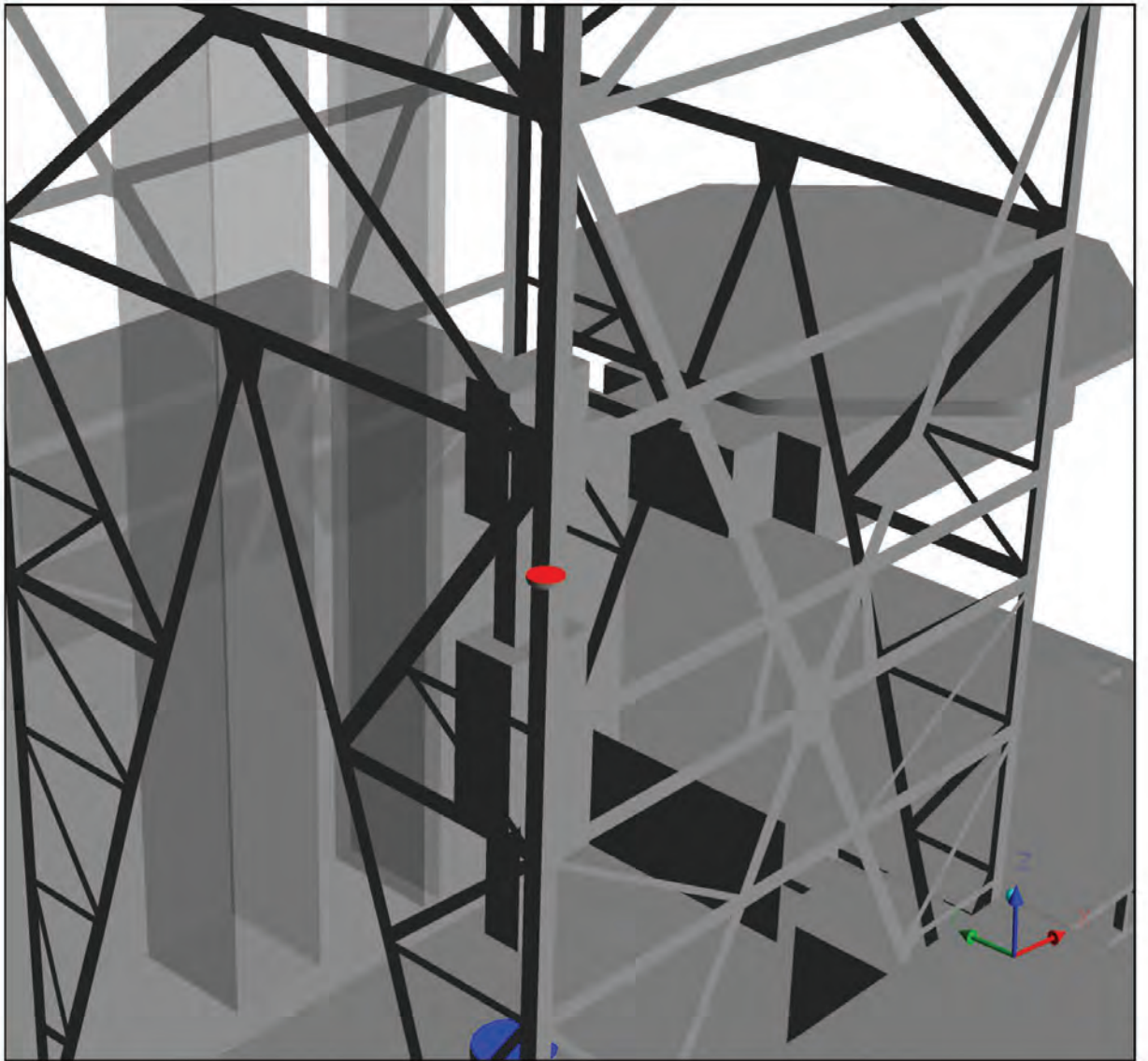


Figure 48 Release point at vacuum breaker, on starboard aft leg of drilling derrick

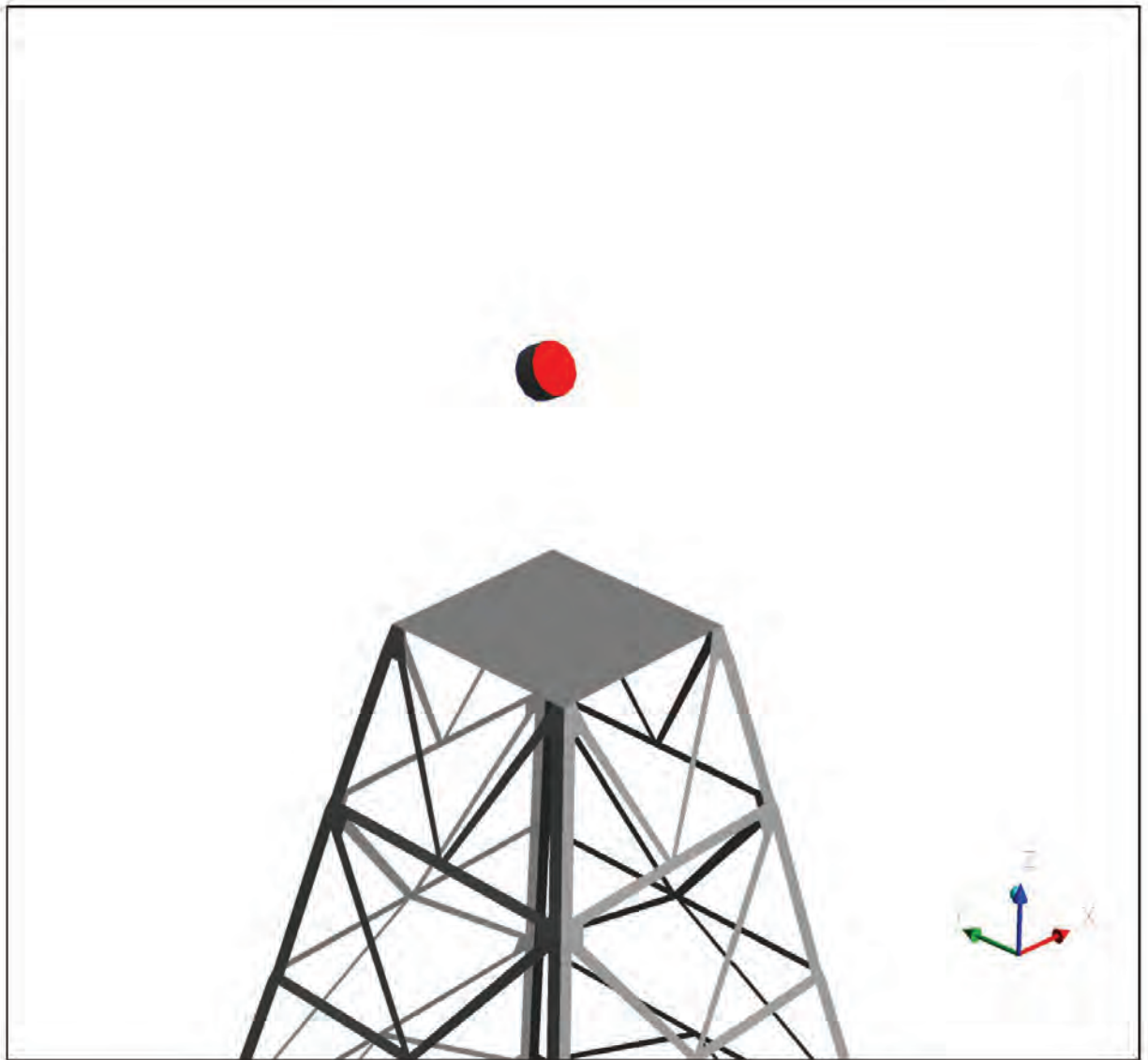


Figure 49 MGS outlet at top of drilling derrick, looking towards the port bow

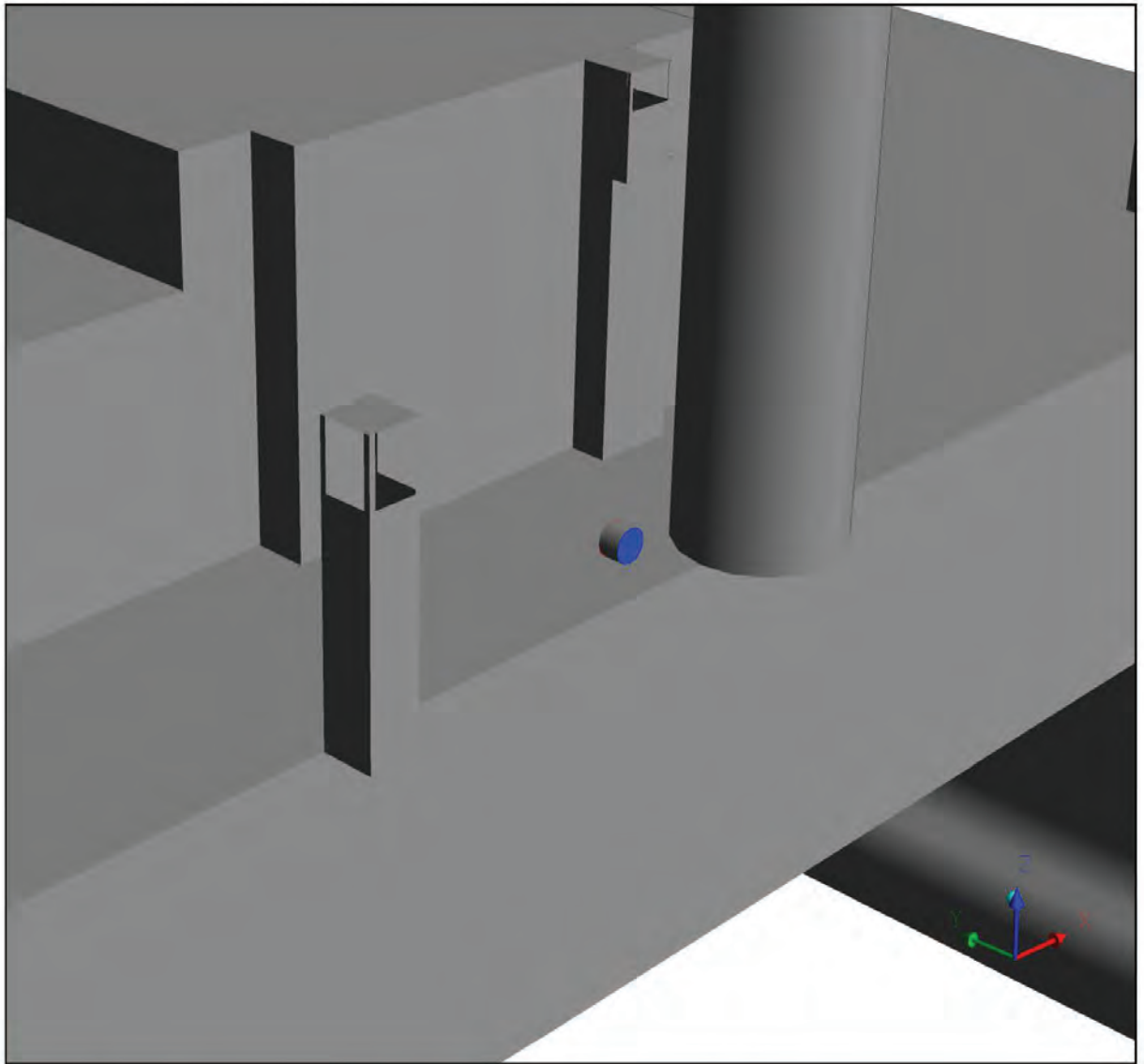


Figure 50 MGS starboard relief line, looking towards the port bow

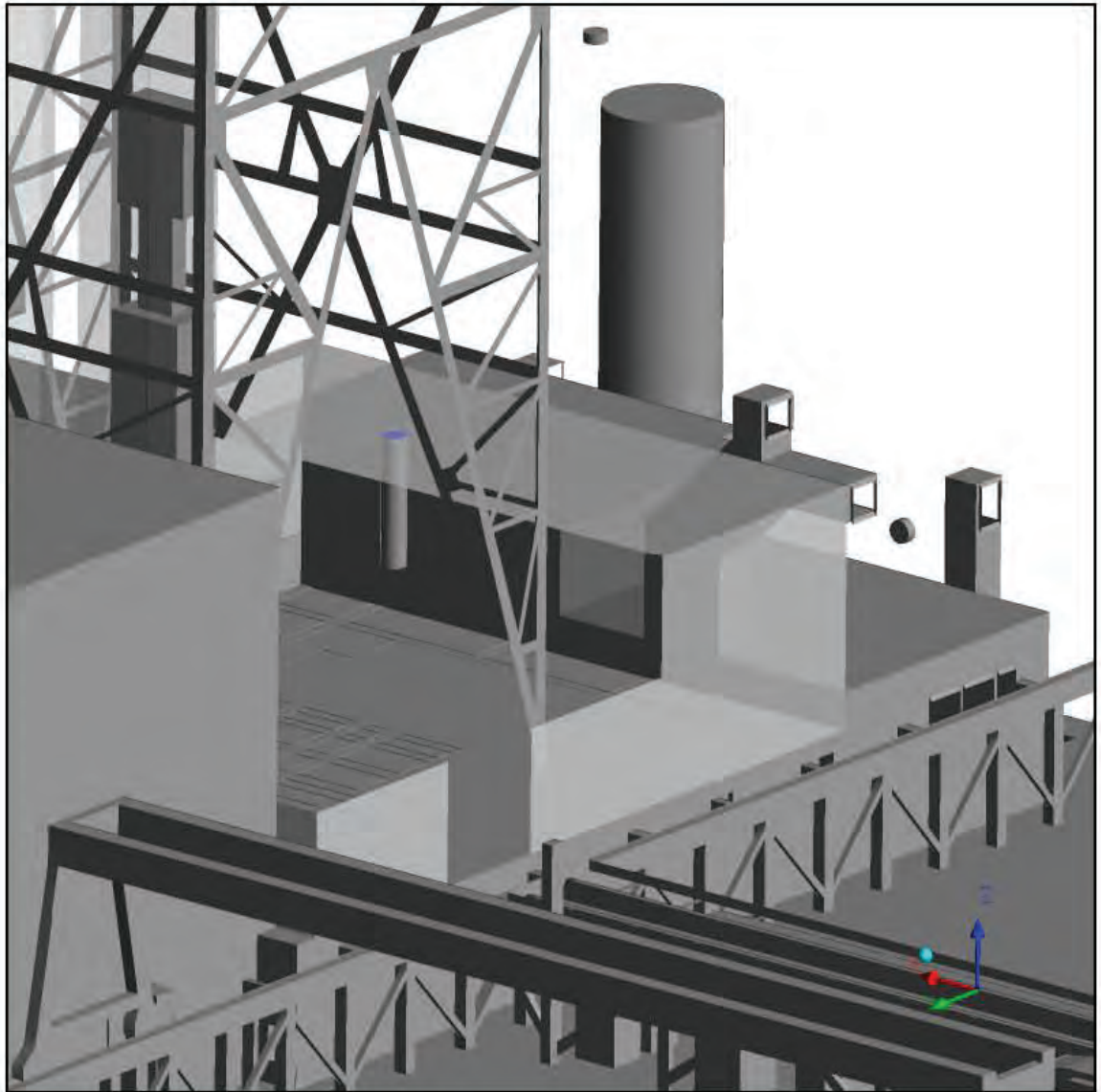


Figure 51 Mini trip tank, looking into the drawworks towards the starboard bow

APPENDICES

APPENDIX A RESULTS FOR CASE A

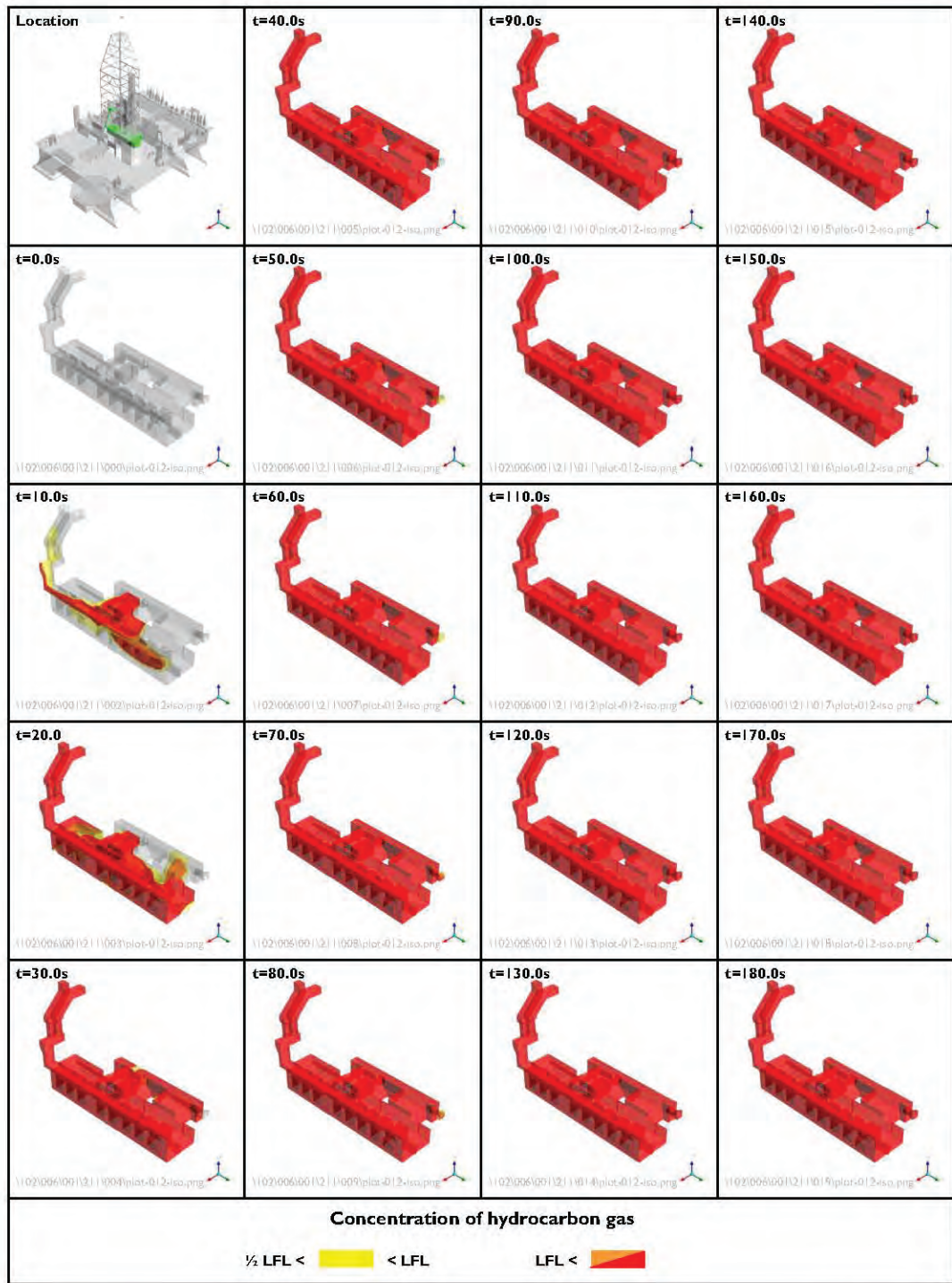
APPENDIX B RESULTS FOR CASE B

APPENDIX C RESULTS FOR CASE C

APPENDIX A RESULTS FOR CASE A

FIGURES

- Figure 52 Extent of hydrocarbon gas within shale shaker house – Case A
- Figure 53 Extent of hydrocarbon gas within shale shaker house – Case A
- Figure 54 Extent of hydrocarbon gas within moonpool – Case A
- Figure 55 Extent of hydrocarbon gas within moonpool – Case A
- Figure 56 Extent of hydrocarbon gas outside the rig – isometric view – Case A
- Figure 57 Extent of hydrocarbon gas outside the rig – top view – Case A
- Figure 58 Extent of hydrocarbon gas outside the rig – port view – Case A
- Figure 59 Extent of hydrocarbon gas outside the rig – aft view – Case A
- Figure 60 Extent of hydrocarbon gas on external rig surfaces – isometric view – Case A
- Figure 61 Extent of hydrocarbon gas within engine room 1 – Case A
- Figure 62 Extent of hydrocarbon gas within engine room 2 – Case A
- Figure 63 Extent of hydrocarbon gas within engine room 3 – Case A
- Figure 64 Extent of hydrocarbon gas within engine room 4 – Case A
- Figure 65 Extent of hydrocarbon gas within engine room 5 – Case A
- Figure 66 Extent of hydrocarbon gas within engine room 6 – Case A
- Figure 67 Extent of hydrocarbon gas within mud pump rooms – Case A
- Figure 68 Extent of hydrocarbon gas within HVAC rooms – Case A
- Figure 69 Extent of hydrocarbon gas within port transformer room – Case A
- Figure 70 Extent of hydrocarbon gas within starboard transformer room – Case A
- Figure 71 Extent of hydrocarbon gas within sack storage room – Case A
- Figure 72 Extent of hydrocarbon gas within warehouse – Case A
- Figure 73 Extent of hydrocarbon gas within mud tank room – Case A
- Figure 74 Extent of hydrocarbon gas within cement room – Case A
- Figure 75 Extent of hydrocarbon gas within cement room – Case A



Peak flow rate:

500 MMscfd

Wind speed:

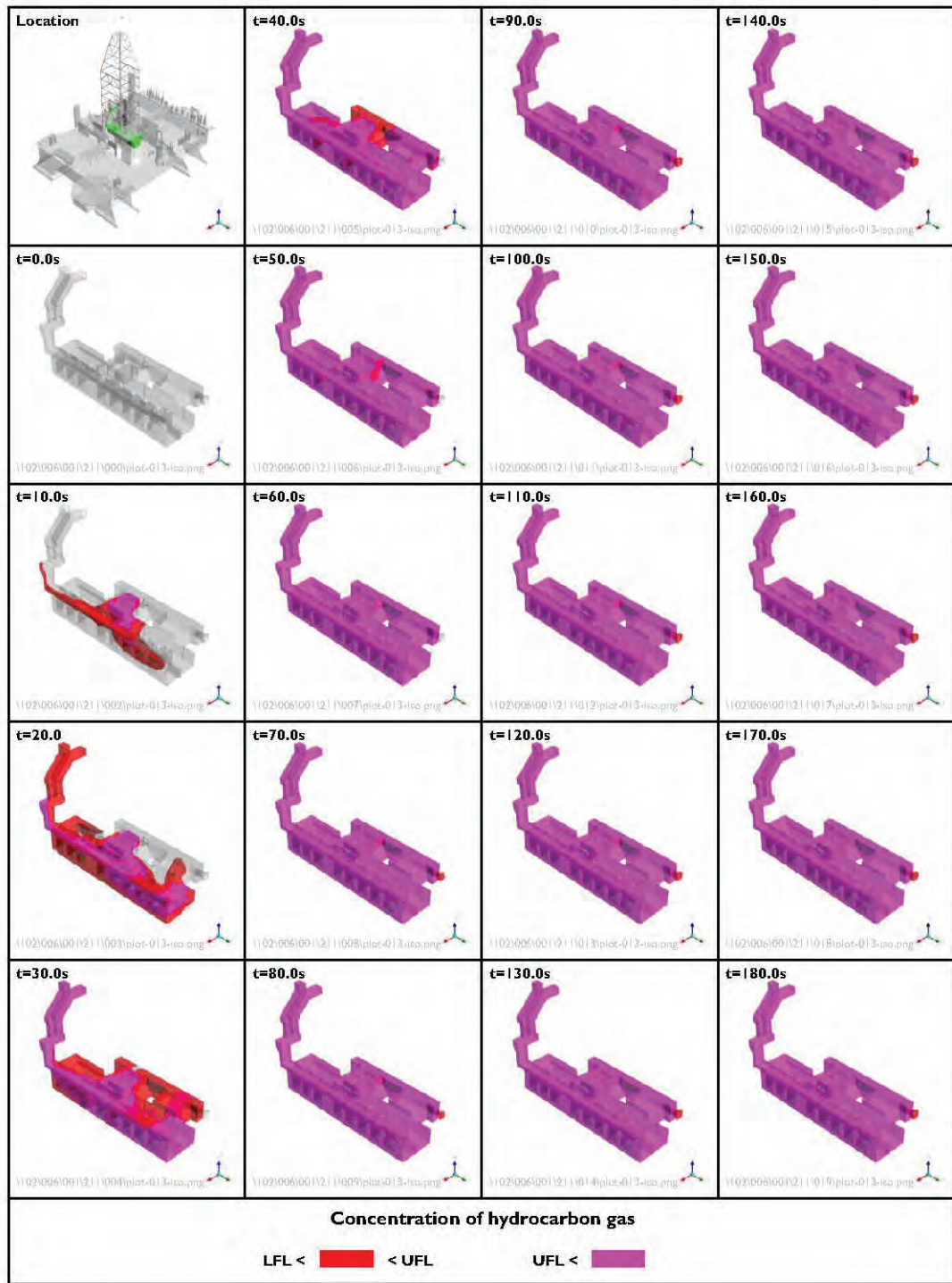
1.5 m/s

Wind direction:

90°

Figure 52

Extent of hydrocarbon gas within shale shaker house – Case A



Peak flow rate:

500 MMscfd

Wind speed:

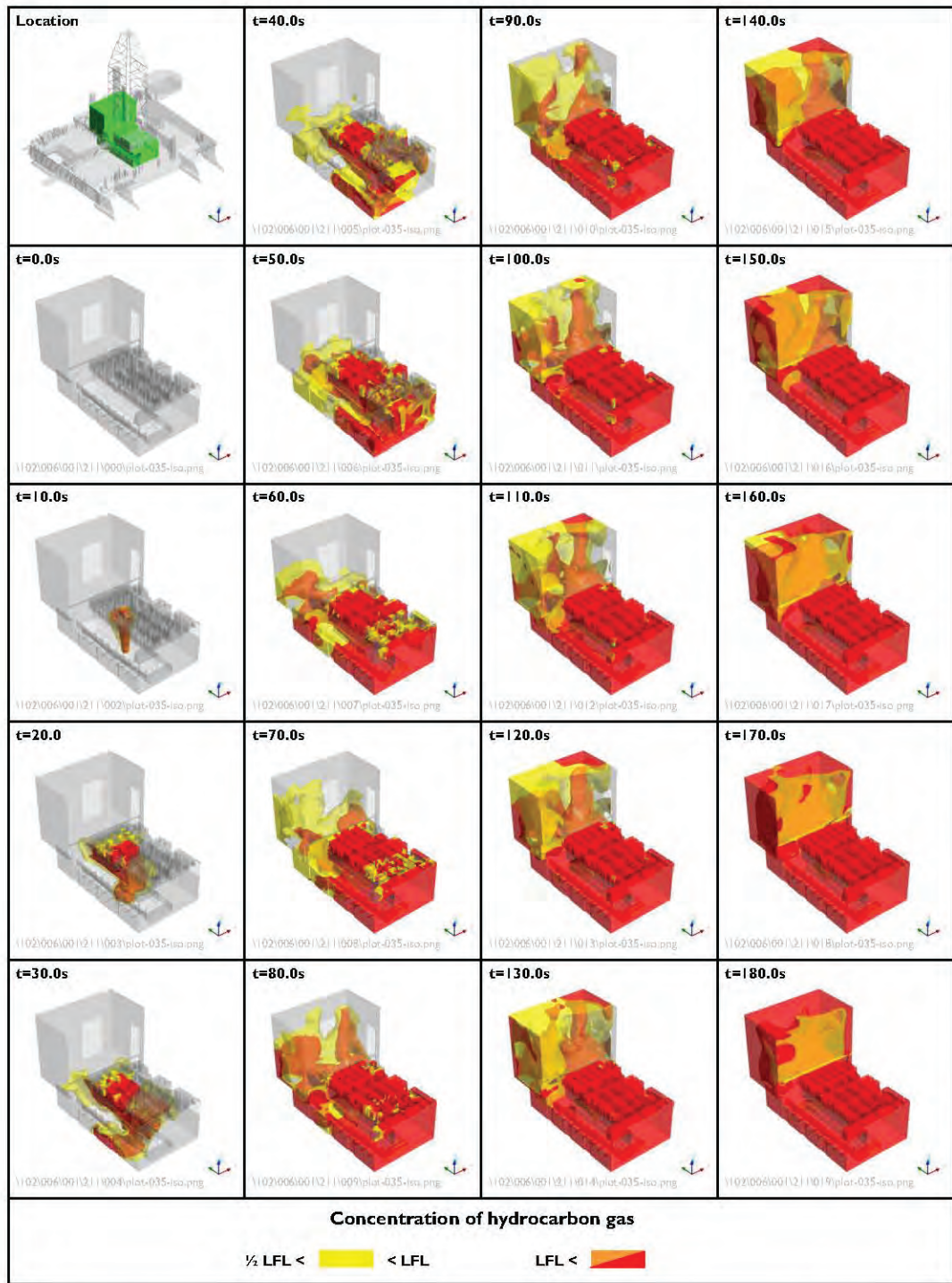
1.5 m/s

Wind direction:

90°

Figure 53

Extent of hydrocarbon gas within shale shaker house – Case A



Peak flow rate:

500 MMscfd

Wind speed:

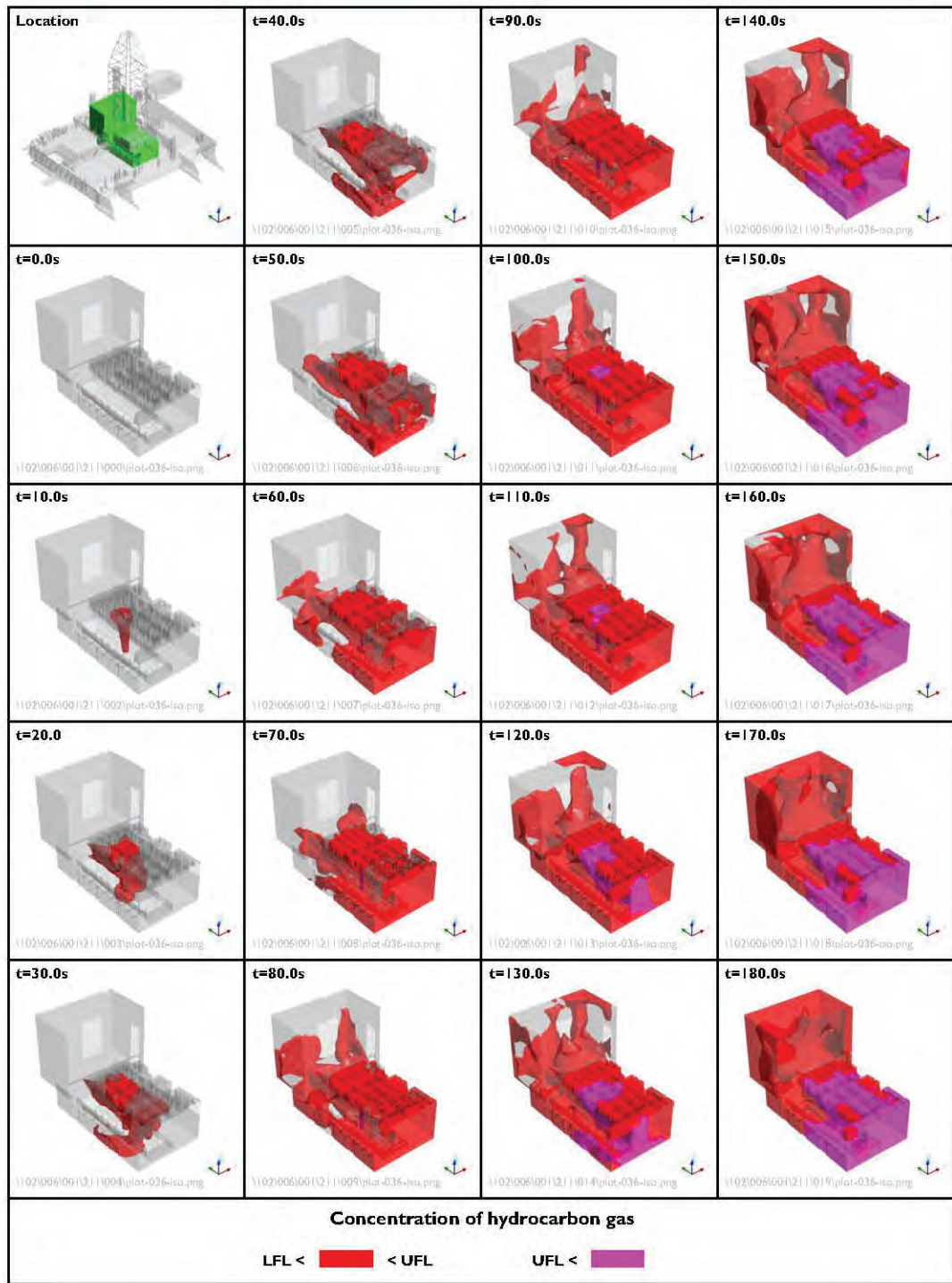
1.5 m/s

Wind direction:

90°

Figure 54

Extent of hydrocarbon gas within moonpool – Case A



Peak flow rate:

500 MMscfd

Wind speed:

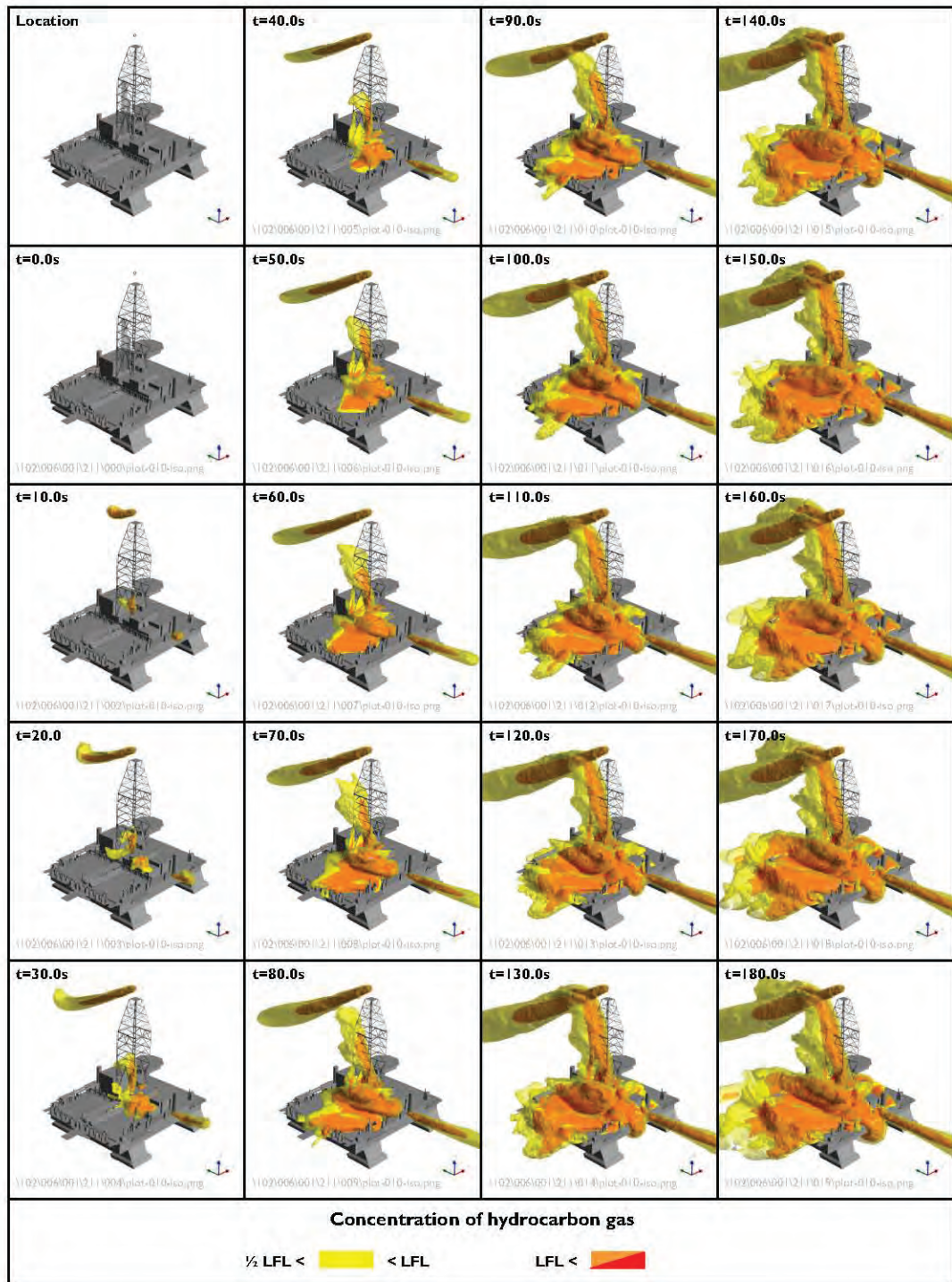
1.5 m/s

Wind direction:

90°

Figure 55

Extent of hydrocarbon gas within moonpool – Case A



Peak flow rate:

500 MMscfd

Wind speed:

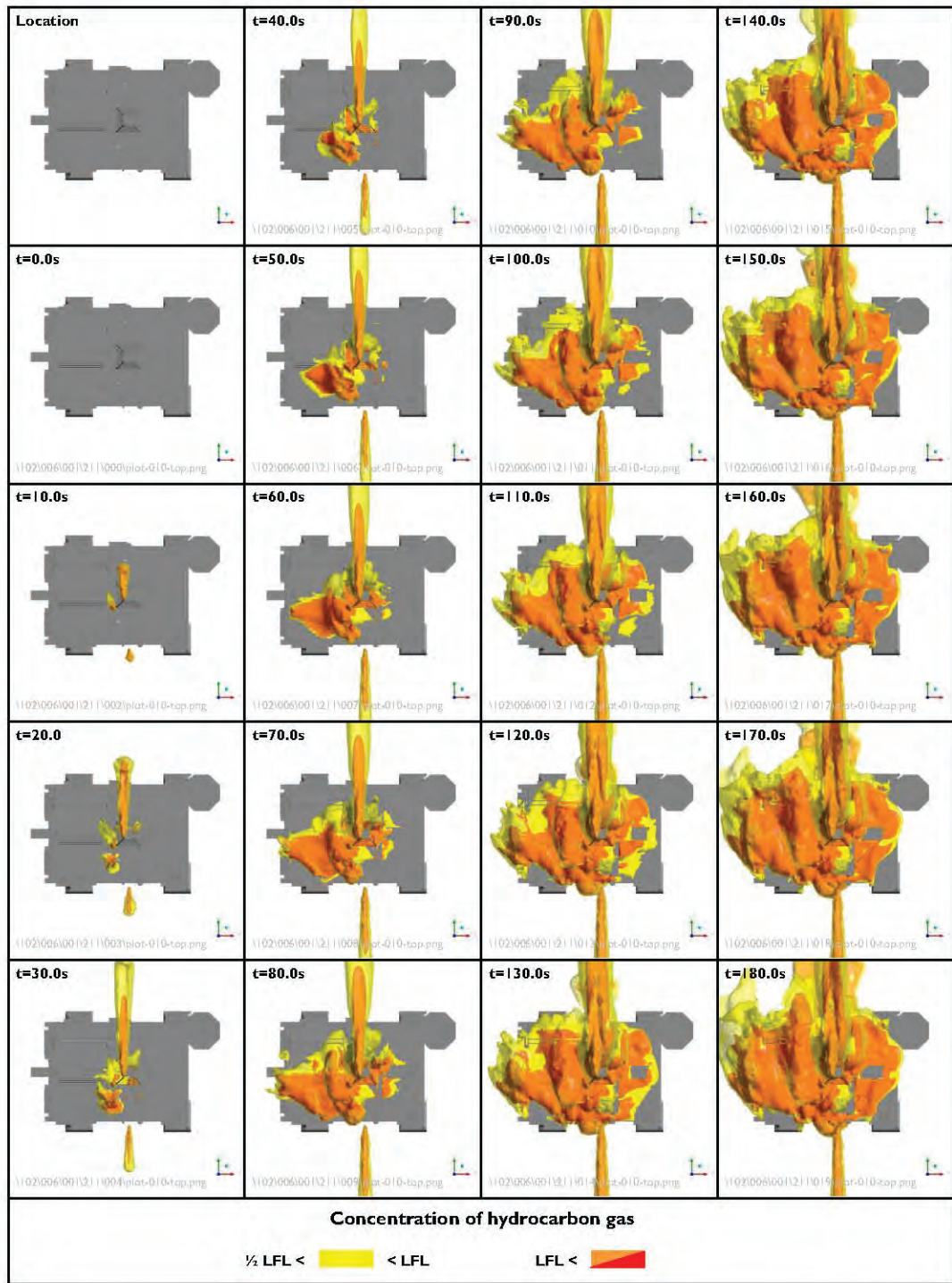
1.5 m/s

Wind direction:

90°

Figure 56

Extent of hydrocarbon gas outside the rig – isometric view – Case A



Peak flow rate:

500 MMscfd

Wind speed:

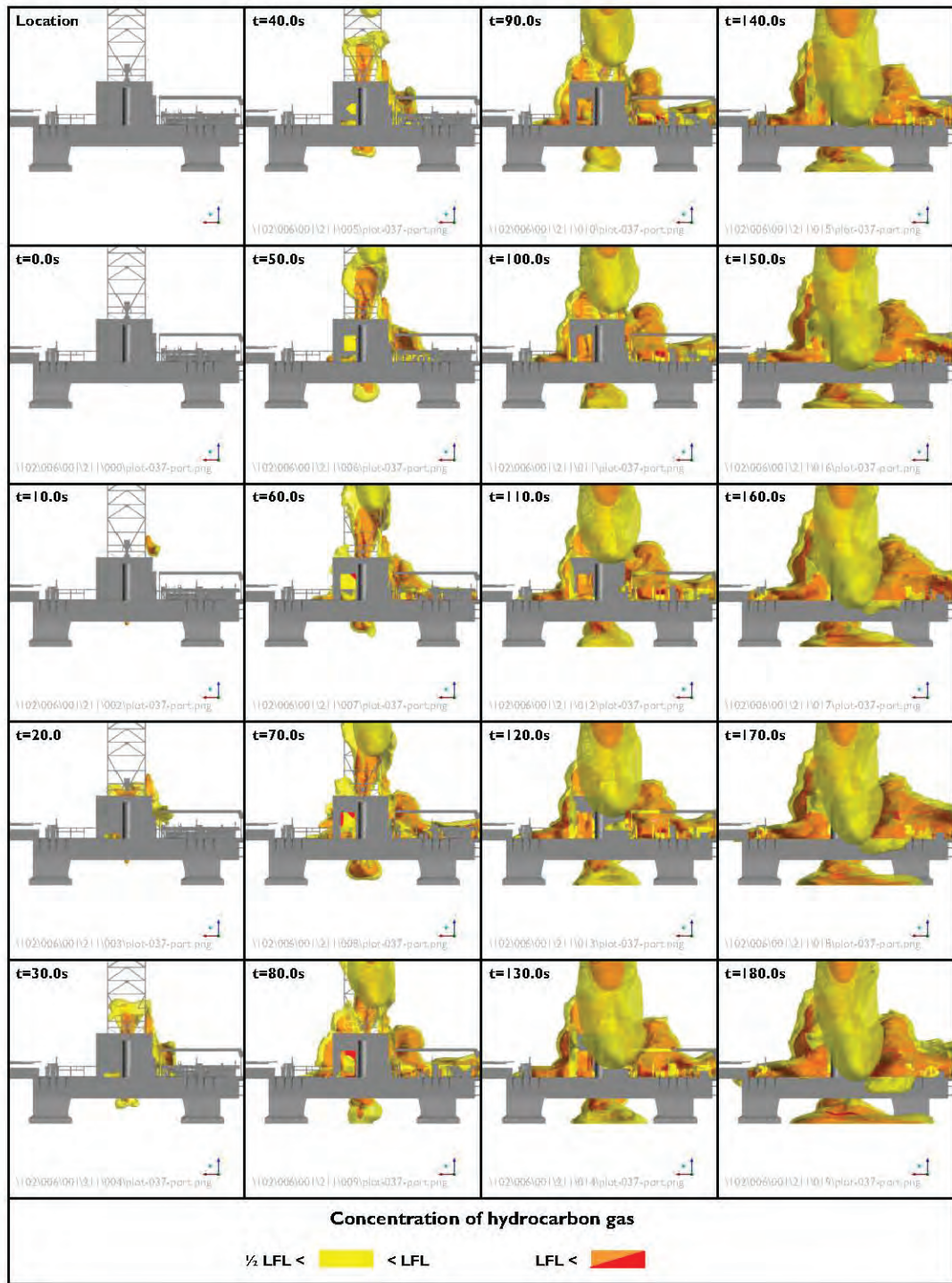
1.5 m/s

Wind direction:

90°

Figure 57

Extent of hydrocarbon gas outside the rig – top view – Case A



Peak flow rate:

500 MMscfd

Wind speed:

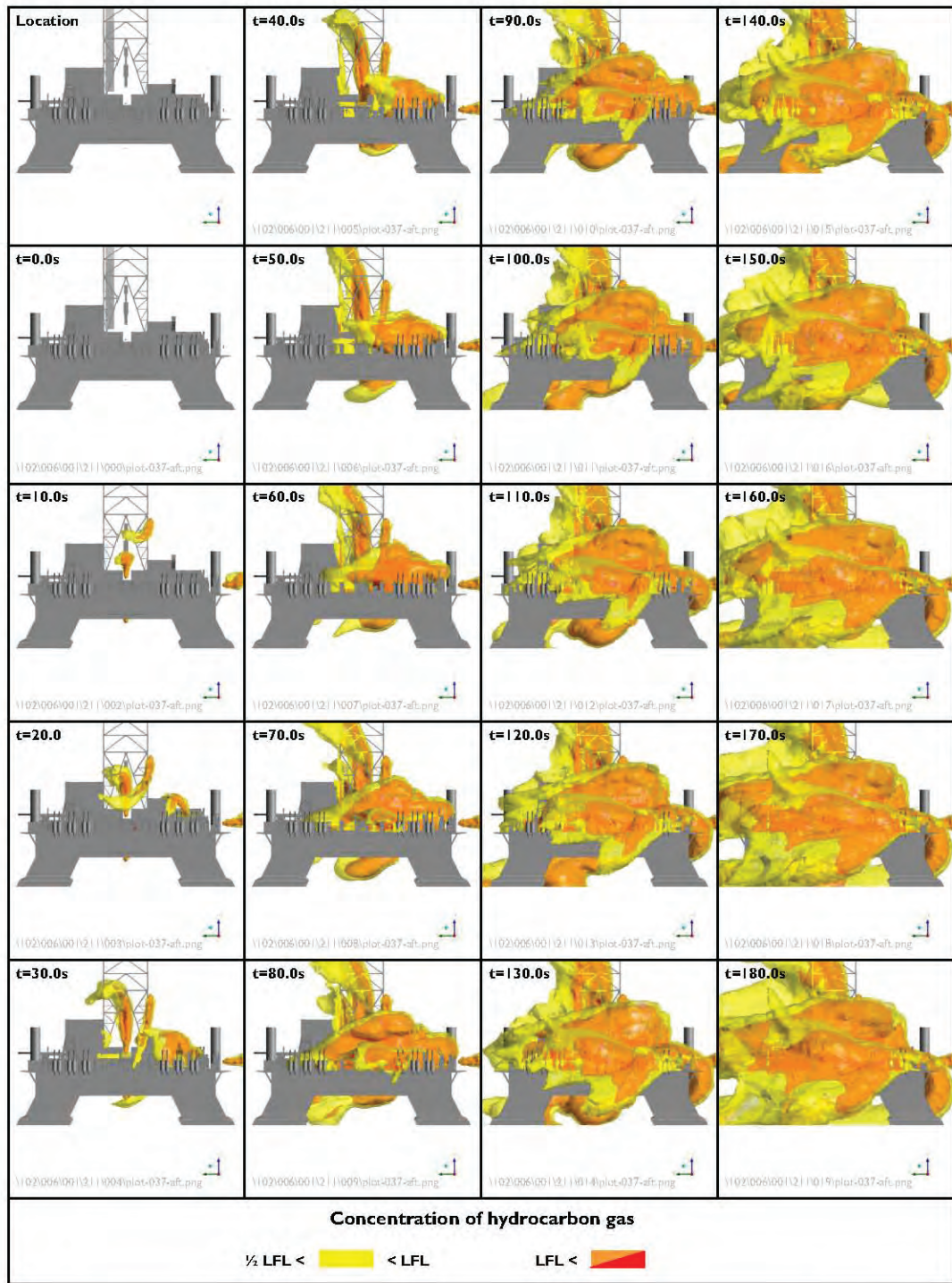
1.5 m/s

Wind direction:

90°

Figure 58

Extent of hydrocarbon gas outside the rig – port view – Case A



Peak flow rate:

500 MMscfd

Wind speed:

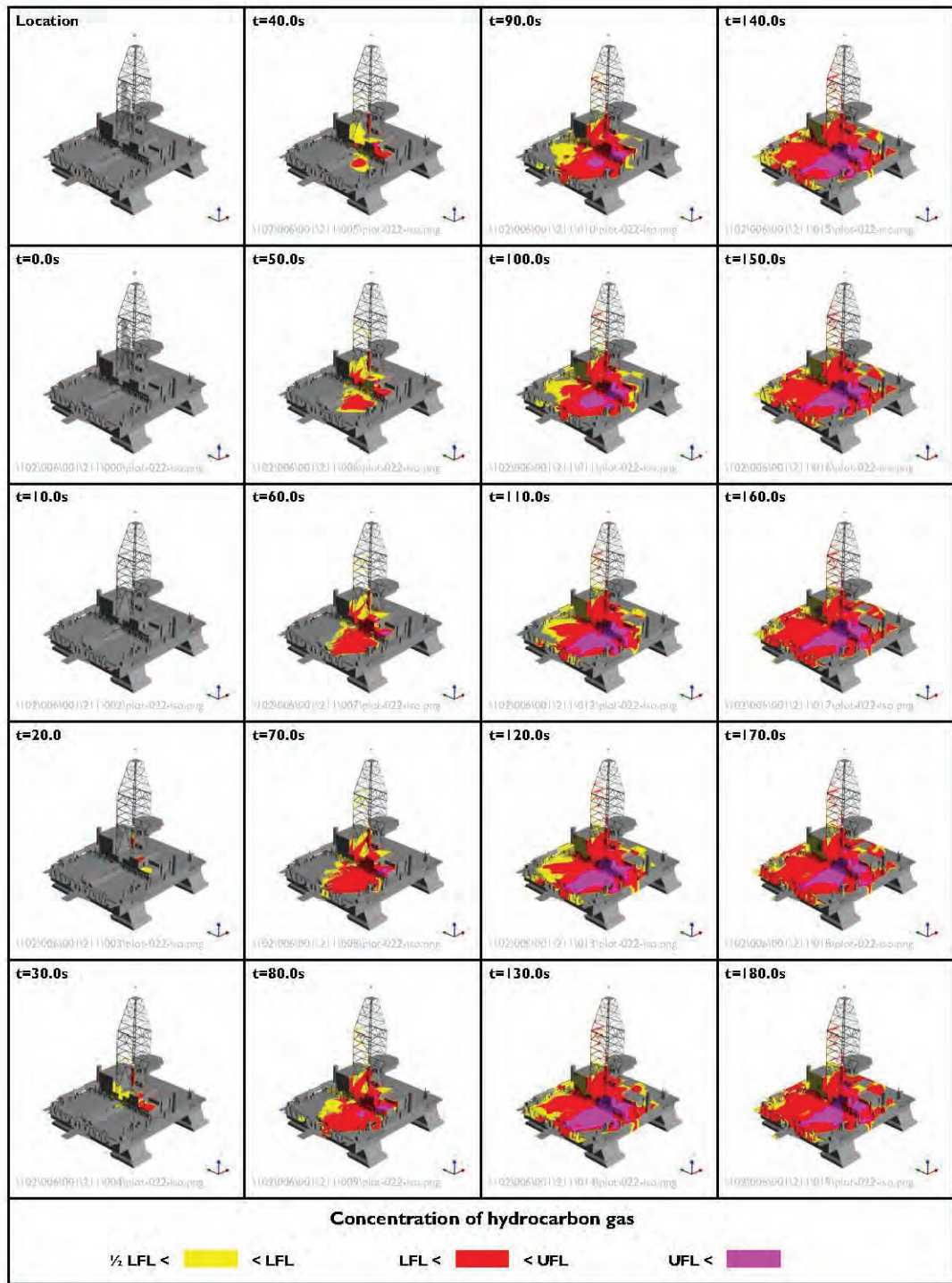
1.5 m/s

Wind direction:

90°

Figure 59

Extent of hydrocarbon gas outside the rig – aft view – Case A



Peak flow rate:

500 MMscfd

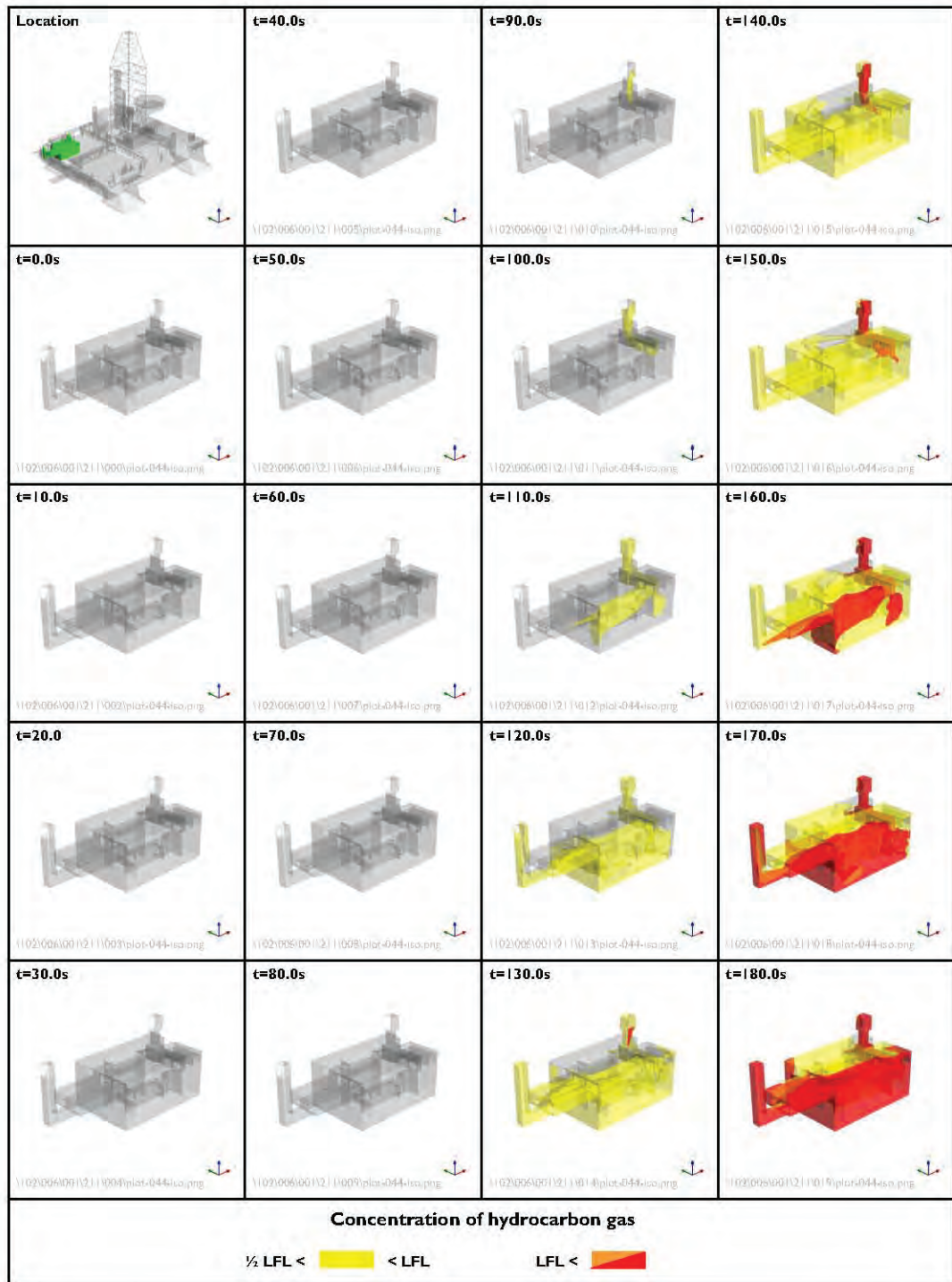
Wind speed:

1.5 m/s

Wind direction:

90°

Figure 60 **Extent of hydrocarbon gas on external rig surfaces – isometric view – Case A**



Peak flow rate:

500 MMscfd

Wind speed:

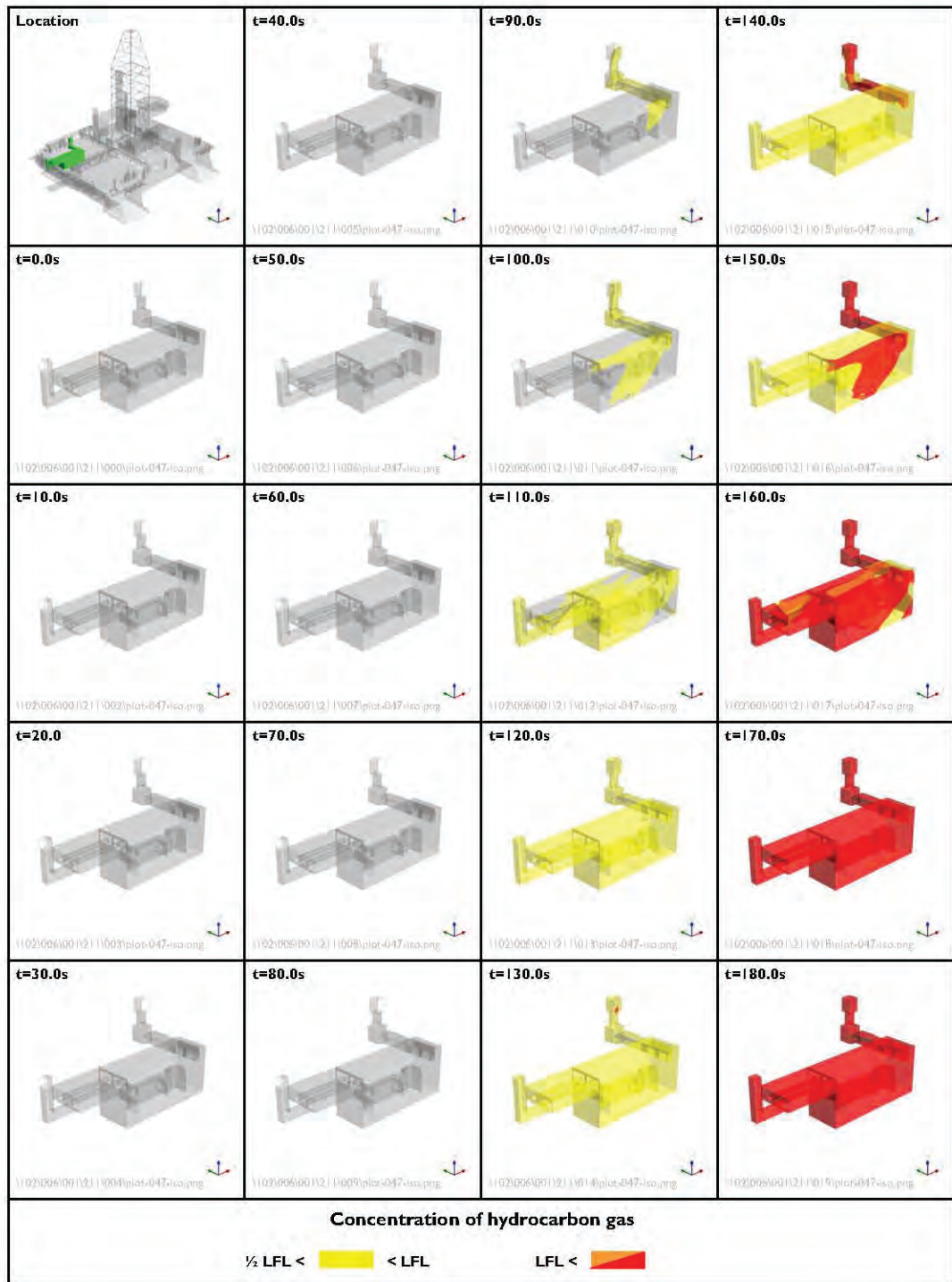
1.5 m/s

Wind direction:

90°

Figure 61

Extent of hydrocarbon gas within engine room I – Case A



Peak flow rate:

500 MMscfd

Wind speed:

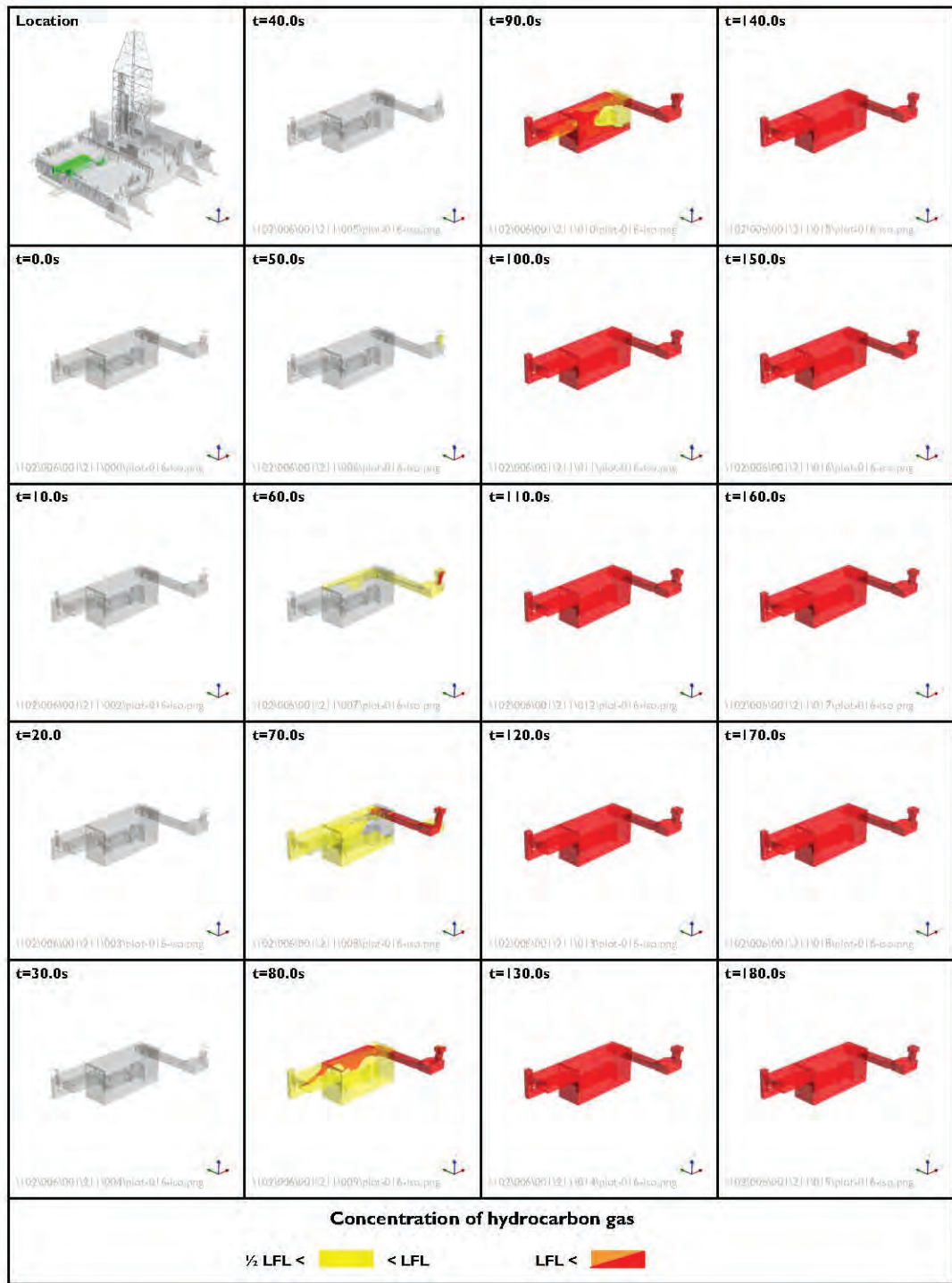
1.5 m/s

Wind direction:

90°

Figure 62

Extent of hydrocarbon gas within engine room 2 – Case A



Peak flow rate:

500 MMscfd

Wind speed:

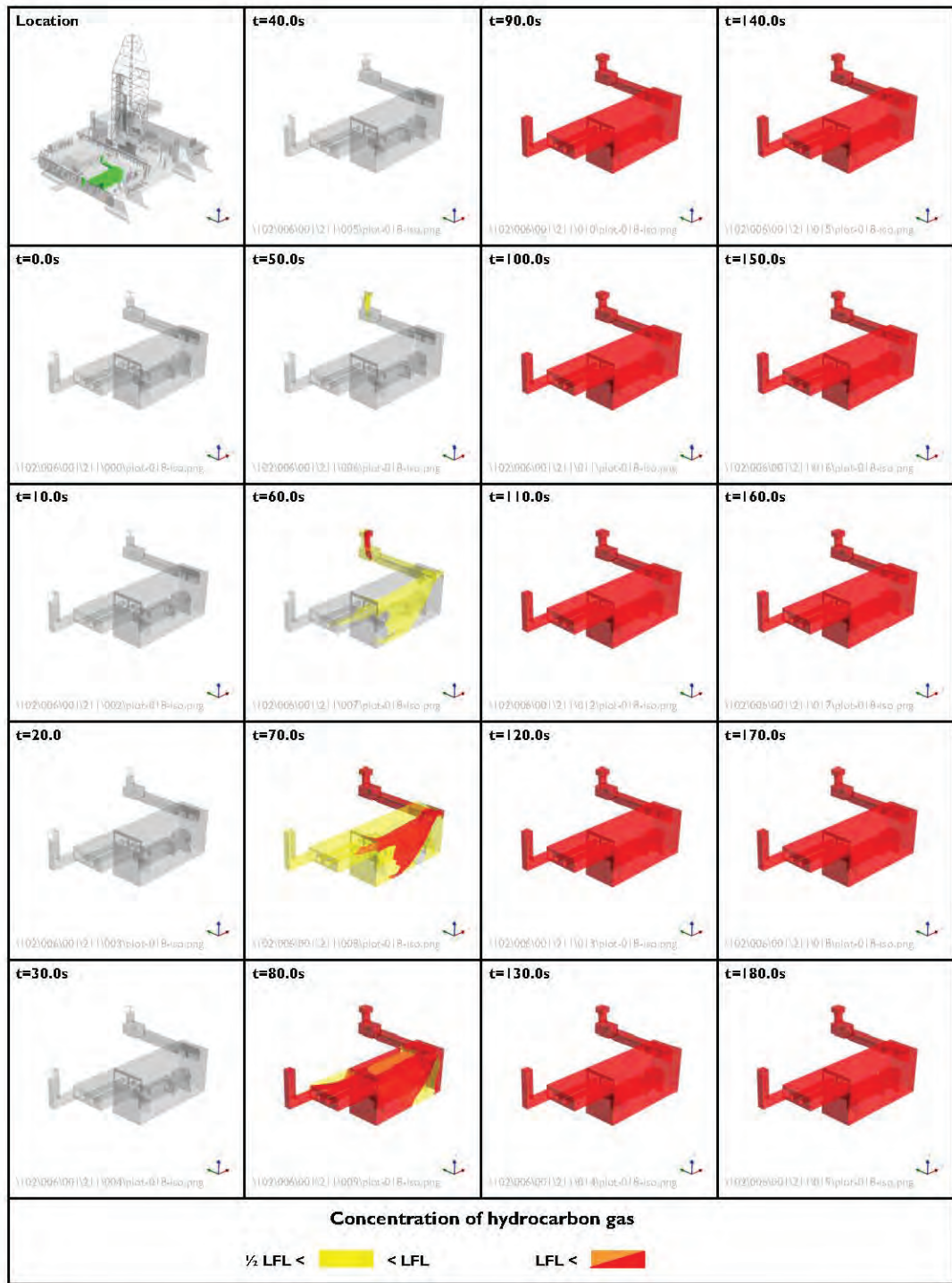
1.5 m/s

Wind direction:

90°

Figure 63

Extent of hydrocarbon gas within engine room 3 – Case A



Peak flow rate:

500 MMscfd

Wind speed:

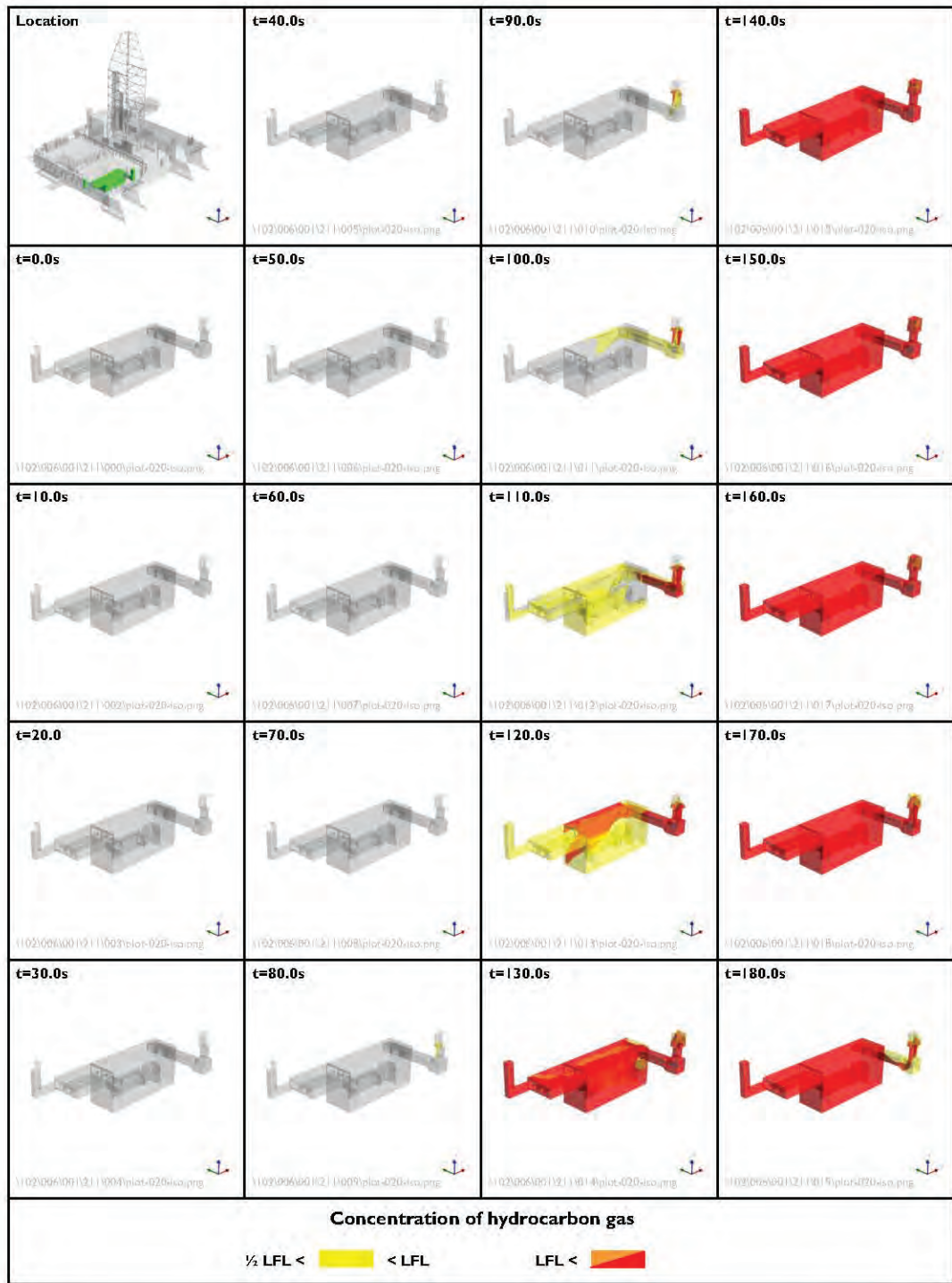
1.5 m/s

Wind direction:

90°

Figure 64

Extent of hydrocarbon gas within engine room 4 – Case A



Peak flow rate:

500 MMscfd

Wind speed:

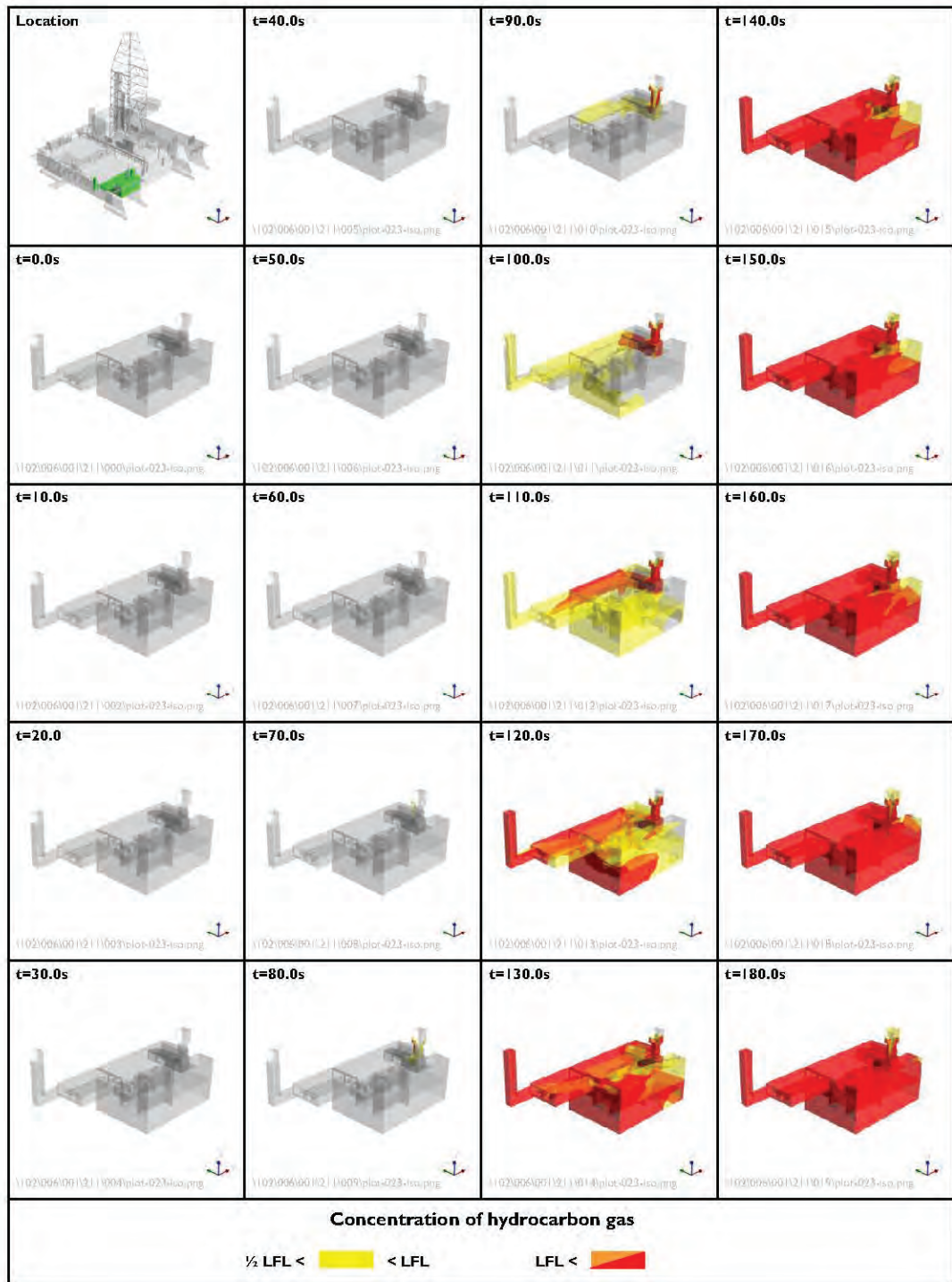
1.5 m/s

Wind direction:

90°

Figure 65

Extent of hydrocarbon gas within engine room 5 – Case A



Peak flow rate:

500 MMscfd

Wind speed:

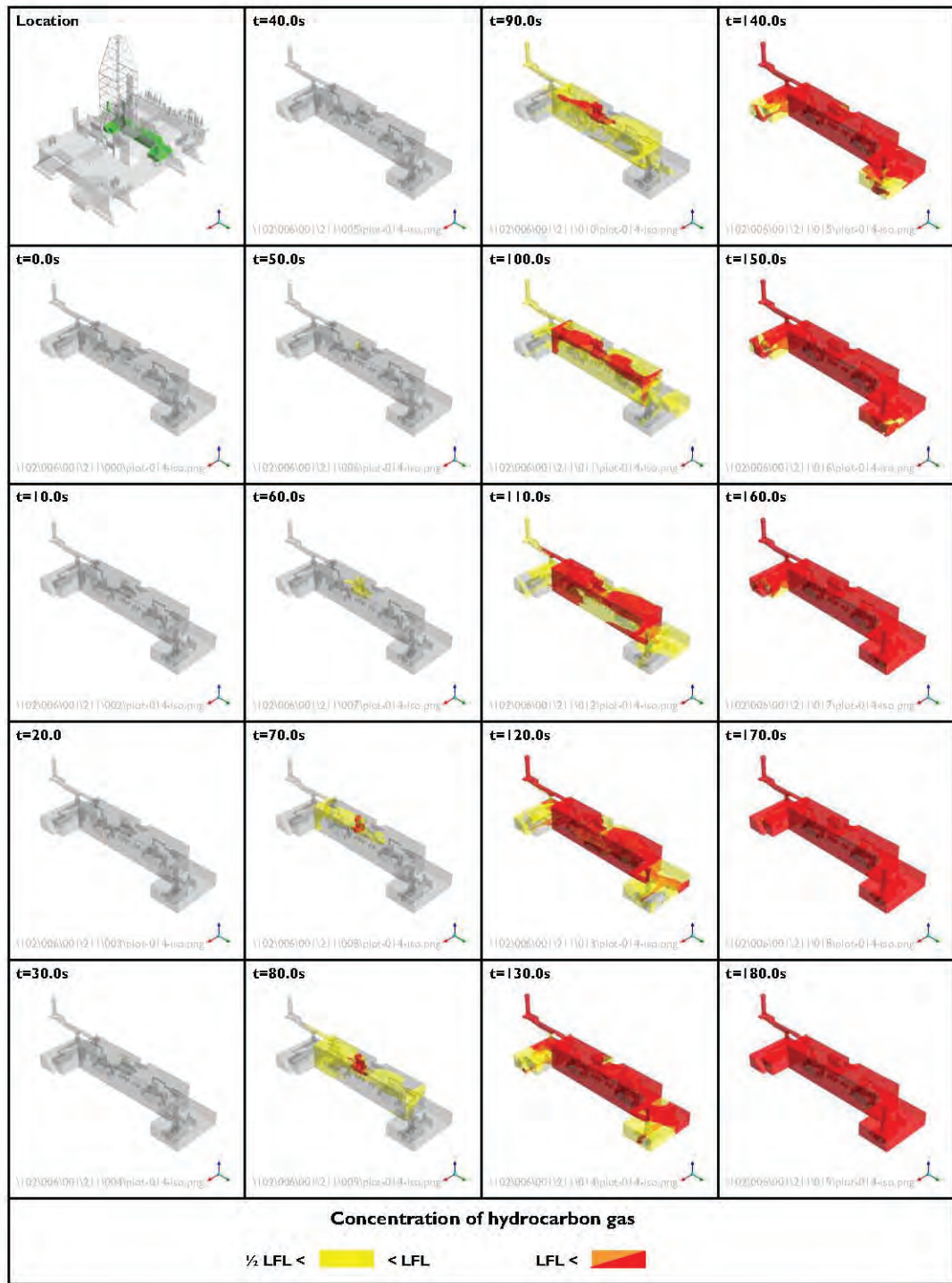
1.5 m/s

Wind direction:

90°

Figure 66

Extent of hydrocarbon gas within engine room 6 – Case A



Peak flow rate:

500 MMscfd

Wind speed:

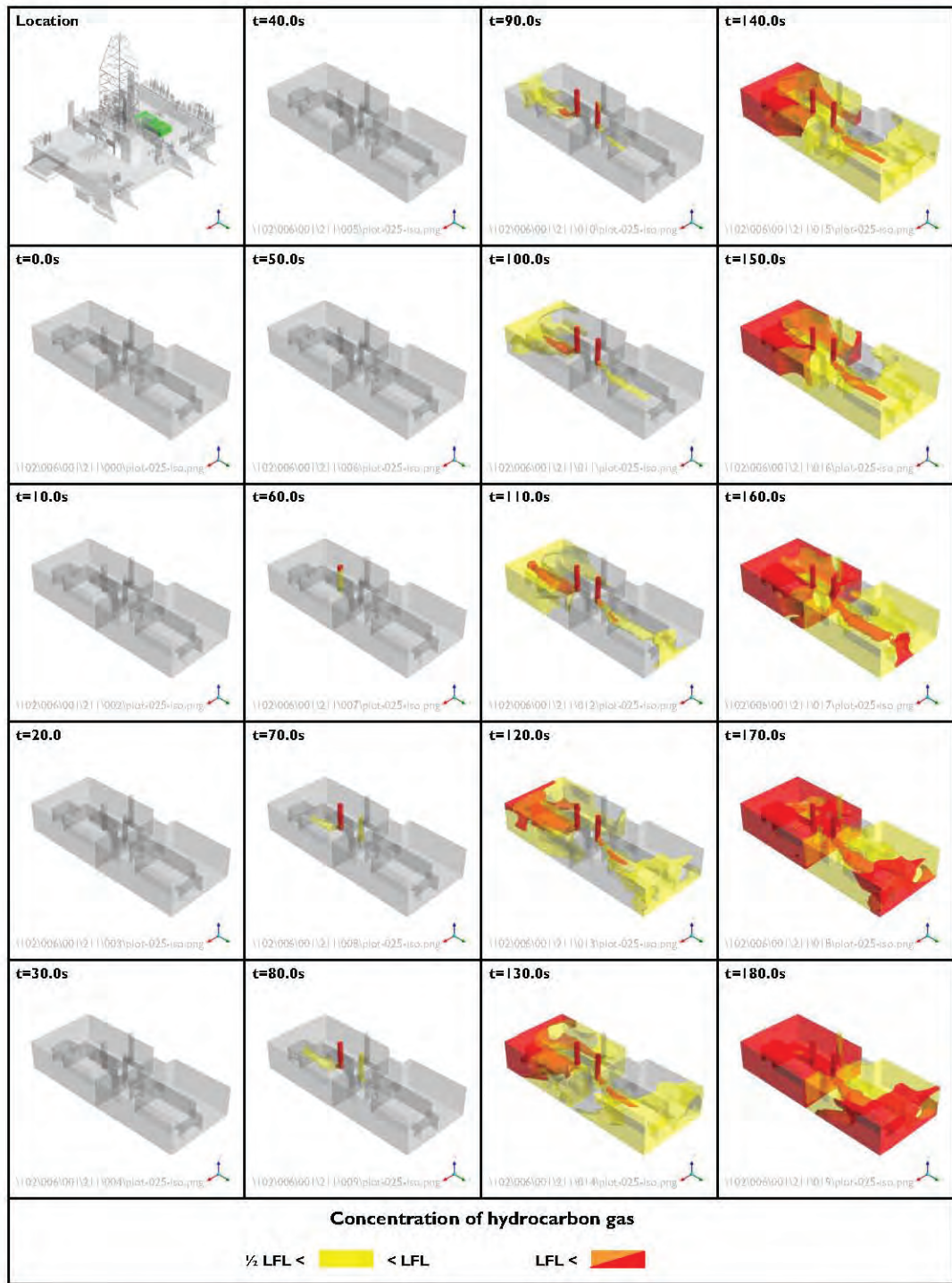
1.5 m/s

Wind direction:

90°

Figure 67

Extent of hydrocarbon gas within mud pump rooms – Case A



Peak flow rate:

500 MMscfd

Wind speed:

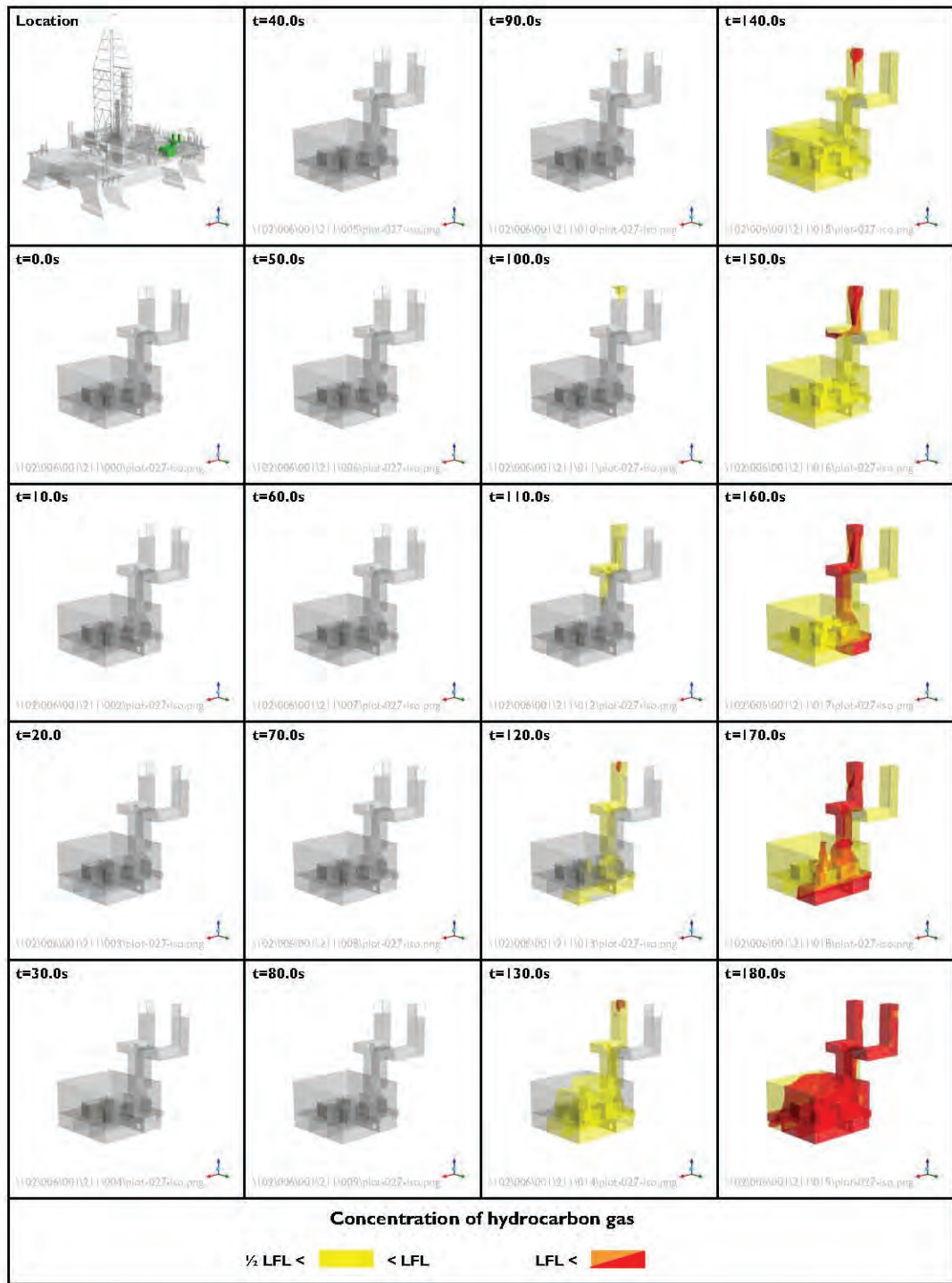
1.5 m/s

Wind direction:

90°

Figure 68

Extent of hydrocarbon gas within HVAC rooms – Case A



Peak flow rate:

500 MMscfd

Wind speed:

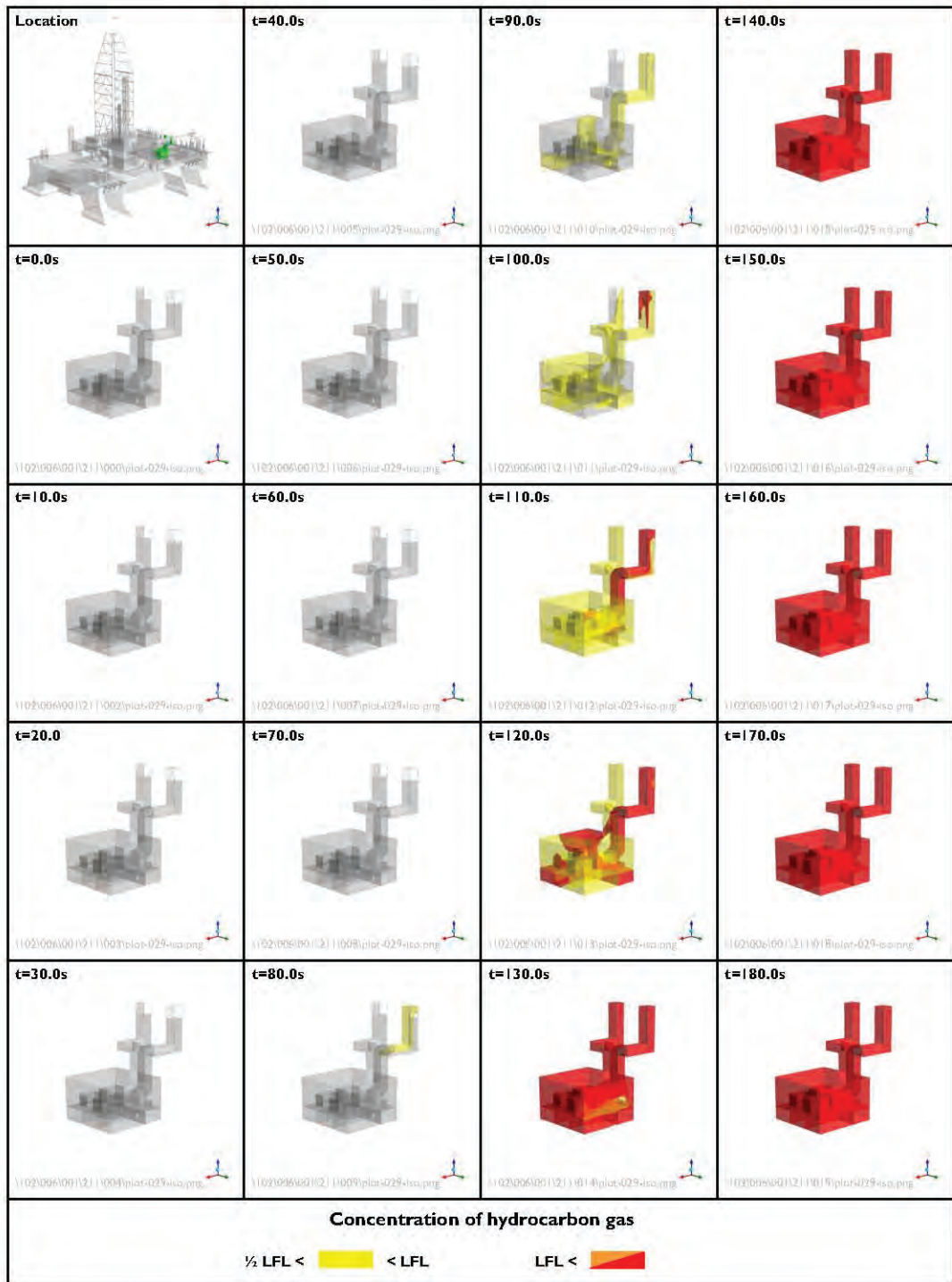
1.5 m/s

Wind direction:

90°

Figure 69

Extent of hydrocarbon gas within port transformer room – Case A



Peak flow rate:

500 MMscfd

Wind speed:

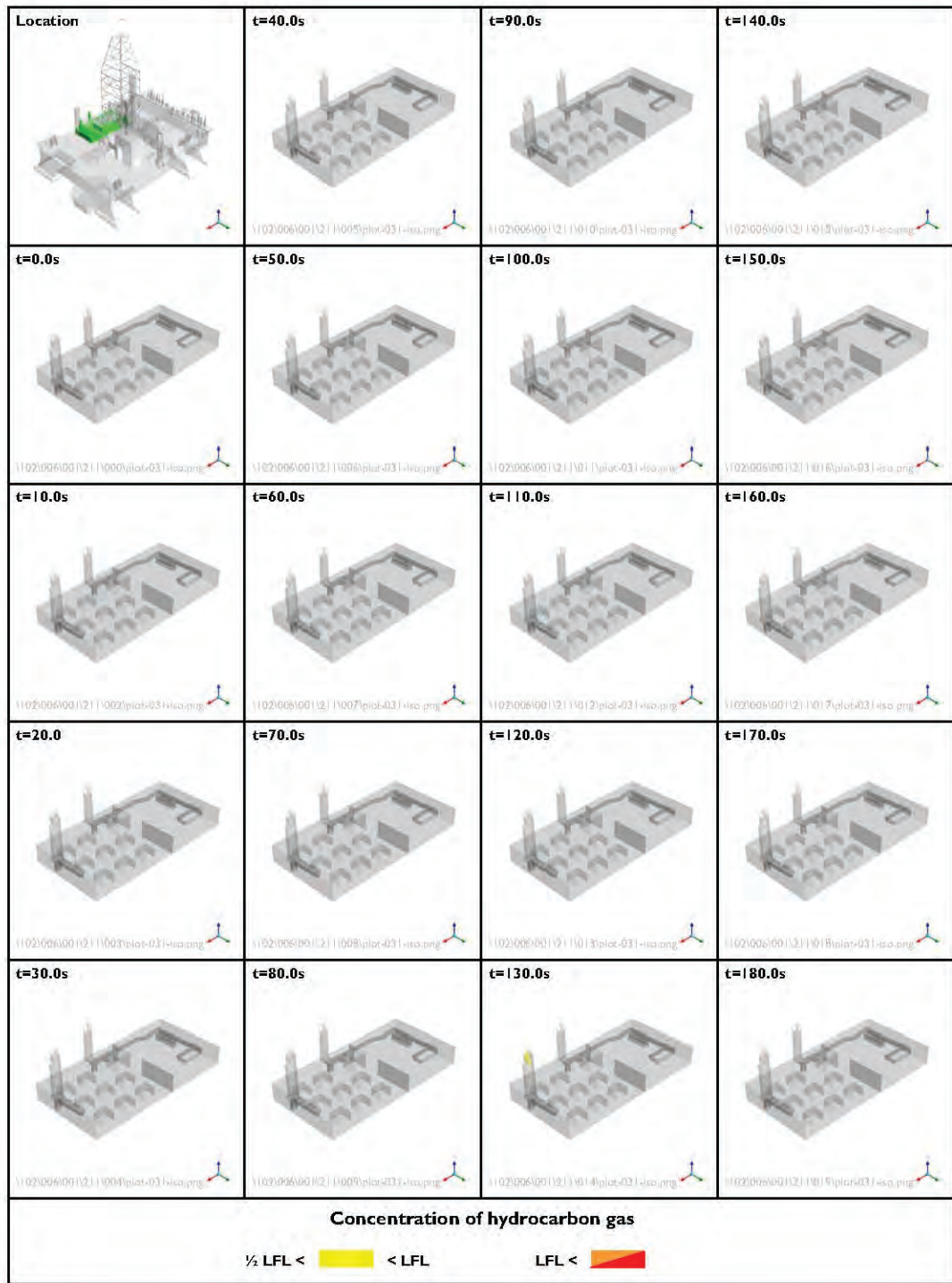
1.5 m/s

Wind direction:

90°

Figure 70

Extent of hydrocarbon gas within starboard transformer room – Case A



Peak flow rate:

500 MMscfd

Wind speed:

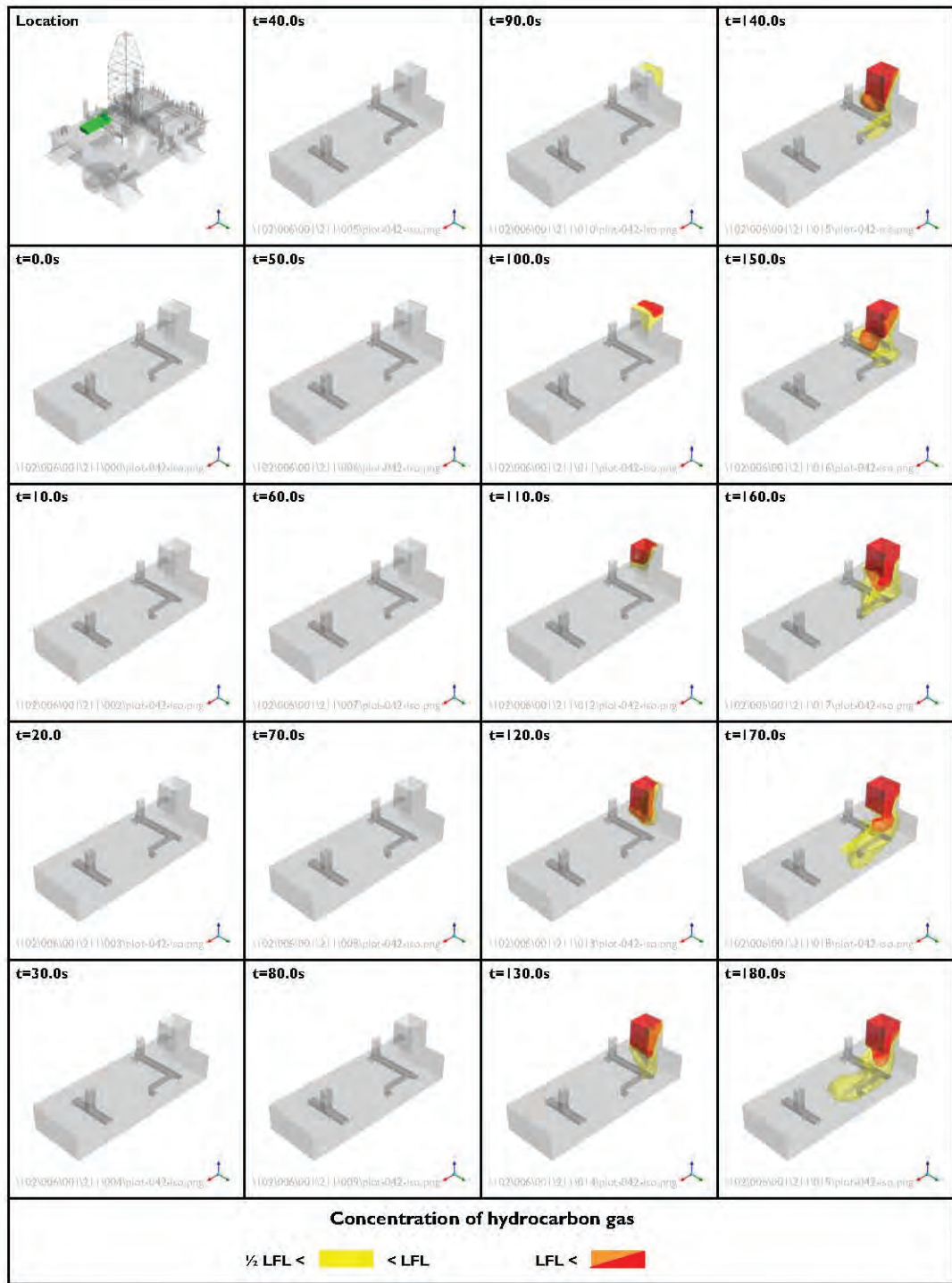
1.5 m/s

Wind direction:

90°

Figure 71

Extent of hydrocarbon gas within sack storage room – Case A



Peak flow rate:

500 MMscfd

Wind speed:

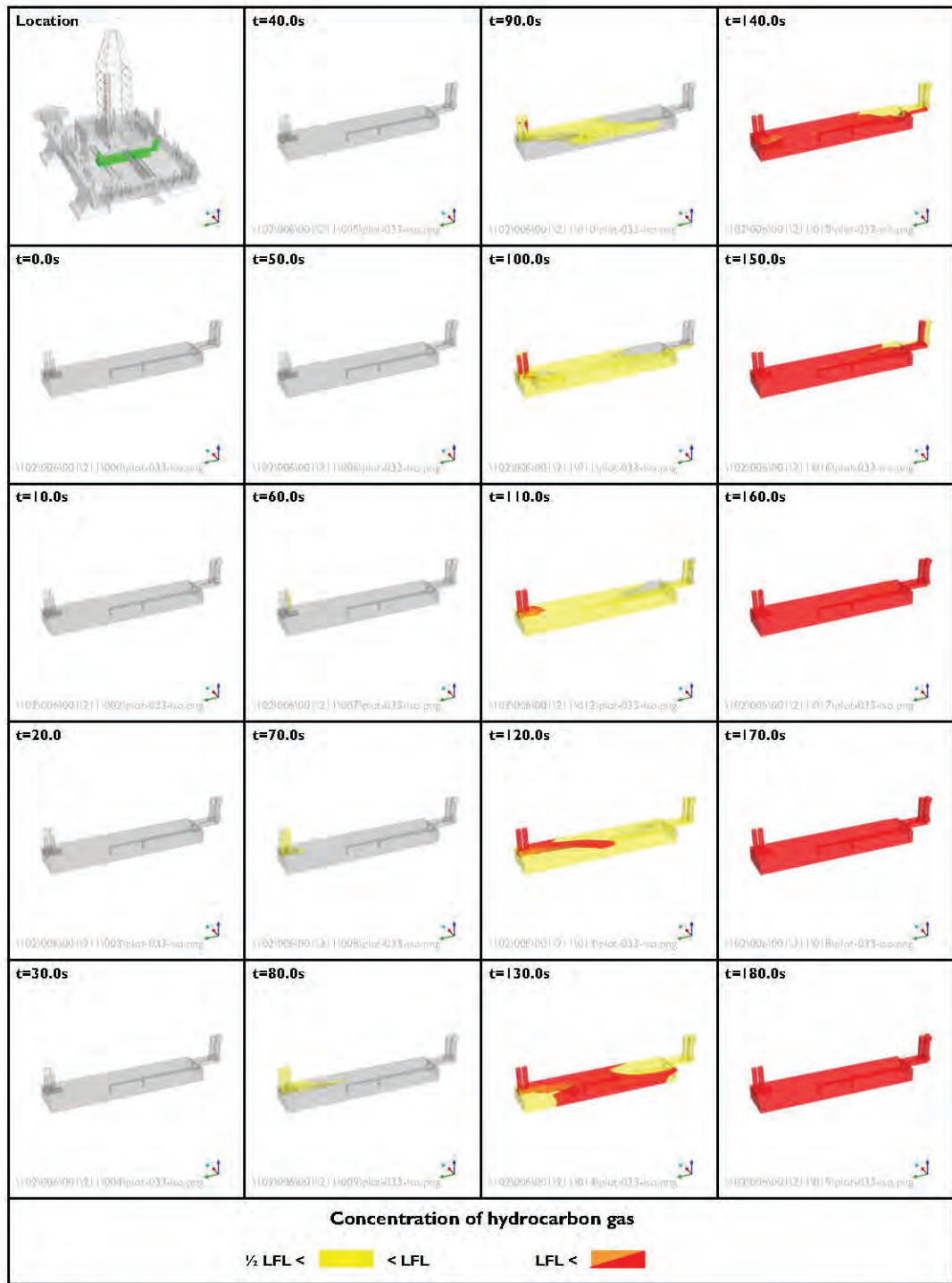
1.5 m/s

Wind direction:

90°

Figure 72

Extent of hydrocarbon gas within warehouse – Case A



Peak flow rate:

500 MMscfd

Wind speed:

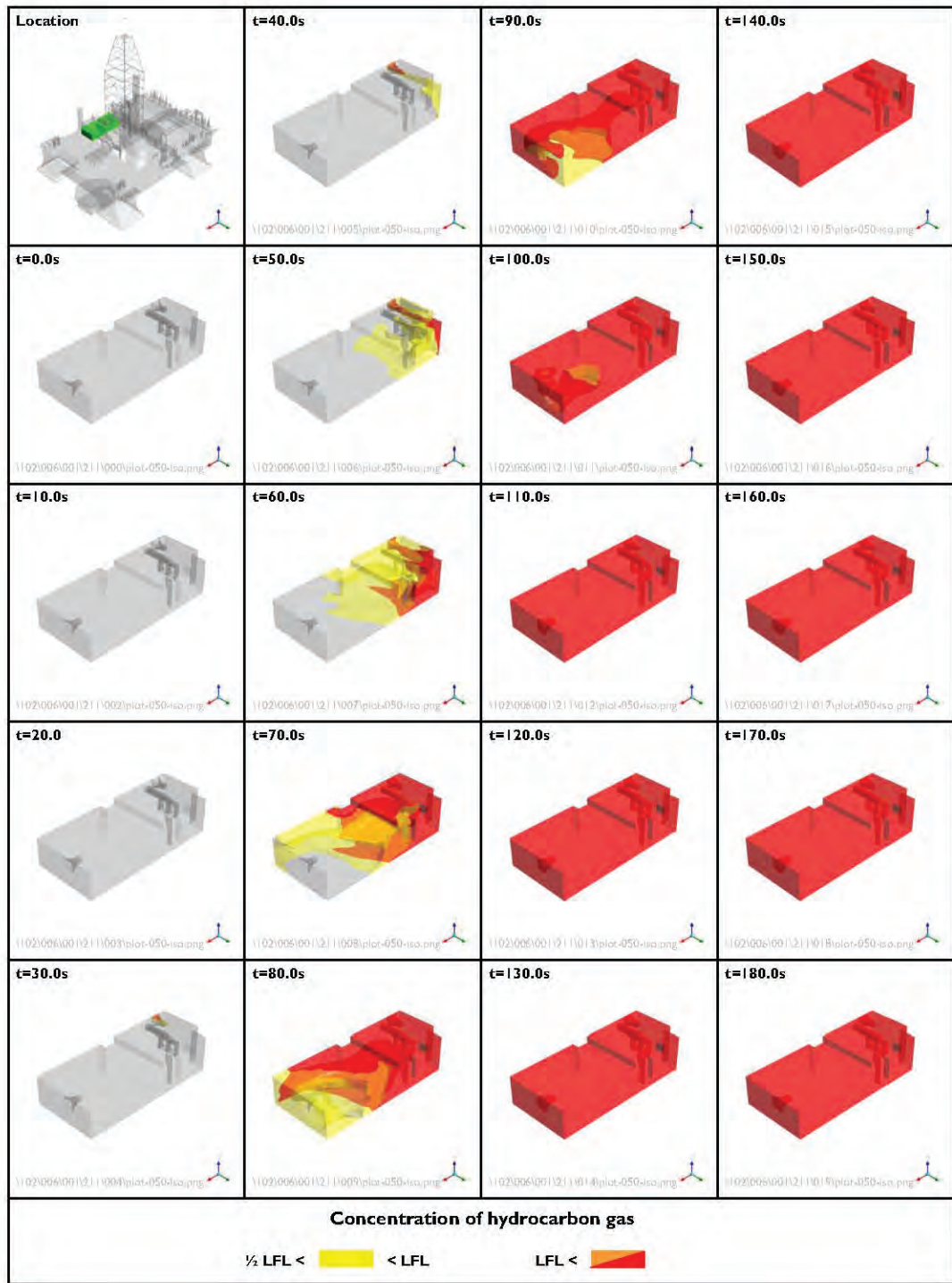
1.5 m/s

Wind direction:

90°

Figure 73

Extent of hydrocarbon gas within mud tank room – Case A



Peak flow rate:

500 MMscfd

Wind speed:

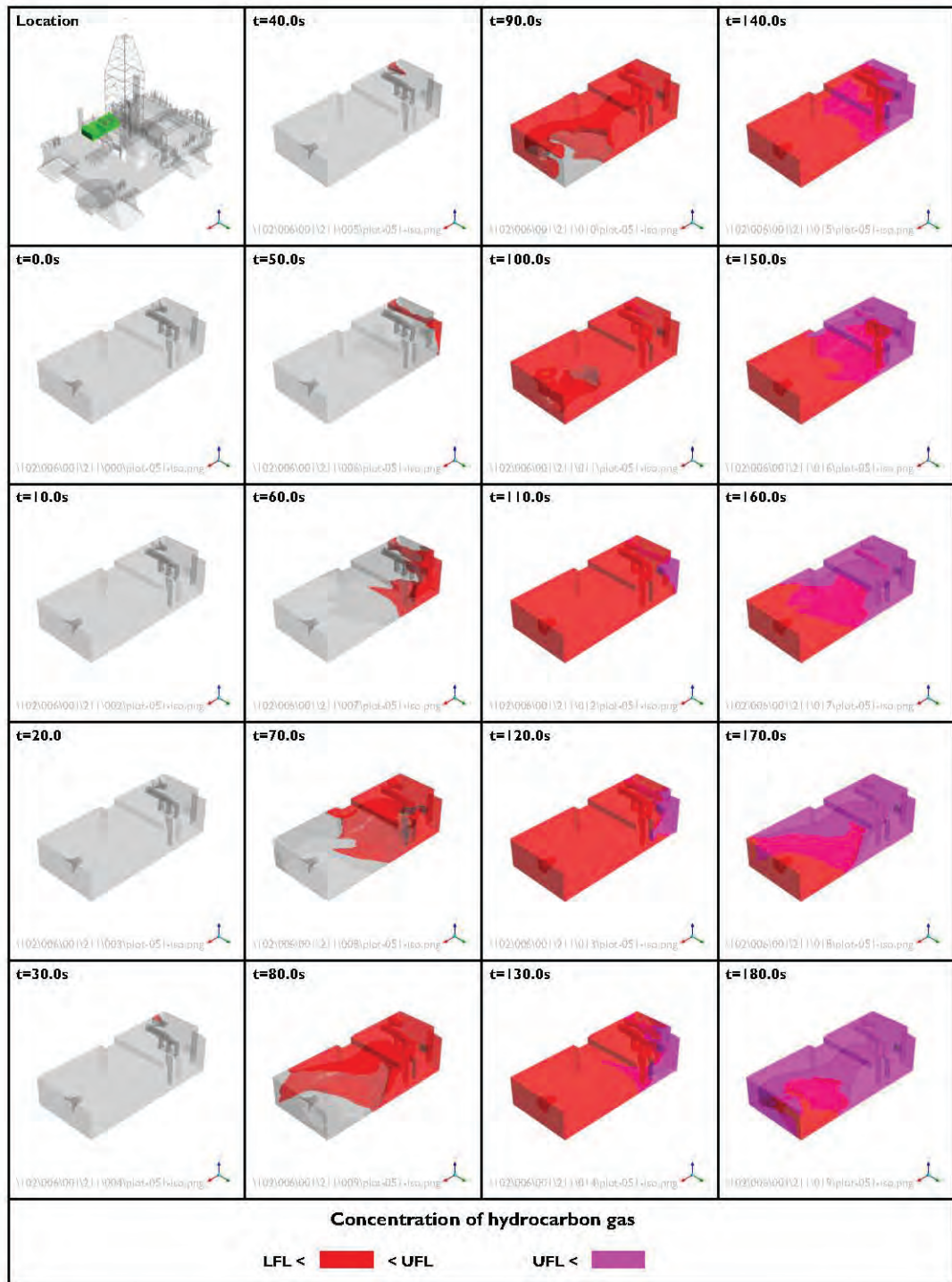
1.5 m/s

Wind direction:

90°

Figure 74

Extent of hydrocarbon gas within cement room – Case A



Peak flow rate:

500 MMscfd

Wind speed:

1.5 m/s

Wind direction:

90°

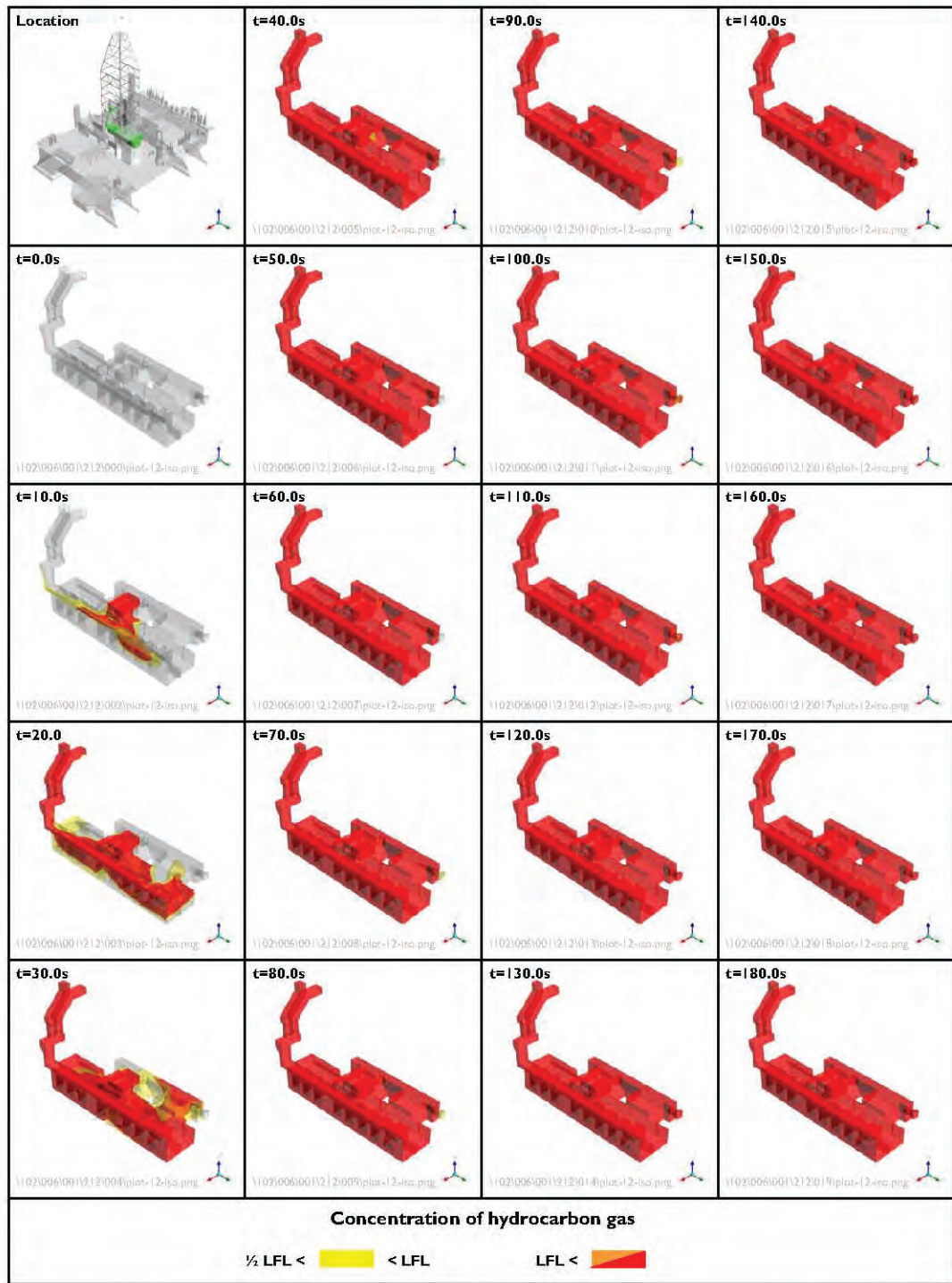
Figure 75

Extent of hydrocarbon gas within cement room – Case A

APPENDIX B RESULTS FOR CASE B

FIGURES

- Figure 76 Extent of hydrocarbon gas within shale shaker house – Case B
- Figure 77 Extent of hydrocarbon gas within shale shaker house – Case B
- Figure 78 Extent of hydrocarbon gas within moonpool – Case B
- Figure 79 Extent of hydrocarbon gas within moonpool – Case B
- Figure 80 Extent of hydrocarbon gas outside the rig – isometric view – Case B
- Figure 81 Extent of hydrocarbon gas outside the rig – top view – Case B
- Figure 82 Extent of hydrocarbon gas outside the rig – port view – Case B
- Figure 83 Extent of hydrocarbon gas outside the rig – aft view – Case B
- Figure 84 Extent of hydrocarbon gas on external rig surfaces – isometric view – Case B
- Figure 85 Extent of hydrocarbon gas within engine room 1 – Case B
- Figure 86 Extent of hydrocarbon gas within engine room 2 – Case B
- Figure 87 Extent of hydrocarbon gas within engine room 3 – Case B
- Figure 88 Extent of hydrocarbon gas within engine room 4 – Case B
- Figure 89 Extent of hydrocarbon gas within engine room 5 – Case B
- Figure 90 Extent of hydrocarbon gas within engine room 6 – Case B
- Figure 91 Extent of hydrocarbon gas within mud pump rooms – Case B
- Figure 92 Extent of hydrocarbon gas within HVAC rooms – Case B
- Figure 93 Extent of hydrocarbon gas within port transformer room – Case B
- Figure 94 Extent of hydrocarbon gas within starboard transformer room – Case B
- Figure 95 Extent of hydrocarbon gas within sack storage room – Case B
- Figure 96 Extent of hydrocarbon gas within warehouse – Case B
- Figure 97 Extent of hydrocarbon gas within mud tank room – Case B
- Figure 98 Extent of hydrocarbon gas within cement room – Case B
- Figure 99 Extent of hydrocarbon gas within cement room – Case B



Peak flow rate:

400 MMscfd

Wind speed:

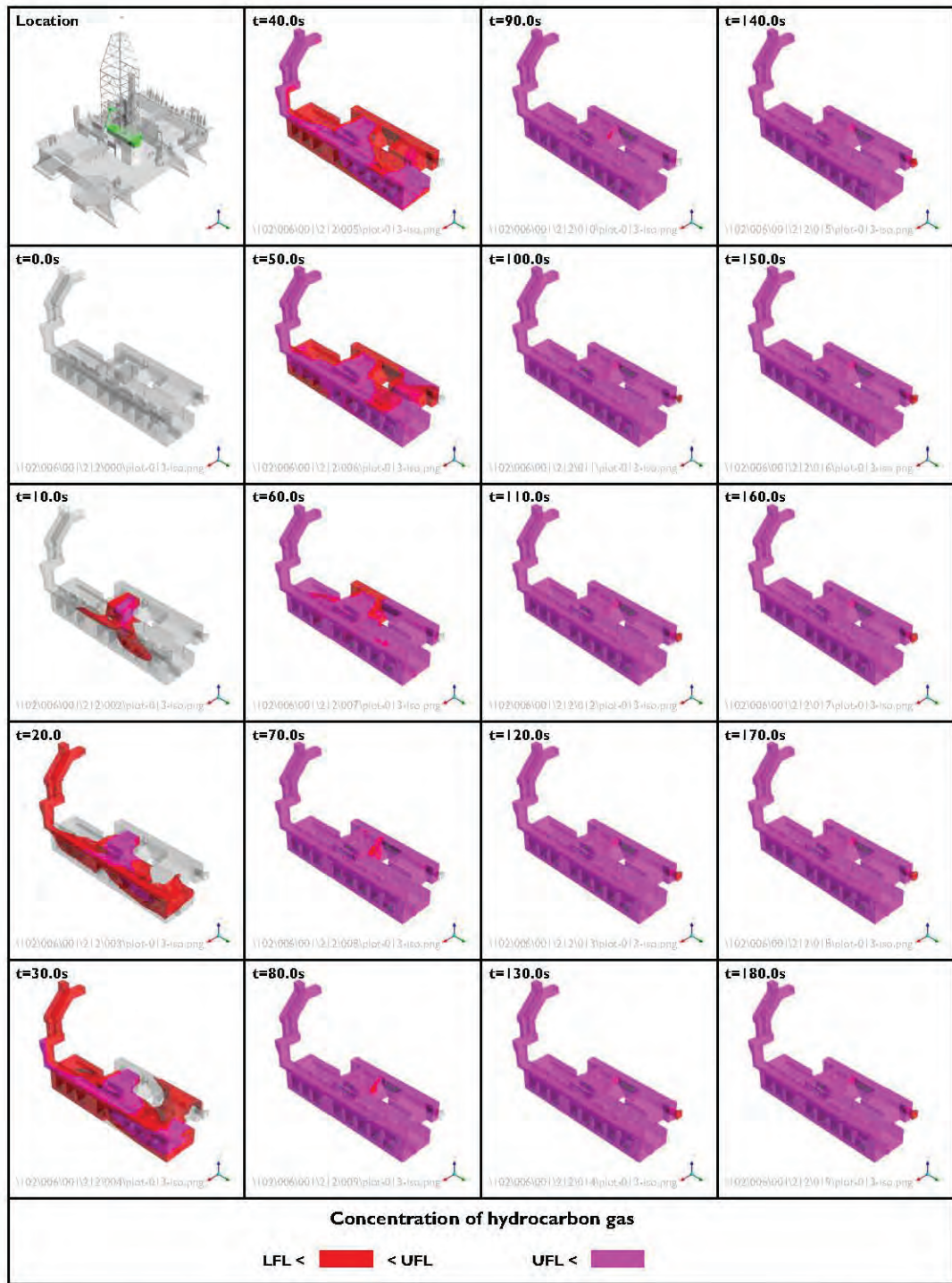
1.5 m/s

Wind direction:

90°

Figure 76

Extent of hydrocarbon gas within shale shaker house – Case B



Peak flow rate:

400 MMscfd

Wind speed:

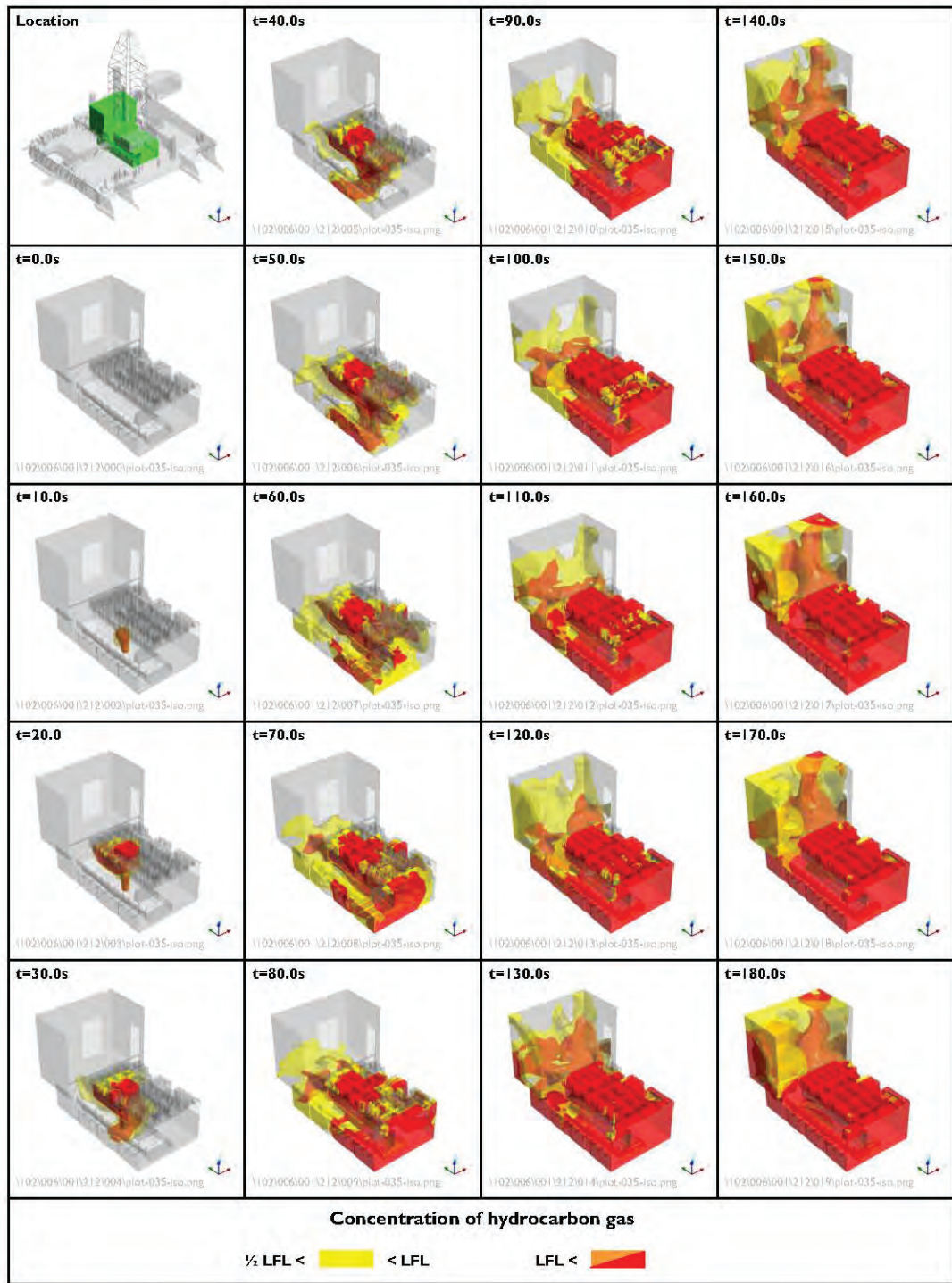
1.5 m/s

Wind direction:

90°

Figure 77

Extent of hydrocarbon gas within shale shaker house – Case B



Peak flow rate:

400 MMscfd

Wind speed:

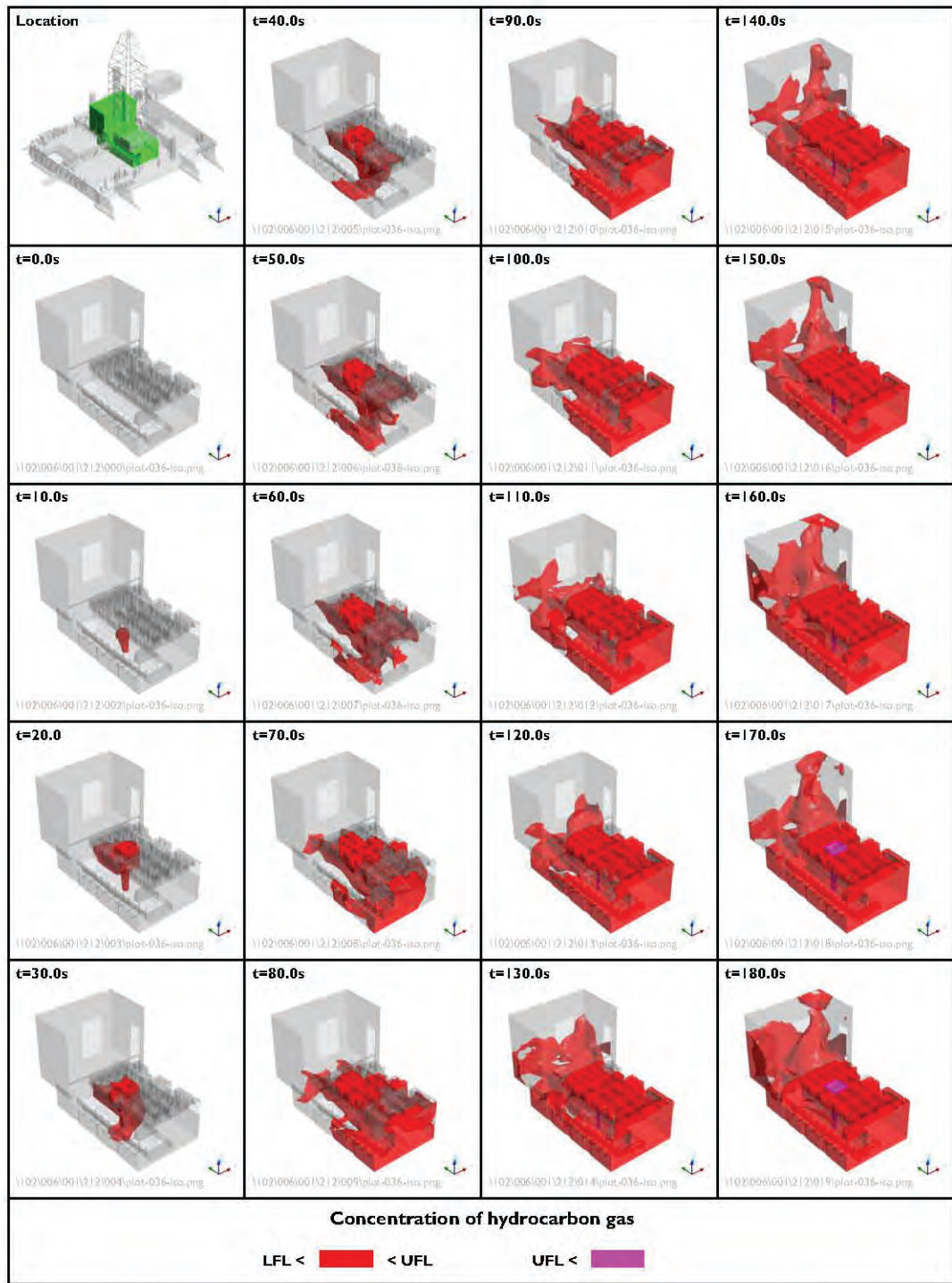
1.5 m/s

Wind direction:

90°

Figure 78

Extent of hydrocarbon gas within moonpool – Case B



Peak flow rate:

400 MMscfd

Wind speed:

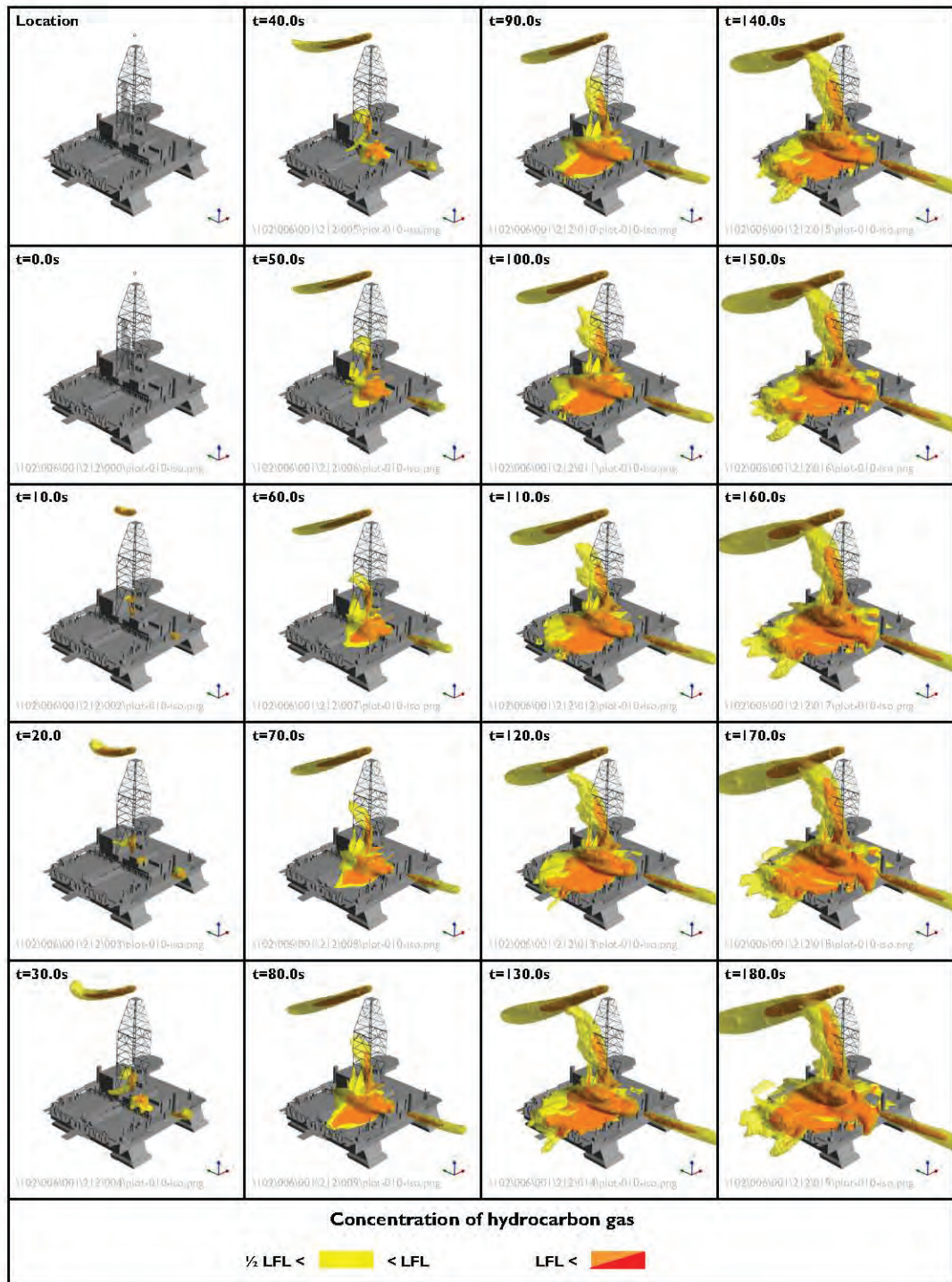
1.5 m/s

Wind direction:

90°

Figure 79

Extent of hydrocarbon gas within moonpool – Case B



Peak flow rate:

400 MMscfd

Wind speed:

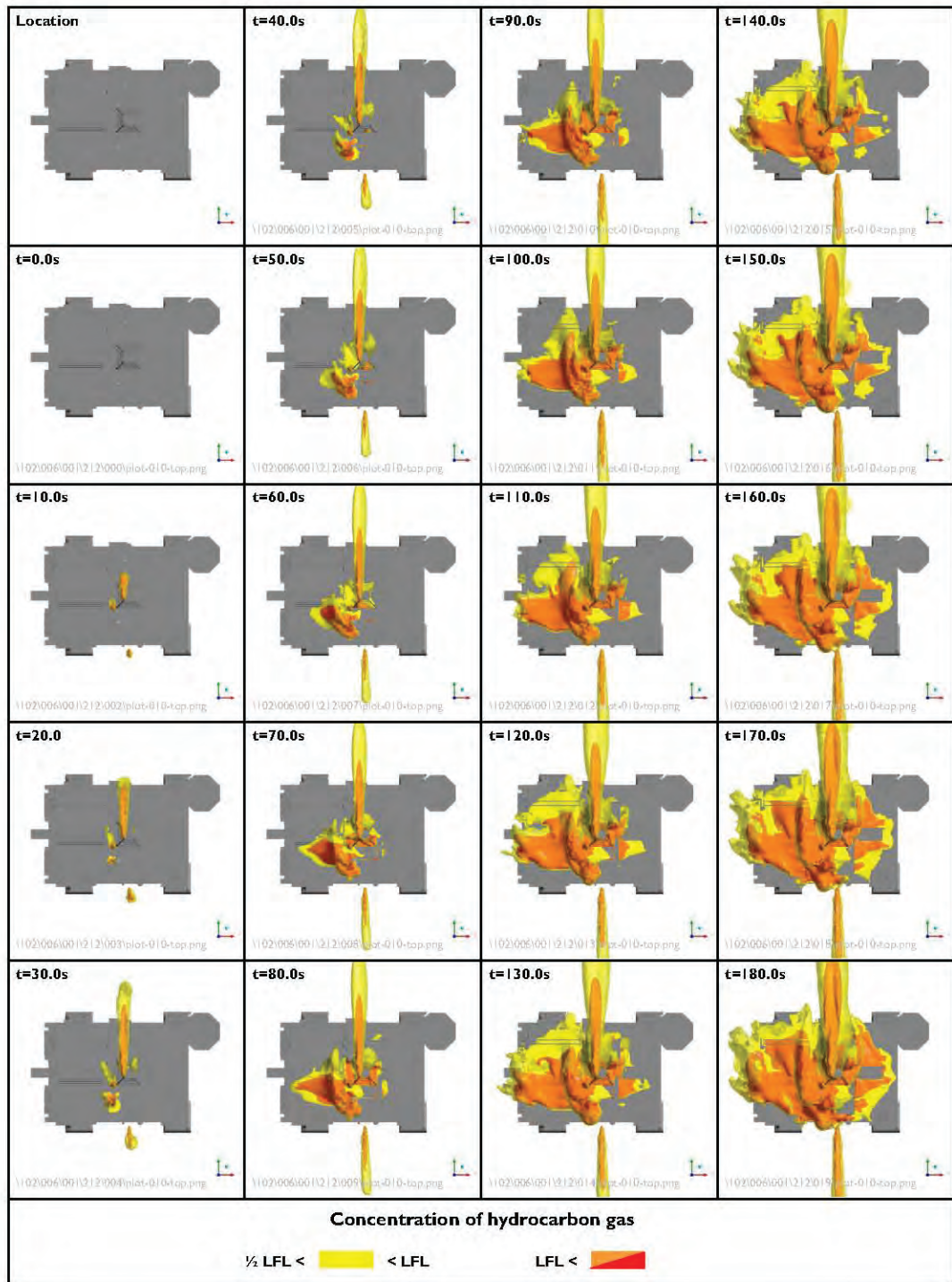
1.5 m/s

Wind direction:

90°

Figure 80

Extent of hydrocarbon gas outside the rig – isometric view – Case B



Peak flow rate:

400 MMscfd

Wind speed:

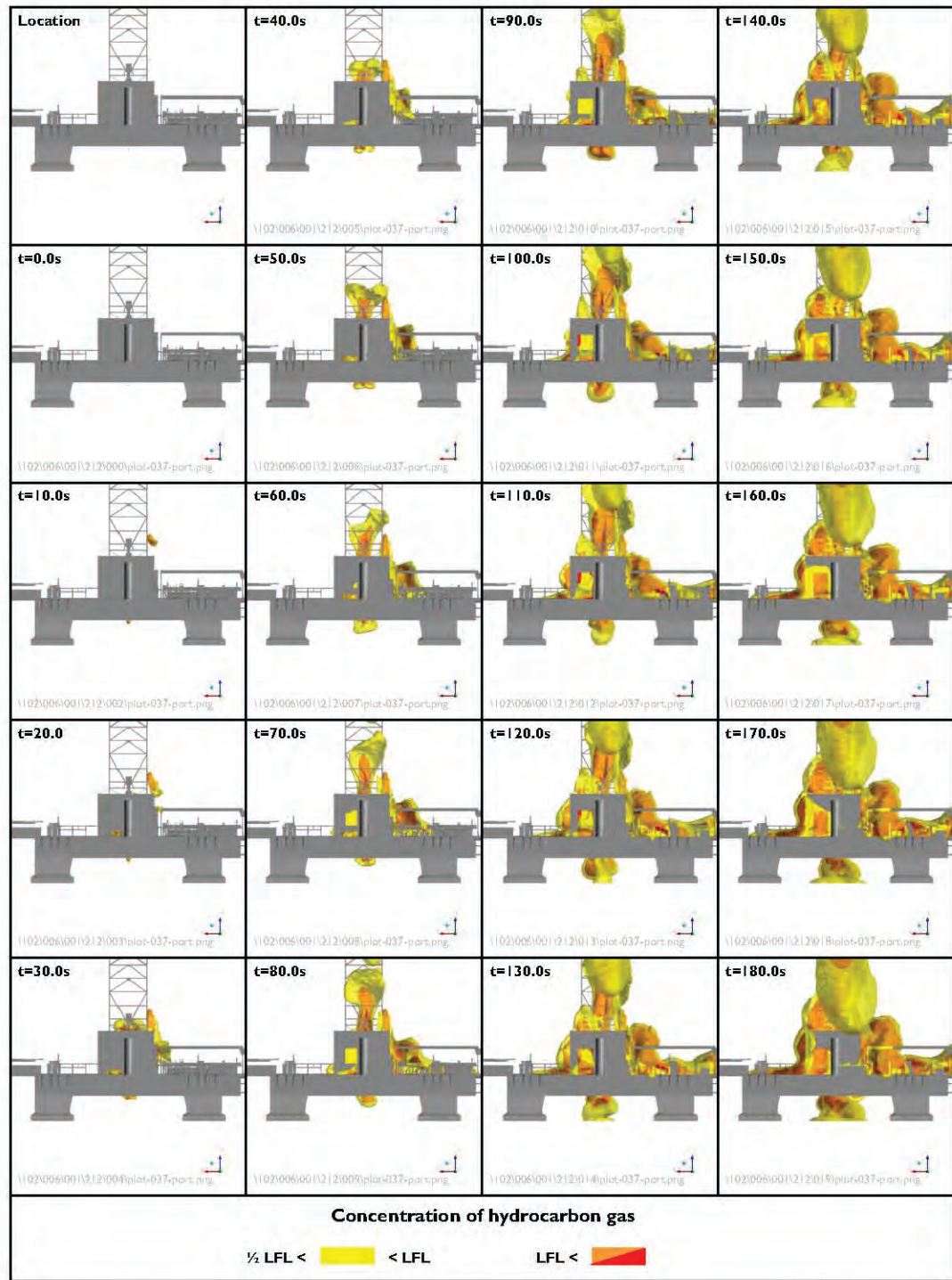
1.5 m/s

Wind direction:

90°

Figure 8 I

Extent of hydrocarbon gas outside the rig – top view – Case B



Peak flow rate:

400 MMscfd

Wind speed:

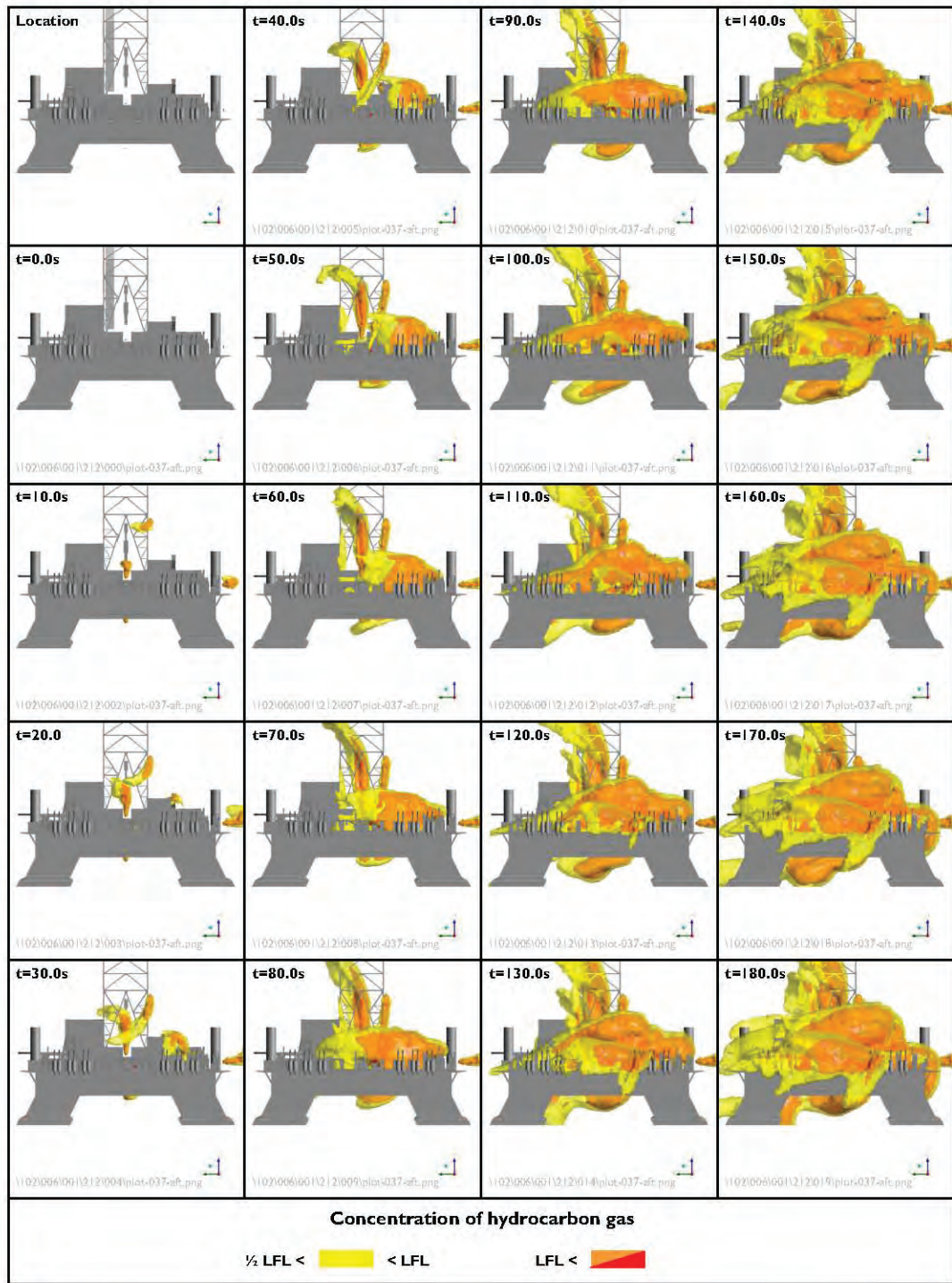
1.5 m/s

Wind direction:

90°

Figure 82

Extent of hydrocarbon gas outside the rig – port view – Case B



Peak flow rate:

400 MMscfd

Wind speed:

1.5 m/s

Wind direction:

90°

Figure 83

Extent of hydrocarbon gas outside the rig – aft view – Case B

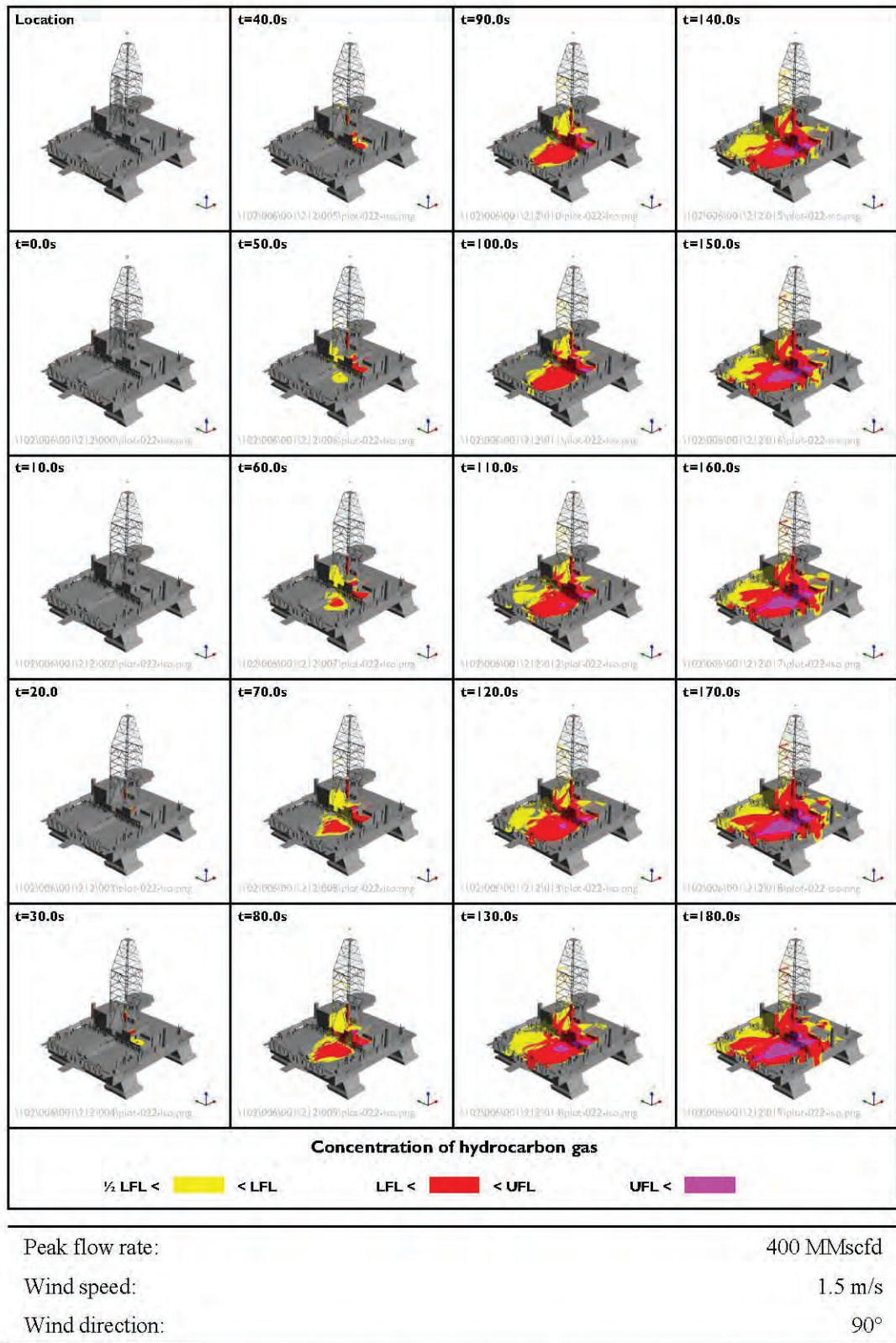
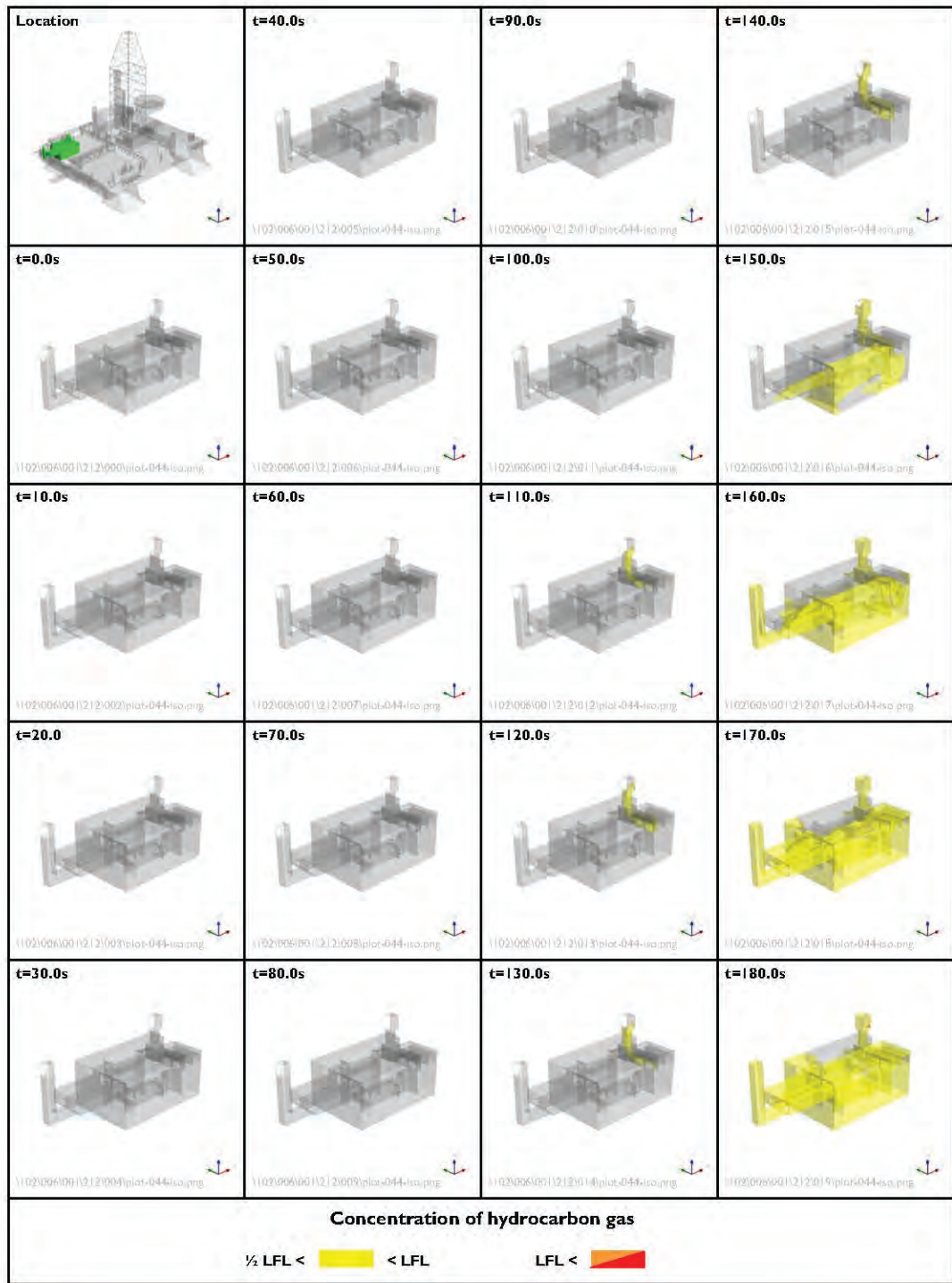


Figure 84 Extent of hydrocarbon gas on external rig surfaces – isometric view – Case B



Peak flow rate:

400 MMscfd

Wind speed:

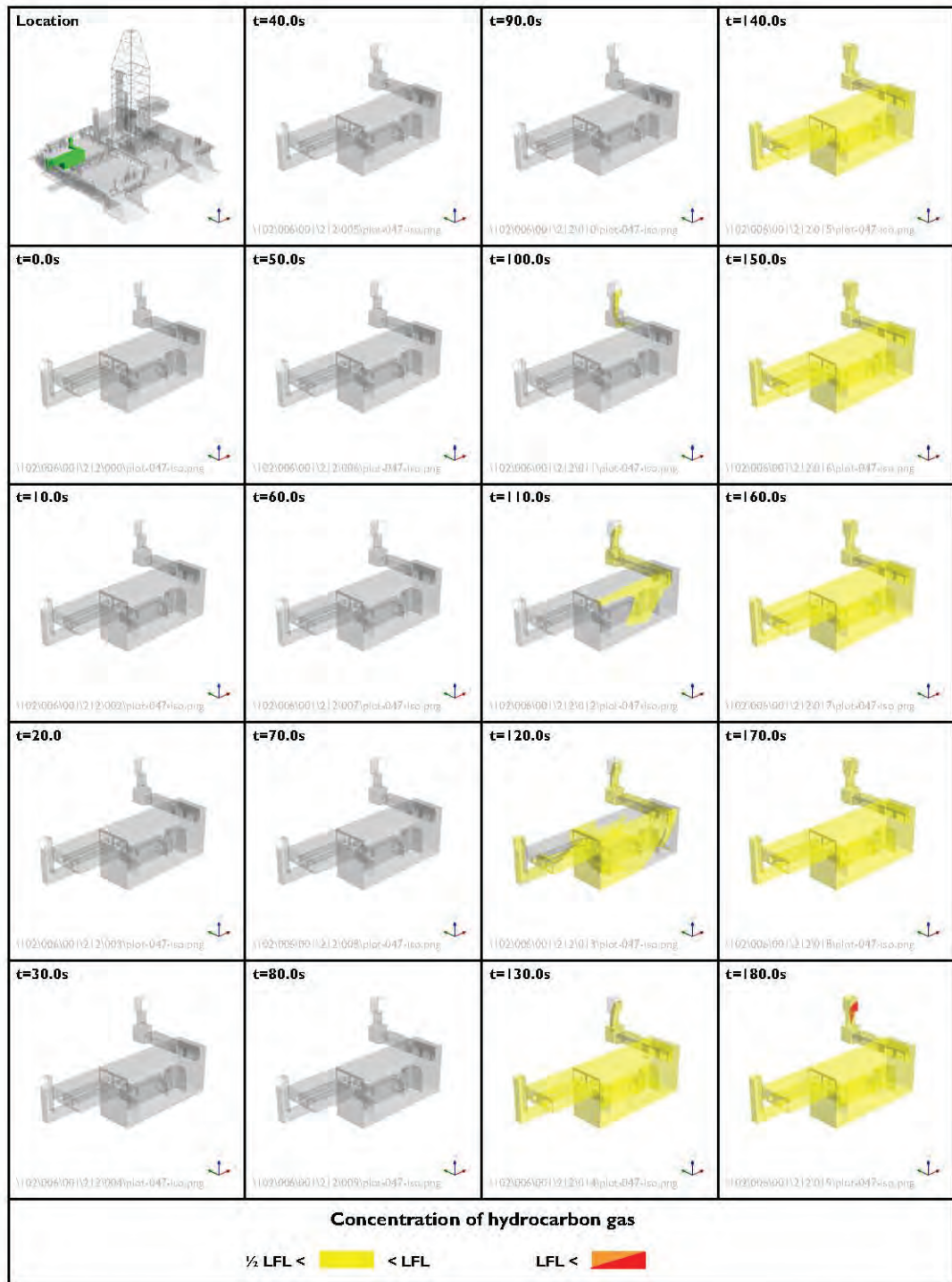
1.5 m/s

Wind direction:

90°

Figure 85

Extent of hydrocarbon gas within engine room I – Case B



Peak flow rate:

400 MMscfd

Wind speed:

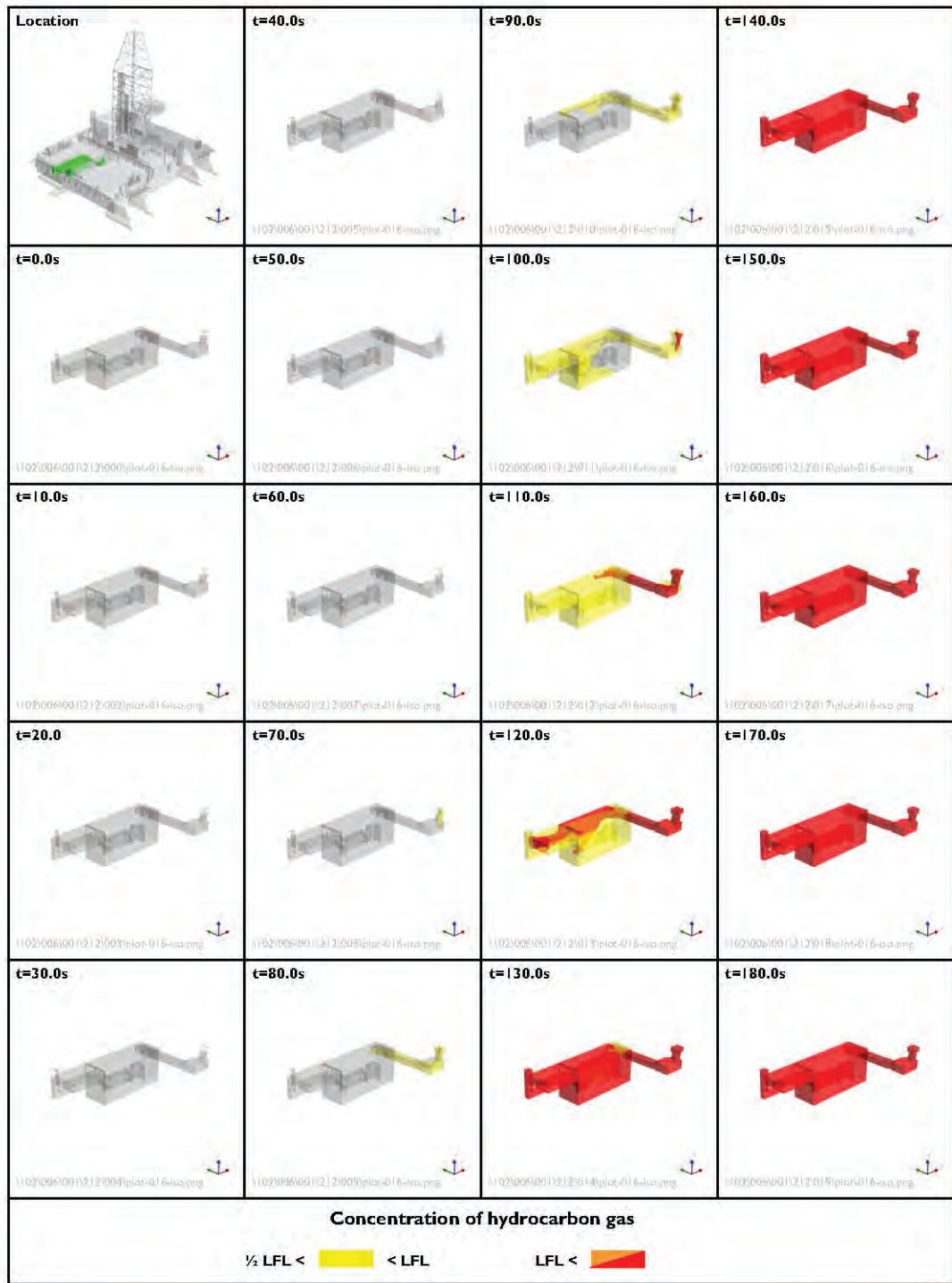
1.5 m/s

Wind direction:

90°

Figure 86

Extent of hydrocarbon gas within engine room 2 – Case B



Peak flow rate:

400 MMscfd

Wind speed:

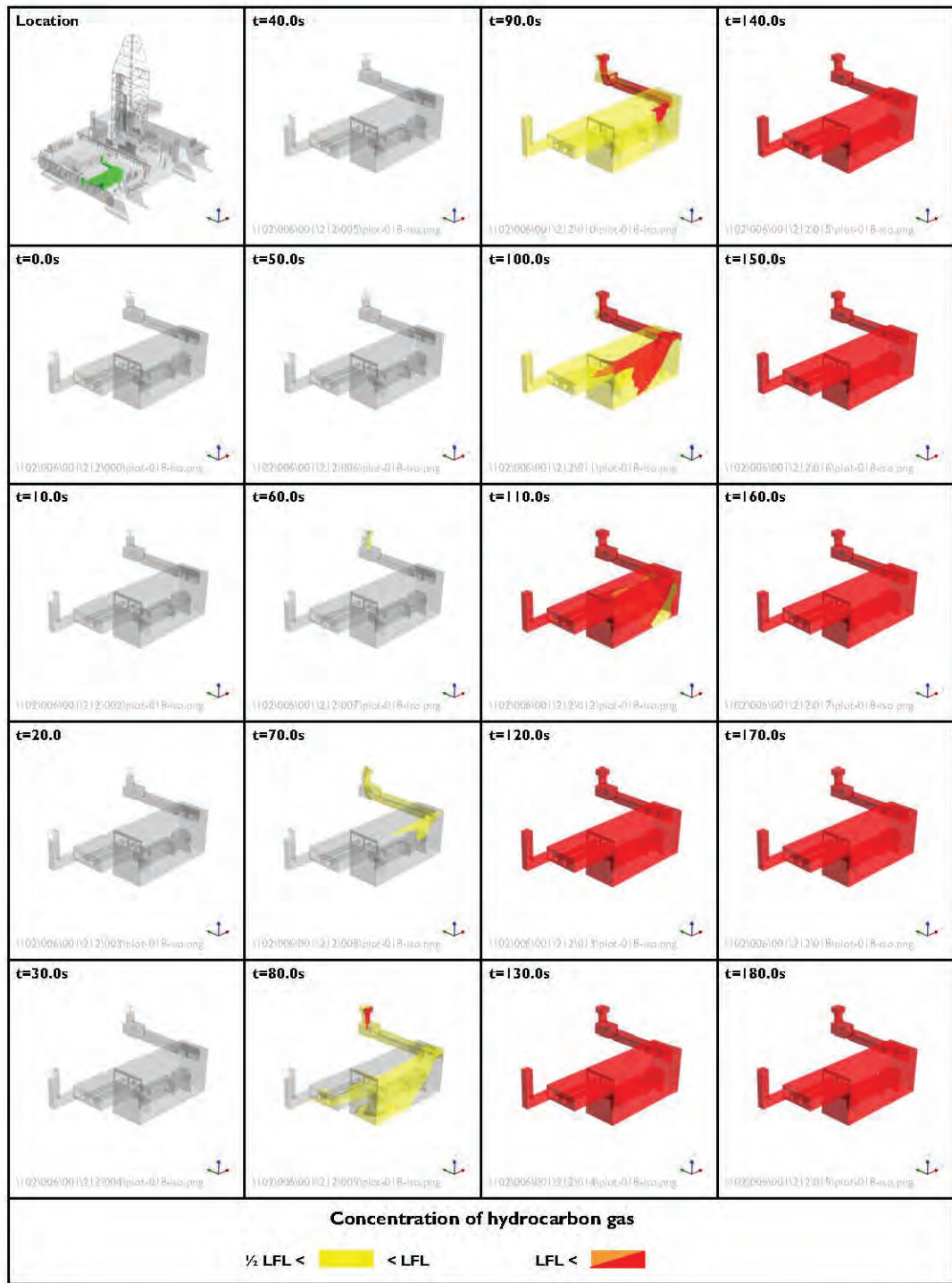
1.5 m/s

Wind direction:

90°

Figure 87

Extent of hydrocarbon gas within engine room 3 – Case B



Peak flow rate:

400 MMscfd

Wind speed:

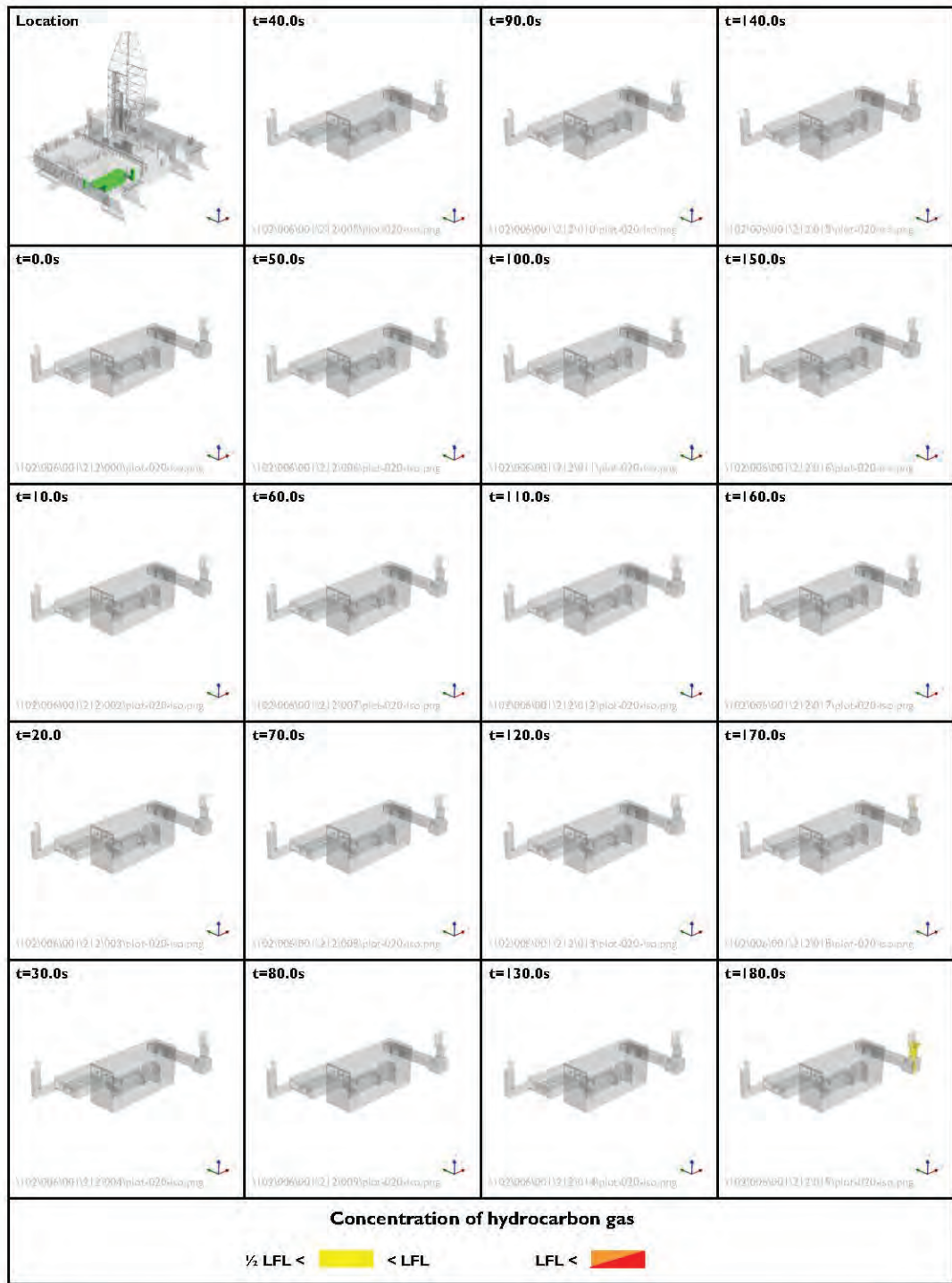
1.5 m/s

Wind direction:

90°

Figure 88

Extent of hydrocarbon gas within engine room 4 – Case B



Peak flow rate:

400 MMscfd

Wind speed:

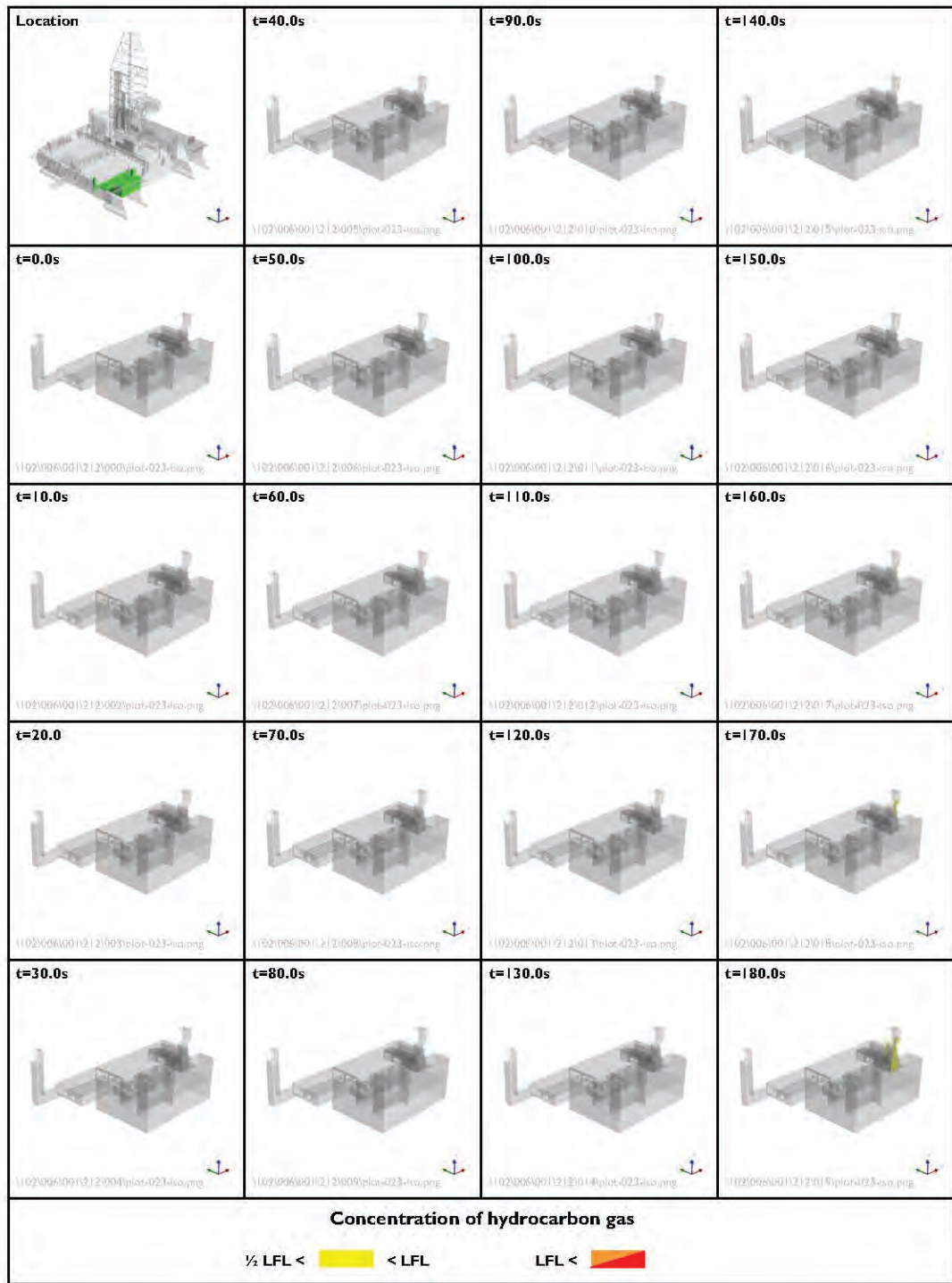
1.5 m/s

Wind direction:

90°

Figure 89

Extent of hydrocarbon gas within engine room 5 – Case B



Peak flow rate:

400 MMscfd

Wind speed:

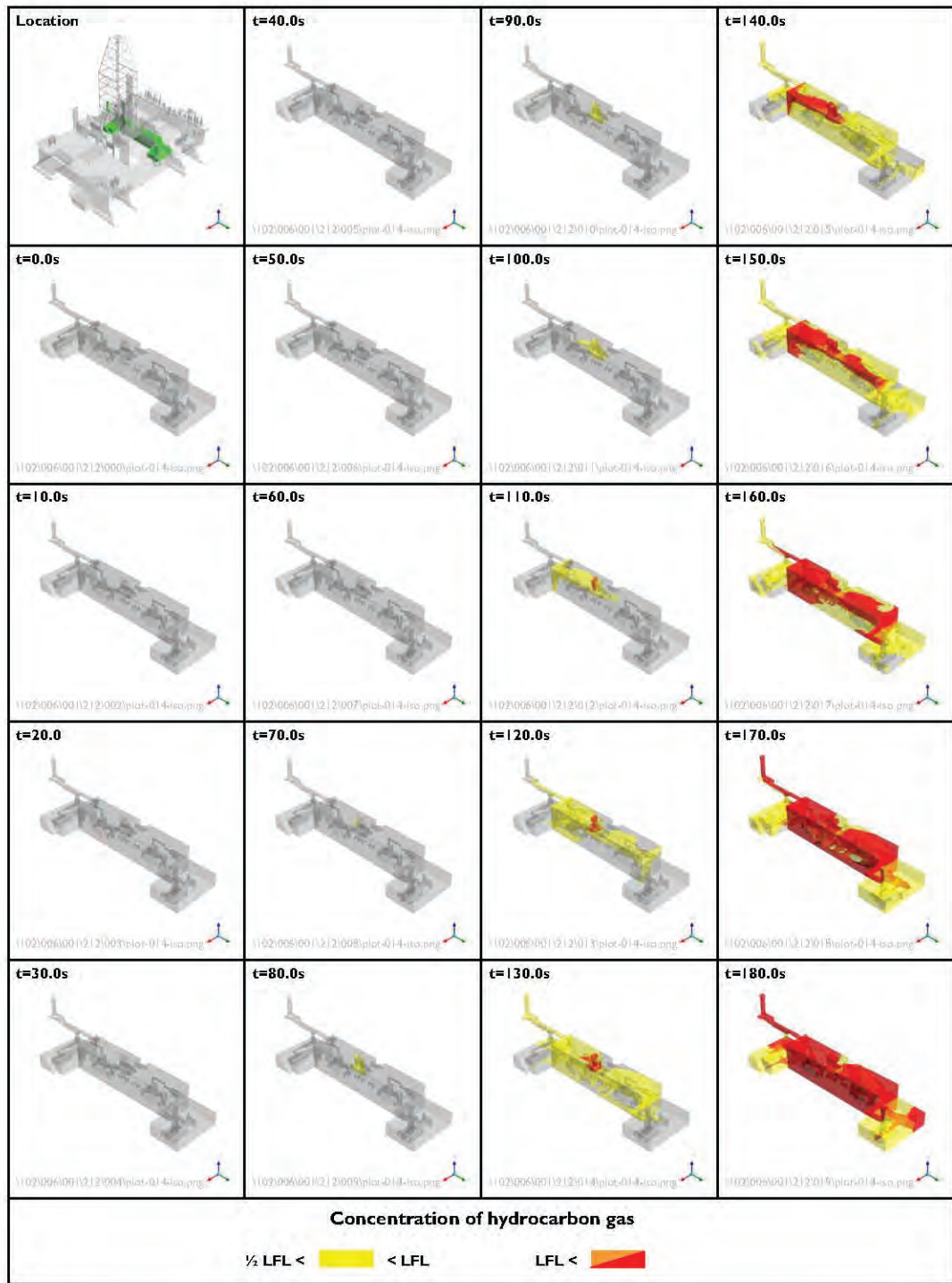
1.5 m/s

Wind direction:

90°

Figure 90

Extent of hydrocarbon gas within engine room 6 – Case B



Peak flow rate:

400 MMscfd

Wind speed:

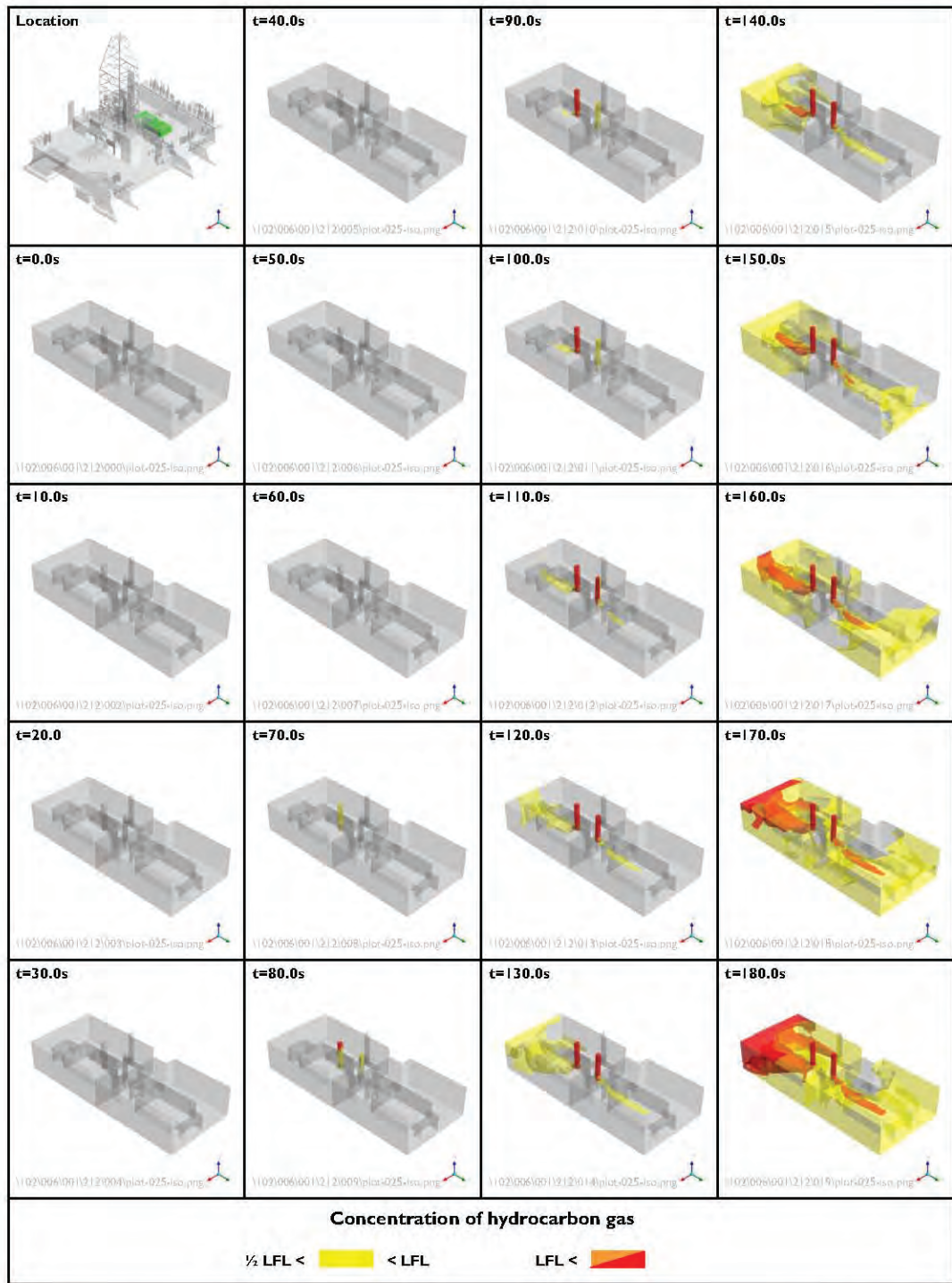
1.5 m/s

Wind direction:

90°

Figure 91

Extent of hydrocarbon gas within mud pump rooms – Case B



Peak flow rate:

400 MMscfd

Wind speed:

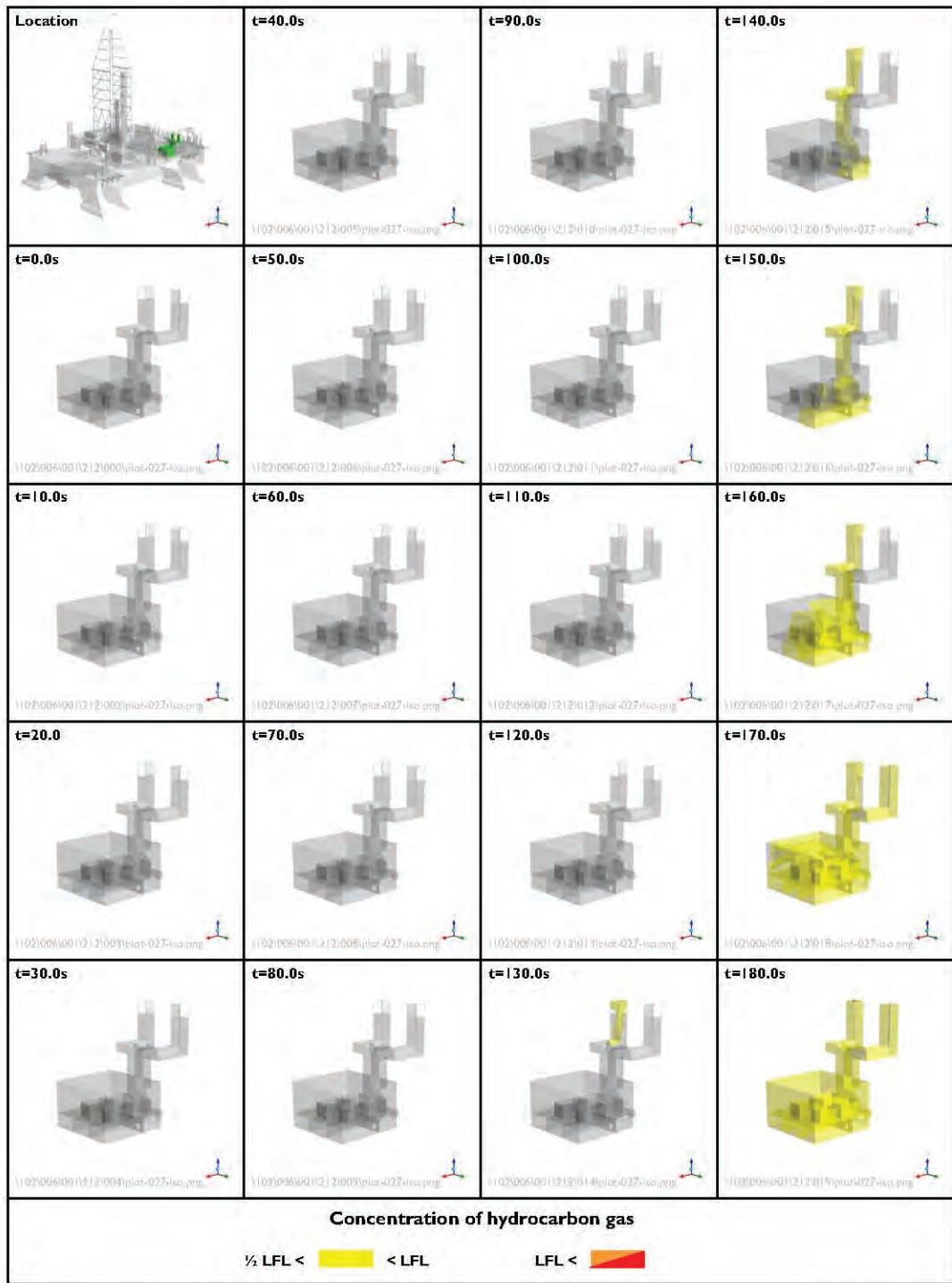
1.5 m/s

Wind direction:

90°

Figure 92

Extent of hydrocarbon gas within HVAC rooms – Case B



Peak flow rate:

400 MMscfd

Wind speed:

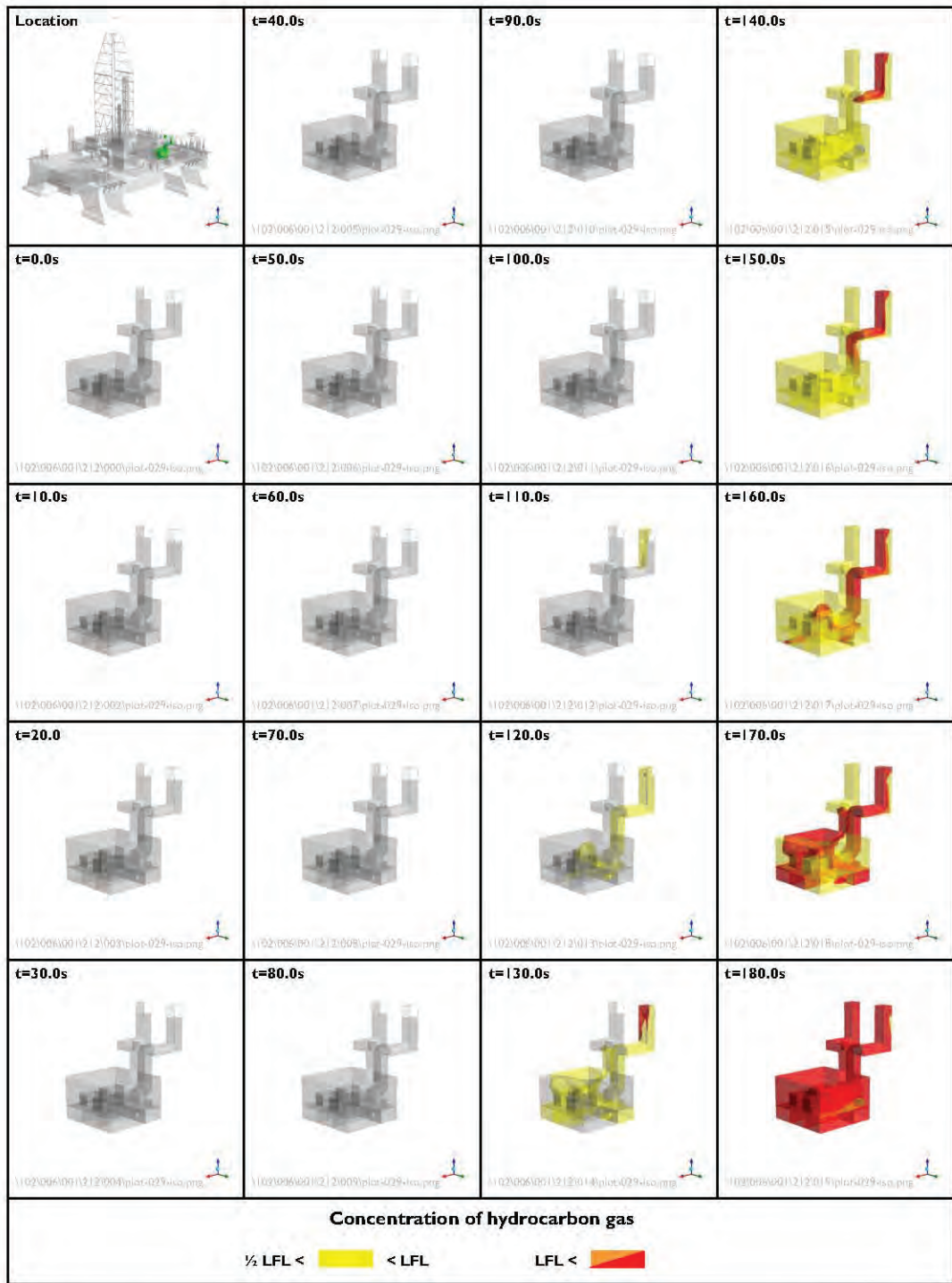
1.5 m/s

Wind direction:

90°

Figure 93

Extent of hydrocarbon gas within port transformer room – Case B



Peak flow rate:

400 MMscfd

Wind speed:

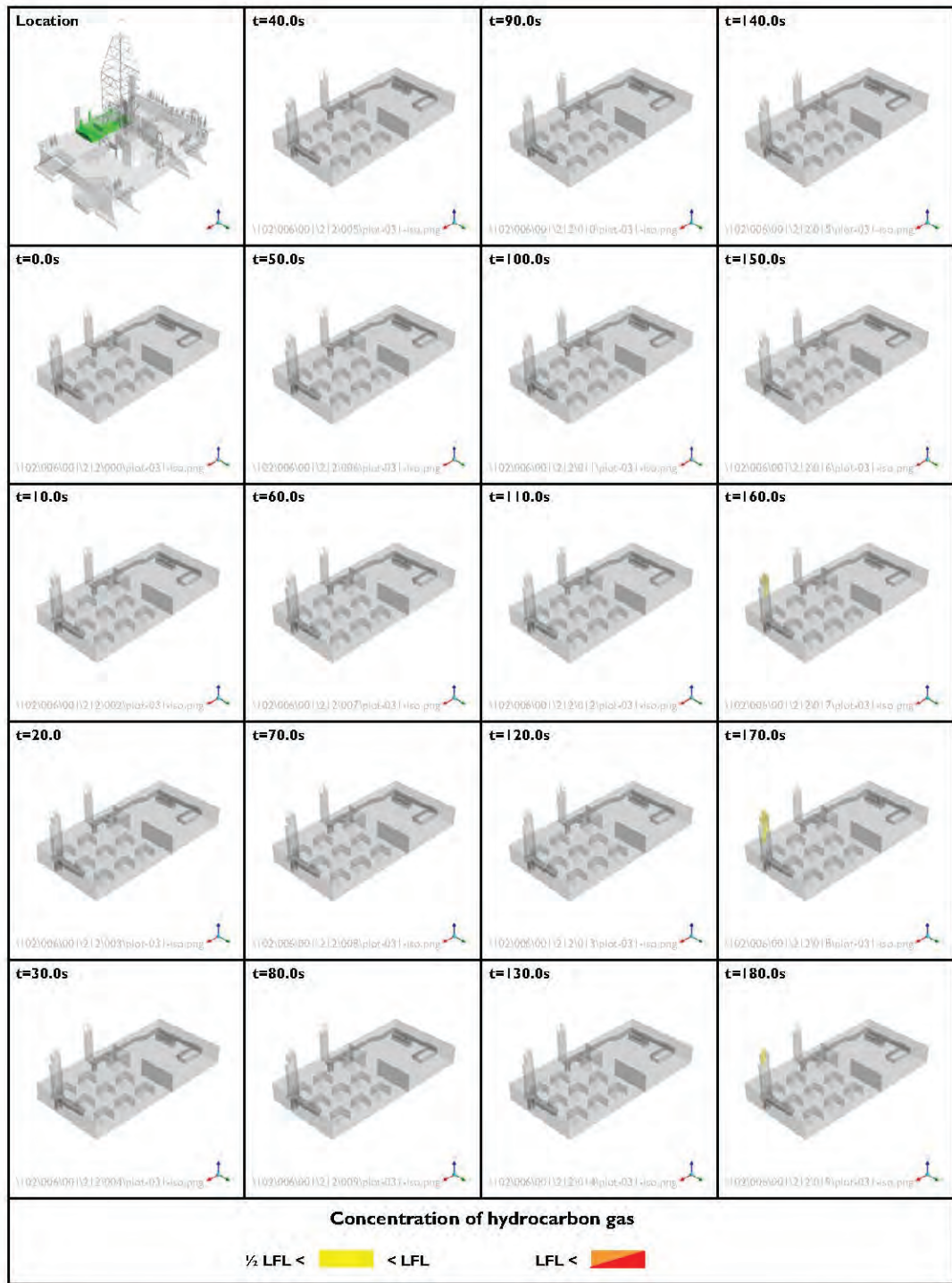
1.5 m/s

Wind direction:

90°

Figure 94

Extent of hydrocarbon gas within starboard transformer room – Case B



Peak flow rate:

400 MMscfd

Wind speed:

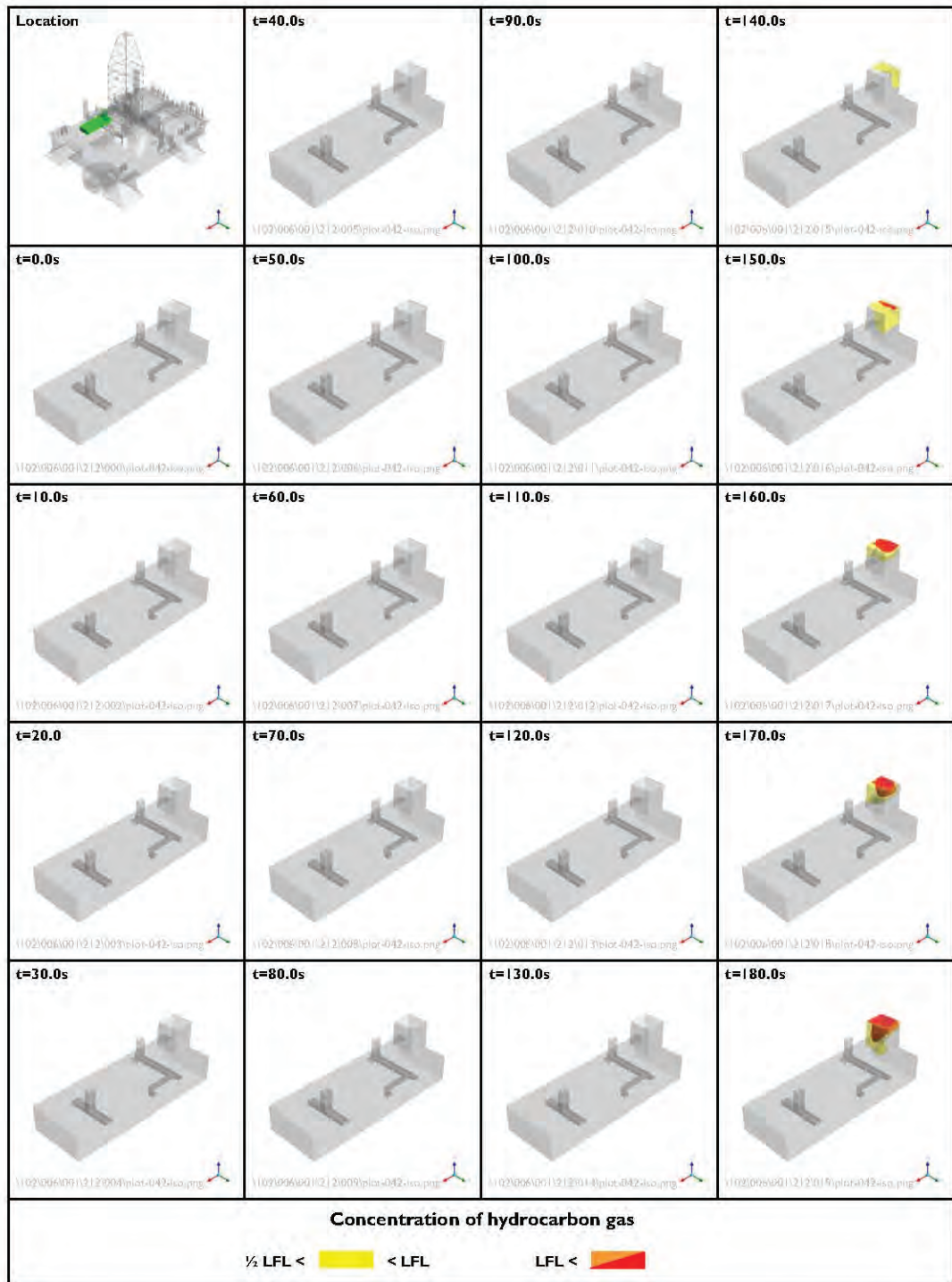
1.5 m/s

Wind direction:

90°

Figure 95

Extent of hydrocarbon gas within sack storage room – Case B



Peak flow rate:

400 MMscfd

Wind speed:

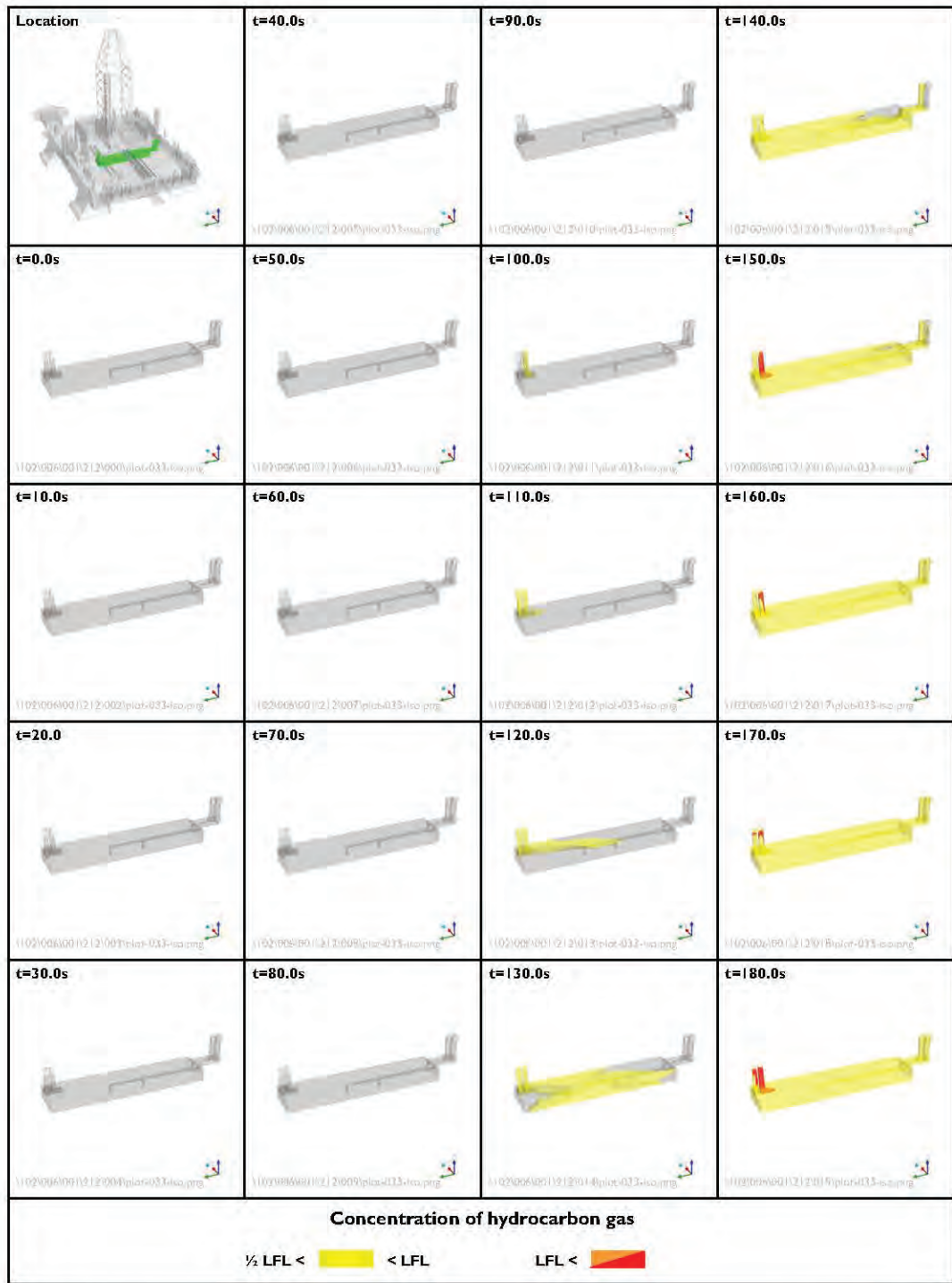
1.5 m/s

Wind direction:

90°

Figure 96

Extent of hydrocarbon gas within warehouse – Case B



Peak flow rate:

400 MMscfd

Wind speed:

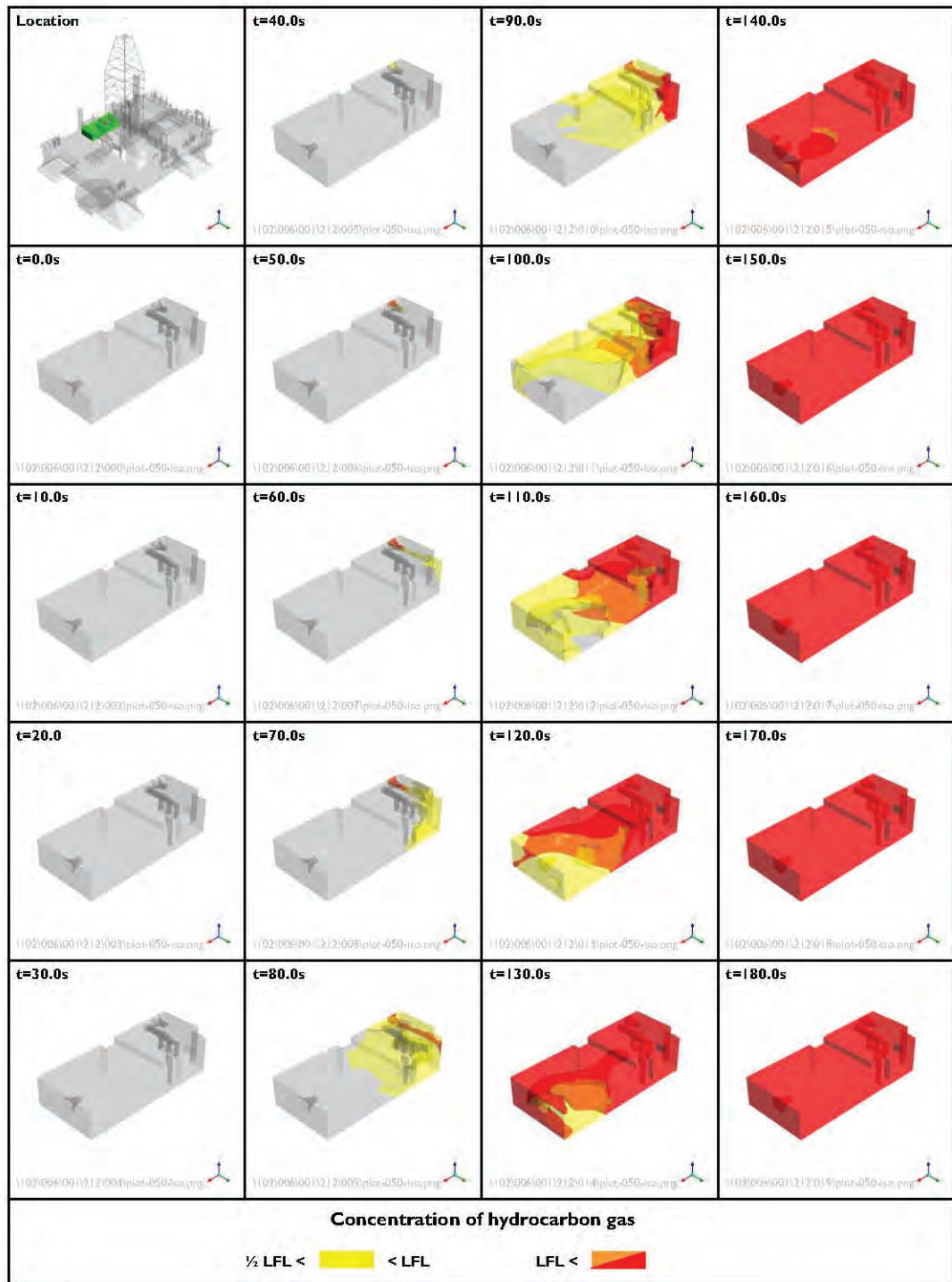
1.5 m/s

Wind direction:

90°

Figure 97

Extent of hydrocarbon gas within mud tank room – Case B



Peak flow rate:

400 MMscfd

Wind speed:

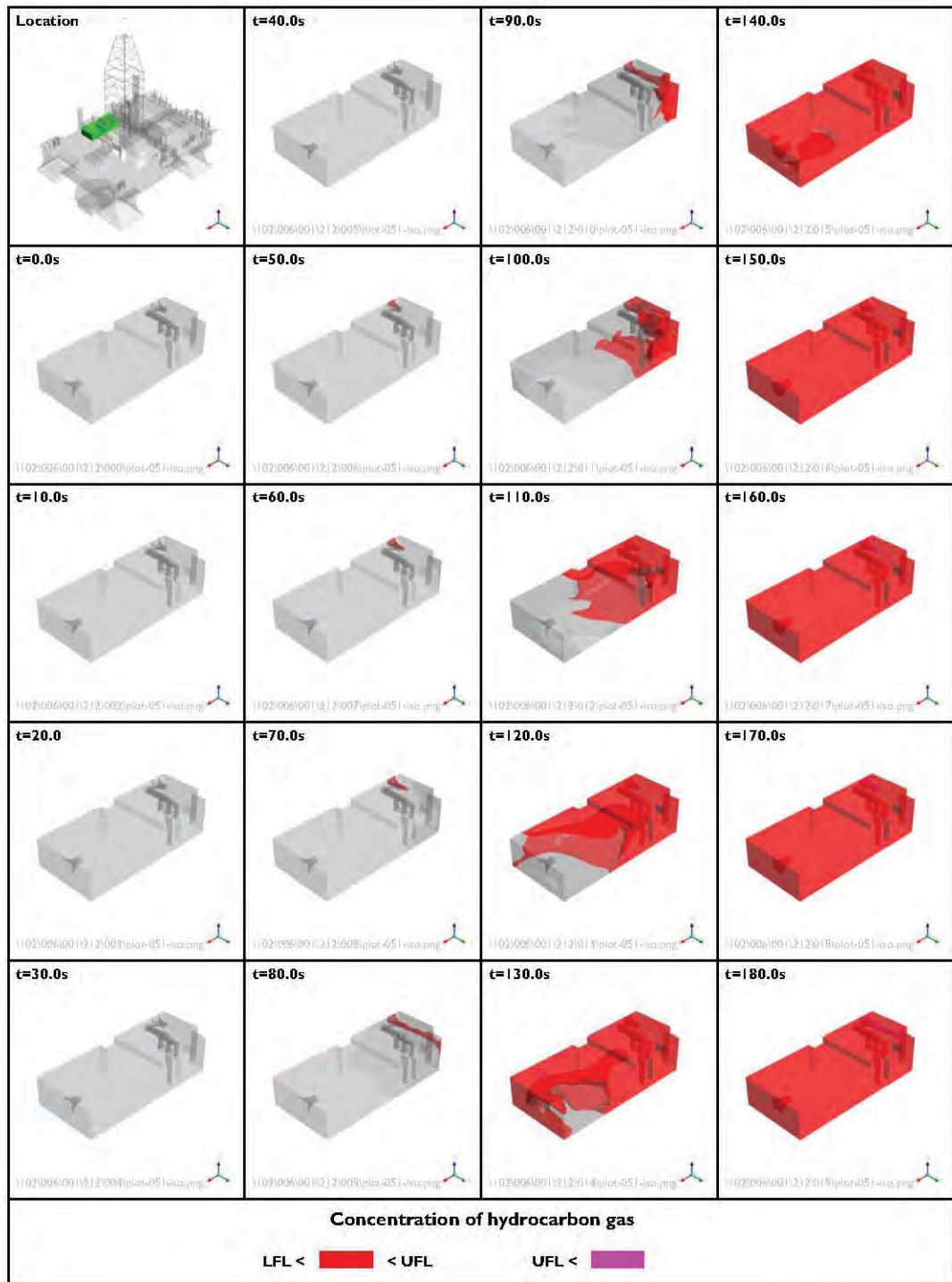
1.5 m/s

Wind direction:

90°

Figure 98

Extent of hydrocarbon gas within cement room – Case B



Peak flow rate:

400 MMscfd

Wind speed:

1.5 m/s

Wind direction:

90°

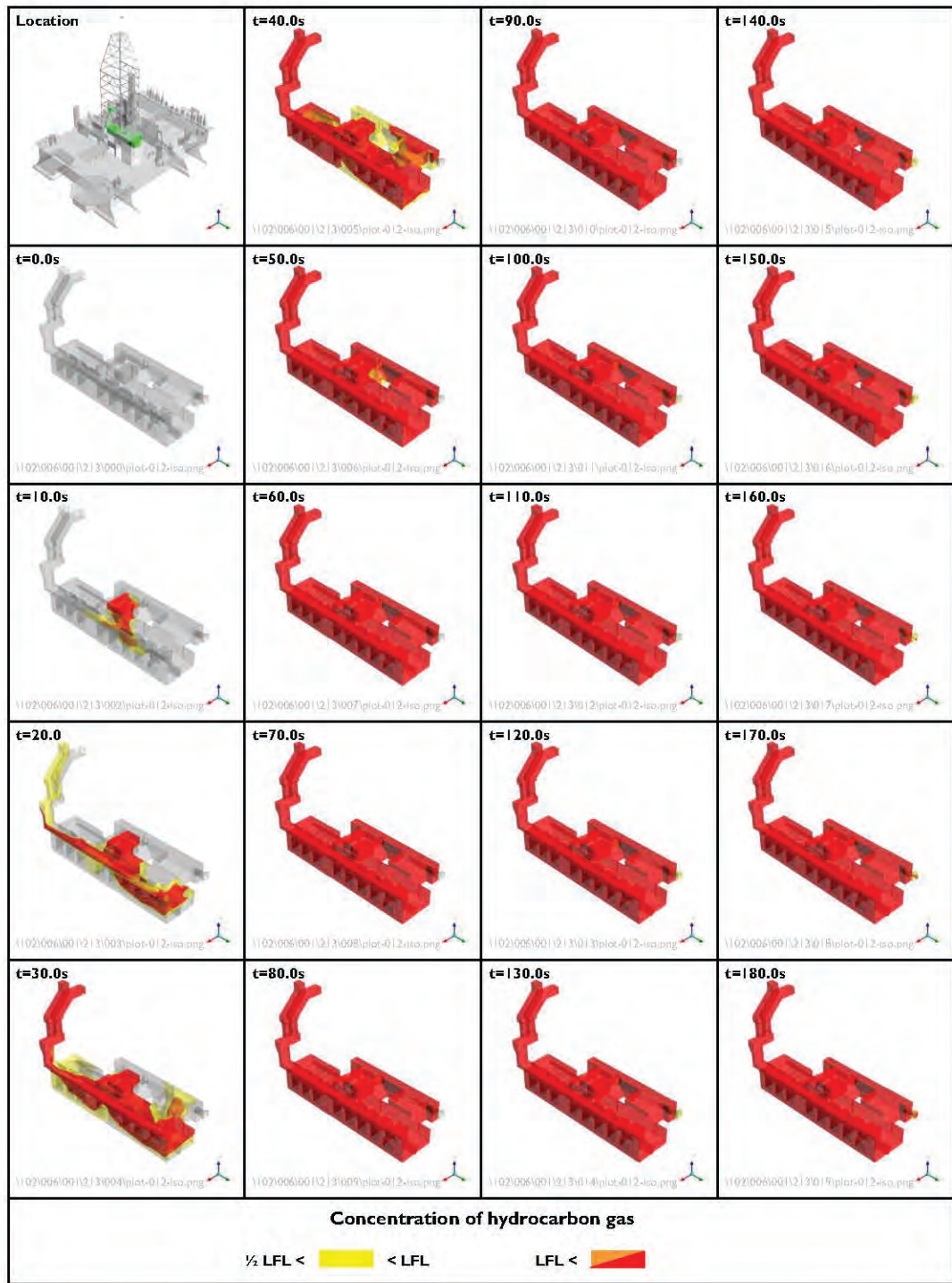
Figure 99

Extent of hydrocarbon gas within cement room – Case B

APPENDIX C RESULTS FOR CASE C

FIGURES

Figure 100	Extent of hydrocarbon gas within shale shaker house – Case C
Figure 101	Extent of hydrocarbon gas within shale shaker house – Case C
Figure 102	Extent of hydrocarbon gas within moonpool – Case C
Figure 103	Extent of hydrocarbon gas within moonpool – Case C
Figure 104	Extent of hydrocarbon gas outside the rig – isometric view – Case C
Figure 105	Extent of hydrocarbon gas outside the rig – top view – Case C
Figure 106	Extent of hydrocarbon gas outside the rig – port view – Case C
Figure 107	Extent of hydrocarbon gas outside the rig – aft view – Case C
Figure 108	Extent of hydrocarbon gas on external rig surfaces – isometric view – Case C
Figure 109	Extent of hydrocarbon gas within engine room 1 – Case C
Figure 110	Extent of hydrocarbon gas within engine room 2 – Case C
Figure 111	Extent of hydrocarbon gas within engine room 3 – Case C
Figure 112	Extent of hydrocarbon gas within engine room 4 – Case C
Figure 113	Extent of hydrocarbon gas within engine room 5 – Case C
Figure 114	Extent of hydrocarbon gas within engine room 6 – Case C
Figure 115	Extent of hydrocarbon gas within mud pump rooms – Case C
Figure 116	Extent of hydrocarbon gas within HVAC rooms – Case C
Figure 117	Extent of hydrocarbon gas within port transformer room – Case C
Figure 118	Extent of hydrocarbon gas within starboard transformer room – Case C
Figure 119	Extent of hydrocarbon gas within sack storage room – Case C
Figure 120	Extent of hydrocarbon gas within warehouse – Case C
Figure 121	Extent of hydrocarbon gas within mud tank room – Case C
Figure 122	Extent of hydrocarbon gas within cement house – Case C
Figure 123	Extent of hydrocarbon gas within cement house – Case C



Peak flow rate:

300 MMscfd

Wind speed:

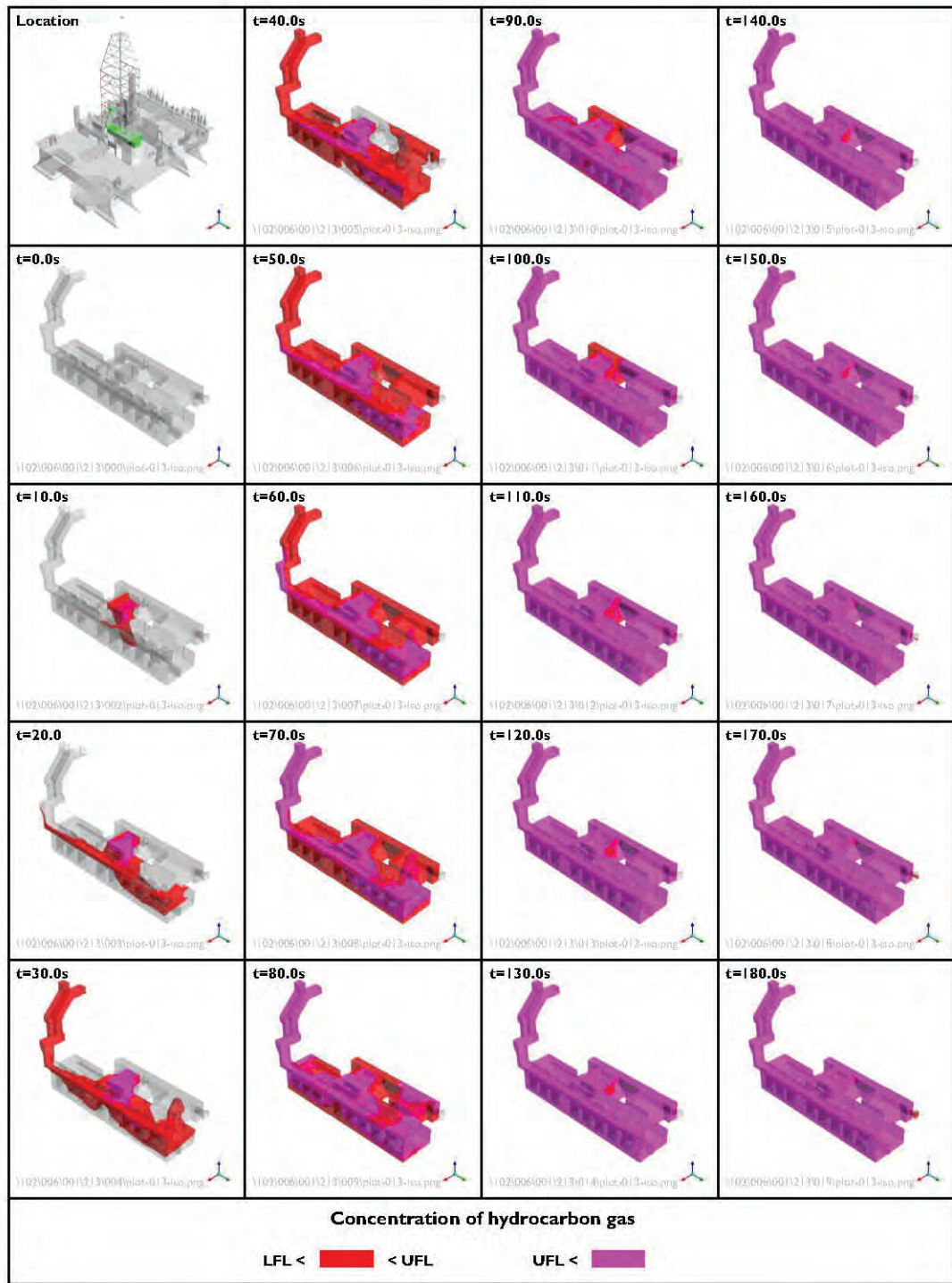
1.5 m/s

Wind direction:

90°

Figure 100

Extent of hydrocarbon gas within shale shaker house – Case C



Peak flow rate:

300 MMscfd

Wind speed:

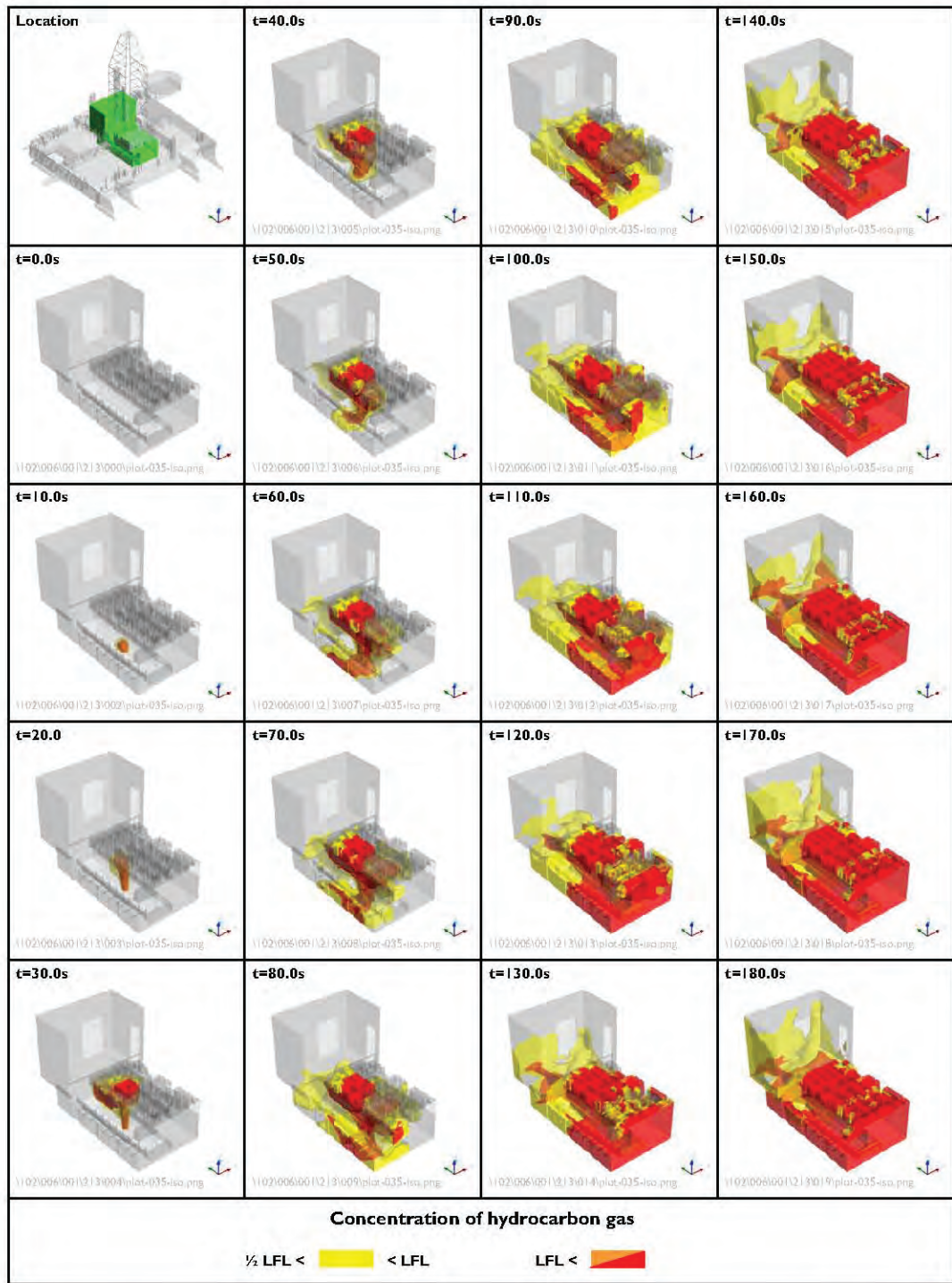
1.5 m/s

Wind direction:

90°

Figure 101

Extent of hydrocarbon gas within shale shaker house – Case C



Peak flow rate:

300 MMscfd

Wind speed:

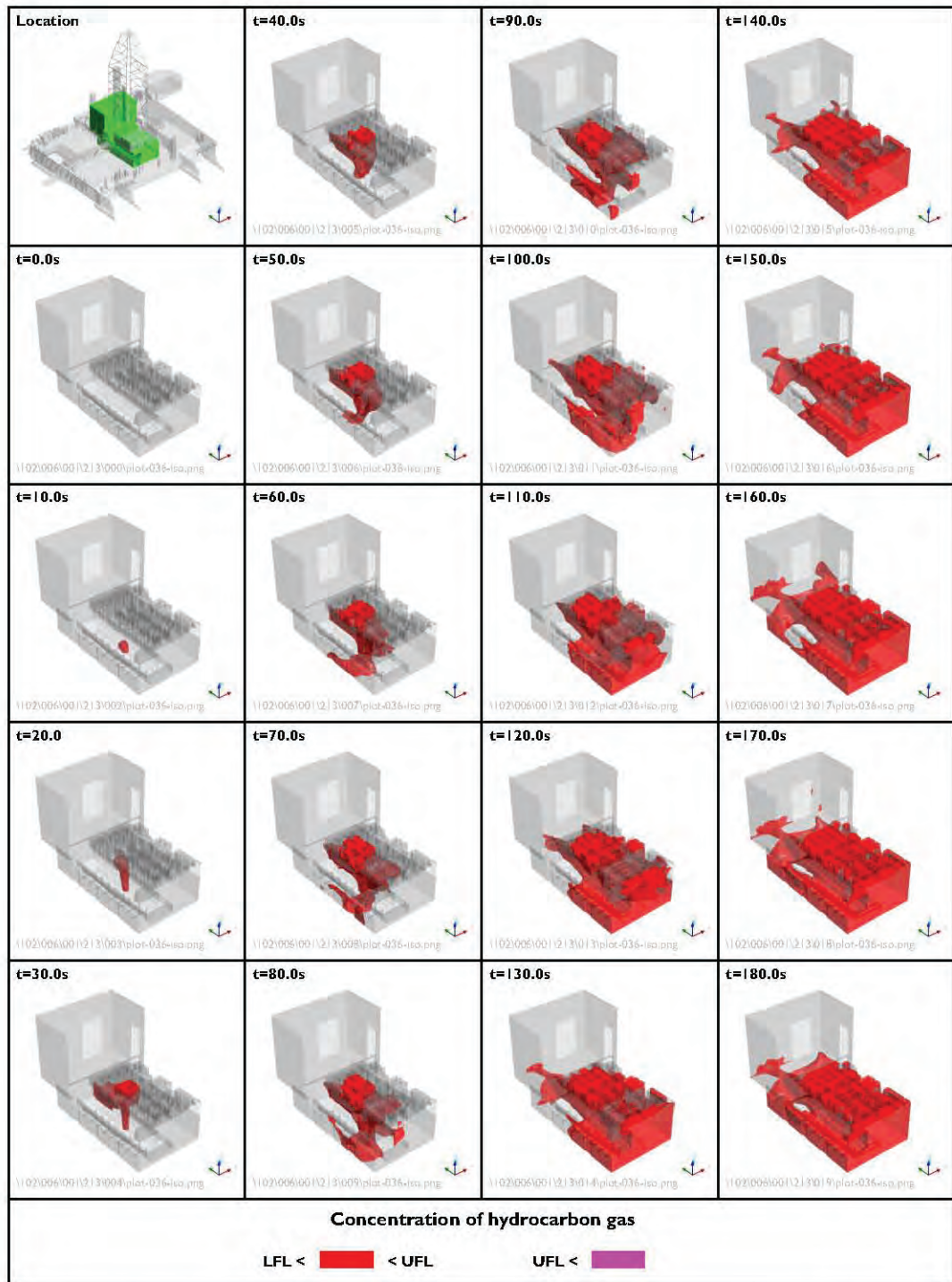
1.5 m/s

Wind direction:

90°

Figure 102

Extent of hydrocarbon gas within moonpool – Case C



Peak flow rate:

300 MMscfd

Wind speed:

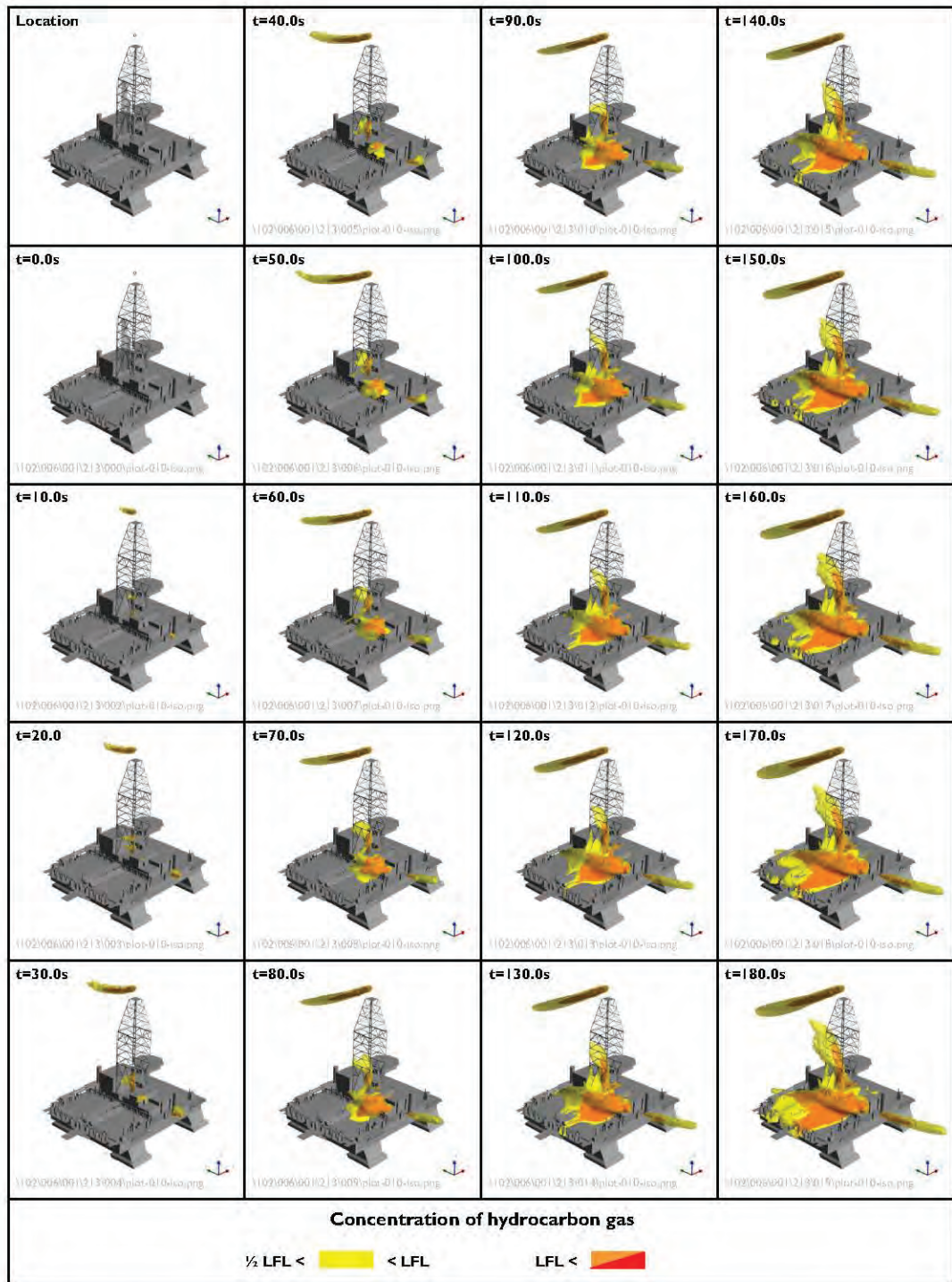
1.5 m/s

Wind direction:

90°

Figure 103

Extent of hydrocarbon gas within moonpool – Case C



Peak flow rate:

300 MMscfd

Wind speed:

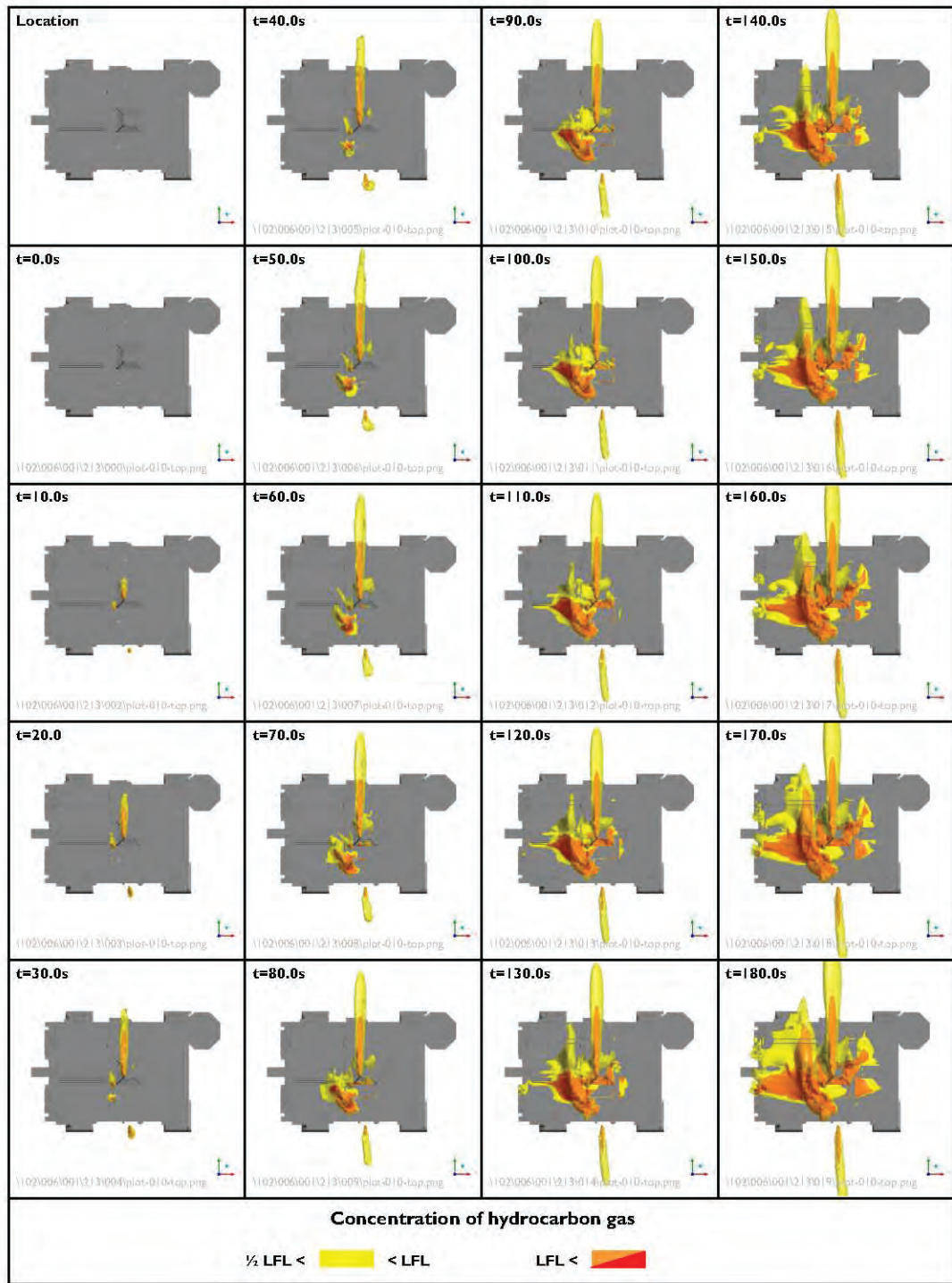
1.5 m/s

Wind direction:

90°

Figure 104

Extent of hydrocarbon gas outside the rig – isometric view – Case C



Peak flow rate:

300 MMscfd

Wind speed:

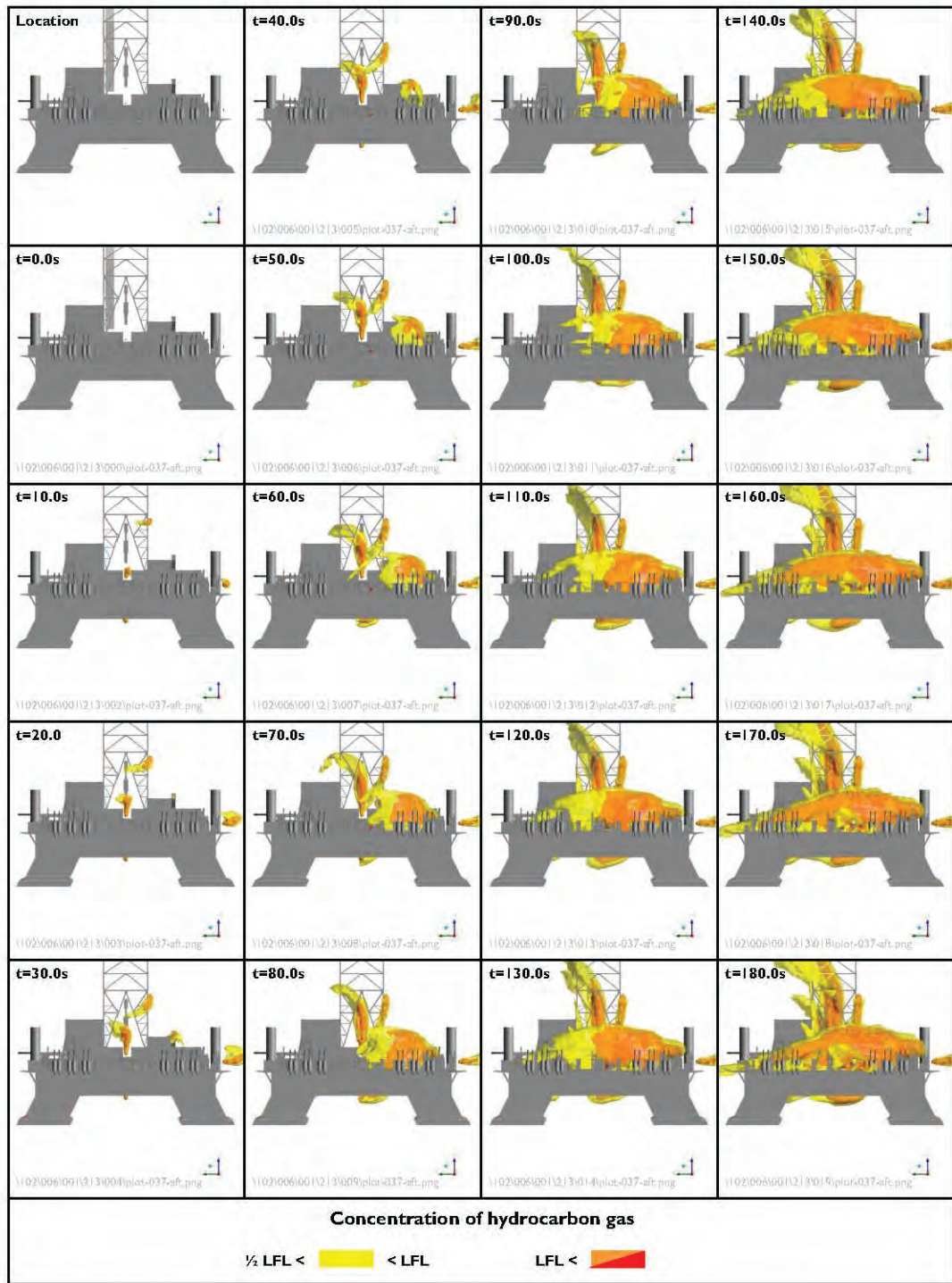
1.5 m/s

Wind direction:

90°

Figure 105

Extent of hydrocarbon gas outside the rig – top view – Case C



Peak flow rate:

300 MMscfd

Wind speed:

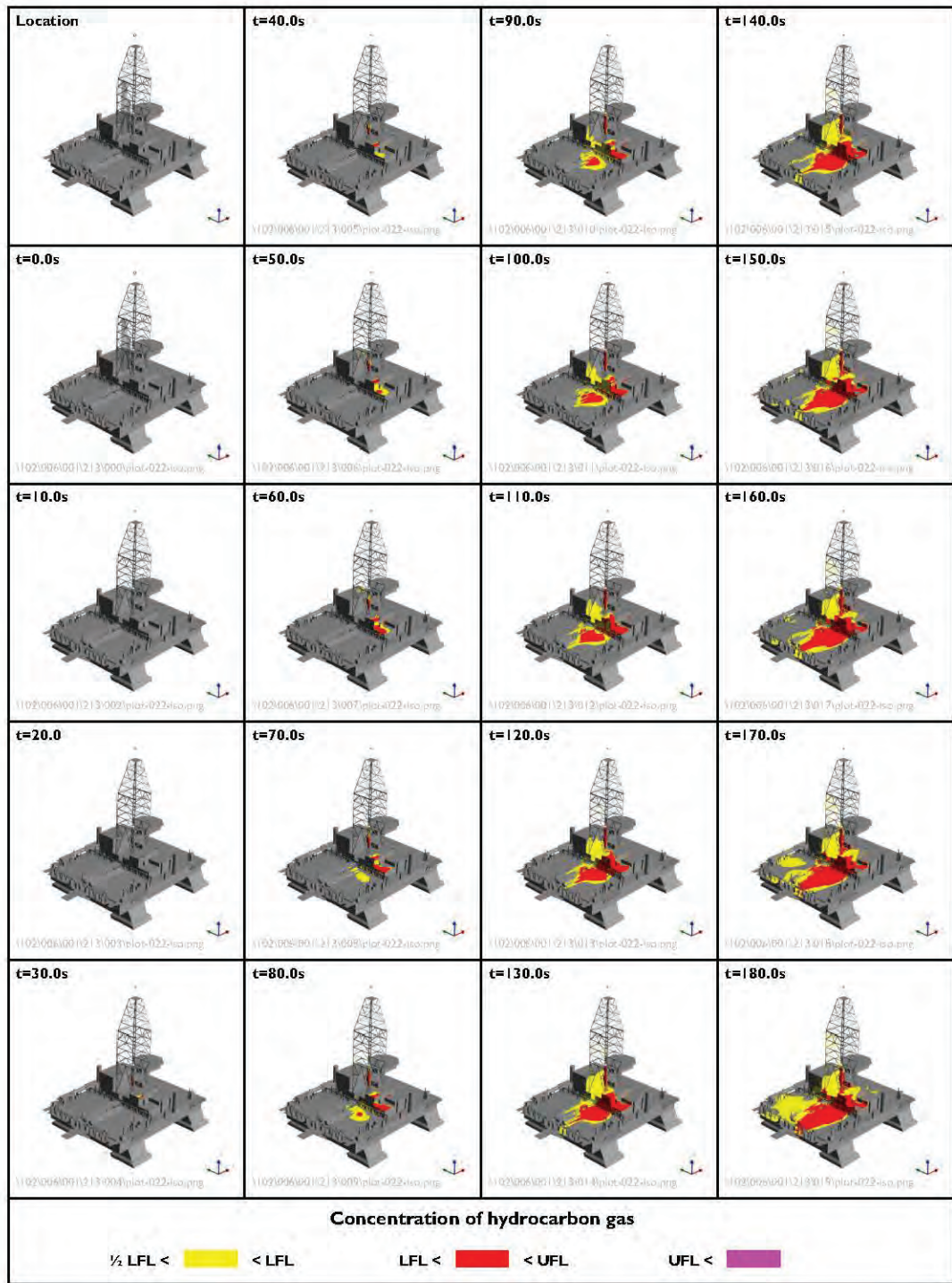
1.5 m/s

Wind direction:

90°

Figure 107

Extent of hydrocarbon gas outside the rig – aft view – Case C



Peak flow rate:

300 MMscfd

Wind speed:

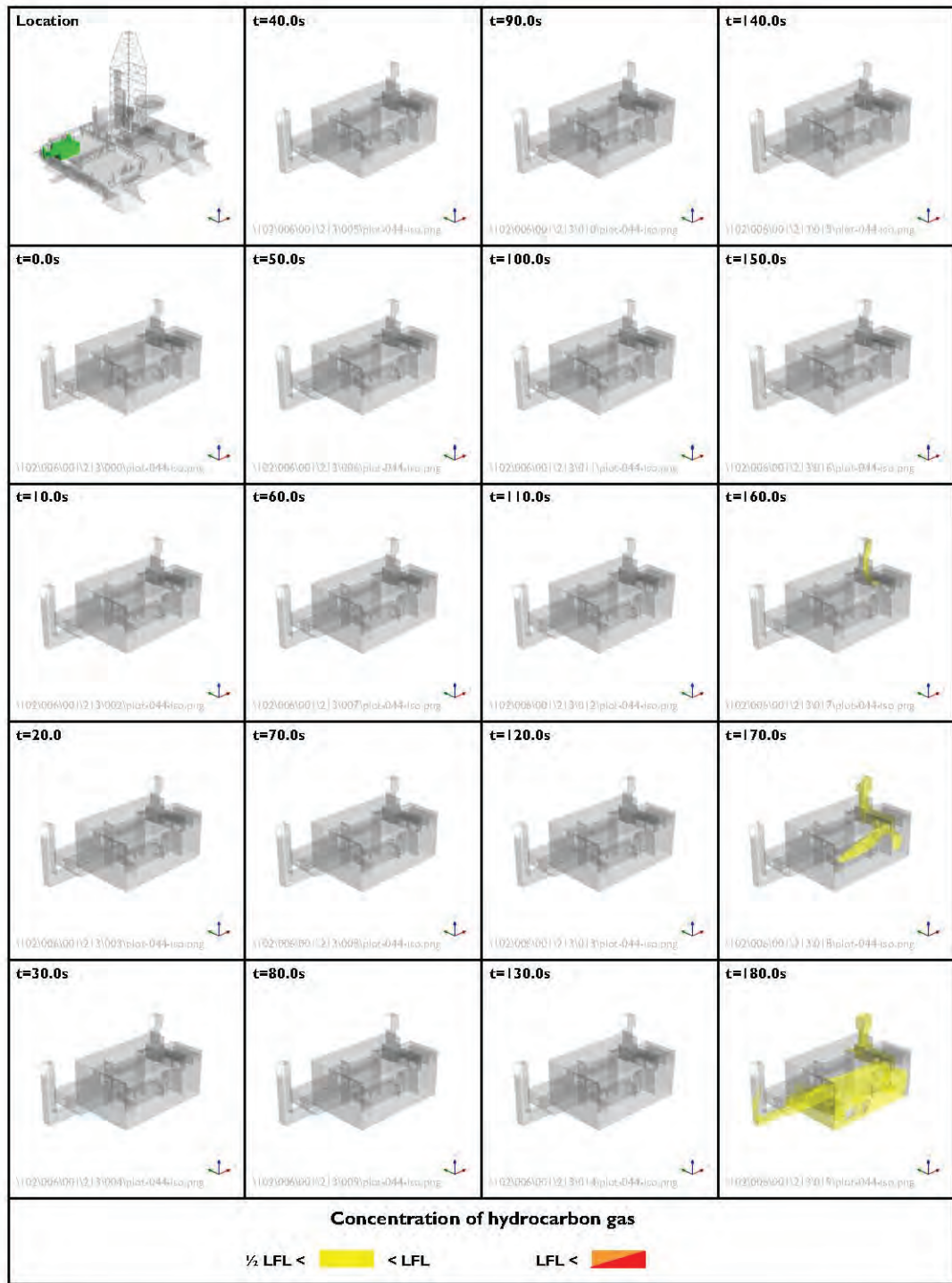
1.5 m/s

Wind direction:

90°

Figure 108

Extent of hydrocarbon gas on external rig surfaces – isometric view – Case C



Peak flow rate:

300 MMscfd

Wind speed:

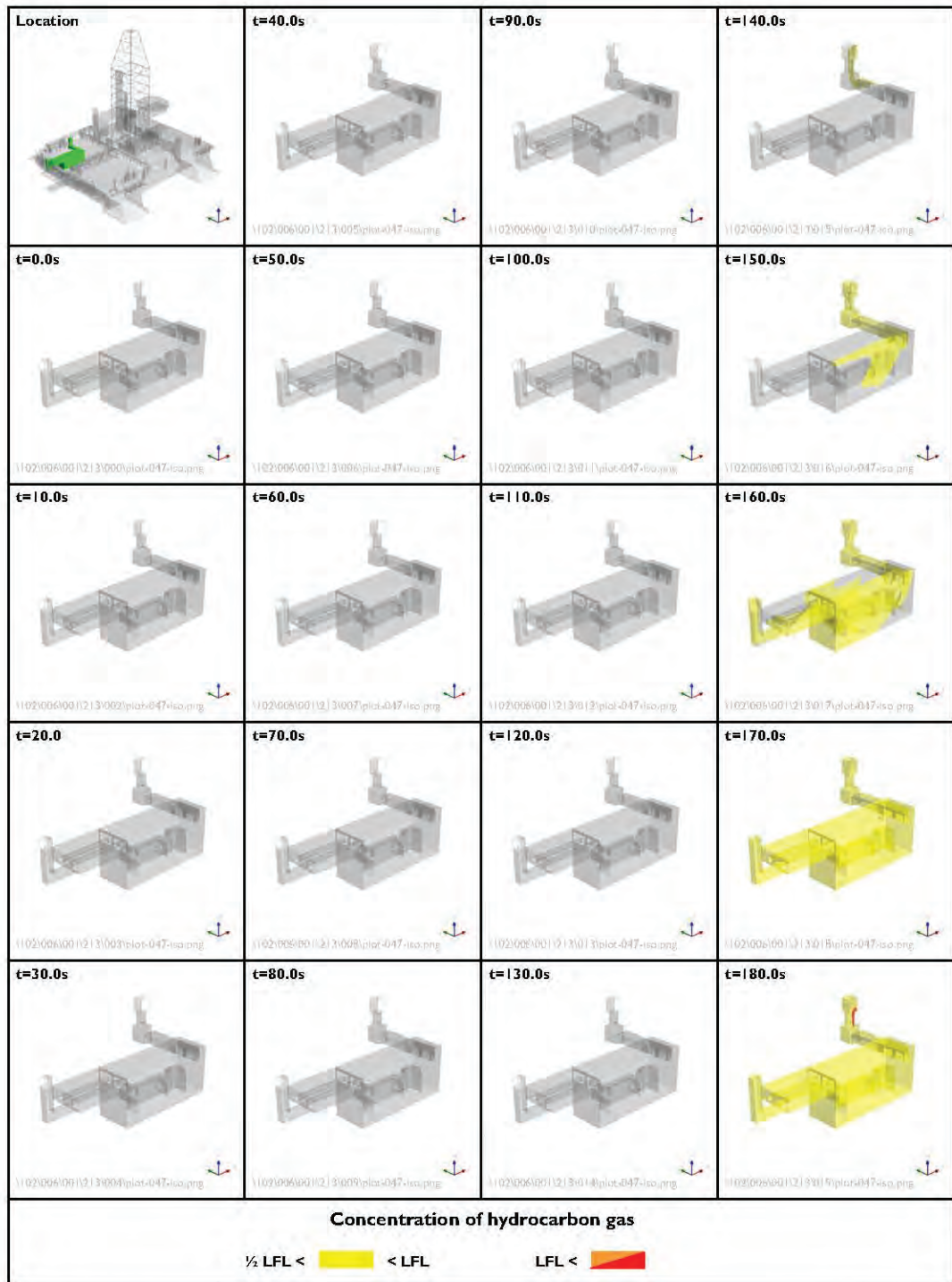
1.5 m/s

Wind direction:

90°

Figure 109

Extent of hydrocarbon gas within engine room I – Case C



Peak flow rate:

300 MMscfd

Wind speed:

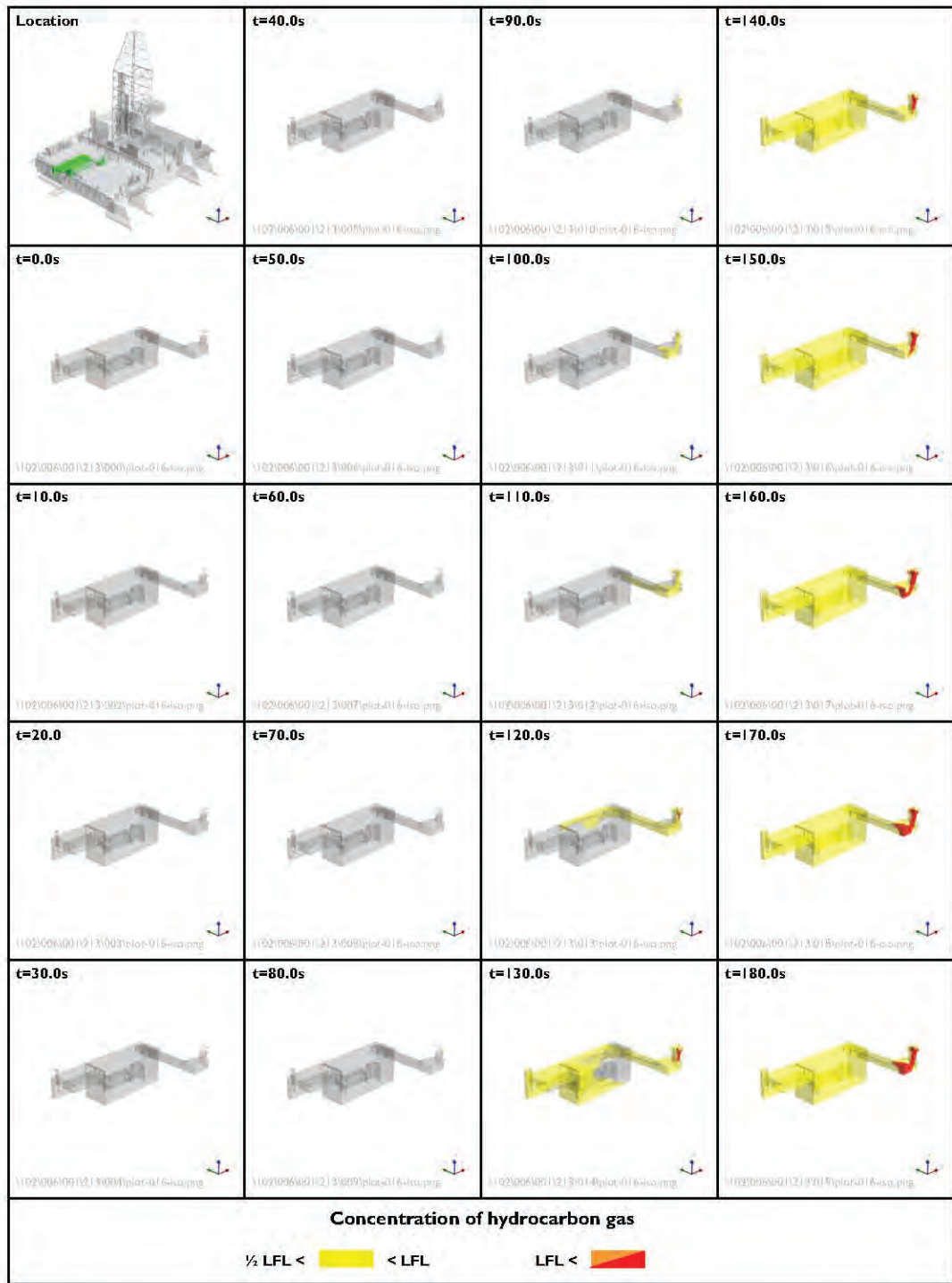
1.5 m/s

Wind direction:

90°

Figure I 10

Extent of hydrocarbon gas within engine room 2 – Case C



Peak flow rate:

300 MMscfd

Wind speed:

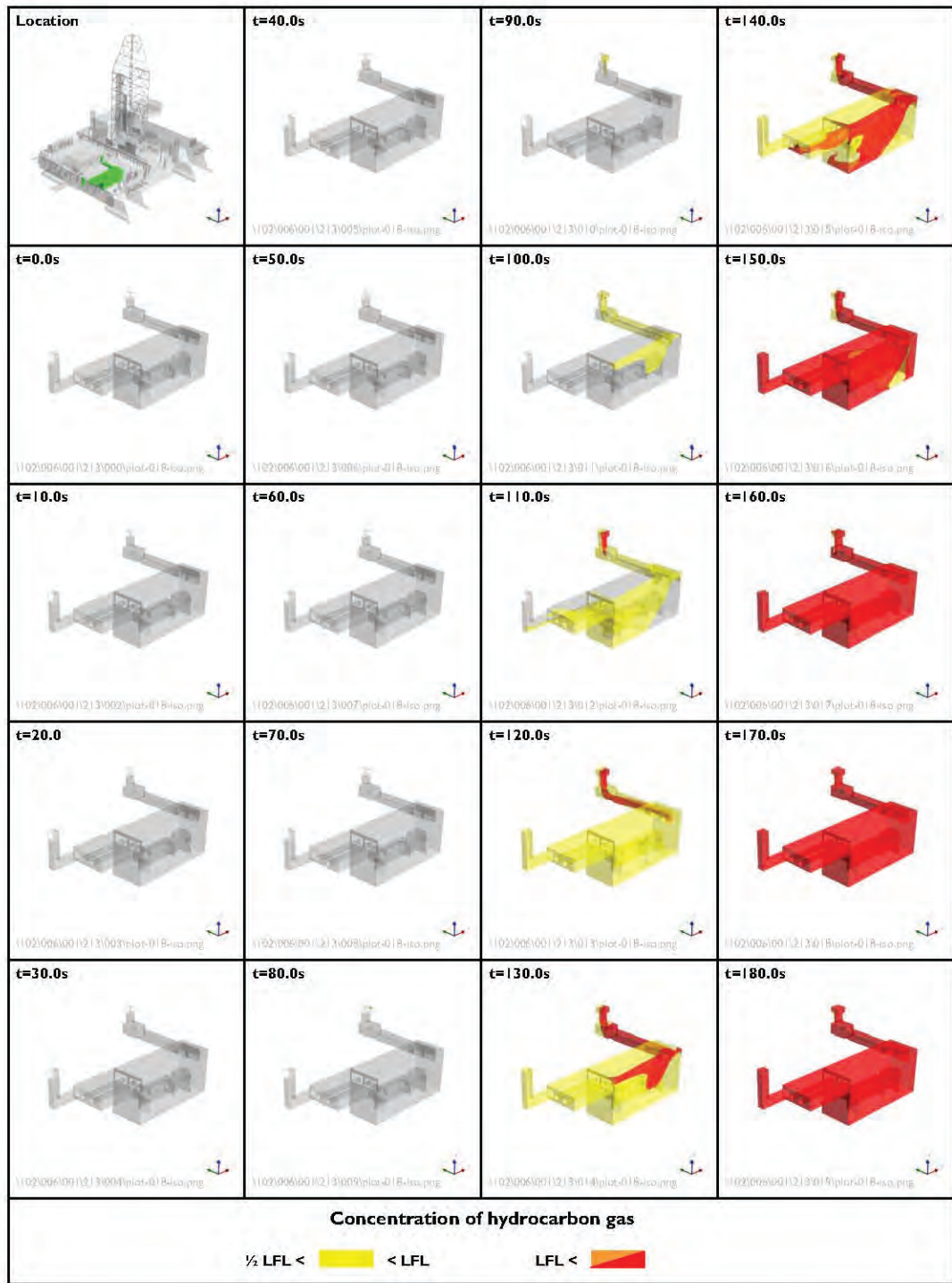
1.5 m/s

Wind direction:

90°

Figure III

Extent of hydrocarbon gas within engine room 3 – Case C



Peak flow rate:

300 MMscfd

Wind speed:

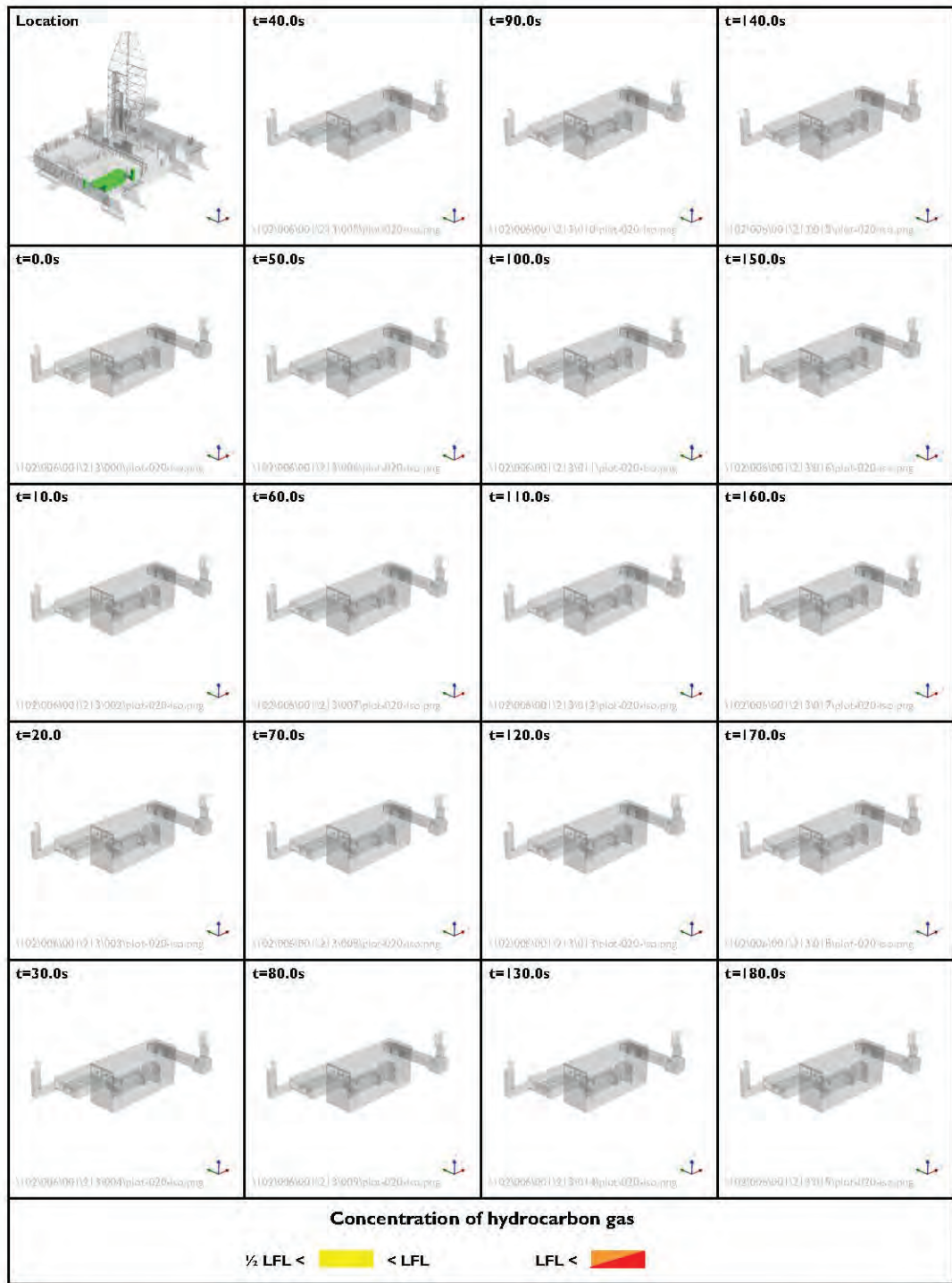
1.5 m/s

Wind direction:

90°

Figure I 12

Extent of hydrocarbon gas within engine room 4 – Case C



Peak flow rate:

300 MMscfd

Wind speed:

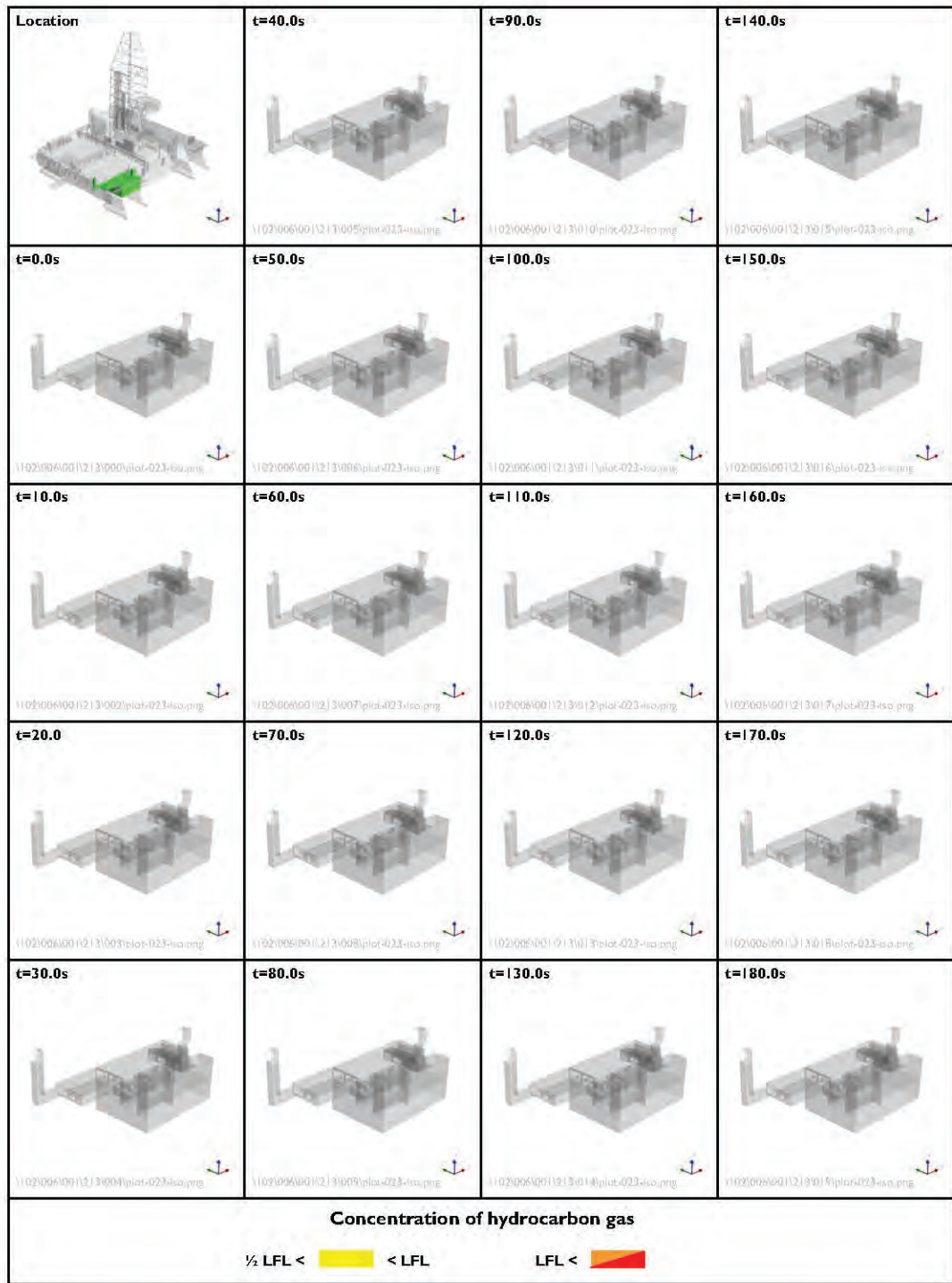
1.5 m/s

Wind direction:

90°

Figure I 13

Extent of hydrocarbon gas within engine room 5 – Case C



Peak flow rate:

300 MMscfd

Wind speed:

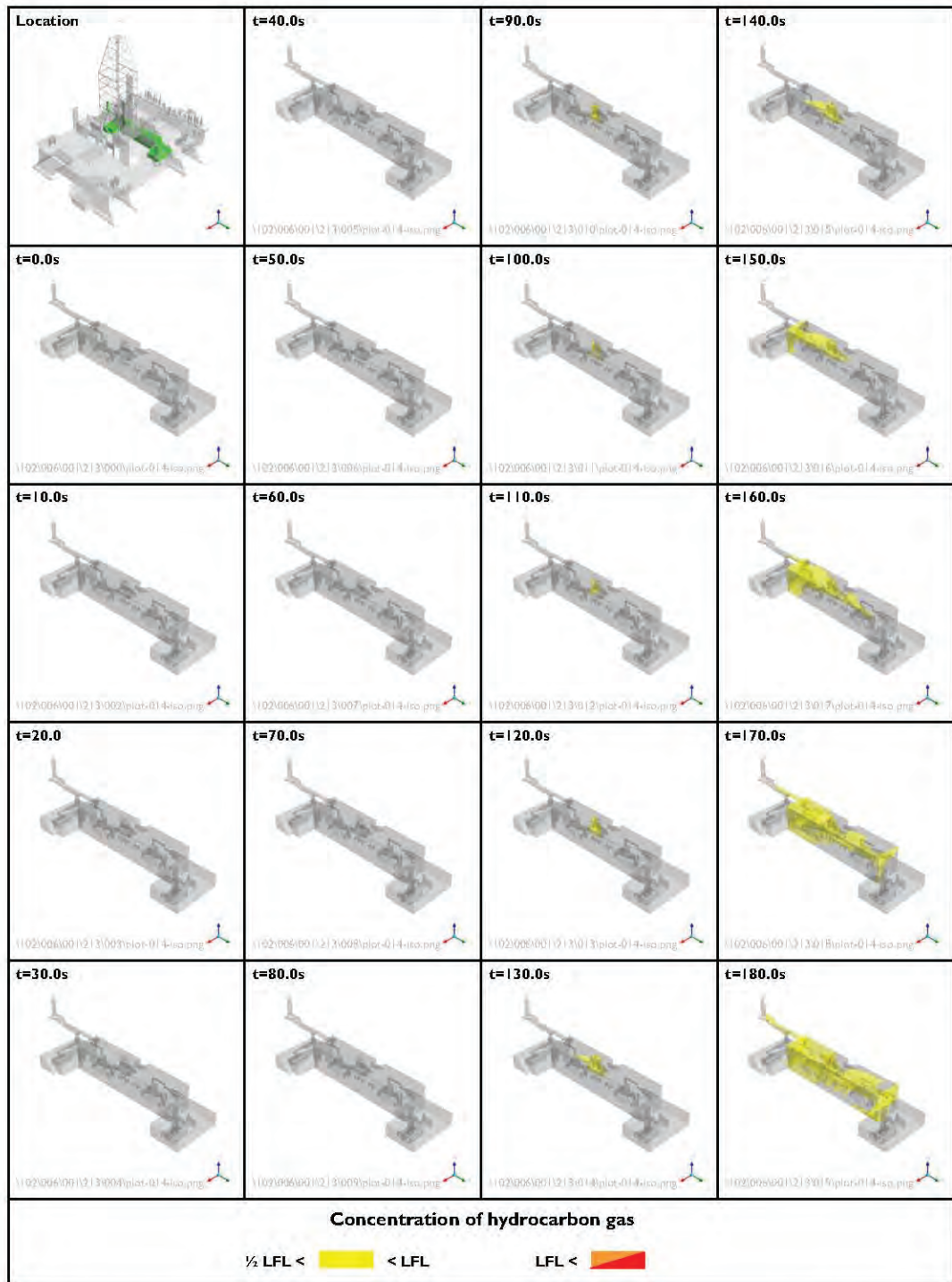
1.5 m/s

Wind direction:

90°

Figure I 14

Extent of hydrocarbon gas within engine room 6 – Case C



Peak flow rate:

300 MMscfd

Wind speed:

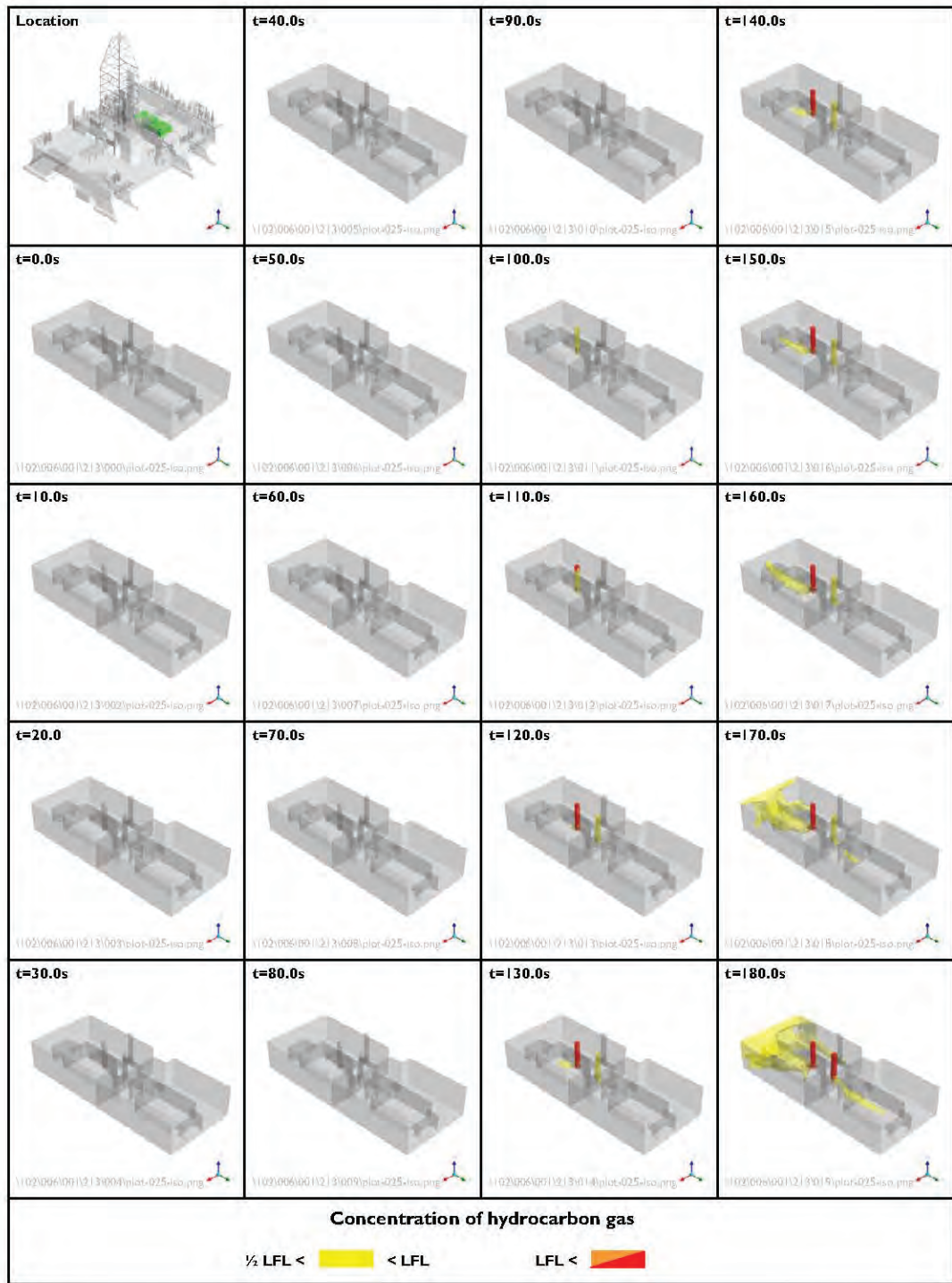
1.5 m/s

Wind direction:

90°

Figure I 15

Extent of hydrocarbon gas within mud pump rooms – Case C



Peak flow rate:

300 MMscfd

Wind speed:

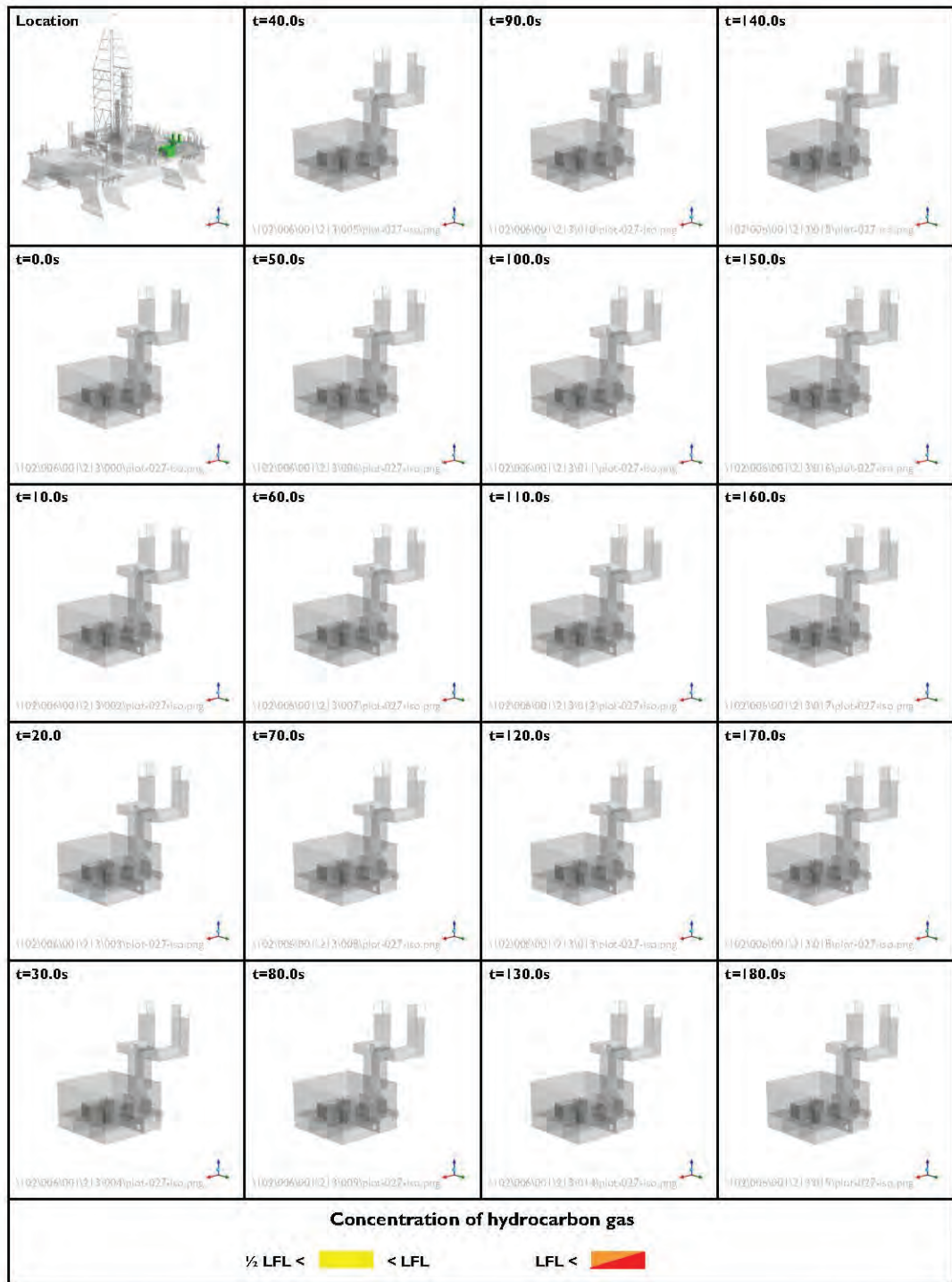
1.5 m/s

Wind direction:

90°

Figure I 16

Extent of hydrocarbon gas within HVAC rooms – Case C



Peak flow rate:

300 MMscfd

Wind speed:

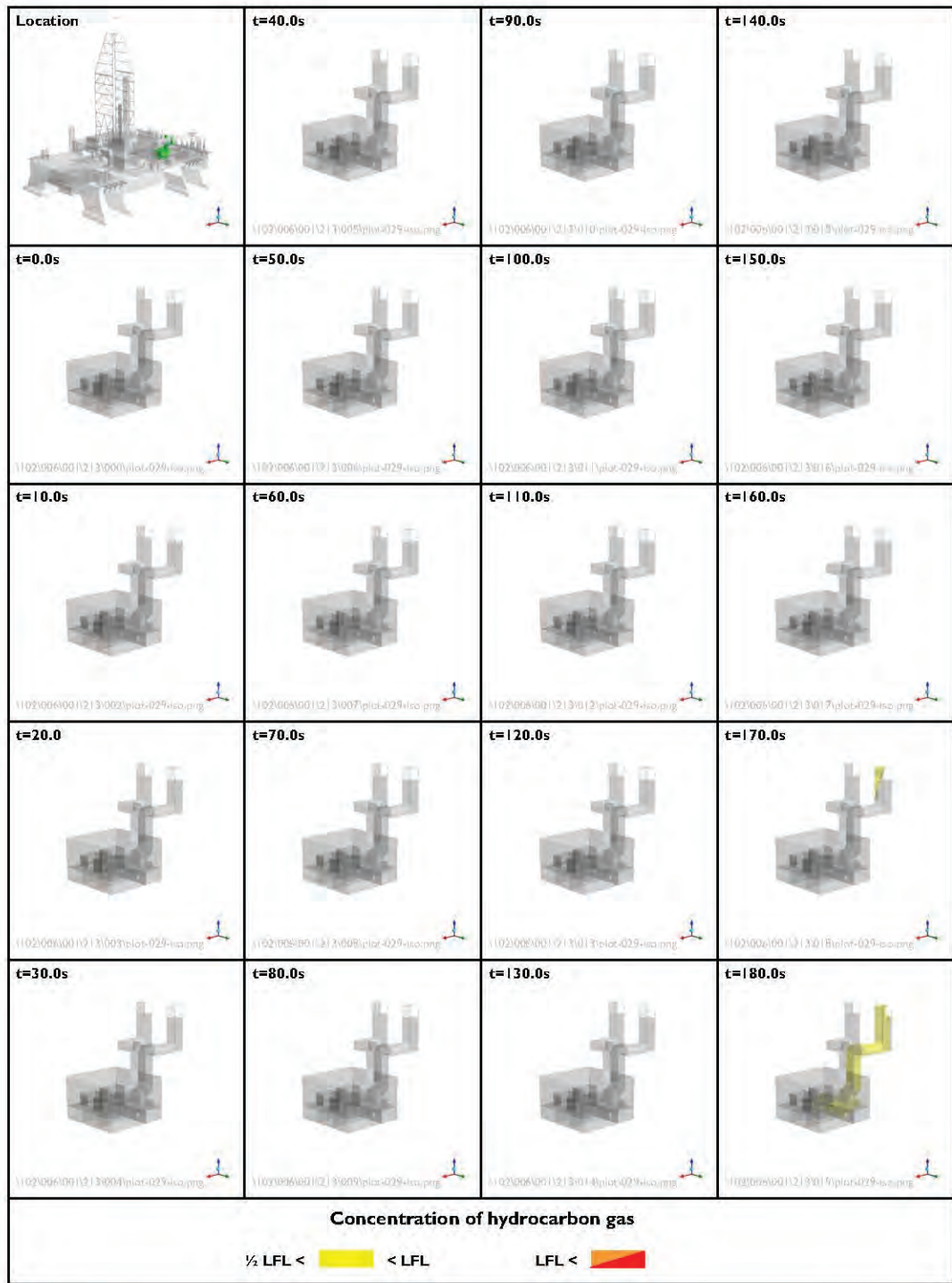
1.5 m/s

Wind direction:

90°

Figure I 17

Extent of hydrocarbon gas within port transformer room – Case C



Peak flow rate:

300 MMscfd

Wind speed:

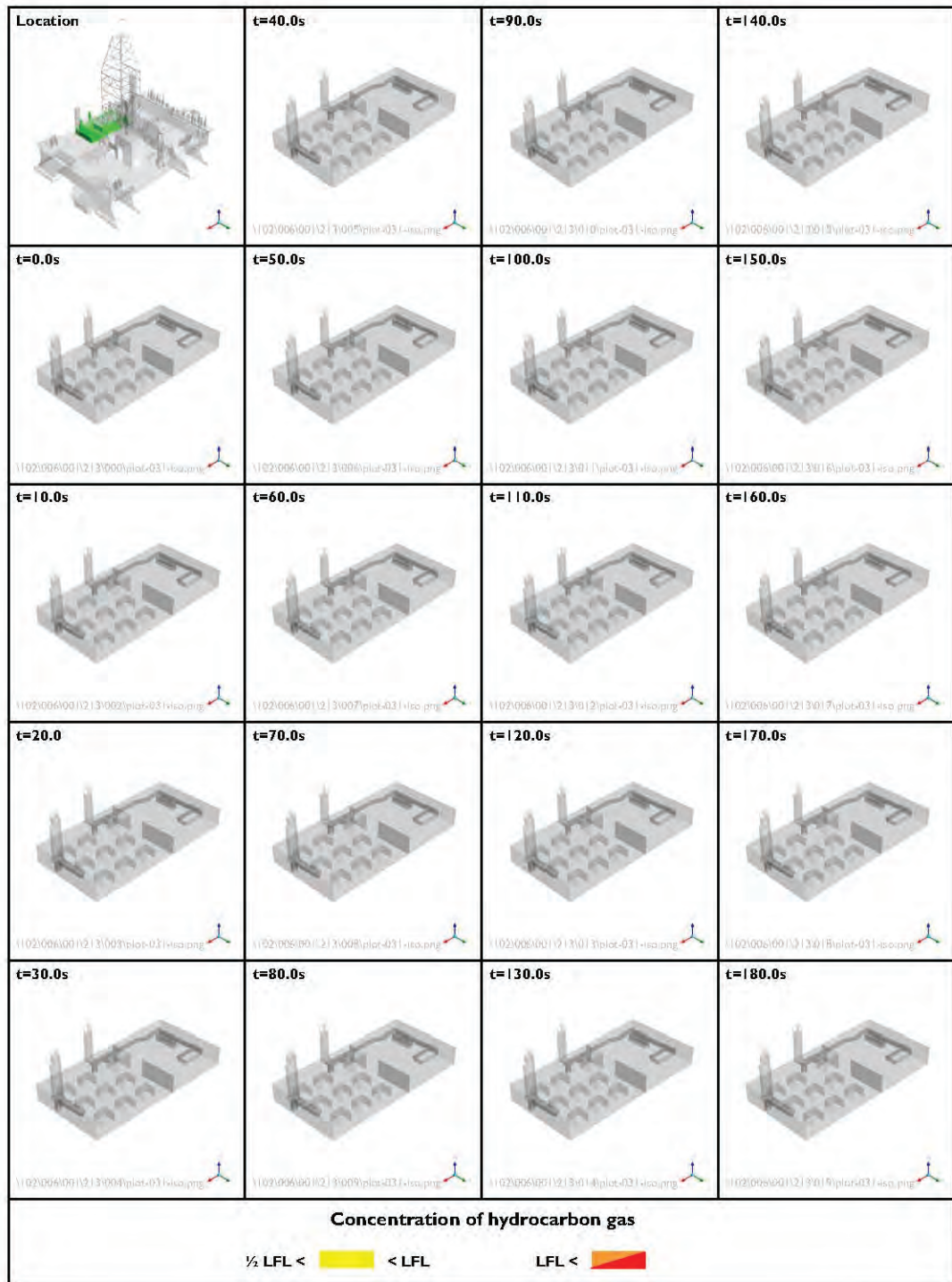
1.5 m/s

Wind direction:

90°

Figure I 18

Extent of hydrocarbon gas within starboard transformer room – Case C



Peak flow rate:

300 MMscfd

Wind speed:

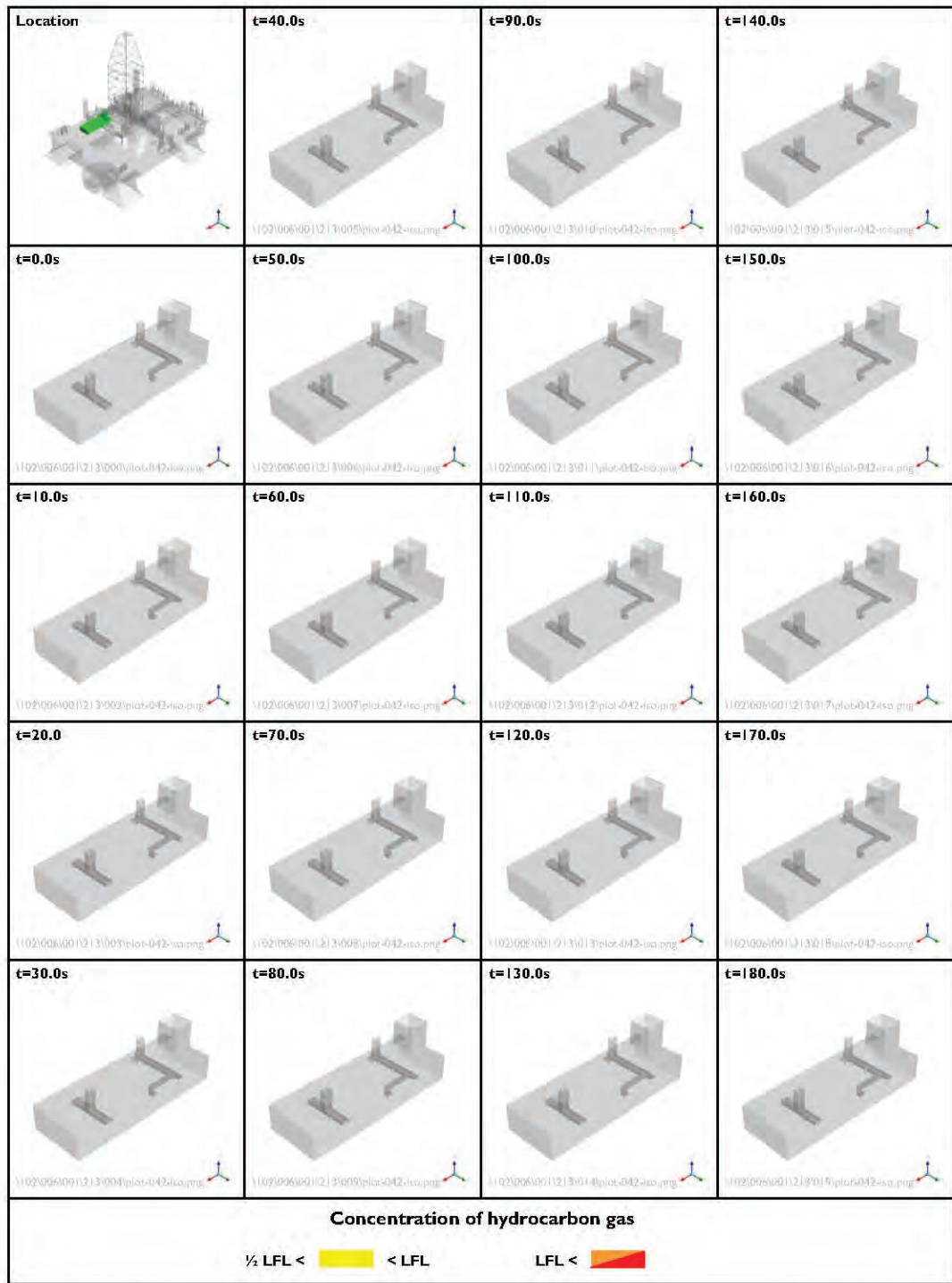
1.5 m/s

Wind direction:

90°

Figure I 19

Extent of hydrocarbon gas within sack storage room – Case C



Peak flow rate:

300 MMscfd

Wind speed:

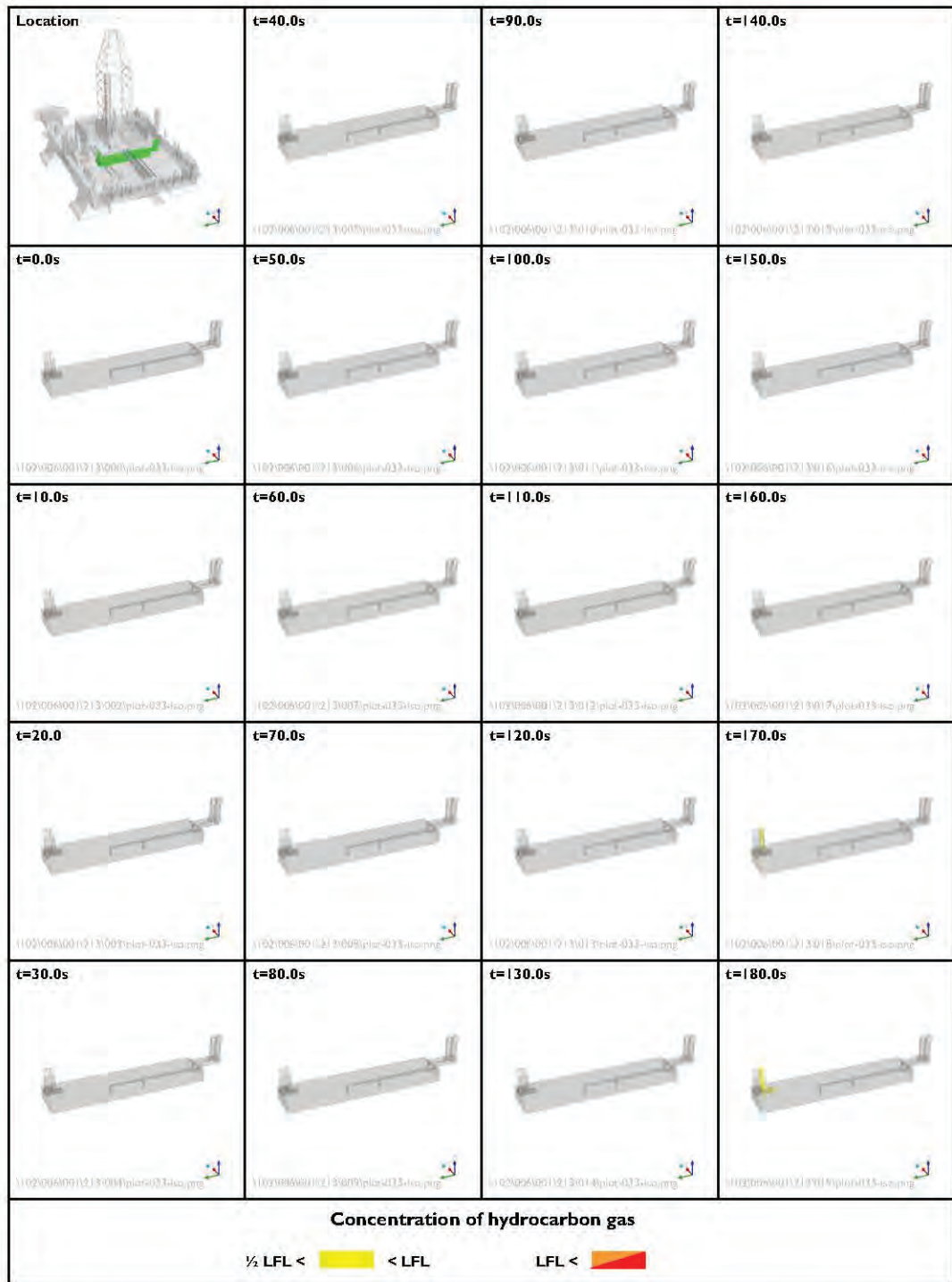
1.5 m/s

Wind direction:

90°

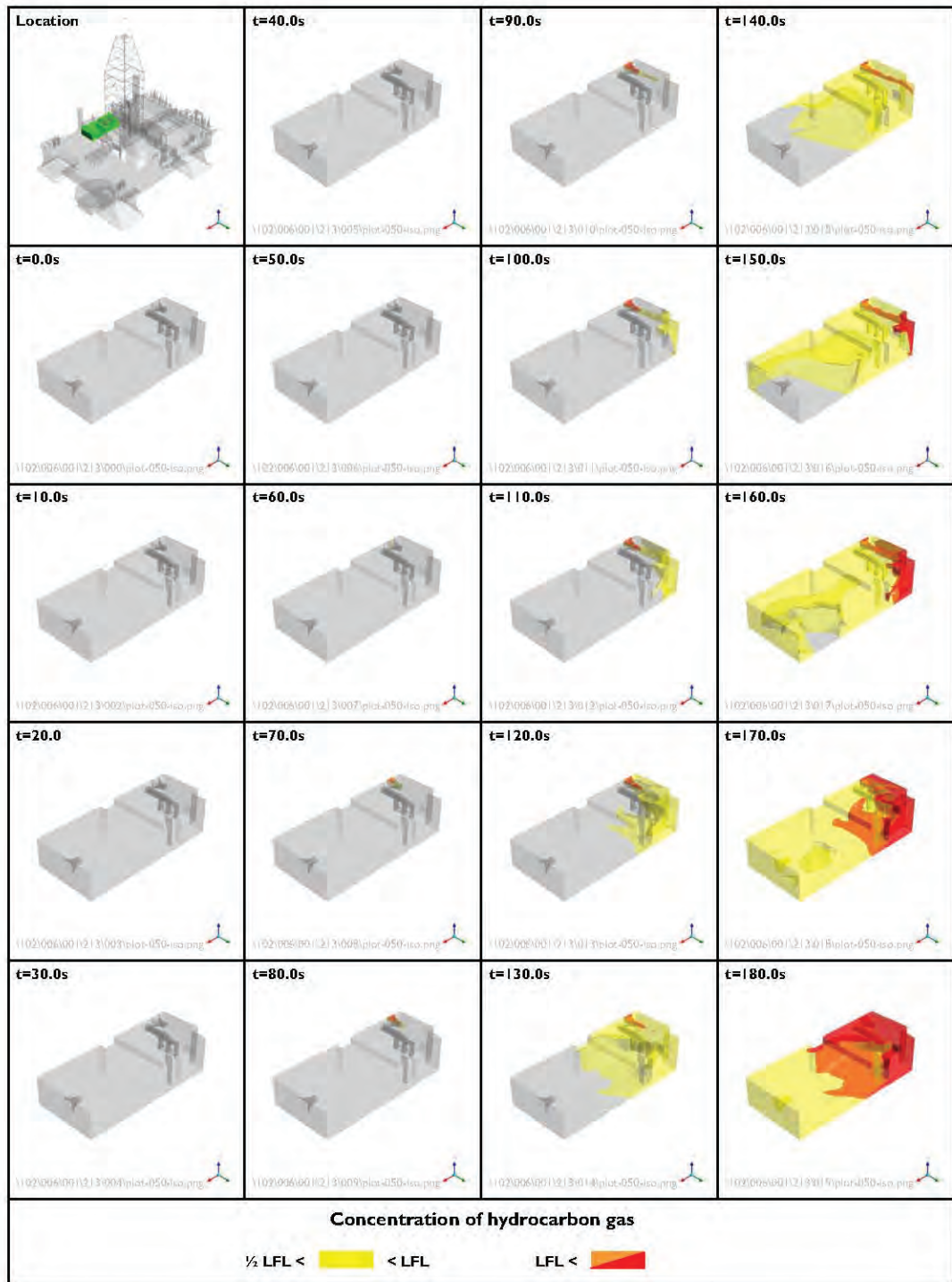
Figure 120

Extent of hydrocarbon gas within warehouse – Case C



Peak flow rate: 300 MMscfd
 Wind speed: 1.5 m/s
 Wind direction: 90°

Figure 121 Extent of hydrocarbon gas within mud tank room – Case C



Peak flow rate:

300 MMscfd

Wind speed:

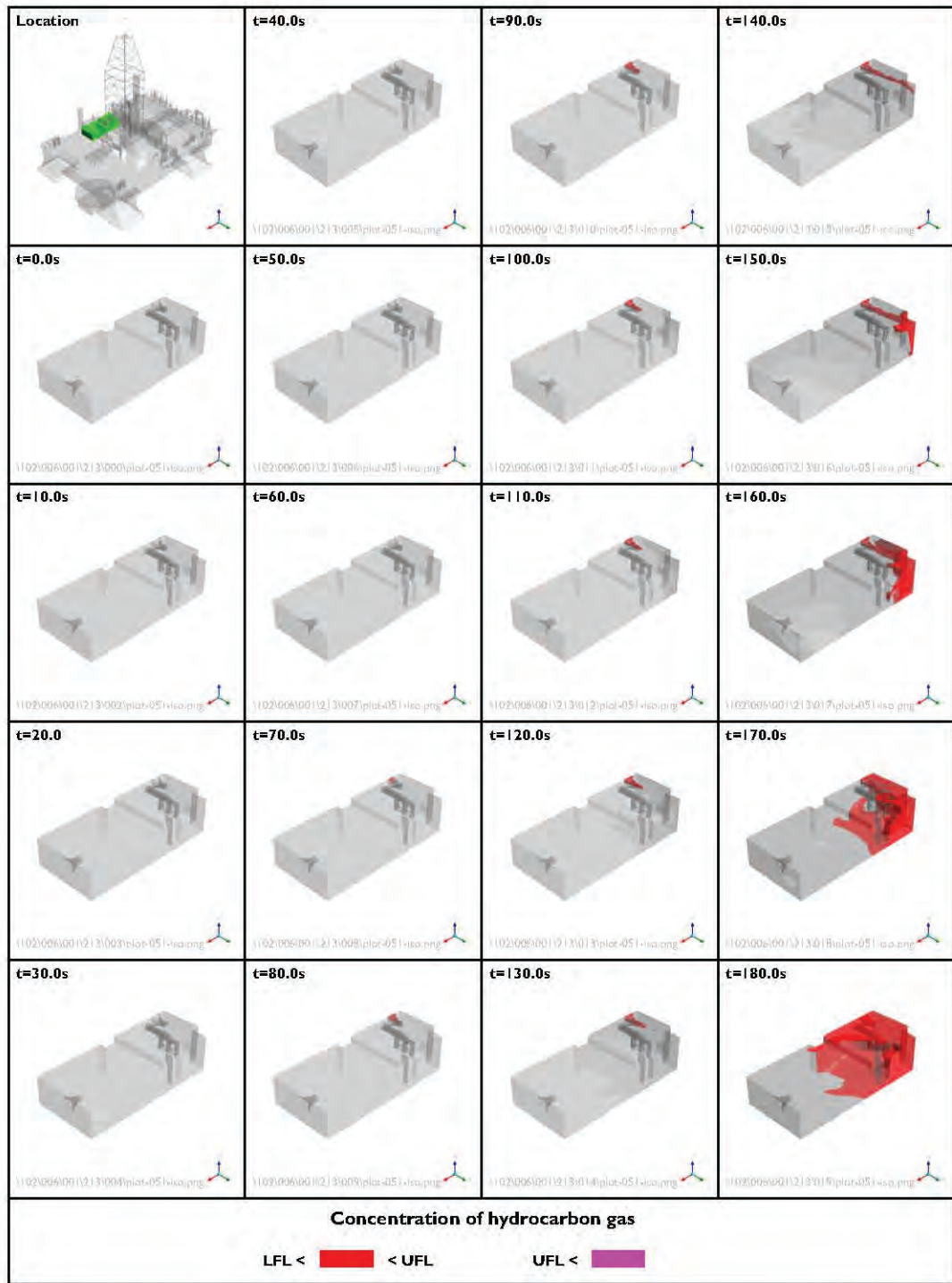
1.5 m/s

Wind direction:

90°

Figure I22

Extent of hydrocarbon gas within cement house – Case C



Peak flow rate:

300 MMscfd

Wind speed:

1.5 m/s

Wind direction:

90°

Figure 123

Extent of hydrocarbon gas within cement house – Case C

Appendix Q

Possible Ignition Sources

Appendix Q Possible Ignition Sources

The size of the flammable gas cloud that enveloped the *Deepwater Horizon* made an explosion almost inevitable. While the investigation team cannot specify what source or sources caused the gas to ignite, the investigation team has identified and analyzed possible ignition sources.

Engine Spaces (Likely)

Scope and Method of Investigation

Identification of potential ignition sources located in the engine room(s) by:

- Review of gas dispersion analysis and the extent of gas cloud
- Assessments of witness statements
- Review of technical drawings and rig schematics
- Review of engine operating procedures and instruction manuals

Summary of Investigation

No crew members were reported as working in the engine rooms at the time of the incident; however, crew members were present in the adjacent engine control room and electronic technician's workshop. The engine rooms were not classified as hazardous areas. The gas dispersion analysis (*See Appendix P*) shows that hydrocarbons had entered engine rooms 3 and 4 within 60 seconds after the initial release. Of the six engine rooms, engine rooms 3 and 4 are the most likely to have presented an ignition source.

During normal operation, an engine exhaust temperature is likely to exceed 420°C.¹ Hence, it is possible for hydrocarbons to self ignite when in contact with the exhaust covers. Should an engine start over-speeding, the exhaust temperature is very likely to spike to even higher levels, thus increasing the likelihood of self-ignition on the exhaust system.

Another potential scenario for ignition arises from an engine being started. When starting an engine, the air pressure in the start-air system will drop from 30 bar, therefore initiating the start-air compressor. The compressor is electrically driven and not explosion-proof and could be a potential source for sparks. Additionally, the effects of compressing hydrocarbons to such a high degree could lead to an ignition.

Two scenarios are most likely for initiation of an engine start sequence:

- Investigation indicates it is likely that an engine fueled by an uncontrolled source will take on all load and therefore trip the other running engine to prevent reverse power. After an engine has tripped, the Power Management System (PMS) will initialize start-up of an additional engine to maintain dynamic position (DP) status.
- Additionally, after a blackout, the PMS will start all generators on standby to recover power.

A witness stated that he saw an engine "changeover" and witnessed the blackout before the first explosion.²

Every time an engine is connected to the electrical bus or disconnected from it breakers will cause electrical sparks. Since this occurs in the switchboard rooms adjacent to each engine room these have been reviewed as a possible ignition sources; however, indications are that the hydrocarbon gas did not reach its low flammable limit in these rooms before the first explosion and are therefore considered as an unlikely ignition source.

The investigation team has identified a number of ignition sources within an engine room and that ignition was likely from one or more engine rooms. The team believes that an ignition and subsequent explosion would most likely be from within the engine room space rather than an actual engine.

Main Deck (possible)

Scope and Method of Investigation

Identification of potential ignition sources on the main deck by:

- Review of gas dispersion analysis and the extent of gas cloud on main deck, excluding areas in which hydrocarbon gas was not present
- Assessments of witness statements
- Review of technical and hazardous area drawings

Summary of Investigation

The main deck of the *Deepwater Horizon* was divided into four quadrants to refine the areas containing a potential ignition source. None of these areas were classified as a hazardous area.

An ignition of the hydrocarbons on the Main Deck was possible, but a specific location could not be identified.

(1) Port Forward (unlikely)

No crew members were reported working in this area at the time of the incident. The gas dispersion analysis shows hydrocarbon gas migrating into the port forward area after the initial release. The overall coverage of gas was low compared to other parts of the main deck (See *Appendix P*), therefore reducing the likelihood of providing an ignition source. The port forward area was mostly covered by pipe storage and the bridge; these areas were unlikely to provide an ignition source. The ventilation fans for lower decks, columns, and pontoons normally would have been running, but the gas cloud was unlikely to have reached its LFL at these vents before the first explosion occurred.

No viable ignition source was identified within this area.

(2) Port Aft (inconclusive)

It was determined that crew members were working with a bucking machine port aft, and their crane operator was in the gantry crane.³ The gas dispersion shows gas migrating into the port aft quadrant after the initial release. See *Appendix P*. This indicates only a short period of time when ignition could have been possible. There are contradicting witness statements from those working in this area about presence of gas in port aft area;⁴ however, the dispersion analysis indicates the gas cloud did not reach them within its flammable range before the first explosion.

Ventilation fans, the bucking machine, and the gantry crane were all possible ignition sources.

(3) Starboard Forward (possible)

Crew members were reported working in this area at the time of the incident.⁵ Some crew members were working on the starboard side of the rig with the starboard main deck crane. As the incident started, the crane operator was in the process of trying to lay the crane boom into the boom rest. From pictures taken after the incident, this task was not completed, so it can be assumed that the starboard crane engine was running.⁶ Other crew members were in this area but not performing any work that could create a viable ignition source. The gas dispersion analysis shows limited gas migrating into the starboard forward quadrant after the initial release, which allows for a short period in which ignition would be possible. See *Appendix P*. The ventilation fans for lower decks, columns, and pontoons would normally have been running, but the gas cloud was unlikely to have reached its LFL at these vents before the first explosion occurred.

If the starboard crane engine was running it could have provided a spark or hot surfaces for ignition.

(4) Starboard Aft (inconclusive)

No crew members were reported working in this area at the time of the incident. The gas dispersion analysis shows gas migrating into the starboard aft quadrant in the area of the riser skate (probably from the mud-gas separator and shale shaker ventilation) from very early on after the initial release (*See Appendix P*), which allows for a short period in which ignition would be possible. Electrical motors for various ventilation systems were covered in gas early after the initial release, and those motors could have ignited the hydrocarbons before they reached the engine rooms. However, witness statements show indication of gas entering some engine rooms (i.e., engines in engine rooms 3 and possibly 6 revving up); therefore, an ignition source from these electrical motors does not fit in with the sequence of events and are considered to be an unlikely source of ignition.⁷ The ventilation fans for lower decks, columns, and pontoons normally would have been running, and the gas cloud was likely to have reached its LFL at these vents before the first explosion occurred. However, for the same reason as with the electrical motors, these ventilation fans have been disconnected as an ignition source.

Non-explosion proof lights and junction boxes were a possible ignition source. The transformer room and its ventilation system are not believed to have provided an ignition source. The equipment located in the transformer room is very unlikely to have created an exposed spark or a significant hot surface.

Drilling Areas (Possible)

Scope and Method of Investigation

Identification of potential ignition sources located in the drilling areas by:

- Review of gas dispersion analysis and the extent of the gas cloud
- Assessments of witness statements
- Review of technical and hazardous area drawings and rig schematics
- Review of equipment lists

Summary of Investigation

Most of the drilling areas on the *Deepwater Horizon* were classified as Zone 2 Hazardous Areas and, therefore, all equipment had to be in compliance with American Bureau of Shipping (ABS) rules for that area; no evidence has been found that this was not the case.⁸ Though rated (classified) to only contain explosion-proof equipment, it is possible that an ignition point could exist in the area due to the presence of foreign objects or damage from well debris. The drilling area was divided into five parts for investigation purposes as follows:

- Shale Shaker Area (classified as a Zone 1 Hazardous Area)
- Mud Pump Room (not classified as a Hazardous Area)
- Mud Pit Area (classified as a Zone 2 Hazardous Area)
- Drilling Floor Area (classified as a Zone 2 Hazardous Area)
- Mud-Gas Separator (within a classified Zone 2 Hazardous Area)

Possible ignition points existed in various locations within the drilling area, but the investigation team has been unable to determine an exact ignition point

(1) Shale Shaker Area (unlikely)

Crew members reported working in this room prior to the incident. The shale shaker area was classified as a Zone 1 hazardous area, and all equipment had to be in compliance with ABS rules for this room; no evidence has been found that this was not the case.⁹ The drill crew had emptied the sand traps prior to the incident, but at the time of the incident, neither they nor any third party were believed to be working in (cleaning) the sand traps.¹⁰ Therefore, it is very unlikely that zoned equipment was exposed or unzoned equipment was present in the area. Gas entered this room shortly after it was released onto the rig (back feeding from the gumbo box into the shaker room) and activated the gas detection system.¹¹ It should be noted that the gas concentration quickly rose above its upper flammable limit (UFL), certainly before the first explosion. *See Appendix P.* An ignition source due to damage to equipment within the area is possible, but the possibility of flying debris is considered unlikely.

Ignition within this area is considered unlikely.

(2) Mud Pump Room (possible)

Crew members were working in this room prior to the incident. The mud pump room was not classified as a hazardous area. Leading up to the time of the incident, three of four pumps were operational, and a witness reports that repair work on the fourth pump had been completed prior to the explosions;¹² therefore, this work is not deemed to be a likely cause of ignition. Gas entered this room shortly after it was released onto the rig and was in the region of its LFL at the time of the first explosion. *See Appendix P.* After one of the explosions, a witness opened a door and looked into the room, but did not enter due to the damage he observed.¹³ It is unknown if the explosion in this room originated from within it or initiated in another space such as an engine room.

Ignition within this area is considered possible.

(3) Mud Pit Room (unlikely)

No crew members were reported working in this area at the time of the incident. The mud pit room was classified as a Zone 2 hazardous area, and all equipment had to be in compliance with ABS rules for this room; no evidence has been found that this was not the case.¹⁴ As far as can be established, no maintenance work was being undertaken in this room at the time of the incident. Gas entered this room less than 90 seconds after it was released onto the rig and was near its LFL at the time of the first explosion. *See Appendix P.*

Ignition within this room is considered unlikely.

(5) Drilling Area (possible)

Crew members were working in this area during the incident. The drilling area was classified as a Zone 2 hazardous area, and all equipment had to be in compliance with ABS rules for this area; no evidence has been found that this was not the case.¹⁵ Gas was present within the drilling area almost immediately after it was released onto the rig and activated the gas detection system.¹⁶ *See Appendix P.* This gas almost certainly was coming from the rotary table and overflowing from the top of the mini trip tank.

The drilling area had several possible ignition sources. The drill floor and derrick were likely subject to damage during the incident due to debris flying from the rotary table under pressure. The possibility of damage to lighting and equipment existed, which could cause an open electrical circuit and exposed spark. Well debris striking against objects on the drill floor or in the derrick could also cause a spark due to contact. The drawworks motors could also provide a source of ignition by drawing hydrocarbons into the blower motors. The driller's work station was a positive pressure environment,¹⁷ but once power was lost, any opening due to open doors or damage from debris could pose a potential spark due to non-zoned equipment located in the space. Any third-party equipment located in the area would require hazardous-area classification and was not determined to be a possible source of ignition.

Ignition within the drilling area is considered possible.

(6) Mud-Gas Separator (unlikely)

The investigation team found that the mud-gas separator (MGS) was overloaded, as evidenced by the design information and Macondo well hydraulic analysis performed by Stress Engineering Services. The MGS was contained within the drill floor Zone 2 hazardous area and had few parts that could have caused an ignition source. Although the MGS was overloaded beyond its design limits, and witnesses describe seeing a flash/explosion in the area of the MGS, the investigation team does not believe that the MGS itself exploded, and it is thought to be an unlikely ignition source.¹⁸

Ignition from the MGS is considered unlikely.

Moon Pool Area (Possible)

Scope and Method of Investigation

Identification of potential ignition sources located in the moon pool area by:

- Reviewing equipment and maintenance of equipment in the moon pool
- Assessing the potential of mechanical sparks due to well debris
- Review of witness statements and interviews
- Review of gas dispersion analysis

Summary of Investigation

The moon pool was classified as a Zone 2 hazardous area and therefore all equipment had to be in compliance with ABS rules for that area; no evidence has been found that this was not the case.¹⁹ The gas dispersion analysis indicates that a flammable gas cloud was forming within the first 30 seconds after the first release of gas onto the rig. *See Appendix P.* A witness describes “gas pressure” in the moon pool prior to the first explosion;²⁰ this is believed to be fluid/gas escaping through the slip joint packer, which probably failed due to the pressure of fluid/gas exerted onto it.²¹ The chief engineer describes an enormous fire in the moon pool when he went to try and start the standby generator.²²

Witness statement and review of the slip joint rating indicates that the slip joint packer likely failed and did not maintain a seal of the slip joint. Hence, it is possible that well debris was shooting out of the slip joint, potentially damaging equipment in the moon pool area and causing electrical sparks. Furthermore, debris impacting on the metal structure of the moon pool with such high velocity is capable of creating mechanical sparks and possibly impacting the integrity of equipment that was classified for use in a hazardous area.

The additional equipment, such as equipment provided by a third party, in the moon pool is not believed to be a potential ignition source.

Based on the evidence, the moon pool area has to be considered as a possible ignition source, although an exact location(s) within the area has not been identified.

Off Rig (Unlikely)

Scope and method of investigation Introduction

Identification of potential ignition sources located off rig by:

- Evaluating the likelihood of the sports fishing boat *Endorfin*, the supply vessel *Damon B. Bankston*, and any other vessel in the immediate area of the *Deepwater Horizon*
- Reviewing witness statements, interviews, and information provided by Tidewater Marine

Summary of Investigation

(1) *Endorfin* (unlikely)

Although the *Endorfin* had been under the rig prior to and at the start of the incident, according to the fishermen's statements, "They were about 100 yards from the *Deepwater Horizon* when the lights went out, and the first of a series of massive booms shook the rig."²³ Therefore this fishing boat is unlikely to have been a source of ignition.

(2) *Damon B. Bankston* (unlikely)

The supply vessel *Damon B. Bankston* was about 40 ft. away from the *Deepwater Horizon* on the port side of the rig with oil-based mud (OBM) hose connected and waiting to receive OBM back from the rig when the incident started.²⁴ The following potential ignition sources on the *Bankston* have been identified:

- Sparks from its exhaust stacks
- Hot work (burning and welding)
- Hot surfaces within its engine room

Information provided by Tidewater Marine indicates that the *Bankston* was equipped with working spark arrestors on its exhaust stacks.²⁵ From testimony by members of the *Bankston* crew, there is no indication that hot work was being performed on the vessel at the time of the incident. Had hydrocarbon gas entered the engine room of the *Bankston* and ignited, there would have been significant damage to the vessel; there is no evidence this happened. The *Bankston* crew did report to *Deepwater Horizon* survivors that a bridge window was broken, but this is believed to have been as a result of an explosion on the *Deepwater Horizon*.²⁶ Based on assessment of this information, the *Bankston* is not considered a viable ignition source.

(3) Other Vessels in the Area (unlikely)

There were other vessels within the immediate area of the *Deepwater Horizon* at the time of the incident, as confirmed by the response to the distress messages sent by the rig.²⁷ However, none of these vessels has been identified as being closer than 500 meters to the *Deepwater Horizon* at the start of the incident and, therefore, cannot be considered a viable ignition source.

Based on the information available, the investigation team considers it unlikely that the source of ignition for the hydrocarbon gas cloud on the *Deepwater Horizon* originated from a source "off rig."

Appendix Q Possible Ignition Sources

1. *Deepwater Horizon* – Exhaust Gas Temperatures, #1 and 2 Main Engines, Aug. 1, 2007.
2. Testimony of William Stoner, Hearing before the *Deepwater Horizon* Joint Investigation Team, May 28, 2010, 340:22–25.
3. Testimony of Micah Sandell, Hearing before the *Deepwater Horizon* Joint Investigation Team, May 29, 2010, 8:7–8, 12:2–4.
4. Transocean Investigation Team Interview of Cole Jones, June 1, 2010.
5. Transocean Investigation Team Interview of Caleb Holloway, May 28, 2010.
6. Picture of unknown source of *Deepwater Horizon*, taken approximately two hours after the start of the incident.
7. William Stoner Witness Statement, April 21, 2010; The United States Coast Guard, Doug Brown Witness Statement, April 21, 2010 *Deepwater Horizon*.
8. *Deepwater Horizon* Operations Manual, Section 9.1, March 2001.
9. *Deepwater Horizon* Operations Manual, Section 9.1, March 2001.
10. Sperry Sun data.
11. Testimony of Andrea Fleytas, Hearing before the *Deepwater Horizon* Joint Investigation Team, Oct. 5, 2010, 13:11–14; Testimony of Yancy Keplinger, Hearing before the *Deepwater Horizon* Joint Investigation Team, Oct. 5, 2010, 150:22–151:7.
12. Testimony of Chad Murray, Hearing before the *Deepwater Horizon* Joint Investigation Team, May 27, 2010, 314:2–9.
13. Testimony of Chad Murray, Hearing before the *Deepwater Horizon* Joint Investigation Team, May 27, 2010, 309:2–10.
14. *Deepwater Horizon* Operations Manual, Section 9.1, March 2001.
15. *Deepwater Horizon* Operations Manual, Section 9.1, March 2001.
16. Testimony of Andrea Fleytas, Hearing before the *Deepwater Horizon* Joint Investigation Team, Oct. 5, 2010, 13:11–14; Testimony of Yancy Keplinger, Hearing before the *Deepwater Horizon* Joint Investigation Team, Oct. 5, 2010, 150:22–151:7.
17. HITEC FDS Driller's work station ST3784-FDS-100; R&B Falcon., Safety Systems Design Philosophy, Aug. 23, 2000, TRN-MDL-00402475.
18. Testimony of Micah Sandell, Hearing before the *Deepwater Horizon* Joint Investigation Team, May 29, 2010, 10:5–11:24.
19. *Deepwater Horizon* Operations Manual, Section 9.1, March 2001.
20. Transocean Investigation Team Interview of Cole Jones, June 1, 2010.
21. ABB Vetco Gray, Telescopic Joint with Hydraulic Latch and Fluid Assist Bearing Operating and Service Procedure 6210, June 2000, 2; ABB Vetco Gray, Field Service Manual for Reading & Bates Drilling Co., RBS8D, *Deepwater Horizon*, HMF-H; Marine Riser System and Wellhead Connector, P.O. # MR-87-00023 Co's #C54927.
22. Testimony of Stephen Bertone, Hearing before the *Deepwater Horizon* Joint Investigation Team, July 19, 2010, 41:5–1423
Transocean Investigation Team Interview of Cole Jones, June 1, 2010.
23. Transocean Investigation Team Interview of Cole Jones, June 1, 2010; Huffington Post, May 9, 2010, marine biology student Albert Andry III and three friends had come to the *Deepwater Horizon* to fish.
24. Weekly Leader Episode 68 podcast of Captain Alwin Landry Interview, Oct. 5, 2010; *Damon Bankston* Log, April 20, 2010, TDW-0020.
25. Harold Wilson e-mail message to Billy Brown, Oct. 13, 2010, TWD-06611; Beaird Industries Inc – MSA1 Maxim Spark Arrestor Silencer.
26. Transocean Investigation Team Interview of Kennedy Cola, June 17, 2010; Transocean Investigation Team Interview of Mike Mayfield, June 3, 2010.
27. *Damon Bankston* Log, April 20, 2010, TDW-0020.

